The University Of Sheffield.

Synthesis and characterisation of nitroazoles, azidonitroazoles and azolyltriazenes and their use as explosophoric ligands for the synthesis of novel lead-free energetic materials

Bradley James Westwater

A thesis submitted in partial fulfilment of the requirements for the degree of Doctor of Philosophy

The University of Sheffield
Faculty of Science
Department of Chemistry

September 2022

Abstract

Conventional primary explosives such as lead azide ($Pb(N_3)_2$) and lead styphnate (LS), while offering enviable characteristics, are hazardous to health due to their lead content. Lead toxicity has been well studied and chronic lead poisoning has been shown to affect long term users of these compounds. Therefore, research has focused on the replacement of lead azide and lead styphnate with more environmentally friendly options. As a promising lead-free initiatory compound, copper (I)-nitrotetrazolate (DBX-1) has received much attention as the go to lead azide replacement, However, difficulties in consistently producing pure DBX-1 have prevented its full adoption in initiatory formulations

An investigation into the synthesis of DBX-1 has been conducted. It has been discovered that the nitrotetrazolate transfer reagent, sodium-nitrotetrazolate, must be purified as its tetrahydrate before DBX-1 can form. The formation of DBX-1 is heavily dependent on the state of the reactor vessel used and seed crystals play a dominant role in product selection. $Cu_3(NT)_2Cl$ (DBX-X) was found to form prior to any DBX-1 formation and is the first well defined compound produced from the Cu(II)/Cu(I) reduction system. The crystal structure of DBX-X has been determined during this investigation. DBX-X can be exclusively synthesised though the seeding effect of DBX-X crystals but this is much less effective than intentional seeding to form DBX-1 making large scale synthesis challenging. DBX-X proves to be much more sensitive to impact than DBX-1 however its lower thermal stability and liability to hydrolyse prevent it from being a viable alternative to DBX-1 and lead azide.

Six novel Cu(I)-nitroazolates have been synthesised as competitors to DBX-1. The synthesis of all six have been confirmed by elemental analysis and FTIR spectroscopy while some have also been identified through the use of Cu content analysis. Three of the compounds have also had their crystal structure determined: Cu_4(3,5-dinitrotriazolate)$_3$Cl ($Cu_4(DNT)_3Cl$), copper (I)-4-amino-3,5-dinitropyrazolate (Cu-ADNP) and copper (I)-3,5-dinitropyrazolate (Cu-3,5-DNP). Thermal behaviour and detonation performance parameters have been determined. All compounds prove to be highly thermally stable with some rivalling or surpassing the thermal stability of DBX-1. The calculated detonation velocities and pressures show all compounds to be of interest as primary explosives with most surpassing the recorded values for detonation velocities and pressures of DBX-1 and $Pb(N_3)_2$. Biscopper (I)-tetranitroimidazolate (Cu_2-TNBI), Cu-ADNP and $Cu_4(DNT)_3Cl$ have had their sensitiveness towards impact tested and all prove to be highly sensitive materials, far more sensitive than DBX-1 when recorded on the same instrument. Cu_2-TNBI and Cu-ADNP can be considered as viable alternatives to DBX-1 while $Cu_4(DNT)_3Cl$ will presumably suffer similar long term stability problems to DBX-X, preventing a practical use. Cu-3,5-DNP, Cu-2,4-DNI (copper(I)-2,4-dinitroimidazolate) and Cu-4,5-DNI (copper(I)-4,5-dinitroimidazolate) are untested with regard to impact sensitiveness but the other recorded properties of these compounds should warrant further investigation into their use as lead free initiatory compounds. Copper(I)-3,4-dinitropyrazolate (Cu-3,4-DNP) does not form as a crystalline precipitate but instead forms a suspected metallogel.

Triazenes have a short history of synthesis in the field of energetic materials and so research into their potential as explosophoric ligands was conducted. Bis(1-methyl-tetrazol-5-yl)triazene (B1MTT) was used due to its absence from the literature as a ligand. Sodium-bis(1-methyl-tetrazol-5-yl)triazene.5H_2O was reacted with six metal salts to form coordination compounds in all cases. Fe/Co/Ni(bis(1-methyl-tetrazol-5-yl)triazenide)$_2$ have all been crystallised as their acetone solvates. Pb/Zn(bis(1-methyl-tetrazol-5-yl)triazenide)$_2$ formation is proven by elemental analysis. All compounds had their thermal behaviour and detonation parameters determined. All compounds are proven to be highly thermally stable with some (Ni and Co compounds) proving more thermally stable than DBX-1. Impact sensitiveness has not been determined for the compounds. The reaction of $CuCl_2$ with Na-bis(1-methyl-tetrazol-5-yl)triazenide.5H_2O results in the formation of the mixed ligand coordination polymer Cu(B1MTT)(Cl)(H_2O). The chloride can be further substituted with other explosophores. The novel nitroazolyltriazene (only the second reported synthesis in this class of compound) bis(1-methyl-3-nitro-1,2,4-triazol-5-yl)triazene (B1M3NTT) is reported and has been characterised as its bis(triphenylphosphine)iminium (PPN) salt.

Like the triazenes, azidonitroimidazoles and pyrazoles have also been neglected in energetic materials research and so were investigated as energetic alkali metal salts. 2-Azido-4-nitroimidazole was synthesised as reported, however reports regarding the synthesis of 2-azido-4,5-dinitroimidazole have had doubt cast on them as a result of the work in this investigation. Potassium-2-azido-4-nitroimidazole has been synthesised and its crystal structure determined. Two azidonitropyrazolates have been shown not to form as their azido containing moieties but instead tautomerise to form pyrazolo-tetrazolates. The crystal structures of these compounds, K-4-nitropyrazolo[1,5 d]tetrazolate.H_2O and Na_2-3-oxido-4-nitropyrazolo[1,5 d]tetrazolate.5H_2O , were determined. The thermal behaviour and detonation parameters of the three novel alkali metal salts were determined with K-4-nitropyrazolo[1,5 d]tetrazolate.H_2O and Na_2-3-oxido-4-nitropyrazolo[1,5 d]tetrazolate.5H_2O potential being useful energetic compounds. K-4-nitropyrazolo[1,5 d]tetrazolate.H_2O also had its impact sensitiveness determined and proved to be almost as sensitive to impact as DBX-1.

Acknowledgements

First and foremost, I would like to thank my supervisor Dr. Peter Portius. Without your guidance throughout first my masters research project and now my PhD research project, I would not have been to complete the work I have. I am immensely grateful for the time spent discussing research ideas and for pushing me to become a better chemist.

During my time within the department, I have received training from many skilled staff members and for this I offer my thanks. A special thank you goes to Dr Craig Robertson without whom the determination of the crystal structures discussed in this thesis would not have been possible. Thanks also go to Dr. Tom Roseveare of the University of Sheffield and Dr. Inigo Victorica-Yrezabal of the University of Manchester for their help in the structural determination of Cu(I)-nitroazolates.

Thank you to group members past and present for making the Portius group into a positive place to conduct research. In particular, Dr. Rory Campbell and Dr. Zoe Smallwood were of great help during my time in the research group. Thanks go to the friends I've made during my time in the Department of Chemistry at Sheffield but especially to Evelin Csanyi and Mike Harris who have been here every step of the way from our time as undergraduates.

Thanks to all my friends from back home for all their support over the years especially to Jack, Nick and Connor for the many evenings of entertainment and to Jacob, Harry and Natalee for the organisation of countless meetups throughout my PhD project, without these the past four years would have been far less enjoyable. Looking forward to our next annual meeting.

To my parents, I would not be writing this thesis without the endless encouragement you have given me throughout my time at university. For that, I'll be forever grateful.

And finally, to my girlfriend, Georgie, who has been endlessly patient during the writing of this thesis. It would not have been possible to finish this work without your love and support over the past 3 years.

Author's Declaration

This research has been performed between the months of October 2018 and September 2022, within the Department of Chemistry at the University of Sheffield, under the supervision of Dr Peter Portius.

I, the author, confirm that the Thesis is my own work. I am aware of the University's Guidance on the Use of Unfair Means (www.sheffield.ac.uk/ssid/unfair-means). This work has not previously been presented for an award at this, or any other, university.

List of Publications

Published Manuscripts

1. B. Westwater, H. J. Lloyd, I. J. Vitorica-Yrezabal, A. Fong, P. McMaster, M. Sloan, B. M. Coaker, C. R. Pulham, P. Portius, Synthesis and characterization of the mixed-ligand coordination polymer $Cu_3Cl(N_4C\text{-}NO_2)_2$, *Dalton Trans*., 2020,49, 14975-14984

Contents

List of Abbreviations

2-A-4-NIm	2-azido-4-nitroimidazole
2-AIm	2-azidoimidazole
3-A-4,5-DNP	3-azido-4,5-dinitropyrazole
3-A-4-NP	3-azido-4-nitropyrazole
3-O-4-NPT	3-oxido-4-nitro-pyrazolo[1,5 d]tetrazolate
ADNP	4-amino-3,5-dinitropyrazolate
ANT	3-azido-5-nitro-triazole
APC	Atom Pair Contribution
B1M3NTT	Bis(1-methyl-3-nitro-triazol-5-yl)triazene
B1MTT	Bis(1-methyl-tetrazol-5-yl)triazene
B2MNTT	Bis(2-methyl-4-nitro-2H-1,2,3-triazole)triazene
B2MTT	Bis(2-methyltetrazolyl)triazene
BAM	Bundesanstalt fuer Materialforschung
BATT	1,3-bis-[3-(5-amino-1,2,4-triazolyl]triazene
BBB	Blood-brain barrier
BPT	1,3-bis(pyrazol-3-yl)triazene
CEA	Chemical Equilibrium with Applications
DBX-1	Copper(I)-nitrotetrazolate
DBX-X	$Copper(I)_3$-$(nitrotetrazolate)_2$-Chloride
DDT	Deflagration to Detonation transition
dmpz	3,5-dimethylpyrazolate
DNI	Dinitroimidazolate
DNP	Dinitropyrazolate
DNT	3,5-dinitrotriazolate
DSC	Differential scanning calorimetry
EI	Electron Impact Ionisation
EA	Elemental analysis
en	Ethylenediamine
ESD	Electrostatic discharge
ESI	Electrospray ionisation
FS	Friction sensitiveness
FTIR	Fourier transform infrared
GC-MS	Gas Chromatography-Mass spectrometry
IPA	Propan-2-ol
IS	Impact Sensitiveness
K_2DNABT	potassium-1,1'-dinitramino-5,5'-bistetrazolate
KDNBF	potassium 4,6-dinitro-7-hydroxy-7-hydrobenzofurazan-1-oxide
KDNP	potassium-5,7-dinitro-[2,1,3]-benzoxadiazol-4-olate 3-oxide
KW	Kistiakowsky-Wilson
LA	Lead Azide
LFI	Lead-free initiator
LS	Lead Styphnate
MALDI	Matrix-Assisted Laser Deposition Ionisation
MF	Mercury fulminate
MOF	Metal-organic framework
MS	Mass spectrometry
NaNT	Sodium nitrotetrazolate

NMR	Nuclear magnetic resonance
NPT	4-nitro-pyrazolo[1,5 d]tetrazolate
NT	Nitrotetrazolate
NTZ	3-nitro-1H-1,2,4-triazole
PETN	Pentaerythritol tetranitrate; 2,2-Bis[(nitrooxy)methyl]propane-1,3-diyl dinitrate; penthrite
PPN	Bis(triphenylphosphine)iminium
PXRD	Powder X-ray diffraction
RDX	1,3,5-trinitro-1,3,5-triazacyclohexane; hexogen; cyclo-trimethylenetrinitramine
ROS	Reactive oxygen species
SCXRD	Single crystal X-ray diffraction
SEM	Scanning electron microscopy
SET	Single Electron Transfer
SR	Springall Roberts
TEM	Transmission electron microscopy
TGA	Thermogravimetric analysis
TNBI	Tetranitrobisimidazolate
TNI	Trinitroimidazolate
TNP	Trinitropyrazolate
TNT	Trinitrotoluene
TOF	Time of Flight
UN	United Nations
UV-vis	Ultraviolet-visible

Structure, names and abbreviations of compounds relevant to the work conducted

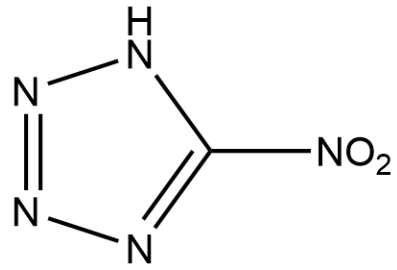

Nitrotetrazole (NT)

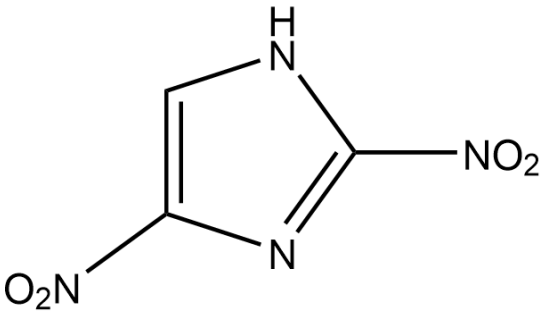

2,4-Dinitroimidazole (2,4-DNI)

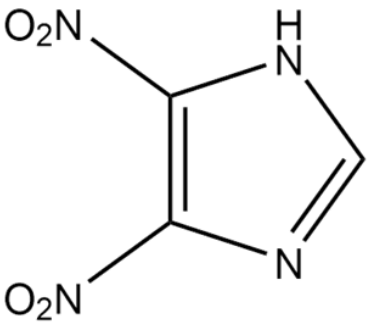

4,5-Dinitroimidazole (4,5-DNI)

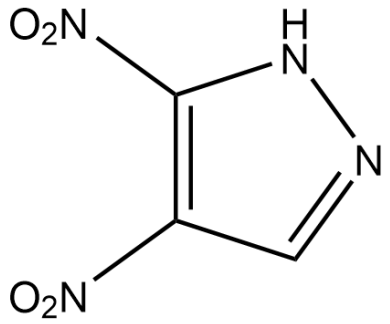

3,4-Dinitropyrazole (3,4-DNP)

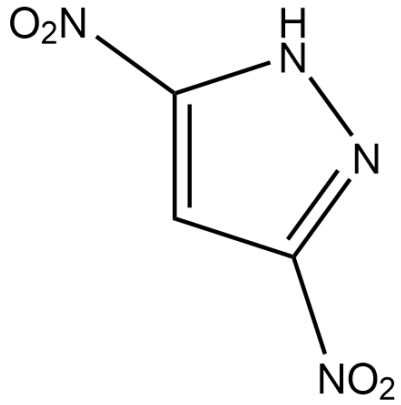

3,5-Dinitropyrazole (3,5-DNP)

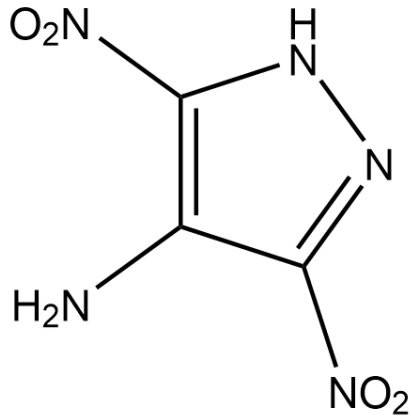

4-Amino-3,5-dinitropyrazole (ADNP)

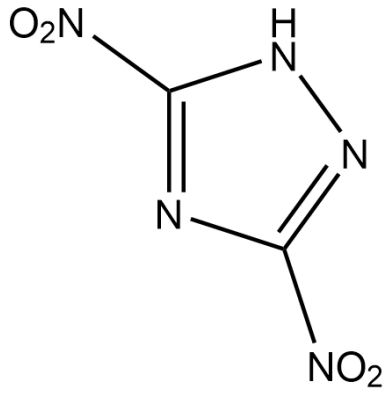

3,5-Dinitrotriazole (3,5-DNT)

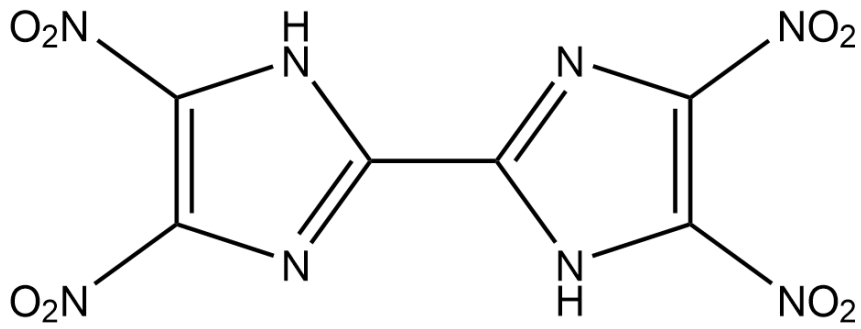

4,4’,5,5’-Tetranitrobisimidazole (TNBI)

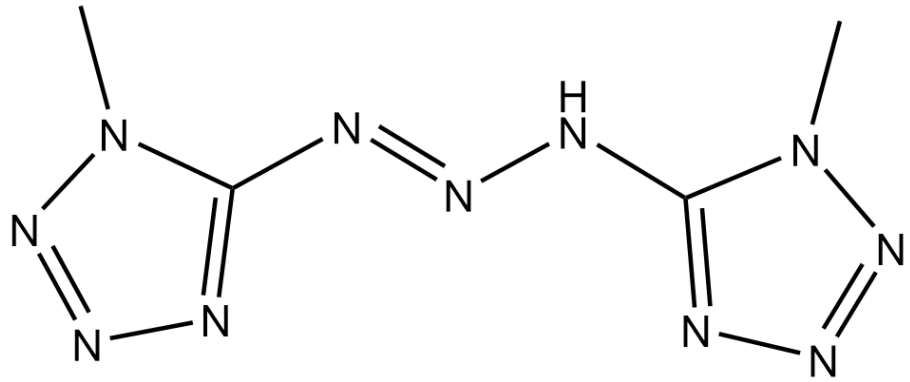

Bis(1-methyltetrazol-5-yl)triazene (B1MTT)

x

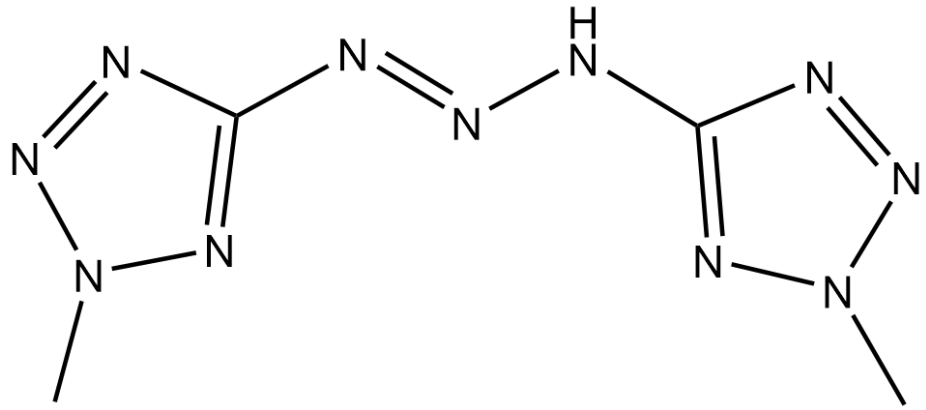

Bis(2-methyltetrazol-5-yl)triazene (B2MTT)

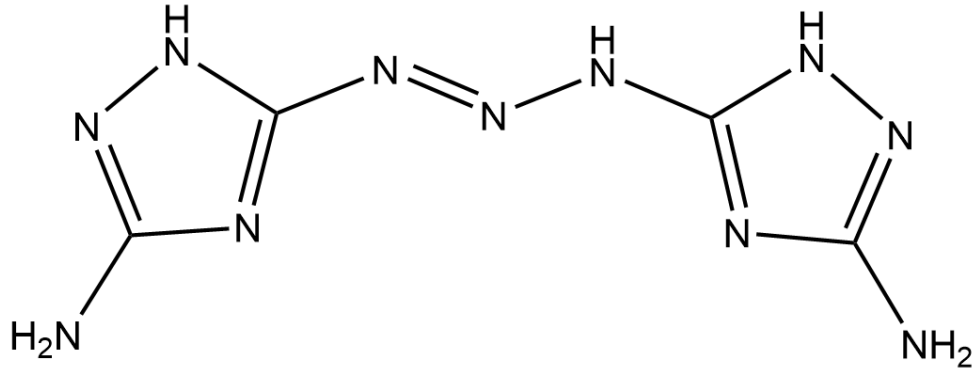

Bis(5-amino-1,2,4-triazol-3-yl)triazene (BATT)

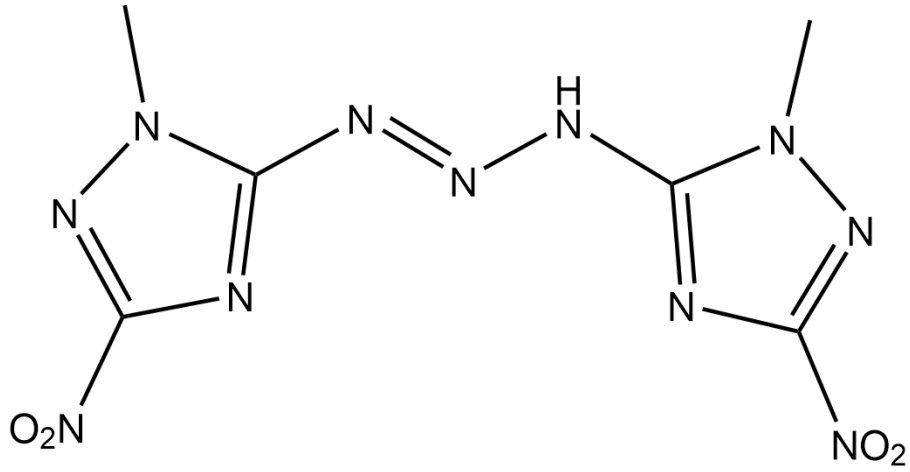

Bis(1-methyl-3-nitro-1,2,4-triazole)triazene (B1M3NTT)

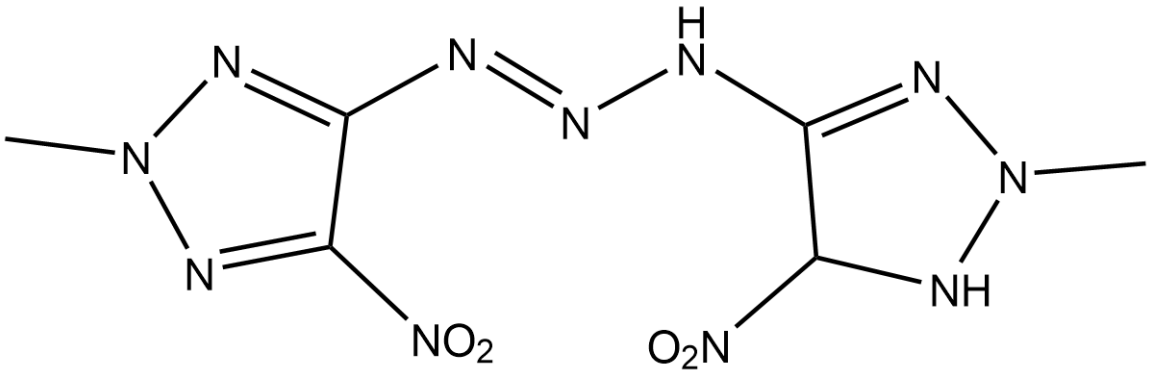

Bis(2-methyl-4-nitro-1,2,3-triazole)triazene (B2MNTT)

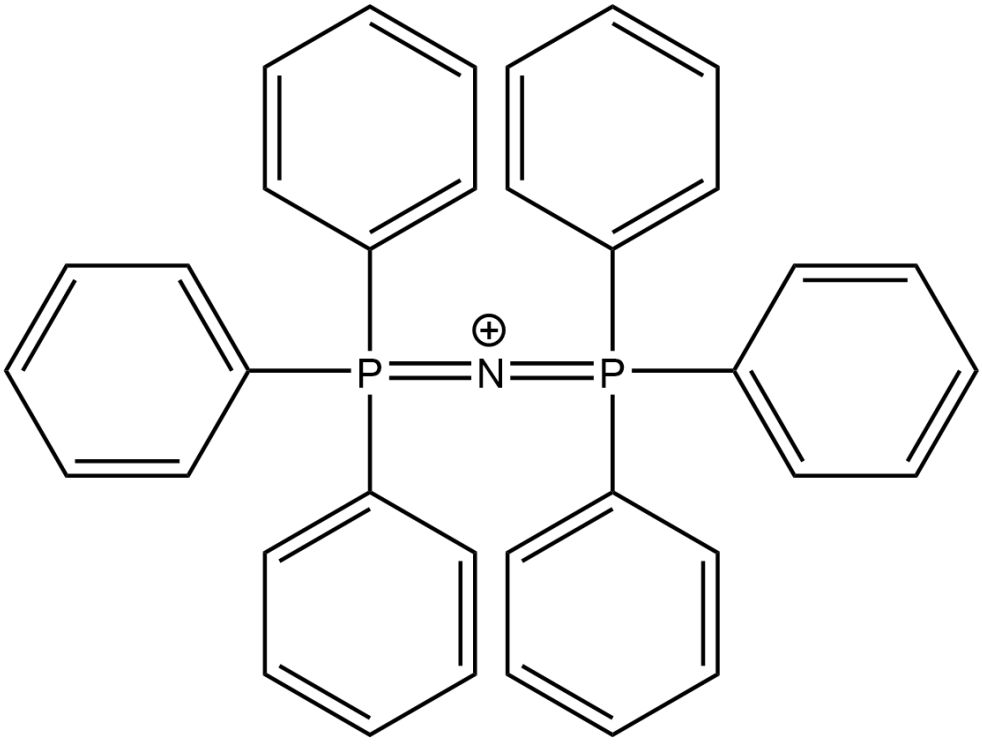

Bis(triphenylphosphine)iminium cation (PPN)

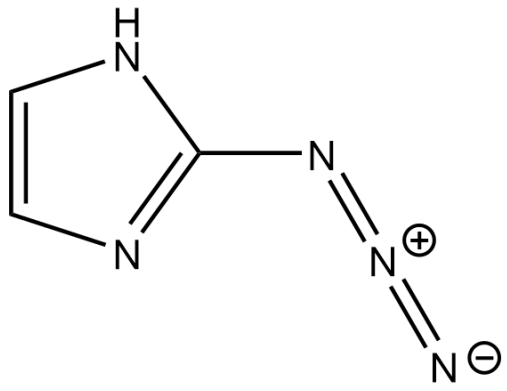

2-Azidoimidazole (2-AIm)

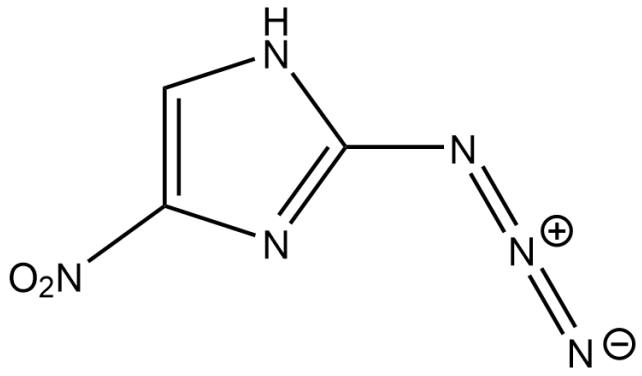

2-Azido-4-nitroimidazole (2-A-4-NIm)

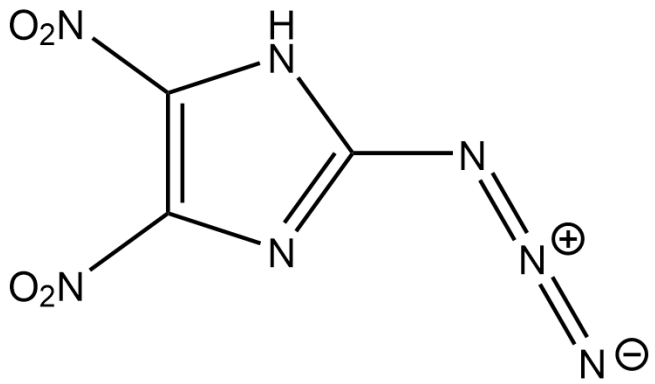

2-Azido-4,5-dinitroimidazole (2-A-4,5-DNI)

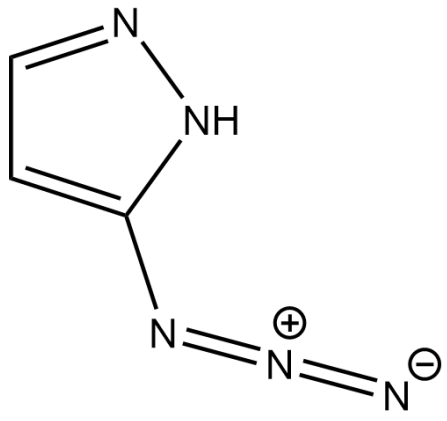

3-Azidopyrazole (3-AP)

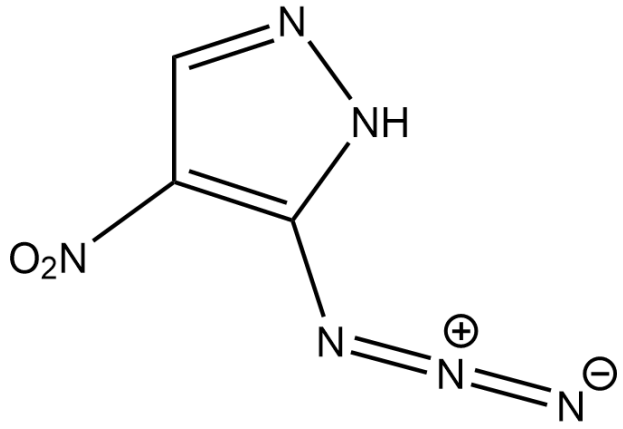

3-Azido-4-nitropyrazole (3-A-4-NP)

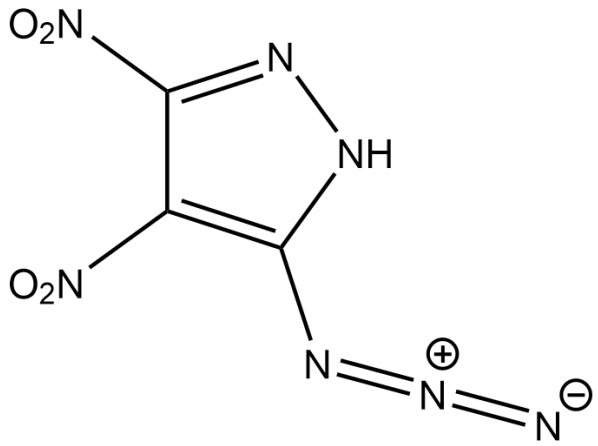

3-Azido-4,5-dinitropyrazole (3-A-4,5-DNP)

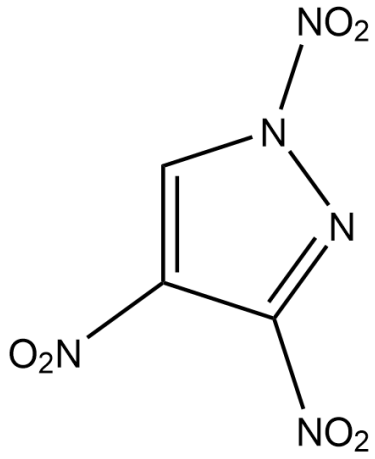

1,3,4-Trinitropyrazole (1,3,4-TNP)

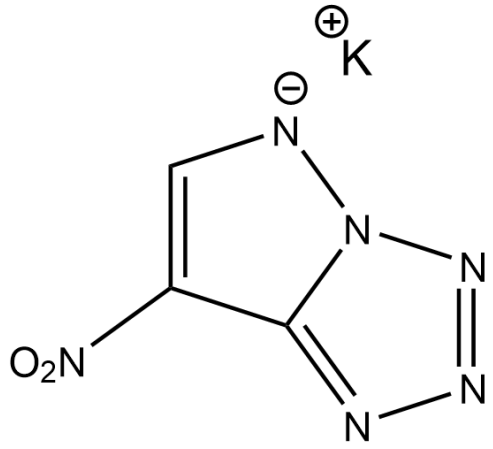

Potassium-4-nitropyrazolo[1,5 d]tetrazole (K-NPT)

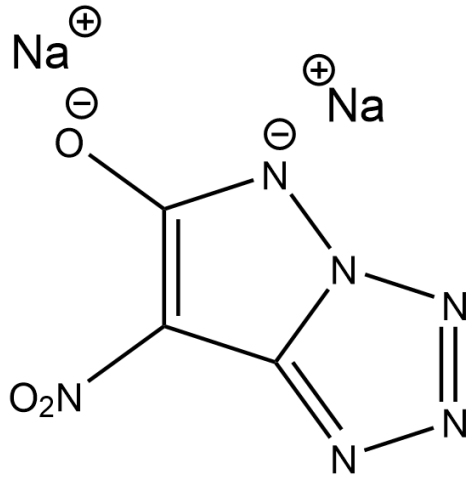

Disodium-3-oxido-4-nitropyrazolo[1,5 d]tetrazole (Na_2-3-O-4-NPT)

Theses

1. What are the difficulties in the synthesis of DBX-1 preventing its full adoption as the replacement for lead azide? Can DBX-1 be consistently synthesised in a pure crystalline state? Can the identities of by-products in the reaction to form DBX-1 be identified and characterised (crystallographically or spectroscopically)?

2. Can novel copper(I)-nitroazolato compounds be formed using the same reaction system as for DBX-1? Can the detonation performance parameters of these compounds be recorded? Do the synthesised copper(I)-nitroazolates have properties that allow them to be seen as DBX-1/$Pb(N_3)_2$ replacements?

3. Can the known triazene, bis(1-methyl-tetrazol-5-yl)triazene, be used in the synthesis of energetic coordination compounds? Can crystal structures of novel metal-triazenido compounds be determined and how do they compare to related known metal-triazenides? Do the novel metal-triazenides possess the detonation performance parameters and long-term stability expected of primary explosives? Can novel nitroazolyl-triazenes be formed and characterised?

4. Can known azidonitroazoles be synthesised in good yield and purity? Can the alkali metal salts of these azoles be synthesised and their crystal structures determined? Do the alkali metal salts possess similar detonation performance parameters to other known alkali metal LFI's?

1. Introduction

The subjects discussed during this introduction have been chosen due to their relevance to the work carried out and communicated throughout this thesis. Classification of energetic materials is introduced to explicitly state the criteria used to define explosives as either primary or secondary explosives. Knowledge of these criteria is required to assess the later classification of novel compounds synthesised during this research project. Information contained within this section is built upon a general review of the common books in the field of energetic materials (ref[1-5]) and also research papers discussing the chemical classification of explosives. Characterisation of energetic materials is covered to give a general guide to the tests common to energetic materials. Information is once again built upon a review of books common to the field but also upon the UN published guidelines regarding characterisation of energetic materials alongside research articles dealing with particular characterisation techniques. A brief history of the legacy primary explosives and the problems associated with their use and a summary of the current replacements of these materials is discussed. It can be said that this discussion is integral to the understanding of why the research presented in this thesis was conducted. Information in this section is developed from the various review articles published regarding these topics alongside the book *Primary Explosives* by Matyáš and Pachman which gives a comprehensive account of the history of legacy primary explosives. Methods of introducing the nitro group into azolates and mechanisms of nitration are covered extensively during the introduction as nitroazolates feature heavily in this work. Information regarding methods of introducing the nitro group to azoles has predominantly come from the book *Nitroazoles: Synthesis, Structure and Applications* and from the various papers that have come to be known to the author over the course of this research project. The FTIR spectroscopy of NO_2 groups is also discussed at length in the introduction. FTIR has been used extensively as a way to probe the bonding present in metal salts and coordination compounds of energetic ligands to assert if reactions have progressed as expected. Information in this section has been developed by a thorough review of the available literature and books specifically regarding the vibrational spectroscopy of the NO_2 group. Finally, a review of the characterisation techniques used during this PhD research project has been discussed.

1.1 Classification of energetic materials

Energetic materials are primarily classified based upon their uses. These classes are *explosives*, *propellants* and *pyrotechnics*. Pyrotechnics are defined as energetic materials that, when burned, release large amounts of light, heat, smoke, sound or a combination of these.[1] Pyrotechnics find common use as road flares, fire extinguishers and fireworks.[1] Propellants are compounds or mixtures of compounds which, when burned, expel gaseous products, provide thrust and impart momentum when initiated in a rocket motor, for instance. A key characteristic of propellants is that they must combust in a controlled manner (*i*) and must not be able to undergo a deflagration-to-detonation transition (DDT) (*ii*).[2] Explosives are further divided into two classes according to their sensitiveness: *primary* and *secondary* explosives. It is important to define the difference between sensitivity and sensitiveness. Sensitiveness to stimuli is with respect towards accidental initiation and the determination of probabilities of initiation by stimuli whereas sensitivity is related to the reliability of a function (such as in tests more applicable to real world applications).[3] However, throughout the chemical literature the terms are used somewhat interchangeably (the use of either word during this thesis is with respect to the above definition). Primary explosives are energetic materials which display a very rapid transition from deflagration (defined as a subsonic combustion of a material after ignition from a flame, shock, spark, friction etc. Deflagrating substances burn faster and more violently, accompanied by flames/spark/crackling noises, than ordinary combustible materials) to detonation (defined as the propagation of a chemical reaction zone through an energetic material by the action of a shock-wave at a speed faster than sound).[3][4] Primary explosives generate large amounts of heat or a shockwave which can then be used to induce either deflagration in propellants and pyrotechnics, or detonation in other, more powerful explosives.[4] Primary explosives are exceptionally sensitive towards initiation through impact, friction, electrostatic discharge and heat in general – all of which can cause detonation. Secondary explosives (also referred to as high explosives), unlike primary explosives, cannot be easily initiated through impact, friction, electrostatic discharge and heat. Instead, the detonation of a secondary explosive requires the transfer of a shockwave from a

primary explosive. Secondary explosives also usually have explosive performance parameters greater than those of primary explosives.[4]

Explosive materials can also be classified according to their chemical composition. Classification depending on the chemical composition of explosives can prove useful with regards to the identification of classes of explosophores. Explosophores are functional groups that can be incorporated into molecules to imbue energetic or explosive properties. Knowledge of common explosophores also drives theoretical studies into the property prediction of novel compounds which concentrates on the thermal stability and sensitiveness to initiation. The structure-property relationships derived from these studies are sometimes explicitly used to guide design of novel explosive materials. Chemical classification also finds use in the detection of explosive materials where the knowledge of common explosophores is key to deciding upon the analytical methods required for detection of these materials. Various iterations of these chemical classes have been issued by different authors since van't Hoff first proposed classes based upon the seven types of chemical bonds that usually provide explosive properties to molecules in 1909.[5] Each subsequent list of classes further subdivides or reclassifies the chemical commonalities of explosives into ever more niche categories.[5] However, common groupings of chemical classes are agreed upon and can be used for broad definitions of the chemical classes of explosives (**Figure 1.1**). Explosives can at first be divided between pure/single explosives and explosive mixtures. Pure/single explosives refer to pure unimolecular explosives whose decomposition may result in an explosion.[6] Explosive mixtures are combinations of two or more explosives to produce composite explosive mixtures such as Composition B (RDX (60%) and TNT 40%) or Semtex H (PETN (50%) and RDX (50%)). While explosive mixtures can be subcategorised, due to the focus of the work of this thesis only single explosives will be discussed further. Single explosives can be divided between organic and inorganic explosives. Organic explosives are explosive molecules that contain at least one atom of carbon and only C, H, O, N or halogen in their structures. The organic explosives can be broken down into six classes:[6]

- Nitro explosives: Nitro explosives are organic explosives characterized by having in their structure one or more nitro groups (R-NO_2). These can be further divided into nitro aromatics (R-NO_2 groups bound to a carbon atom that is part of an aromatic ring system), nitro aliphatics (R-NO_2 bound to a carbon atom as

part of an aliphatic chain), nitramines (R-NO_2 group bound to a nitrogen atom) and nitrate esters (R-NO_2 bound to an oxygen atom)[7]

- Organic azides: Characterised by having at least one azido group (R-N_3) bound to a carbon[3][7]
- Peroxide explosives: Characterised by having one or more peroxido groups (-O-O-) in their structure[8]
- Organic halogen amino explosives: explosives that contain at least one carbon and one halogen amino group (-NX_2, X=F, Cl…) in their structure[6]
- Azo/diazonium explosives- Explosive compounds containing at least one carbon atom with an azo (-N=N-) or diazonium group (-$N{\equiv}N^+$)[3][7]
- Miscellaneous organic explosives- explosives containing at least one carbon atom which do not fit in any other classification

Inorganic explosives differ in that they contain no carbon atoms and/or contain an atom in their structure different to C, H, N, O or the halogens. Inorganic explosives can be further subcategorised into non-metal and metal containing inorganic explosives. Non-metal inorganic explosives are explosives that do not contain either carbon or metal atoms in their structure and can commonly be found in the form of ammonium salts (inorganic ionic salts composed of the ammonium cation and an anion such as nitrate, dinitramide, perchlorate…), nitrogen halides (NI_3, NCl_3…) and as hydrazine derivatives.[3][9] Metal containing inorganic explosives are simply those explosives that contain one or more metal atoms per formula unit. These can be further sub-divided as shown below:[6]

- Metal azides- Metal azides are the combination of the azide anion bound to a metal cation such as $Pb(N_3)_2$[3][6]
- Metal fulminates- Metal fulminates are the combination of a metal cation and a fulminate anion, $(C{=}N{=}O)^-$, such as silver fulminate(AgCNO) or mercury fulminate ($Hg(CNO)_2$). [3][6]
- Metal acetylides- Metal acetylides are characterised as containing a metal atom and an acetylide group (-C≡C-) such as cuprous acetylide (Cu_2C_2)[3][6]
- Organometallic explosives- Organometallic explosives consist of metal centres surrounded by already high energy ligands. This class of compounds is very

broad with many examples such as the nitrotetrazolate coordination compounds[3][6]

- Metal Salts- energetic organic or inorganic ligands bound to a metal centre by ionic interactions[3][6]

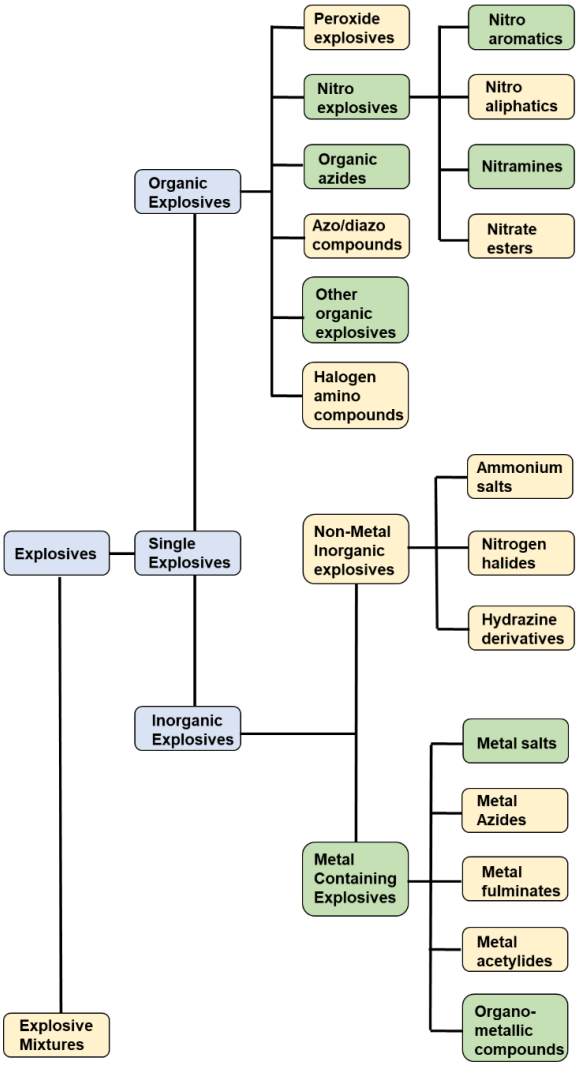

Figure 1.1: *Chemical classification of explosives, categories highlighted in green are of interest to this thesis*

1.2 Ignition, hot-spots and phonon-mode up-pumping

Chemical explosions can be divided into five stages: Ignition, growth of deflagration, deflagration to detonation transition, detonation and then the propagation of detonation.[4] Ignition can lead directly to detonation if the initiating impulse is able to impart a large amount of energy onto an explosive. Heat produced from adiabatic

compression then causes the shockwave to propagate detonation (NB: the conditions required for this usually occur only in specially-formulated explosive compositions).[2] It is thought that the ignition of explosives is a thermal process. Ignition occurs when a material is heated to or above its ignition temperature, T_{ign}, which is specific to individual substances.[2] Ignition temperature is defined as the minimum temperature required for the process of initiation to be self-sustaining. The action of external stimuli (friction, impact, electron static discharge etc.) on explosive materials inputs energy into the explosive and results in a rise in its temperature. Once stimulated, the rise in temperature induces a series of pre-ignition reactions (transitions in crystalline state, liquid phased becoming gaseous, thermal decomposition etc.) which lead to a self-sustaining combustion of the material termed 'ignition'.[2] Energy from external stimuli can be converted to thermal energy in a variety of ways. The heat produced from stimuli is concentrated in small transient, regions of the material termed 'hot spots'. There is no single mechanism of formation of hot spots as the mechanism/isms that operate depend upon the energy input and physical properties of the material. A non-exhaustive list of hot spot formation mechanisms is detailed below:[10]

- Adiabatic compression of trapped gas bubbles
- friction between explosive crystals and/or grit particles in an explosive
- rapid heating of other components of the explosive mixture (polymer binder etc.) causing catastrophic failure of the component and energy release
- localized adiabatic shear of the material during mechanical failure
- heating at dislocation pileups
- heating at crack tips

Hot spots formed via friction readily form on the surface of crystals due to their relatively low thermal conductivity (in comparison to metals). The temperature of the hot spots must be greater than 430 °C for ignition to occur but the maximum temperature of hot spots formed through friction is determined by the melting point of the crystals (explosives with melting points below 430 °C will not achieve ignition through the frictional formation of hot spots).[2] Frictionally generated hot spots have a lifetime of 10^{-5} to 10^{-3} seconds. It is important to note that not all hot spots lead to

detonation. If the energy lost to the surroundings is greater than the energy generated by the hot spot formation then the micro-explosion will die away without propagation of the detonation.[2]

Hot spots formed via impact will have different mechanisms of formation depending on the phase and form of the explosive. When liquid explosives are impacted, trapped gas bubbles experience adiabatic compression and collapse and produce local heating above the T_{ign} of the explosive (NB: degassing of liquid explosives can therefore lead to desensitisation). When solid explosives are subjected to impact, hot spots form through either the compression and heating of gas bubbles or through inter-crystalline friction. Primary explosives ignite only below the melting temperature of the crystals and thus primarily ignite due to inter-crystalline friction whereas secondary explosives ignite above their melting point. When exposed to impact, secondary explosives will flow (plastic flow), entrapping gas bubbles. Hot spots then form in a similar way to that described in liquid explosives.[2][4][10]

The thermal energy produced from hot spots must be efficiently converted to molecular bond breaking vibrations to induce decomposition and propagate detonation.[4] This occurs through a process called vibrational ‘up-pumping’. In this model, energy (either from hot spots or directly from shock waves) is transferred into the phonon modes (phonon defined as a quantum mechanical description of the uniform vibrational motion of the atoms that make up the crystal lattice) that are specific to a material.[11-13] These low frequency phonon modes must efficiently convert (‘up pump’) this vibrational energy into higher frequency (>1000 cm^{-1}) molecular vibrations relevant to bond breaking. The dominant mechanism by which up-pumping occurs is the anharmonic coupling of excited phonon modes with low frequency molecular vibrations (known as doorway modes). The efficiency with which up-pumping occurs has great control over the sensitiveness of an explosive, with any process that leads to dissipation of energy (diffusion, rotational modes etc.) having a desensitising effect on the sensitiveness of an explosive. In contrast, any feature of a compound that leads to more efficient up-pumping (NB: it has been reported that defects in the crystal can lead to a local increase in the anharmonic coupling of excited phonon modes with low frequency molecular vibration)[11] will have a sensitising effect.

1.3 Characterisation of energetic materials

To determine whether an explosive can be classified as a secondary or primary explosive, sensitiveness tests to certain stimuli are used. Impact sensitiveness (IS) is one of the simplest and easiest methods of assessing sensitiveness with references for its use dating back to the early 20th century.[14] The United Nations (UN) recommended impact sensitiveness tester is the BAM drop hammer (BAM = Bundesanstalt fuer Materialforschung and –pruefung, federal authority for materials research and materials testing of the FRG) (**Figure 1.2**).[15] A typical tester will consist of an impactor of known mass, *m*, and an anvil. The tested substance is placed between two steel cylinders and then onto the anvil. The impactor is then released from a known height and guided to strike the metal cylinder. The impactor is dropped multiple times from a series of drop heights onto a fresh sample each time. Each drop is recorded as a “go” (i.e., flash, smoke, and / or audible report) or “no go”, depending on how the energetic material has reacted.[3][4][16-18] The data is then converted to an observed probability of samples initiated vs. drop height plot, from which the h_{50} height (at which 50% of drops resulted in initiation) and the E_{50} energy (energy required for 50% of drops to initiate) can be interpolated. These values are essential in the discussion of impact sensitiveness. Compounds with E_{50} above 40 J are considered to be insensitive; note that primary explosives typically have E_{50} below values of 4 J.[4][15][17] A compound is considered insensitive at a certain drop height only if none of the drops result in a “go”. The minimum impact energy required for any initiation is defined as the height at which one out of six drops initiate the sample.[4] While h/E_{50} are useful for describing the impact sensitiveness of explosives one must also consider the limitation of such values. Due to differences in tester design (mass of weight used, drop height, sample mounting procedure, use of grit paper, shape of striking pin etc.) values of h/E_{50} for explosives should not be seen as infallible and true for all laboratories. Instead, the h/E_{50} for a specific explosive is true only for the laboratory in which the impact test was done. Even with the UN recommended BAM tester (used by many laboratories around the world) one cannot assume that values between BAM testers will be consistent. Sample morphology can also play an important role in the obtained sensitiveness values with differences in crystal size and shape greatly affecting the value recorded. Therefore, not only are h/E_{50} specific to

the laboratory and equipment used to record the values, but it should also be said that the recorded value is specific only to the particular batch of explosive used for the test.[19][20] The use of a standard on the specific tester used is imperative for contextualising the values for h/E_{50}. While values for sensitiveness can change between labs, by recording a value for sensitiveness for a standard (RDX, PETN etc.) one can at least draw general trends of sensitiveness useful enough for discussion of the safety one must employ for safe handling of the explosive in question. For example, RDX (reported IS of ~7J) is a useful standard when the impact sensitiveness of primary explosives is being assessed due to the proximity to the typical value for primary explosives (~4J). Any compound found to have a higher sensitiveness towards impact than RDX can be seen as a potential primary explosive and must therefore be treated appropriately.

Figure 1.2: *Specialised apparatus for standard, quantitative testing of energetic materials. Left: BAM Falhammer for impact sensitiveness testing(Image copyright ref[18]); Top Right: Spark generator for electrostatic sensitiveness testing (Image copyright ref[18]); Bottom Right: BAM friction sensitiveness tester (Image copyright ref[21])*

Another important test for sensitiveness is the friction test. Friction sensitiveness (FS) testers measure the frictional force required to initiate an explosive reaction. The BAM friction tester (**Figure 1.2**) is probably the most widely used commercial instrument and is part of the UN-recommended testing procedure for determining friction sensitiveness.[15] In this test a porcelain plate loaded with 20 mg of the sample being tested is moved beneath a porcelain peg through which a load can be applied by suspending weights on the loading arm. The test proceeds through loads ranging from 0.1 N to 360 N with six trials conducted at each load.[4][16][17][22] The friction sensitiveness of an energetic material is then defined as the lowest frictional load at which one explosion occurs during six trials.[4][16] Compounds with friction sensitiveness's of above 360 N are regarded as *friction insensitive* while compounds with sensitiveness's of under 80 N will be designated as too sensitive for transport. Primary explosives typically have friction sensitiveness's of below 10 N.[4][15] Materials must also be sieved prior to being tested; the particles for the test should pass through a sieve with 0.5±0.05 mesh size (NB: while particle size is not specified for the other energetic material tests, sieving to ensure uniform particle size should also be performed for all tests) .[15]

Sensitiveness to electrostatic discharge (ESD) is one of the most frequent causes of accidents with energetic materials, hence, determining this type of sensitiveness is a critical and increasingly important test for any energetic material,[23] especially, given that the human body can become electrostatically charged and generate spark energies of 0.005 to 0.02 J [4]. ESD is measured using an ESD test apparatus (**Figure 1.2**) whereby spark energies, typically ranging from 0.001 J to 20 J, are applied to a material sample.[4] ESD values are highly particle size-dependant, and samples must therefore be sieved prior to measurement to ensure sufficient homogeneity in particle size.[4] Materials with ESD values less than 0.1 J are considered *sensitive* and those with sensitiveness's above 0.1 J are described as *insensitive.*[4]

The Koenen test, devised by Koenen and Ide in 1956 is another test used for the evaluation of energetic materials.[24] This test is used to determine the effect of intense heat on a *confined* solid or liquid.[11] The result of this test is used to determine transport safety.[4] For this test, a sample is loaded into a steel tube with defined material and geometric parameters, which is then sealed with a nozzle plate containing

a nozzle with defined opening diameter. The tube is then heated by three gas burners in a particular geometric, fixed, arrangement (**Figure 1.3**) until the sample tube either ruptures, or until a minimum of 5 minutes has passed uneventfully. After each test the fragments (if any) are collected and weighed. A reaction is recognised as an explosion if the tube has fragmented into three or more pieces.[15][24][25] Since the fragmentation of the tube plays a significant role in this test, meaningful comparisons of test results can only be made under conditions where the bursting pressure of the tube is roughly constant.[4]

While not an important parameter in the *classification* of new energetic materials, thermal stability is nevertheless critical for an assessment of chemical stability which has a large impact on potential practical applications of a given material. Differential scanning calorimetric measurements (DSC) are usually performed as a simple and quick method that requires only small amounts of material (1 to 10 mg) at a time, to determine both decomposition temperatures and reaction heats.

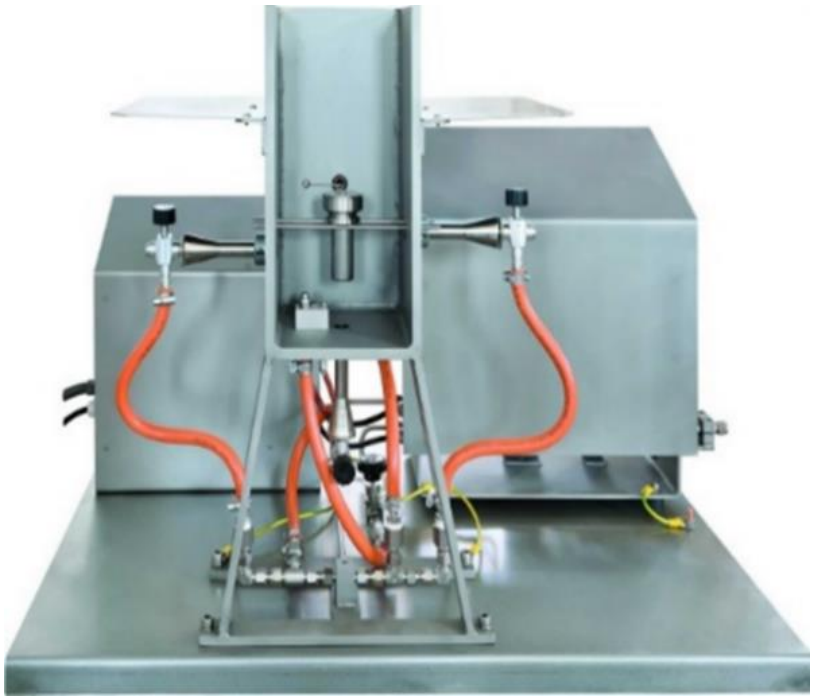

Figure 1.3: *Koenen Test apparatus (Image copyright ref[25])*

Typically, samples are confined either in perforated aluminium crucibles allowing for pressure release, or in hermetically sealed stainless-steel capsules equipped with a burst disc. In either case, samples are heated at rates at or below 10

K min^{-1}. Sufficiently low heating rates must be chosen to avoid sample explosion which damages the calorimeter sample heating stage. However, longer-term stabilities require more involved measurements. These can, for instance, be performed by isothermal calorimetry which requires time periods of 48 hours or longer. Alternatively, isoperibolic calorimetry can be applied where the stability of substances in a cell with controlled internal temperature is investigated.[4]

The Kneisl-Test is another method of testing long-term thermal stability. In this test a known quantity of a substance is sealed in a glass ampoule and then placed in an oven for a duration of 100 hours at the temperature for which thermal stability is needed. At the end of the heating period, the ampoule is opened, the mass of the remaining product recorded, and any gaseous products analysed by standard methods (FTIR, MS, GC-MS). If less than 2% of the original mass of the substance is lost to decomposition, then the substance is deemed to have passed the test for that temperature.[4][16]

1.4 Primary explosives: Uses and legacy primary explosives

Primary explosives find use in initiatory devices. These devices can be classified as either detonators or igniters.[26] Detonators are designed to generate a shockwave which can be transferred to a secondary explosive (*vide supra*).[3] Igniters are designed to produce a flame and / or molten slag which generates sufficiently large amounts of heat to allow the ignition of propellant / pyrotechnic assemblies without shocking the propellant.[26] Because of the different outputs of detonators and igniters, different formulations of chemical compounds are required in each. The formulations are typically combinations of primary explosives with various pyrotechnic fuels and oxidisers.[3] Both detonators and igniters themselves are initiated in a variety of ways such as flame, heat, impact, stab, friction and electric spark. Detonators and igniters are used as the second phase of what has come to be known as the explosive train (**Figure 1.4**).[3]

The explosive train is an arrangement of explosive components through which initiation from a primer is transferred into the main charge of the train.[3] Primers deliver an initiating impulse to either the detonator or igniter. This impulse is fed into the output charge of the detonator or igniter which creates either a shockwave or heat output

which, depending on the intended use, can be fed to the main charge containing either secondary explosive or propellant / pyrotechnic. In the case of very insensitive secondary explosives, the output of the detonator will be fed into a booster charge which then feeds into the main charge. [3]

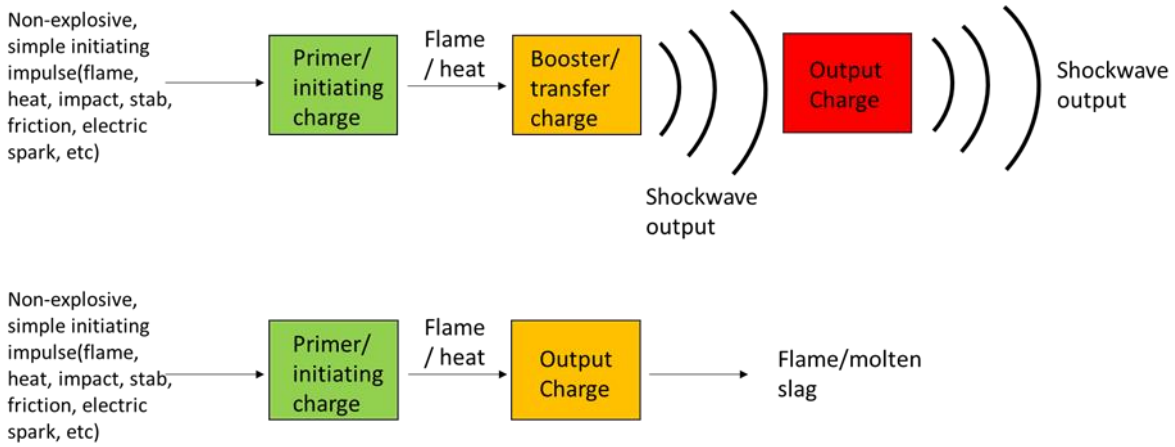

Figure 1.4: *Schematic representation of the two most common types of explosive trains*

1.4.1 Legacy primary explosives

Mercury fulminate (MF) is one of the oldest known compounds suitable as a primary explosive. References go back to as early as the 17th century, including details of its synthesis.[27] Mercury fulminate found extensive use in the 19th and early 20th century. The first patent for its use as an initiator was issued in 1807.[3] Thanks in part to the work of Alfred Nobel in developing his “Fulminate Blasting Caps”, and due to its desirable characteristics, such as high density, flammability, stability, brisance and desired sensitivity, MF became the most widely used primary explosive of its time and maintained this status until alternatives with greater initiating efficiency, lower toxicity and cheaper technical syntheses became available.[3] Research into the use of MF has waned over the years and it was only in 2007 that the first crystal structure was published (**Figure 1.5**).[28]

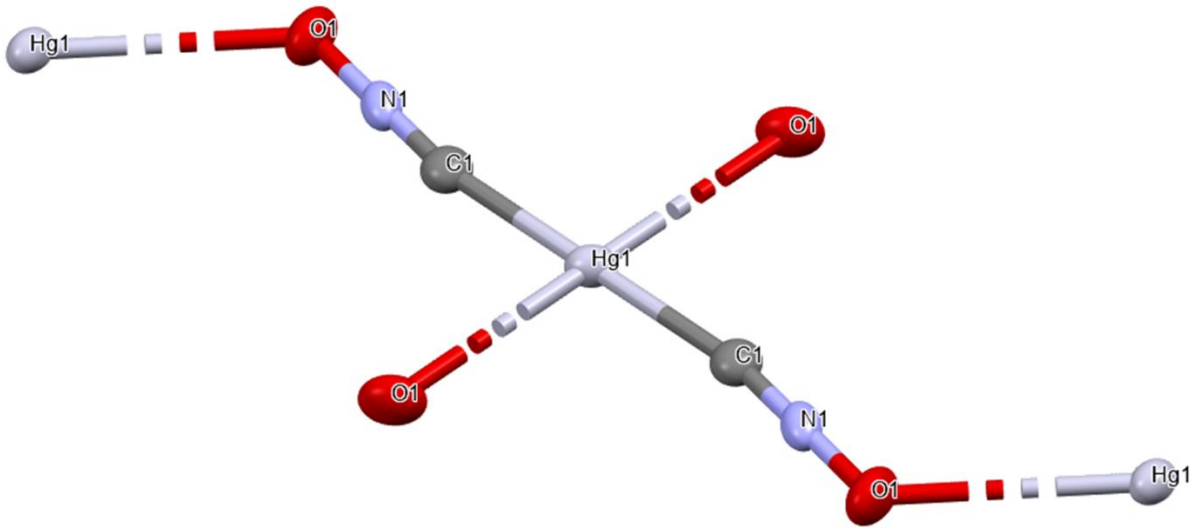

Figure 1.5: *Projections of the thermal ellipsoids in the molecular structure of mercury fulminate (set at the 67% probability level) showing the asymmetric unit; Atoms colour coded as follows: Red=Oxygen; Blue=Nitrogen; Grey=Carbon; White=Mercury, image produced from data available in ref*[28]

Lead azide (LA) (**Figure 1.6**) is the compound that eventually replaced MF in initiator formulations. The synthesis of LA is first attributed to Curtius in 1889.[29] It involves the addition of lead acetate to a solution of sodium or ammonium azide, resulting in the precipitation of LA. Initially, lead azide did not replace the more expensive mercury fulminate. It was not until 1907, when interest was once again sparked, [30] and not until 1920 when the problems with industrial application of LA, mostly related to its high sensitiveness, were overcome.[5] Following this, LA, due to its lower cost and superior initiating efficiency compared to mercury fulminate, gradually replaced the latter as the primary explosive of choice and has yet to be fully displaced from this position by modern primary explosives. While an important part of initiatory formulations, the future use of lead azide in these formulations is currently under review. The review is necessitated by two key issues: (1) The lead content – as a heavy metal, lead is highly toxic and detrimental to humans and most organisms in general, and (2) concerns over its stability in long-term storage. Dry LA is stable under normal atmospheric conditions. However, if LA is exposed to air, it will slowly decompose in a reaction with CO_2 and H_2O.[3]

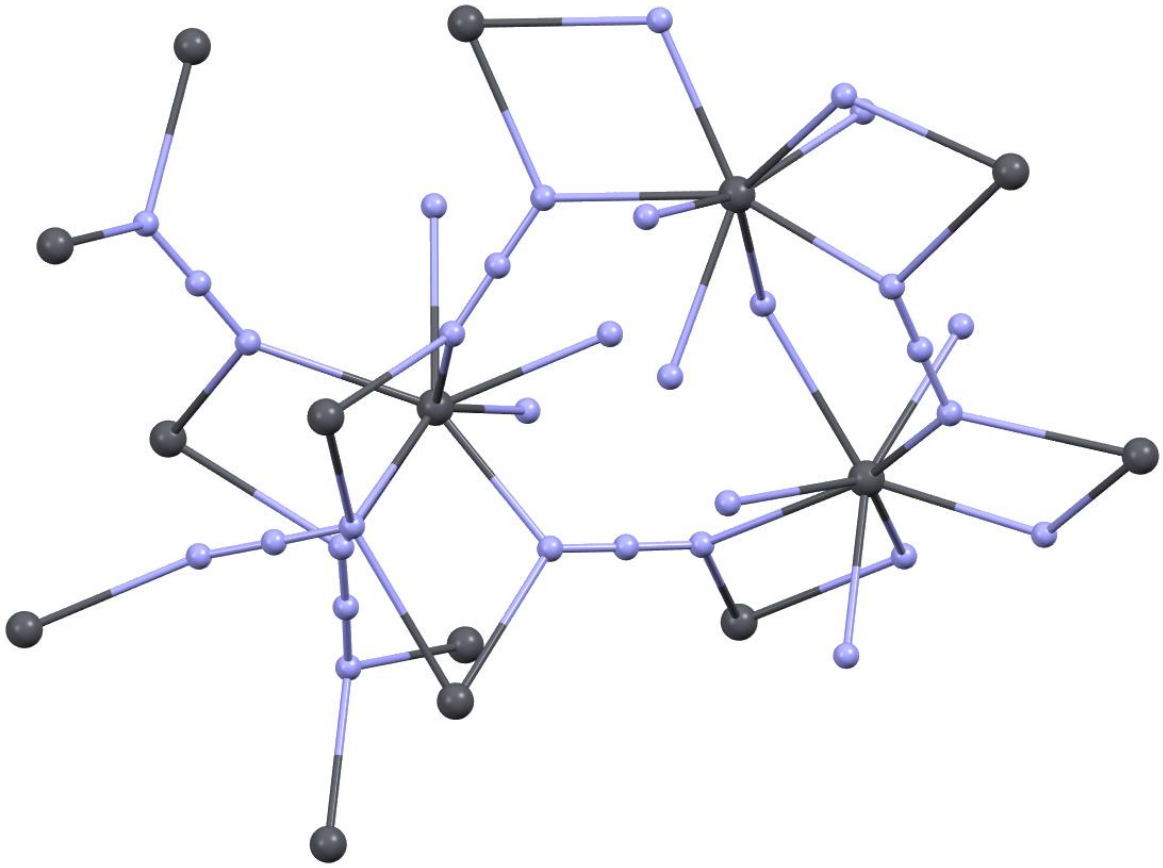

Figure 1.6: *Ball and Stick diagram of the molecular structure of Lead Azide, $Pb(N_3)_2$. Atoms colour coded as follows: Grey=Lead; Blue=Nitrogen, image produced from data available in ref*[31]

If the partial pressure of CO_2 is lower than 1.2 kPa, basic lead azide ($PbO.Pb(N_3)_2$) forms along with hydrazoic acid (HN_3).[3] At higher CO_2 partial pressures, dibasic lead carbonate ($2PbCO_3 \cdot Pb(OH)_2$) forms next to HN_3. If the LA-containing explosive mixture is not sealed well, then the HN_3 evaporates resulting in a gradual conversion of LA to one of the two lead hydroxide compounds detailed above.[3] Whilst it was feared initially that this would impact the initiation efficiency and, hence, decrease the overall ability of LA to perform with the desired strength, it was found that the formation of a lead carbonate layer helped to protect the bulk of the LA from further decomposition and consequently had a much lower impact on performance.[3] The more pressing issue with LA decomposition is the proclivity of HN_3 towards reactions with metals other than the lead.[32] HN_3 can react with various metals to produce metal

azides such as copper azide, which have a greater sensitiveness than LA with serious consequences to the handling requirements and safety.[3]

Lead styphnate (LS) is another well-known lead-based primary explosive. It found extensive use alongside LA in initiator device formulations. LS has been used in two different forms as either normal lead styphnate, or monobasic lead styphnate (**Figure 1.7**). The interest in normal lead styphnate stems from research conducted around the same time as LA. While the first patent for LS was issued in 1915[33], its synthesis had already been detailed 40 years earlier by Stenhouse.[34] Stenhouse synthesised LS through the reaction of lead acetate with an aqueous solution of styphnic acid. The currently employed syntheses, however, predominantly rely on the reaction of a soluble styphnate salt with either lead acetate or lead nitrate.[2] LS has been shown to have poor initiating efficiency with the only high explosive it can detonate being PETN (NB: PETN constitutes one of the most sensitive commercial high explosives). The need for LS arises from its high sensitivity to flame and ESD initiation compared to lead azide. While lead styphnate cannot initiate many secondary explosives, it is able to easily *initiate* other primary explosives, such as lead azide, which do not initiate as easily from flame and ESD.[3] Thus, lead styphnate finds uses in mixtures with lead azide. A typical formulation contains a mixture of 30 % lead styphnate and 70 % lead azide which combine the high sensitivity to flame and ESD of lead styphnate with the high initiating efficiency of lead azide.[3]

While forming many different basic salts, only the monobasic salt of lead styphnate has found practical use. Monobasic lead styphnate was first synthesised by Griese in 1874.[35] Monobasic lead styphnate is prepared by reaction of the sodium or magnesium salt of 2,4,6-trinitroresorcine in an alkaline reaction medium with lead nitrate.[3] Monobasic lead styphnate has similar properties to lead styphnate with a high sensitiveness to ESD and flame but has a higher sensitiveness to impact and a higher temperature of ignition. Monobasic lead styphnate also finds use in initiatory mixtures with other primary explosives, binders and fuels.[26]

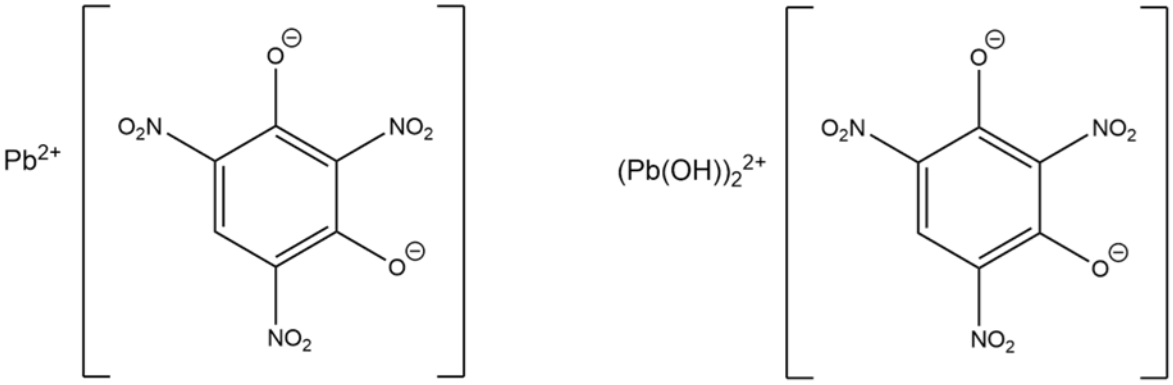

Figure 1.7: *Left: Normal Lead Styphnate; Right: Basic Lead styphnate*

The extreme sensitiveness towards ESD of both normal and basic lead styphnate presents a significant problem in the production of these compounds. This has resulted in accidents during LS production and handling.[3] Operations that involve movement of the material, such as mechanical grain size and shape modifications and sieving, can result in electrostatic charge build-up, which, therefore, have to be performed with the utmost care during large-scale (patents exist detailing syntheses of tens of kilograms of “wet” lead styphnate[36]) synthesis of LS. Attempts had been made at synthesising graphite-coated lead styphnate to help desensitise the compound and overcome these issues. However, no noticeable difference in its ESD sensitiveness was observed.[3]

By far the biggest issue with both lead azide and lead styphnate is, again, the use of lead (*vide supra*). The toxicity of lead azide has been investigated as early as 1943 by Fairhall *et al.*[37] In rats it was found that, while the accumulation of lead in tissue was similar to other lead salts, the toxicity of lead azide was greatly increased due to the azide anion and the subsequent production of azidyl radicals (**Figure 1.8**).[38] Even though acute lead poisoning is uncommon, chronic lead poisoning from repeated low-level exposure, such as that found in long-term handlers or users of initiators, leads to a variety of health problems including persistent vomiting, encephalopathy, lethargy, delirium, convulsions and cancer.[39][40]

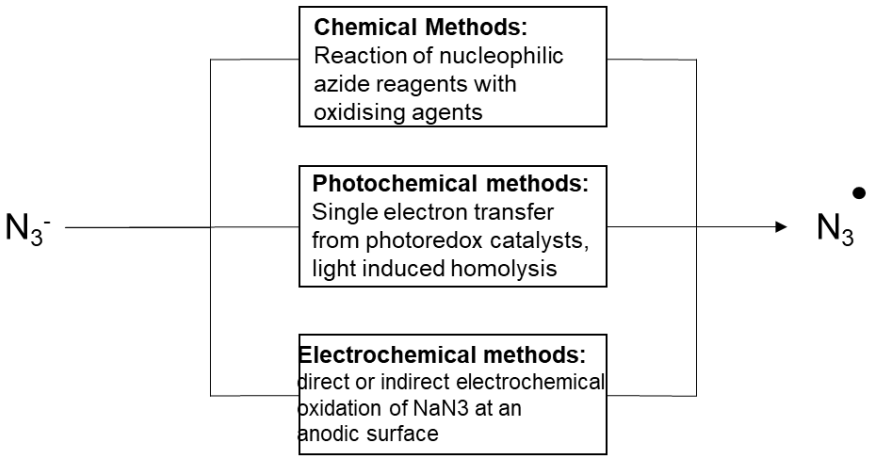

Figure 1.8: *Production of the azidyl radical from the azide anion*

The reasons for the high toxicity (toxicity defined as the degree to which a chemical substance can damage an organism) of lead itself has a large history of research behind it. Oxidative stress has been reported to be a major cause of lead toxicity.[39][40] Oxidative stress is a phenomenon caused by an imbalance between production and accumulation of reactive oxygen species (ROS) in cells and tissues. The presence of lead leads to a reduction in the number of antioxidants available in cells to quench radicals (**Figure 1.9**).[39][40]

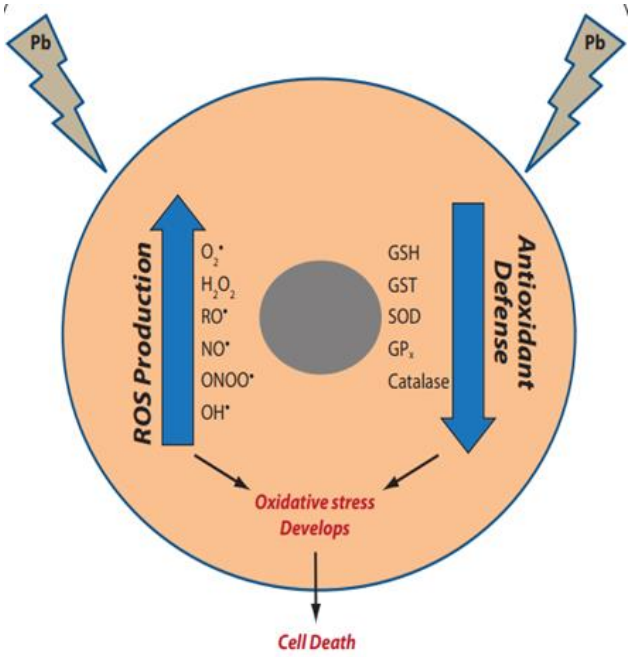

Figure 1.9: *Mechanism underlying the development of oxidative stress in a cell on lead exposure, (Image reproduced with permission from [40])*

Glutathione, a key intracellular antioxidant, is deactivated by lead due to the formation of bonds between lead and the thiol group present in glutathione (**Figure 1.10**).[40][41]

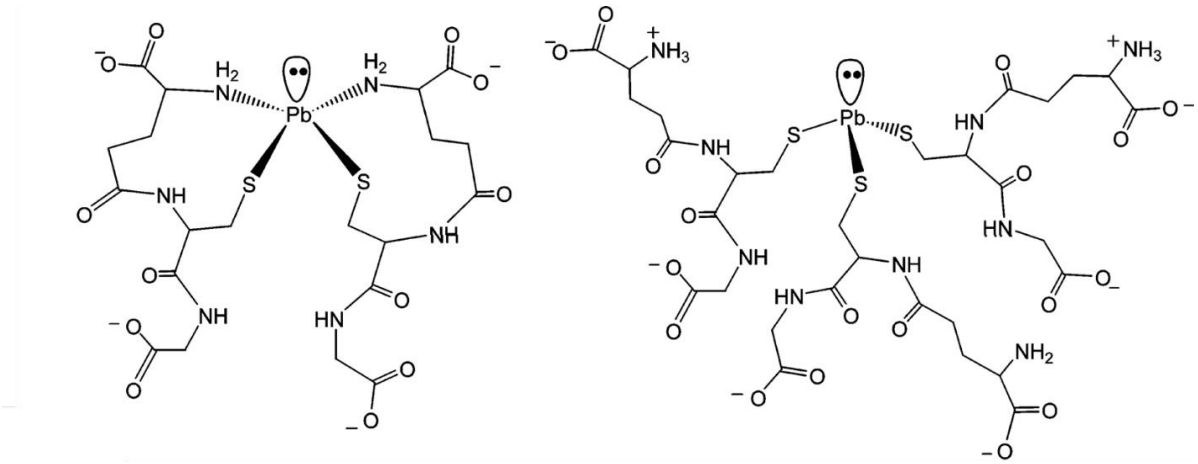

Figure 1.10: *Glutathione-lead binding modes, Reprinted with permission from* V. Mah, F. Jalilehvand, Inorg. Chem. 2012, 51, 6285−6298, *Copyright 2012 American Chemical Society [41])*

The toxicity of lead arising from an ionic mechanism of action mainly arises due to its ability to substitute out other metals such as Ca^{2+}, Mg^{2+}, Fe^{2+} and Na^{+}, affecting various fundamental biological processes of the body.[40] Significant effects have been found on various cellular processes like intra- and intercellular signalling, cell adhesion, protein folding and maturation, apoptosis, ionic transportation, enzyme regulation, release of neurotransmitters, etc.[42] The ionic mechanism contributes principally to neurological deficits, as lead, after replacing calcium ions, becomes able to cross the blood-brain barrier (BBB) at an appreciable rate, thereby affecting key neurotransmitters such as the protein kinase C, which regulates long-term neural excitation and memory storage.[40]

1.5 Replacements for lead-based primary explosives

Because of the hazards associated with lead exposure, large research efforts have been dedicated to finding a synthesis of alternative primary explosives with lesser health and environmental concerns. Any lead-free primary explosive (the term lead

free initiator (LFI), commonly used in the chemical literature, is used interchangeably with lead-free primary explosive) would have to fulfil the following criteria to be regarded as a viable alternative to lead azide and lead styphnate[42]:

- must have performance equal to or greater than that which can be expected of current lead-based formulations
- must lend itself to safe and reliable synthesis
- insensitivity towards moisture and light
- sensitivity towards initiation (ideally low sensitiveness towards unwanted stimuli while retaining a high sensitivity in specific devices)
- thermally stable up to at least 200 °C
- chemically stable for extended periods toward carbon dioxide and water
- devoid of toxic metals such as lead, mercury, silver, barium, or antimony
- must be free of perchlorate due to perchlorates ability to affect the function of the thyroid gland

1.5.1 Potassium-based primary explosives

One of the more promising areas in replacements for lead-based energetic materials is the synthesis of potassium salts of energetic ligands. The combination of heterocyclic-based nitrogen-rich energetic ligands with environmentally friendly potassium metal has proven to be a successful route to viable lead-free energetic materials. One of the first reported synthesis in this area revealed the synthesis of potassium 4,6-dinitro-7-hydroxy-7-hydrobenzofurazan-1-oxide (KDNBF) (**Figure 1.11**), which was communicated in 1899 by Drost.[43] In Drost's paper, the salt is described as the product of replacement of an aromatic ring hydrogen, located on the phenyl ring, by a metal. Further work by Gaughran[44] showed that this product was unlikely to possess the suspected structure and Boulton[45] showed that the originally obtained compound was in fact the Jackson-Meisenheimer adduct (a Jackson–Meisenheimer complex is a 1:1 reaction adduct between an arene carrying electron-withdrawing groups and a nucleophile) between potassium hydroxide and 4,6-dinitro-benzofuroxan, which forms by the reaction of 4,6-dinitrobenzofuroxan with potassium bicarbonate. While still known as a viable lead-free primary explosive, thermal analysis

has shown that KDNBF cannot be regarded as an alternative to lead-based energetic materials because its thermal stability is insufficient.[46]

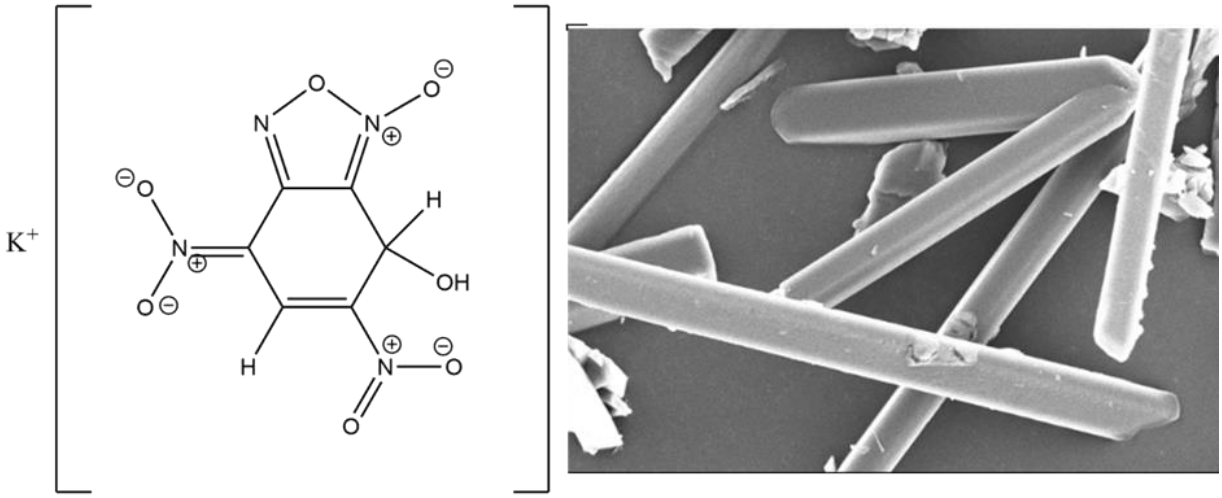

Figure 1.11: *Left: Structure of KDNBF; Right: SEM image of crystalline KDNBF, (Image reproduced with permission from ref[47])*

Another potassium-based replacement described in the open literature is potassium-1,1'-dinitramino-5,5'-bistetrazolate(K_2DNABT).[48] This compound was first synthesised in a seven-step procedure by Klapötke *et al.* in 2014 (**Figure 1.12**).[48] K_2DNABT was found to be essentially non-toxic and therefore held potential as a lead azide replacement.[48] Both standard analysis and unique-to-energetic materials-analysis was done to determine whether K_2DNABT has potential as a primary explosive. K_2DNABT was shown to have high sensitiveness in the impact, friction and ESD tests, with values for all of these tests at levels around those found for lead azide.[48] Instant detonation of the material that came into contact with flame or a hot needle alongside the successful ignition of 1 g of RDX by 40 mg K_2DNABT shows K_2DNABT to be a lead azide replacement candidate.[48] When heated to a temperature of 100 °C and held for 48 h, K_2DNABT shows no sign of mass loss or decomposition (Kneisl test, vide supra) highlighting the desired high stability for this compound. While violent decomposition of the material was reported if the temperature reached 200 °C, this is still within the acceptable range for a lead azide replacement and thus K_2DNABT remains in consideration for detonator and primer formulations of the future.[48]

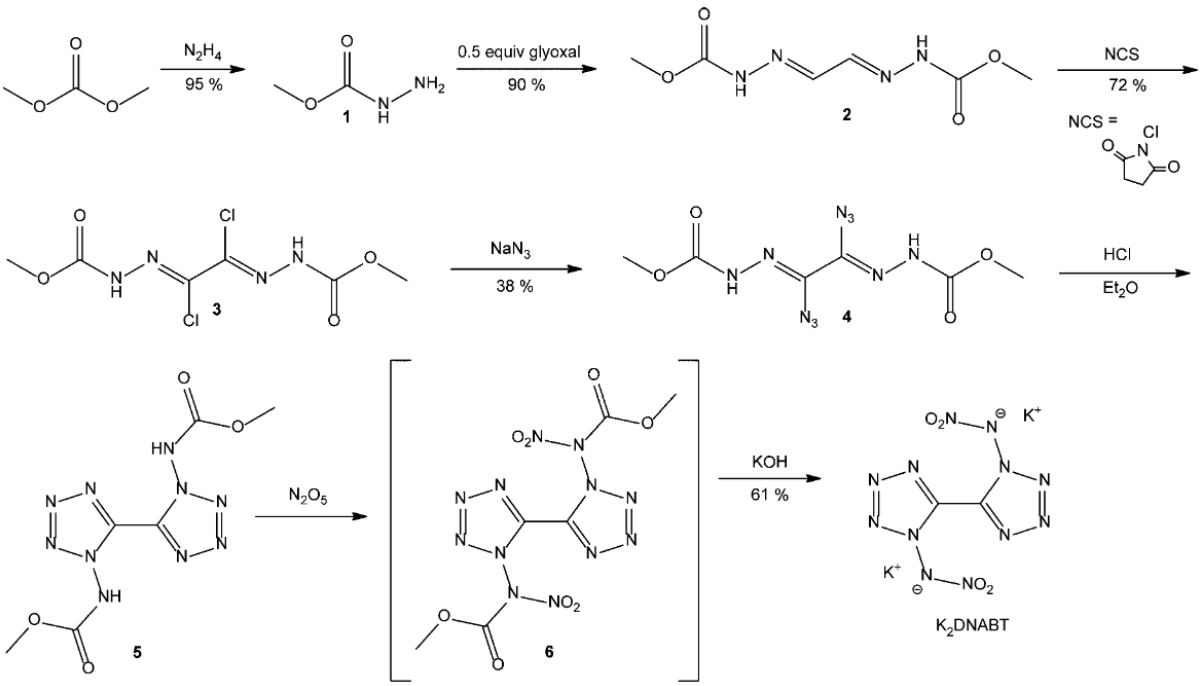

Figure 1.12: *Synthesis of K_2DNABT, (Image reproduced with permission from ref[48])*

While KDNBF and K_2DNABT are prospective replacements for $Pb(N_3)_2$, potassium-based replacements for lead styphnate are also known and have shown comparable explosive performance in igniters and comparable thermal stabilities. The most promising of these is potassium-5,7-dinitro-[2,1,3]-3-oxide-benzoxadiazol-4-olate (KDNP) (**Figure 1.13**). KDNP has been known since 1983 with the first synthesis published by Norris *et al.*[49] KDNP is a remarkably similar compound to KDNBF, with the only difference being the removal of one ring hydrogen and subsequent restoration of aromaticity over the entire ring structure. While use of KDNBF is rare due to its low thermal stability, KDNP possess a greatly increased thermal stability and so has attracted further investigation as a LS replacement. A variety of synthetic procedures are known to produce KDNP including the original preparation by Norris and the Boulton-Katritzky rearrangement of 5-chlorobenzofuroxan.[50] However, preparation by these routes leads to KDNP which retains the water used as reaction solvent and gives needle-shaped crystals that are very friction/impact sensitive. A better method devised by Fronabarger *et al.* shows that the synthesis of KDNP can be achieved by nitration of 3-bromoanisole to form 3-bromo-2,4,6-trinitroanisole which can be heated with potassium azide in methanol at reflux to displace the bromine for an azido group. Once

this solid has been isolated, it is then heated to reflux in diethyl carbonate at 134 °C to form the furoxan ring and afford a KDNP polymorph which is comparably less hygroscopic.[51] KDNP can be initiated easily from a variety of methods. Its impact sensitiveness is like that of LS, but the friction sensitiveness is significantly lower than that of LS. Overall, KDNP has chemical, physical, safety and performance properties which allow it to be regarded as a drop-in replacement (NB: drop-in refers to the requirement that no redesign of existing explosive devices is needed beyond the use of KDNP as a volumetric replacement for LS) for LS in a variety of applications. KDNP also offers environmental improvements over lead styphnate in manufacture, use and disposal.

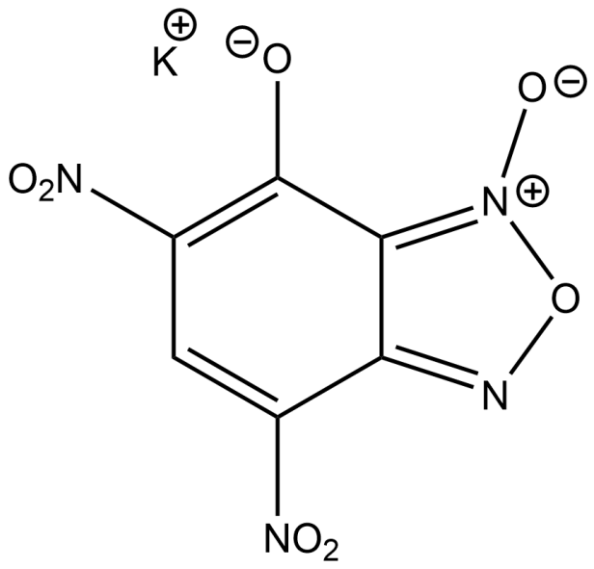

Figure 1.13: *Lewis structure of KDNP*

1.5.2 Copper(I) nitrotetrazolate

One of the most promising replacement candidates thus far, however, is copper(I) nitrotetrazolate (from here referred to as DBX-1 as per the convention set by Fronabarger *et al.*) (**Figure 1.14**).[52] While a synthetic method has been known for a long time[16], DBX-1 has recently been the subject of renewed interest due to its potential as a lead azide replacement. A large body of literature reporting new research has been published recently detailing the synthesis of DBX-1 through two

main methods. The first synthesis was detailed in a 2007 patent filed by Fronabarger et al.[53] The synthesis involves the reaction of copper (I)-chloride (CuCl) with sodium-nitrotetrazolate dihydrate(NaNT.$2H_2O$) at various temperatures in the range 80 °C to 130 °C. Product identity was proved by digestion of a sample in 1 M aqueous NaOH and subsequent UV/vis determination of 5-nitrotetrazolate content. A nitrotetrazolate content of 62.25% was taken as confirmation of the identity of the material as Cu(I) 5-nitrotetrazolate (theoretical value of 64.22%). Clearly, the material has an unidentified impurity, though, my analysis of the supplied IR spectra suggests that the discrepancy could be due to inefficient drying of the product.[53] This synthetic method has been used in related research published elsewhere;[54] however, it has lost popularity in favour of alternative synthetic methods.

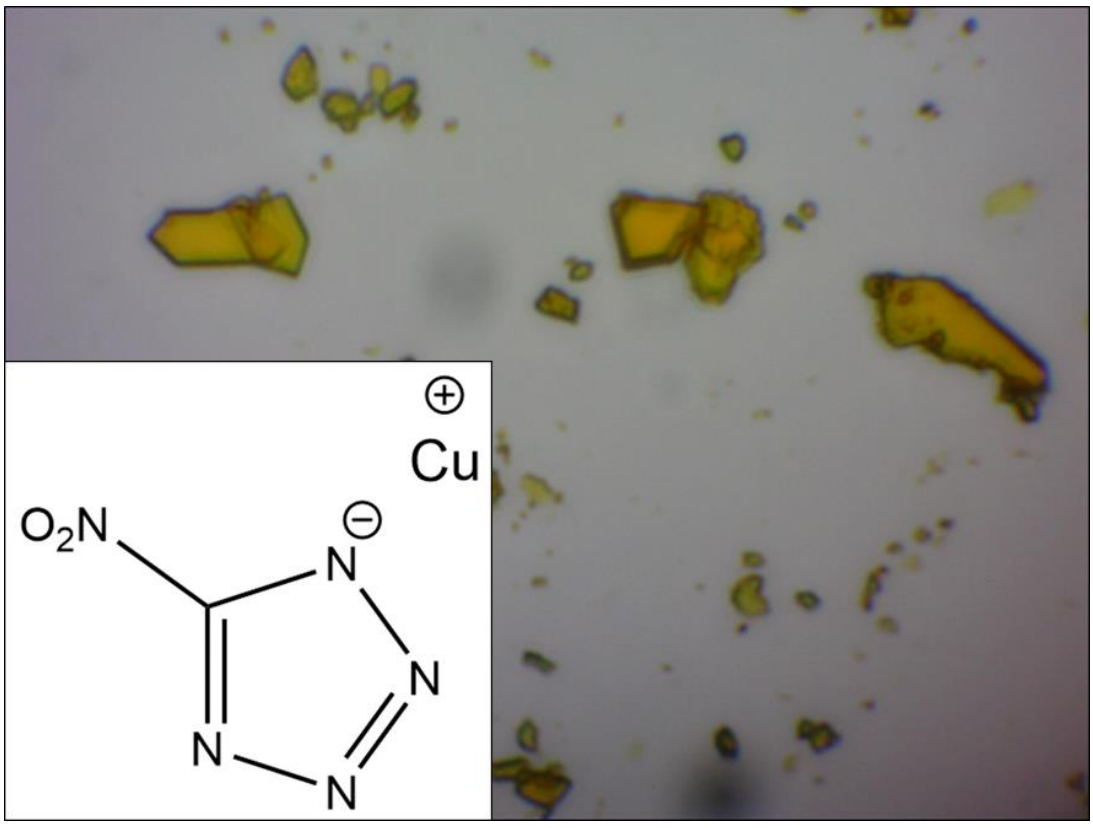

Figure 1.14: *Inset bottom left: Structure of Cu(I)-Nitrotetrazolate; Right: Crystals of Cu(I)-Nitrotetrazolate, viewed under optical microscope 100x zoom, Images taken at The University of Sheffield*

Recent papers have detailed the synthesis of DBX-1 that relies instead on the reaction between sodium nitrotetrazolate (NaNT) and $CuCl_2$ to form a Cu(II)-nitrotetrazolate

species *in situ* which is then reduced at 90 °C by the addition of sodium ascorbate.[52] This method has been favoured by some research groups as it relies on the cheaper $CuCl_2$ instead of CuCl as a starting material.[52] Fronabarger *et al.* detail the batch synthesis of DBX-1 up to a 2.5 g scale. In this paper, DBX-1 was also investigated as a drop-in replacement for lead azide.[52] Thermal analysis demonstrated that DBX-1 is thermally highly stable and outperforms common lead azide-based detonator formulations in a multitude of tests such as humidity, high and low temperature tests and high resolution TGA. Various performance tests were also performed with DBX-1 which demonstrate that it possesses performance characteristics equal to, or greater than, those found for lead azide.[52]

The synthesis that relies on the reduction method has also been detailed and improved upon in a paper by Ford *et al.*[55] In this paper, a flow reactor method for the synthesis of DBX-1 is explored, which allows for its production without the need to handle its explosive precursor, sodium nitrotetrazolate, and without the need for NaNT purification (**Figure 1.15**).[56]

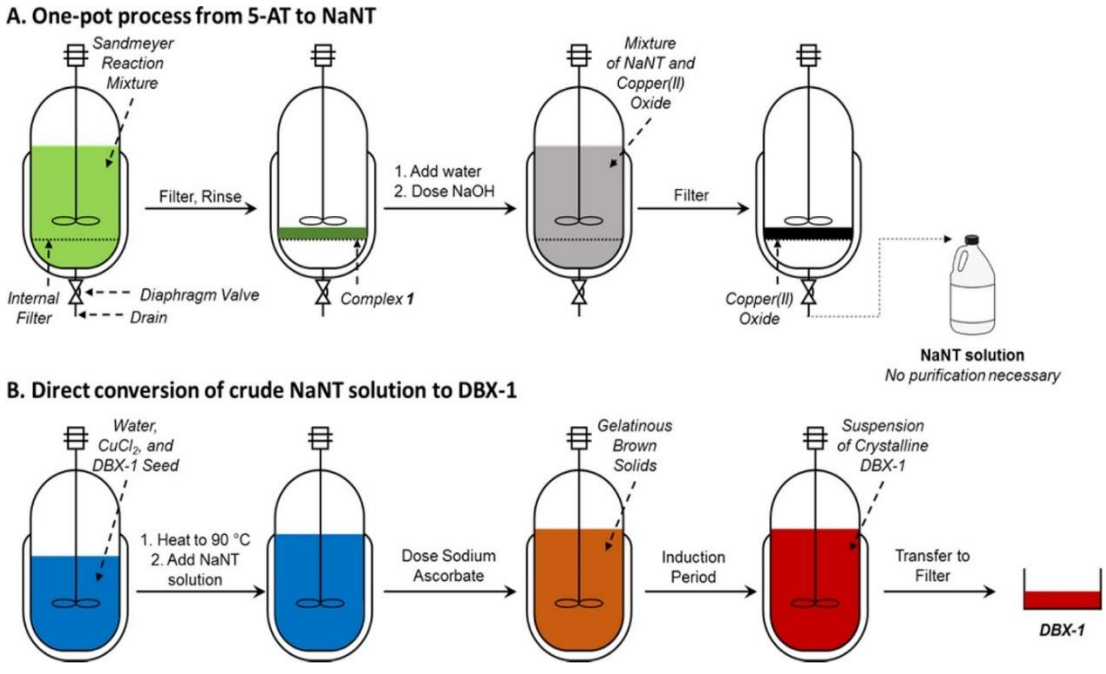

Figure 1.15: *Top: Process to NaNT utilizing reactor with internal filter for synthesis of NaNT without manual manipulation of 1; Bottom: Process for converting crude NaNT solution to DBX-1 without prior purification (Image reproduced with permission from ref[55])*

While a highly promising lead-free initiator (LFI), DBX-1 is considered still problematic in its potential to replace the conventionally used explosives due to existing hurdles in its suggested production process. Irreproducibility of published results has been a major problem that prevented the full adoption of DBX-1 as the go-to lead azide replacement. Some attempted reactions never converted the starting material to pure, crystalline DBX-1.[55] The reasons for these outcomes are still unknown. Purity of NaNT, dosing rate of reductant, and presence of seed crystals have all been raised as potential variables that need tight control to produce high purity DBX-1.[55] Purity of NaNT has been investigated in a recent paper[56] comparing the effects of impure *vs*. pure NaNT in the synthesis of DBX-1. It was found that the NaNT synthesised by classic methods has substantial impurities present, some of which have been identified as 5,5'-bistetrazole, 5-aminotetrazole and 1*H*-tetrazole.[56] The impurities in this material evidently prevents (inhibits) DBX-1 formation in the reduction reaction. An improved synthesis of NaNT is also detailed in the paper and gives a product which is sufficiently pure to allow its use in the reduction reaction. It produces DBX-1 to a level of purity comparable to that found in genuine DBX-1 used in detonators.[56] Only the method published by Ford has proven capable of using impure NaNT as a starting material.[55] Work with DBX-1 has revealed other potential problems: in the presence of certain oxidisers, such as sodium periodate, decomposition of DBX-1 is observed with formation of Cu(II) salts and water soluble nitrotetrazolate salts. This implies that, in certain detonator / initiator formulations, DBX-1 cannot be combined with additional oxidisers due to the formation of Cu(II) salts.[57]

1.6 Strategies for the synthesis of novel energetic materials

When designing new energetic materials, certain design principles are used to narrow down the list of potential target compounds. A high nitrogen content (defined as the nitrogen mass fraction (%) of an energetic material being above 60%) is regarded as desirable since high nitrogen compounds typically possess large, positive heats of formation which lead to high energy output upon detonation (chemical potential).[4] It is also desirable to realise near-zero oxygen balances. Oxygen balance is used to determine the degree to which an explosive can fully oxidise its content to the standard

oxides (CO_2, H_2O, metal oxides, etc.). A molecule, compound or materials is said to have a positive oxygen balance if it contains more oxygen than is needed and a negative oxygen balance if it contains less oxygen than is needed for complete combustion without external oxygen (without afterburn if used in air, for instance). An oxygen balance of zero is desired as it is at this point that the heat of explosion (Q, defined as the difference between the energies of formation of a material and the energies of formation of the explosion products) reaches a maximum as this corresponds to the oxidation of all carbon to carbon dioxide and all hydrogen to water.[2] A small oxygen deficiency has often less dramatic effects on the actual performance parameters of H_{det} (heat of detonation, amount of energy that can be liberated on the detonation of explosives) and V_0 (volume of gas produced after explosion) due to afterburn which during the stage of expansion of the hot product mixture leads to atmospheric oxygen to mix in and burn carbon and carbon monoxide.[58] High densities are also a desired characteristic for energetic materials. For homogeneous explosives, the velocity of detonation (*D*) increases as the compaction density (*loading density*) of the explosive material increases. Velocity of detonation is defined as the velocity at which the shock wave front travels through a detonated explosive. Velocity of detonations vary greatly depending on the class of explosive used with primary explosives usually found in the range 3500-5500 ms^{-1} and secondary explosives found in the range 5500-9000 ms^{-1}.[4] Maximum velocity of detonation is therefore achieved at the maximum density of the explosive which, for a crystalline material, will be limited by the density of the crystal. While *primary* explosives are generally desired to have the aforementioned properties, achieving high values for the characteristic explosive parameters is less important than showing the ability for the generation of a shockwave and the ability to transfer this to more powerful secondary explosives.[3] Nevertheless, these design principles have driven the research into novel primary explosives. Azoles have been heavily investigated for their suitability in this respect due to their presence imparting high heats of formation, nitrogen contents and densities on novel materials (**Figure 1.16**).[59] They have also displayed high thermal stabilities which is one of the key requirements of primary explosives (*vide supra*).

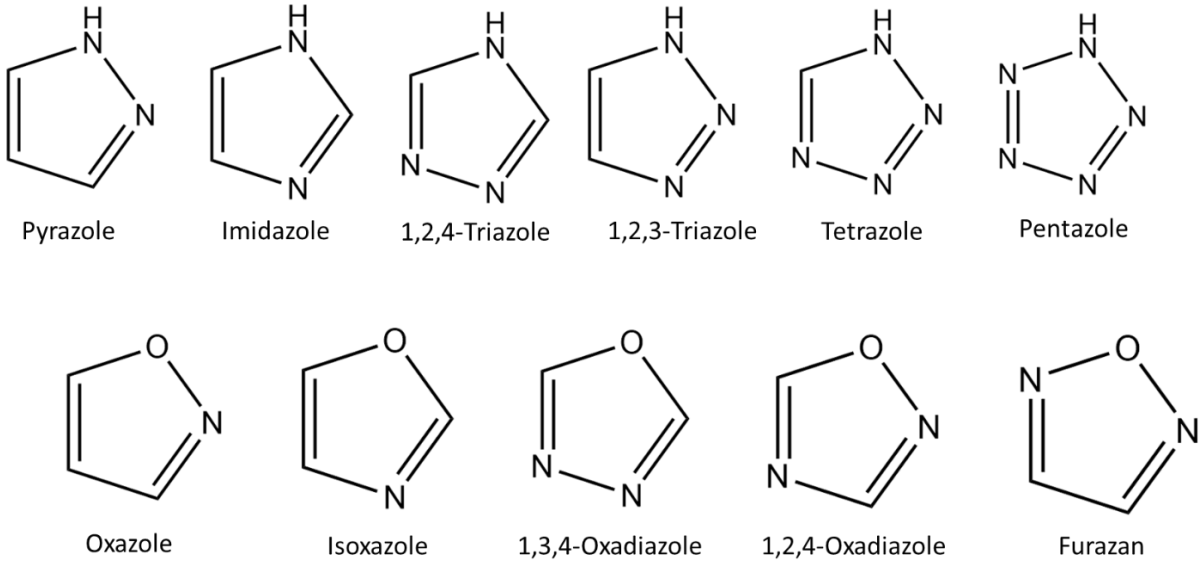

Figure 1.16: *Known CHN and CHNO azoles*

Azole rings contain C-sites and N-sites that can be further modified by introducing explosophores, obtaining high performance energetic materials.[60] One of the most widely used explosophores in azole chemistry is the nitro group. Nitro groups are commonly incorporated into azole molecules *via* four key methods: a) direct nitration of the carbon backbone of an azole (C-nitration),[61] b) nitration of the N-H function of the azole to form an N-nitro compound (N-nitration),[61] c) nitration of an amino group attached to the azole forming a nitramino group,[62] d) direct nitration of an acetonyl group to form the trinitromethyl moiety.[63] The most common method of introducing a nitro group to the carbon backbone of pyrrole, imidazole or pyrazole rings relies on the electrophilic substitution mechanism. In this mechanism, the nitronium ion, NO_2^+, serves as the attacking electrophilic moiety.[64] The nitronium ion can be formed by protonating nitric acid with sulphuric acid in "mixed acid", a H_2SO_4 / HNO_3 acid mixture (**Figure 1.17**).[65] The nitronium ion as the active nitrating agent was confirmed by the work of Bennett [66] and Westheimer *et al*.,[67] who stated that in mixtures of HNO_3 and H_2SO_4 an “ionisation of the nitric acid was involved in the determination of the maximum rate of nitration” and that only ionisation that produced a nitronium cation could account for the “thousand-fold increase in rate of nitration that accompanies an increase in sulphuric acid concentration”.[67]

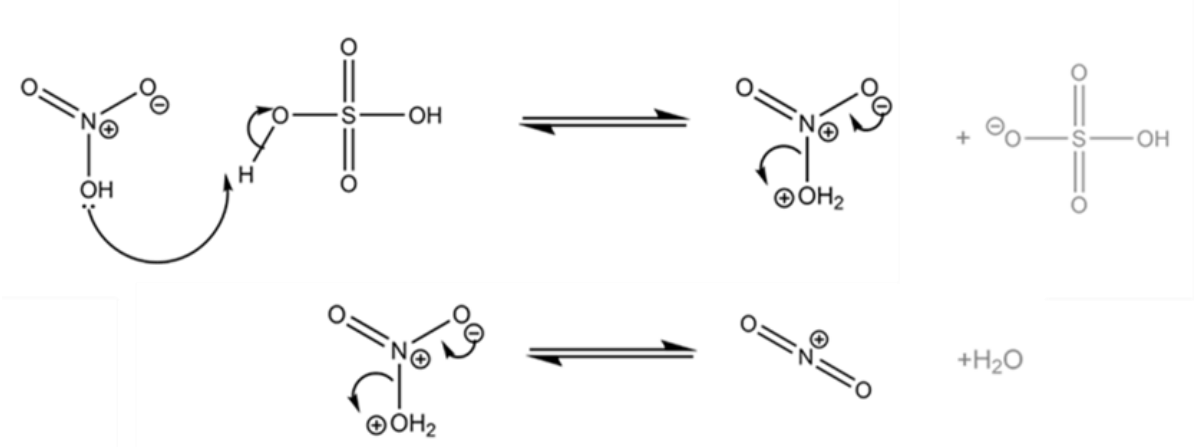

Figure 1.17: *Formation of the nitronium cation from HNO_3 and H_2SO_4*

Nitronium cations can also be formed by the addition of metal nitrates to HNO_3, using 100% nitric acid or by the use of nitronium salts such as nitronium tetrafluoroborate, which provides a preformed nitronium cation directly.[68] Nitration reactions relying on HNO_3 only, form the nitronium ion by autoprotolysis formally between two HNO_3 molecules (**Figure 1.18**).[69]

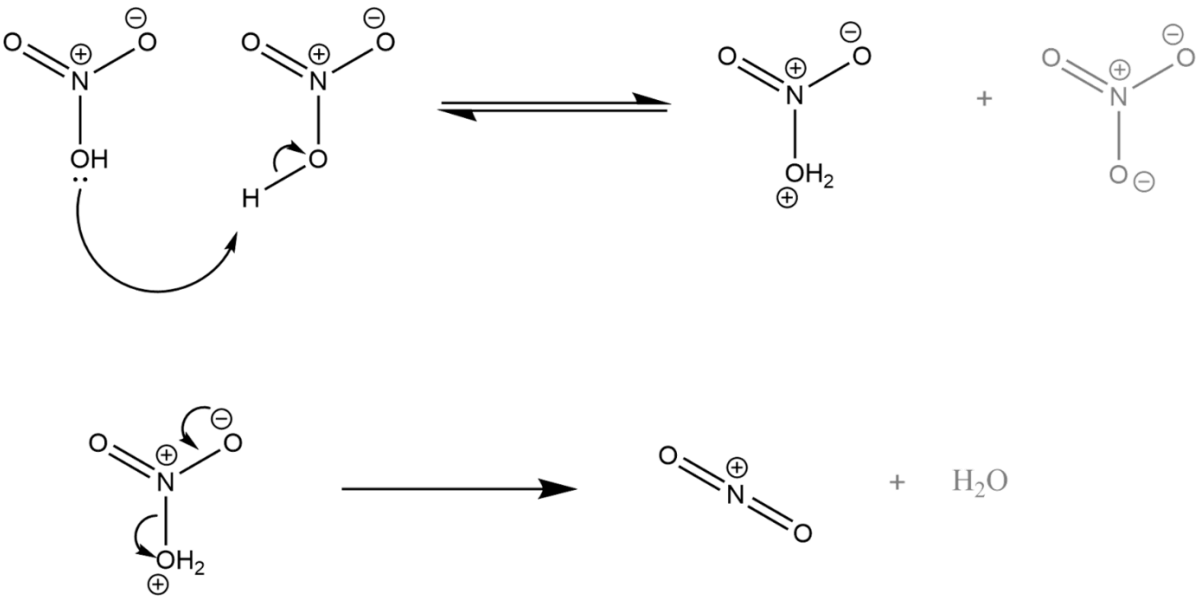

Figure 1.18: *Formation of the nitronium cation via autoprotolysis of HNO_3*

Following the work of Ingold, Hughes and Reed,[70] it was commonly thought that both nitronium cation and aromatic substrate take part in a reversible, bimolecular reaction

to form a σ-complex (**Figure 1.19**),[70] the so called Wheland intermediate, which subsequently undergoes fast deprotonation to form the aromatic nitro compound. This mechanism was developed further by the work of Dewar,[71] who proposed that π-complexes represent transition states that lie between the starting materials and σ-complexes and between σ-complexes and final product. Numerous theoretical and experimental studies have been conducted for the purpose of understanding better the mechanism of aromatic nitration.[72-74] While commonly accepted as the mechanism by which aromatic nitration occurs, the Ingold-Hughes mechanism has been shown to not fully explain the experimental data available for aromatic nitrations.[72-74] While kinetic investigations have shown the π-complex to be a transition state blocked by only low activation energy and a high reaction rate towards forming σ-complexes, nitrations by nitronium salts do not share this behaviour.

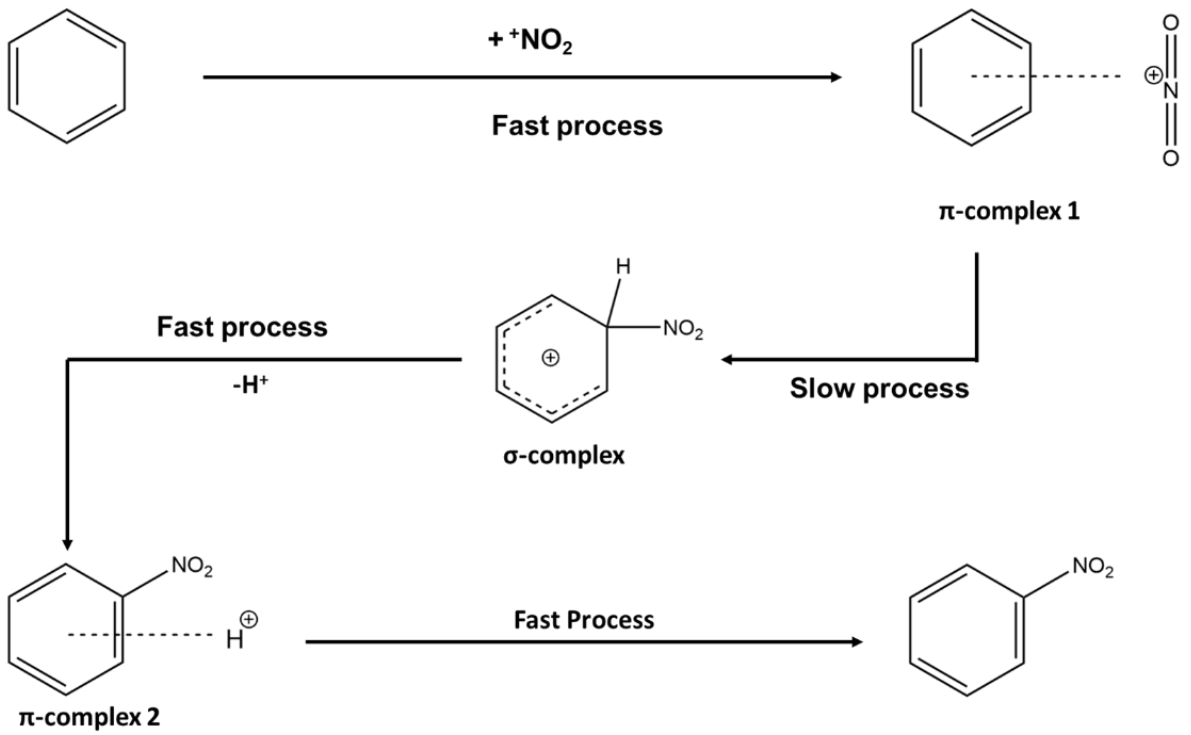

Figure 1.19: *Electrophilic aromatic substitution by the nitronium cation*

Olah *et al.* have found that nitronium salts have a reaction rate limited by the formation of the much more stable π-complex followed by conversion to the unstable σ-complex.[68] This provoked much discussion of a reaction mechanism previously deemed sound. Alongside this, alternative explanations for the nitration mechanism

involving the nitronium cation have been presented since the nitronium ion was first identified as the active nitrating agent. A single electron transfer (SET) mechanism is also seen as having merit when discussing this reaction scheme (**Figure 1.20**). First proposed in separate papers by Kenner[75] and Weiss[76], this mechanism requires the transfer of an electron from the aromatic π system to the nitronium cation during formation of the π-complex resulting in the formation of an ion-radical pair intermediate.[77] Recombination of the two radicals then results in formation of the same σ-complex as seen in the Ingold-Hughes mechanism.[77] This mechanism attracted renewed interest thanks to the work of Perrin[78], who showed that electrochemical nitration of naphthalene resulted in the same ratio of products as that achieved through acidic nitration.[78] Further experimental results have also pointed to a SET mechanism firmly promoting it as a rival to the Ingold-Hughes mechanism.[79] More recently, computational modelling of this class of reaction points firmly to the SET mechanism being the dominant one especially in the case of electron-rich aromatics.[77] These calculations have shown that significant electronic charge transfer to the nitronium cation occurs at the π-complex formation stage seemingly proving that the SET mechanism is the one taking place.[77]

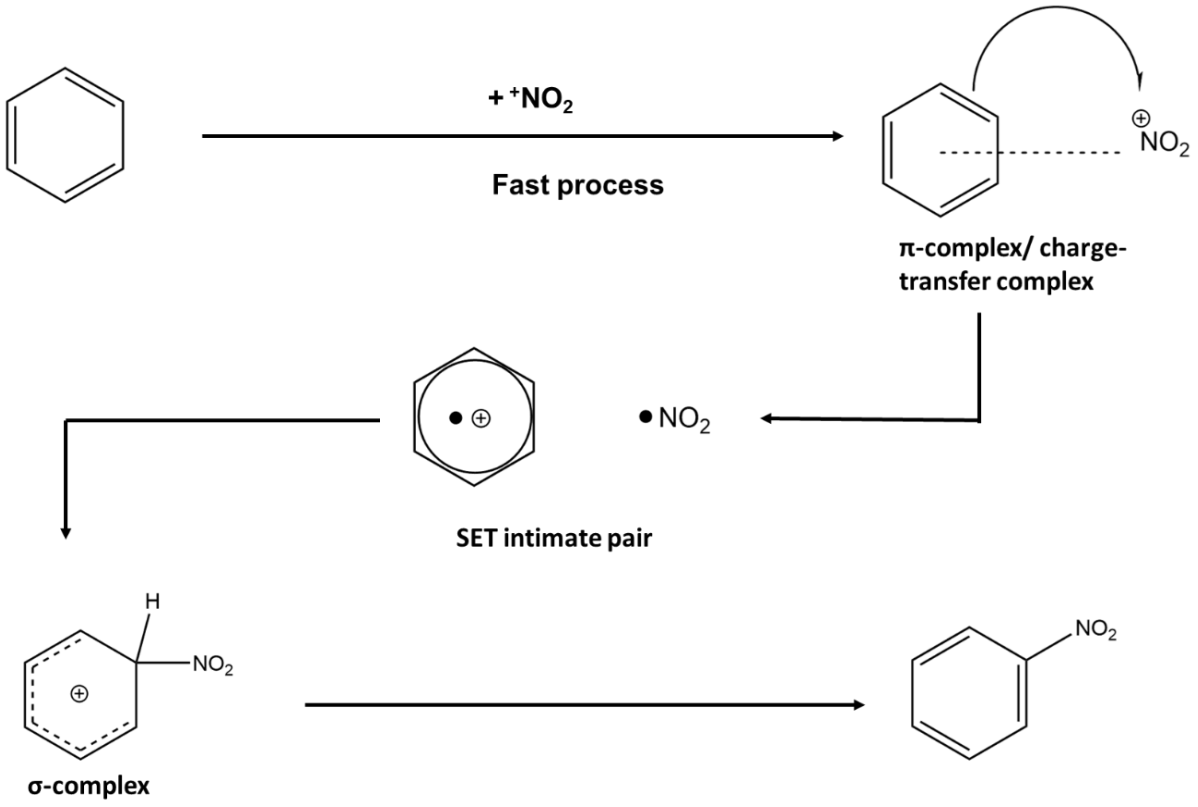

Figure 1.20: *Nitration of benzene via the SET mechanism*

It must, however, be stated that these calculations consider the reaction in the gas phase. A 2016 paper by Galabov *et al.*[80] has shown that when solvent effects are included, *no* significant charge transfer takes place between arenes and nitronium cations in the reaction in HNO_3 / H_2SO_4 mixtures, and that the mechanism present is in fact the Ingold-Hughes.[80] The conclusion one can draw from this is that the mechanism by which the nitronium cation nitrates aromatic systems is still very much debated. It has been suggested, and seems likely, that both mechanisms are viable and the specific mechanism occurring heavily depends on the nature of the nitrated compound, electron deficient vs. electron rich aromatic rings being an example.[80]

While the nitronium ion nitration mechanism is still much debated, the nitronium ion as the active nitrating agent has been invoked heavily in the syntheses of nitropyrroles, imidazole and pyrazoles. Mono-nitrated pyrrole, imidazole, pyrazole, dinitrated pyrrole, imidazole, trinitrated imidazole, pyrazole and tetranitropyrrole have all been synthesised through nitration with the nitronium cation.[61][81-84] The benefits of using this reaction arise from the ease of the reaction set up, wide availability of the starting materials and the good yields achieved in almost all cases. This reaction method does have its disadvantages: certain sites on the azolate ring, most notably the 2- and 3/5-positions in imidazole and pyrazole, respectively,[61][82] cannot be nitrated in this way. Forming these nitro derivatives has been achieved through different means which are detailed below.

Acetyl nitrate (formed upon the addition of HNO_3 to acetic anhydride) is also widely used as a nitrating agent for azoles.[85] Addition to azoles without a “pyrrole” nitrogen result in nitration similar to that seen with electrophilic substitution. When added to azoles containing a “pyrrole” nitrogen, N-nitro compounds are formed (**Figure 1.21**).[86]

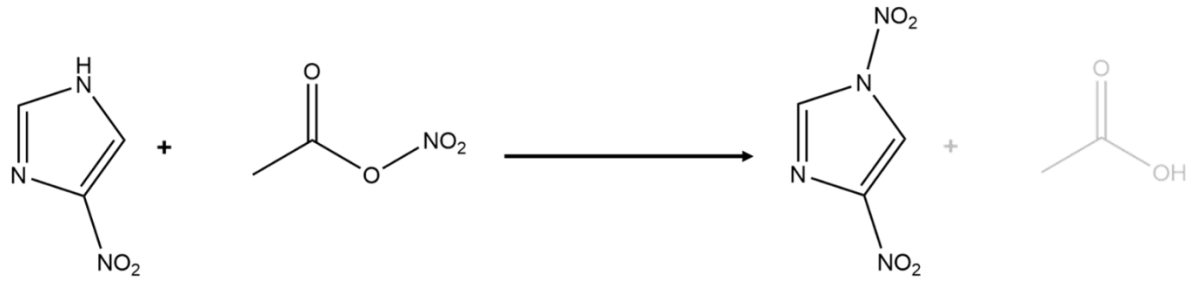

Figure 1.21: *Formation of acetyl nitrate*

In cases where N-nitration can occur at multiple sites, steric hindrance has a large effect on which site is nitrated. Nitration generally proceeds at the least sterically hindered nitrogen. In some cases, N-nitration can even be prevented completely by using large bulky substituents (protecting groups) adjacent to “pyrrole” nitrogen atoms.[87] N-nitro azoles have been shown to isomerise at high temperature to their C-nitro isomers due to the thermodynamic driving force of forming C-NO_2 bonds over N-NO_2 ones (**Figure 1.22**).[61][82] This allows for the isolation of nitroazoles that could not previously be accessed by direct azole nitration with the nitronium cation. N-nitro compounds in H_2SO_4 solution are also a nitronium cation source.[88]

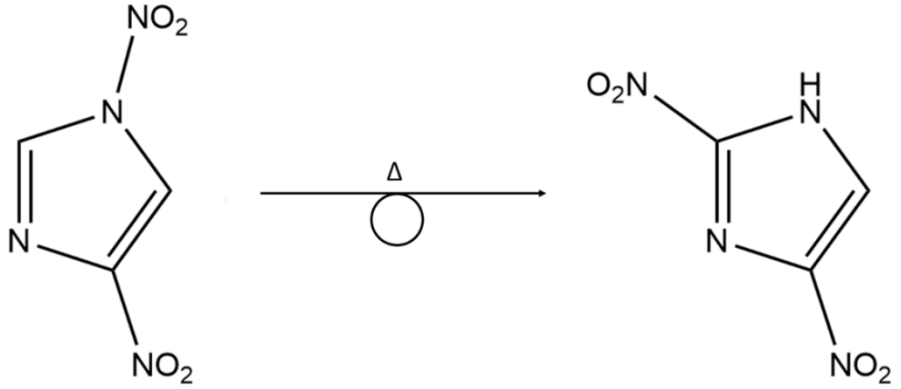

Figure 1.22: *High temperature isomerisation of N-Nitro azoles to form their C-Nitro isomers*

Ipso electrophilic aromatic substitution, whereby the entering group binds at a position in an aromatic compound already carrying a substituent group,[89] by a nitronium cation has also been exploited extensively in the synthesis of nitroazoles (**Figure 1.23**). Here, the nitration of iodoimidazoles is covered in great detail in a series of reports which show that diiodo- and triiodoimidazoles can be converted to their di- and trinitro derivatives in a one-pot reaction as opposed to the stepwise nitration used to form dinitro and trinitroimidazole reported elsewhere.[90]

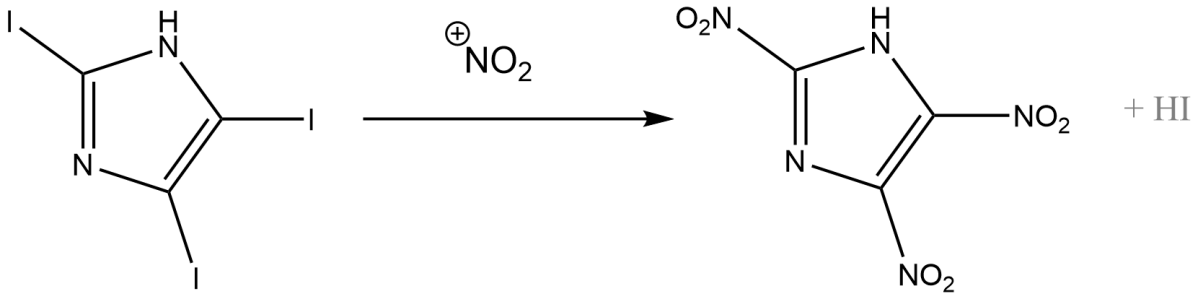

Figure 1.23: *Ipso nitration to form trinitroimidazole*

Beside some known special cases such as for triazolone, the direct nitration of azoles containing both carbon and nitrogen atoms can only occur in azoles bearing one or two nitrogen atoms.[69] For azoles with three or more heteroatoms, other methods of nitration must be used. Amino-nitro functional group interconversion has proven to be amongst the most popular methods of forming the higher-order nitroazoles (nitro-tetrazoles and triazoles). Here, the Sandmeyer reaction is the key method.[91] The latter relies on the conversion of an aromatic amine into its diazonium salt, followed by the displacement of the $-N_2^+$ group by a nucleophile.[91] Many of these reactions proceed only in the presence of a Cu(I) catalyst.[91] Diazonium salts are formed *in situ* by the action of the nitrosonium cation (NO^+). The nitrosonium ion is generated by the reaction of sodium nitrite with acid.[92] The Sandmeyer reaction then commences with the transfer of an electron from a Cu(I) salt to the diazonium salt. This results in the breakdown of the diazonium with loss of N_2 and the formation of an aromatic ring radical.[93][94] This reacts with the Cu(II) catalyst via two routes: a) reductive elimination from a formally Cu(III)-aromatic ring species,[93][94] or b) via direct transfer of an X atom / group with reformation of the Cu(I) salts (**Figure 1.24**).[93][94] This method has been used to great effect when introducing nitro groups to azoles, with the Sandmeyer reaction representing one of the few methods of introducing the nitro group into tetrazole rings.[91][93][94]

Even though it is a viable approach, the oxidation of amines is not widely used in the synthesis of nitroazoles. Mononitro-pyrazole, imidazole, triazole and tetrazole have all been isolated through the use of oxidising agents such as peroxytrifluoroacetic acid, Caro's acid, and diazotisation of amine followed by oxidation through addition of H_2SO_4.[68] While these reactions proceed, it appears that oxidation of amino groups can only be used in the case where one nitro group is desired. There are no examples of sequential or simultaneous oxidation of diamino azoles to dinitro azoles.[68] In some select cases it is also possible to synthesise a nitroazole from cyclisation of two reagents, one of which already contains a nitro group.[68] Nitro and dinitro pyrazoles have been synthesised from the reaction of sodium nitromalonaldehyde with substituted hydrazines and 1,2-dinitro-2-phenylethene with diazoalkanes.[68] 1,2,3-nitrotriazoles can also be synthesised through cyclisation with 4-nitro-5-methyl-1,2,3-triazole synthesised through the reaction of trinitropropane with sodium azide.[68]

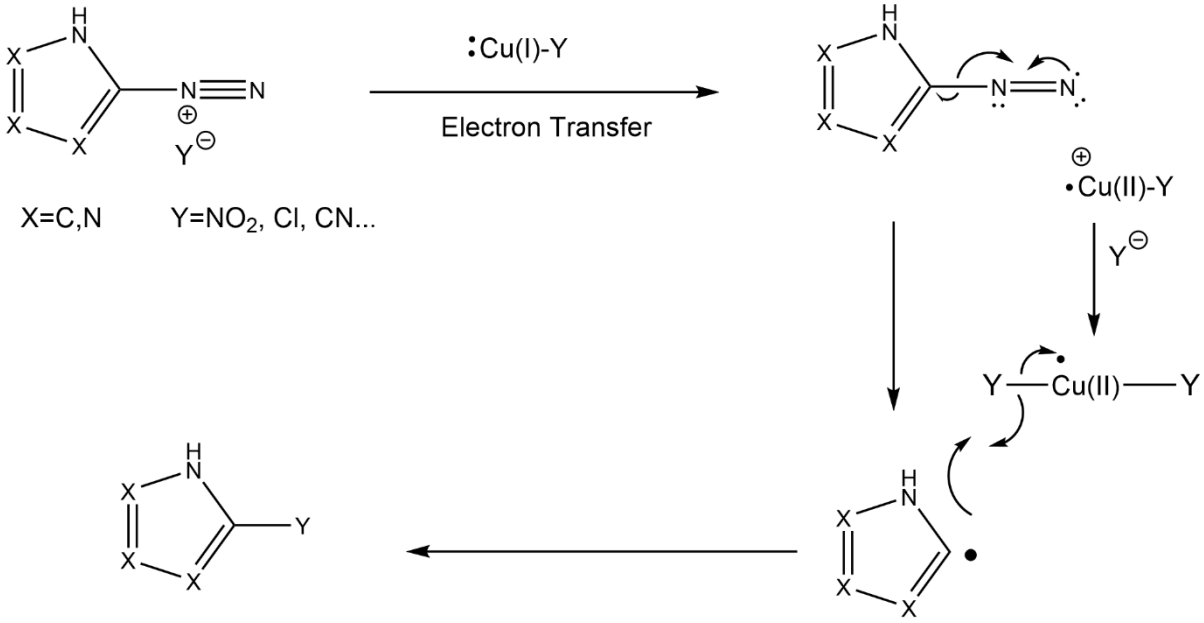

Figure 1.24: *Mechanism B of the Sandmeyer reaction*

1.7 Infrared spectroscopic properties of the -NO_2 group

1.7.1 NO_2 Group vibrational modes

Fourier transform infrared (FTIR) spectroscopy is one of the simplest and most informative ways of characterising nitro aromatic compounds. The nitro functional group, including the atom to which it is attached, can exhibit six distinct molecular vibrations (**Figure 1.25**), three of which are relatively intense and can be used for identification of the nitro group. Absorption of the asymmetric NO_2 stretch (ν_{as}) typically appears in the spectral range 1500–1650 cm^{-1}. A spectral distinction is possible between C and N-bound -NO_2 groups. C-bound -NO_2 groups in aromatic compounds have asymmetric stretches that appear in the region 1490-1580 cm^{-1}, whereas those for the N-NO_2 moiety can generally be found in the range 1600-1650 cm^{-1}.[68] A characteristic of the spectra of nitroimidazoles is a splitting of the absorption bands of the antisymmetric N-O stretching vibration in the nitro group into multiple bands, independent of the number of nitro groups. Therefore, it is impossible to determine the number and positions of nitro groups in the imidazole ring from the IR spectra alone.[95] This effect has also been noticed in polynitropyrazoles and it is reasonable to suggest that it can occur in any polynitroazole.[96] However, this phenomenon has not been

explicitly studied outside of imidazole. The symmetric stretch (ν_{sym}) in general appears from 1260–1400 cm^{-1}, but once again, C-NO_2 and N-NO_2 have different expectation ranges for ν_{sym}. The symmetric stretch for C-NO_2 can be found from 1310-1400 cm^{-1} and that of N-NO_2 from 1260-1294 cm^{-1}.[68]

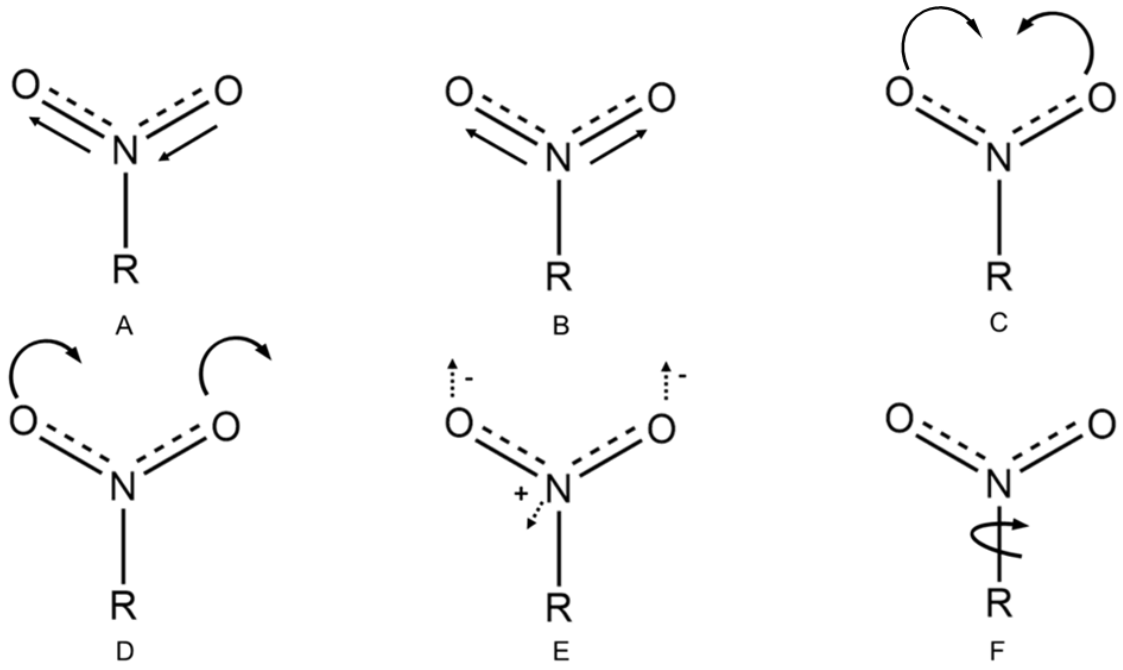

Figure 1.25: *Molecular vibrations of the NO_2 group: A) Asymmetric stretch, B) Symmetric stretch, C) Symmetric bend/ Scissor, D) asymmetric bend/Pivot, E) Out-of-plane deformation, F) Torsion motion/Twist*

The nitro group is planar and contains π bonds. As a result, vibrational frequencies in an X–NO_2 unit are sensitive to conjugation or resonance effects with the X group causing the nitro groups bonded to conjugated systems to absorb at lower frequencies than those of non-conjugated systems. The *asymmetric* stretch is much more directly affected by changes to conjugation than the *symmetric* stretch. It is known that the frequency of the asymmetric stretch is affected by conjugation and, through conjugation, by substitution. Electron-donating X groups attached to the aromatic ring decrease the frequency while electron-accepting groups increase it. If the nitro group is rotated out of the plane of the ring, then the frequency of the asymmetric stretch increases as a result of reduced conjugation with the ring. It has also been shown that for the six-membered rings, coupling of the asymmetric stretch to ring motions can

result in the appearance of a “double peak” with a lower intensity forepeak visible and the main, higher intensity peak separated by up to 80 cm^{-1}.[97-101]

The symmetric stretch is known to couple to the X-N bond vibration and so, while having a frequency range similar to that of the asymmetric stretch, is more difficult to make direct correlations between ring substituents and frequency. Studies have shown that the position of the absorption seems to be only slightly affected by the electron-withdrawing or -donating characteristics of the substituent. While coupling to ring motions can explain the slight effect ring substituents have on the frequency of the symmetric stretch, it cannot explain the wide range of values the symmetric stretch frequency can assume. Instead, it must be explained through coupling to the X-N bond. Calculations have shown that the N–O bonds stretch while the N–X bond compresses. Studies have also shown that the nitro group symmetric stretch always couples with the N–X stretch and as such it has been suggested that, instead of two coupled motions, the N-X stretch and N-O symmetric stretch could be considered as a single concerted normal mode. Within compounds that have more than one nitro group, coupling of the symmetric stretches can occur. Depending on the number of nitro groups, and the synchronisation of their respective symmetric stretches, this can greatly change the spectrum in the region 1260-1400 cm^{-1} with two nitro groups leading to either reduced or increased intensity of the symmetric absorption depending on constructive or destructive interference of the two symmetric stretches. Compounds with more than two nitro groups can lead to multiple symmetric stretches depending on the synchronicity of the coupled symmetric stretches.[97-101]

The symmetric bend and out-of-plane deformation motions have lower frequencies and are less intense than the stretching modes in the infrared spectrum. While this can lead to the symmetric bend and out-of-plane motions being incorrectly assigned, in nitro group containing aromatics the symmetric bend can still prove to be a useful diagnostic band of the nitro group. The pivot and torsion motions are known to occur at even lower frequencies than the symmetric bend or out-of-plane deformation and are rarely observed. The nitro group bend is much less studied than either ν_{as} or ν_{sym} but still proves to be a valuable characteristic stretch of the aromatic nitro group. The symmetric bend refers to a change of the interior angles of the O-N-O. Much like the symmetric stretch the $-NO_2$ bend can also couple with the N-X stretch. Unlike the symmetric stretch, which couples with the N–X stretch in only one way, the

scissoring motion usually couples with the N–X stretch in two ways both with different associated energy. For both C and N bound nitro groups the higher energy absorption band corresponds to the bending motion where the O-N-O angle decreases and the X-N bond compresses. In the lower energy absorption band, the interior angle decreases while the N–X bond stretches. The higher energy band appears in the range 750-900 cm^{-1} and is generally the absorption band identified when one refers to the nitro group symmetric bend. The lower energy band appears below 750 cm^{-1} but with its lower intensity is usually not used as a diagnostic NO_2 group band.[97-101]

The out-of-plane deformation is frequently grouped with the symmetric bend and referred to only as "-NO_2 skeletal motions". The absorption band can be found in the range 700-800 cm^{-1} but is more commonly found in the range 710-760 cm^{-1}. The overlap of this band with the lower energy symmetric bend can make the out of plane deformation difficult to distinguish. While this band has been frequently shown to not couple with other bands, when coupling *does* occur, it is most often with other nitro group out-of-plane motions, or with the bending motions involving atoms in the backbone of the aromatic system. Studies have shown the out of plane deformation to be only slightly affected by the electron-withdrawing or -donating characteristics of nearby groups, or by the nitro group geometry. It is for this reason that the out-of-plane deformation can be found in a relatively small spectral range. However, it is likely that neighbouring groups which can sterically hinder out of plane motion would have a noticeable effect on the position of this absorption band.[97-101]

1.7.2 Effects of nitroazole salt formation on infrared absorption bands

While the absorption bands of nitroazoles fall into the expected ranges for nitro aromatic compounds, formation of nitroazolate salts can have a large effect on the expected ranges for some of the absorption bands. Investigations into the FTIR spectra of known nitroimidazoles and their respective Na/K salts were done by Epishina et al.[95] It is known that upon deprotonation of nitroimidazoles, the electron density does not remain localised on the nitrogen atom from which the proton disengages but is instead distributed over the entire aromatic ring. It has been shown in the case of nitroimidazoles that the nitro groups can also participate in this electron

delocalisation. Depending on the extent to which electron density is concentrated on either the ring or the nitro group two structures can be theorised:

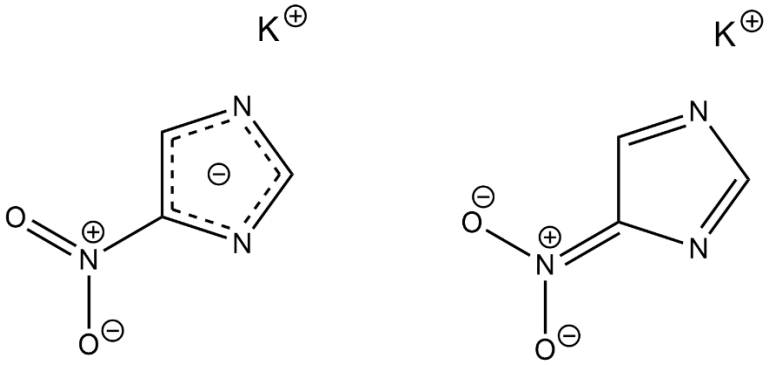

Figure 1.26: *Charged (Right) versus uncharged (Left) nitro group resonance forms of potassium-4-nitroimidazolate*

When salt formation occurs with 'uncharged' nitro groups (**Figure 1.26, Left**), only a small shift in band position is expected with the previously established trends for ν_{as} and ν_{sym} holding true. However, when salt formation occurs with 'charged' nitro groups **(Figure 1.26, Right)**, characteristic bands of the charged nitro group must occur. These are reported at ~1180 and ~950 cm^{-1} for mononitroimidazolates. Formation of the charged nitro group also results in conversion of the imidazole ring to an isoimidazole ring which can also give rise to changes to bands associated with imidazole ring vibrations with at least 3 strong-medium intensity bands associated with formation of isoimidazole for some mononitroimidazolate salts. The salts of polynitroimidazole are also affected by the formation of charged NO_2 salts. When deprotonated, the disappearance of absorption bands at both ~1550 and ~1350 cm^{-1} and the development of new bands in the same regions as for the mononitroimidazolates can be observed.[95] However as not all the bands associated with the ν_{as} and ν_{sym} of polynitroimidazoles disappear it can be theorised that in these cases electron density is not evenly split between nitro groups and instead is localised over a select few giving rise to both charged and uncharged -NO_2 stretches. The phenomenon of charged -NO_2 groups has only been directly reported in imidazoles.[95] However, while no report has been made of the existence of such resonance forms for nitropyrazolates, triazolates or tetrazolates simple assessment of the resonance

forms available to these compounds does show potential charge delocalisation over the NO_2 group. Therefore, this should be considered when assigning the absorption bands of nitroazoles other than imidazoles.

1.8 Instrumental analytical characterisation of inorganic energetic materials

Inorganic explosives require characterisation not only through methods common to energetic materials but also to those common to coordination chemistry. Many techniques exist for the characterisation of coordination compounds. X-ray crystallography is one of the key techniques used for the characterisation of pure crystalline coordination complexes in the solid state. Crystals are materials in which the atoms are arranged in a highly ordered structure which extends in all directions. In single crystal X-ray diffraction, a crystal of a compound is mounted on a goniometer which can be used to orientate the crystal so that it can be analysed from multiple angles. X-rays are generated from an X-ray tube and filtered so that they are monochromatic. When the crystal is placed in the path of the X-ray beam the electrons surrounding each atom in the crystal act as secondary X-ray sources and emit X-rays as spherical waves (Thomson scattering).[102-104] Thomson scattering is an elastic scattering of electromagnetic radiation and so the emitted X-rays have the same energy as the incident X-rays that are fired at the sample. As the crystal is comprised of repeating unit of scatterers this results in a regular array of secondary spherical waves. These waves can combine either destructively or constructively, determined by the relationship specified in Bragg's Law. The specific regions where constructive interference occurs can be detected and appear as spots of intensity on a 2D diffraction pattern for a particular crystal orientation. The crystal mounted on the goniometer is rotated in the beam so that a series of 2D diffraction patterns can be recorded. From these 2D diffraction patterns, computation is used to develop a 3D electron density map of the crystal which can then be used to build and refine a model of the arrangement of atoms in the crystal.[102-104] Powder X-ray diffraction (PXRD) is built upon similar theory to single crystal X-ray diffraction (SXCRD). However, in a crystalline powder every possible crystalline orientation is said to be present in an equal amount assuming the sample is randomly arranged. In practice samples are

rotated to reduce the effects of any ordering of the crystallographic orientations. As all orientations are present, diffraction results not in the formation of discrete spots of intensity but instead as rings (Debye-Scherrer Rings). While structural determination from PXRD patterns remains challenging for complex compounds, important information such as phase identification, crystallinity and lattice parameters can be found from PXRD analysis.[104]

FTIR spectroscopy is also an important technique for the characterisation of coordination compounds and is valuable for probing the environment in which the ligand is coordinated. Upon coordination to a metal centre, electron density is donated from ligand orbitals into metal centred orbitals. This transfer of electrons can have dramatic effects on the electronic configuration of the ligand and result in shifts of absorption bands to higher or lower frequencies all of which can be observed by FTIR monitoring. Not only does the delocalisation of electron density away from ligand orbitals play a role in absorption band shifts, back donation from metal d-orbitals into ligand p-orbitals can greatly affect the ligand vibrations.

Mass spectrometry can also be used for the characterisation of energetic coordination compounds. A mass spectrometer generates multiple ions from the sample being investigated, it then separates them according to their specific mass-to-charge ratio (m/z), and then records the relative abundance of each ion type. The first phase of this process is generation of ions from the sample which can be done in a multitude of ways depending on the information about the sample the user is looking to find. In electron impact ionization (EI), a vaporized sample is passed through a beam of electrons. The high energy (typically 70 eV, the kinetic energy of the bombarding electrons should have higher energy than the ionization energy of the sample molecule) beam strips electrons from the sample molecules leaving a positively charged radical species. The molecular ion is typically unstable and undergoes decomposition or rearrangement to produce fragment ions. Due to the high degree of fragmentation from EI this ionisation method is considered a “hard” ionisation technique. In electrospray ionisation (ESI) the sample being investigated is dissolved in a solvent. The solution is then passed through a charge capillary needle which produces a liquid jet emitting from the capillary tip. This leads to the formation of highly charged droplets which disperse from each other due to coulombic repulsion resulting in the formation of an aerosol. As the aerosol is pumped towards the mass analyser

desolvation occurs through the use of a drying gas or heat. As the droplets decrease in size the charge density increases until it reaches the Rayleigh limit at which point the droplets break apart into smaller charged droplets with this process continuing until individual ions of the sample are generated. ESI is regarded as a soft ionisation technique as it does not lead to a high degree of fragmentation. Matrix Assisted Laser Deposition Ionisation (MALDI) is another popular ionisation technique. MALDI uses a laser energy absorbing matrix to produce ions from large molecules while being a relatively soft ionisation technique. In MALDI mass spectrometry analyte is mixed with a laser absorbing matrix and deposited on a target surface. After a laser pulse, the irradiated spot absorbs the laser energy and the matrix-analyte mixture is thought to desorb from the surface and become ionised. The matrix is then thought to transfer protons to the analyte leading to charged analyte molecules. All these methods of ionisation then pump the now ionised analyte molecules to the mass analyser. Mass analysers are used to determine the mass-to-charge ratio (m/z), this ratio is used to differentiate between molecular ions that were formed in the ionisation process. Time of flight (TOF) mass analysers are some of the most widely used. TOF determines an ion's mass-to-charge ratio by measuring the time taken for analyte ions to reach the detector. By accelerating ions in an electric field of known strength one can accelerate the ions. This acceleration results in an ion having the same kinetic energy as any other ion that has the same charge. The velocity of the ion depends on the mass-to-charge ratio (heavier ions of the same charge reach lower speeds, although ions with higher charge will also increase in velocity). The time that it subsequently takes for the ion to reach a detector at a known distance is measured, and therefore, the mass-to-charge ratio is recorded.[105][106]

Measurement of magnetic susceptibilities (χ, the ability of a substance to be attracted to or repelled by an external magnetic field) can be an effective tool in coordination compound characterisation in cases where the oxidation state of the metal centre needs to be verified. Compounds can be split into two categories according to their response to the applied magnetic field: Paramagnetic compounds which align with the magnetic field (a property of compounds having nonzero spin or orbital angular momentum), $\chi > 0$, or diamagnetic compounds which align against the field, $\chi < 0$. While paramagnetism arises from the presence of unpaired electrons in a molecule, all electrons, whether paired or unpaired, cause diamagnetism. Magnetic

susceptibility is therefore defined by the competing effects of attractive paramagnetism and the repulsion of diamagnetism. The measured magnetic susceptibility of a coordination compound, χ_{meas}, is defined as:

$$\chi_{meas} = \chi_{Paramagnetic\ susceptibility} + \chi_{Diamagnetic\ susceptibility}$$

The paramagnetic susceptibility can be used to determine the number of unpaired electrons in the compound through the equation:

$$\chi_P T = \frac{N_A g^2 \beta^2}{3k_B}[S(S+1)]$$

The number of unpaired electrons can then be used to determine metal oxidation state provided the metal spin state can be determined.[107][108]

Elemental analysis is a simple characterisation method that provides important information on coordination compounds. The most common form of elemental analysis, CHNX analysis, is accomplished by combustion analysis. CHNX analysis is the determination of the mass fractions of carbon, hydrogen, nitrogen, and heteroatoms (X) in the sample. Combustion analysis works by heating an element quickly to a sufficiently high temperature (>1000°C) so that it completely combusts. In this combustion process carbon is converted to carbon dioxide; hydrogen to water; nitrogen to nitrogen gas/ oxides of nitrogen and any other elements to their respective combustion products. These products are then purified, usually by passing over high temperature high purity copper to remove any oxygen not consumed in the initial combustion and to convert oxides of nitrogen to nitrogen gas. Detection of the purified gases by a variety of means is then used to determine the final mass fraction of each element in the sample. Quantification of the elements requires calibration for each element by using high purity standards.[109]

Differential scanning calorimetry (DSC) is another important characterisation method of energetic materials. DSC refer both to the technique of measuring calorimetric data and to the instrument itself. DSC relies on the measurement of heat flow and there are two different types of DSC instruments that can be used to measure this: Heat-flux DSC which measures the difference in heat flux between the sample and a reference and Heat flow DSC which measures the difference in power supplied

to the sample and a reference. In Heat flux DSC, a sample and a reference crucible are placed on a sample holder in a temperature-controlled furnace with temperature sensors for temperature measurement of the crucibles. The two crucibles will heat at approximately the same rate (NB: the reference crucible will generally heat faster due to the additional heat capacity of the sample crucible) until a thermal event occurs. At this point the sample crucible will either increase or decrease in temperature relative to the reference. Once the event finishes the two pans once again continue to heat until the programmed experiment end. The heat flow is calculated by integrating the $\Delta T(T_s - T_r)$ / time curve. Heat flow DSC instead uses a double furnace design in which the sample and reference crucible are placed in thermally insulated furnaces and not next to each other as in Heat-flux-DSC. The temperature of both chambers is controlled so that the same temperature is always present on both sides. The power required to obtain and maintain this state is then recorded rather than the temperature difference between the two crucibles. Once heat flow as a function of temperature can be recorded analyse of the thermal events (glass transition temperature, melting point, decomposition temperature etc..) can begin.[110][111]

1.9 References

1. J. J. Sabatini, *Propellants, Explos. Pyrotech*., 43 (1) (2018), pp. 28-37
2. J. Akhavan, 2011, *The Chemistry of Explosives*, 3rd edition, Published by The Royal Society of Chemistry, Thomas Graham House
3. R. Matyas, J. Pachman, Primary Explosives, 2013, Springer
4. T. Klapötke, Chemistry of High-Energy Materials, 2015, De Gruyter, Berlin, Boston
5. T. Urbanski, Chemistry and technology of Explosives, Vol.1., 1964, Pergamon Press, Oxford and Polish Scientific Publishers, Warsaw
6. F. Zapata, C. Garcia-Ruiz, Crit. Rev. Anal. Chem, 2021, 51, 7, 656-673
7. J. P. Agrawal, R. D. Hodgson, Organic Chemistry of Explosives, Wiley, Weinheim, 2007
8. M. Marshall, J. C. Oxley, Aspects of Explosives Detection, Elsevier, Oxford, 2009
9. J. P. Agrawal, High Energy Materials: Propellants, Explosives and Pyrotechics, Wiley, Weinheim, 2010
10. J. E. Field, Acc. Chem. Res., 1992, 25, 11, 489-496
11. D. D. Dlott, M. D. Fayer, J. Chem. Phys., 1990, 92, 3798-3812
12. G. S. Hong, C. X. Lu, W. L. Sha, Y. X. Dong, J. Mol. Struct., 2007, 809, 1-3, 55-60
13. A. A. L. Michalchuk, P. T. Fincham, P. Portius, C. R. Pulham, C. A. Morrison, *J. Phys. Chem. C* 2018, 122, 34, 19395–19408
14. C. S. Coffey, V. F. Devost, June 1992*, Impact Testing of Explosives and Propellants*, AD-A267 391, Naval surface Warfare Center
15. United Nations, 2009, *Part 1: Classification procedures, Test methods and Criteria relating to Explosives of Class 1*
16. R. Meyer, J. Köhler, A. Homburg, 2007, *Explosives*, 6th Edition, Published by Wiley-VCH Verlag GmbH, Weinheim
17. M. H. Keshavarz, T. M. Klapötke, 2018, *The properties of Energteic Materials: Sensitivity, Physical and Thermodynamic Properties*, 1st edition, De Gruyter, Berlin
18. OZM Research, 2020, BFH-10 BAM Fall Hammer(Impact tester) Product datasheet, OZM Research, Viewed on 03/05/2022, https://mueller-

instruments.de/fileadmin/Downloads/instruments-medien/BAM_Fallhammer_-_BFH_10.pdf
19. F. W. Marrs, V. W. Manner, A. C. Burch, J. D. Yeager, G. W. Brown, L. M. Kay, R. T. Buckley, C. M. Anderson-Cook, M. J. Cawkwell, *Ind. Eng. Chem. Res.,* 60, 13 (2021), pp. 5024-5033
20. P. J. Rae, P. M. Dickson, J. Dynamic Behaviour. Mat, 2021, 7, 414-424
21. OZM Research, 2020, FSKM 10 BAM friction apparatus Product datasheet, OZM Research, Viewed on 03/05/2022, https://www.ozm.cz/files/explosives-and--propellants-testing-instruments/sensitivity-and-explosibility-tests/friction-sensitivity-tester-fskm10/friction-sensitivity-tester-fskm10.pdf
22. L. R. Simpson, M. F. Foltz, June 1996, *LLNL Small Scale Friction Sensitivity (Bam) Test*, Lawrence Livermore National Laboratory
23. D. Skinner, D. Olson, A, Block-Bolten, *Propellants, Explos. Pyrotech.,* 23, 1997, pp. 34-42
24. H. Koenen, K. H. Ide, Explosivstoffe, 1956, 6, pp. 119-125
25. a)SMS, 2022, Koenen Test Apparatus, SMS, https://smsenergetics.com/koenen, b) OZM Research, 2022, Koenen tester KT 300, Viewed on 20/09/2022, https://www.ozm.cz/sensitivity-and-explosibility-tests/koenen-heat-tester-kt300/,
26. K. D. Oyler, N. Mehta, G. Cheng, Overview of Explosive Initiators, 2015, ARMET-TR-15017
27. J. Kunckel, Collegium Physico Chymicum oder Laboratorium Chymicum Engelleder, Hamburg & Leipzig, 1716; p 213
28. W. Beck, J. Evers, M. Gobel, G. Oehlinger, T. M. Klapötke, Z. Anorg. Allg. Chem., 2007, 633, 1417-1422
29. T. Curtius, R. Radenhauser, J. Prakt. Chem., 1891, 43, 207–208
30. B. T. Fedoroff, O. E. Sheffield, S. M. Kaye, Encyclopedia of Explosives and Related Items, New Jersey (1960–1983)
31. C.S. Choi, E. Prince, W. L. Garrett, Acta Crystallographica,Section B:Struct.Crystallogr.Cryst.Chem., 1977, 33, 3536,
32. L.F. Audrieth, Chem. Rev. 1934,15, 169–224
33. E. Herz, British Patent 17961, 29 October 1915.
34. J. Stenhouse, Proc. R. Soc. Lond., 1870-1871, 19, 410–417

35. P. Griess, Berichte der deutschen chemischen Gesellschaft 7, 1223–1228 (1874)
36. J. F. Kenney, 1976, US Patent No. 4029530A
37. : L.T. Fairhall, W .V. Jenrette, S. W. Jones, E. A. Pritchard, Public Health Reports (1896-1970), 1943, Vol. 58, No. 15 pp. 607-617
38. M. Shee, N. D. P. Singh, Chem. Soc. Rev., 2022, 51, 2255-2312
39. A. L. Wani, A. Ara, J. A. Usmani, Interdiscip Toxicol. 2015, 8, 2, 55–64
40. G. Flora, D. Gupta, A. Tiwari, Interdiscip Toxicol. 2012, 5, 2, 47–58
41. V. Mah, F. Jalilehvand, Inorg. Chem. 2012, 51, 6285−6298
42. M. H. V. Huynh, M. D. Coburn, T. J. Meyer, PNAS, 2006, 103, 27, 10322-10327
43. V. P. Drost, Justus Liebigs Ann. Chem .,1899, 307, 49
44. R. J. Gaughran, J. P. Picard, J. V. R. Kaufman, *J. Am. Chem. Soc.* 1954, 76, 8, 2233–2236
45. A. J. Boulton, D. P. Clifford, J. Chem. Soc. 5414–5416 (1965)
46. Q. Nisa-Tariq, S. Manzoor, M. Nisa-Tariq, W. Cao, J. Zhang, Defence Technology, 2021
47. J. Li, F. Chen, H. Yang, K. Lu, Propellants Explos. Pyrotech., 2020, 45, 1313–1325
48. D. Fischer, T. M. Klapötke, J. Stierstorfer, Angew. Int. Ed., 2014, 53, 31, 8172-8175
49. W. P. Norris, A. Chafin, R. J. Spear, R. W. Read, *Heterocycles* **1984**, *22*, 271.
50. A. J. Boulton, P. B. Ghosh, *Benzofuroxans in Advances in Heterocyclic Chemistry*, Academic Press, New York, 1969, Vol. 10, pp. 1–41.
51. J. W. Fronabarger, M. D. Williams, W. B. Sanborn, D. A. Parrish, M. Bichay, Propellants Explos. Pyrotech.2011,36, 459 – 470
52. J. W. Fronabarger, M. D. Williams, W. B. Sanborn, J. G. Bragg, D. A. Parrish, M. Bichay, Propellants Explos. Pyrotech.2011,36, 541 – 550
53. J. W. Fronabarger, M. D. Williams, W. B. Sanborn, 2007, US Patent WO2008048351A2
54. W. Li, K. Tseng, T. Yang, J. Li, K. Lu, Propellants Explos. Pyrotech. 2020, 45, 1–11

55. D. D. Ford, S. Lenahan, M. Jorgensen, P. Dube, M. Delude, P. E. Concannon, S. R. Anderson, K. D. Oyler, G. Cheng, N. Mehta, J. S. Salan, *Org. Process Res. Dev.* 2015, 19, 6, 673–680
56. T. M. Klapötke, D. G. Piercey, N. Mehta, K. D. Oyler, M. Jorgensen, S. Lenahan, J. S. Salan, J. W. Fronabarger, M. D. Williams, Z. Anorg. Allg. Chem.2013,639, (5),681–688
57. T. M. Klapötke, D. G. Piercey, N. Mehta, K. D. Oyler, J. J. Sabatini, Z. Naturforsch. 2014, 69b, 125 – 127
58. S. Alves, A. Kuhl, F. Najjar, J. Tringe, L. McMichael, L. Glascoe, 2012, LLNL-PROC-528333
59. V. Ghule, R. Sarangapani, P. M. Jadhav, S. P. Tewari, J. Mol. Model, 2011, 17, 6, 1507-15
60. P. Yin, J. M. Shreeve, Advances in heterocyclic Chemistry Chapter Four: Nitrogen-Rich Azoles as High Density Energy Materials: Reviewing the Energetic Footprints of Heterocycles, 2017, 121, 89-131
61. J. Cho, K. Kim, J. K. Kim, Het. Comp., 2002, 33, 31,
62. T. Fendt, N. Fischer, T. M. Klapötke, J. Stierstorfer, Inorg. Chem., 2011, 50, 4, 1447–1458
63. J. Singh, R. J. Staples, J. M. Shreeve, ACS Appl. Mater. Interfaces, 2021, 13, 51, 61357–61364
64. C. K. Ingold, Structure and Mechanism in Organic Chemistry, 1953, Cornell Univ. Press
65. J. W. Chapman, A. N. Strachan, 1974, J. Chem. Soc., Chem. Commun., 293-294
66. R. M. Schramm, F. H. Westheimer, Z. Physik. Chem., 1948, 50, 385, 1782-1784
67. G. A. Olah, S. C. Narang, J. A. Olah, K. Lammertsma, Proc. Natl. Acad. Sci. USA., 1982, 79, 14, 4487-4494
68. L. Larina, V. Lopyrev, Nitroazoles: Synthesis, Structure and applications, 2009, Springer Science, New York
69. E. D. Hughes, C. K. Ingold, R. I. Reed, J. Chem. Soc., 1950, 2400-2440
70. M. J. S. Dewar, E. W. T. Warford, J. Chem. Soc., 1956, 3570-3572

71. R. J. Schmitt, D. S. Ross, S. E. Buttrill, J. Am. Chem. Soc., 1981, 103, 5265-5267
72. D. S. Ross, K. F. Kuhlmann, R. Malhotra, J. Am. Chem. Soc., 1983, 105, 4299-4302
73. R. J. Schmitt, D. S. Ross, S. E. Buttrill, J. Am. Chem. Soc., 1984, 106, 926-930
74. J. Kenner, Nature, 1946, 157, 340
75. J. Weiss, Trans. Faraday Soc., 1946,42, 116-121
76. J. F. Queiroz, J. W. M. Carneiro, A. A. Sabino, R. Sparrapan, M. N. Eberlin, P. M. Esteves, . Org. Chem. 2006, 71, 16, 6192–6203
77. C. L. Perrin, J. Am. Chem. Soc., 1977, 99, 5516-5518
78. A. S. Morkovnik, Russ. Chem. Rev., 1988, 57, 144
79. B. Galabov, D. Nalbantova, P. R. Schleyer, H. F. Schaefer, Acc. Chem. Res. 2016, 49, 6, 1191–1199
80. A. R. Cooksey, K. J. Morgan, D. P. Morrey, Tetrahedron, 1970, 26, 21, 5101-5111
81. M. F. Bolter, A. Harter, T. M. Klapötke, J. Stierstorfer, Chem Plus Chem., 2018, 83, 8, 804-811
82. I. L. Dalinger, I. A. Vatsadze, T. L. Shkineva, G. P. Popova, S. A. Shevelev, Y. V. Nelyubina, J. Het. Chem., 2013, 50, 4, 911-924
83. J. C. Hinshaw, W. Wayne Edwards, C. George, R. Gilardi, J. Het. Chem., 1992, 29, 7, 1721-1724
84. F. G. Bordwell, E. W. Garbisch Jr, J. Org. Chem. 1962, 27, 7, 2322–2325
85. J. W. A. M. Janssen, H. J. Koeners, C. G. Kruse, C. L. Habrakern, J. Org. Chem., 1973, 38, 10, 1777-1782
86. I. L. Dalinger, V. A. Litosh, S. A. Shevelev, Russ. Chem. Bull., 1997, 46, 1149-1153
87. G. A. Olah, S. C. Narang, A. P. Fung, J. Org. Chem., 1981, 46, 13, 2706-2709
88. R. B. Moodie, K. Schofield, Acc. Chem. Res. 1976, 9, 8, 287–292
89. P. Ravi, C. K. Reddy, A Saikia, G. M. Gore, A. K. Sikder, S. P. Tewari, Propellants Explos. Pyrotech.2012, 37, 167 – 171
90. T. M. Klapötke, D. G. Piercey, N. Mehta, K. D. Oyler, M. Jorgensen, S. Lenahan, J. S. Salan, J. W. Fronabarger and M. D. Williams, Z. Anorg. Allg. Chem., 2013, 639, 681–688

91. R. Akhtar, A. F. Zahoor, N. Rasool, M. Ahmad, K. G. Ali, Mol. Div., 2022, 26, 1837-1873
92. L. Bering, A. P. Antonchick, Tetrahedron, 2019, 75, 9, 1131-1143
93. E. V. Anslyn, D. A. Dougherty, Modern Physical Organic Chemistry, 2006, University Science Books, Mill Valley California
94. K. P. C. Vollhardt, N. E. Schore, Organic Chemistry: Structure and Function, 2018, W.H. Freeman, Macmillan Learning, New York
95. L. V. Epishina, V. I. Slovetskii, V. G. Osipov, O. V. Lebedev, L. I. Khmel'ntiskii, V. V. Sevost'yanova, T. S. Novikova, Khim. Getero. Soed., 1967, 3, 4, 716-723
96. P. Ravi, J. Mol. Struc., 2015, 1079, 5, 433-447
97. R. W. Beal, T. B. Brill, Applied Spectroscopy., 2005, 59, 10, 139-153
98. J. F. Brown, J. Am. Chem. Soc. 1955, 77, 23, 6341–6351
99. V. G. Osipov, V. A. Shlyapochnikov, E. F. Ponizovtsev, Zhurnal Prikladnoi Spektroskopii, 1968, 8, 6, 1003-1005
100. V. I. Slovetskii, Izvestiya Akademii Nauk SSSR, Seriya Khimicheskaya, 1970, 10, 2215-2221
101. R. D. Kross, V. A. Fassel, J. Am. Chem. Soc. 1956, 78, 17, 4225–4229
102. W. L. Bragg, The Crystalline State: A General Survey, 1966, G. Bell and Sons Ltd., London
103. M. Ladd, R. Palmer, Structure Determination by X-ray Crystallography, 4th Ed., 2003, Kluwer Academic/Plenum Publishers, New York
104. A. I. Kitaigorodskii, The Theory of Crystal Structure Analysis, 1961, Consultants Bureau, New York
105. T. Niwa, Clin. Chim. Acta., 1995, 241-242, 3-413
106. K. L. Busch, G. L. Glish, S. A. McLuckey, Mass Spectrometry: Techniques and Applications of Tandem. John Wiley & Sons, 1989
107. G. A. Bain, J. F. Berry, J. Chem. Ed., 2008, 85, 4, 532-536
108. H. Landolt, R. Bornstein, Landolt-Börnstein, Numerical Data and Functional Relationships in Science and Technology, New Series, II/16, Diamagnetic Susceptibility, Springer-Verlag, Heidelberg, 1986.
109. Royal Society of Chemistry (Website) AMC technical briefs – CHNS Elemental Analysers, Viewed 12/09/22, https://www.rsc.org/images/CHNS-elemental-analysers-technical-brief-29_tcm18-214833.pdf

110. Perkin Elmer, DSC FAQ, Viewed 20/09/22, https://resources.perkinelmer.com/corporate/cmsresources/images/44-74542gde_dscbeginnersguide.pdf
111. P. Gabbott, Principles and Applications of Thermal Analysis, 2008, Blackwell Publishing

2. Synthesis of novel Cu (I)-nitrotetrazolate coordination polymer and insights into the formation of DBX-1

2.1 Introduction

DBX-1 is a member of a family of energetic copper nitrotetrazolates consisting of $Cu(en)_2(NT)_2$,[1] $Cu(NH_3)_3(NT)_2$,[1] $(M')_2[Cu_2(NT)_4 \cdot (H_2O)_2]$,[2] copper(I) nitrotetrazolate[3][4] or DBX-1,[5][6] $Cu(NT)_2$[7] and $Cu(H_3O)(NT)_3 \cdot 3H_2O$[8][9][10] (en= ethylene diamine, NT = 5-nitrotetrazolate).The synthesis of DBX-1 is not straightforward and reproducibility of results has prevented the adoption of DBX-1 as the unanimous lead azide replacement (vide supra). There is a lack of insight into the mechanism of its formation in the presence of sodium 5-nitro-tetrazolate (NaNT) by reduction of either copper(II) chloride with sodium ascorbate, Na(HAsc), in an aqueous reaction,[3][4][11] or from copper(I) chloride directly.[4][12] Efforts to achieve repeatable, consistent and efficient synthesis of DBX-1 have driven research into testing specific preparative methods.[5][6][8] Below is detailed an investigation into the synthesis of DBX-1 and the conditions needed for consistent synthesis of high purity DBX-1.

Research Questions

- Can DBX-1 be synthesised in high yield and purity by the methods reported in the literature?

- Which factors control the reaction outcome?

- Can any other by-products be characterised to obtain a better understanding of the reaction system?

2.2 Results and Discussion

2.2.1 First attempted synthesis of DBX-1 and synthesis of high-purity NaNT.4H₂O

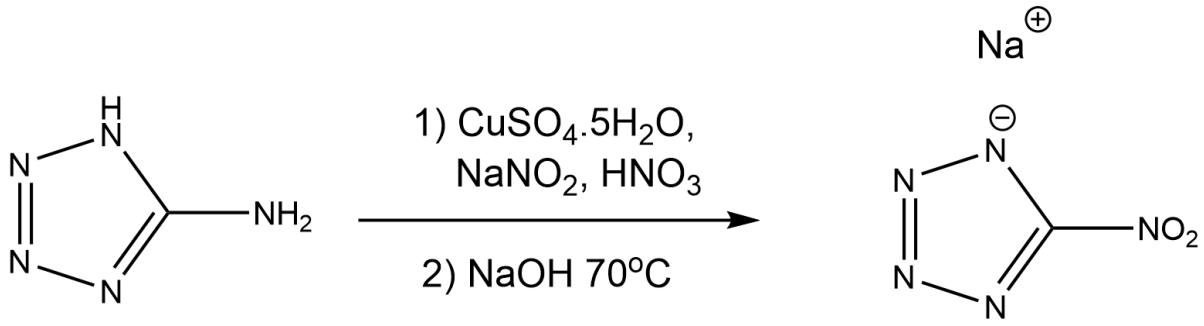

Figure 2.1: *Synthesis of NaNT*

To elucidate the exact conditions under which DBX-1 forms, the precursor, sodium-nitrotetrazolate (NaNT), had to first be synthesised in high purity and yield. NaNT was synthesised according to a modified procedure published by Klapötke *et al.*[6] Briefly, 5-aminotetrazole underwent a Sandmeyer reaction to form 5-nitrotetrazole in solution (**Figure 2.1**). This was then treated with NaOH, and the solvent removed, to afford a light yellow crystalline solid. According to the reports of Klapötke, this product contains $NaNT.2H_2O$ contaminated with a large amount of $NaNO_3$.[6] To purify this solid, a Soxhlet extraction with hot acetone was used. This purification technique makes use of the partial solubility of components of the solid phase in hot solvents to extract the desired components into the liquid phase, leaving behind a residue comprised of unwanted by-products. It was found that extraction of “wet”, crude NaNT resulted in large amounts of $NaNO_3$ also being extracted during the Soxhlet extraction process. Recrystallisation of the $NaNO_3$ on the underside of the sinter bed resulted in slow extraction and a noticeable browning of the crude material (decomposition due to the extended extraction time and prolonged exposure to hot acetone). NaNT must therefore be dry prior to any extractions attempts (dry in this instance refers to the crude NaNT being in a state whereby crystals are flaky, free flowing and not sticking to the walls of any container with no noticeable solvent residues apparent if sample is manipulated on filter paper). Due to the energetic nature of NaNT and warnings from published procedures regarding its sensitiveness to stimuli in the dry state,[6] the rotary

evaporation of the crude material prior to extraction was performed behind a blast shield and carefully monitored to ensure that, while dry, the product was not so dry as to needlessly increase its sensitiveness (drying to the extent of removal of any water present in the crystal). No unexpected explosions of this now dry material were experienced when handling and loading into the Soxhlet extraction apparatus. The solid was extracted as previously attempted with boiling acetone as the liquid phase. After 12 hours of extraction, all yellow colourations had left the solid, leaving behind only a white solid ($NaNO_3$). This was taken as the end point of extraction. The acetone solution was then evaporated under reduced pressure to leave a pale-yellow oil. As all other reported syntheses of NaNT had reported the compound to be a solid, the identity of the yellow oil was a mystery. Critical analysis of the reaction setup led us to the belief that an aldol condensation reaction between acetone molecules had led to the formation of the viscous oil comprised of mesityl oxide (**Figure 2.2**).[13] Leaving the oil exposed with a vigorous airflow passed over its surface led to evaporation of the oil and the formation of a pale yellow crystalline solid. FTIR spectroscopy confirmed the identity of this material as now pure $NaNT.2H_2O$ by comparison to values reported by Klapötke et al.[6]

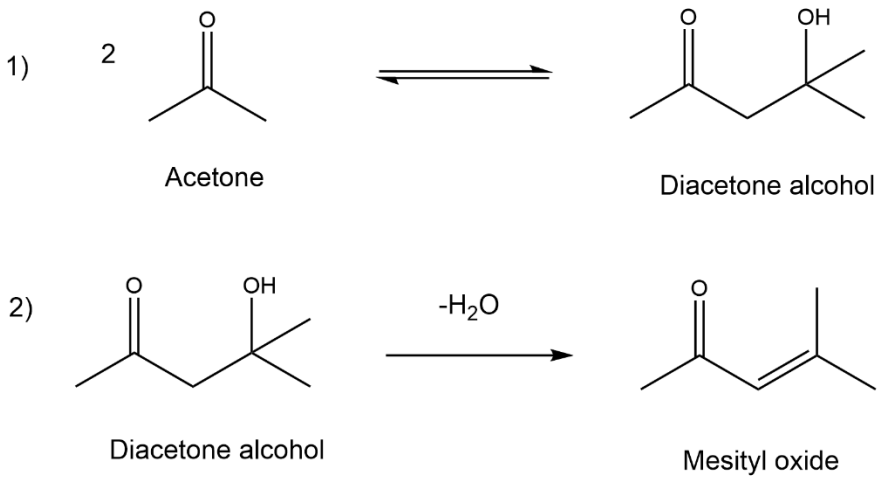

Figure 2.2: *Top: Aldol condensation of acetone to form diacetone alcohol; Bottom: Dehydration of diacetone alcohol to form mesityl oxide*

The $NaNT.2H_2O$ obtained from this extraction was then used in the attempted formation of DBX-1. The reaction to form DBX-1 was adapted from the procedure published by Fronabarger with small differences to reaction scale and setup.[5] $CuCl_2$

was dissolved in water to form a clear, slightly turbid blue solution and placed in a 100ml borosilicate glass beaker with a Teflon coated stirred bar. The reaction solution was then heated to 75-80 °C at which point an aqueous solution of NaNT.2H_2O was added in one portion to form a clear, green solution. This was then heated to 90 °C before a solution of sodium ascorbate in water was added dropwise for 1.5 minutes. The reaction was allowed to dwell at constant temperature and stirring speed for 3 minutes before addition was resumed at the same rate as before until all sodium ascorbate was added for a total reaction time of 15 minutes. The application of the crystallised NaNT·2H_2O as the nitrotetrazolyl reagent in adaptation to the previously published reaction regime, afforded an orange, suspended material that readily blocked D4 sinter filter and discoloured over time in air to form an olive-green, highly explosive powder of as yet unknown composition. FTIR analysis of this powder shows large differences to the published data for DBX-1 and so it was apparent that the reaction had not worked as intended.

It was hypothesised that a low NaNT.2H_2O purity had been the cause of the failure in DBX-1 synthesis and that this low purity could not be identified through FTIR spectroscopy alone. NaNT.2H_2O was further recrystallized from H_2O. At a crystallization temperature of 0 °C, NaNT forms a tetrahydrate as transparent, completely colourless, needle-shaped crystals the IR spectrum of which is closely related to that of the previously reported NaNT·2H_2O. [14]

The indicative region of the IR spectra comes at 1030-1070 cm^{-1} with a shift in two absorption bands (1035 to 1041 cm^{-1} and 1058 to 1066 cm^{-1}, **Figure 2.3**) proving the identity of the recrystallised material as solely the tetrahydrate (Previous work in the research group elucidated the structure and band positions of NaNT.4H_2O [14]). Under vacuum and at room temperature, NaNT.4H_2O readily converts into NaNT.2H_2O, and then into water-free NaNT. The dehydration process can be monitored easily in the infrared using the peak absorption cross sections at ν / cm^{-1} = 1191, 1178, 1068, 1057, 1040 (water-free NaNT), 1193, 1173, 1066 1041 (NaNT.4H_2O) and 1183, 1173, 1058, 1035 (NaNT.2H_2O). In a sealed vessel at room temperature and ambient pressure, NaNT.4H_2O is stable indefinitely.[14]

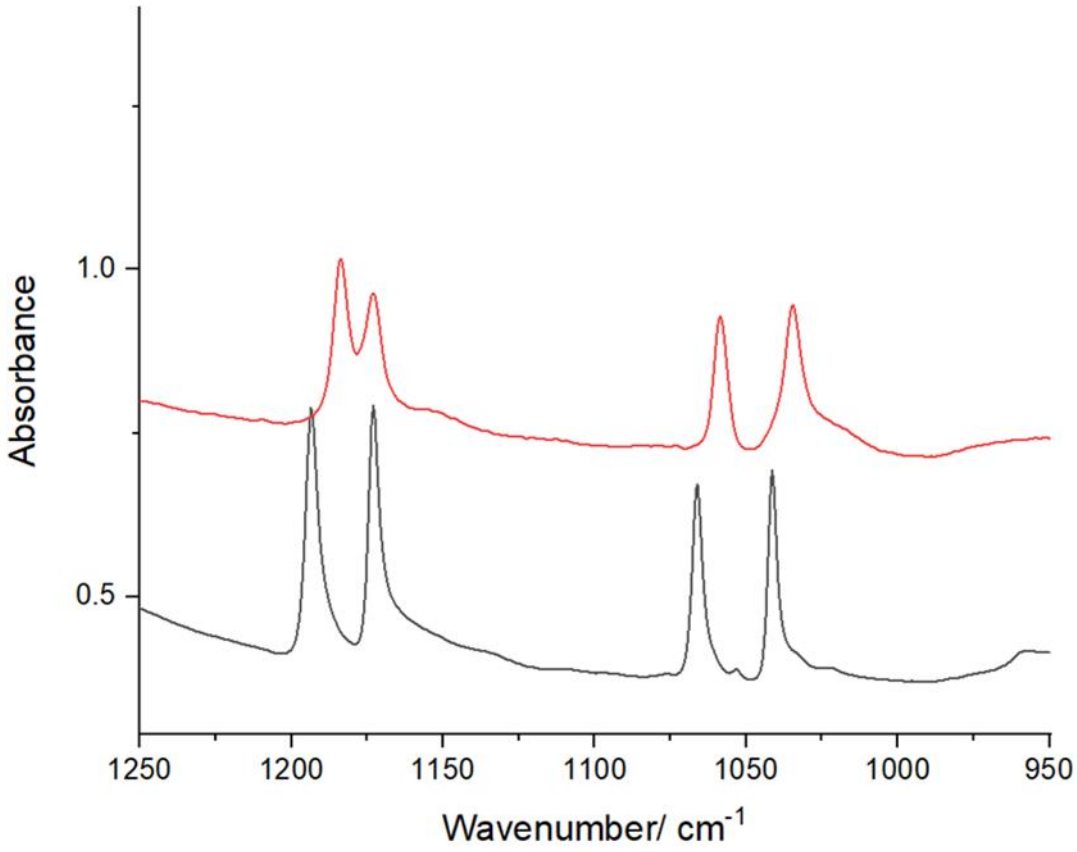

Figure 2.3: *Series of FTIR spectra comparing the indicative regions of NaNT.2H₂O(red) and NaNT.4H₂O(black) in the range 1250-950 cm⁻¹*

2.2.2 Further investigation into the synthesis of DBX-1

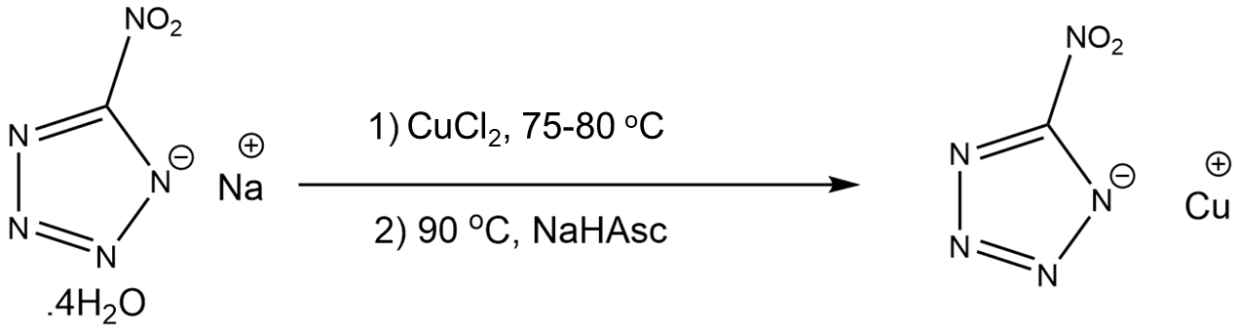

Figure 2.4: *Reaction to form DBX-1 using purified NaNT.4H₂O*

With pure NaNT.4H₂O available to us, the synthesis of DBX-1 was again attempted (**Figure 2.4**). The first attempt at forming DBX-1 with the now purified NaNT.4H₂O elected to forgo the incubation period of 3 minutes and instead the sodium ascorbate solution was added at 1ml min^{-1} for a total reaction time of 9 minutes.

Addition of $NaNT.4H_2O$ to $CuCl_2$ resulted in no colour change unlike that reported by Fronabarger and as seen by ourselves when using impure $NaNT.2H_2O$. This is most likely due to a difference in the impurities present due to a difference in purification method (ion exchange column vs. recrystallisation). Following this, sodium ascorbate addition resulted in a precipitation of a solid which over the 9 minutes addition period changed colour from dark green-yellow-bright orange. The solution proved difficult to filter and left behind an orange filter cake which when left under air flow slowly darkened until a dark green to black highly energetic solid was left (black solid assumed to be CuO with nitrotetrazolate also present). Both inspection of the material and comparison of the FTIR spectra to values reported by Fronabarger led to the conclusion that DBX-1 had not been formed.[5][14] From this it became apparent that stricter control of reaction conditions were needed to more closely resemble that of Fronabarger with the incubation period during addition a possible key step that cannot be excluded.

A second attempt at the reaction was made, more closely following that of Fronabarger. The Fronabarger paper upon which our experiments were based is explicit in its stating of reaction conditions (See **Experimental, 2.4.2.1)** and so further experiments more rigorously followed this procedure.[5] After 1.5 minutes of sodium ascorbate addition an opaque green colour was present in the reaction vessel. During the incubation period this gradually changed colour until we were left with a dark wine-red coloured solution which did not change appearance during the rest of the reaction. Subsequent filtering, washing with H_2O and isopropyl alcohol and drying under vacuum resulted in the isolation of a wine-red microcrystalline powder (**Figure 2.5**) (identified as $Cu_3(NT)_2(Cl)$ from SCXRD, See **2.2.7 Identity of DBX-X: Structure determination of $Cu_3(NT)_2Cl$)**, from here referred to as DBX-X) which, when exposed to a flame, exploded. An FTIR spectrum was recorded and compared to the values reported for DBX-1. It became apparent from this comparison that the wine-red compound was not DBX-1 with an indicative region of the spectrum from 1200-1000 cm^{-1} showing that all peaks had seemingly shifted to lower wavenumbers than for DBX-1(**Figure 2.6**).[14]

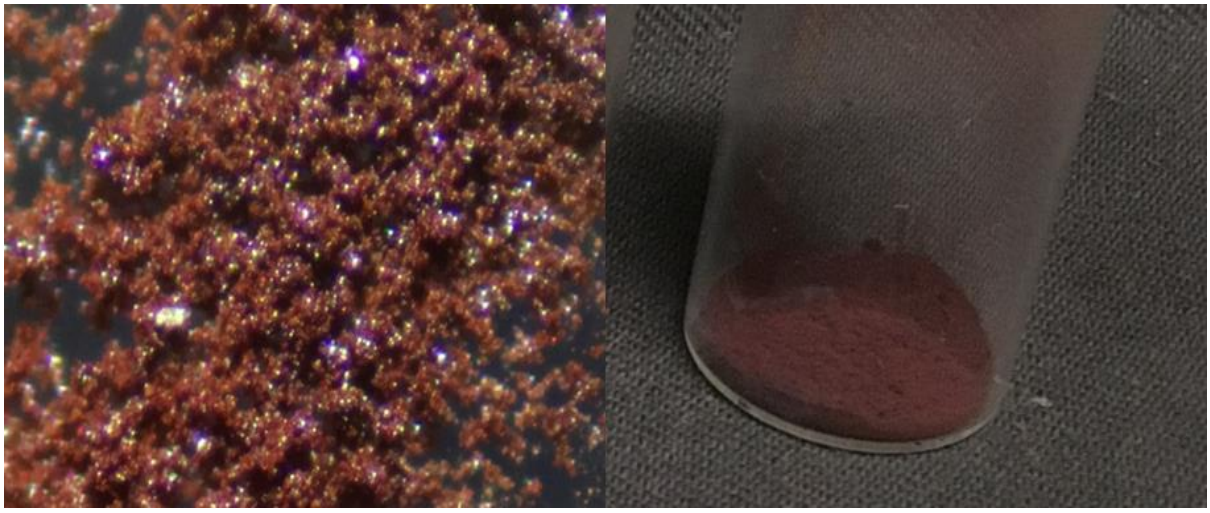

Figure 2.5: *Left: Photograph of DBX-X under optical microscope, Image taken at 7x Zoom; Right: Photograph of DBX-X under normal laboratory lighting*

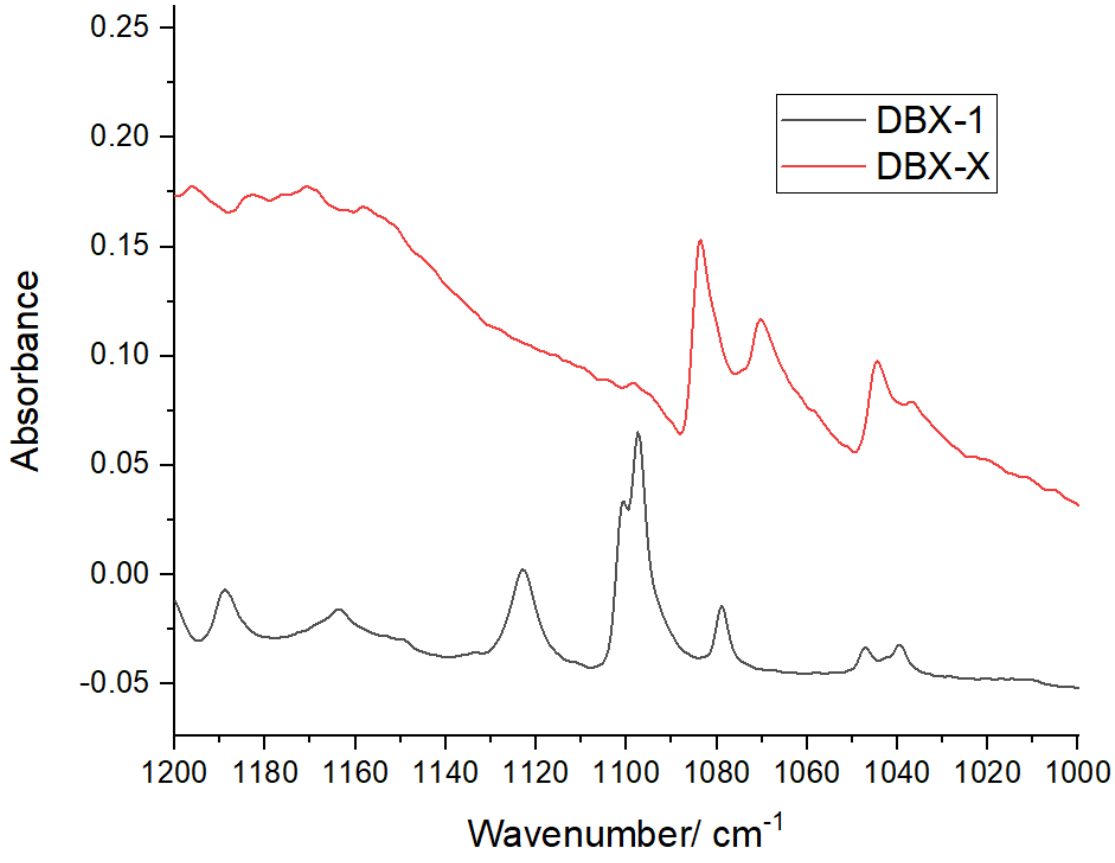

Figure 2.6: *Series of FTIR spectra of DBX-1(Black) and DBX-X (Red) in the range 1200-1000 cm^{-1}*

The experiment was repeated multiple times with no changes to reaction set up or stoichiometry to rule out the potential for human error having affected the reaction output. Formation of DBX-X once again would imply that this was a consistent reaction product and not the result of a one-time error which caused the formation of DBX-X. The reaction vessel was cleaned only with water/acetone and mechanical agitation of any material stuck to the sides of the vessel. Unexpectedly, and after two further syntheses of DBX-X, a third different product formed. During the reaction, addition of sodium ascorbate led to a much lighter coloured solid in suspension than any previously seen. When filtered and washed as done previously a light brown, microcrystalline powder (**Figure 2.7**) was obtained which did not darken over time when exposed to air (vide supra). While inspection of the new compound implied a different reaction product had formed the identity of the product only became clear upon analysis of its FTIR spectrum. A comparison of the region 1200-1000 cm^{-1} for both the spectrum of DBX-X and the reported values for DBX-1 showed absorption bands present from both compounds in the spectrum of the new product (**Figure 2.8**). This showed that repeats of the experiment with no changes to reaction set up or stoichiometry had now produced a mixed DBX-1/DBX-X powder.

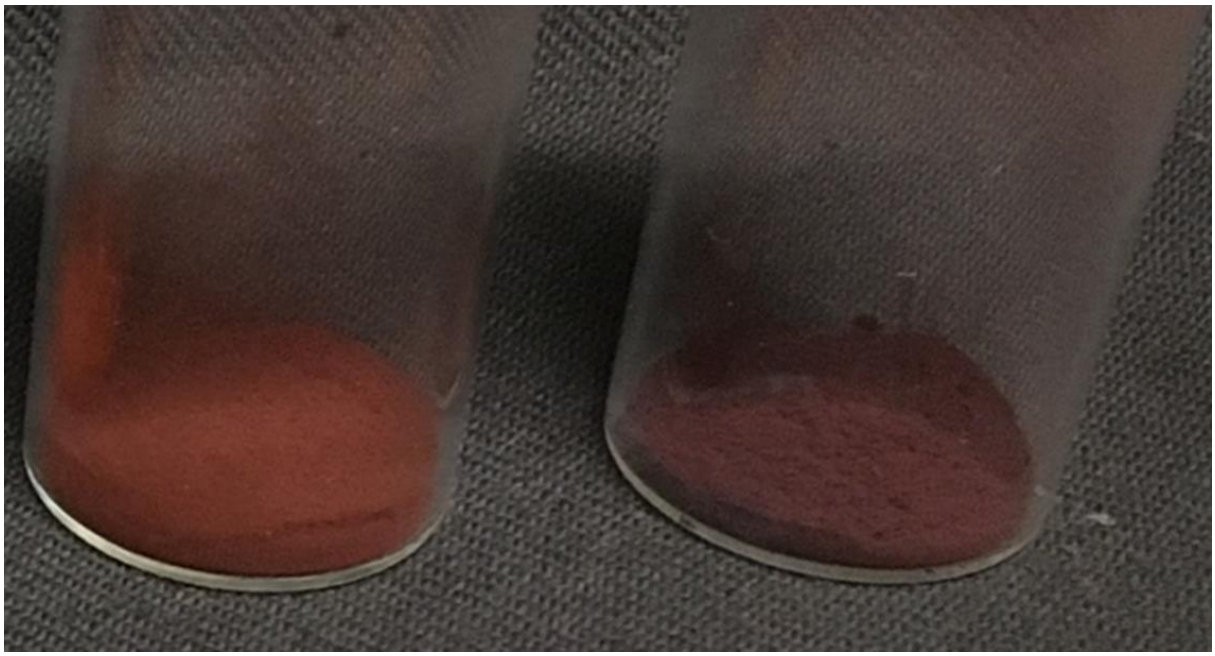

Figure 2.7: *Mixed product formed during second experiment (left) and its comparison to DBX-X (Right), photograph taken under normal laboratory lighting*

With the synthesis of the mixed DBX-1/DBX-X powder showing that DBX-1 could be formed, albeit as an impure powder, following the published procedure we elected to try and alter the experimental conditions to try and produce only DBX-1. The first experimental alteration made was to use a sodium ascorbate solution at half the concentration as previously used (237 mg in 2.4 ml H_2O) (**Appendix 7.8**). The effects of the change were immediately noticeable. On addition of sodium ascorbate and following the 3 minutes of incubation the reaction solution possessed a bright orange colour which persisted until the end of the addition period. Following filtration and washing as specified in earlier reactions we obtained a microcrystalline solid with a bright orange colour which did not darken over time (**Figure 2.8**).

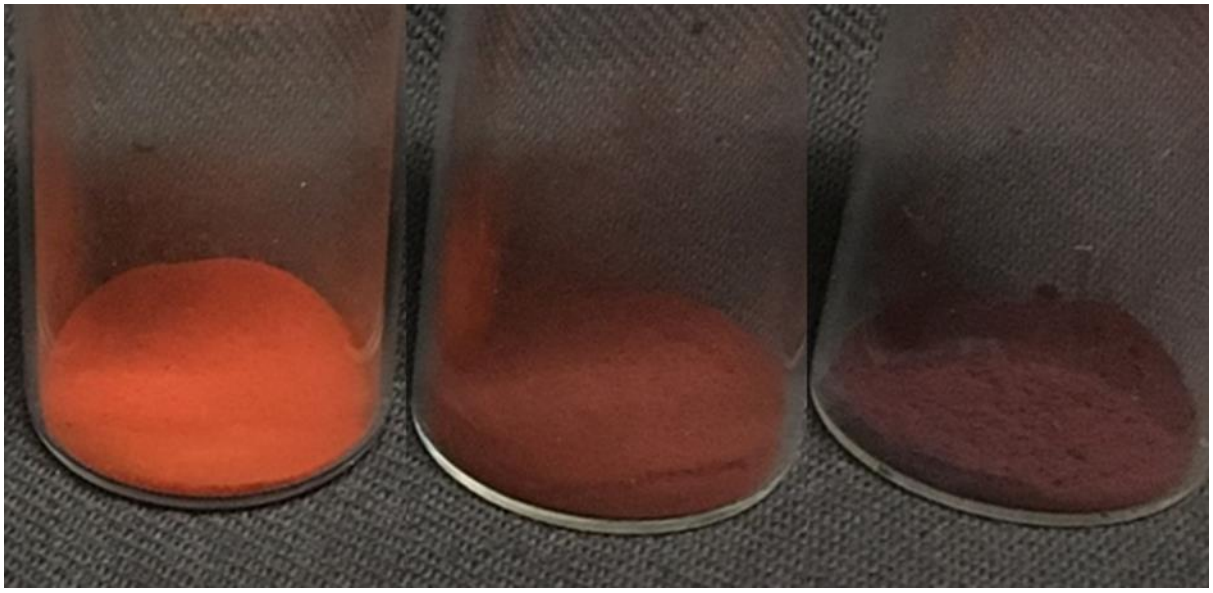

Figure 2.8: *Left: DBX-1; Middle: DBX-1:DBX-X mixed product; Right: DBX-X, all photographs taken under standard laboratory lighting*

An FTIR spectrum was recorded and compared to that for DBX-X and the mixed DBX-1/DBX-X powder. The bright orange crystalline material contains none of the bands specific to DBX-X (**Figure 2.9**) and seemingly only contains those absorption bands unique to DBX-1 confirming the identity of the sample as DBX-1. With the crystals formed being too small for single crystal structural determination, a PXRD diffractogram was recorded and compared to a PXRD diffractogram calculated from the SCXRD data recorded by Fronabarger et al. [5] Comparison of the datasets shows

that the crystalline material contains only the peaks of DBX-1(albeit with some small shifts in peak position) and can be considered purely as one phase (**Figure 2.10**). This result seemed to suggest that it had been the concentration of the sodium ascorbate solution which had been the cause of formation of DBX-X. Repeats of this experiment with the same concentration of sodium ascorbate solution again produced DBX-1 proving its consistency in synthesis.

With the synthesis of DBX-1 confirmed, the reaction was repeated with the original concentration of ascorbate solution. A return to the original concentration of reducing agent should, provided our theory was correct, once again produce only the DBX-X product. However, when using the original concentration (237 mg of sodium ascorbate in 1.2 ml of H_2O) only DBX-1 was produced. The outcome of this reaction stood in contrast to our proposed theory and suggested that another factor was controlling reaction product formation.

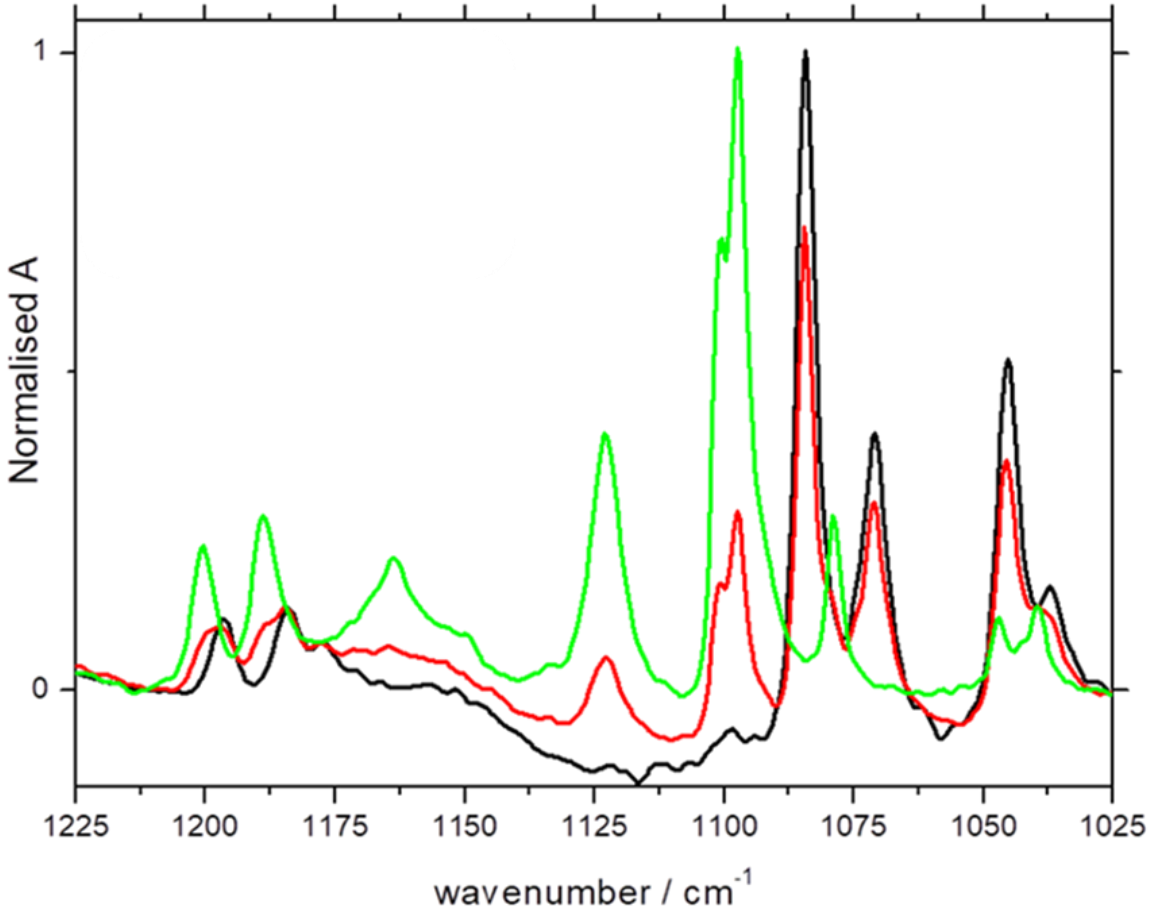

Figure 2.9: *Series of baseline-corrected, normalised FTIR spectra (range 1225-1025 cm^{-1}), Black= DBX-X, Red= Mixed DBX-1/DBX-X powder, Green= DBX-1*

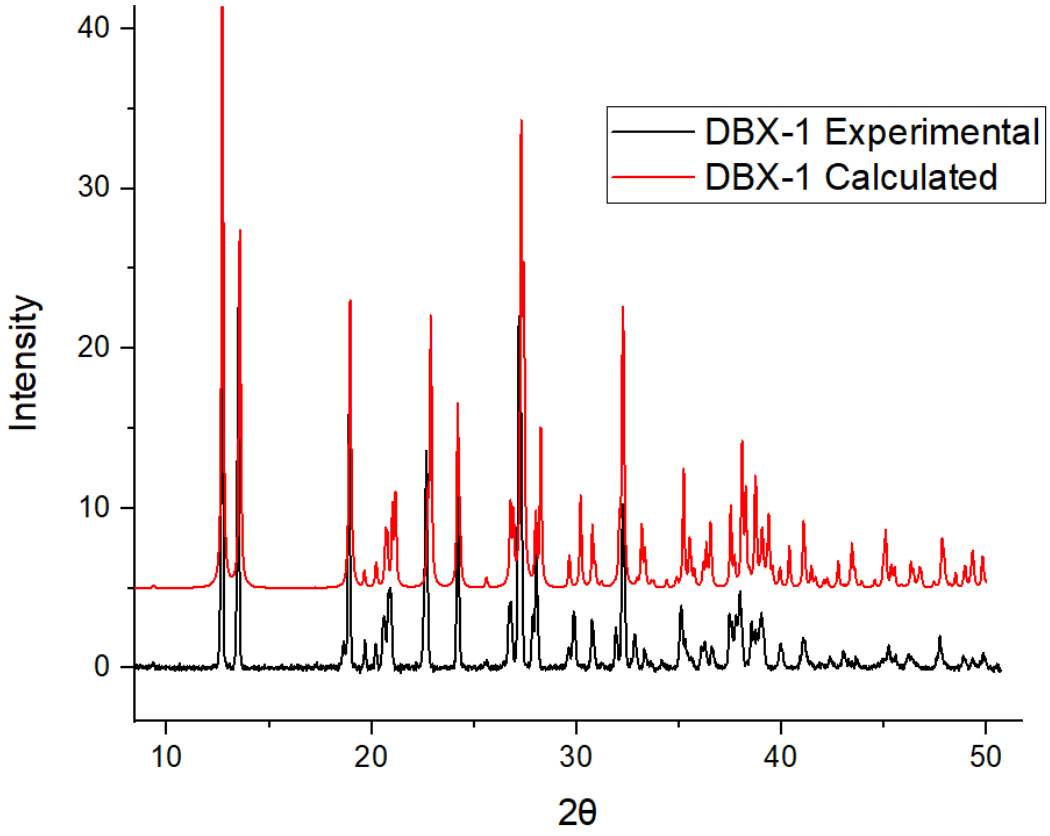

Figure 2.10: *Comparison of the experimentally determined PXRD pattern of DBX-1 (red, recorded in Sheffield) versus that calculated from single crystal data (black, from ref[5])*

Opinions on the identity of this factor were finalised upon careful inspection of the paper by Ford *et al.*[8] This paper is the first instance of seed crystals of DBX-1 being added to the reactor vessel to ensure product formation and states that 'The amount of seed used, the dosing rate of the reducing agent and the purity of NaNT have been identified as important factors for predicting whether a reaction will be successful'.[8] Having purified the NaNT starting material and with dosing rate of reducing agent being consistent throughout the experiments, the unintended presence of seed crystals controlling reaction product formation appeared to be the most logical answer to the changing reaction products observed. Following this conclusion, it was identified that throughout all these reactions, the same reaction vessel had been used between each DBX-X, mixed DBX-1/DBX-X and DBX-1 synthesis. With the vessel only being washed between experiments with water/acetone and mechanical agitation it was plausible to suggest that microscopic seed crystals present in the vessel were controlling reaction outcome and so further experiments were done to determine this effect.

2.2.3 Determining the effect of seed crystals

With the observation that reaction vessel history seemed to be controlling product formation, efforts were made to conduct a series of experiments with a reaction vessel intentionally seeded with small amounts of either DBX-X or DBX-1. Between each reaction, the reactor vessel, stirrer bar and thermometer were cleaned by immersion in boiling 68% HNO_3 as this had proven able to destroy samples of both DBX-X and DBX-1. After an initial clean of the reactor vessel, stirrer bar and thermometer with HNO_3, the first reaction was attempted with no intentional seeding applied. As expected, this reaction resulted in the formation of the amorphous solid seen during earlier attempts to form DBX-1 (**Table 2.1, Trial 1**). Following this, the reactor vessel, stirrer bar and thermometer were cleaned only with H_2O/acetone/mechanical agitation and used immediately in the next reaction. This again led to the formation of an amorphous solid that was spectroscopically distinct to either DBX-1 or DBX-X (**Table 2.1, Trial 2**). This seemed to confirm our suspicion that in the absence of seed crystals neither DBX-X nor DBX-1 would form. This also suggested that the presence of the amorphous solid does not induce DBX-X formation. However, due to the ill-defined nature of this product it could be that multiple different compounds are present in this material and the presence of one is key to formation of DBX-X. It is plausible that the amorphous solid must be synthesised an unspecified number of times before either DBX-X seed crystals build up in the material or before a certain, currently unidentified compound has been formed which then induces bulk DBX-X formation. The reactor vessel, stirrer bar and thermometer were then returned to a pristine state through HNO_3 immersion. A third reaction (**Table 2.1, Trial 3**) was then performed with the only difference experimentally being the intentional seeding of the reaction solution with 10 mg of DBX-1. This resulted in the precipitation of microcrystalline DBX-1 (**Figure 2.11**) which had an FTIR spectrum identical to that of the sample used to seed the reaction vessel. This result showed that the presence of DBX-1 seed crystals was crucial for bulk DBX-1 production. After this result, the reaction equipment was once again cleaned with HNO_3 before the reaction was twice repeated (**Table 2.1, Trials 4 and 5**), with HNO_3 cleaning between reactions, this time with intentional seeding by DBX-X.

Trial No	*n*(Cu^{2+}) / mmol	*n*(NT^-) / mmol	*n*(NaHAsc) / mmol	comment	Product and yield
1	2.39 ($CuCl_2$, 16.3 ml of H_2O)	2.39 ($NaNT{\cdot}4H_2O$, 5.2 ml)	1.20 (1.22 ml)	beaker treated with 65% aqueous HNO_3	amorphous solid
2	2.38 ($CuCl_2$, 16.1 ml of H_2O)	2.88 ($NaNT{\cdot}2H_2O$, 5.1 ml)	1.20 (1.21 ml)	Washed only with H_2O/Acetone	amorphous solid
3	2.39 ($CuCl_2$, 16.4 ml of H_2O)	2.40 ($NaNT{\cdot}4H_2O$, 5.2 ml)	1.20 (1.23 ml)	Seeded with 10 – 15 mg DBX-1	277 mg DBX-1, 65%
4	2.38 ($CuCl_2$, 16.4 ml of H_2O)	2.40 ($NaNT{\cdot}4H_2O$, 5.2 ml)	1.19 (1.20 ml)	Seeded with 10 – 15 mg DBX-X	291 mg DBX-1, 69%
5	2.38 ($CuCl_2$, 16.4 ml of H_2O)	2.40 ($NaNT{\cdot}4H_2O$, 5.2 ml)	1.20 (1.22 ml)	Seeded with 10 – 15 mg DBX-X (different batch to previous seeding)	285 mg DBX-X / DBX-1, 67-79%
6	2.39 ($CuCl_2$, 16.2 ml of H_2O)	2.39 ($NaNT{\cdot}4H_2O$, 5.1 ml)	1.20 (1.23 ml)	beaker only rinsed with deionized water	258 mg DBX-1, 61%

Table 2.1: *Results of intentionally seeding reaction vessel to induce DBX-X/ DBX-1 formation*

Two different samples of DBX-X were used in the seeding process. The first reaction resulted in the formation of only DBX-1 (identified by FTIR) and the second resulted in the formation of a mixed DBX-1: DBX-X phase (ratios of products unknown)(**Figure 2.11**). There are two plausible explanations for the formation of DBX-1 from a DBX-X seeded experiment. It could be the case that due to the presence of DBX-1 in our laboratory, seed crystals of DBX-1 unintentionally entered the reaction system and induced DBX-1 formation. A second explanation could be that the DBX-X used to seed the reaction already had enough DBX-1 seeds present, formed during DBX-X production, but not so many as to be spectroscopically observable to induce solely DBX-1 formation. This then resulted in a competition between the seeding effects of DBX-X and DBX-1, in which the seeding effect of DBX-1 outcompetes that of DBX-X.

The second reaction which produced the mixed compound was seeded with a different batch of DBX-X. It should also be noted that the batch used was formed one reaction prior to the first recorded synthesis of the mixed DBX-1/DBX-X powder. The fact that this DBX-X then seeded for a mixed phase product seems to suggest that this DBX-X sample had enough DBX-1 seed crystals present to partially seed for DBX-1 production but not fully convert the system. These results imply that DBX-1 is formed alongside bulk DBX-X formation, albeit in very small quantities. Differences in the composition of DBX-X can then result in formation of either DBX-X or a DBX-X/DBX-1 mixed phase, if the number of DBX-1 seed crystals is small, or can result in formation of DBX-1 provided it has a comparably high number of DBX-1 seeds. The lower limit of seed crystal amount required for successful seeding of DBX-1 is currently unknown.

One final experiment was done to determine the effects of seeding (**Table 2.1, Trial 6**). A pristine reactor, stirrer bar and thermometer were taken and 10 mg of the previously produced mixed phase solid was added. The experiment was then performed with no other changes. This resulted in the formation of only DBX-1 (**Figure 2.11**) and was free of any DBX-X when assessed using FTIR. This seemed to show that when a comparable amount of DBX-1 and DBX-X are present the reaction will only produce DBX-1 potentially due to the greater ability of DBX-1 to seed for itself in a reaction system

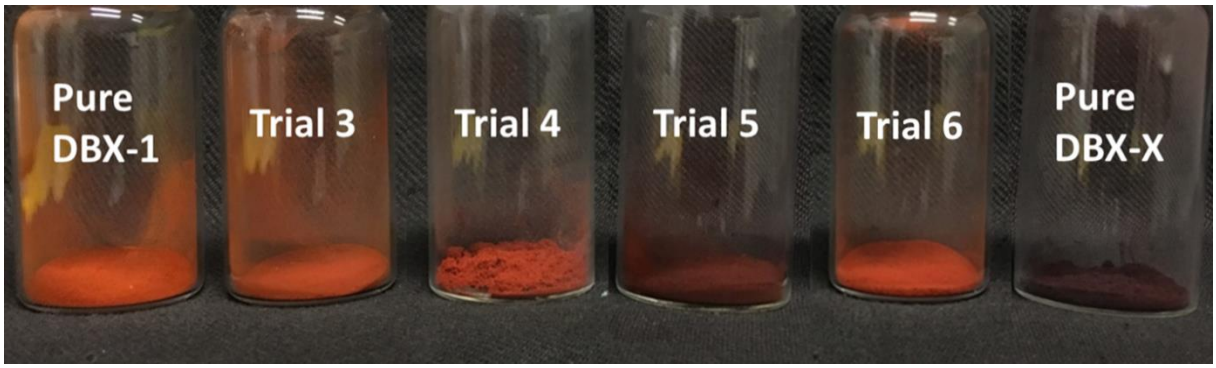

Figure 2.11: *Comparison of the products of seeding experiments, photographs taken under normal laboratory lighting*

2.2.4 Selective formation of DBX-X

With the seeding experiments proving that DBX-1 can be consistently synthesised with strict control of reactor vessel and reagent purity, attention turned to production of DBX-X. As the reaction system seemingly will eventually result in DBX-1 production, assuming that small amounts of DBX-1 are formed alongside bulk DBX-X formation, we investigated whether the reaction can be forced into production of only DBX-X. The first attempt at selective formation of DBX-X was attempted solely with changes to the stoichiometric ratio of the products to ensure a 3 : 2 Cu : NT ratio (**Table 2.2, Trial 1**). These changes seemed to only result in the production of the familiar amorphous solid that did not contain appreciable amounts of DBX-X or DBX-1. The vessel was then washed only with H_2O / acetone / mechanical agitation and intentionally seeded with a sample of DBX-X before the reaction was repeated with the now altered reactant ratios (**Table 2.2, Trial 2**). This resulted in the formation of once again the amorphous material however inspection of the reaction vessel showed a small amount, but more than that which was used to seed the reaction, of wine-red material stuck to the sides of the vessel. Taking this vessel, washing only with H_2O and repeating the reaction with the original stoichiometry of reagents resulted in the production of more wine-red material (**Table 2.2, Trial 3**) (~64 mg) alongside production of the amorphous material. FTIR spectroscopy confirmed its identity as DBX-X thus proving that while DBX-X can be selectively seeded for, the process was less efficient than the easier seeding for DBX-1 formation. It is currently unclear as to why using the original stoichiometry of reagents resulted in more DBX-X production than using the altered stoichiometry. Repeated reactions with this system would still be expected to eventually produce enough seed crystals of DBX-1 to outcompete DBX-X seed crystals and once again only produce DBX-1. From these reactions it became apparent that while it was possible to selectively form DBX-X instead of DBX-1, its non-facile synthesis potentially makes DBX-X an inferior alternative to DBX-1.

Trial No.	Conditions	R 1	v	R 2	v	R 3	v	Product	Yield/ %
1	*a*	$CuCl_2$	1.00	*d*	0.67	Na H-Asc	0.50	amorphous air sensitive solid	-
2	*b*	$CuCl_2$	1.00	*d*	0.67	Na H-Asc	0.50	amorphous solid; red material deposited on vessel walls	-
3	*c*	$CuCl_2$	1.00	*d*	1.00	Na H-Asc	0.50	amorphous solid; 64 mg dark red material deposited on vessel walls	15

Table 2.2: *Results of trials to intentionally form DBX-X, v denotes stoichiometric coefficient, R=Reagent, a= vessel and stir bar rinsed with water and mechanically cleaned with cellulose paper, b= seeded with 10 to 15 mg* $Cu_3Cl(N_4CNO_2)_2$*, c= beaker only rinsed with deionized water, d=* $NaNT(H_2O)_4$

2.2.5 Factors influencing the outcome of the reduction reaction

Using the results from both the initial investigation into DBX-1 synthesis along with the results obtained from intention control of the reaction vessel's seeding, the following conclusions can be drawn:

1. Application of crystallised $NaNT.2H_2O$ without further purification as the nitrotetrazolate transfer reagent leads to the formation of powders that are neither DBX-X nor DBX-1 - an outcome attributed previously to the presence of trace-impurities that act in a catalytic mechanism inhibitive of the formation of either DBX-X or DBX-1. Within the conditions investigated by us, formation of either DBX-X or DBX-1 requires the use of purified NaNT in the form of $NaNT.4H_2O$

2. Provided seeding is in place, changing the concentration of the reductant solution has no significant effect on the course of the reduction

3. Using pure starting material and solvent, the outcome of the reduction reaction depends on the state of the reactor and the presence or absence of microscopic seed crystals

4. The formation of the desired product requires the presence of the appropriate seed crystals, which induce the crystallisation of DBX-X and DBX-1, respectively

5. DBX-X is kinetically preferred (barrier to final substitution of Cl^- large enough to prevent reaction prior to precipitation); forms when enough seed crystals are available; it is the first well-defined phase that forms spontaneously in a pristine reactor that has been repeatedly exposed to the reaction conditions

6. The formation of DBX-X requires the absence of large or even low quantities of seed crystals of DBX-1, the lower limit of DBX-1 contamination which still results in bulk DBX-X formation is unknown

7. DBX-1 is thermodynamically preferred (formation of stronger Cu(I)-$N_{tetrazole}$ bond over Cu(I)-Cl bond); forms exclusively when enough seed crystals are available (on reactor walls, stir bar etc.). If seed crystals of both products are present then the majority product will be DBX-1

8. DBX-X seeds less effectively than DBX-1 seed crystal

9. Hot nitric acid destroys all seed crystals, returning the reactor to a pristine state in which no well-defined copper nitrotetrazolate forms.

2.2.6 Hypothesised reaction scheme for DBX-1 formation

With the effects of seeding established by the control experiments conducted, the reaction to form DBX-1 appears much more complex than first thought. It can be concluded that when using reactants of the purity used during this research project, DBX-1 is not the first well defined micro crystalline compound formed. Instead, it is the final product produced after at least two other products are synthesised and have left their seed crystals on the reactor vessel. At first, an untainted vessel using pure reactants will produce only an amorphous solid. Following this and using the same reactor vessel, treated with only water/acetone/mechanical agitation, DBX-X will form. As seeding with amorphous material to intentionally form DBX-X has not been tested it is currently unknown how many times the amorphous material must be formed before DBX-X starts to be produced. It is also impossible to currently state whether

DBX-X formation is seeded by microscopic (and spectroscopically invisible amounts) amounts of DBX-X formed alongside the amorphous material or if the amorphous material itself is stimulating DBX-X production, potentially by the formation of nucleation sites.[20] Alongside bulk DBX-X formation, spectroscopically invisible amounts of DBX-1 are also formed. Following this, DBX-X will continue to form until a point at which, enough DBX-1 seed crystals have formed to reach a tipping point, at which point seed crystals of each compound compete and lead to the production of a mixed phase DBX-1:DBX-X mixture with the ratios of each product currently unknown. Once formed, any subsequent reaction using the same reaction vessel, provided it is not cleaned with nitric acid, will only produce DBX-1 and the seed crystals outcompete those of DBX-X. It is also possible to not produce a mixed phase and instead form DBX-1 straight away after DBX-X formation provided enough seed crystals have formed during DBX-X formation.

What currently cannot be said however, is whether this reaction is common to all DBX-1 syntheses or if this phenomenon is unique to the work detailed in this thesis. With starting material purity having been shown to have a large effect on the reaction outcome, it is plausible to suggest that small differences in the respective purities of the NaNT.4H_2O used in our syntheses and the NaNT.2H_2O used by various other research groups could have led to differing reaction pathways. The presence of spectroscopically invisible amounts of unknown impurities in either our or other groups starting materials could have many possible effects such as serving as nucleation sites or as catalysts for certain reaction pathways to occur all of which could allow for the reaction pathway discussed here or for different ones found by other research groups.

2.2.7 Structure determination of $Cu_3(NT)_2Cl$

The identity of DBX-X was discovered using single crystal X-ray diffraction (SCXRD). SCXRD measurements were performed using selected crystals from one batch of DBX-X. The small crystal size required a high-flux rotating anode as X-ray source. The rotating anode allows for better heat dissipation than with a standard anode and thus allows higher flux which leads to better resolution of the diffraction pattern. Crystalline DBX-X is composed of copper, chlorine and 5-nitrotetrazolato moieties which are distributed over three, one and two unique crystallographic sites in the stoichiometric

ratio of 3 : 1 : 2, respectively. These proportions, in combination with the measured magnetic properties, imply that copper is exclusively present in the oxidation state +1 forming the compound $Cu_3Cl(NT)_2$.

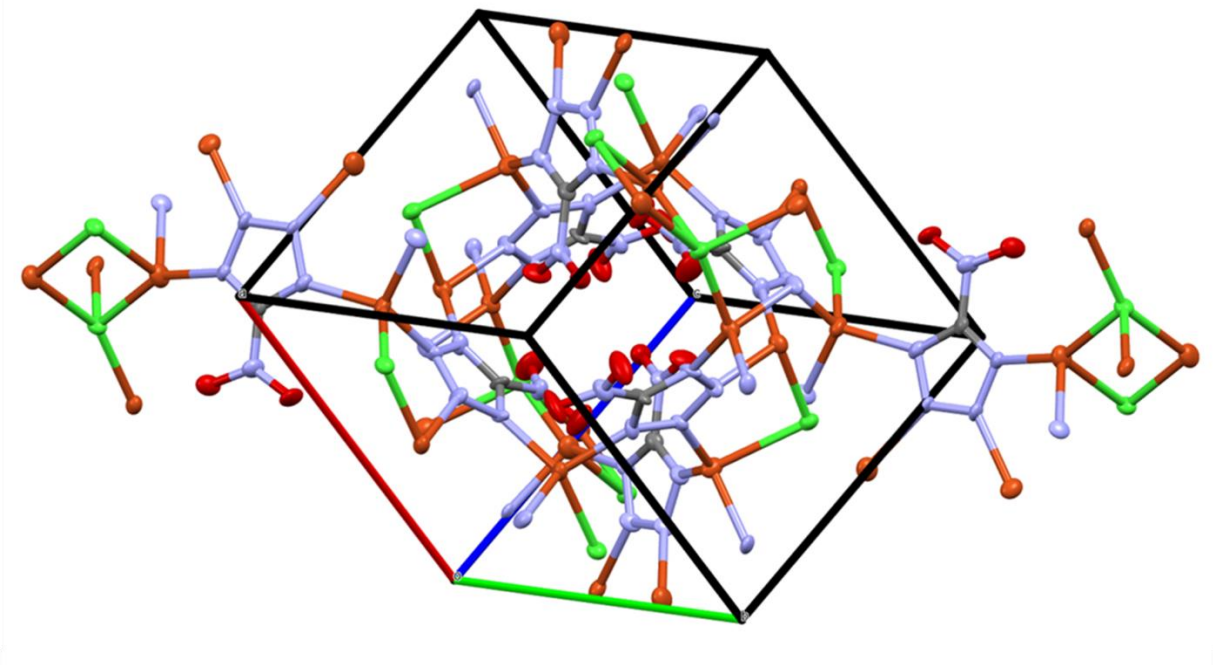

Figure 2.12: *Projections of the thermal ellipsoids in the molecular structure of the crystals of DBX-X (set at the 67% probability level) showing the unit cell (top down 1, 1, -1 axis)*

The compound presents as an infinitely extending, 3D coordination polymer built around the bonding interactions between Cu, Cl, ring nitrogen of nitrotetrazolate and a weak interaction between Cu and oxygen of the nitro group of nitrotetrazolate (**Figure 2.12**). Copper is coordinated in three chemically distinct distorted tetrahedral environments to at least one chloro- and up to three nitrotetrazolato ligands, forming $Cu(\kappa(N_\alpha)\text{-}NT)(\kappa(N_\beta)\text{-}NT)Cl_2$, $Cu(\kappa(N_\alpha)\text{-}NT)(\kappa(N_\beta)\text{-}NT)_2Cl$ and $Cu(\kappa(N_\alpha)\text{-}NT)_2(\kappa(N_\beta)\text{-}NT)Cl$ that constitute a mixed-ligand coordination polymer. The nitrotetrazolate anion is present in the unit cell in two crystallographically independent sites. Differently to $NaNT.4H_2O$ and DBX-1, all ring-nitrogen atoms are engaged in the coordination network involving $\mu4(N_\alpha,N_\alpha',N_\beta,N_\beta')$-NT bridges. As in DBX-1, the coordinative Cu-N_α/N_α' bonds are slightly shorter (1.968(7)-2.027(7) Å) than those involving N_β/N_β' ring-atoms (1.996(7)-2.100(7) Å). This is explained by the resonance forms of the nitrotetrazolate anion.

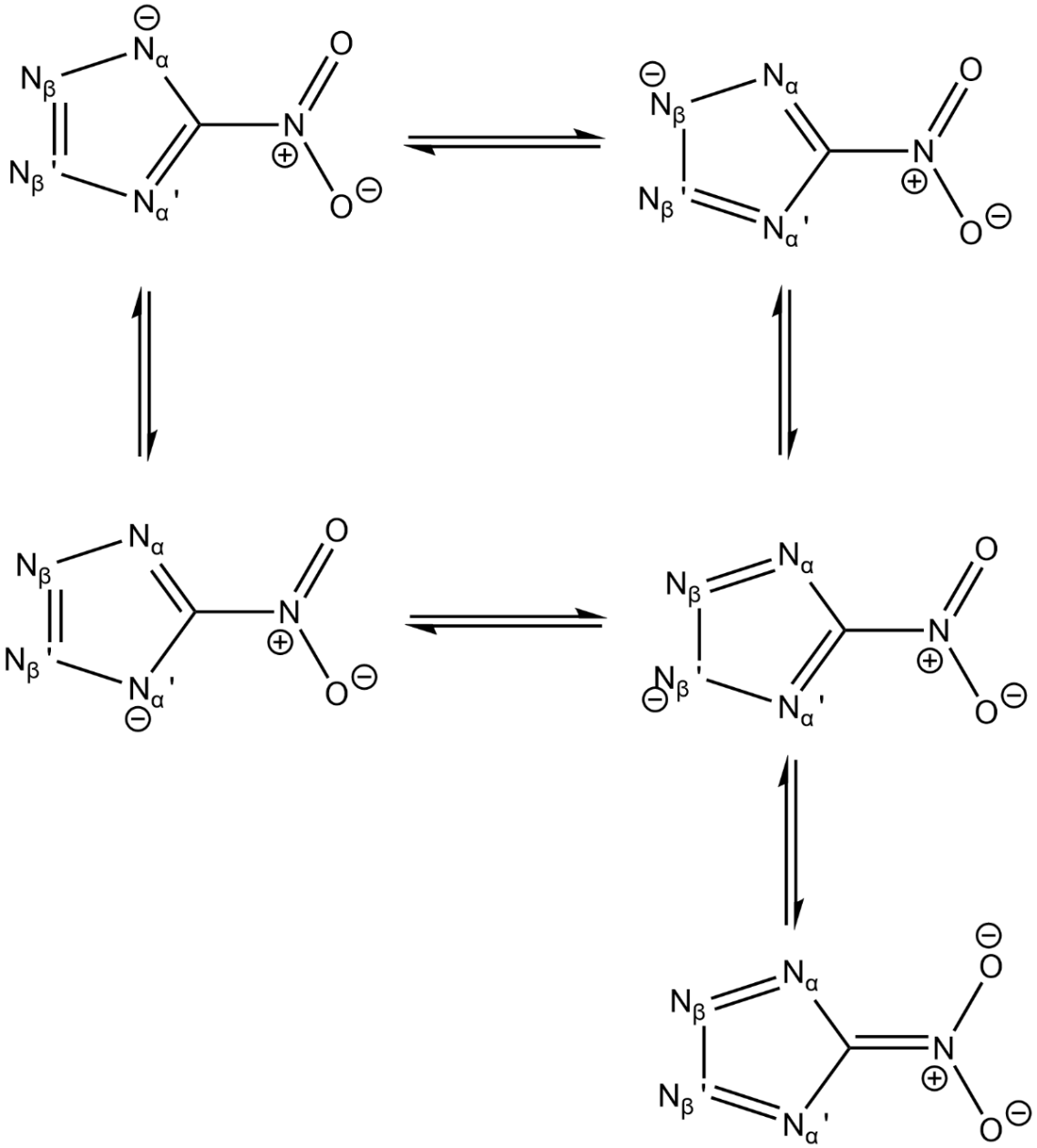

Figure 2.13: *Resonance forms of nitrotetrazolate anions*

Nitrotetrazole is comprised of five different resonance forms, in two of these (**Figure 2.13**) the negative charge sits on the N_α/N_α' ring nitrogen atoms and in another two (**Figure 2.13**) the negative charge is situated on the N_β/N_β' ring nitrogen. The thermodynamically favoured resonance forms are those with the negative charge situated on the N_α/N_α' nitrogen which explains the shorter Cu-N bond length as a greater relative charge density sits on the N_α/N_α' resulting in stronger attraction to the Cu(I) centre. Chloride is present in only one crystallographically independent site with each chloride making four bonds to copper atoms (**Figure 2.14**).

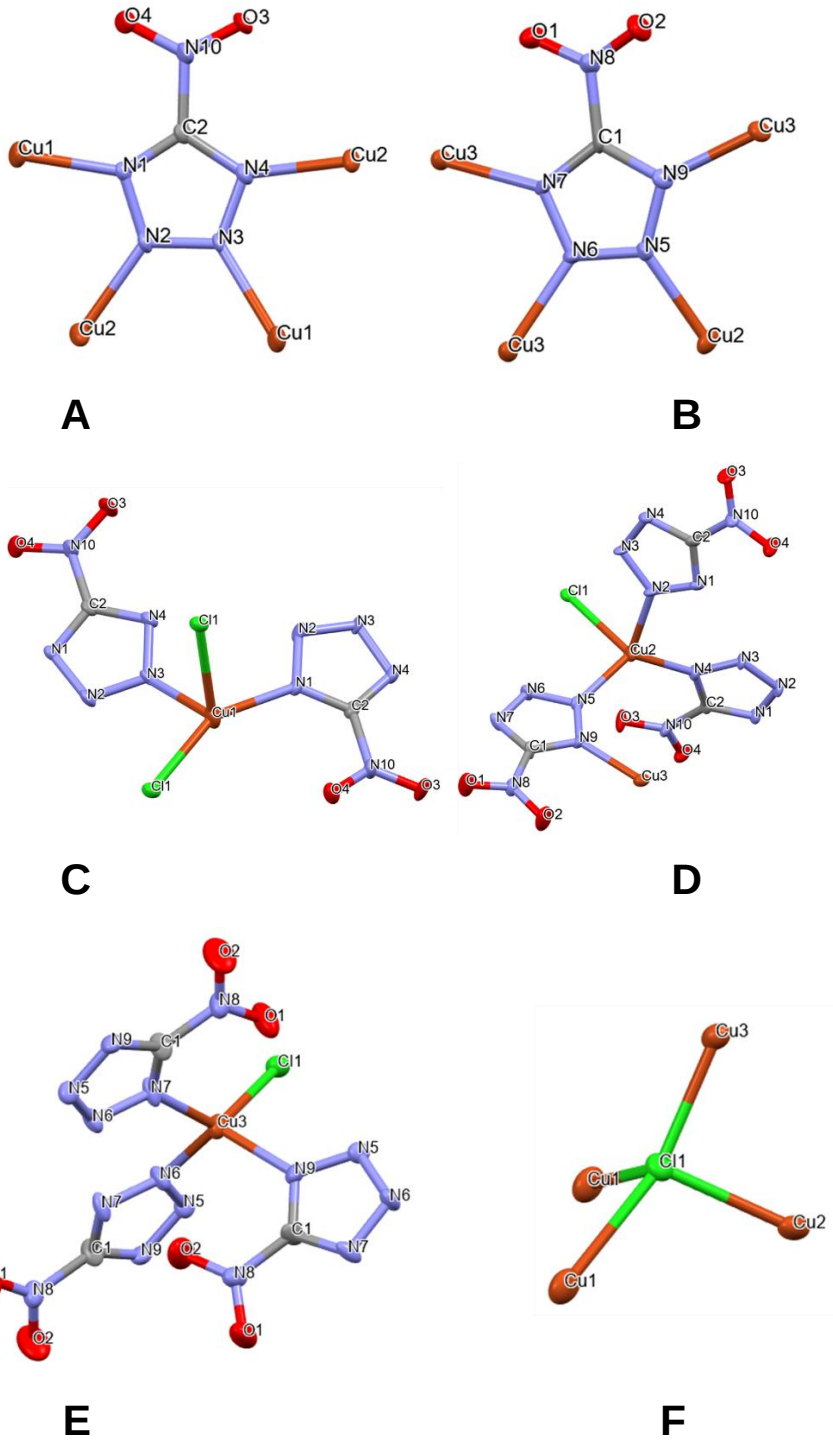

Figure 2.14: *Projections of the thermal ellipsoids in the molecular structure of the crystals of DBX-X (set at the 67% probability level) showing the coordination of copper to the tetrazolato ligands (A and B), primary coordination sphere of copper (Cu(1), C; Cu(2), D; Cu(3), E), and chlorine (F); Atom Colours: Red = Oxygen, Blue = Nitrogen, Grey = Carbon, Orange = Copper, Green = Chlorine, selected bond lengths:Cu3–N7 2.027(8), Cu3–N6 2.065(7), Cu3–N9 2.039(7), Cu2–Cl1 2.561(3), Cu2–N4 2.028(7), Cu2–N2 2.067(7), Cu2–N5 1.996(7), Cu1–Cl1 2.245(2), Cu1–Cl1 2.622(3), Cu1–N3 2.100(7), Cu1–N1 1.968(7), Cl1–Cu3 2.371(2), Cl1–Cu2 2.561(3), Cl1–Cu1 2.622(3), N3–Cu1 2.101(7), N2–Cu2 2.067(7), N6–Cu3 2.065(7), N9–Cu3 2.039(7)*

All analogous bond lengths between DBX-X and DBX-1 are close in value with the only major difference being that the shortest Cu···O contact in DBX-X (2.836 Å) is somewhat longer than that found in DBX-1 (2.745 Å) (**Table 2.3**). Similar to the finding made in the structures of NaNT.2H_2O and NaNT.4H_2O,[14] the different coordination environments have only negligible effects on the molecular structure of the N_4C-NO_2 ligand, as neither the presence of Cl^- (DBX-X vs. DBX-1) nor the replacement of $Na(H_2O)^{4+}$ by Cu^+ (NaNT.4H_2O vs. DBX-X) change its internal bond lengths and angles in any significant way. The X-ray powder diffractogram predicted from the single crystal data is consistent with all those diffractograms obtained from direct measurement of the crystalline material produced during the synthesis of DBX-X (**Figure 2.15**).

Bond	**Bond lengths of NaNT.4H_2O,[14] Å**	**Bond lengths of DBX-X, Å**	**Bond lengths of DBX-1,[5] Å**
M-N_1	-	1.968(7)-2.039(7)	1.924-2.026
M-N_2	2.576(13)	1.996(7)-2.100(7)	1.981-2.139
M-Cl	-	2.245(2)-2.622(2)	-
M···M	3.505(1)	3.104(2)	3.467
C-NO_2	1.447(4)	1.434(12), 1.457(11)	1.447, 1.448
N-O	1.221(8), 1.231(7)	1.205(10)-1.224(10)	1.216-1.227
C-N	1.322(3), 1.338(3)	1.289(11)-1.340(12)	1.320-1.333
N_1-N_2	1.340(10), 1.341(14)	1.337(10)-1.358(10)	1.331-1.355
N_2-N_2	1.347(12)	1.339(10), 1.344(10)	1.317, 1.325

Table 2.3: Comparison of the key bond lengths of NaNT.4H_2O[14], DBX-X and Bond lengths of DBX-1[5]

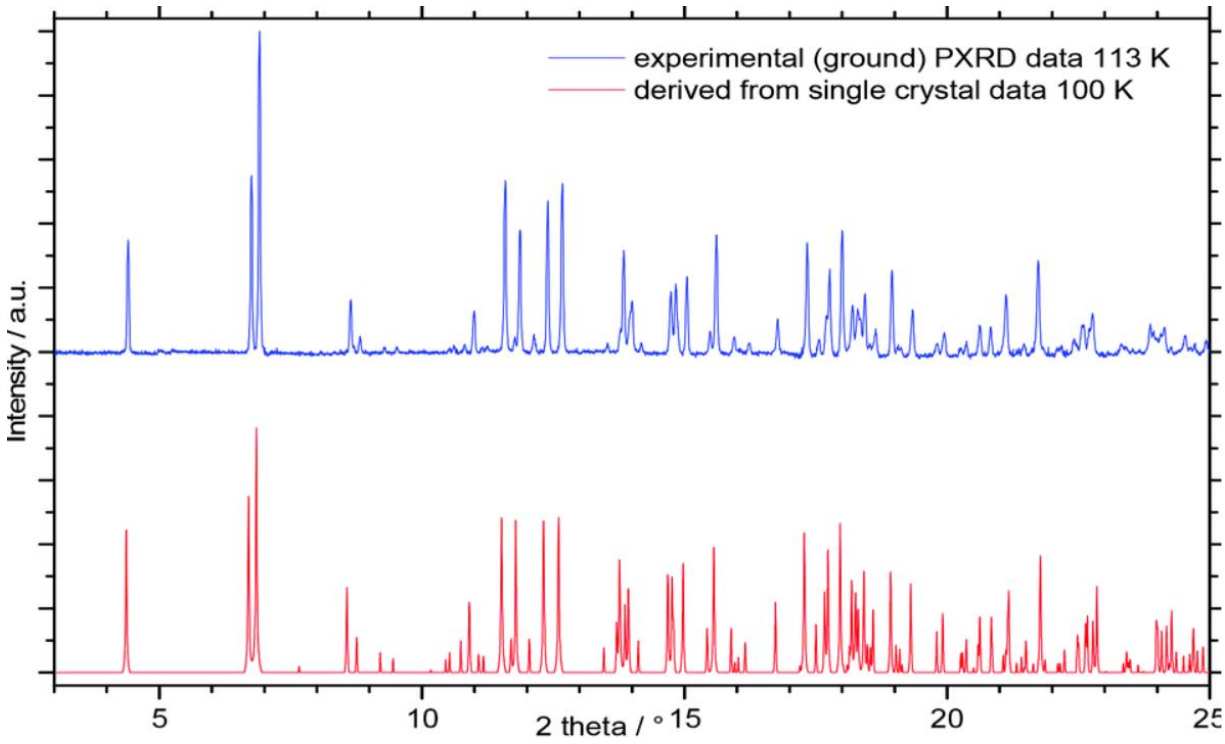

Figure 2.15: *Comparison of a simulated powder X-ray diffractogram of DBX-X based on the single crystal structure solution (red) with that obtained from measurement (blue)*

2.2.8 DBX-X versus DBX-1: Detonation performance parameter comparison for determination of eligibility as lead free initiators

With the conditions affecting reaction outcome determined, it was important to evaluate and compare key properties of DBX-X with those of DBX-1 and $Pb(N_3)_2$.

2.2.8.1 Thermal Behaviour and impact sensitiveness

A comparison of data originating from different research groups (laboratories) needs to take account of variations in the experimental conditions and parameters. These consist of varying sample mass (i), the type of sample container (ii), the instrument response characteristics (iii) and the calibration methods (iv) to name the most prominent one. Because of this, the thermoanalysis of DBX-1 was repeated (see ref. 5 for the original data) using freshly made material on the Sheffield DSC calorimeter

(see **General experimental methods and instrumentation** for instrument characteristics and analytical details).

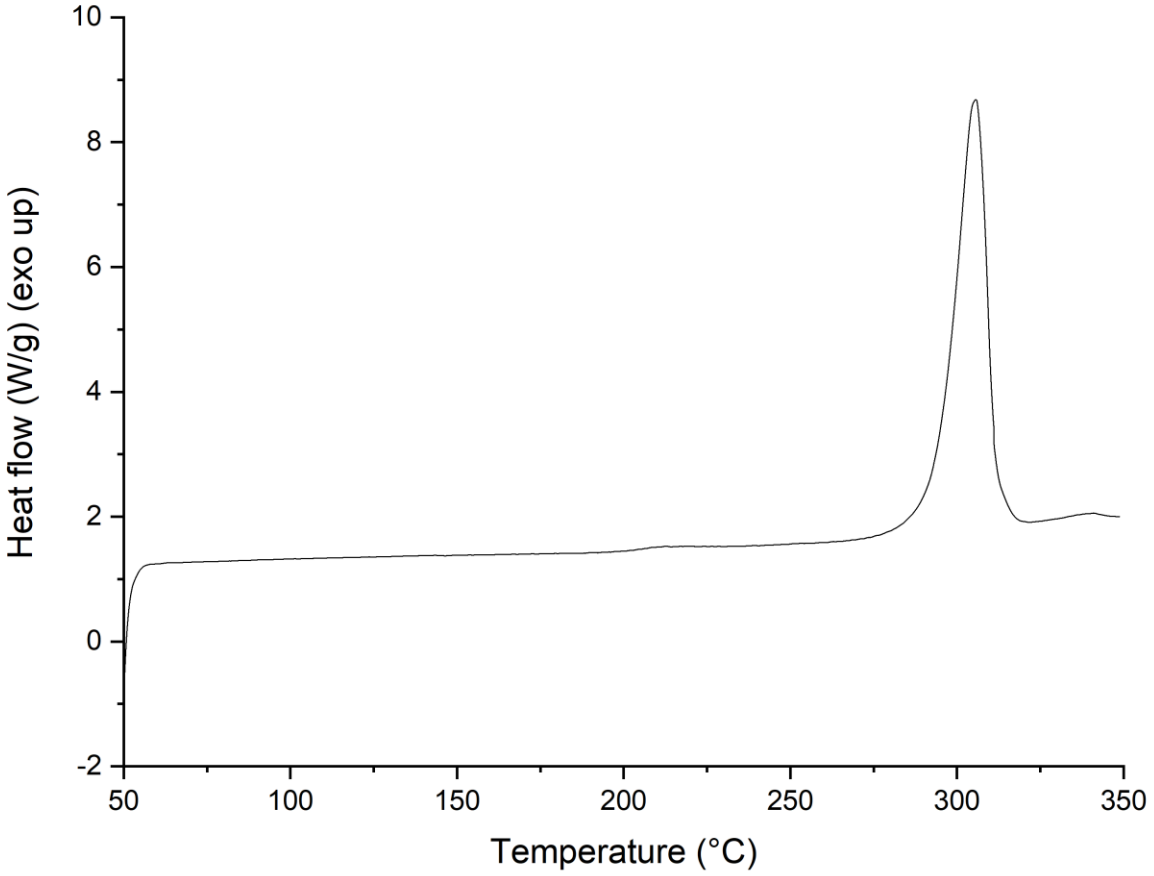

Figure 2.16: *DSC calorigram for DBX-1 (exothermic events show as an increase of heat flow).*

Purity and identity of the analyte material was ascertained by a combination of IR spectroscopy and powder X-ray crystallography, which returned data fully consistent with the literature.[5][14] The DSC trace of a sample of this batch of DBX-1 is shown in **Fig. 2.16**. It displays an exothermic peak with an extrapolated onset temperature and peak temperature of DBX-1 at 294.0 °C and 305.6 °C, respectively; NB: the onset temperature defined as the intersection point of the extrapolated baseline and the inflectional tangent of the decomposition peak; the peak temperature is defined as the temperature reached at maximum heat flow. The calorigram (DSC trace) shows no other peak at lower temperature. The lack of additional thermal effects allows the conclusion that *i*) the exotherm at 294.0 °C is caused by the controlled slow decomposition of DBX-1, and *ii*) that the material does not undergo any phase

changes prior to its decomposition. These conclusions are contingent on the method of sample encapsulation and the heating rate (3 K min^{-1}). Therefore, the decomposing phase is the same as that present at room temperature. Fronabarger observed an onset and peak (maximum) temperature of 329.8 °C and 337.7 °C, respectively, using the much increased heating rate of 20 K min^{-1}. These temperatures are much higher than those obtained at Sheffield. It is important to consider that Fronabarger et al. encapsulated their samples in sealed aluminium containers.[5] In the theory of thermal analysis it is stated that, all other parameters being identical (material morphology and purity, confinement) and using an ideal calorimeter, the *onset* temperature of a given thermal (calorimetric) effect is independent of both sample mass and heating rate. If potential systematic errors caused by deviating detector response functions are excluded, the deviation in the measured thermal characteristics (lower temperature of decomposition obtained at Sheffield) must be caused by either an undetected impurity catalysing the decomposition of the copper(I) nitrotetrazolate, or an autocatalytic process that induced thermal decomposition which leads to an earlier onset when lower heating rates are applied. It should also be considered that the pressure inside the stainless-steel capsule (Sheffield) will be much higher than in the aluminium capsule which will expand when gas production occurs. Increased pressure may accelerate decomposition reactions.

The calorigram of DBX-X (**see Fig. 2.17**) was obtained under identical conditions to that of DBX-1 and indicates a similar decomposition pattern consisting of a single exothermic peak which is interpreted in terms of a thermally induced decomposition that produces heat. Once again, the lack of any thermal effects below this temperature (other than the slowly decreasing apparent heat capacity of the sample-container assembly – a linearly rising base line) suggests that the compound undergoes decomposition *without* any prior phase change.

The onset and peak temperatures of thermally induced decomposition of DBX-X were found to be 273.2 °C and 282.8 °C, respectively. It is important to note the increased broadness of the exothermic peak of DBX-X compared to that of DBX-1. The appearance of a shoulder to the peak implies a more complex decomposition process than that operating in DBX-1.

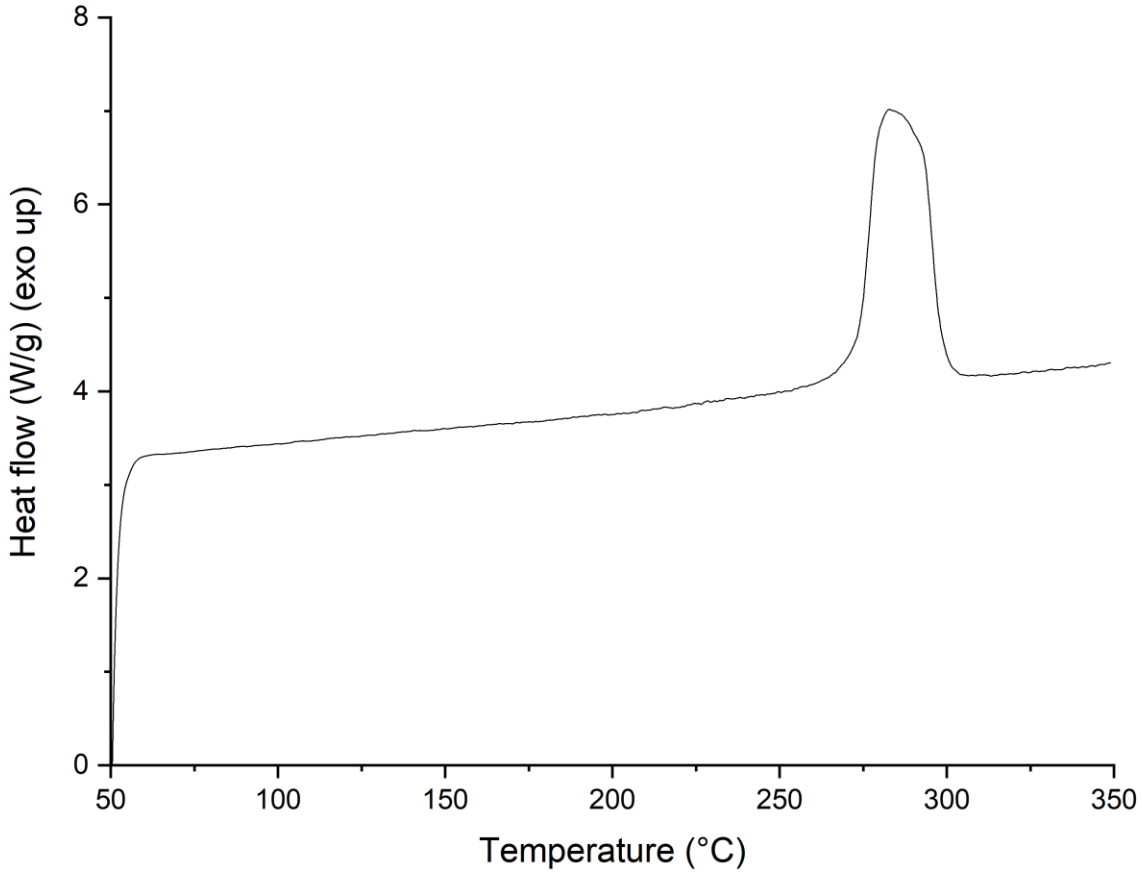

Figure 2.17: DSC calorigram for DBX-X (exothermic events show as an increase of heat flow).

Under identical conditions, the onset of decomposition of DBX-X occurs at a temperature which is approximately 20 K below that of DBX-1 (Sheffield). Furthermore, DBX-X has a specific heat of decomposition (1201 J g^{-1}) which is 38% lower than that of DBX-1 (1653 J g^{-1}), a molar heat of decomposition (based on Cu) that is only two thirds as large as that found for DBX-1 (DBX-X: 181.8 kJ mol^{-1}, DBX-1: 293.6 kJ mol^{-1}), and an energy density of the crystals that is 19% below that of DBX-1 (DBX-X: 3.5 kJ cm^{-3}, DBX-1: 4.3 kJ cm^{-3}). The ratio of molar heats of decomposition can thus be closely estimated by the ratio of stoichiometric proportions of copper and nitrotetrazolato groups in both compounds, (DBX-1, 1 : 1) / (DBX-X, 3 : 2) ≈ 0.67 (theory) vs. 0.62 (observed).

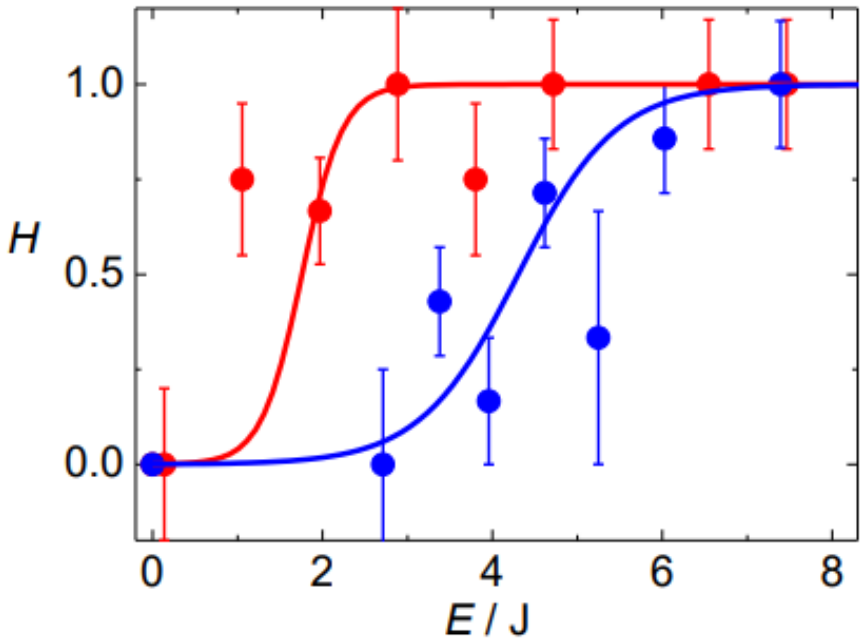

Figure 2.18: *Graph of results of drop-weight testing for DBX-1 (Blue) and DBX-X (Red)*

Preliminary drop weight testing reveals that the microcrystals of DBX-X have significantly higher impact sensitiveness than those of DBX-1 (**Figure 2.18**). The impact sensitiveness (IS) is determined as the energy (E_{50}) at which 50% of the impacted samples react (initiate). The E_{50} value is interpolated from the data points using a Weibull function, E = a - (a - b)exp(-(k x)^d). The measurement resulted in the values 1.8 (± 0.2) J for DBX-X vs. 4.3 (± 0.3) J for DBX-1. For comparison, $Pb(N_3)_2$ has IS values in the range 2.5 – 4.0 J. The variation of $Pb(N_3)_2$ sensitiveness is influenced by formulation changes, *i.e.* reaction conditions, additives, morphology, crystal size distribution etc. In conclusion, DBX-X can be regarded as having high impact sensitiveness with an E_{50} that exceeds that typically found for $Pb(N_3)_2$ (**Table 2.4**)

The increased sensitiveness towards impact of DBX-X compared to DBX-1 can be explained via two different explanations: a) crystals of DBX-X are more likely to form hot spots (See **Introduction, 1.1 Ignition, hot spots and phonon mode up-pumping**) resulting in more thermal events that can be up-pumped to bond breaking molecular vibrations resulting in a greater chance of detonation propagation or b) the presence of Cl^- in the crystal results in a higher vibrational energy up-conversion

efficiency, which again leads to a higher chance of thermal events leading to bond breaking and thus a greater chance of detonation propagation. Further experimentation is required to verify the cause of the increased sensitiveness of DBX-X.

	$Cu_3Cl(N_4C\text{-}NO_2)_2$ (DBX-X)	$Cu(N_4C\text{-}NO_2)$ (DBX-1)	$\alpha\text{-}Pb(N_3)_2$ (lead azide)
T_{dec}^{on} / °C	274 [a]	293 [a]	313 [b]
ΔH_{exo}/(kJ mol^{-1})	546 [c]	294 [c]	443 [d]
ΔH_{exo} / (kJ g^{-1})	1.20 [a]	1.65 [a]	1.52 [e]
ΔH_{exo} / (kJ cm^{-3})	3.5 [f]	4.3 [f]	7.2 [f]
E_{50} / J (impact)	1.8(±0.2) [g]	4.3(±0.3) [g]	2.5 - 4.0 [h]
$\rho_{crystal}$(calc.) / (g cm^{-3})	2.939 [i]	2.584 [j]	4.763 [k]
M / (g mol^{-1})	454.18	177.59	291.24

Table 2.4: *Comparison of key energetic material parameters of DBX-X, DBX-1 and Lead azide. [a]obtained by DSC, heating rate 3 K min^{-1}; [b]ref[15]; [c]ΔH_{exo} / (kJ mol^{-1}) = [ΔH_{exo} / (kJ g^{-1})] x [M / (g mol^{-1})]; [d]ref[16]; [e]ΔH_{exo} / (kJ g^{-1}) = [ΔH_{exo} / (kJ mol^{-1})] / [M / (g mol^{-1})], ref[17]; [f]ΔH_{exo} / (kJ cm^{-3}) = [ΔH_{exo} / (kJ mol^{-1})] / [M / (g mol^{-1})] x [$\rho_{crystal}$ / (g cm^{-3})]; [g]values obtained from material as synthesised without further processing, apparatus used for testing DBX-X and DBX-1 is different to those used for LA; [h] ref [1]; [i] ref [18]; [j]ref [5]; [k]using a = 6.63, b = 16.25, c = 11.31 Å, Z = 12 given in ref[19]*

As energetic materials, it is essential to estimate the performance parameters of these compounds. The outcome of such an evaluation has profound influence on the classification and potential application. Two commonly used concepts are the Chapman Jouguet detonation velocities (D_{CJ}) and detonation pressures (p_{CJ}). To calculate these for DBX-1 and DBX-X, the heat of formation (ΔH_f) and the loading density (r) are required. In these calculations, the crystal density (ρ) is used as the upper limit for the loading density, hence the calculated D_{CJ} and p_{CJ} values must be regarded as upper limits, too. The crystallographically determined density of DBX-X is significantly higher than that of DBX-1 (2.939 g cm^{-3} vs. 2.584 g cm^{-3}) and also slightly greater than what can be predicted from the densities of DBX-1 and CuCl (2.817 g cm^{-3}). This suggests that the packing in DBX-X is more efficient than in a simple mixed

crystal with the 2 : 1 stoichiometry of Cu(N_4C-NO_2) and CuCl. A similar argument can be made using the spatial demand of the Cu(N_4CNO_2) moiety. Using the published values for the density of DBX-1, an effective volume of the Cu(N_4C-NO_2) moiety can be calculated. The effective volume of Cu(N_4C-NO_2) in DBX-1 is found to be 114.1 $Å^3$. Calculating the effective volume of DBX-X in the same manner and subtracting the value found for Cu(N_4C-NO_2) shows that the volume available for Cu and Cl in DBX-X would only be 28.4 $Å^3$, which is much less than what is available in CuCl crystals (58.35 $Å^3$, calculated from the density of CuCl). As the crystal density is the limiting density in explosive formulations, the higher density of DBX-X could potentially lead to higher detonation pressures and velocities than that which could be found in DBX-1 based formulations.

Heats of formation (ΔH_f) can be determined experimentally by way of bomb calorimetry and has been done so for DBX-1 by Fronabarger *et al.* with a recorded heat of formation of -49.9 kJ mol^{-1}. Without access to a bomb calorimeter, one can make reasonable estimations of the heat of formation by using specific heats of decomposition as determined by DSC. If decomposition products are assumed to be the same as the detonation products, and by using the heats of formation of these products at the onset temperature of thermal decomposition, one can apply Hess's Law to estimate the heat of formation of novel explosives without accurate bomb calorimetry measurements. With estimations of $\Delta H_{f(explosive)}$, and assuming the crystal density to be the limiting density, detonation velocities and pressures can be calculated. The accuracy of this estimation depends on the accuracy of the DSC measured enthalpy of decomposition (ΔH_d) and the method of assigning detonation products. Multiple different rulesets exist to assign detonation products including Kistiakowsky-Wilson Rules, Modified Kistiakowsky-Wilson Rules, Springall Roberts Rules and by use of the NASA chemical equilibrium code CEA. NASA CEA is a reactionless computer code that minimizes free energies using a Newton Raphson method with ideal gases and pure condensed phases to determine chemical equilibria (such as those found at high temperature in detonations) at defined temperatures. Values for $\Delta H_{f(explosive)}$ for DBX-1 were calculated using the different sets of detonation products and ΔH_d recorded for a sample of DBX-1 synthesised in Sheffield. The value for $\Delta H_{f(explosive)}$ was then compared to that recorded via bomb calorimetry to determine which method of assigning detonation products gave the most accurate value for

$\Delta H_{f(explosive)}$. Values for heats of formation at 290 °C of detonation products were used in the calculations. The methods of detonation product assignment are generally used for CHNO compounds only. Therefore, generally accepted rules regarding the treatment of metals do not exist. In this thesis the problem of the detonation products of DBX-1 is treated in two ways: a) assuming that only metallic Cu is formed (as shown in the work of Zhang[21]), b) assuming that Cu_2O is formed. Within CEA, however, a method of assigning detonation products exists allowing for a much more accurate estimation of $\Delta H_{f(explosive)}$ compared to the other methods of detonation product treatment (**Table 2.5**).

Method of Det. Prod Assignment	**Detonation Products**	**$\Delta H_{f(products)}$/ kJ mol^{-1}**	**$\Delta H_{f(explosive)}$/ kJ mol^{-1}**	**% Difference from Bomb. Cal derived value**
KW Rules(Cu)	Cu + CO_2 + 2.5 N_2	-361.5	-67.9	+36.1
SR Rules(Cu)	Cu + CO_2 + 2.5 N_2	-361.5	-67.9	+36.1
KW(Cu_2O)	0.5Cu_2O + 0.5CO_2 + 0.5CO + 0.5N_2	-307.0	-13.4	-73.2
SR (Cu_2O)	0.5Cu_2O + 0.583CO_2 + 0.33CO + 0.083C + 2.5N_2	-321.7	-28.1	-43.7
CEA	0.5Cu_2O + 0.75CO_2 + 0.25C + 2.5N_2	-351.1	-57.5	+15.3%

Table 2.5: *Comparison of the detonation products predicted via different methodology and the $\Delta Hf_{explosive}$ associated to these products*

Using CEA for the estimation of heat of formation from DSC calorigrams for DBX-1 gives an error in $\Delta H_{f(explosive)}$ of -7.55 kJ mol^{-1}. The estimates of Q, D and P can be compared to those calculated from experimentally determined values for DBX-1 in order to assess the accuracy of this method. As a result, Q, D and P values were found to be within 2.75%, 0.63% and 1.26% of the values calculated using the bomb calorimetrically determined heat of formation. Using these results, we calculated $\Delta H_{f(explosive)}$, heat of explosion(Q), Chapman Jouguet detonation velocities (D_{CJ}) and detonation pressures (P_{CJ}) values for DBX-X to compare to those values known for DBX-1.

Compound	**$\Delta H_{f(explosive)}$/ kJ mol^{-1}**	**ρ/ g cm^{-3}**	**Q/ J g^{-1}**	**D_{CJ}/ km s^{-1}**	**P_{CJ}/ kbar**
DBX-1	-49.9	2.584	1696.7	6.341	219.97
	Estimated $\Delta H_{f(explosive)}$/ kJ mol^{-1}	**ρ/ g cm^{-3}**	**Q/ J g^{-1}**	**D_{CJ}/ km s^{-1}**	**P_{CJ}/ kbar**
DBX-1	-57.5	2.584	1654.2	6.301	217.19
DBX-X	-197.2	2.939	1199.1	5.944	204.42

Table 2.6: *Comparison of the values for Q, D and P calculated for DBX-1 and DBX-X from estimated $\Delta H_{f(explosive)}$ and the comparison of these values to those known for DBX-1 from Bomb calorimetry, loading density ρ assumed to be the same as the crystal density therefore the calculated values of can be seen as an upper limit*

Applying this method to DBX-X shows that DBX-X decomposes in a more exothermic process ($\Delta H_{f(explosive)}$) per Cu compared to DBX-1 (**Table 2.6**). Using the estimated $\Delta H_{f(explosive)}$ and the crystal density values for Q, D and P could be calculated. This results in reduced Q, D and P values compared to DBX-1 but all values are above the minimum thresholds associated with primary explosives. Clearly the increased density of DBX-X does not result in increased D and P due to the increased exothermicity of ΔH_f because of the loss of 1/3 nitrotetrazolate in favour of chloride. This contradicts our previous published findings [14] in which DBX-X was predicted to have higher

Chapman Jouguet detonation velocities (D_{CJ}) and detonation pressures (P_{CJ}). This is due to a reassessment of the likely detonation products and the use of CEA in determining these.

2.2.8.2 Stability of DBX-1 and DBX-X

Stability towards atmospheric moisture is a crucial characteristic of any prospective lead-free initiator (**See Introduction, Replacements for lead-based primary explosives).** The stability of DBX-1, DBX-X and a DBX-1 / DBX-X mixed phase (1 : 1 mass fractions) were tested in lab air. For this purpose, samples of each compound were kept in open vials and the solids monitored by IR spectroscopically as nujol mulls. The state of the samples after 21 days exposure time is shown in **Fig. 2.19** (DBX-1), **Fig. 2.20** (DBX-X) and **Fig. 2.21** (DBX-1 / DBX-X mixed phase). In all three layered FTIR spectra the number of peaks and the peak positions remain unchanged. Apparent changes in the spectra of DBX-1 and DBX-X, most noticeable in the region 3000-1600 cm^{-1}, are the result of the Christiansen effect due to the poorer grinding of the microcrystalline materials in the process of sample preparation. With poor grinding, large particles are present in the suspension being investigated. The Christiansen effect occurs when a suspension of particles in a transparent medium (in this instance nujol) is observed at a wavelength where the refractive indices of the particles and of the medium are equal, thus producing an optically homogeneous medium.[22][23] The Christiansen effect is the increase of the crystalline powder transmittance at those wavelengths where the sample and medium refractive indices are equal. This results in the formation of Christiansen peaks, regions of high transmittance, which can most commonly be seen either side of adsorption bands. While equal refractive index of both particles and medium can occur at adsorption band maxima, the observation of this effect is quite difficult. This effect is minimized by grinding of particles to below 2 µm but can never be completely eliminated.[24][25] All apparent changes in the FTIR spectra can be explained by the appearance of Christiansen peaks as a result of poor sample preparation. Furthermore, visual and physical inspection of the samples revealed no changes to either colour or sample crystallinity. Both DBX-X and DBX-1 can therefore be said to be stable for prolonged periods when exposed to air.

In order to test stability when immersed in water, standard glass vials were charged with samples of DBX-1, DBX-X and a 50 : 50 DBX-1 / DBX-X mixture under deionised water and the setup left unsealed over the course of 2 months. Additional deionised water was added whenever the samples neared dryness. Within 21 days decomposition was already visible in both DBX-X and the mixed sample. This decomposition is revealed by the slight blue colouration of the aqueous phase over DBX-X. The decomposition of the mixed phase presented with the same blue colouration, which, upon evaporation, deposited a ring of blue material. After 61 days, DBX-X appears to have fully decomposed and left behind a material that contains neither DBX-X nor DBX-1 (according to a visual inspection, the characteristic dark wine-red colour had vanished and a yellow-brown voluminous new solid phase had formed, **Figure 2.22**).

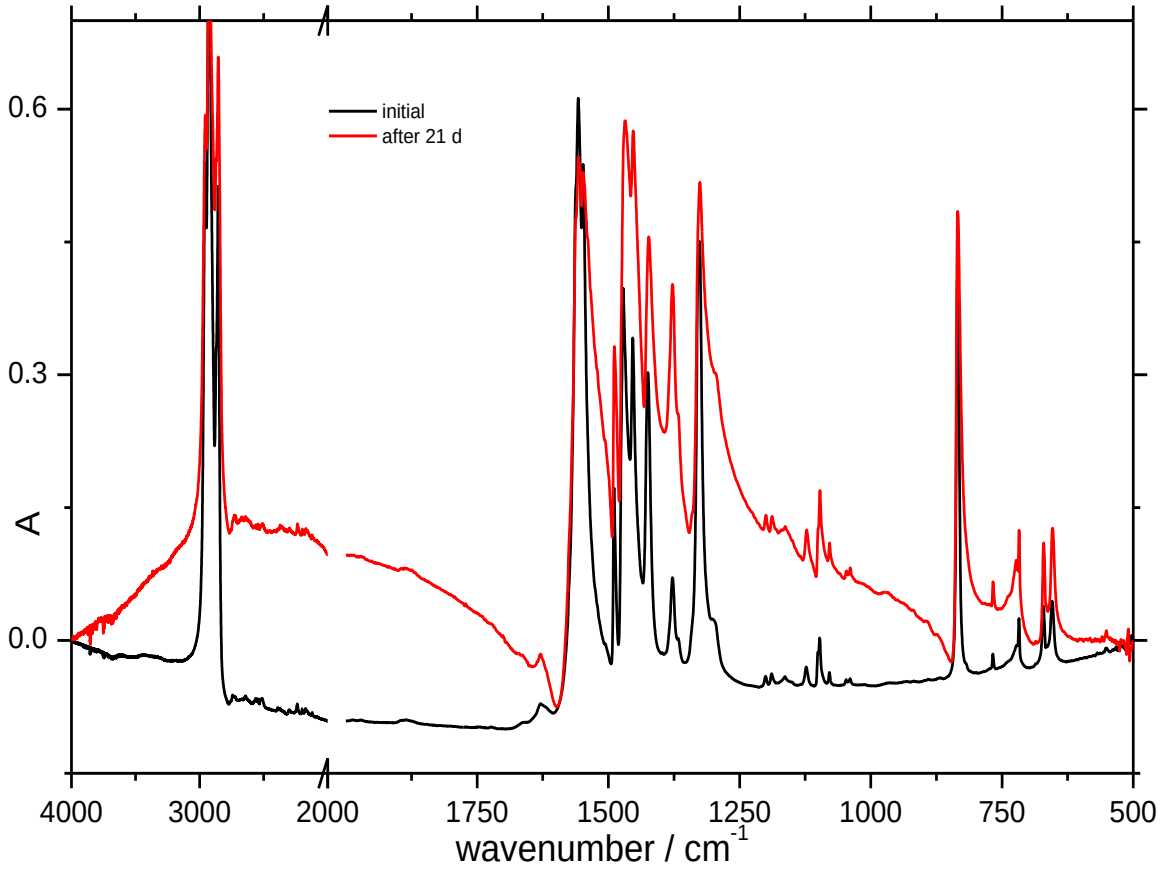

Figure 2.19: *Comparison of IR spectra of DBX-1 before (black) and after (red) stability testing in air.*

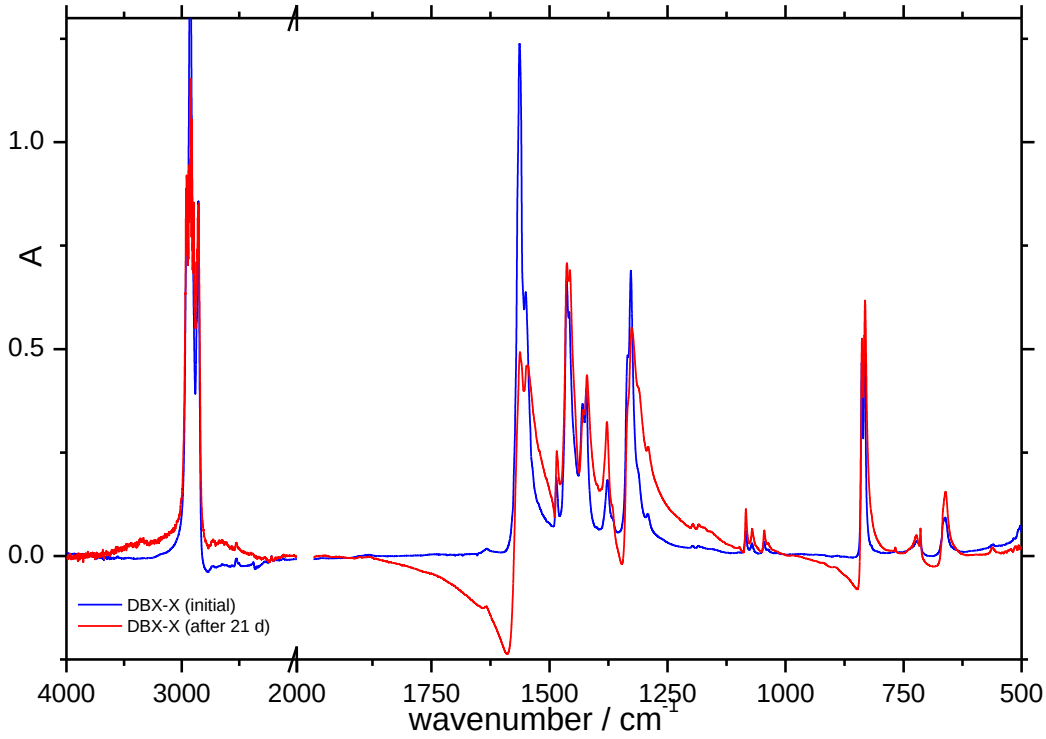

Figure 2.20: *Series of baseline corrected IR spectra of DBX-X before (blue) and after (red) stability testing in air.*

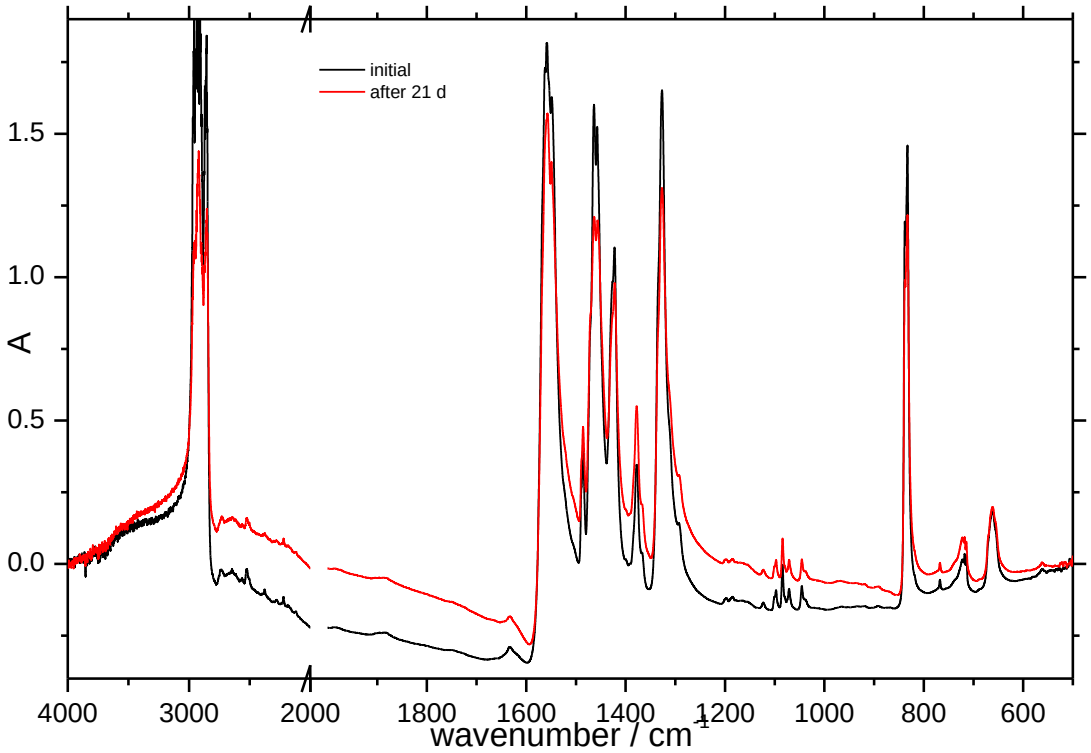

Figure 2.21*: Series of IR spectra of a mixed DBX-1 / DBX-X phase before (black) and after (red) stability testing in air*.

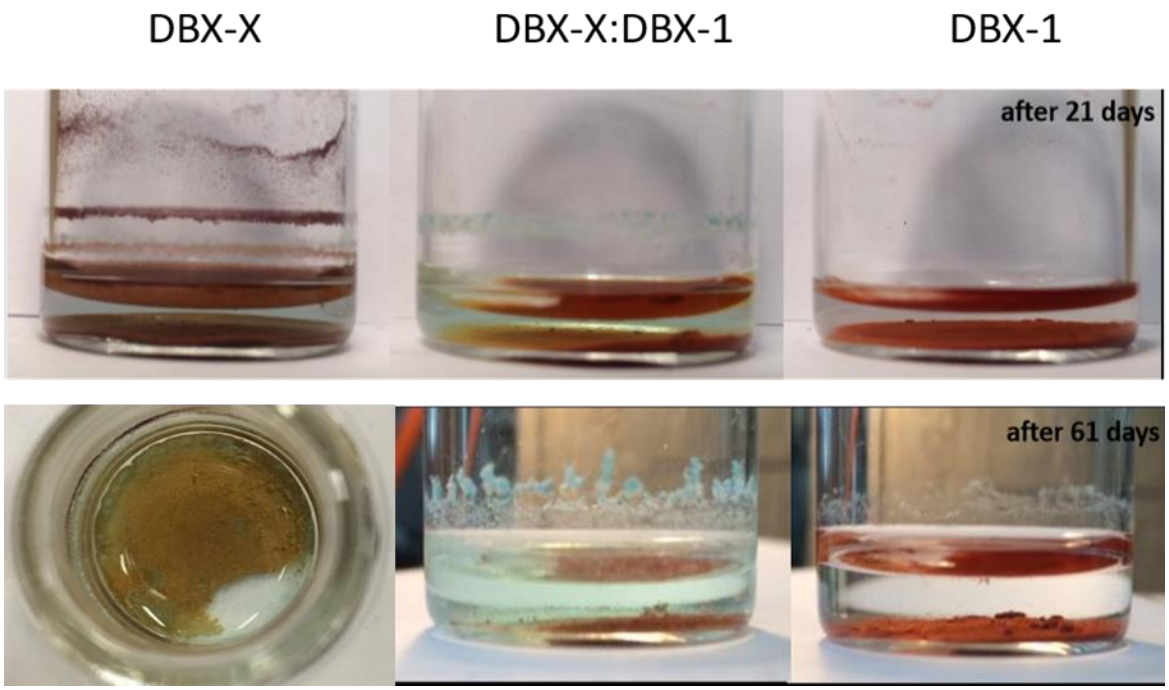

Figure 2.22: *Top: State of samples after 21 days under water; Bottom: State of samples after 61 days under water*

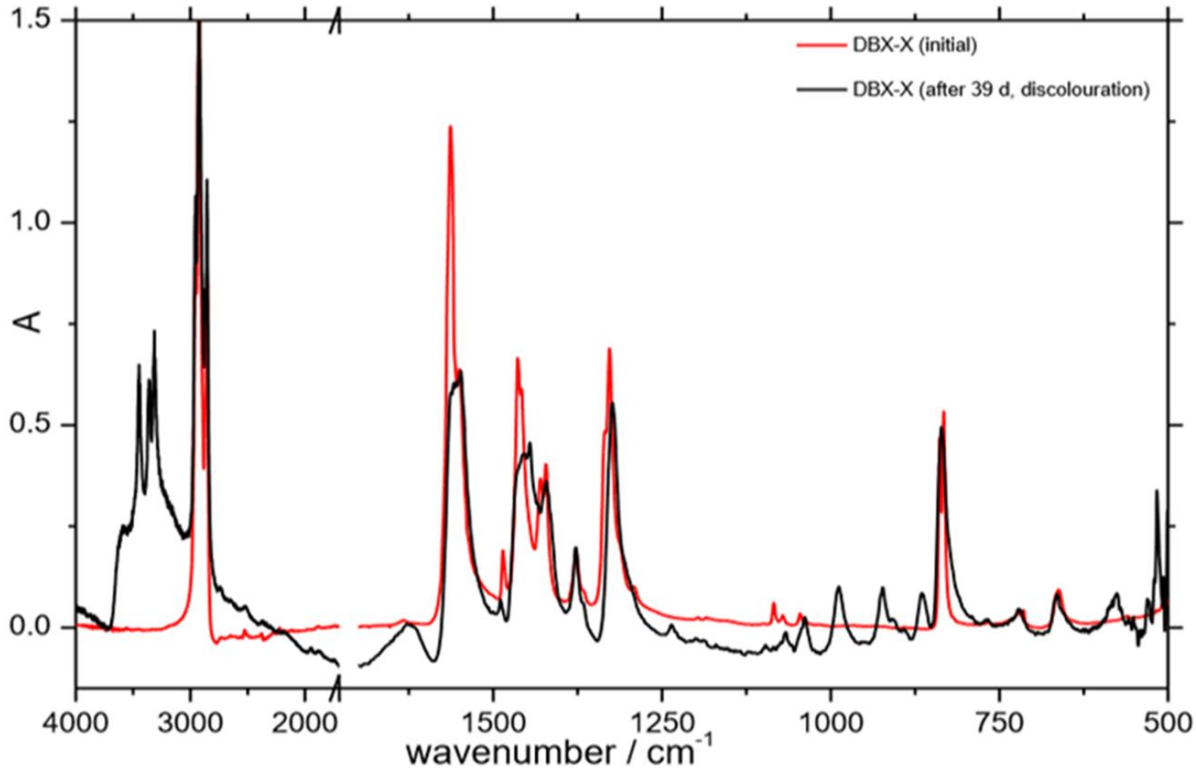

Figure 2.23: *Series of FTIR spectra of pure DBX-X (red)(spectrum is baseline corrected) and the brown product following discolouration of DBX-X (black)*

Accordingly, IR spectra before and after the 61 days clearly show the hydrolysis of DBX-X (**Figure 2.23**). Shifts in the peak positions of the absorption bands relating to the nitrotetrazolate anion can be identified throughout the spectral region 1600-500 cm^{-1}, with the indicative region of 1100-1000 cm^{-1} completely changed post decomposition. Multiple new absorption bands can also be seen, most prominently in the region 1125-500 cm^{-1}. The appearance of intense absorption from 3700-3300 cm^{-1} points towards water coordinating to the copper, possibly as a result of forming basic copper carbonate ($Cu_2CO_3(OH)_2$), a compound with a characteristic blue colouration.

After 61 days the mixed phase, too, appeared to show decomposition. The brown solid obtained after DBX-X decomposition was present alongside DBX-1 and the same blue solid as before which was assumed to be basic copper carbonate, forming as a result of CO_2 from the air dissolving in the aqueous solution. While full decomposition of DBX-X seems to have occurred it does appear that less of the brown solid and more basic copper carbonate has formed. The reason for this is unclear as it is not known whether the DBX-X present in the mixed phase decomposes solely due to contact with water or whether the presence of DBX-1 in the mixture promotes a different decomposition pathway.

Intriguingly, under the same conditions, pure DBX-1 did not show any visible decomposition. IR spectra recorded before and after the water exposure were identical except for the previously mentioned Christiansen effect which depends on the crystal size. [22-25] The difference in water stability of the two compounds can be rationalised by the presence of chlorine in DBX-X, which is tentatively suggested to promote the hydrolysis of Cu compounds in a similar manner to that seen in copper(I) chloride in water. With Cu(I) being a soft acid de-coordination of the hard Cl^- could occur more easily than for the softer nitrotetrazolate. This open coordination site could allow for oxidation of Cu(I) by dissolved O_2 leading to the formation of Cu(II) and the higher water instability of DBX-X vs DBX-1.[26] If the Cl^- could be substituted for a different ligand, potentially an explosophore with a stronger binding affinity for Cu(I), a novel compound could be formed which reduces the likelihood of hydrolysis occurring.

Overall, while both DBX-X and DBX-1 share similarities in their respective properties, there are key differences which would exclude DBX-X from being viewed as either a

DBX-1 alternative or as a prospective LFI. DBX-X possess good thermal stability, a high impact sensitiveness but not so high as to prevent safe handling and has a crystal density higher than that of DBX-1. However, the apparent lack of stability in water compared to DBX-1 does show that the long-term storability of DBX-X could potentially be an issue (though DBX-X does appear to be stable for long periods of time with regard to atmospheric moisture). DBX-X also possesses a lower enthalpy of decomposition which results in lower detonation performance parameters than for DBX-1. Questions also remain over the feasibility of preventing DBX-1 formation when one is aiming solely for DBX-X production, casting doubts over the potential manufacture of DBX-X on a large scale. These issues all suggest that DBX-X cannot be considered a viable DBX-1 alternative or prospective LFI.

2.3 Conclusion

The use of $NaNT.2H_2O$, purified only through Soxhlet extraction, in the Cu(I) reduction reaction to form DBX-1 only results in the formation of an amorphous solid which is unstable in air. $NaNT.2H_2O$ was purified by recrystallization in water at 0 °C to form $NaNT.4H_2O$. When using this solid in the reduction reaction of copper(II) chloride, a wine-red chlorine-containing copper nitrotetrazolate, $Cu_3Cl(N_4C\text{-}NO_2)_2$, was discovered. This result indicates that the seemingly simple synthesis of DBX-1 produces a number of well-defined energetic materials. The formation of $Cu_3Cl(N_4C\text{-}NO_2)_2$ shows that mixed-ligand coordination frameworks are possible and lends weight to the notion that more efficient lead-free primary initiators are potentially accessible in which Cl^- is replaced by a different, potentially explosophoric group with the aim to reduce sensitivity toward water, and to tune sensitiveness toward shock, friction and temperature. The selectivity of the $CuCl_2$ – sodium ascorbate – explosophoric group-transfer reduction reaction can be controlled by the action of seed crystals and this can be exploited to direct the reaction pathway towards formation of DBX-1. The crystals of $Cu_3Cl(N_4C\text{-}NO_2)_2$ consist of an elaborate void-less coordination network with a density exceeding that of DBX-1. It has higher friction and impact sensitiveness than either DBX-1 ($Cu(N_4C\text{-}NO_2)$) or lead azide and decomposes violently upon rapid heating or shock. $Cu_3Cl\ (N_4C\text{-}NO_2)_2$ is a powerful explosive but has lower energetic parameters than DBX-1. Even though stable in air indefinitely, $Cu_3Cl(N_4C\text{-}NO_2)_2$ decomposes under water within weeks. Due to this, its lower decomposition temperature, and its lower detonation performance parameters $Cu_3Cl(N_4C\text{-}NO_2)_2$ cannot be considered as a viable alternative to DBX-1 or $Pb(N_3)_2$.

2.4 Experimental

2.4.1 Synthesis of Sodium nitrotetrazolate dihydrate, NaNT.4H_2O

To a 100 ml plastic beaker, sodium nitrite (6.906 g, 100 mmol) and copper sulphate (2.324 g, 14.6 mmol) were added before 33.1 ml of H_2O was added. The solids dissolved to form a dark green solution. The solution was cooled to 12 °C with the use of an ice bath. To a separate vessel, aminotetrazole monohydrate (3.245 g, 33.2 mmol) and copper sulphate (0.046 g, 0.266 mmol) were added along with 20 ml of H_2O and 3 ml of 68% of HNO_3. This formed a light blue-white suspension (solution is light blue, solid in suspension is white) which was stirred for 10-15 minutes but no further dissolution occurred. This suspension was added to the dark green sodium nitrite-copper sulphate solution via addition in portions with care paid to maintaining temperature below 15 °C (note that temperatures as high as 18 °C have been observed with no difference in product purity). Immediately on addition, bubbling can be observed (indicative of N_2 gas formation). Continued addition results in the bubbling continuing to increase which results in large amounts of foam formation. Stirring (reaction mixture used a Teflon stirrer bar) also becomes noticeably poorer on addition of each portion. The addition was paused after each portion to allow stirring to recover to an acceptable level and to allow foam to fall back into solution. The solution was stirred for 30 minutes at the same temperature before the addition of a solution of nitric acid (4.65 mL, 68 %, diluted with an additional 2 ml of H_2O, 6.65 ml total volume) in one portion whilst the beaker was still immersed in the ice bath. The solution was allowed to warm to room temperature and was stirred at this temperature for 1 h. After 1 hour, the contents of the plastic beaker were transferred to a 100 ml glass beaker. A concentrated NaOH solution (50:50 w/w with H_2O) was added to the solution with vigorous stirring until a pH of 8 was seen using indicator paper. During addition of the NaOH solution the colour of the solution in the glass beaker gradually changes and at pH 8 has a turquoise colour. The turquoise solution was then heated to 70 °C with vigorous stirring for 2 hours. The solution gradually darkens until it becomes a black colour. After 2 hours, the solution was allowed to cool to room temperature and the pH checked to ensure pH 8 was maintained. Once at room temperature, the solution was filtered through a layer of Celite packed onto a sinter bed. A black solid is collected on the Celite and a pale-yellow filtrate is obtained. The filtrate was evaporated using a

rotary evaporator with a bath temperature of 50 °C to give a pale yellow solid. This solid was extracted using a continuously running Soxhlet extraction apparatus and acetone as the extraction solvent. The extraction end point was after 12-18 hours. This left a colourless solid on the sinter which upon heating showed no energetic character (presumed to be $NaNO_3$). The extraction solvent was filtered and then evaporated to leave a viscous yellow oil (comprised of $NaNT.2H_2O$ and mesityl oxide) which evaporated when left under intense airflow, leaving large, pale-yellow crystals of $NaNT.\ 2H_2O$.Identity of crystals proven by comparison of FTIR spectra to ref[6]. Indicative IR absorption bands (nujol) v/cm−1 = 1183, 1173, 1058, 1035. In a glass beaker, a saturated solution of sodium 5-nitrotetrazolate was prepared by stirring $NaNT{\cdot}2H_2O$, (173.02 g mol^{-1}, 7.905 g, 45.7 mmol) in deionised water (ca. 18 ml) at 20 to 25 °C. By immersing the beaker in an ice bath, the solution was then cooled to 0 °C for the duration of 2 h, after which needle-shaped colourless crystals had formed. Cold-filtration, washing of the filter residue with small amounts of ice-cold water (×2) and then acetone (×2), followed by brief air-drying of the wash residue, affords $NaNT.4H_2O$ ($CH_8N_5NaO_6$, 209.04 g mol^{-1}, 5.943 g, 28.4 mmol, 62% with respect to $NaNT.2H_2O$) as a white crop of colourless, odourless, free-flowing crystals. $NaNT.4H_2O$ can be stored in a sealed vessel without decomposition at r.t. for several months. Under a dynamic vacuum (ca. 1 mbar) at r.t., however, it dehydrates readily to convert into $NaNT.2H_2O$ and upon further dehydration to NaNT. The yield of $NaNT.4H_2O$ afforded by this preparative method is highly sensitive to temperature and solvent volumes, and ranges between 29% and 62%. IR (nujol) v/cm^{-1} = 3592s, 3399s, br, 1643w, 1551s, 1453vs, 1426vs, 1325s, 1183m, 1058w, 1035w, 842m, 597vs, br. Magnetic susceptibility χmeas/(emu mol^{-1}) = −4.2 (±0.7) × 10^{-4} .

2.4.2 General reaction scheme for the synthesis of DBX-1 and DBX-X

$CuCl_2$ was reduced using the method given by Fronabarger et al.[5]Method restated here for the sake of clarity:

2.4.2.1 Fronabarger synthesis

$CuCl_2$(18 mL of 1m, 18 mmol) was added to water(100 mL) in a 400 mL beaker containing a 50 mm magnetic stir bar at 500 RPM. The solution was heated to approx. 81 °C and an aqueous solution of NaNT (approx.18 mmol, 32 mL of a 0.097 g mL^{-}

[1]aqueous solution at ambient temperature) was added. On addition the clear blue solution became light green. Heating was continued until the mixture was at 90 °C and addition of an aqueous sodium ascorbate (9 mL of 1M solution, 9 mmol, 1.0 equiv.) solution was started at the rate of 1 mL min^{-1}. Initially the green solution remained clear and darkened in colour. At 1.5 minutes into the addition, solids started to form and the mixture became an opaque olive green. The addition of ascorbate was paused. Over the next 4.5 minutes the mixture went from olive green to orange-green to brown and finally to rust red. Solid particles of DBX-1 were apparent at the meniscus and the addition of the remaining ascorbate was started, again at 1 mL min^{-1}. The suspension was maintained at 90–92 °C throughout the addition and was stirred after the addition was complete for additional 1.5 minutes (14 minute total reaction time). The suspension was removed from the hot plate, the magnetic stirrer was removed, and the supernatant was decanted leaving solid DBX-1 behind. The solids were washed twice with water and afterwards filtered through Whatman #1 filter paper. The precipitate was washed with water (2X) followed by 2-propanol (3X) and afterwards dried in a convection oven at 65 °C until dry (approx. 30 minutes).

2.4.2.2 Sheffield Synthesis

The following modifications to apparatus and reagents have be made to allow for the experimental work to be performed at the University of Sheffield (i–iv): a 100 ml beaker made from borosilicate glass acts as the reaction vessel (i), a Teflon-coated magnetic bar with the dimensions 25 mm × 6 mm is employed for agitation (ii), NaNT.$2H_2O$/NaNT.$4H_2O$ is used as the nitrotetrazolyl group transfer reagent (iii), and the aqueous Na(HAsc) reductant is added dropwise into the reaction mixture using a Pasteur pipette (iv). NB: previous publications noted colour changes upon addition of the nitrotetrazolyl group transfer reagent. We have found that they are dependent on the purity of the NaNT solution; addition of NaNT.$2H_2O$ results in a colour change from light blue to green; however, the addition of aqueous solutions of NaNT.$4H_2O$ to those of $CuCl_2$ causes a slight deepening of the blue colour. The Na(HAsc) addition regime was (points in time stated in minutes, reaction mixture stirred continuously): 0 to 1.5 addition, 1.5 to 6 dwell time, 6 to 13.5 addition, 13.5 to 15 dwell time. Multiple experiments were done following this general reaction scheme and the results are tabulated in **Appendix 8.8**. The isolated yields of DBX-X and DBX-1 with respect to

$CuCl_2$ range from 67% to 86%. Caution (!), careful grinding of a 10 mg batch of DBX-X obtained by this preparative procedure, using an agate mortar and pestle, caused initiation events (audible as loud crackling sound), which subsided once the crystal size had reduced sufficiently through milling action.

DBX-X $Cu_3Cl(N_4CNO_2)_2$, M = 454.18 g mol^{-1} ; DSC, T_{on} = 274 °C (dec.), T_{peak} = 283 °C, ΔH_{exo} = 1201 J g^{-1} , 3 K min^{-1} , NB: heating DBX-X at a high rate (10 K min^{-1}) causes decomposition at around 300 °C and breaks the sample container. Cu content as Cu^{2+} 41.97(± 0.04)% (calcd), 41.7 (± 2.4)% (found). In three crops of crystals, the magnetic susceptibility χ_{meas}/(emu mol^{-1}) was found to range from −8.4 (±0.5) × 10^{-4} to +1.8(±0.2) × 10^{-4} . IR (nujol) v/cm^{-1} = 1563vs, 1550m, 1486w, 1430w, 1422w, 1328s, 1292vw, 1197vw, 1084vw, 1071vw, 1045vw, 838m, 833m, 768vw, 715w, 662w, 502vw; TOF LD(+) MS m/z = 652 (2) $[Cu_2(CN)(DCTB)_2]$ + , 563 (8) $[Cu(DCTB)_2]$ + , 502 (4) $[Cu_4(DCTB)]$+ , 418 (9) $[Cu_2O(CN)\ (DCTB)]$+ , 411 (11) $[Cu_2Cl(DCTB)]$+ , 402 (21) $[Cu_2(CN)(DCTB)]$+ , 313 (100) [Cu(DCTB)]+ , 241 (8) $[Cu_3(CN)_2]$ + , 152 (5) $[Cu_2(CN)]$+ . PXRD data and single crystal data are given in the appendix (8.7, 9.1). A suitably sized, but small, specimen crystal was used for single crystal XRD measurement (vide supra). Impact sensitiveness E_{50} = 1.8(± 0.2) J.

For comparative purposes, analogous analytical data for $Cu(N_4CNO_2)$ (DBX-1, M = 177.59 g mol^{-1}), obtained at Sheffield under identical conditions, are given here: DSC, T_{on} = 293 °C (dec.), T_{peak} = 305 °C, ΔH_{ex} = 1653 J g^{-1} , 3 K min^{-1} . IR (nujol) v/cm^{-1} = 1558vs, 1548vs, 1489m, 1472s, 1454s, 1425s, 1327vs, 1201vw, 1189vw, 1164vw, 1123vw, 1098w, 1079vw, 1047vw, 1040vw, 835vs, 768vw, 718w, 671w, 655w, 552w; impact sensitiveness E_{50} = 4.3(±0.3) J. PXRD data is given in Appendix 8.6. Single crystal data available for DBX-1 in the cited literature[5]: DSC: T_{on}/°C = 302.8 (5 K min^{-1}), 329.8 (20 K min^{-1}), T_{peak}/°C = 337.7 (20 K min^{-1}), ΔH_{ex} = 1967 J g^{-1} , (20 K min^{-1}); IR (KBr) v/cm^{-1} = 1556vs, 1470s, 1451m, 1422s, 1325vs, 1123w, 1096w, 832s; crystal structure see ref[5], PXRD ref[8]

2.5 References

1. T. M. Klapötke and C. M. Sabate, Dalton Trans., 2009, 1835–1841
2. M. H. V. Huynh, M. A. Hiskey, T. J. Meyer and M. Wetzler, Proc. Natl. Acad. Sci. U. S. A., 2006, 103, 5409–541
3. Y. Pu, D. Sheng, Y. Zhu, L. Chen, B. Yang, Y. Wang and M. Xu, Huogongpin, 2009, 43–45
4. Y.-L. Pu, D.-L. Sheng, Y.-H. Zhu, L.-K. Chen, B. Yang, Y.-L. Wang and M.-H. Xu, Hanneng Cailiao, 2010, 18, 654– 659
5. J. W. Fronabarger, M. D. Williams, W. B. Sanborn, J. G. Bragg, D. A. Parrish and M. Bichay, Propellants, Explos., Pyrotech., 2011, 36, 541–550
6. T. M. Klapötke, D. G. Piercey, N. Mehta, K. D. Oyler, M. Jorgensen, S. Lenahan, J. S. Salan, J. W. Fronabarger and M. D. Williams, Z. Anorg. Allg. Chem., 2013, 639, 681–688
7. T. Klapoetke and C. M. Sabaté, Cent. Eur. J. Energ. Mater., 2010, 7, 161–173
8. D. D. Ford, S. Lenahan, M. Jorgensen, P. Dube, M. Delude, P. E. Concannon, S. R. Anderson, K. D. Oyler, H. Chen, N. Mehta and J. S. Salan, Org. Process Res. Dev., 2015, 19, 673–680.
9. E. v. Herz, Verfahren zur Herstellung von Nitrotetrazol, Patentschrift, DE1931H127723D 19310711 Nr 562511, 1931.
10. M. Krawiec, S. R. Anderson, P. Dube, D. D. Ford, J. S. Sala, S. Lenahan, N. Mehta and C. R. Hamilton, Propellants, Explos., Pyrotech., 2015, 40, 457–459
11. J. W. Fronabarger, M. D. Williams and S. Hartman, Copper (I) 5-nitrotetrazole Synthesis Optimization, NSWC-IH Contract 2010. May 25, VSE Corporation Customer, Pacific Scientific EMC, Chandler AZ, USA, PO F060467.
12. J. W. Fronabarger, M. D. Williams and W. B. Sanborn, PCT Int. Appl., WO 2008048351 A2 20080424, 2008.
13. X. Xu, H. Meng, Y. Lu, C. Li, *RSC Adv*., 2018,8, 30610-30615
14. B. Westwater, H. J. Lloyd, I. J, Vitorica-Yrezabal, A. Fong, P. McMaster, M. Sloan, B. M. Coaker, C. R. Pulham, P. Portius, Dalton Trans., 2020, 49, 14975-14984
15. D. J. Whelan, R. J. Spear, R. W. Read, Thermochim. Acta, 1984, 80, 149-163
16. Bowden, F. P.; Williams, H. T., Proc. R. Soc. Lon. Ser.-A, 1951, 208, 176-188

17. R. Meyer, J. Köhler, A. Homburg, Explosives, 6th ed. Wiley-VCH, Weinheim, 2007
18. T. M. Klapötke, C. M. Sabate, J. M. Welch, Dalton Trans. 2008, 6372-6380
19. L. V. Azaroff, Z. Kristallog. – Cryst. Mater., 1956, 107, 362-369
20. K. Sangwal, Nucleation and Crystal Growth: Metastability of Solutions and Melts, 2018, Wiley
21. Y. Wang, J. Zhang, H. Su, S. Li, S. Zhang, S. Pang, *J. Phys. Chem. A* 2014, 118, 25, 4575–4581
22. H. R. Carlon, Applied Optics, 1979, 18, 21, 3610-3614
23. R. Prost, Clays and Clay Minerals, 1973, 21, 363-368
24. R. A. Nyquist, Interpreting Infrared, Raman and Nuclear Magnetic Resonance Spectra Volume 2, 2001, Academic Press
25. B. H. Stuart, Infrared Spectroscopy: Fundamentals and Applications, 2005, Wiley
26. R. R. Conry, K. D. Karlin, Encyclopaedia of Inorganic Chemistry, First Edition: Copper: Inorganic and Coordination Chemistry, 2006, Wiley

3. Synthesis and characterisation of novel Cu(I)-nitroazolates

3.1 Introduction

Many copper containing energetic materials are known such as $Cu(N_3)$,[1] $Cu(N_3)_2$,[2-6] polyazido cuprates,[7] and $[Cu_2(dmpz)(N_3)_2]_n$.[8] Copper azolates have also seen attention as they appear to have a fortuitous combination of energy density and chemical stability. Apart from the aforementioned Cu(NT) (DBX-1),[9] and $Cu_3Cl(NT)_2$ (DBX-X),[10] there are copper-containing energetic metal-organic framework (MOF, defined as a one-, two- or three-dimensional coordination network held together by bonds between metal cations and organic linker ligands) structures such as $Cu(NTZ)(N_3)(solv)]_n$,[11] tetraamminebis(3,5-dinitro-1,2,4-triazolato-N1)copper(II),[12] hydronium copper(II) tris(5-nitrotetrazolate) trihydrate[13] ($[Cu(N_3)_2$(1-methyl-5H-tetrazolyl)],[14] as well as $Cu(N_3)_2(L)_n$ containing a series of azolate groups.[15] Notably, most research has concerned the Cu (II) azolates with Cu(I) azolates less well researched. As previously discussed, copper 5-nitrotetrazolate (DBX-1) shows advantageous properties regarding its long-term stability, sensitiveness, specific volume and energy density making it a viable alternative to lead azide.[9] However, the difficulties in its synthesis (vide supra) and the recent discovery of $Cu_3(NT)_2(Cl)$ (DBX-X), a compound possessing high sensitiveness towards impact, raises questions regarding its suitability for large industry scale synthesis.[10] Therefore, efforts turned towards the formation of novel energetic Cu(I)-azolates as shockwave generating (**See Introduction, 1.3: Primary Explosives**), DBX-1 alternatives as this could result in the formation of coordination compounds with detonation properties matching or exceeding those of DBX-1 and $Pb(N_3)_2$ whilst also having a more straightforward synthesis. A list of targetable Cu(I)-azolates was developed according to some key principles:

1. Pro-ligands must have facile, well detailed synthetic procedures available
2. All pro-ligands must have shown the ability to form alkali metal salts that can be readily purified through common laboratory methods or have readily deprotonatable sites for novel alkali metal salt formation

3. Ligands should have previously shown the ability to form highly thermally stable salts of coordination compounds
4. Ligands should be of a similar size to nitrotetrazolate while also displaying a similar number of coordination sites. This is to hopefully form similar water insoluble coordination polymers
5. Ligand should have proven energetic character through either calculation or the use of said ligand in forming energetic compounds
6. Ligands cannot show sensitivity to light or air exposure
7. Salts/energetic compounds of the ligands should have shown the appropriate sensitiveness towards impact/friction/ESD expected of primary explosives

The known dinitroazolates fit all the above criteria. Dinitrotriazoles,[16] dinitroimidazoles[17-20] and dinitropyrazoles[21-24] have been investigated heavily as energetic materials as they feature explosophoric group properties akin to those of nitrotetrazole. Seven dinitroazoles as their sodium/potassium salts were chosen for the attempted formation of Cu(I) compounds (**Figure 3.1**). As for 5-nitrotetrazole, 2,4/4,5-dinitroimidazole (2,4-DNI/4,5-DNI), 3,4/3,5-dinitropyrazole (3,4-DNP/3,5-DNP), 3,5-dinitro-1H-1,2,4-triazole (3,5-DNT) and 4-amino-3,5-dinitropyrazole (ADNP)[25] have known and well-defined syntheses, proven ability to form alkali metal salts, have been proven to form highly energetic compounds of high thermal stability and possess a similar size to nitrotetrazole whilst also having multiple coordination sites/modes available to them which hopefully will result in the formation of 3D coordination polymers. Tetranitrobisimidazole (TNBI) was also targeted alongside these dinitroazolates as it shares many of these targeted characteristics.[26]

Research Questions

- Can novel Cu(I)-nitroazolates be formed when their respective sodium/potassium salts are used as an alternative to nitrotetrazolate in the Cu(II)/Cu(I) reduction?

- Do these novel Cu(I)-nitroazolates possess explosive properties and stabilities that match or exceed DBX-1?

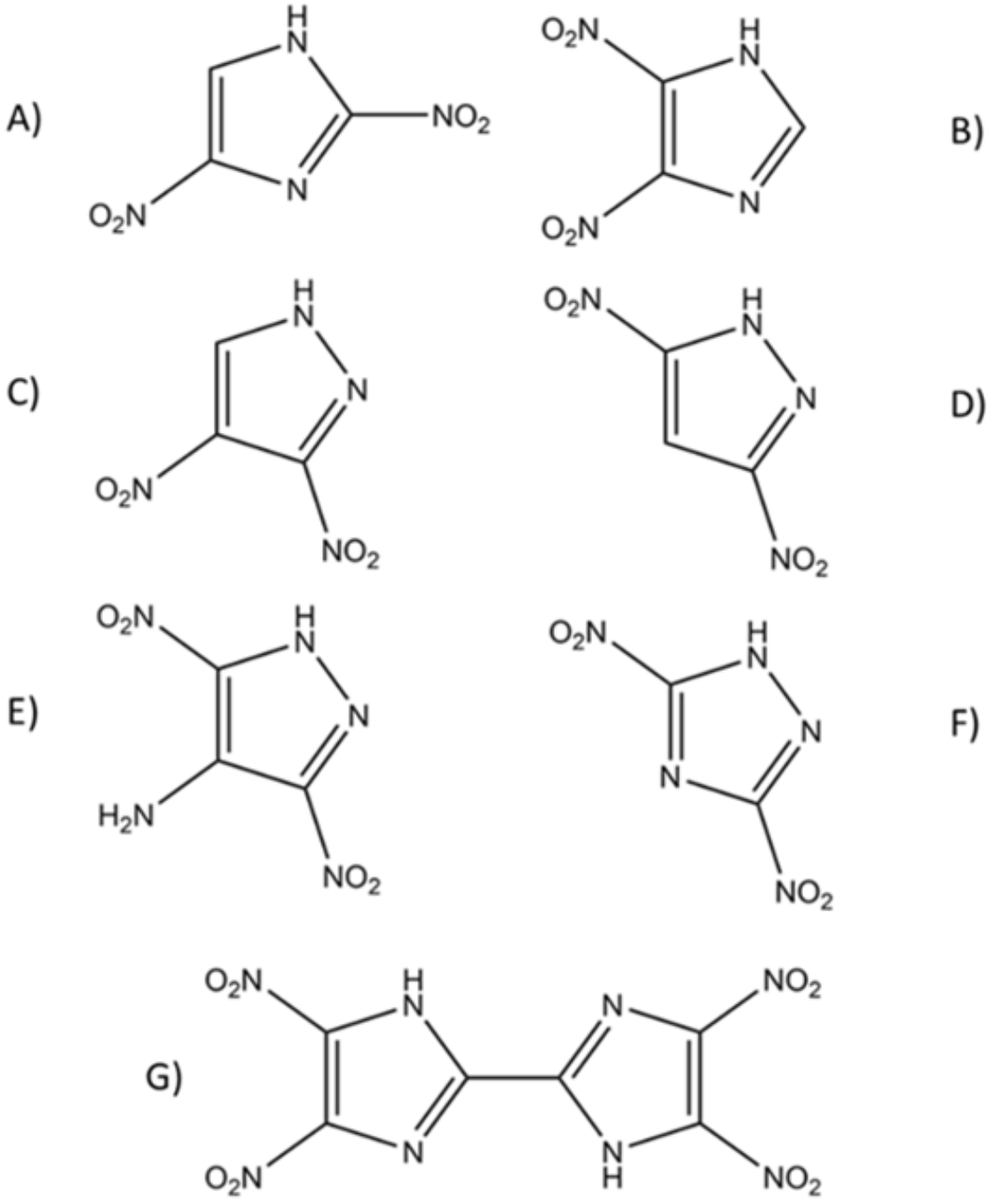

Figure 3.1: *Nitroazoles targeted for replacement of 5-nitrotetrazole in the Cu(II)/Cu(I) reduction reaction used to form DBX-1, A= 2,4-dinitroimidazole (2,4-DNI), B= 4,5-dinitroimidazole (4,5-DNI), C= 3,4-dinitropyrazole (3,4-DNP), D= 3,5-dinitropyrazole (3,5-DNP), E= 4-amino-3,5-dinitropyrazole (ADNP), F= 3,5-dinitro-1H-1,2,4-triazole (3,5-DNT), G= tetranitrobisimidazole (TNBI)*

3.2 Results and Discussion

3.2.1 Synthesis of $Cu(I)_4(DNT)_3Cl$

Dinitrotriazolate (DNT) was the first nitrotetrazolate alternative identified in this project. Its high nitrogen content, perfect oxygen balance and similarity to nitrotetrazolate (one ring nitrogen replaced by a C-NO_2 unit), led to the conclusion that DNT had the best chance of forming a viable alternative to DBX-1. Sodium-3,5-dinitro-1,2,4-triazolate was synthesised according to the method of Liu et al. (**Figure 3.2**). [27]

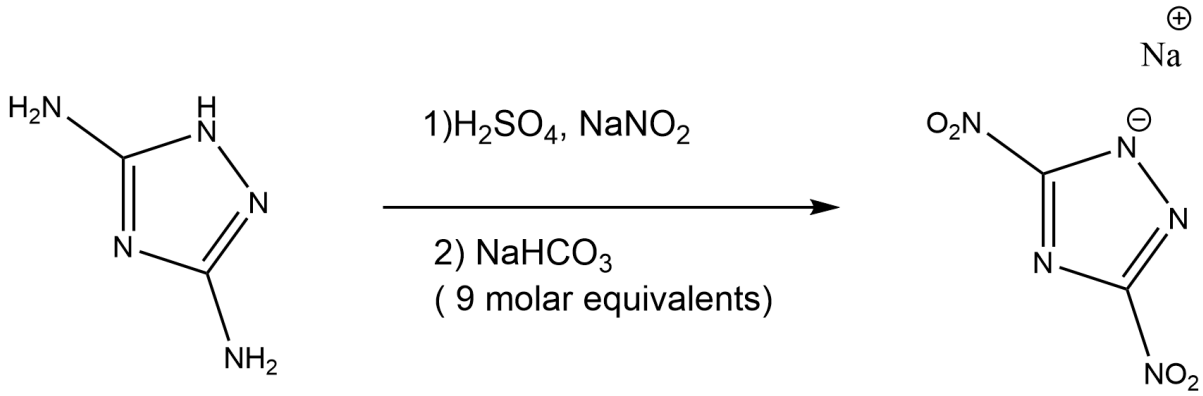

Figure 3.2: *Reaction to form sodium-dinitrotriazolate, synthesis reported in ref[27]*

This allowed for isolation of the crude sodium-dinitrotriazolate (NaDNT). Crystalline NaDNT.2H2O was formed according to the methods of Haiges.[16] Na-DNT was proven to be present as its dihydrate by comparison of absorption band position in a FTIR recorded in Sheffield to that reported by Haiges.[16] This compound was then used in the Cu(II)/Cu(I) reduction reaction used for synthesis of DBX-1 and DBX-X (**Figure 3.3**). Addition of an aqueous solution of NaDNT.$2H_2O$ to an aqueous solution of $CuCl_2$ resulted in the formation of a clear green solution. Addition of an aqueous sodium ascorbate solution at 90 °C resulted in the precipitation of a wine-red coloured solid. The colour of the precipitate was consistent throughout the entire reaction time of 14 minutes. The precipitate was filtered and washed with both water and isopropanol (IPA) to afford a wine-red coloured micro crystalline solid. FTIR spectra of Na-DNT.$2H_2O$ and the reaction product were compared to look for signs of substitution of Cl^- for DNT.

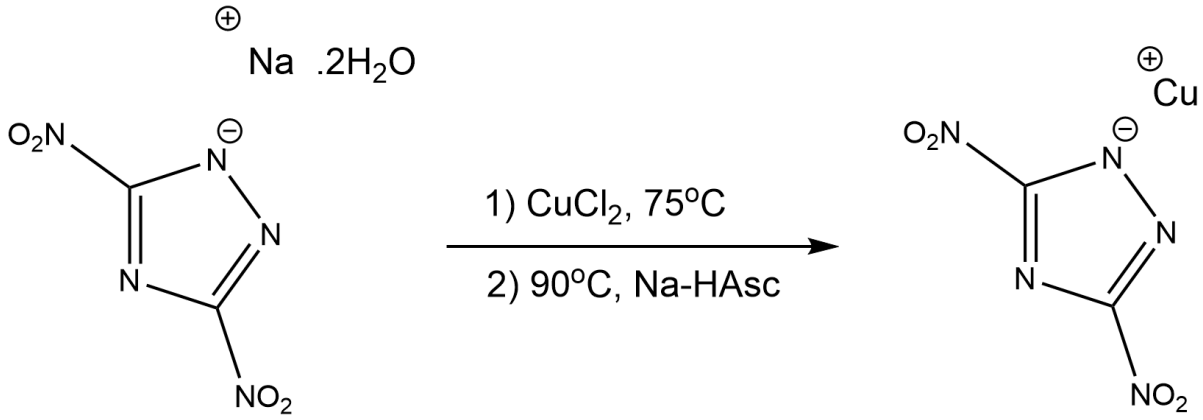

Figure 3.3: *Reaction scheme for the attempted synthesis of CuDNT*

3.2.2 Vibrational Spectroscopy

NaDNT.2H_2O has strong absorption from the stretching vibrations of H_2O present in the crystal at 3564, 3369 and 3262 cm^{-1}. The H_2O bend can also be viewed at 1646 cm^{-1}. These absorption bands have completely disappeared from the spectrum of the wine-red precipitate apart from a very low intensity peak at 1650 cm^{-1} which could be a weak ring vibration previously masked by the H_2O bending absorption. These observations confirm that the wine-red product crystallises as a water free compound. NaDNT has absorption bands associated with the stretching modes of the NO_2 group at 1550 (Asymmetric NO_2 stretching vibration, $\nu_{as}(NO_2)$), 1541 ($\nu_{as}(NO_2)$), 1394 (Symmetric NO_2 stretching vibration, $\nu_{sym}(NO_2)$) and 1377 ($\nu_{sym}(NO_2)$) cm^{-1}. Large changes to the absorption bands assigned to the symmetric stretching vibration can be seen in the spectrum of the wine-red precipitate with two bands at 1394 and 1377 cm^{-1} coalescing into a much broader single band found at 1376 cm^{-1} with a noticeable shoulder at 1366 cm^{-1}(likely to be a ring vibration as a similar band is found in the spectrum of NaDNT.2H_2O) (**Figure 3.4**). Likewise similar changes can be found for the $\nu_{as}(NO_2)$ stretching vibration. Formation of a new band at 1562 cm^{-1} and a general broadening of the bands in this region of the spectrum are observed. Two absorption bands at 1108 and 1053 cm^{-1} are present in the spectrum of NaDNT.2H_2O. The loss of these bands in the spectrum of the wine-red solid could indicate the loss of a 'Charged' NO_2 group (See Introduction, **IR spectroscopic properties of the -NO_2 group**) but as this phenomenon has not been observed in nitrotriazoles before this is speculative band assignment. Absorption bands for the NO_2 bending mode can be found in both spectra with little

difference in band shape and intensity but for a relative increase in intensity of the band at 846 cm^{-1} versus the band at 826 cm^{-1}. Ring vibrational absorption bands can likewise be found in both spectra with small shifts in wavenumber found for almost all bands. Overall, the analysis indicates that the dinitrotriazolate moiety is still present in the wine-red compound but changes to the absorption bands assigned to NO_2 stretching vibrations along with shifts in ring vibrations indicates a change in the bonding present within the DNT moiety as one would expect upon going from a predominantly ionically bound compound (NaDNT) to that of a covalently bound compound (CuDNT). The crystal structure of the compound was investigated to definitively prove the identity of the wine-red solid.

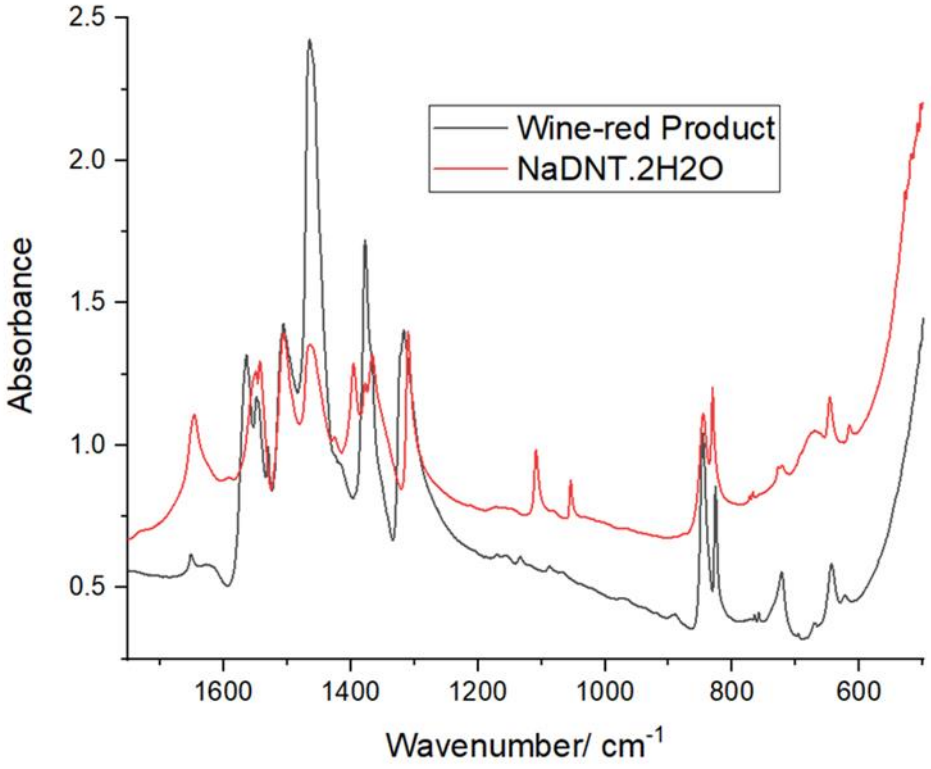

Figure 3.4: *Series of FTIR spectra in the range 1750-500 cm^{-1}, Black= Product of the reaction intended to form CuDNT, Red= NaDNT.2H_2O*

3.2.3 SEM and structure determination of $Cu_4(DNT)_3Cl$

SEM images were recorded to determine the size of the crystals in the wine-red crystalline powder. SEM images showed that the compound crystallised as kite shaped single crystals with the largest crystals found to be approximately 10 microns in length (**Figure 3.5**).

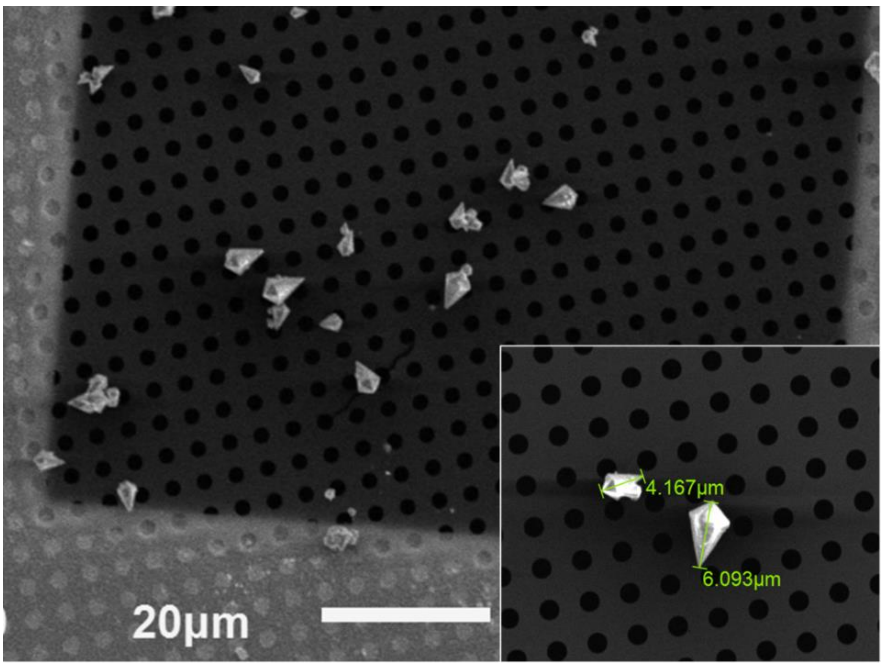

Figure 3.5: *SEM images of the wine-red crystalline product*

The structure of the wine-red solid was confirmed following a partial structure determination from a single crystal followed by subsequent structure solution from Rietveld fitting of the recorded PXRD pattern. Structure determination confirmed that, rather than the 1;1 CuDNT compound we had in fact synthesised $Cu_4(DNT)_3Cl$. $Cu_4(DNT)_3Cl$ crystallises in the P 6_3 space group. Crystalline $Cu_4(DNT)_3Cl$ is composed of copper, chlorine and 3,5-dinitrotriazolato moieties which are distributed over two, one and one unique crystallographic sites in the stoichiometric ratio of 4 : 1 : 3, respectively (**Figure 3.6**). These ratios, alongside the measured magnetic properties, imply that copper is exclusively present in the oxidation state +1. Copper is coordinated in two chemically distinct crystallographic sites. Cu (1) is coordinated in a slightly distorted tetrahedron to one ring nitrogen from three dinitrotriazolato moieties and to one chlorine forming a $Cu(\kappa(N1)\text{-}DNT)_3Cl$ unit. Cu(2) is present as a 3 coordinate “T” shaped moiety with bonds to N(2) and N(3) or DNT and one bond to chlorine. For each Cu(1) tetrahedral unit there are 3 associated “T” shaped Cu(2) units. The dinitrotriazolato moiety is present in only one crystallographically independent site. All ring nitrogens take part in the bonding with the adjacent N(1) and N(2) bridging between Cu(1) and Cu(2) respectively. The third ring nitrogen atom (N (3)) on each DNT ligand links to the next $Cu_4Cl(DNT)_3$ unit. Bonds from N(1)

to Cu(1) and N(3) to Cu(2) are of a similar length (1.933 vs 1.942 (1) Å) with the bond from N(2) to Cu(2) being substantially shorter at 1.847(2) Å. Chlorine is present only in a distorted trigonal bipyramidal coordination geometry. Each chloride binds to three T-shaped Cu coordination centres and one distorted tetrahedral Cu centre. The Cu-Cl distance changes depending on the coordination geometry with the T-shaped Cu-Cl distance (ca. 2.66 Å) being longer than that of the pseudo tetrahedral Cu-Cl distance (ca. 2.54 Å). While in $NaDNT.2H_2O$[16] the nitro groups sit almost co-planar with the ring, upon coordination to Cu both nitro groups are twisted out of plane by 8.8° and 25.96° degrees. The internal bond distances of dinitrotriazolate also all change with all ring bond distances increasing in $Cu_4(DNT)_3Cl$ compared to $NaDNT.2H_2O$ and both nitro group C-N bond distances becoming substantially shorter on coordination to Cu. N-O bond distances also change in each nitro group with N(5)-O(3) becoming slightly longer and N(4)-O(20) becoming substantially shorter and N(5)-O(4) becoming shorter and N(4)-O(1) becoming longer than in $NaDNT.2H_2O$. Comparisons can also be made to DBX-X as the only other Cu(I) azolate-chloride coordination compound known.[10] $Cu_4(DNT)_3Cl$ has on average much longer Cu-Cl bonds (2.538-2.657Å) than DBX-X (2.245-2.622Å). Cu-Cl bonds from the “T” coordinated Cu atoms have a Cu-Cl bond length (2.657Å) comparable to that of the Cu-Cl found in DBX-X where the Cu is coordinated in manner C (See **2.2.7 Structure determination of $Cu_3(NT)_2Cl$**). Tetrahedrally coordinated Cu in $Cu_4(DNT)_3Cl$ result in a Cu-Cl bond (2.538Å) of similar length to that found in DBX-X where Cu is found to be in coordination mode D. $Cu_4(DNT)_3Cl$ features nitro groups which are twisted to a greater degree out of plane of the ring(8.80-21.7°, 15.01-25.96°) than those found for the nitrotetrazolate found in DBX-X (6.85-8.11°, 11.96-13.7°). This could be due to the greater steric demands of two $C\text{-}NO_2$ groups versus the one found in DBX-X. This can be seen in the space filling model of $Cu_4(DNT)_3Cl$ which shows the close packing nature of the $C\text{-}NO_2$ groups thus requiring a greater twist out of plane to accommodate the $C\text{-}NO_2$ groups of neighbouring DNT ligands. $Cu_4(DNT)_3Cl$ also features much shorter C-N bonds for each $C\text{-}NO_2$ unit (1.257-1.347 Å) than that of DBX-X (1.434-1.457 Å). This could indicate that the $C\text{-}NO_2$ of DBX-X is much closer to the transition state for decomposition with regards to loss of NO_2 than $Cu_4(DNT)_3Cl$.

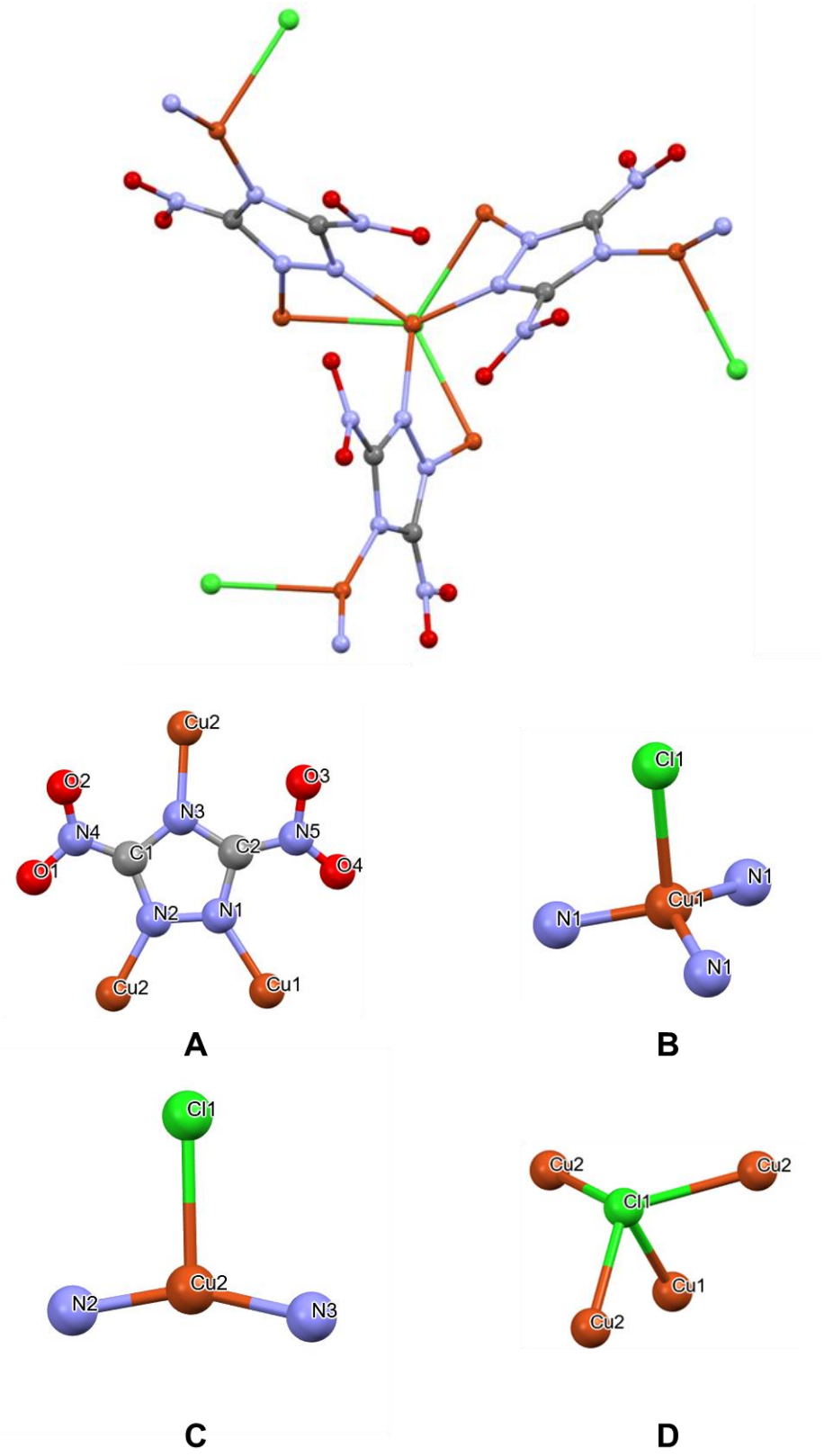

Figure 3.6: *Projections of the thermal ellipsoids in the molecular structure of the crystals of $Cu_4(DNT)_3Cl$ (set at the 67% probability level) showing the bonding present in the crystal (top) and the DNT, Cu and Cl binding environments*

3.2.4 Synthesis of Cu(I)-dinitropyrazolato compounds

3,4-dinitropyrazole, 3,5-dinitropyrazole were proposed as candidate ligands for use in the Cu(II)/Cu(I) reduction reaction. Efforts were made to synthesise these proposed pro-ligands before deprotonation and purification to isolate them as their alkali metal salts, ready for use in the Cu(II) reduction reaction. 3,4/3,5-DNP were synthesised according to the published procedures.[21][22]Na-3,5-DNP.2H_2O was formed according to a synthesis published by Klapotke et al. (**Figure 3.7**).[21] Product identity was proven by comparison of the unit cell data, FTIR and $^{1}H/^{13}C$ NMR to the values reported by Klapotke et al.[21]

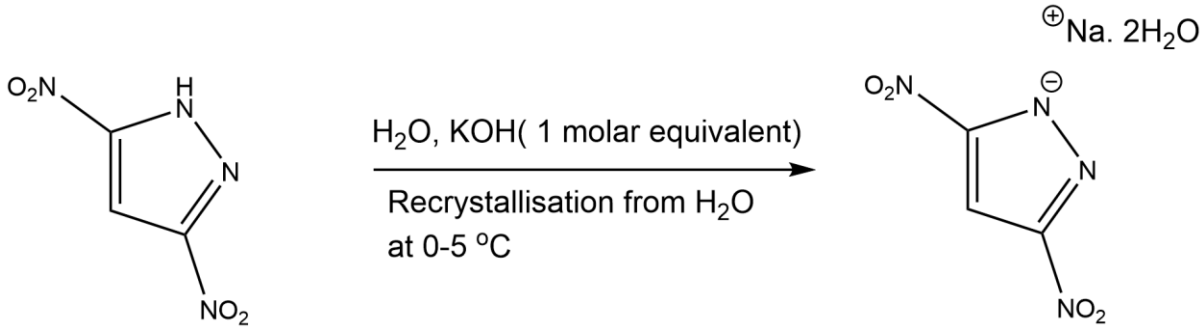

Figure 3.7: Synthesis of Na-3,5-DNP.2H_2O

3.2.5 Synthesis of Cu(I)-3,5-DNP

Na-3,5-DNP.2H_2O was used in the synthesis of Cu-3,5-DNP. Cu-3,5-DNP was synthesised using the same procedure as that used for DBX-1 (**Figure 3.8**). Addition of an aqueous solution of Na-3,5-DNP.2H_2O to an aqueous solution of $CuCl_2$ resulted in the formation of a clear green solution. Addition of an aqueous sodium ascorbate solution at 90 °C resulted in the precipitation of an orange coloured solid. The colour of the precipitate was consistent throughout the entire reaction time of 14 minutes. The precipitate was filtered and washed with both water and IPA to afford an orange coloured micro crystalline solid.

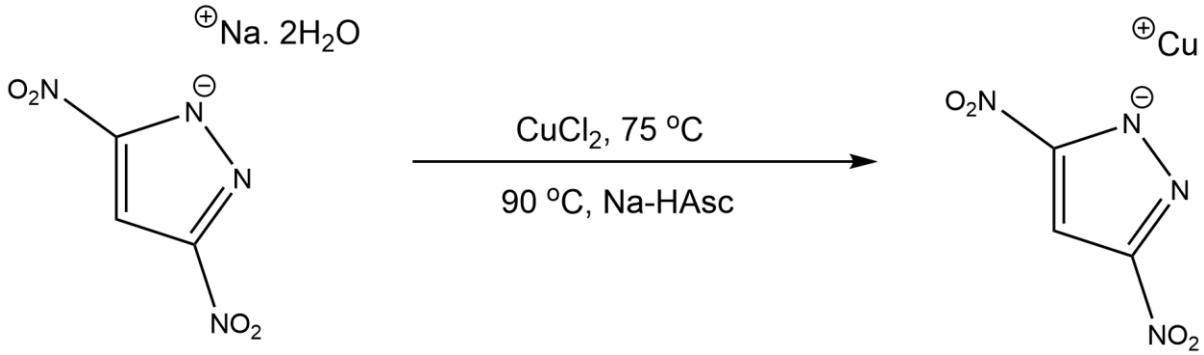

Figure 3.8: *Synthesis of Cu-3,5-DNP*

3.2.6 Vibrational Spectroscopy

FTIR spectra of Na-3,5-DNP.2H_2O and the orange reaction product were compared to look for signs of substitution of Cl^- for DNP (**Figure 3.9**). Observations upon reaction with $CuCl_2$ and Na-HAsc are similar to that seen for $Cu_4(DNT)_3Cl$. All absorption bands assigned to H_2O stretching and bending modes are not present in the spectrum of the product. The C-H stretch of the 3,5-dinitropyrazolato moiety can be found in the spectra of both product and Na-3,5-DNP.2H_2O. Absorption bands assigned to ring vibrations are found to shift in wavenumber but it general are still present in the FTIR spectrum of the orange reaction product. Bands in the region 1550-1500 cm^{-1} assigned to $\nu_{as}(NO_2)$ are now found in the region 1570-1550 cm^{-1} and have broadened. The band at 1356 cm^{-1} is split and now appears at 1369 and 1343 cm^{-1}. The NO_2 symmetric bend can also still be found in the spectrum of the orange product with little change to band position. Overall, the FTIR spectra point to the 3,5-DNP moiety being present in the product. With the precipitation of a water insoluble compound as seen for other Cu(I) nitroazolates, the product was tentatively assigned as water free, Cu-3,5-DNP.

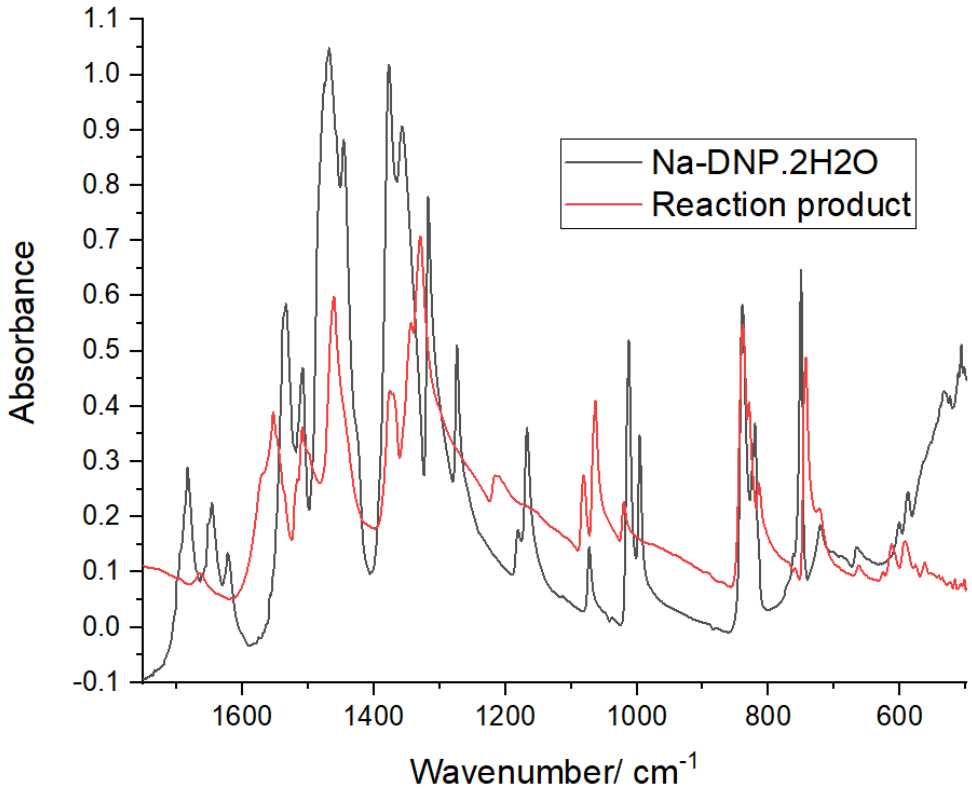

Figure 3.9: *Series of FTIR spectra in the range 1750-500 cm^{-1}, Black = Na-3,5-DNP.2H$_2$O, Red = Reaction product of the attempt to form Cu-3,5-DNP*

3.2.7 SEM and crystal structure determination

Crystal structure determination was used to determine the reaction product. When the orange crystalline product was observed under a microscope, two crystal types were observed: large yellow crystals as the minor product and smaller orange crystals forming the bulk of the solid. SEM images were recorded to determine crystal size (**Figure 3.10**). SEM shows the smaller orange crystals had formed as rectangular rod-shaped crystals with the yellow crystals present as large irregularly shaped plates. Both of the crystal types were investigated with SCXRD. The structure solution obtained for the small orange crystals proved that they were Cu-3,5-DNP (**Figure 3.11**). Cu(I)-3,5-DNP crystallised in the space group P2$_1$/c. Cu(I)-3,5-DNP is made up of two crystallographically independent 3,5-dinitropyrazolte units and two crystallographically independent Cu(I) cations bound together to form an infinitely extending 3D coordination polymer. Cu1 binds to three nitro group oxygens and two ring nitrogens in a heavily distorted square pyramidal coordination geometry.

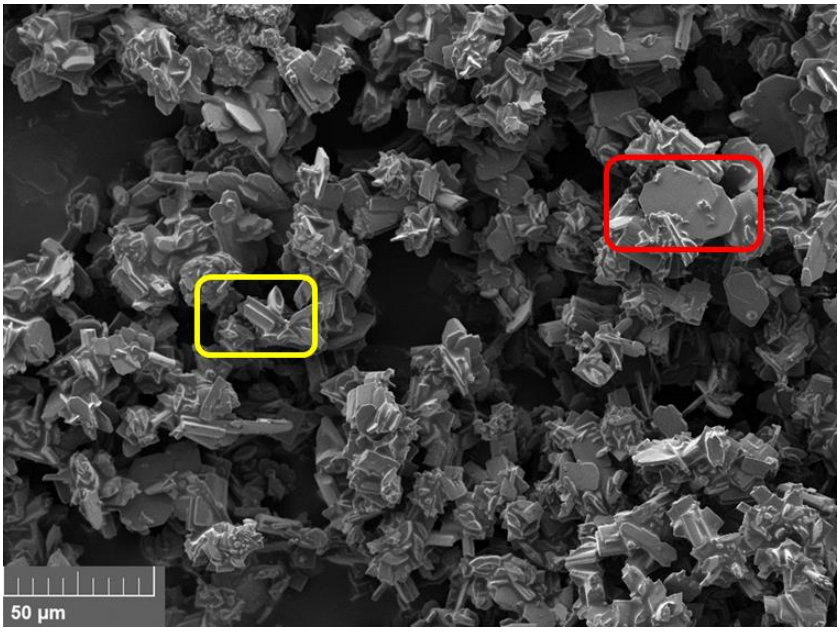

Figure 3.10: *SEM Images of the reaction product obtained in attempts to form Cu-3,5-DNP, small orange rod crystals show by yellow box, large yellow plate crystals show in red box*

The base of the square pyramid is formed from two non-related 3,5-DNP units which chelate the metal centre through κ2 coordination modes. Ring nitrogens bind to the metal centre with Cu-N bond lengths of 1.862-1.892. Oxygen from a nitro group, bound to the carbon atom adjacent to the binding ring nitrogen, also bind to the same Cu completing the κ2 coordination mode. A third oxygen atom, found on the nitro group adjacent to the ring nitrogen not involved in coordination to Cu1, binds to Cu1 to form the square pyramid. The base of the square pyramid is heavily distorted with O-Cu-N bond angles of 67.44-69.29°. The O2-Cu-N3 bond is also distorted away from that expected for a square pyramid with an angle of 105.49. Cu2 is found to have a coordination number of three and is found in a heavily distorted trigonal planar geometry not too dissimilar from the T-shaped coordination geometry found for one of the Cu atoms in $Cu_4(DNT)_3Cl$. Two bonds are formed to ring nitrogens with one bond also formed to an oxygen atom of a nitro group adjacent to one of the binding nitrogen atoms once again forming a chelating κ2 coordination mode. Cu-N distances are consistent for both nitrogens at 1.900Å. Coordination to Cu2 serves to bind neighbouring Cu1 based square pyramids to each other allowing for the 3D coordination polymer to form. 3,5-DNP can be found in one of two coordination environments in the crystal.

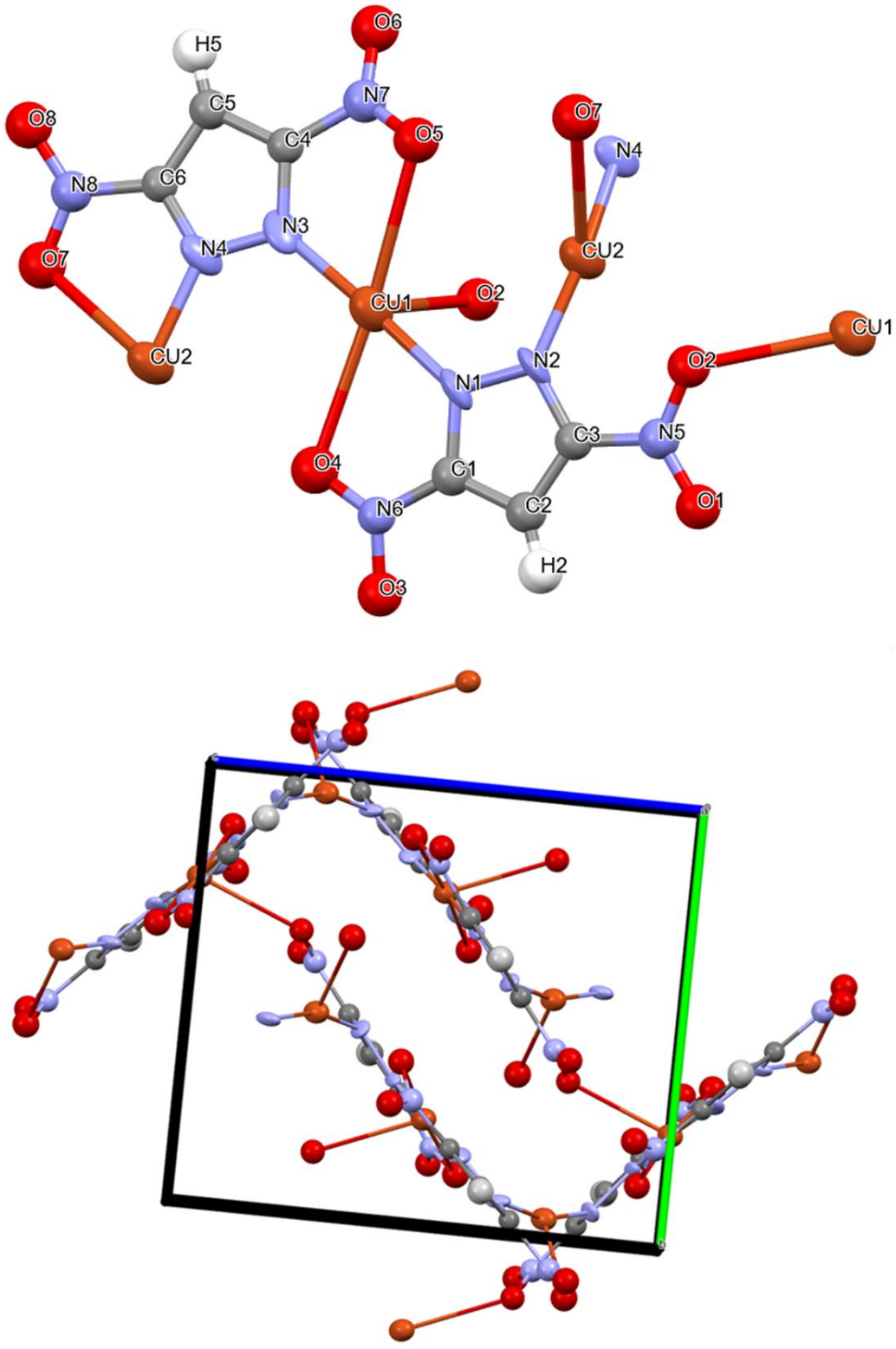

Figure 3.11 : *Crystal structure of Cu-3,5-DNP, Cu and N atoms modelled anisotropically (ellipsoids set at the 67% probability level), all other atoms modelled isotropically (Top), Unit cell packing (Bottom)*

Both 3,5-DNP units bind to Cu1 only through ring nitrogen N1 with ring nitrogen N2 forming bonds only to Cu2. For each unit O4 binds to the Cu centre whereas O2 differs depending on which of the unique 3,5-DNP units it originates from. For one of the units O2 forms the final bond of the square pyramid formed from the bonds to Cu1, for the other it binds to Cu2 and form the k2 coordination mode. For both crystallographically independent 3,5-DNP moieties, O1/O3 are not involved in any significant bonding to any of the other atoms present. The degree of out of plane twist of each nitro group also differs between moieties. 3,5-DNP A has twists out of plane of 10.64-15.44° whereas 3,5-DNP B has twists out of plane of 4.62-9.28°

The larger yellow crystals proved to diffract poorly and only a low-quality structure could be obtained with most atoms non-positive definite (NPD) (NB: Non-positive definite atoms are defined as a physically impossible state in which one or more of the atomic displacement parameters have become negative during refinement). The large yellow crystals were identified as 1-methyl-4-hydroxy-3,5-dinitropyrazole (1-M-4H-3,5-DNP) (**Figure 3.12**). Hydrogen atoms could not be located on either the methyl or hydroxy group. The mechanism by which this by product forms is currently not understood.

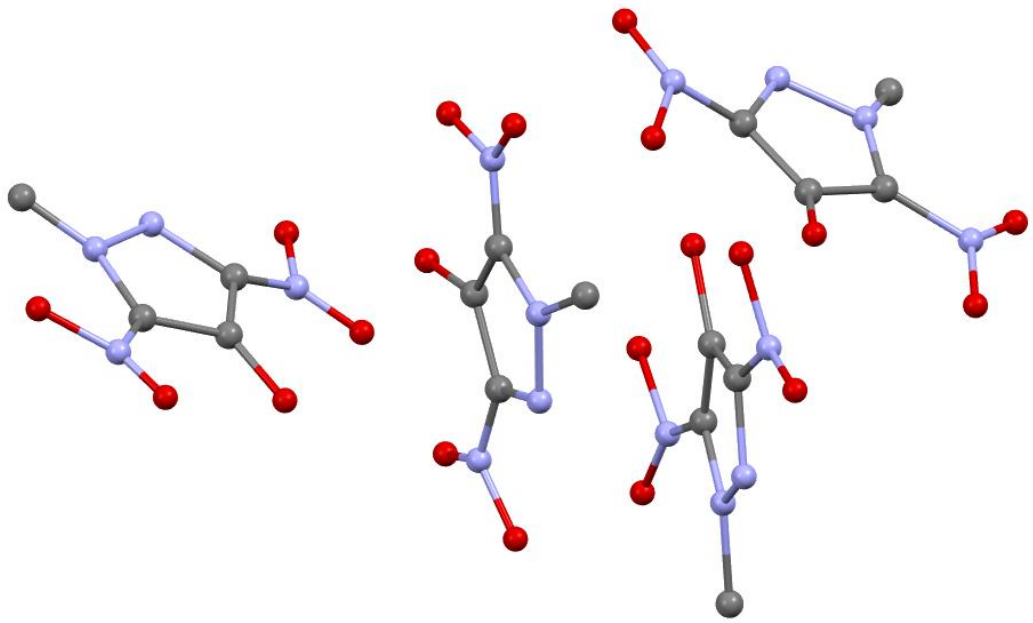

Figure 3.12: *Ball and stick diagram of the crystal structure of 1-methyl-4-hydroxy-3,5-dinitropyrazole*

3.2.8 Elemental Analysis

Knowing that two products are formed during the reaction, elemental analysis was used to determine the ratios of the two products.

		C%	H%	N%
	Found	17.10	0.54	25.23
Cu-3,5-DNP	**Expected**	16.33	0.46	25.40
	Difference to found	-0.77	-0.08	0.17
1-M-4H-3,5-DNP	**Expected**	20.46	2.29	31.82
	Difference to found	3.36	1.75	6.59
96%(Cu-3,5-DNP): 4% 1-M-4H-3,5-DNP	**Expected**	16.50	0.53	25.66
	Difference to found	-0.60	-0.01	0.43

Table 3.1: *Elemental analysis results for Cu-3,5-DNP*

The elemental analysis clearly shows that the product is neither pure Cu-3,5-DNP nor 1-M-4-H-3,5-DNP, corroborating the findings of the SCXRD studies (**Table 3.1**). Scaled addition of CHN values for the two products was used to determine a crude product composition. The composition with the lowest standard deviation when using the sum of squares of the differences on various formulations of X%(Cu-3,5-DNP): Y% 1-M-4H-3,5-DNP results in the lowest standard deviation for the formulation 96%(Cu-3,5-DNP): 4% 1-M-4H-3,5-DNP. The CHN values for this compound are close to the usually accepted tolerances for elemental analysis (<0.5%) with only C% being slightly over the acceptable tolerance. Tentatively, the product of this reaction is therefore assigned as Cu-3,5-DNP with a 4% minor product of 1-methyl-4-hydroxy-3,5-dinitropyrazole

3.2.9 Synthesis of Cu(I)-3,4-DNP

K-3,4-DNP.2H_2O was synthesised by the reaction of 3,4-DNP with K_2CO_3 in ethanol at room temperature according to the published procedure.[23] Product purity was proven by comparison of unit cell data and ^{1}H and ^{13}C NMR to known values.[23] Pure, crystalline K-3,4-DNP.2H_2O was then used in the Cu(II)/Cu(I) reduction reaction. However, this led to some unexpected results which had not been seen in the other reduction reactions tried so far. Addition of K-3,4-DNP.2H_2O to $CuCl_2$ in water leads to the formation of bright blue precipitate which partially redissolves in 90 °C water (**Figure 3.13**). Addition of NaHAsc leads to the formation of a dark red gel-like material (**Figure 3.13**). Temperature had no effect on the reaction outcome as either reactions at room temperature or at 90°C produced the same reaction product. This product as thought to be a metallogel. Cu(I) metallogels are not unknown in the literature and have been shown for a variety of systems.[28] Inversion of the gel stored in a sample vial resulted in no flow of material towards the bottom of the vial (**Figure 3.13**), this being an important test as the retardation of flow of materials is a key qualitative test for assigning compounds as gels.[28] The solid was not investigated further as an energetic material.

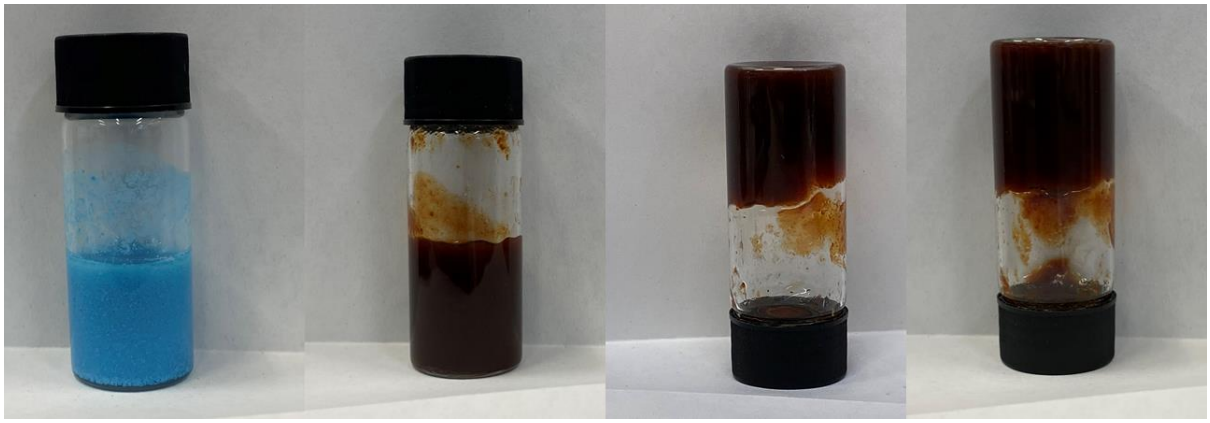

Figure 3.13: *Left: Product formed on addition of K-3,4-DNP.2H_2O to solutions of $CuCl_2$, Left Middle: Product formed on addition of Na-HAsc to solutions of $CuCl_2$ + K-3,4-DNP.2H_2O, Right Middle: Inversion test 1 hours, Right: Inversion test 6 hours*

3.2.10 Synthesis of Cu(I)-Nitroimidazolates

2,4-Dinitroimidazole (2,4-DNI) and 4,5-dinitroimidazole (4,5-DNI) were also proposed as candidate ligands for use in the Cu(II)/Cu(I) reduction reaction. 2,4-DNI was synthesised as detailed by Cho et al. (**Figure 3.14**). [17]

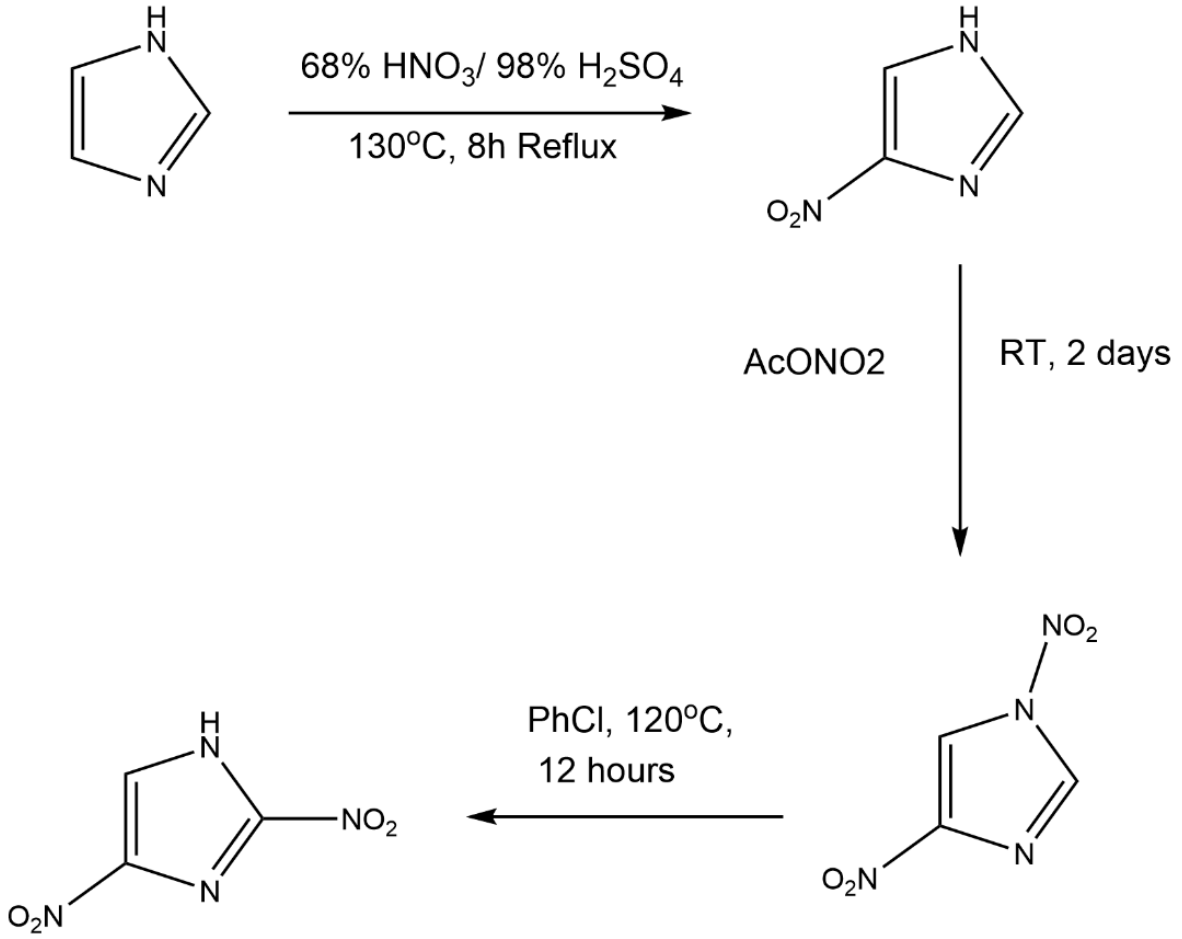

Figure 3.14: *Synthesis of 2,4-DNI*

The potassium salt of 2,4-DNI was synthesised according to the methods of Zhang et al[19]. An aqueous solution of 2,4-DNI was heated to 60 °C at which point an equimolar amount of KOH was added and the solution was stirred for a further hour. Removal of the solvent and recrystallization of the solid remaining in ethanol resulted in the growth of yellow block crystals of anhydrous K-2,4-DNI. Product identity was confirmed by comparison of ^{1}H and ^{13}C NMR to the published data of Zhang et al.[19]

3.2.11 Synthesis of Cu(I)-2,4-DNI

Upon addition of K-2,4-DNI to solutions of $CuCl_2$ at 75 °C, a light blue solution forms. The light blue solution was heated to 90 °C and sodium ascorbate was added under the same addition scheme as used for the formation of previous Cu(I)-nitroazolates (**Figure 3.15**). During the addition a red/orange solid begins to precipitate out and by the end of addition an orange suspension is formed. Filtering and washing with water (2X) and IPA (2X) afforded Cu(I)-2,4-DNI as an orange/red amorphous solid. Product identity was proved by FTIR and elemental analysis.

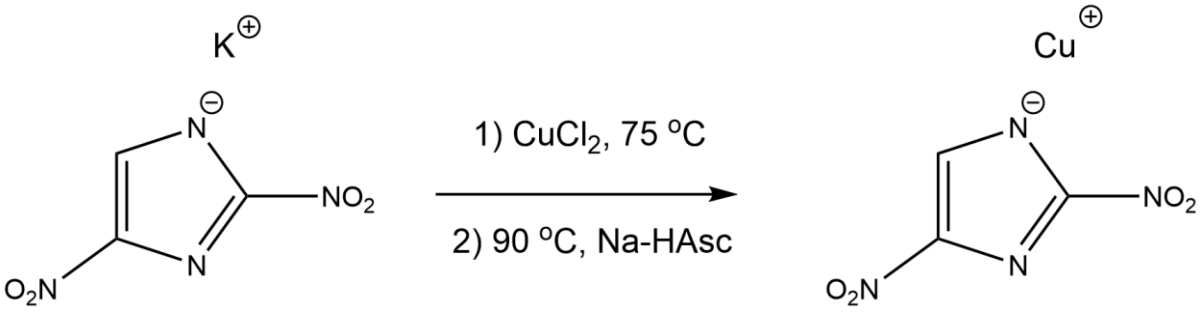

Figure 3.15: *Synthesis to form Cu-2,4-DNI*

3.2.12 Vibrational Spectroscopy

Not discussed in the work of Epishina regarding the infrared spectra of salts of nitroimidazoles, K-2,4-DNI shows differences to the other nitroimidazole salts.[30] No absorption bands indicative of 'charged' NO_2 groups can be observed. These absorption bands are still present in the spectrum of the orange/red reaction product proving them to more likely be ring vibrations. Absorption bands associated with uncharged NO_2 stretching and bending modes can be found in the spectrum of Cu(I)-2,4-DNI further proving this theory. Overall, as the 2,4-DNI moiety appears to be present in the orange/red reaction product analysis of the FTIR spectra help to tentatively assign the product as Cu(I)-2,4-DNI (**Appendix 8.19 and 8.20**). Elemental Analysis was used to confirm product identity.

3.2.13 Elemental analysis

As shown in **Table 3.2**, values for CHN are all within the acceptable tolerances and confirm the product identity as Cu-2,4-dinitroimidazolate. Cu content could not be determined during the timeframe of this project.

	C%	H%	N%
Expected	16.33	0.46	25.40
Found	16.49	0.82	25.26
Difference(Found-Exp)	+0.16	+0.36	-0.14

Table 3.2: *Elemental analysis results for Cu-2,4-DNI*

3.2.14 Synthesis of Cu(I)-4,5-dinitroimidazolate

4,5-Dinitroimidazole (4,5-DNI) was synthesised according to the methods of Katritzky et al (**Figure 3.16**).[18] Unlike 2,4-DNI, 4,5-DNI can be isolated via direct nitration of 4-nitroimidazole.

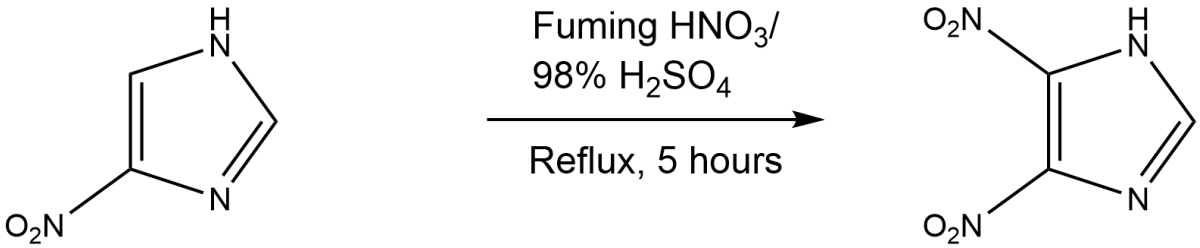

Figure 3.16: *Synthesis of 4,5-DNI*

Product identity was confirmed by comparison of ^{1}H and ^{13}C NMR to the values published by Katritzky.[18] Formation of the potassium salt of 4,5-dinitroimidazole was done according to the methodology of Katritzky.[18] 4,5-dinitroimidazole was dissolved in acetone to give a pale-yellow solution and reacted with potassium carbonate over 24 hours. Following filtration and evaporation of the acetone solution long, rectangular, bright yellow crystals of K-4,5-dinitroimidazolate monohydrate was obtained as confirmed by comparison of the ^{1}H and ^{13}C NMR spectra to reported

values.[18] Pure K-4,5-dinitroimidazolate monohydrate was used in the synthesis of Cu(I)-4,5-DNI (**Figure 3.17**).

3.2.15 Synthesis of Cu(I)-4,5-DNI

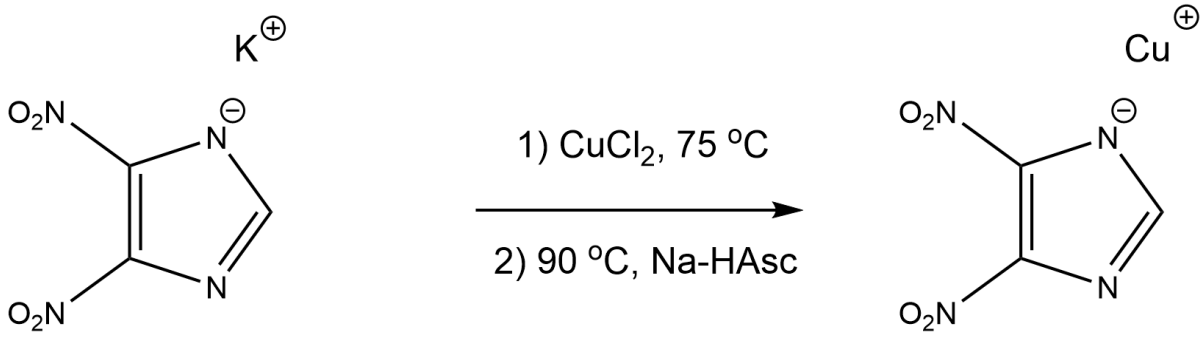

Figure 3.17: *Synthesis to form Cu-4,5-DNI*

Upon addition of K-4,5-DNI to solutions of $CuCl_2$ at 75 °C, a light blue solid precipitated from the solution (presumably the Cu(II) salt of 4,5-DNI). The now light blue suspension was heated to 90 °C and sodium ascorbate was added under the same addition scheme as used for the formation of previous Cu(I)-nitroazolates. During the addition, a colour change from blue to brown could be observed and at the end of the reaction a brown suspension was obtained. Filtering and washing with water (2X) and IPA (2X) afforded Cu(I)-4,5-DNI as a light brown solid. Product identity was proved by FTIR and elemental analysis.

3.2.16 Vibrational Spectroscopy

The band assigned to the C-H stretching mode in K-4,5-DNI.H_2O has both moved to higher wavenumbers and increased in intensity in the spectrum of Cu(I)-4,5-DNI (**Figure 3.18**). As stated previously, K-4,5-DNI has four absorption bands associated with NO_2 stretching modes; 1528 cm^{-1} and 1366 cm^{-1}, associated with the uncharged NO_2 group and 1187 cm^{-1} and 960 cm^{-1}, associated to the charged NO_2 Group. Upon coordination to Cu(I) both absorptions associated with the charged NO_2 group disappear from the spectrum of Cu-4,5-DNI. Instead, the band at 1528 cm^{-1} becomes much broader and features multiple peaks all of a similar intensity. This is indicative of the formation of an uncharged NO_2 group, presumably due to the change in bonding from ionic in K-4,5-DNI.H_2O to covalent in Cu-4,5-DNI. The band

at 1366 cm^{-1} can be seen to become sharper upon coordination to Cu(I). Bands assigned to NO_2 deformation modes can still be seen in the spectrum of Cu-4,5-DNI with both having shifted to lower wavenumbers. Bands associated with ring vibrations are still present in the spectrum of Cu-4,5-DNI with the familiar shifts and intensity changes that accompany coordination to metal centres.

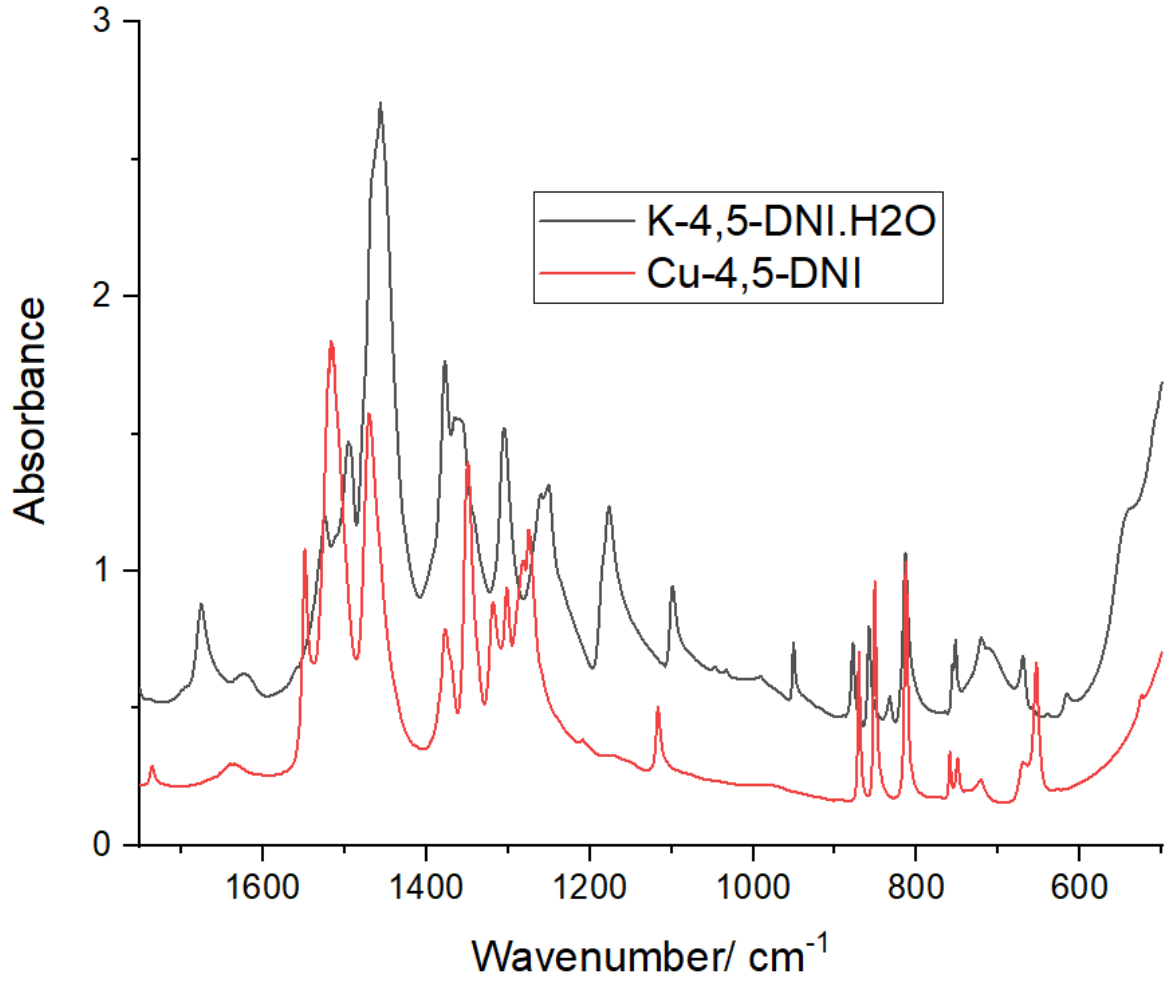

Figure 3.18: *Series of FTIR spectra in the range 1750-500 cm^{-1}, Black = K-4,5-DNI.H2O, Red = Cu-4,5-DNI*

3.2.17 Elemental analysis

	C%	H%	N%
Expected	16.33	0.46	25.40
Found	16.38	0.84	24.94
Difference(Found-Exp)	+0.05	+0.38	-0.46

Table 3.3: *Elemental analysis results for Cu-4,5-DNI*

As shown in **Table 3.3**, values for CHN are all within the acceptable tolerances and confirm the product identity as Cu-4,5-dinitroimidazolate. Cu content could not be determined during the timeframe of this project.

The crystal structure of Cu-4,5-DNI could not be recorded as the crystals proved too small for a dataset to be recorded on the diffractometers present at Sheffield. SEM proves the maximum crystal size to be approximately 10 μm (**Figure 3.19**). PXRD could be recorded for the sample (**Figure 3.20**), however unit cell data has not yet been obtained from the diffractogram

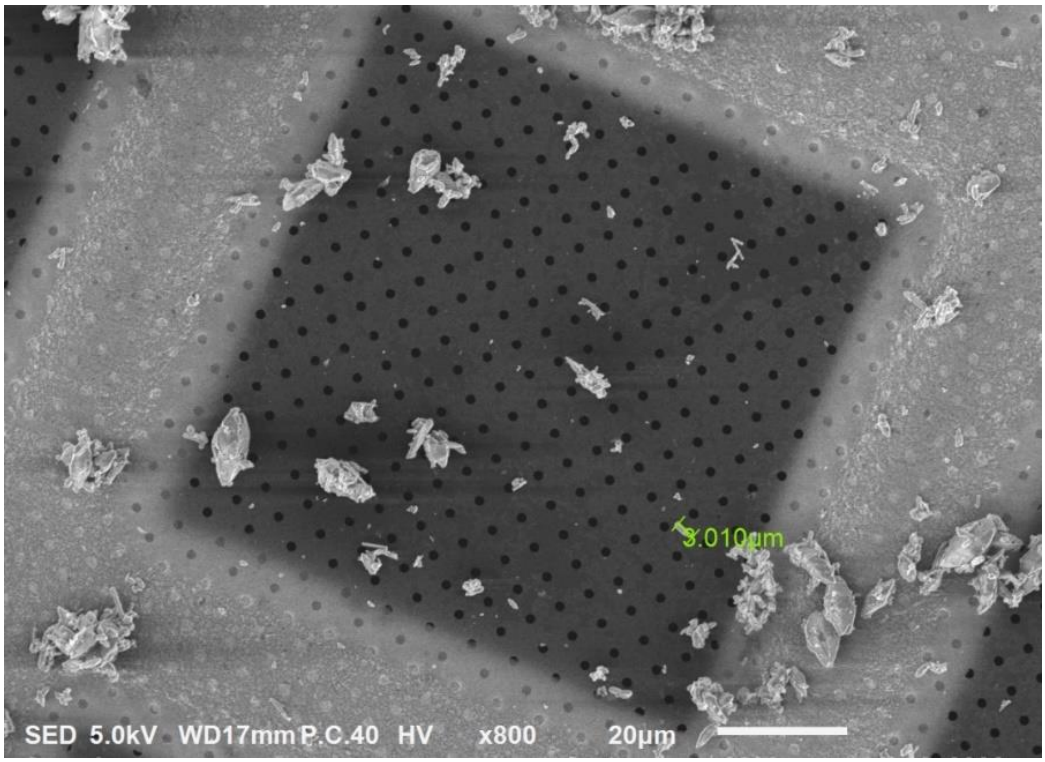

Figure 3.19: *SEM images of Cu-4,5-DNI*

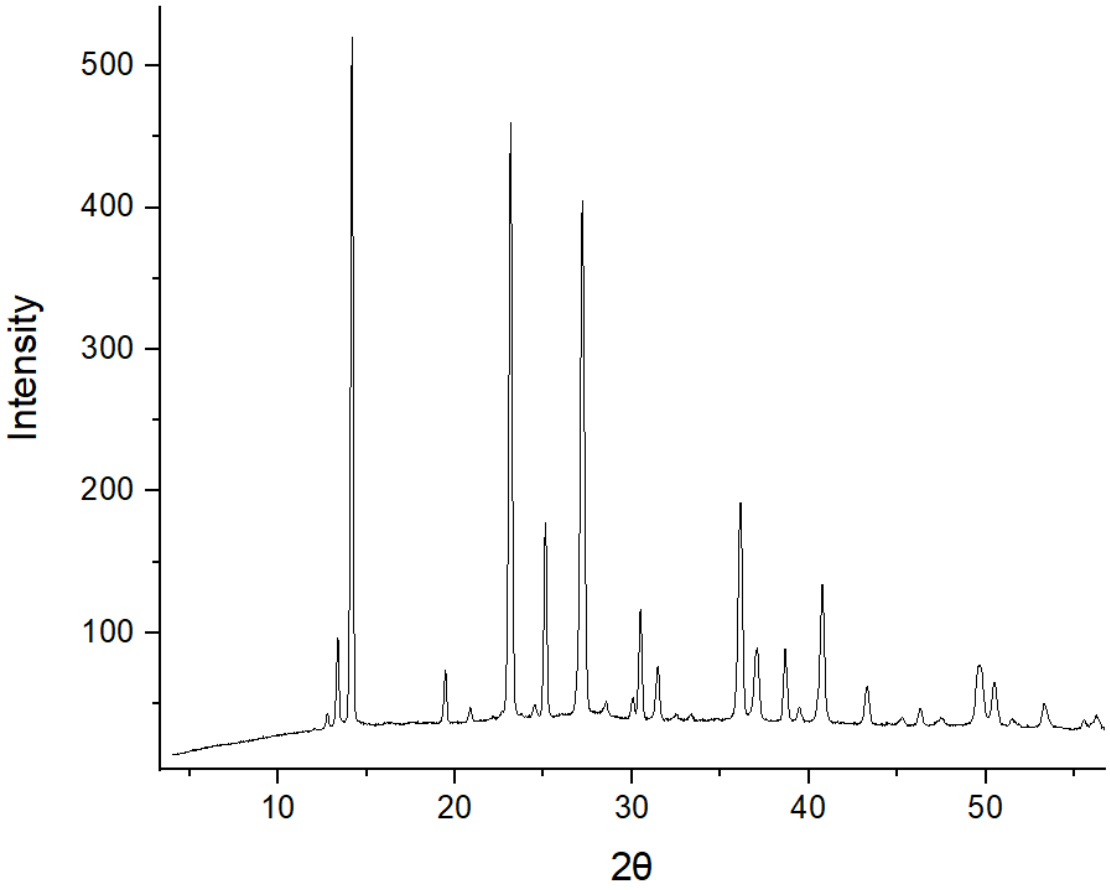

Figure 3.20: *PXRD Diffractogram of Cu-4,5-DNI, recorded in the range 5-60 2Θ*

3.2.18 Synthesis of Cu(I)- 4,4-,5,5-Tetranitro-2,2-bisimidazolate

4,4-,5,5-Tetranitro-2,2-bisimidazole(TNBI) is an energetic compound with little research conducted into its ligand properties.[26] With energetic characteristics similar to that of the dinitroazolates, we elected to use TNBI as its potassium salt in the synthesis of its Cu(I) compound.

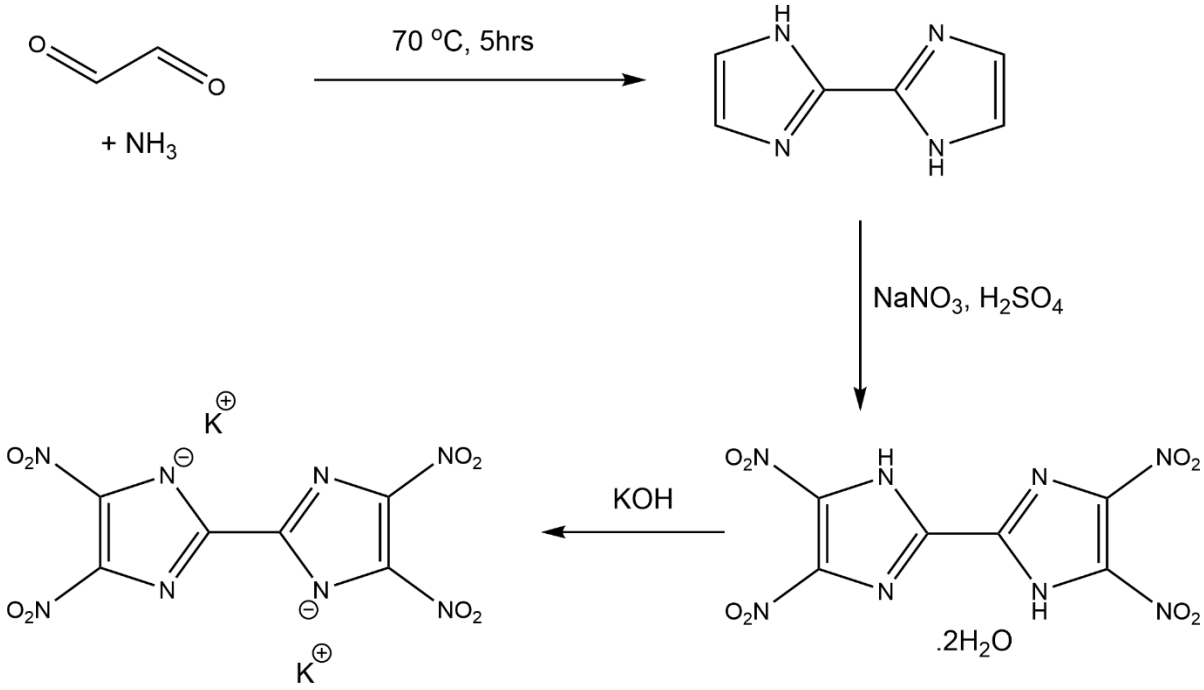

Figure 3.21: *Synthesis of K_2-TNBI*

K_2-TNBI was synthesised according to the published procedure (**Figure 3.21**).[26] Synthesis and purity of K_2-TNBI was confirmed by comparison of ^{1}H and ^{13}C NMR data to published values.[26] With the NMR spectra proving product purity, K_2-TNBI was used in the Cu(II)/Cu(I) reduction reaction (**Figure 3.22**).

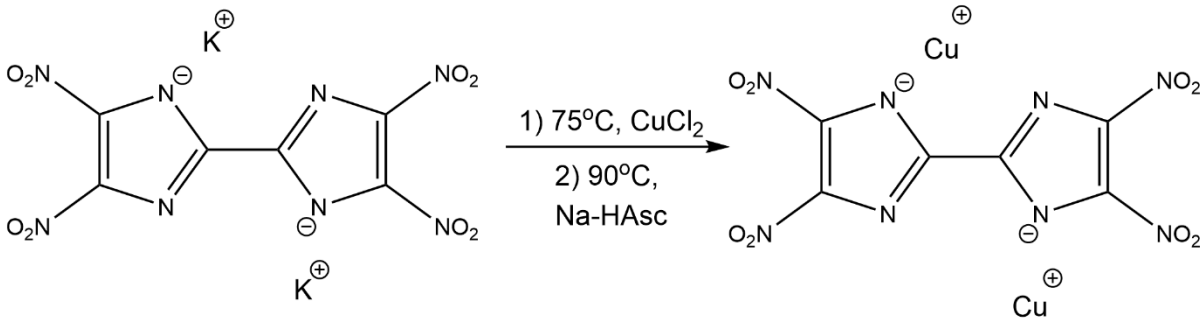

Figure 3.22: *Synthesis attempted to form Cu_2-TNBI*

Addition of an aqueous suspension of K_2-TNBI to an aqueous solution of $CuCl_2$ resulted in the formation of a pale orange suspension. Addition of Na-HAsc under the same addition regime used for previous syntheses resulted in the gradual formation of Cu_2-TNBI as a brown precipitate. The reaction mixture was filtered and washed with both water and IPA to afford a similar coloured micro crystalline solid. Product identity was confirmed by FTIR spectroscopy and elemental analysis.

3.2.19 Vibrational Spectroscopy

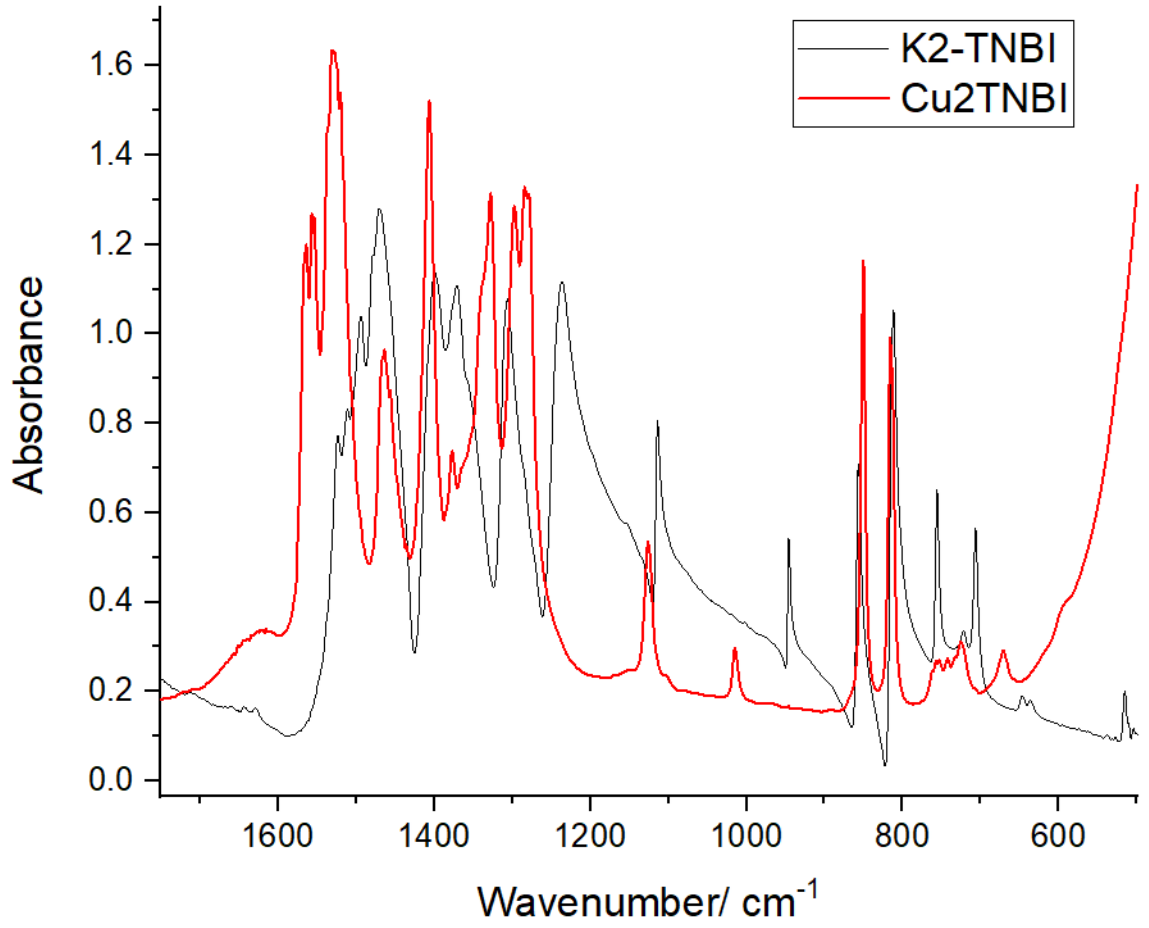

Figure 3.23: *Series of FTIR spectra in the range 1750-500 cm^{-1}, Black = K_2-TNBI, Red = Cu_2-TNBI*

FTIR spectra of potassium salt and product were compared (**Figure 3.23**). K_2-TNBI has the characteristic absorption bands of both charged and uncharged NO_2 groups. The FTIR spectrum of Cu_2-TNBI shows a large increase in intensity of both $\nu_{as}(NO_2)$ and $\nu_{sym}(NO_2)$ for uncharged NO_2 groups. It can also be claimed that both of the

absorption bands of charged NO_2 groups are missing from the spectrum. The reduced intensity and large shift in band position of the absorption band at 1013 cm^{-1} is unlikely to be the shifted $v_{sym}(NO_2)$ and more likely to be a now IR active ring vibration. Likewise, the band at 1124 cm^{-1} is more likely the shift in position of the band at 1153 cm^{-1} than the continued presence of v_{as} of the charged NO_2 groups. Uncharged NO_2 deformation modes likewise see a large increase in intensity, signalling the presence of more uncharged NO_2 groups. This is strong evidence to suggest the substitution reaction has worked and TNBI is now bound to two Cu(I) cations (similar effects seen in formation of both Cu-2,4-DNI and Cu-4,5-DNI). Ring vibrations are seen to shift in wavenumber and some heavily reduce in intensity. Disappearance of an absorption band that could be assigned to an isoimidazole ring (as would be formed with charged NO_2 groups) at 1494 cm^{-1} is yet more evidence (albeit tentative) for the successful substitution of Cl^- by TNBI to form Cu_2-TNBI.

3.2.20 Elemental analysis and Cu content determination

Product identity was conclusively proven by elemental analysis and with copper content analysis by UV/vis spectroscopy.

	C%	**H%**	**N%**
Expected	16.41	0	25.51
Found	16.28	0	25.13
Difference(Found-Exp)	-0.13	0	-0.38

Table 3.4: *Elemental analysis results for Cu_2-TNBI*

C, H and N values are all found to be within the accepted errors (± 0.5%) of the expected values for Cu_2-TNBI (**Table 3.4**). This is strong evidence to suggest formation of Cu_2-TNBI. Cu content was recorded by dissolving a sample of Cu_2-TNBI in 68% HNO_3. This decomposes the solid into H_2TNBI and $Cu(H_2O)_6^{2+}$. $Cu(H_2O)_6^{2+}$ has a strong absorbance in the UV/vis spectrum.[29] By performing the same digestion on a sample of $Cu(SO)_4.5H_2O$ of known mass we can use this as a

standard for the $Cu(H_2O)_6^{2+}$ UV/vis absorption and from this we can determine the Cu content of other Cu(I) salts. Using this method, we determine the Cu content of Cu_2-TNBI to be 28.82%(Theory states 28.94%). This corroborates the findings of elemental analysis and allows for confirmation of the first synthesis of Cu_2-TNBI.

The crystal structure of Cu_2-TNBI could not be determined. SEM images proved the crystal size to be below 1µm (**Figure 3.24**). PXRD diffractograms prove the sample to be a microcrystalline powder (**Figure 3.25**) but unit cell data has yet to be determined.

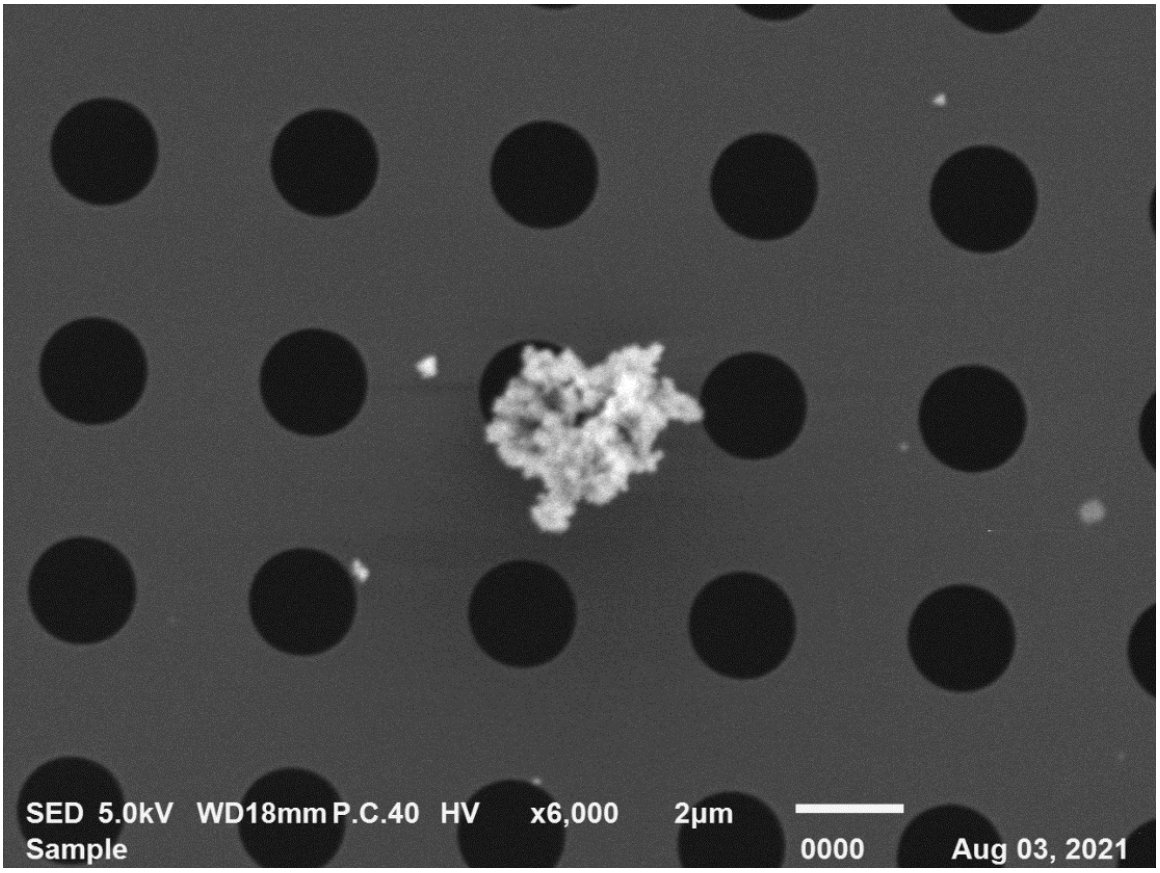

Figure 3.24: *SEM Image of a cluster of Cu_2-TNBI crystals*

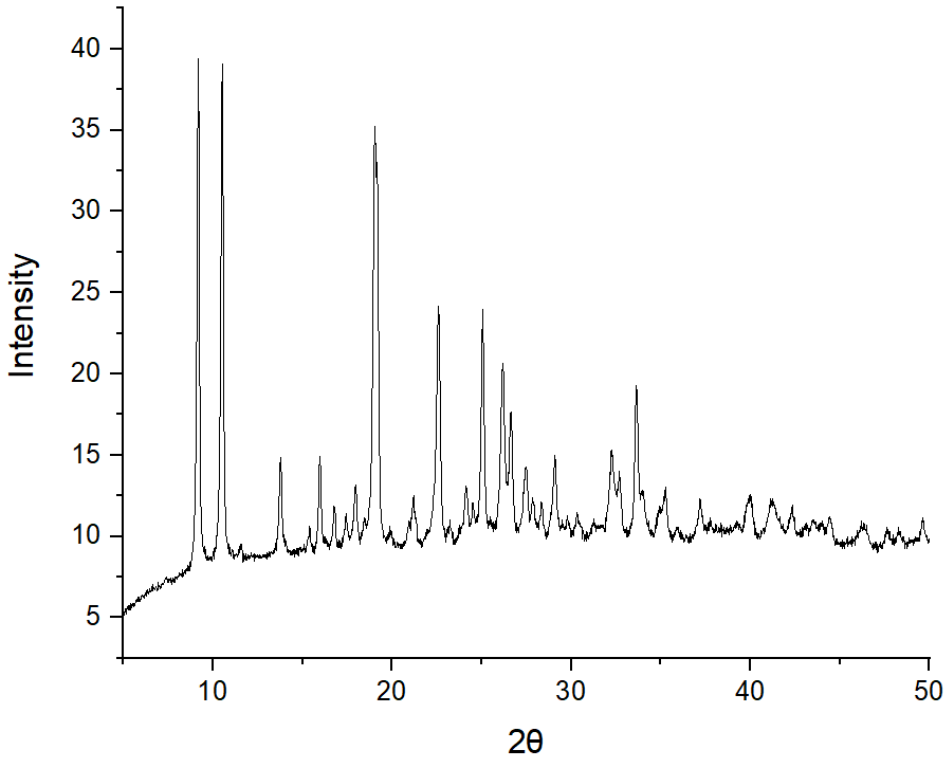

Figure 3.25: *PXRD diffractogram of Cu_2-TNBI recorded in the range 5-50 2Θ*

3.2.21 Synthesis of Cu(I)-ADNP

4-Amino-3,5-dinitropyrazole (ADNP) was also chosen as a ligand for the formation of Cu(I) salts. ADNP was synthesised through the stepwise nitration and amination of chloropyrazole according to the work of Ek.[25] A solution of potassium-4-amino-3,5-dinitropyrazole was made by addition of stoichiometric amounts of KOH to a 5 ml aqueous solution of ADNP. This was then added to a solution of $CuCl_2$ at 75 °C resulting in the formation of a dark orange solution. The solution was heated to 90 °C and sodium ascorbate was added under the same addition scheme as used for the formation of previous Cu(I)-nitroazolates (**Figure 3.26**).

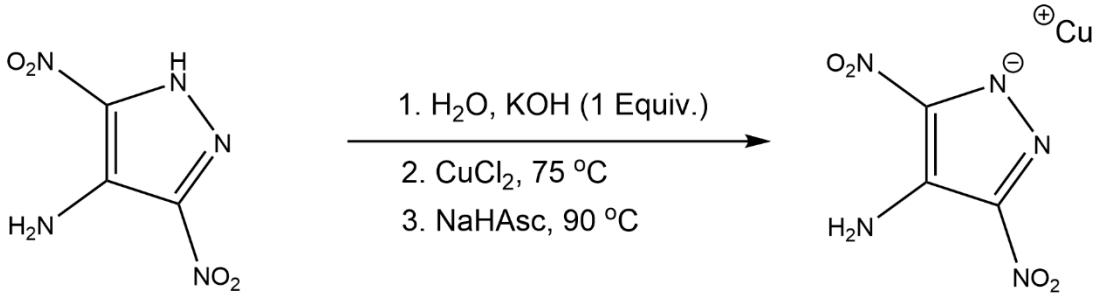

Figure 3.26: *Synthesis to form Cu(I)-ADNP*

During the addition an orange solid precipitates within the first minute of addition. Upon completion of the addition an orange suspension is obtained. Filtering and washing with water (2X) and IPA (2X) afforded Cu(I)-4-amino-3,5-dinitropyrazolate (Cu(I)-ADNP) as a bright orange solid. Product identity was proved by elemental analysis, Cu content determination and determination of the crystal structure.

3.2.22 Elemental Analysis and Cu Content

	C%	**H%**	**N%**
Expected	15.29	0.86	29.72
Found	15.35	1.19	29.62
Difference (Found-Exp)	+0.06	+0.33	-0.10

Table 3.5: *Elemental analysis results for Cu(I)-ADNP*

As shown in **Table 3.5**, values for CHN are all within the acceptable tolerances for the values assumed for Cu(I)-ADNP. Cu content was also used to determine product identity. Cu Content was recorded using the method described for other novel Cu(I)-nitroazolates by using $CuSO_4.5H_2O$ as a standard for UV/vis and digesting Cu(I)-ADNP in 68% HNO_3.

	Cu Content
Expected	26.97
Found	27.07
Difference	+0.10

Table 3.6: *Cu content analysis of Cu(I)-ADNP*

The Cu content of the sample of Cu(I)-ADNP used was 27.07, a result within +0.10% of the expected value (**Table 3.6**). This, alongside the element analysis results, proved the identity of the bright orange solid as Cu(I)-ADNP.

3.2.23 Structural determination of Cu(I)-ADNP

When a sample of Cu(I)-ADNP was viewed under a microscope 3 crystal types could be observed: Large yellow crystals, small orange crystals and a <5 μm microcrystalline powder. The sample was also viewed with SEM. Here the largest of the yellow crystals can be seen to be approximately 25 μm (**Figure 3.27**). The smaller orange crystals are hard to distinguish from the microcrystalline powder in the SEM image but some relatively large crystals can be seen to be ~10 μm. It is also clear that the large crystals make up only a small proportion of the crystalline material.

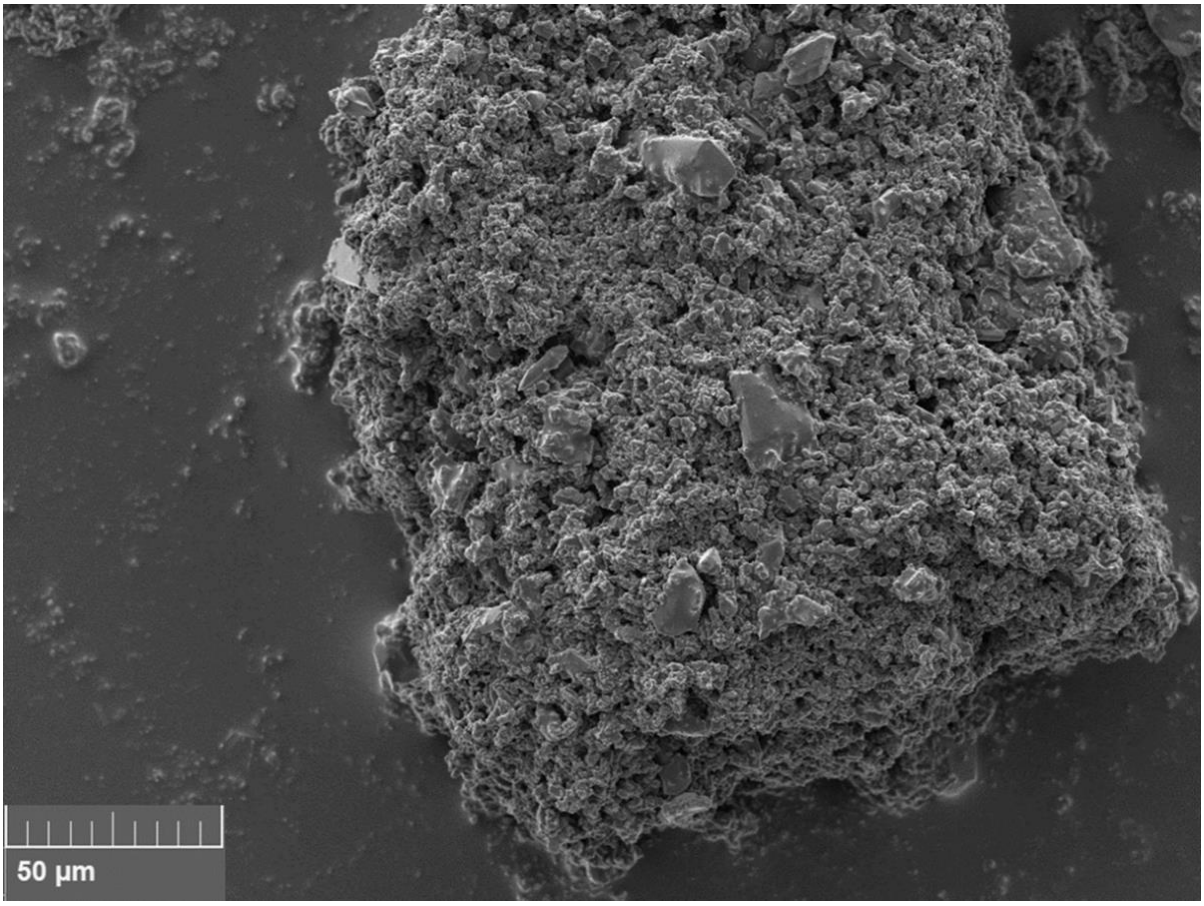

Figure 3.27: *SEM image of a sample of Cu(I)-ADNP*

Both the orange crystals and the yellow crystals were investigated with SCXRD. The orange crystals were composed of copper and 4-amino-3,5-dinitropyrazolyl moieties in a 1:1 ratio. This, along with the measured magnetic properties, implies that that copper is only observed in the 1+ oxidation state. Each copper binds to two ADNP moieties which results in unusual trimers forming with ADNP compounds bridging

between copper centres (**Figure 3.28, Top**). Hydrogen bonds can be found between the oxygens of the 3- and 5-NO_2 groups towards the adjacent amino group ranging from 2.297-2.414 Å. Weak hydrogen bonding can be found between trimers from nitro group oxygen atoms to amino group hydrogens (2.865 Å). Bonds between Cu atoms and nitro group oxygens can also be observed. Cu 2 and Cu 3 feature one long bond to a nitro group oxygen (2.816-2.994 Å) and one short bond (2.436-2.488 Å). Cu1 features two bonds to nitro group oxygens of similar length (2.747 Å, 2.787 Å). Nitro groups are found to be in plane with the pyrazolato moiety with only small twists (5.81-16.44° out of plane. This is similar to the behaviour seen in the structure of Cu-3,5-DNP. Neither of these structures are seen to have one extremely twisted NO_2 group as seen for $Cu_4(DNT)_3Cl$. Cu-N bond lengths for Cu(I)-ADNP (1.821-1.889 Å) are also found to be similar to that seen for the bonding found in the distorted square pyramidal moieties found in Cu(I)-3,5-DNP(1.862-1.892 Å).

The large yellow crystals were also found to diffract and a crystal structure was recorded. The yellow crystals were found to be 1-methyl-4-amino-3,5-dinitropyrazole (**Figure 3.28, Bottom**). The crystal structure was not investigated further and was used only for product identification. This is a very similar by-product to what is found in the reaction forming Cu(I)-3,5-DNP, but with the 4-amino group preventing hydrolysis of the pyrazole ring. Likewise, the mechanism for formation of the methylated product is currently unknown however this being the second observation of a methylated pyrazole product, it is clear that the pyrazole moiety is affected by the reducing conditions present in the reaction solution. With no other sources of carbon present in the reaction mixture (baring sodium ascorbate which is present in all reduction reactions performed so far), it is likely that the pyrazole moiety is the source of the methyl group. It is not unreasonable to suggest a similar by-product will form for other nitropyrazolates used in this reaction system.

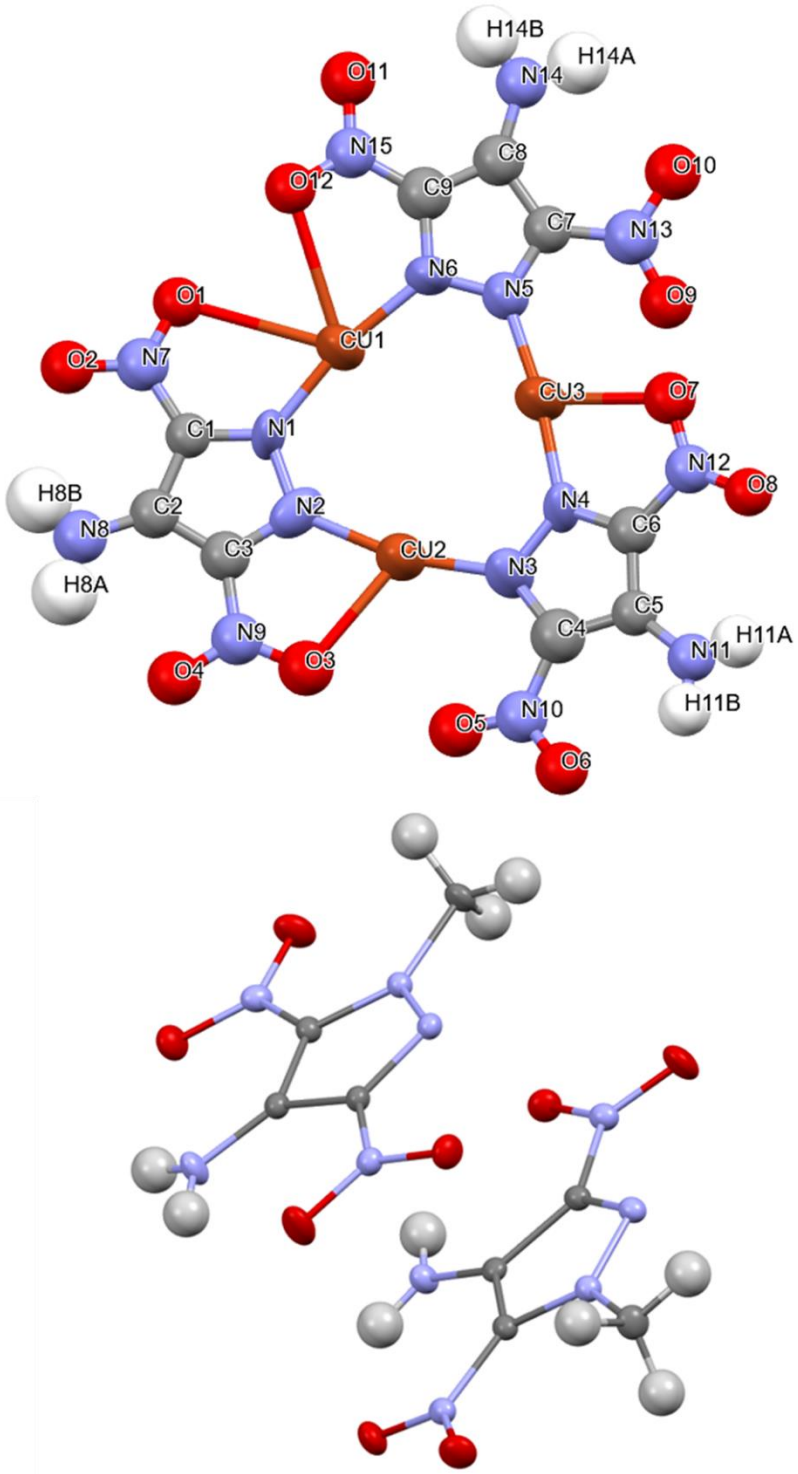

Figure 3.28: Top: *Projections of the thermal ellipsoids in the molecular structure of the crystals of Cu-ADNP (set at the 67% probability level), Bottom: Projections of the thermal ellipsoids in the molecular structure of the crystals of 1-methyl-4-amino-3,5-dinitropyrazole (set at the 50% probability level)*

3.2.24 Thermal Behaviour and detonation performance parameters of Cu(I)-nitroazolates

3.2.24.1 Thermal behaviour

All novel Cu(I) salts were investigated by DSC calorimetry (**Table 3.7**) with both thermal decomposition temperatures and enthalpies of decomposition (ΔH_d) recorded. None of the materials showed phase transitions or chemical reactivity between r.t. and the onset of decomposition. Therefore, the decomposing phase is the same as that present at r.t. $Cu_4(DNT)_3Cl$, Cu_2-TNBI and Cu-ADNP were heated at rate of 5 K min $^{-1}$ until 200 °C was reached, after which a heating rate of 1-2 K min $^{-1}$ was used to allow for a controlled (slower) decomposition. Cu-2,4-DNI, Cu-4,5-DNI and Cu-3,5-DNP were heated at 3 K min^{-1} for the entire temperature range. DSC traces can be found in the Appendix (**8.54-8.59**).

Compound	**T_{on}/ °C**	**T_{peak}/ °C**	**ΔH_d/ J g^{-1}**	**ΔH_d/ kJ mol^{-1}, Per Cu**	**ΔH_d/ kJ mol^{-1}, Per azolyl ring**
DBX-1	293	305	1653	294	294
DBX-X	274	283	1201	182	273
$Cu_4(DNT)_3Cl$	267	269	2347	447	596
Cu_2-TNBI	287	300	2425	533	533
Cu-3,5-DNP[a]	324	325	1583	349	349
Cu-2,4-DNI	336	344	1793	396	396
Cu-4,5-DNI	281	300	1734	383	383
Cu-ADNP[b]	298	300	2576	686	686

Table 3.7: *Comparison of the thermal behaviour of known Cu(I)-nitroazolates, [a]Compound contains 4% 1-methyl-4-hydroxy-3,5-dinitropyrazole, [b]Compound contains an unknown amount of 1-methyl-4-amino-3,5-dinitropyrazole*

The onset of exothermic decomposition of $Cu_4(DNT)_3Cl$ occurs at T_{on} = 267 °C within a very sharp peak (T_{peak} = 269 °C). In contrast, compound Cu_2-TNBI possesses a greater thermal stability and decomposes less rapidly as shown by both onset and peak temperature exceeding $Cu_4(DNT)_3Cl$ by over 20 K and with greater

separation (T_{on} = 287 °C, T_{peak} = 300 °C). Cu-ADNP displays an even higher thermostability (T_{on} = 296 °C, T_{peak} = 300 °C) but with a narrower temperature range than Cu_2-TNBI. Cu-2,4-DNI and Cu-3,5-DNP show the highest thermal stabilities of any of the novel Cu(I)-nitroazolates (Cu-2,4-DNI: T_{on}:336 °C, T_{peak}: 343 °C; Cu-3,5-DNP: T_{on}: 324 °C, T_{peak}: 325 °C) while Cu-4,5-DNI has thermal decomposition temperature comparable to Cu_2-TNBI (T_{on}: 281 °C, T_{peak}: 299.8 °C) (**Table 3.7**). The thermal decomposition of Cu-4,5-DNI also appears to occur in two stages with the associated exotherm having two distinct peaks. The thermostability of the investigated materials is thus close to that observed for DBX-1 and DBX-X which decompose at 293 °C and 274 °C respectively. All solids greatly exceed the minimum threshold for thermal stability expected of LFI's. Specific heats of decomposition vary greatly amongst the novel Cu(I)-nitroazolates. Cu-ADNP, Cu_2-TNBI and $Cu_4(DNT)_3Cl$ have similar specific heats of decomposition (2576 J g^{-1}vs. 2425 J g^{-1} vs. 2342 J g^{-1}) and these are substantially higher than those found for DBX-1 and $Cu_3Cl(NT)_2$ (1653 and 1201 J g^{-1} , respectively). Cu-3,5-DNP, Cu-2,4-DNI and Cu-4,5-DNI all have specific heats of decomposition similar to those found for DBX-1 (1583 J g^{-1} vs. 1793 J g^{-1} vs. 1734 J g^{-1}). When calculated per Cu atom or per azolyl moiety, the novel Cu(I)-nitroazolates all have higher molar heats of decomposition than DBX-1. This suggests that the number of C-NO_2 groups is critical for increasing the heat of decomposition. Incorporation of C-H groups over N atoms can be said to have a negative effect on the heat of decomposition as can be seen by the much small increases in molar heat of decomposition per azolyl group for Cu-3,5-DNP, Cu-2,4-DNI and Cu-4,5-DNI over DBX-1 compared with that of $Cu_4(DNT)_3Cl$.The specific heat of decomposition and the molar heat of decomposition per azolyl group in Cu-ADNP are both substantially larger than that of Cu_2-TNBI or $Cu_4(DNT)_3Cl$ (2912 J g^{-1} , 686 kJ mol^{-1}) which suggests that the NH_2 group has an additional exothermic effect in the exothermic decomposition of nitroazolates.

3.2.24.2 Detonation parameters

Detonation parameters were calculated to help with explosive classification of the novel Cu(I)-nitroazolates and to see if they meet the required standards of a lead free initiator/DBX-1 alternative (Detonation parameters on par with $Pb(N_3)_2$ or DBX-

1). With crystal structures known for $Cu_4(DNT)_3Cl$, Cu-ADNP and Cu-3,5-DNP, crystal densities can be calculated and taken as the limiting density. In the case of Cu_2-TNBI, Cu-2,4-dinitroimidazolate and Cu-4,5-dinitroimidazolate determination of the crystal structure could not be achieved. In these cases, Q,D and P cannot be calculated due to the lack of a crystal density. However, one can make estimates of the crystal density according to the methods of Ammon and Hofmann.[31][32] In these papers, average volumes for specific atoms, and in the method of Ammon for atoms in specific binding environments, are calculated from large (over 1000 datasets) sets of crystal structures obtained from the CCDC. From the average volumes an estimated volume for individual moieties can be calculated additively which in turn can be used to calculate an estimated density for the compound in question. This was applied to the Cu(I)-nitroazolates with known structures to assess the validity of the density estimation when compared against values calculated from the crystal structures.

Compound	**ρ, determined from crystal structure/ g cm^{-3}**	**ρ, estimation[31][32]/ g cm^{-3}**	**Difference/ g cm^{-3}**	**% Difference**
DBX-1	2.584[9]	2.39	-0.194	-7.5%
DBX-X	2.939	2.53	-0.409	-13.9%
$Cu_4(DNT)_3Cl$	2.574	2.39	-0.184	-7.15%
Cu-ADNP	2.446	2.22	-0.226	-9.24%
Cu-3,5-DNP	2.520	2.18	-0.340	-13.49

Table 3.8: *Estimated crystal density versus that determined from the crystal structure*

The methods of Hofmann and Ammon underpredict the density of all Cu(I)-nitroazolate compounds with recorded crystal structures (**Table 3.8**). This discrepancy is less than 10% except for DBX-X and Cu-3,5-DNP in which the methods of Hofmann and Ammon cannot account for the efficient packing present in the crystal. [10] These methods can therefore be used for estimation of crystal densities for Cu_2-TNBI, Cu-2,4-dinitroimidazolate and Cu-4,5-dinitroimidazolate

however these values should be taken as lower limits of the theoretical maximum values. Using these estimated crystal densities and the calculated values for $Cu_4(DNT)_3Cl$, Cu-ADNP and Cu-3,5-DNP, we can calculate detonation performance parameters for these compounds and compare them to DBX-1 and $Pb(N_3)_2$ (**Table 3.9**).

Compound	**T_{dec}/ °C**	**$\Delta H_{fexplosive}$/ kJ mol^{-1}**	**ρ/ g cm^{-3}**	**Q/ J g^{-1}**	**D/ km s^{-1}**	**P/ kbar**
$Cu_4(DNT)_3Cl$	267	-248.0	2.574	2342.7	7.868	338.05
Cu-ADNP[a]	298	-85.7	2.446	2700.0	7.242	279.59
Cu-3,5-DNP[b]	324	-407.5	2.520	1583.3	6.147	204.30
Cu_2-TNBI	287	-203.9	2.27[c]	2425.1	7.562	293.86
Cu-2,4-DNI	336	-361.1	2.18[c]	1793.3	5.686	162.71
Cu-4,5-DNI	281	-374.0	2.18[c]	1734.8	5.639	160.04
DBX-1	293	-49.9[9]	2.584	1695.6	6.341	219.97
$Pb(N_3)_2$	313[33]	-	4.763[34]	-	5.920[33]	338[33]

Table 3.9: *Comparison of the detonation performance parameters for known Cu(I)-nitroazolates and $Pb(N_3)_2$, [a]Compound contains an unknown amount of 1-methyl-4-amino-3,5-dinitropyrazole,[b]Compound contains 4% 1-methyl-4-hydroxy-3,5-dinitropyrazole, c= estimated densities*

Estimated values for the density of Cu_2-TNBI, Cu-2,4-dinitroimidazolate and Cu-4,5-dinitroimidazolate are similar to the predicted density for Cu-ADNP/ Cu-3,5-DNP and lower than predicted values for the other Cu(I)-nitroazolates. While this value can be taken as a lower limit for density, this does imply that unless these compounds have highly efficient packing they may have similar actual densities to Cu-ADNP/ Cu-3,5-DNP. All compounds are predicted to have favourable detonation performance parameters. Cu-2,4/4,5-dinitroimidazolate have the lowest predicted values for both D and P, however the values for D are within 4.7% of the value for lead azide. Assuming that the predicted density is a lower limit, Cu-2,4/4,5-DNI could possess values for D that rival that of lead azide and DBX-1. On account of their high thermal stabilities (Cu-2,4-DNI found to have T_{dec} over 40 °C above that of DBX-1) and their predicted detonation parameters, Cu-2,4/4,5-DNI can both be seen as potential lead-

free initiators. Cu-3,5-DNP is found to have D and P values similar to that found for DBX-1 while also having a decomposition temperature which is 30 °C higher. This suggests that Cu-3,5-DNP could be a viable alternative to DBX-1 in initiatory formulations. $Cu_4(DNT)_3Cl$, Cu-ADNP and Cu_2-TNBI are all predicted to have detonation velocities and pressures far exceeding that of DBX-1. This is primarily due to the larger amounts of CO_2 produced by these compounds upon detonation and the much higher values for ΔH_d recorded for these compounds. The detonation pressures of these materials also much more closely match that for lead azide than does DBX-1. With high thermal stabilities in all cases, these compounds should be further investigated as replacements for both DBX-1 and lead azide.

3.2.25 Long term Stability

In all cases the novel Cu(I)-nitroazolates have desirable detonation parameters. However long-term storability has not been investigated for these compounds. On account of the chloride present in $Cu_4(DNT)_3Cl$, it can be assumed that a similar decomposition to that seen for DBX-X will be present upon long term water immersion. The chloride free Cu(I)-nitroazolates should prove stable upon water immersion but these tests must be conducted to conclusively prove this.

3.2.26 Impact Sensitiveness

The impact sensitiveness of $Cu_4(DNT)_3Cl$, Cu_2-TNBI and Cu-ADNP were recorded and compared to the values recorded for DBX-1 and DBX-X and for the known range of values for $Pb(N_3)_2$ (**Table 3.10**).

Compound	**IS/ J**
$Cu_4(DNT)_3Cl$	1.8(±0.1) J
Cu_2-TNBI	1.7(±0.1) J
Cu-ADNP	2.5(±0.1) J
DBX-1	4.3(±0.3) J
DBX-X	1.8(±0.2) J
$Pb(N_3)_2$	2.5-4 J[35]

Table 3.10: *Impact sensitiveness of known Cu(I)-nitroazolates and lead azide*

Preliminary drop weight testing reveals that the tested novel Cu(I)-nitroazolates possess high sensitiveness towards impact. Cu_2-TNBI is found to have the highest sensitiveness with an IS of 1.7(±0.1) J. In all compounds, sensitiveness's are found to be much lower than that recorded for DBX-1 and even the least sensitive (Cu-ADNP) is found to be as sensitive as the most sensitive batches of $Pb(N_3)_2$ (($Pb(N_3)_2$ sensitiveness is influenced by formulation changes, *i.e.* reaction conditions, additives, morphology, crystal size distribution etc). It should be noted that both Cu(I)-chlorido-nitroazolato compounds (DBX-X and $Cu_4(DNT)_3Cl$) have the same IS. This could indicate that inclusion of chlorides into these compounds may have a sensitising effect (See **2.2.8.1 Thermal Behaviour and impact sensitiveness**) , albeit at the cost of some detonation performance parameters. Overall, Cu_2-TNBI, Cu-ADNP and $Cu_4(DNT)_3Cl$ should all be considered as possessing a high sensitiveness towards impact, exceeding that of other know primary explosives.

3.3 Conclusion

Seven nitroazoles with known syntheses of their respective alkali metals salts were targeted for use in the Cu(II)/Cu(I) reduction reaction system used in the synthesis of DBX-1. Six of the nitroazolates have been shown to form Cu(I) salts though the products vary between nitroazolates. TNBI, 2,4-DNI and 4,5-DNI form Cu_2-TNBI, Cu-2,4-DNI and Cu-4,5-DNI respectively. Use of DNT in the Cu(II)/Cu(I) reduction reaction results in the formation of the mixed ligand coordination polymer $Cu_4(DNT)_3Cl$. This is remarkably similar to that seen in DBX-X and is likely similar to suffer from similar long term stability issues. Further investigation into the synthesis of this compound could reveal similar reaction trends to that seen with DBX-X/DBX-1 potentially resulting in the formation of 1:1 Cu-DNT. Cu-ADNP and Cu-3,5-DNP both form from their respective alkali metal salts but both have multiple side products also forming. Cu-ADNP has a minimum of 3 different products forming: 2 polymorphs of Cu-ADNP and 1-methyl-4-amino-3,5-DNP. Elemental analysis confirms that the major product is Cu-ADNP. Similarly, the use of K-3,5-DNP also results in multiple products forming with two identified as Cu-3,5-DNP and 1-methyl-4-hydroxy-3,5-dinitropyrazole. The use of K-3,4-DNP does not result in the formation of a solid precipitate but instead forms as a suspected metallogel. The crystal structures of Cu-ADNP, Cu-3,5-DNP and $Cu_4(DNT)_3Cl$ have all been determined. Thermal behaviour and detonation performance parameters have been determined for all compounds. All compounds are shown to be highly temperature stable with all but $Cu_4(DNT)_3Cl$ rivalling the thermal stability of DBX-1. For compounds without defined crystal densities, the methods of Hofmann and Ammon have been shown to give lower limit of the expected crystal density. All compounds are predicted to have detonation velocities approaching that of lead azide and DBX-1 with some(Cu_2-TNBI, Cu-ADNP, $Cu_4(DNT)_3Cl$) predicted to have performance parameters much higher than expected of primary explosives. The impact sensitiveness of Cu_2-TNBI, Cu-ADNP and $Cu_4(DNT)_3Cl$ have also been tested and all were found to have sensitiveness's towards impact exceeding that of other know primary explosives(DBX-1 and $Pb(N_3)_2$). All six compounds can be considered a potential DBX-1 alternatives, however complete characterisation(impact sensitiveness of Cu-2,4/4,5-DNI, Cu(I)-

3,5-DNP) and long term stability studies must be conducted before an accurate assessment can be made.

3.4 Experimental

Syntheses of Na-DNT.2H_2O,[16][27] K_2-TNBI,[26] Na-3,5-DNP.2H_2O,[21] K-3,4-DNP.H_2O,[23] K-2,4-DNI,[19] K-4,5-DNI.H_2O[18] and ADNP.H_2O[25] were performed as specified in the references given. Product purity was proven by comparison of $^{1}H/^{13}C$ NMR, FTIR spectra and unit cell data to the reported values before use in the Cu(II)/Cu(I) reduction reaction. FTIR spectra of the alkali metal salts of nitroazoles can be found in the Appendix.

General Synthesis of Cu(I)-nitroazolates

$CuCl_2$ (320 mg) was added to a beaker and dissolved in 16ml of H_2O to form a light blue solution. The solution was heated to 75 °C at which point the sodium/potassium nitroazolate (1 equivalent) was added in two portions, letting the solution heat back up to 75 °C before the second portion was added. Heating is then continued until the mixture was at 90 °C at which point sodium ascorbate (237 mg in 1.2 ml of water) was added. Addition was made at a rate of 0.133 ml min^{-1}. After addition for 1.5 minutes the solution was allowed to stir for 4.5 minutes. Addition was then continued at the same rate as before. Once addition was complete reaction was stirred for 1.5 minutes for a total reaction time of 14 minutes. Precipitates were filtered and washed with water and IPA before drying under vacuum.

$Cu_4(DNT)_3Cl$

Following the above procedure afforded a filter residue consisting of $Cu_4(DNT)_3Cl$ as a wine-red, microcrystalline, free flowing powder. The procedure was carried out three times with yields ranging from 49.0 to 51.6%, (0.222 to 0.234 g) with respect to $CuCl_2$. IR (nujol) v / cm^{-1} = 1653, 1625, 1565, 1546, 1530, 1504, 1314, 844, 826, 646. Elemental analysis: calcd. for $Cu_4C_6N_{15}ClO_{12}$ cf. $Cu(DNT)_{0.75}Cl_{0.25}$, M = 763.79 g mol^{-1}, C 9.44, H 0, N 27.51%; found: C 9.54, H 0.00, N 26.36% (note: the experimental values fit best for $Cu(DNT)_{0.7}Cl_{0.3}$, C 9.10, H 0, N 26.53%). Copper analysis found 30.26(±0.56)%, value fits best for $Cu(DNT)_{0.9}Cl_{0.1}$, 30.36%. Impact sensitiveness E_{50} = 1.6(±0.1) J. PXRD data are given in Fig. S2.2. DSC T_{on} = 267 °C (dec.), T_{peak} = 269 °C, ΔH = 2343 J g^{-1}, 1 K min^{-1}. MALDI (LD+) m/z = 784 ($[Cu(DCTB)_2(DNT)]^+$), 563 ($[Cu(DCTB)_2]^+$), 534 ($Cu_2(DCTB)(DNT)]^+$), 313.3

([Cu(DCTB)]$^{+}$); MALDI (LD–) m/z = 599.8 ([$Cu_2(DNT)_3$]$^{-}$), 507.8 ([$Cu_2(DNT)_2(C_2N_3]^{-}$), 467.8 ([$Cu_2(DNT)_2(CN)]^{-}$), 378.9 ([$Cu(DNT)_2]^{-}$), 286.9 ([$Cu(DNT)(C_2N_3)]^{-}$), 158 (DNT^{-}).

Determination of the crystal structure of $Cu_4(DNT)_3Cl$:

Crystal structure was solved by Tom Roseveare of the University of Sheffield. Below is a summary of the methods used to determine the structure.

Powder X-ray diffraction data was recorded at the University of Sheffield using a D8 Advance powder X-ray diffractometer with a Cu-K α sealed source. Data was recorded using a rotating capillary stage between $4 \leqslant 2\theta \leqslant 80$. Data was initially analysed using Pawley refinement methods [36] using TOPAS software; [37-39] followed by Rietveld methods[40] once suitable unit cell dimensions had been determined. Rietveld Refinement: Powder diffraction data was initially fitted using Pawley refinement methods [36] in order to obtain suitable unit cell parameters and peak shape information for fitting using Rietveld methods.[37] Preliminary Rietveld fitting refined the atom coordinates of the two copper atoms and one chloride atom with the DNT ligand being modelled using a rigid body, by refining six parameters (three translational and three rotational), which was produced using previously reported single crystal data of an uncoordinated ligand.[41] From this preliminary fit it was apparent that Cu1 and Cl1 were in fact located along a 3-fold rotation (1/3, 2/3, z). This prompted a second Rietveld fit where x and y for Cu1 and Cl1 were fixed to 1/3 and 2/3, respectively, allowing for z to refine freely. The second copper atom (Cu2) was allowed to freely refine (x, y and z) and the rotational/translational parameters of the DNT ligand were also allowed to refine. These eleven parameters were refined to convergence, randomise and re-refined for 100,000 iterations in order to determine the best fit to the experimental data. Upon determining the best fit further refinement cycles were completed to include refinement of the background, peak shapes and lattice parameters to produce a final fit for the data.

Cu_2-TNBI

The above procedure afforded a brown, microcrystalline, free flowing powder of Cu_2-TNBI (yield 0.400 g, 38.3% with respect to $CuCl_2$). IR (nujol) v / cm^{-1} = 2608, 2576,1563, 1556, 1553, 1536, 1520, 1526, 1524, 1519, 1505, 1455, 1404, 1338,

1326, 1296, 1284,1277, 1125, 1015, 850, 814, 762, 757, 753, 742, 733, 725. Elemental analysis: calcd. for $Cu_2C_6N_8O_8$: C 16.41, H 0.00, N 25.51%; found: C 16.28, H 0.0, N 25.13%. Copper analysis calculated 28.94%, found 28.82(±0.60)%. Impact sensitiveness E_{50} = 1.8(±0.1) . PXRD is given in Appendix 8.21. $\chi = +6\times10^{-7}$ emu g^{-1}. DSC, T_{on} = 287 °C (dec.), T_{peak} = 300 °C, ΔH = 2425 J g^{-1}, 1 K min^{-1}. MALDI (LD+) m/z = 563 ($[Cu(DCTB)_2]^+$), 499 ($[DCTB_2 – H]^+$), 472, 313 ($[Cu(DCTB)]^+$); MALDI (LD−) m/z = 532 ($[Cu_2(DCTB)(C_3N_2(NO_2)_2]^-$), 516 ($[Cu_2(DCTB)(C_3N_2(NO_2)(NO)]^-$), 427 ($[Cu(TNBI)(CN)_2]^-$), 287 ($[Cu(TNBI)(CN)_2 - C_3N_2(NO_2)(NO)]^-$), 236 ($[TNBI – NO_2 – NO]^-$), 182 ($[TNBI – NO_2 – NC\text{-}NO_2]^-$); ESI(+) m/z = 381 ($[TNBI, MeCN, N_2]^+$), 353 ($[TNBI, MeCN]^+$), 313 ($[H\text{-}TNBI]^+$), 145 ($[Cu(MeCN)_2]^+$); ESI(−) m/z = 814.5 ($[Cu_6(TNBI)_4]^{2-}$), 594.6 ($[Cu_4(TNBI)_3]^{2-}$), 473 ($[Cu_2Cl(TNBI)]^-$), 374.8 ($[Cu_2\text{-}TNBI_2]^{2-}$), 312.9 ($[H\text{-}TNBI]^-$).

Cu-ADNP

The above procedure afforded an orange, microcrystalline, free flowing powder of Cu-ADNP. Elemental analysis: calcd. for $C_3H_2CuN_5O_4$ (235.63 g mol^{-1}): C 15.29, H 0.86, N 29.72%; found: C 15.35, H 1.19, N 29.62%. Copper analysis calculated 27.073%, found 26.97%. IR (nujol) v / cm^{-1} = 3464, 3359, 1657, 1457, 1329, 1299, 1266, 1213, 1002, 852, 758, 720, 656 DSC T_{on} = 296 °C (dec.), T_{peak} = 300°C, ΔH_{exo} = 2912 J g^{-1}, 1 K min^{-1}.

Cu-3,5-DNP

The above procedure afforded an orange, microcrystalline, free flowing powder of Cu-3,5-DNP. Yield: 0.293 g, 56.3 % Elemental analysis: C 16.33, H 0.46, N 25.40%; found: C 17.1, H 0.54, N 25.23%. IR (nujol) v / cm^{-1} = 3163, 1547, 1510, 1466, 1378, 1327, 1216, 1084, 1057, 1017, 835, 750. DSC T_{on} = 324 °C (dec.), T_{peak} = 325 °C, ΔH_{exo} = 1583.3 J g^{-1}, 1 K min^{-1}.

Cu-2,4-DNI

The above procedure afforded an orange/red, microcrystalline, free flowing powder of Cu-2,4-DNI. Yield 0.280 g, 53.5%. Elemental analysis: C 16.33, H 0.46, N 25.40%; found: C 16.49, H 0.82, N 25.26%.IR (nujol) v / cm−1 = 3464, 3359, 1657, 1457, 1329, 1299, 1266, 1213, 1002, 852, 758, 720, 656 DSC T_{on} = 336 °C (dec.), T_{peak} = 343 °C, ΔH_{exo} = 1793 J g^{-1}, 1 K min^{-1}.

Cu-4,5-DNI

The above procedure afforded a brown, microcrystalline, free flowing powder of Cu-4,5-DNI. Yield 0.243 g, 46.4 %. Elemental analysis: C 16.33, H 0.46, N 25.40%; found: C 16.38, H 0.836, N 24.94%. IR (nujol) v / cm−1 = 3133, 1548, 1519, 1470, 1350, 1314, 1298,1275, 1119, 878, 849, 806, 754, 657 DSC T_{on} = 281 °C (dec.), T_{peak} = 299 °C, ΔH_{exo} = 1734 J g^{-1}, 1 K min^{-1}.

Methods for SEM Imaging of Cu_2-TNBI, $Cu_4(DNT)_3Cl$, Cu-4,5-DNI:

Cu 200 mesh TEM grids coated with Quantifoil R 2/2 carbon film were glow discharged before application of the sample. A small number of crystals were transferred to a vial containing IPA (2 mL) and agitated by hand. A 2 µL aliquot of the crystal/IPA suspension was pipetted onto the Quantifoil side of the grid and allowed to dry. A custom-made copper shuttle was used to hold the TEM grids during the imaging experiments. Imaging was performed using a JEOL JSM-IT100 Scanning Electron Microscope. An accelerating voltage of 5.0 kV, a working distance of 17 mm and a probe current of 40 (arbitrary units) were used to image the grids

3.5 References

1. 1.L. Xiaohui, G. Janine, M. Stefan, D. Richard, Angew. Chem. Int. Ed, 2015, 54, 6, 1954-9.
2. 2.J. Li, L. Sun, X. Wang, H. Zhu, M. Miao, J. Phys. Chem., C 2018, 122, 39, 22339-22344.
3. K. Dehnicke, Zeitschrift fuer Anorganische und Allgemeine Chemie, 1974, 409, 3, 311-19.
4. S. Ye, Z. Ya-Jing, W. Zhao-Xi, Dalton trans., 2019, 48, 30, 11186-11190.
5. M. Straumanis, A. Cirulis, Zeitschrift fuer Anorganische und Allgemeine Chemie 1943, 251, 315-31.
6. R. Soderquist, Acta Crystallographica, Section A: Crystal Physics, Diffraction, Theoretical and General Crystallography 1968, 24 (Pt. 3), 450-5.
7. M. Straumanis, A. Cirulis, Berichte der Deutschen Chemischen Gesellschaft [Abteilung] B: Abhandlungen 1943, 76B
8. G. Fan, X. Li, Z. Ma, L. Deng, Y. Zhang, J. Guo, Chinese Journal of Structural Chemistry 2015, 34, 10, 1508-1512.
9. J. W. Fronabarger, M. D. Williams, W. B. Sanborn, J. G. Bragg, D. A. Parrish, M. Bichay, Propellants Explos. Pyrotech. 2011, 36, 541-550
10. B. Westwater, H. Lloyd, I. Victorica-Yrezabal, A. Fong, P. McMaster, M. Sloan, C. Pulham, P. Portius, Dalton Trans. 2020, 49, 14975-14984.
11. X. Qu, L. Zhai, B. Wang, Q. Wei, G. Xie, S. Chen, S. Gao, Dalton Trans, 2016, 45, 43, 17304-17311.
12. M. H. Huynh, M. Hiskey, R. Gilardi, Journal of Energetic Materials 2005, 23, 1, 27-32.
13. M. Krawiec, S. Anderson, P. Dube, D. D. Ford, J. Salan, S. Lenahan, N. Mehta, C. Hamilton, 2015, 40, 4, 457-459.
14. M. H. Wurzenberger, M. Lommel, M. Gruhne, N. Szimhardt, J. Stierstorfer, Angew. Chem. Int. Ed., 2020, 59 30.
15. M. Straumanis, A. Cirulis, Zeitschrift fuer Anorganische und Allgemeine Chemie 1943, 251, 341-54.
16. R. Haiges, G. Belanger-Chabot, S. M. Kaplan, K. O. Christe, Dalton Trans., 2015, 44, 16, 7586-7594

17. J. Cho, K. Kim, S. Cho, J. Kim, J. Heterocyclic Chem., 2001, 38, 141-147
18. A. Katritsky, S. Singh, K. Kirichenko, M. Smiglak, J. Holbrey, W. M. Reichert, S. Spear, R. Rogers, Chem. Eur. J., 2006, 12, 4630-4641
19. G. Zhang, Y. Wang, M. Cai, D. Dai, K. Yan, A. Shan, O. Chen, R. Wang, P. Li, J. Yi, J. Coord. Chem., 2010, 63, 9, 1480-1491
20. S. S. Novikov, L. I. Khmel'nitskii, O. V. Lebedev, V. V. Sevost'yanova, L. V. Epishina, Khim. Getero. Soed., 1970, 4, 503-507
21. M. F. Bolter, A. Harter. T. M. Klapotke, J. Stierstorfer, ChemPlusChem, 2018, 83, 804-811
22. J. W. A. M. Janssen, H. J. Koeners, C. G. Kruse, C. L. Habrakern, J. Org. Chem., 1973, 38, 10, 1777-1782
23. A. M. W. Dufter-Munster, A. Harter, T. M. Klapotke, E. Reinhardt, J. Pomer, J. Stierstorfer, Eur. J. Inorg. Chem., 2022, 8, e202101048, 1-9
24. T. M. Klapotke, A. Penger, C. Pflueger, J. Stierstorfer, New J. Chem., 2016,40, 6059-6069
25. 25.S. Ek, N. Latypov, J. Heterocyclic Che., 2014, 51, 1621-1627
26. T. M. Klapotke, A. Preimesser, J. Stierstorfer, Zeitschrift fuer Anorganische und Allgemeine Chemie, 2012, 638, 9, 1278-1286.
27. T. Liu, X. Q, K. Wang, J. Zhang, W. Zhang, Q. Zhang, New. J. Chem., 2017, 41, 9070-9076
28. T. Zhao, S. Chen, K. Kang, J. Ren, X. Yu, Langmuir, 2022, 38, 4, 1398–1405
29. S. Roger Qiu, B. C. Wood, P. Ehrmann, S. Demos, P. Miller, K. Schaffers, T. I. Suratwala, R. Brow, Phys. Chem. Chem. Phys., 2015, 17, 18913
30. L. V. Epishina, V. I. Slovetskii, V. G. Osipov, O. V. Lebedev, L. I. Khmel'ntiskii, V. V. Sevost'yanova, T. S. Novikova, Khim. Getero. Soed., 1967, 3, 4, 716723
31. H. L. Ammon, S. Mitchell, Propellants, Explosives, Pyrotechnics, 1998, 23, 260-265
32. D. W. M. Hofmann, Acta Cryst., 2002, B57, 489-493
33. D. J. Whelan, R. J. Spear, R. W. Read, Thermochim. Acta, 1984, 80, 149-163
34. L. V. Azaroff, Z. Kristallog. – Cryst. Mater., 1956, 107, 362-369
35. T. M. Klapötke, C. M. Sabate, , Dalton Trans., 2009, 1835-1841
36. G. S. Pawley, J. Appl. Crystallogr., 1981, 14, 357–361.
37. A. A. Coelho, Topas Acad. Version 6,see http//www.topas-academic.net.

38. A. A. Coelho, J. Evans, I. Evans, A. Kern and S. Parsons, Powder Diffr., 2011, 26, S22–S25.
39. A. A. Coelho, J. Appl. Crystallogr., 2018, 51, 210–218.
40. H. M. Rietveld, J. Appl. Crystallogr., 1969, 2, 65–71.
41. H. Yang, Y. Liu, H. Ning, J. Lei and G. Hu, RSC Adv., 2017, 7, 33231–33240.

4. Novel metal-triazenido coordination compounds as energetic materials and the synthesis of a new bis(nitroazolyl)triazenide

4.1 Introduction

Few anionic ligands suitable for use in the formation of energetic coordination compounds exist. Azido, azolato and the nitrato anion have been extensively investigated and offer increasingly diminished returns for further research.[1][2] Therefore, the focus of research is shifting towards the attempted discovery of novel classes of energetic ligands and coordination compounds. Research into this field has recently resulted in the synthesis of the pentazolate anion, a new energetic ligand.[3] With a synthetic procedure known after years of attempted syntheses, research now focuses on the formation of novel coordination compounds.[4] While known, a class of ligand that deserves an increased focus from energetic material chemists are the triazenides. The triazenido ligand consists of a negatively charged chain of three nitrogen atoms which bridges two organic groups (**Figure 4.1**).

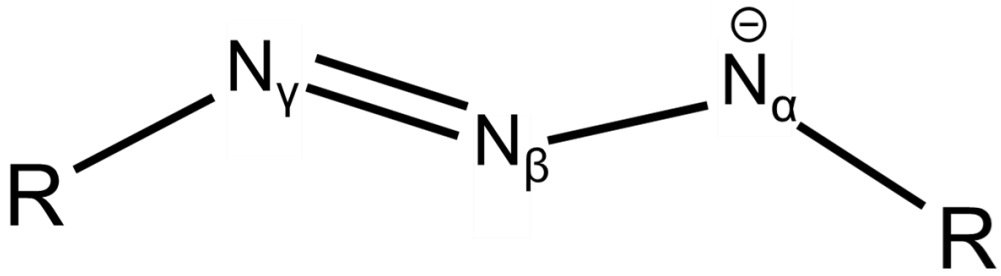

Figure 4.1: *Structure of the triazenide chain*

The coordination chemistry of triazenides is, in general, well understood but little of this research has focused on the synthesis of energetic coordination compounds. Many examples of triazenides binding to metal centres are known and a variety of binding modes have been observed (**Figure 4.2**).[5] Triazenides with non-coordinating R groups are known to coordinate in monodentate, bidentate or chelating bonding modes. N_α,N_α binding has also been observed in at least one triazenido complex.[6] The inclusion of an R group that can engage in bonding results in more coordination

modes becoming available with tetradentate and terdentate bonding modes also known. Known azolyl triazenides show predominantly terdentate N_β binding with R groups binding to the same metal ion as N_β.[7] Other binding modes such as N_α, N_β and the η^3 binding mode, whilst speculated upon, have not been found to occur so far.[5] While not extensively investigated, the IR spectroscopy of triazenido complexes is understood to the extent that information regarding the binding modes of simple triazenido coordination complexes can be extracted from their FTIR spectra. The asymmetric triazenido stretch (ν_{as}(NNN)) gives rise to the characteristic absorption band used for identification of the binding mode.

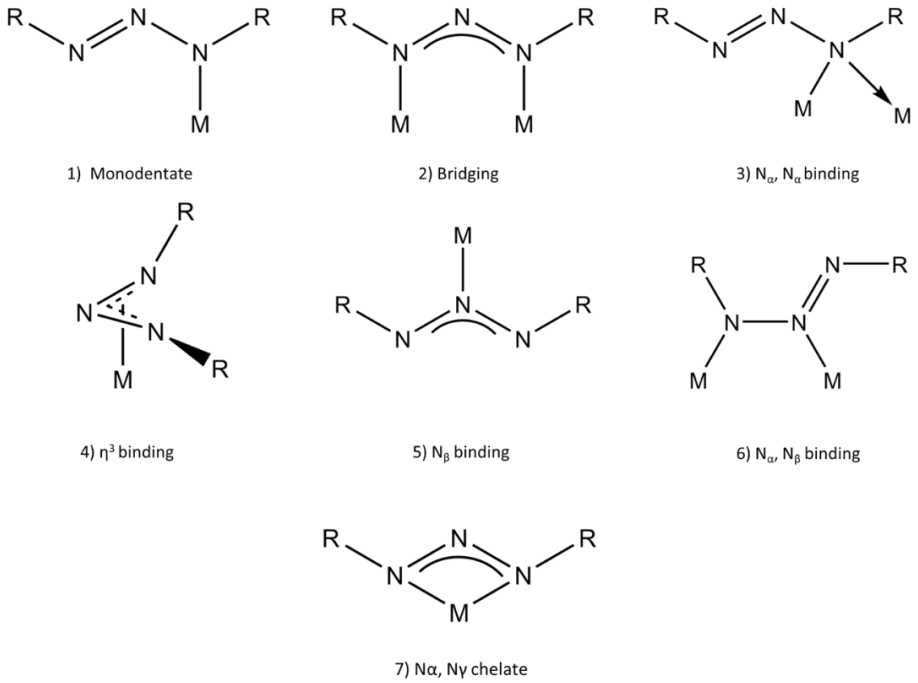

Figure 4.2: *Binding Modes of the triazenido moiety*

It appears that both the chelating and monodentate binding modes have frequencies for ν_{as}(NNN) in the region 1350-1250 cm^{-1}. Reports by Robinson and Uttley reported that monodentate triazenido ligands also absorbed at around 1150, 1190-1210 and 1580-1600 cm^{-1} unlike their chelate analogues which absorbed only at 1260-1350 and 1580-1600 cm^{-1}.[8][9] Absorption bands at 1580-1600 cm^{-1} are heavily debated and presumed by many to be related to the respective R groups of the triazenido moiety.[10] Whilst it is possible that bands found at lower wavenumbers could correspond to vibrations found only in monodentate triazenides, little has been done to corroborate

these claims and so the ν_{as}(NNN) remains as the characteristic band of all triazenido complexes. Kuyper *et al.* reported that bridging triazenido ligands display a characteristic vibration at 1350-1375 cm^{-1} and can be used to distinguish between coordination modes in some simple structures.[10][11] It is so far unclear where one can expect to find ν_{as}(NNN) in cases where the triazenido anion can be found in a non-coordinating environment. With few examples of N_β bound triazenides in the literature it is hard to draw conclusions regarding the position of the ν_{as}(NNN) but it appears to occur at wavelengths around ~1350 cm^{-1}.[7][12]

Triazenes are a group of proligands which have only a short history of use in energetic materials. The high nitrogen content 1,3-bis-[3-(5-amino-1,2,4-triazolyl]triazene was first synthesised in 1964 and had investigations into its coordination chemistry in a series of paper in the 1990s[13][14]. Although these investigations focused on the magnetic properties of its metal coordination compounds, its high nitrogen content and easily functionalised amine groups make it a potentially interesting ligand in the search for novel LFIs. The same researchers also synthesised 1,3-bis(pyrazol-3-yl)triazene in 1996 which is another potentially interesting energetic ligand due to its two ring carbon atoms which could be further functionalised to increase the energetic nature of this ligand (**Figure 4.3**).[15]

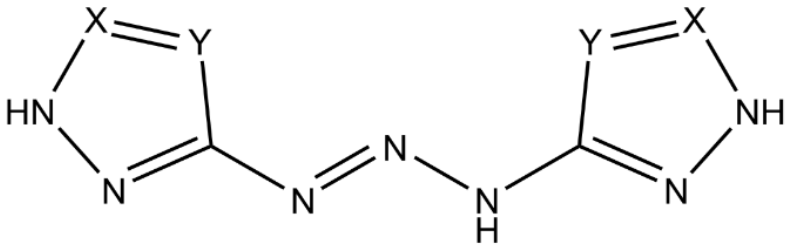

Figure 4.3: *Structure of the bis-azolyltriazenes synthesised by Hanot et al.[15]: A) 1,3-bis-[3-(5-amino-1,2,4-triazolyl]triazene and B) 1,3-bis(pyrazol-3-yl)triazene*

In 2009, the Klapötke group investigated bis(methyltetrazolyl)triazenes[16] as nitrogen-rich ingredients in solid rocket propellants. They found that these pro-ligands show

desirable high positive heats of formation (514 – 792 kJ mol^{-1}), high decomposition temperatures (T_{dec} = 182 to 183 °C), and impact sensitiveness's comparable to known primary explosives (2 J to 3 J). These parameters could make for highly temperature-stable metal compounds whilst also retaining the sensitivity and sensitiveness needed of a potential LFI. One of the isomers of bis(methyltetrazolyl)triazene, bis(2-methyltetrazolyl)triazene, had its coordination chemistry towards metal salts investigated (**Figure 4.4**).[7] IR, NMR, UV-vis, SCXRD and thermal analysis were conducted on the Fe(II), Ni(II) and Co(II) salts of bis(2-methyltetrazolyl)triazene. However, bis(1-methyltetrazol-5-yl)triazene was not investigated with no metal compounds of this ligand currently known. Alongside these azolyltriazenes, only one triazene containing a nitroazole can be found in the literature. Feng et al synthesised bis(2-methyl-4-nitro-2H-1,2,3-triazole)triazene from acidic solutions of 2-methyl-4-nitro-2H-1,2,3-triazole through the addition of $NaNO_2$ at 0-5 °C.[17] With a decomposition temperature (T_{dec}) of 181 °C and other good physical and chemical properties, this compound could find use in energetic formulations. As the use of triazenes as energetic materials has been only briefly investigated, we elected to investigate the synthesis of coordination compounds of the known bis(1-methyltetrazol-5-yl)triazene to form potential LFI's (for use in either detonators or igniters depending on the properties of the compounds) and into the synthesis of novel triazenes.

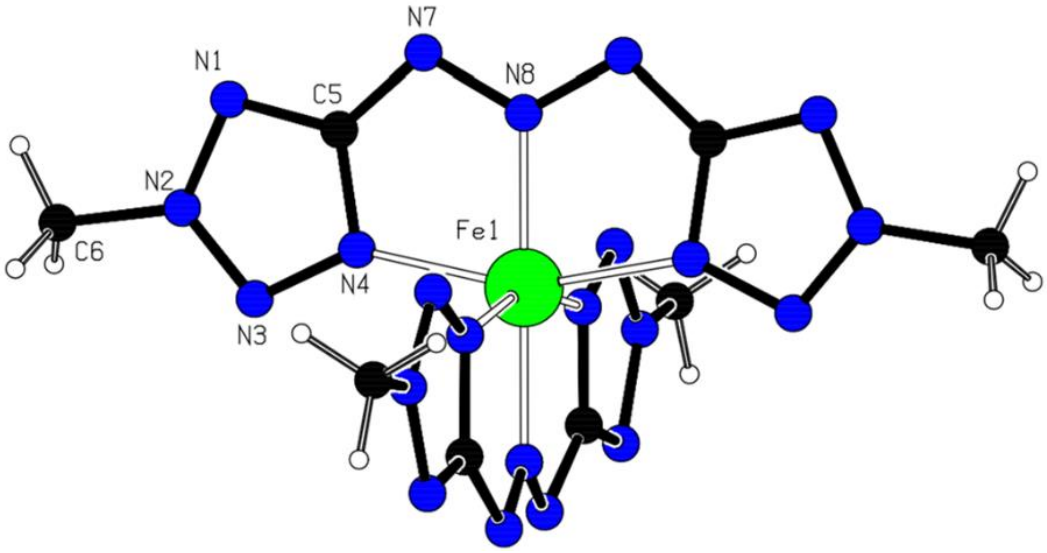

Figure 4.4: *Crystal structure of Fe(bis(2-methyl-tetrazol-5-yl)triazenide)$_2$, Atom Colours: Blue = Nitrogen, Black = Carbon, Green = Iron, White = Hydrogen, image reproduced with permission from ref[7]]*

Research Questions

- Can metal compounds of bis(1-methyl-tetrazol-5-yl)triazene be made, purified and characterised including their crystal structures?
- With the tests available in the research group do any of these metal compounds meet the requirements expected of any potential LFIs?
- Can novel azolyltriazenes be synthesised?

4.2 Results and Discussion

4.2.1 Synthesis of Na- bis(1-methyl-tetrazol-5-yl)triazenide pentahydrate

With a high positive heat of formation and T_{dec}, bis(1-methyl-tetrazol-5-yl)triazene (B1MTT) was an ideal compound to target for synthesis as a precursor to novel energetic metal-triazenides. As described earlier, bis(1-methyl-tetrazol-5-yl)triazene had been prepared as both the free acid and its sodium salt by Klapötke et al.[16] and has been previously synthesised in this research group.[19]

Bis(1-methyl-tetrazol-5-yl)triazene is synthesised by diazotisation of half a molar equivalent of 1-methyl-5-aminotetrazole in HCl and subsequent reaction with the other half of the 1-methyl-5-aminotetrazole starting material to form the triazene chain (**Figure 4.5**). Bis(1-methyl-tetrazol-5-yl)triazene precipitates from solution and is immediately used without further purification to synthesis Na-bis(1-methyl-tetrazol-5-yl)triazenide (Na-B1MTT). Off-white bis(1-methyl-tetrazol-5-yl)triazene is reacted with an equimolar amount of NaOH to form its sodium salt Na-B1MTT. The solvent was removed under vacuum and the pale-yellow residue was recrystallised from water to form the sodium salt as its pentahydrate. Comparison of the FTIR spectrum to internally known values confirmed the identity of this compound.[19] Once Na-B1MTT.5H_2O had been synthesised, its reactions with aqueous solutions of metal ions were investigated.

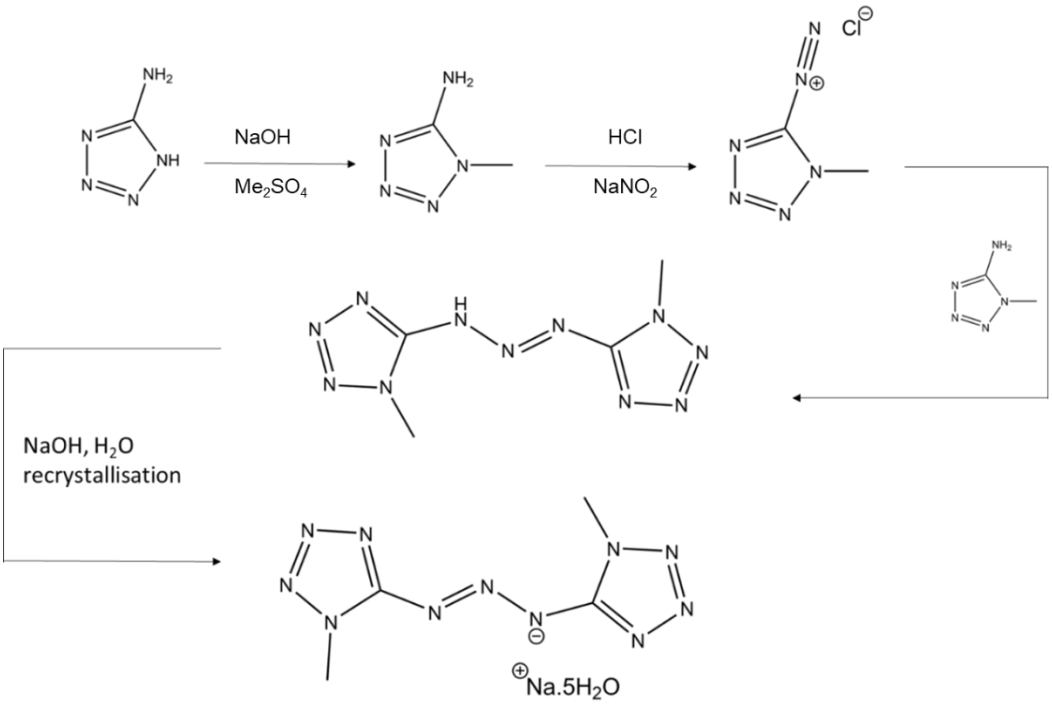

Figure 4.5: *Synthesis of Na-B1MTT.5H_2O*

4.2.2 Synthesis of Metal-triazenido compounds

For $FeCl_2.4H_2O$, Zn(II)Cl_2, Ni(II)Cl_2, Co(II)$(NO_3)_2$ and Pb(II)$(NO_3)_2$ the addition of a two-fold molar amount Na-B1MTT.5H_2O resulted in the immediate precipitation of coloured precipitate (**Table 4.1**).

Metal Salt	**Metal: Triazenide molar ratio**	**Precipitate formation and colour**	**Yield/ % (Assuming formation of $M(B1MTT)_2$)**
$FeCl_2.4H_2O$	1:2	Dark Green precipitate	72.3
$ZnCl_2$	1:2	Light Yellow precipitate	46.6
$NiCl_2$	1:2	Bright Red precipitate	52.2
$Co(NO_3)_2$	1:2	Mauve precipitate	65.3
$Pb(NO_3)_2$	1:2	Bright Yellow precipitate	80.2

Table 4.1: *Reactions of Na-B1MTT.5H_2O with metal salts*

4.2.3 Elemental analysis of metal-triazenides

Elemental analysis was used to inspect the purity of the freshly precipitated metal triazenido compounds prior to any recrystallisation attempts (**Table 4.2**).

		C%	H%	N%
Ni(B1MTT)$_2$	Expected	20.23	2.55	64.87
	Found	**18.58**	**2.90**	**58.06**
Fe(B1MTT)$_2$	Expected	20.35	2.56	65.26
	Found	**19.67**	**2.71**	**63.36**
Co(B1MTT)$_2$	Expected	20.22	2.55	64.84
	Found	**19.41**	**2.84**	**62.80**
Zn(B1MTT)$_2$	Expected	19.95	2.51	63.97
	Found	**18.02**	**3.00**	**55.74**
Pb(B1MTT)$_2$	Expected	15.41	1.94	49.42
	Found	**15.18**	**1.85**	**49.20**

Table 4.2: *Elemental analyses of metal-triazenido complexes*

With the exception of Pb(B1MTT)$_2$, none of the solids precipitate as pure 1 : 2 metal triazenides. For both Co and Fe, the inclusion of one water molecule in the crystal gives expected EA values within the acceptable tolerances (<0.5% difference between expected and found values) and confirms the precipitated solids as Co(B1MTT)$_2$.H_2O and Fe(B1MTT)$_2$.H_2O. With Ni(B1MTT)$_2$ having the exact same number of absorption bands associated to water as the Fe/Co compounds (See ***Vibrational spectroscopy, Figure 4.6***) one can reasonably assume that the precipitate formed on addition of Na-B1MTT.5H_2O to $NiCl_2$ is Ni(B1MTT)$_2$.H_2O albeit in a more impure form than that for Fe/Co as even accounting for the water molecule gives expected EA values outside the acceptable tolerances (Ni(B1MTT)$_2$.H_2O: Expected EA: C, 19.48; H, 2.86; N, 62.48%). Zn(B1MTT)$_2$ seems to precipitate as a similarly impure solid with an unknown impurity present.

4.2.4 Vibrational Spectroscopy

FTIR spectra for all precipitated solids were compared to that recorded for Na-B1MTT.5H_2O (**Figure 4.6**). The assumed triazenide coordination complexes of Co, Fe and Ni all precipitate as hydrates, with the absorption bands associated with H_2O visible at ~1630 cm^{-1} and 3530-3615 cm^{-1}.

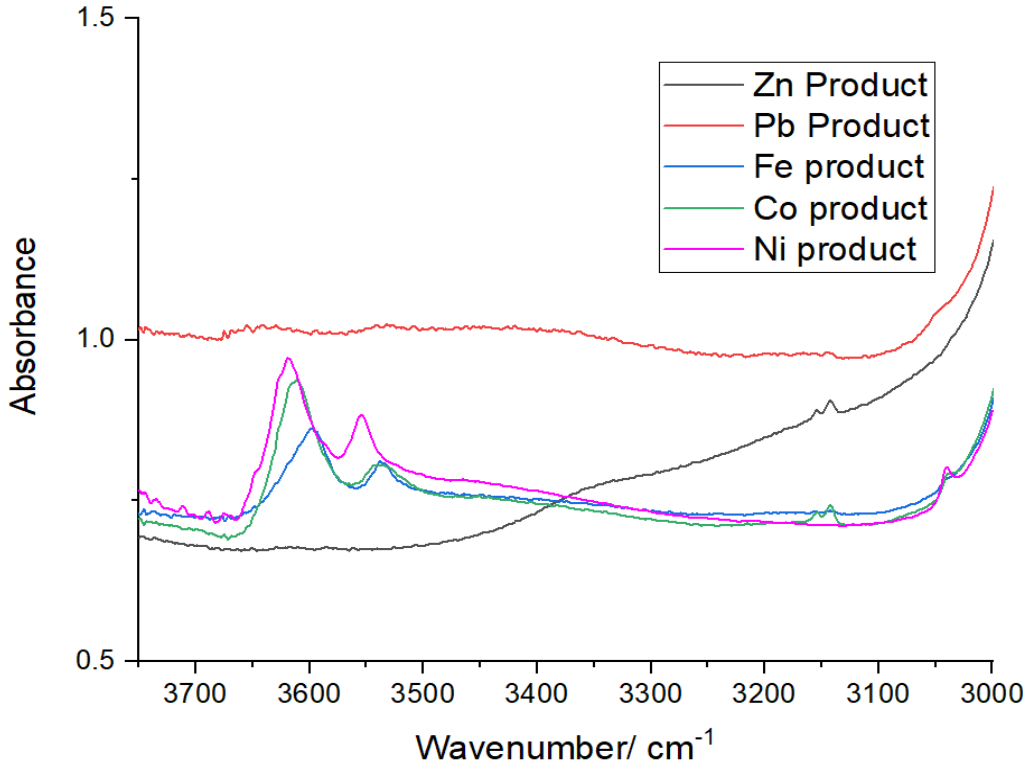

Figure 4.6: *Series of FTIR spectra of metal-triazenido complexes in the range 3700-3000 cm^{-1}, $Ni(B1MTT)_2$ (pink), $Co(B1MTT)_2$ (green), $Fe(B1MTT)_2$ (blue), $Pb(B1MTT)_2$ (red), $Zn(B1MTT)_2$ (black)*

Co and Ni also show a high degree of similarity in their FTIR spectra with only small shifts of peak position from each other and few additional peaks found in their spectra. This suggests that these compounds are found in similar metal : ligand ratios and possibly implies that these compounds form as very similar coordination compounds. While broadly similar to Ni/Co the Fe compound does show larger shifts and more additional bands than that found between Ni and Co. While the number of bands is not so large as to imply a vastly different metal : ligand ratio it does suggest that the Fe compound could have a differing type/strength of interaction with the B1MTT ligand. However, the general trends for the precipitated powders are consistent across these three metal compounds. Coordination to metal cations results in the shift of

absorption bands and in some cases absorption bands found in the spectrum of the sodium salt are now split. Shifts to higher/lower frequency can be attributed to the change from a predominantly ionic salt with coordinatively dominant Na-OH_2 bonds towards a more covalent interaction between metal and ligand with coordination dominated by metal-nitrogen bonds.

Compounds formed from the addition of Na-B1MTT.$5H_2O$ to $ZnCl_2$/$Pb(NO_3)_2$ are distinct from Fe/Co/Ni in the fact that they precipitate out as anhydrous powders. This is clear in the IR spectra of both compounds with a lack of H_2O absorption bands in the regions 3000-3500 cm^{-1} and 1600-1700 cm^{-1}. Both the zinc and lead compounds follow similar trends to each other with bands shifted or split when compared to the sodium salt.

The assignment of ν_{as}(NNN) is important for the interpretation of triazenide binding mode from FTIR data. Bis(1-methyl-tetrazol-5-yl)triazene is reported as having ν_{as}(NNN) in the range 1430-1470 cm^{-1}. As reported for the bis(2-methyl-tetrazol-5-yl)triazenide compounds, deprotonation and coordination of the triazenide results in ν_{as}(NNN) appearing in the region 1310-1340 cm^{-1} (**Figure 4.7**). This effect is also reported by Klapötke for the sodium salt of bis(1-methyl-tetrazol-5-yl)triazene. Therefore, we assign the band at 1305 cm^{-1} in the spectrum of Na-B1MTT.$5H_2O$ as ν_{as}(NNN) and expect to see shifts in this band upon coordination to metal centres. The symmetric stretch of the triazene chain is not assigned due to its reported low intensity in an already crowded part of the FTIR spectra (1200-1350 cm^{-1}). Upon coordination, the band at 1305 cm^{-1} can be seen to shift for all triazenes to higher wavenumbers (Ni:1321 cm^{-1}, Co: 1318 cm^{-1}, Zn: 1326 cm^{-1}, Fe: 1310 cm^{-1}, Pb: 1311 cm^{-1}). Shifts to higher wavenumbers are similar to that seen for the Ni/Co coordination compounds of bis(2-methyl-tetrazol-5-yl)triazenide (Ni: 1320 cm^{-1}, Co: 1327 cm^{-1}) and may indicate that similar binding is present in the metal compounds of bis(1-methyl-tetrazol-5-yl)triazenide (Ni/Co compounds of bis(2-methyl-tetrazol-5-yl)triazenide present as chelating N_β binders with bonds from tetrazole groups to the metal centre). With a shift to 1350-1375 cm^{-1} expected for bridging triazenides and no intense additional bands found in this region of the spectra, we can be certain that this binding mode is not present in these compounds. However, as the observed absorption bands appear in a similar region of the spectra to that expected of triazenides bound in a monodentate fashion it would be unwise to draw definitive conclusions on binding from assignment

of v_{as}(NNN) alone. Evidence for binding interactions of the 1-methyltetrazole side arms can be found in the FTIR spectra of these compounds.

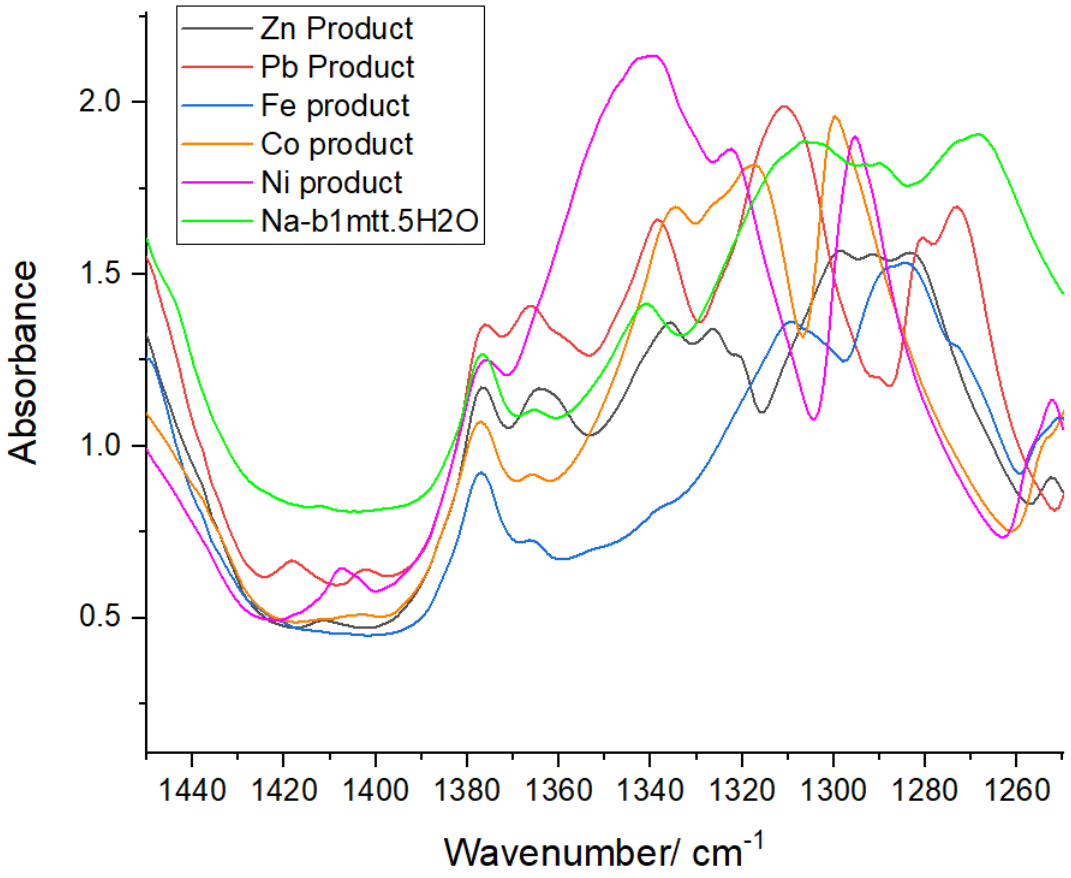

Figure 4.7: *Series of FTIR spectra of metal-triazenido complexes in the range 1440-1250 cm^{-1}, Ni(B1MTT)$_2$ (pink), Co(B1MTT)$_2$ (orange), Fe(B1MTT)$_2$ (blue), Pb(B1MTT)$_2$ (red), Zn(B1MTT)$_2$ (black), Na-B1MTT.5H$_2$O (green)*

As shown by Bigotto et al., 1-methyl-5-amino-tetrazole has easy to identify ring stretches at 1595 cm^{-1} with a relatively intense deformation mode found at 791 cm^{-1} as discussed previously these can be reasonably well correlated with the bands found at 1512 and 809 cm^{-1} in Na-B1MTT.5H$_2$O (**Figure 4.8**). Assuming the band assignment in the sodium salt is correct, these bands can be used to see how coordination to a metal centre has affected the ring vibrations. In all cases shifts of these absorption bands were noted. The band at 1512 cm^{-1} does show shifts to higher frequency in all cases but differs depending on the metal cation with the Fe compound showing the largest shift with the band appearing at 1574 cm^{-1} and Zn showing the

smallest shift with only a 1-2 cm^{-1} shift. The band at 809 cm^{-1} shows less consistent trends upon coordination to metals.

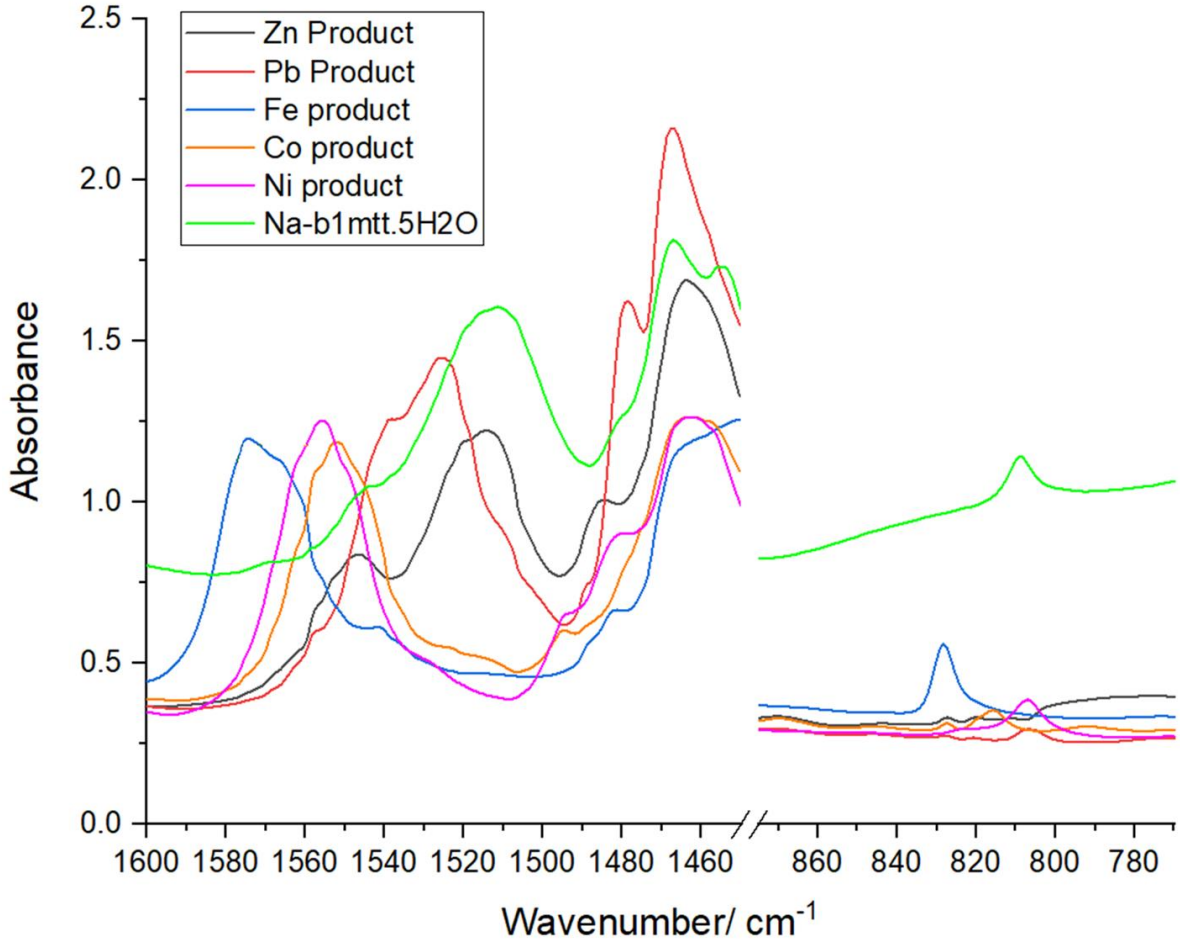

Figure 4.8: *Series of FTIR spectra of metal-triazenido complexes in the range 1600-1460 cm^{-1} and 860-770 cm^{-1}, $Ni(B1MTT)_2$ (pink), $Co(B1MTT)_2$ (orange), $Fe(B1MTT)_2$ (blue), $Pb(B1MTT)_2$ (red), $Zn(B1MTT)_2$ (black), Na-B1MTT.5H_2O (green)*

For some metals (Fe and Co) a shift to higher frequency is recorded, for Ni and Pb only minor shifts of 1-2 cm^{-1} to lower wavenumbers are found and for Zn the band appears to disappear completely and is replaced with a very broad band from 770-810 cm^{-1}. In all cases the ring vibrations are affected by coordination to the metal centre. While speculative, one could argue that the Fe compound has the strongest affinity for B1MTT binding because of the large shifts seen in its absorption bands compared to the other compounds. Zn appears distinct from the other triazenide compounds with disappearance of some ring stretches and shifts to higher frequencies when all other

triazenide compounds shift to lower frequencies. This could indicate that Zn does not bond as strongly as the other compounds or may be found to coordinate differently to the other compounds. Attempts were made at growing single crystals for structural analysis to corroborate the structural information gleaned from FTIR analysis.

4.2.5 Structural determination of $Ni(B1MTT)_2.(CH_3)_2CO$

$Ni(B1MTT)_2.H_2O$ proved to be insoluble in almost all solvents except for DMSO and DMF with the compound also being sparing soluble in acetone. Recrystallisation of $Ni(B1MTT)_2.H_2O$ could be achieved with 30 mg of the crude material dissolving in 150 ml of acetone but this did not result in the growth of crystals of sufficiently quality for structural determination. However, X-ray quality crystals could be formed during attempts at bulk purification of the crude $Ni(B1MTT)_2.H_2O$. When attempting purification via Soxhlet extraction, non-uniform condensation of the acetone vapour on the walls of the Soxhlet extractor resulted in small amounts of the crude solid not meeting a continuous flow of acetone during the course of the extraction. Instead, these uncontacted solids were simply “wet” with condensed acetone vapour. In these areas, large dark red crystals had grown instead of being extracted (**Figure 4.9**). Isolating these crystals and allowing any residual acetone to evaporate resulted in the formation of an air stable, dark red crystalline material with an amount of this material assumed to be inorganic solids insoluble in the acetone extraction solution. SCXRD was used to identify the composition of the crystal. SCXRD proved the composition of the red crystals to be $Ni(B1MTT)_2.(CH_3)_2CO$ (**Figure 4.9**). It therefore appears that for these crystals the acetone has instead extracted the water present in the crude sample and recrystallised the Ni compound as its acetone co-crystal. $Ni(B1MTT)_2.(CH_3)_2CO$ crystallises in the Pbca space group.

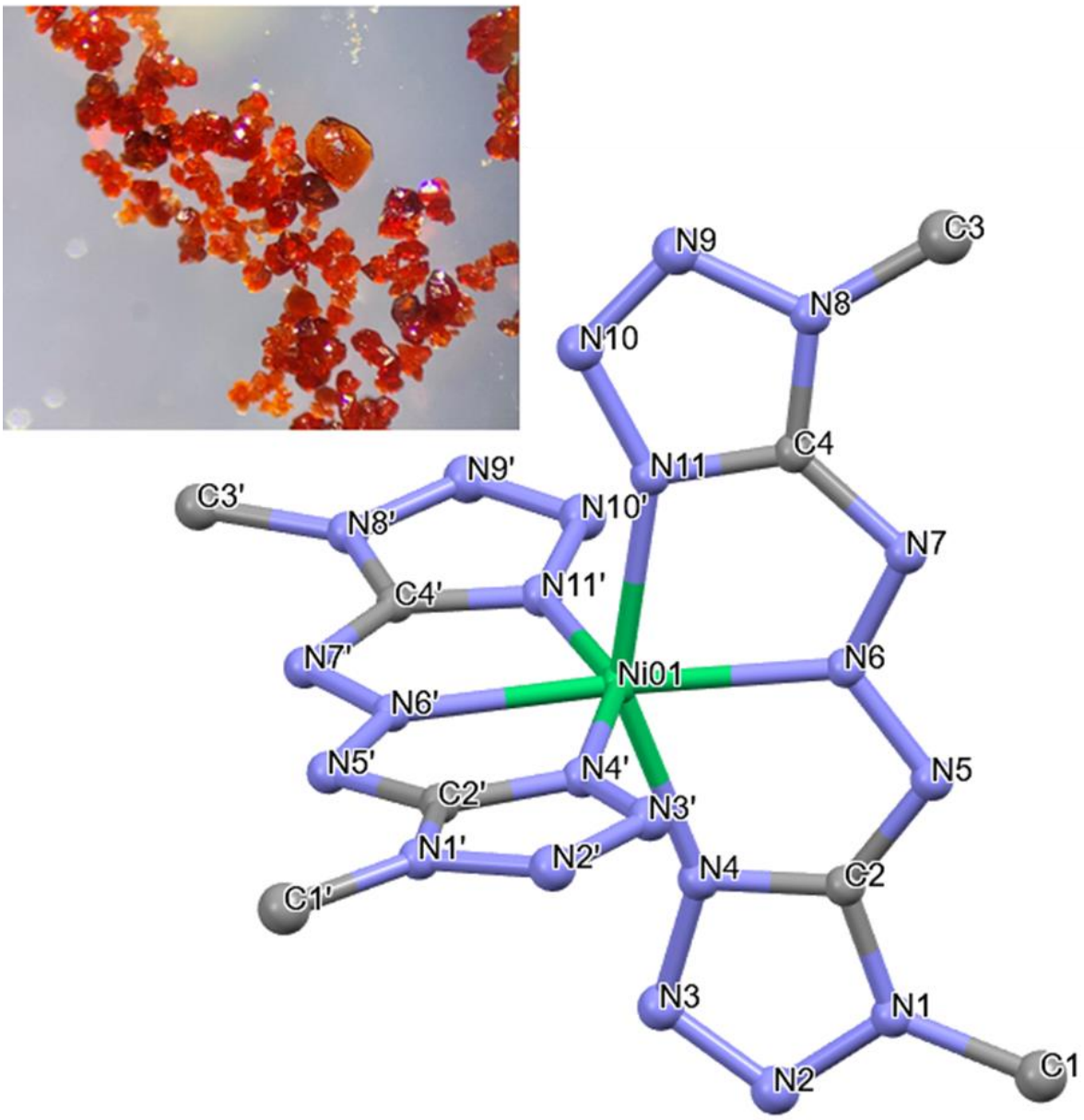

***Figure 4.9**: Top left Inset: Crystals of Ni(B1MTT)$_2$.(CH$_3$)$_2$CO at 4x zoom, Centre: Projections of the thermal ellipsoids in the molecular structure of the crystals of Ni(B1MTT)$_2$.(CH$_3$)$_2$CO, (CH$_3$)$_2$CO and hydrogens removed for clarity, Atom Colours: Blue = Nitrogen, Grey = Carbon, Green = Nickel, White = Hydrogen*

Two triazenido ligands bind to the Ni centre each in a tridentate chelating manner (**Figure 4.9**). Each triazenido ligand binds in the same manner with binding interactions to Ni taking place through N4, N6 and N11. No other binding interactions take place through any of the other nitrogens of the triazenide. Each $Ni(B1MTT)_2$ unit therefore forms as monomeric units with only van der Waals forces determining the crystal packing. Each $Ni(B1MTT)_2$ unit forms as a distorted octahedron with the N6-Ni-N6 angle being 170.41(1)° and the two N4-Ni-N11 angles being 151.51(1)° and 150.97(1)°. N-Ni bonds range from 2.071(3)-2.089(3) Å with ring nitrogen-nickel bond length being very slightly shorter on average than triazenide chain nitrogen-nickel bond length (2.079 vs 2.083 Å). 8 units of $Ni(B1MTT)_2$ sit inside the unit cell with 8 acetone molecules also present. No strong interactions between acetone and $Ni(B1MTT)_2$ can be said to take place, though a weak hydrogen bond between C-H of acetone and N3 of a tetrazole ring can be observed.

4.2.6 Structural determination of $Co(B1MTT)_2.(CH_3)_2CO$

The mauve precipitate proved to be insoluble in most common solvents similar to $Ni(B1MTT)_2.H_2O$ and was also found to be sparingly soluble in acetone. Dissolution of 40 mg of the crude material in 150 ml of acetone followed by slow evaporation of the solvent resulted in the growth of large, thick, hexagonal crystals (**Figure 4.10**). SXRD was used to identify the composition of the crystal. $Co(B1MTT)_2$ crystalises in the space group $P2_1/n$ with a disordered acetone molecule. Each triazenido ligand binds in a tridentate chelating manner through N4, N6 and N11. Each $Co(B1MTT)_2$ unit forms a distorted octahedral shape with no bonding interactions between $Co(B1MTT)_2$ units; only van der Waals interactions define their crystal packing. Three units of $Co(B1MTT)_2$ are present in the unit cell with 3 disordered acetone molecules. Each $Co(B1MTT)_2$ unit forms as a distorted octahedron with the N6-Co-N6' angle being 164.66(2)° and the two N4-Co-N11 angles being 146.56(2)° and 147.69(2)°. N-Co bonds range from 2.101(6)-2.143(6) Å with ring nitrogen-cobalt bond length being shorter on average than triazenide chain nitrogen-cobalt bond length (2.111 vs 2.143 Å).

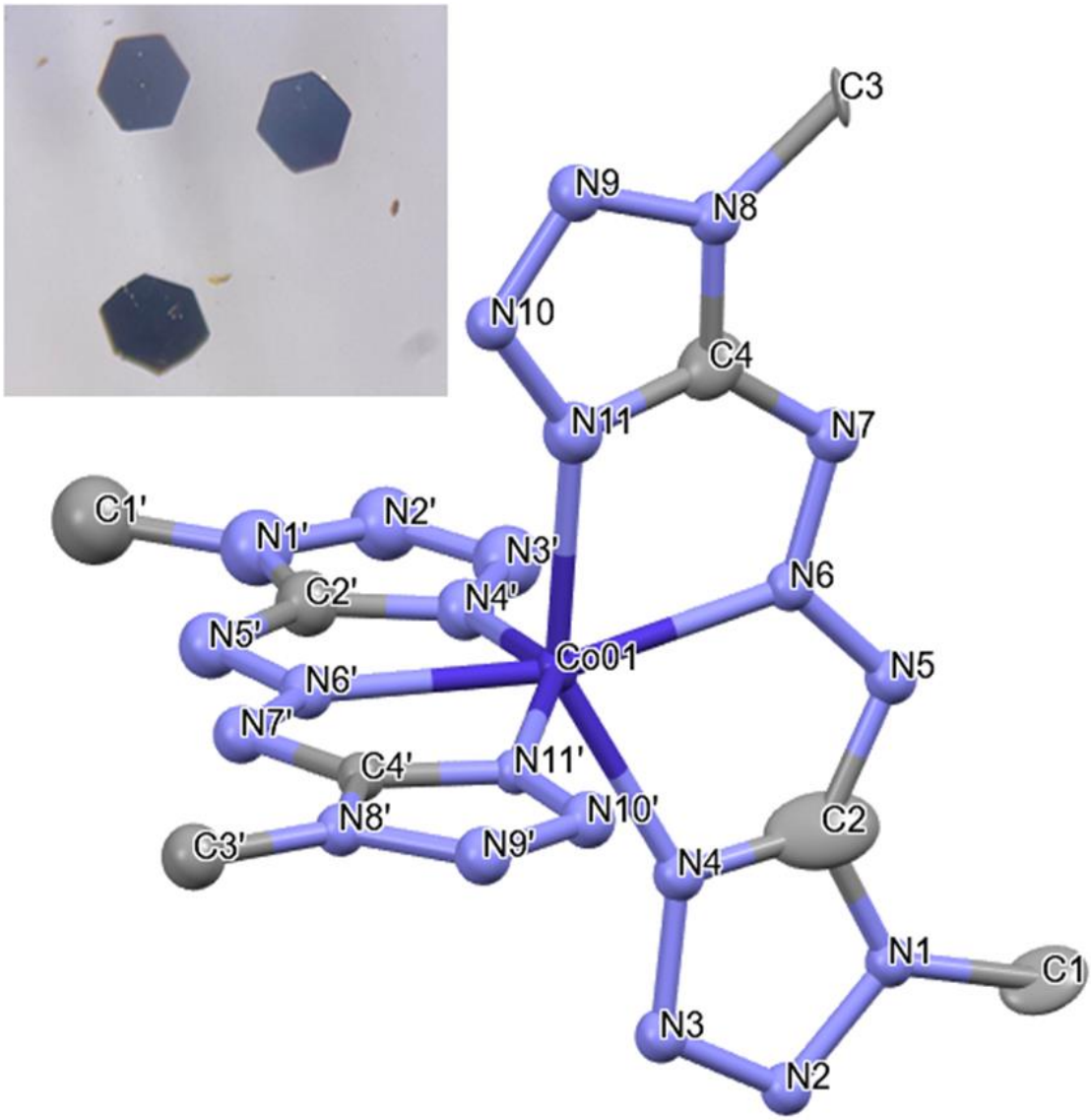

Figure 4.10: *Left: Hexagonal shaped crystals of Co(B1MTT)$_2$.(CH$_3$)$_2$CO at 4x zoom, Right: Projections of the thermal ellipsoid in the molecular structure of the crystals of Co(B1MTT)$_2$.(CH$_3$)$_2$CO, (CH$_3$)$_2$CO and hydrogens removed for clarity, Atom Colours: Blue = Nitrogen, Grey = Carbon, Dark Blue = Cobalt, White = Hydrogen*

4.2.7 Structural determination of $Fe(B1MTT)_2.(CH_3)_2CO$ and comparison to $Ni(B1MTT)_2.(CH_3)_2CO$ and $Co(B1MTT)_2.(CH_3)_2CO$

Unlike the previous triazenide complexes, $Fe(B1MTT)_2.H_2O$ proved to be highly soluble in acetone. Dissolution of 150 mg of the crude material in 150 ml of acetone followed by slow evaporation of the solvent resulted in the growth of large, dark green, rectangular crystals (**Figure 4.11**). SXRD was used to identify the composition of the crystal. SCXRD confirmed the crystallised compound to be $Fe(B1MTT)_2.(CH_3)_2O$. $Fe(B1MTT)_2.(CH_3)_2CO$ crystallises in the $P2_1/n$ space group. Two triazenido ligands bind to the Fe centre each in a tridentate chelating manner (**Figure 4.11**). Each triazenido ligand binds in the same manner with binding interactions to Fe taking place through N1, N7 and N13. No other binding interactions take place through any of the other nitrogen of the triazenide. Each $Fe(B1MTT)_2$ unit therefore forms as monomeric units with only van der Waals forces determining the crystal packing. Each $Fe(B1MTT)_2$ unit forms as a distorted octahedron with the N6-Fe-N6' angle being 175.1(4)° and the two N4-Fe-N11 angles being 157.46(4)° and 157.18(4)°. Three units of $Fe(B1MTT)_2$ sit inside the unit cell with 3 acetone molecules also present. N-Fe bonds range from 1.906(9)-1.948(1) Å with ring nitrogen-iron bond lengths being longer on average than triazenide chain nitrogen-iron bond length (1.936 vs 1.917 Å). No strong interactions between acetone and $Fe(B1MTT)_2$ can be said to take place. Comparisons between the common bond angles, lengths and coordination modes of metal compounds of B1MTT can be made to observe trends across this family of compounds. The internal bond lengths of the tetrazolyl groups of B1MTT follow broadly similar trends across their metal coordination compounds. N1-N2/N8-N9 and N3-N4/N10-N11 bond lengths are on average the longest found with fairly large differences between the shortest and longest values. N1-N2/N8-N9 values vary the most across tetrazoles in each compound but as an average are quite similar in value across each of the metal compounds. Co and Fe have similar average values and ranges for N3-N4/N10-N11, however Ni has the longest average N3-N4/N10-N11 length with a narrower range of values. N2-N3/N9-N10 and $C_{tetrazole}$-$N_{tetrazole}$ bond lengths are found to be shorter on average than N1-N2/N8-N9 and N3-N4/N10-N11 across all coordination compounds and are broadly similar in both range and value

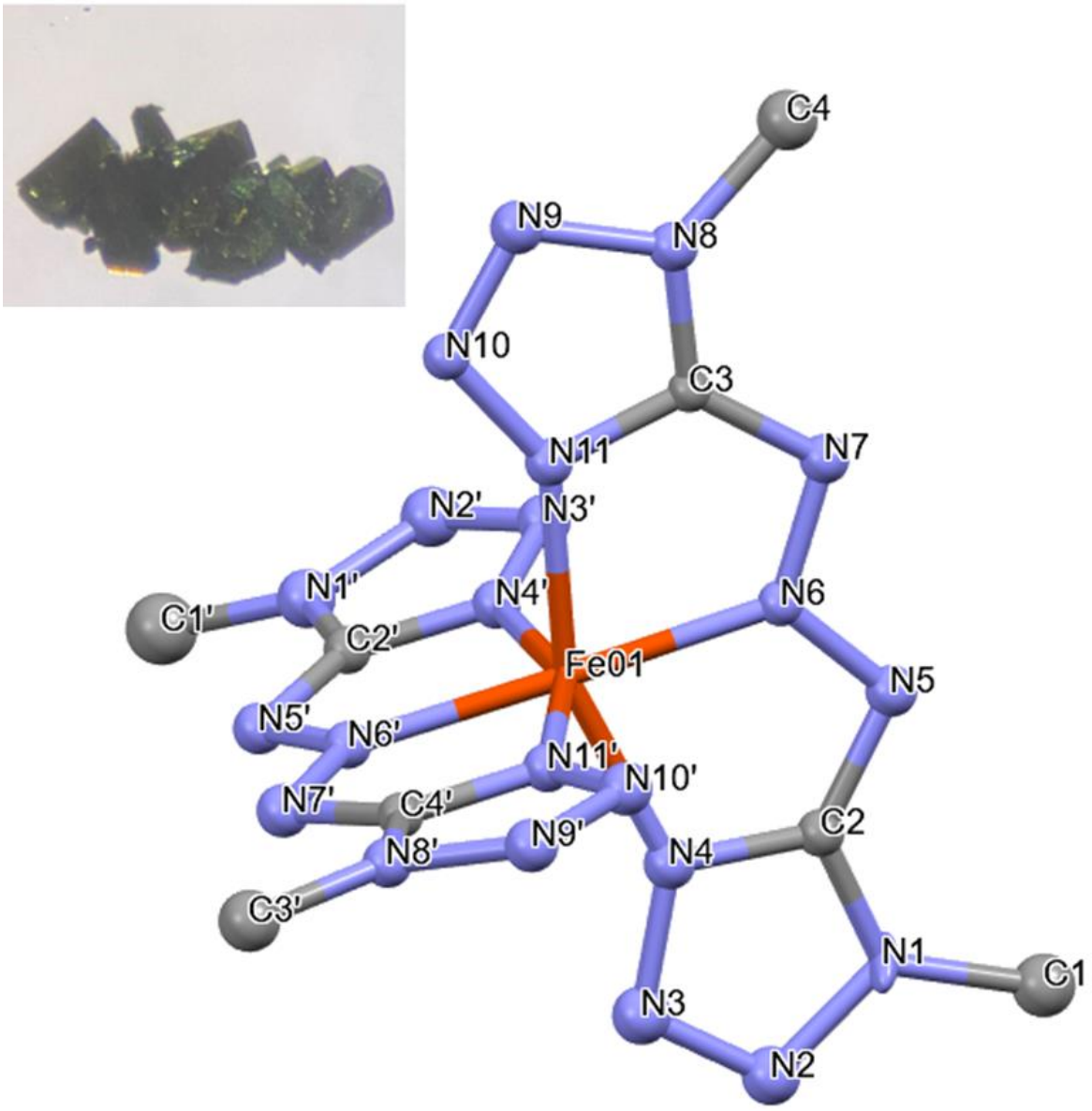

Figure 4.11: *Left: Dark green crystals of Fe(B1MTT)$_2$.(CH$_3$)$_2$CO at 4x zoom; Right: Projections of the thermal ellipsoid in the molecular structure of the crystals of Fe(B1MTT)$_2$.(CH$_3$)$_2$CO, (CH$_3$)$_2$CO and hydrogens removed for clarity, Atom Colours: Blue = Nitrogen, Grey = Carbon, Orange = Iron, White = Hydrogen,*

between Fe, Co and Ni except for two anomalously short $C_{tetrazole}$-$N_{tetrazole}$ bond for Fe at 1.310(1) Å. N2-N3/N9-N10 bond lengths are consistently the shortest across all coordination compounds and breaking this bond is the most likely first step in tetrazole decomposition to form N_2. Ni has the smallest range of values for N2-N3/N9-N10 whilst also having on average the longest N2-N3/N9-N10 bond. Both Co and Fe have a wide range of values for N2-N3/N9-N10 lengths with each possessing at least one N2-N3/N9-N10 length substantially shorter than that of Ni (Shortest bonds: Ni: 1.293(4) Å, Co: 1.275(9) Å, Fe: 1.265(1) Å). Providing that tetrazole decomposition and elimination of N_2 is the first stage of the decomposition of B1MTT this could be an indication that Co and Fe are more thermally unstable than the Ni salt. The length of the N-N bonds in the triazene chain show some similarities for Co and Ni and slight differences for Fe. Both Ni and Co have two types of triazene chain present in their ligands, one chain where both the N5-N6 and N6-N7 bond lengths are near identical and one which features a shortened N5-N6 compared to the N6-N7 bond length. Fe is again different in that the difference between N5-N6 and N6-N7 bond lengths is lower than for either Co/Ni. The average of the N-N bond lengths of the triazene chain for each B1MTT unit is broadly the same for Ni and Co while Fe features a small but much more substantial difference in the bond length averages of the triazene chain of its two B1MTT units.

$Fe(B1MTT)_2$ has much shorter metal-nitrogen bonds than for either Co or Ni. Fe is also unique in the fact that the Fe-N6 bond length is shorter than the average Fe-N4/N4' distance, in both the Co and Ni complexes it is the M-N4/N4' distance which is shorter. As a result of this and to account for steric repulsion $Fe(B1MTT)_2$ has the largest average N-M-N angle at 157.32° compared to Ni (151.22°) and Co (147.125°).

It is important to compare these trends in bond lengths to other related compounds to see if the trends present can be said to originate as a result of the metal present or as a ligand effect. The most closely related compound to the $M(B1MTT)_2.(CH_3)_2CO$ compounds are the coordination compounds of bis-2-methyltetrazol-5-yl)triazenide (B2MTT) for which the Fe, Co and Ni compounds are known.[7] Much like the $M(B1MTT)_2$, compounds $Fe(B2MTT)_2$ has consistently shorter metal-nitrogen bond lengths than for $Co(B2MTT)_2$ or $Ni(B2MTT)_2$. For the Co compounds, $Co(B2MTT)_2$ has substantially shorter Co-N bond lengths than $Co(B1MTT)_2$ regardless of the environment of the coordinating N atom ($N_{tetrazole}$ vs

$Nt_{triazenide}$).[7] Likewise Ni(B2MTT)$_2$ has slightly shorter Ni-$N_{tetrazole}$ bonds substantially shorter Ni-$N_{triazenide}$ bonds. This trend flips for the Fe compounds with Fe(B1MTT)$_2$ having shorter Fe-N bonds than that for Fe(B2MTT)$_2$. Not only are the bond length changes different for each metal, the trends regarding length of M-$N_{tetrazole}$ vs M-$N_{triazenide}$ also change. For Co(B1MTT)$_2$ and Ni(B1MTT)2, the average Co-$N_{tetrazole}$/Ni-$N_{tetrazole}$ bond length is shorter than Co-$N_{triazenide}$/Ni-$N_{triazenide}$ whereas for Co/Ni(B2MTT)$_2$, Co/Ni-$N_{tetrazole}$ is now substantially longer than Co/Ni-$N_{triazenide}$. For Fe this effect does not happen and Fe-$N_{triazenide}$ is consistently the shortest Fe-N bond in both B1MTT and B2MTT compounds. One would expect consistency in regard to these bond lengths with either the B2MTT or the B1MTT compound consistently having longer/shorter M-N bond lengths. It can be reasonably assumed that the changes to both sigma donor capabilities and steric repulsion effects when going from B1MTT to B2MTT have some role to play in this, but these phenomena are still not fully understood.

Comparison to other homoleptic Fe/Co/Ni compounds can also be made to view trends regarding Fe, Co and Ni compounds. The structures of hexaamino-metal(II)-halides were published by Eβman et al. and serve as a good comparison for both Fe vs Ni structures and gives more data for comparisons of Fe vs Co.[20] $[Fe(NH_3)_6]Cl_2$ has longer M-N bonds than that found for $[Ni(NH_3)_6]Cl_2$ (2.207 vs 2.107(2) Å) and $[Fe(NH_3)_6]Br_2$ has longer bonds than that found for $[Co(NH_3)_6]Br_2$ (2.216 vs 2.176 Å). This directly contrasts the results found for Fe(B1MTT)$_2$ and Ni(B1MTT)$_2$ where the Fe compound had the much shorter M-N bonds for both $N_{tetrazole}$ and $N_{triazenide}$. This can be explained by observing the spin states of the metal ions. The hexaamino-metal(II) halides have all been measured to be high spin complexes.[20] High spin Fe has electrons occupying the two degenerate e_g orbitals resulting in greater repulsion along the ligand axis and therefore increased bond lengths. As it is known that the M(B2MTT)$_2$ compounds are low spin it is reasonable to assume a similar spin state for the M(B1MTT)$_2$ compounds due to the similarity of the ligands.[7] If the M(B1MTT)$_2$ are low spin then this would help to explain the apparent differences to the $[M(NH_3)_6]^{2+}$ complexes. Low spin Fe^{2+} would result in occupation of only the t_{2g} set of orbitals resulting in less repulsion along the ligand axis (observed as Fe(B1MTT)$_2$ has the shortest metal-nitrogen bond lengths). Low spin Co^{2+} would have a singly occupied e_g orbital, resulting in Jahn-Teller distortion and a compression or elongation of the

ligands bond lengths (potentially seen with the elongation of the triazenide axis, resulting in $Co(B1MTT)_2$ having the longest metal-triazenide bond). Low spin Ni^{2+} has the same electron configuration as high spin Ni^{2+} and so has the smallest change in both its bond lengths compared to its hexaamino complex and also has the smallest average difference between $M\text{-}N_{triazenide}$ and $M\text{-}N_{tetrazole}$. The spin state of the $M(B1MTT)_2$ compounds should be determined through magnetic measurements to confirm this explanation.

4.2.8 Attempts at recrystallisation of $Zn(B1MTT)_2$ and $Pb(B1MTT)_2$

Much like both the Co and Ni compounds, small amounts of $Zn(B1MTT)_2$ could be dissolved in acetone however, recrystallisation to form single crystals of sufficient quality for SCXRD could not be achieved in this manner. $Pb(B1MTT)_2$ proved insoluble in all solvents except DMF and DMSO and could not be recrystallised to obtain structural information.

4.2.9 Metal compounds of bis(1-methyl-tetrazol-5-yl)triazene as potential lead-free energetic materials

Thermal analysis of the metal compounds of bis(methyltetrazolyl)triazene was investigated with DSC (See **Appendix 8.6-8.64**). Onset temperatures, peak temperature and enthalpies of decomposition were calculated from their data (**Table 4.3**). All compounds proved to be highly temperature stable with the least thermally stable, $Fe(B1MTT)_2.(CH_3)_2CO$, possessing an onset temperature of 268.4 °C and the most thermally stable, $Ni(B1MTT)_2$, possessing an onset temperature of 321.8 °C. The results of thermal analysis are in agreement with the tends predicted from analysis of tetrazole N-N bond length with $Fe(B1MTT)_2.(CH_3)_2CO$ (1.265(1) Å for N2-N3/N9-N10) being far more thermally unstable than the Ni/Co compounds. This result does lend evidence to the theory that N2-N3/N9-N10 cleavage is the first step in metal-triazenide decomposition. Following from this it is reasonable to suggest that $Zn(B1MTT)_2$ may also possess a shortened N2-N3/N9-N10 bond whilst $Pb(B1MTT)_2$ could have a N2-N3/N9-N10 bond length similar to that found in the Ni/Co compounds assuming that the decomposition pathway is the same. All compounds possessed decomposition

temperatures above that required for any potential LFI (T_{on}>200 °C) highlighting the potential for use of these compounds as lead azide or lead styphnate replacements (excluding $Pb(B1MTT)_2$) dependent on the results of other tests.

Metal-triazenide	**Onset temperature, T_{on}/ °C**	**Peak temperature, T_{peak}/ °C**	**Enthalpy of decomposition / J g^{-1}**	**Enthalpy of decomposition / kJ mol^{-1}**
$Fe(B1MTT)_2.(CH_3)_2O$	268.4	279.0	1303	675
$Co(B1MTT)_2.H_2O$	310.5	311.5	1331	681
$Ni(B1MTT)_2.H_2O$ (Crude)	321.8	324.4	1304	667
$Zn(B1MTT)_2$ (crude)	267.7	276.4	1545	744
$Pb(B1MTT)_2$	312.4	319.0	1138	710
DBX-1	294.0	305.6	1653	294

Table 4.3: *Comparison of the onset temperature of decomposition, peak temperature of decomposition and enthalpy of decomposition of metal-triazenide compounds and DBX-1*

The compounds also possessed high enthalpies of decomposition which molar enthalpies of decomposition much greater than that found for the prospective LFI DBX-1. Once more the molar enthalpy of decomposition can be used for estimation of the heat of formation which, alongside crystal densities estimated according to the methods stated previously, can be used for calculation of heat of detonation, detonation velocity and detonation pressure (**Table 4.4**). For all metal triazenido compounds, values for Q, D and P are in the range expected of primary explosives (**Table 4.4**). All compounds are found to have lower predicted detonation velocities and pressures than that found for lead azide and DBX-1. While high values for Q, D and P are not essential for a prospective LFI it is still important to maintain similar values to those found for lead azide and while in all cases the metal triazenides do not match lead azide they are not so low as to rule out these compounds as potential LFI's. The phlegmatizing effect of H_2O and $(CH_3)_2CO$ on the Ni,Co an Fe compounds

is also apparent with all possessing lower detonation pressures and velocities than that found for Zn and Pb. Once desolvated the Fe/Co/Ni compounds could have estimated detonation velocities as high as that calculated for $Pb(B1MTT)_2$. Comparisons to DBX-1 show that across all parameters, DBX-1 proves to be the higher performance explosive. While the metal triazenides possess high heats of formation, the low densities compared to DBX-1 are the cause for the comparably low detonation velocities. However, with the challenges of DBX-1 synthesis shown, the metal triazenides could hold potential as alternative lead azide or lead styphnate replacements.

Metal-triazenide	**ΔH_d/kJ mol^{-1}**	**ΔH_f/kJ mol^{-1}**	**ρ/ g cm^{-3}**	**Q/ J g^{-1}**	**P/ kbar**	**D/ km s^{-1}**
$Fe(B1MTT)_2.(CH_3)_2CO$	675	273.2	1.587	1289.0	91.02	4.667
$Co(B1MTT)_2.H_2O$	681	442.3	1.702	1397.8	105.73	4.919
$Ni(B1MTT)_2.H_2O$	667	428.2	1.713	1369.7	106.07	4.917
$Zn(B1MTT)_2$	744	728.8	1.629	1565.8	108.38	5.050
$Pb(B1MTT)_2$	710	702.2	2.059	1150.5	147.75	5.501
DBX-1	294	-49.9	2.584	1695.6	219.97	6.341
$Pb(N_3)_2$	-	-	4.763	-	338	5.920

Table 4.4: *Comparison of the heats of decomposition (ΔH_d), calculated heats of formation of the metal triazenides (ΔH_f), estimated densities(densities estimated using the methods of Ammon and Hofmann,[21][22] heat of explosion (Q), detonation velocity (D) and detonation pressure (P) values for metal-triazenide compounds compared to know values of DBX-1 and $Pb(N_3)_2$*

4.2.10 Long term water stability

The long-term water stability of each compound was also tested. 20 mg of each salt was added to sealed vials of deionised water and left submerged for two months. After two months the samples were filtered, dried and through both inspection and analysis of FTIR spectra were inspected for signs of decomposition. Samples of $Pb(B1MTT)_2$, $Co(B1MTT)_2.H_2O$ and $Fe(B1MTT).(CH_3)_2CO$ showed no changes in their FTIR spectra

except for a noticeable exchange of acetone for H_2O in the case of Fe(B1MTT).$(CH_3)_2CO$ forming Fe(B1MTT)$_2$.H_2O (**Appendix 8.32, 8.33 and 8.36**). The M(B1MTT)$_2$ moiety can be considered water stable for long periods of time in these cases. Zn(B1MTT)$_2$ shows some minor changes to its absorption bands following water immersion (**Figure 4.12**). Some bands appear less well resolved while others feature more prominently in the spectrum. This could be due to poor mulling during sample preparation or due to decomposition, further investigation of this solid is required. However, as these changes are relatively minor it can be stated that the majority of the Zn(B1MTT)$_2$ has not decomposed during the 2-month immersion in water. Ni(B1MTT)$_2$.H_2O shows the largest changes during its water immersion (**Figure 4.13**). Three new intense absorption bands can be seen in the range 1250-750 cm $^{-1}$. It is unlikely a new hydrate is forming due to no changes appearing in the 4000-3000 cm^{-1} range. It is possible this is indication of decomposition, but the product of this decomposition is currently unknown.

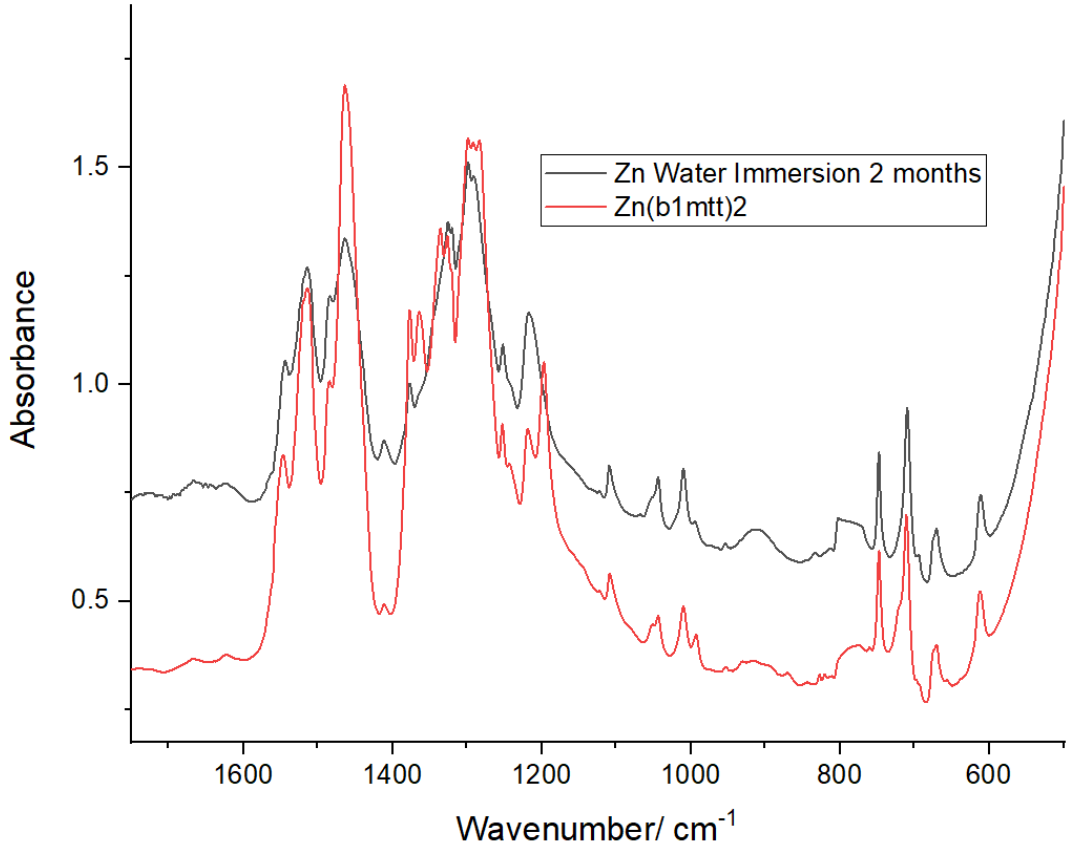

Figure 4.12: *Series of FTIR spectra in the range 4000-500 cm^{-1}, Zn(B1MTT)$_2$ (red), Zn(B1MTT)$_2$ following immersion into water for 2 months (black)*

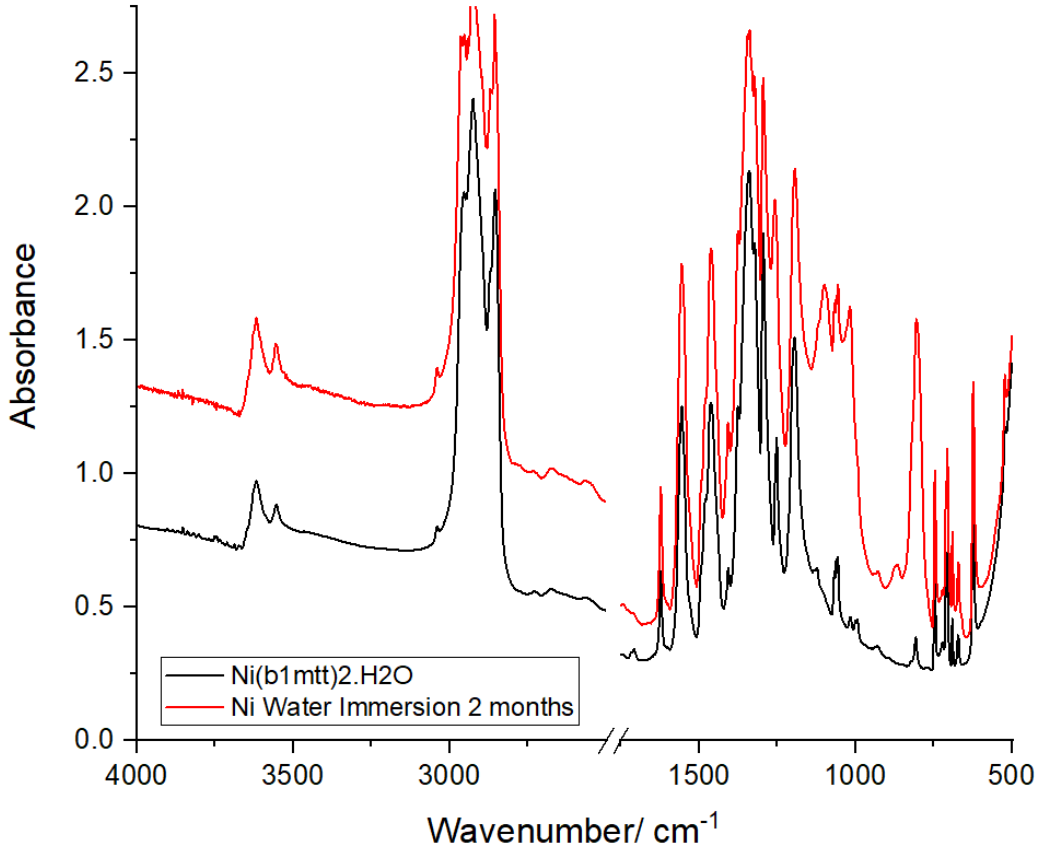

Figure 4.13: *Series of FTIR spectra in the range 4000-500 cm^{-1}, $Ni(B1MTT)_2.H_2O$ (red), $Ni(B1MTT)_2.H_2O$ following immersion into water for 2 months (black)*

With all peaks associated with $Ni(B1MTT)_2.H_2O$ remaining in the spectrum the analysis suggests that the $Ni(B1MTT)_2$ moiety has mostly survived 2 months of water immersion , but this cannot be proven until further analysis in the form of elemental analysis is recorded

4.2.11 Impact Sensitiveness

Impact sensitiveness of the compounds could not be recorded during this research project and so these products have not yet been proven to be initiatory materials. The presence of acetone and H_2O in the Fe/Co/Ni compounds could have an effect on the sensitiveness to impact of the compounds (decrease/increase of phonon mode up-pumping efficiency) so each compound must have its sensitiveness recorded both before and after desolvation to observe the effect of the crystallisation solvent on sensitiveness. For the Ni/Zn compounds, compound purity must also be proven as the

crude materials may also have their sensitiveness towards impact affected by the assumed non energetic inorganic material present in the crude material. Until the sensitivity and sensitiveness of the compounds can be established, the compounds cannot be viewed as viable LFI's for use in either detonators or igniters.

4.2.12 Addition to Cu(II): Formation of a mixed ligand coordination compound

Using $CuCl_2$ as the metal salt gave a change in reaction product. Unlike with the other metals salts, the addition of B1MTT to $CuCl_2$ resulted in the formation of a dark brown solution with no precipitation. Slow evaporation of the dark solution led to the formation of dark brown crystals. Flame tests of the material showed no explosion with just a simple decomposition observed leaving behind a black residue. Single crystal X-ray diffraction helped to prove the identity of the dark brown crystals as Cu(B1MTT)Cl(H_2O). The crystal structure shows the Cu(II) coordination centre to have an octahedral geometry (**Figure 4.14**). The coordination sphere is made up of 3 bonds to the triazenido ligand, two to the ring nitrogen atoms of tetrazole, and one to the central nitrogen of the triazene bridge. The other coordination sites are occupied by Cl and H_2O. Each Cl bridges between two copper atoms and has one short (2.227(9) Å) and one long (2.847(9) Å) bond. Cu(B1MTT)Cl(H_2O) forms as long chains of complexes, bound together through the Cl-Cu bond. Hydrogen bonding is present in the crystal but in both the layers and between layers. Hydrogen bonding in the layer is present between the hydrogen atoms of the water molecule and Cl and hydrogen bonding between layers is found between hydrogen atoms of the water molecules and a nitrogen of the triazene chain. As a mixed azolyltriazenido-chlorido-copper coordination compound it is important to compare bond lengths and angles common to other azolyltriazenido-chlorido-copper coordination compounds if structures are known. Cu(1,3-bis(3-(5-amino-1,2,4-triazolyl)triazenido)Cl.H_2O (Cu(BATT)(Cl).H_2O), first synthesised by Hanot et al.,[18] provides an excellent reference compound to compare alike bonds and structural motifs. Like for Cu(B1MTT)(Cl)(H_2O), the 1,3-bis(3-(5-amino-1,2,4-trizolyl)triazenido (BATT) ligand also coordinates to the Cu atom in a tridentate mode. Both compounds also feature two bonds to from Cu to Cl resulting in a similar chain structure developing.

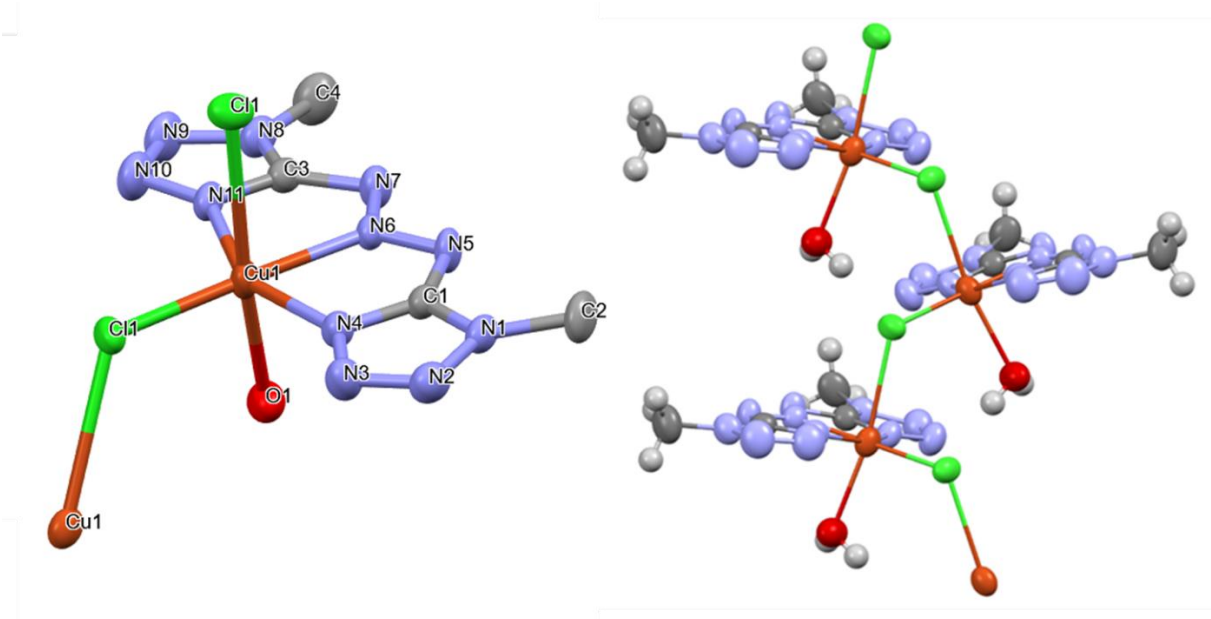

Figure 4.14: *Left: Projections of the thermal ellipsoid in the molecular structure of the crystals of Cu(B1MTT)(Cl)(H_2O), hydrogens removed for clarity; Right: Chains of Cu(B1MTT)(Cl)(H_2O), Atom Colours: Blue = Nitrogen, Grey = Carbon, Orange = Copper, White = Hydrogen, Green = Chlorine, Red = Oxygen*

Unlike Cu(B1MTT)(Cl)H_2O, Cu(BATT)(Cl).H_2O does not see coordination of the water molecule to the Cu atom and instead it is present only in the crystal. This results in the formation of a stair-like chain structure held together only through bonds between Cu and Cl. Cu(B1MTT)(Cl)(H_2O) does not form the stair-like chain and instead forms an infinitely extending skew polygon chain between Cu and Cl with the chain also held together by the weak hydrogen bonds from H_2O towards the Cl (2.39 Å). The effect of the presence of hydrogen bonding on the chain structure can also be seen in the Cl-Cu-Cl bond angles with Cu(BATT)(Cl).H_2O having an angle of 95.06° whereas Cu(B1MTT)(Cl)(H_2O) has two Cl-Cu-Cl bond angles one of 93.37(3)° and one much larger angle at 120.04(4)° with the larger angle being the most closely affected by the presence of H_2O. The Cu-Cl distances of both follow similar trends with a short and long Cu-Cl bond. Whilst the short Cu-Cl bonds are of similar length (2.227(9) vs 2.268 Å) the long Cu-Cl bond of Cu(B1MTT)(Cl)(H_2O) is greatly elongated compared to Cu(BATT)(Cl).H_2O (2.847(9) vs 2.586 Å). This is again most likely due to the steric demands of a coordinated H_2O vs a H_2O present unbound in the unit cell. Both

compounds share similarities in their Cu-N bond lengths with both compounds having a longer Cu-$N_{triazenide}$ bond length for than for Cu-N_{azole}.

Comparisons can also be made between the bonds lengths and angles present in the Copper salt to those present in the other novel metal triazenides discussed previously. Cu(B1MTT)(Cl)(H_2O) has Cu-N distances between that of Fe and Ni and fits the trend of Co and Ni whereby the Cu-$N_{tetrazole}$ bond length is shorter than Cu-$N_{triazenide.}$ N-Cu-N bond angles are also comparable to N-Ni-N with a value of 152.60(1)°. Triazenide chain N-N bond lengths however are identical to the values of one of the triazenide chains of Fe(B1MTT)$_2$. One could argue that the reason Cu takes bond length and angle values between that of Fe and Ni is due to the poorer sigma donor capabilities of Cl^- + H_2O versus that of another B1MTT ligand, thus allowing for stronger bonding of the B1MTT ligand to the Cu atom.

Internal bond lengths of Cu(B1MTT)(Cl)(H_2O) can also be compared to that of the known M(B1MTT)$_2$ complexes discussed previously. Cu broadly follows the same trends as these complexes with longer average N3-N4/N10-N11 and N1-N2/N8-N9 bond lengths compared to N2-N3/N9-N10. The N2-N3/N9-N10 bond length of Cu(B1MTT)(Cl)(H_2O) has a range of 1.282(4)-1.291(4) Å. While the average bond length is similar to that found for Fe and Co the smaller range of values and the absence of one noticeably shorter N2-N3/N9-N10 distance could indicate that Cu(B1MTT)(Cl)(H_2O) represents a more thermally stable compound than either of the Fe or Co compounds, provided that the decompositions of mono substituted triazenide compounds also follow the same decomposition pathway. A PXRD diffractogram was recorded and compared to a PXRD diffractogram calculated from the SCXRD data recorded for Cu(B1MTT)(Cl(H_2O). Comparison of the datasets shows that the crystalline material contains only the peaks calculated from the single crystal(with small shifts in all peak positions) and can be considered purely as one phase (**Figure 4.15**).

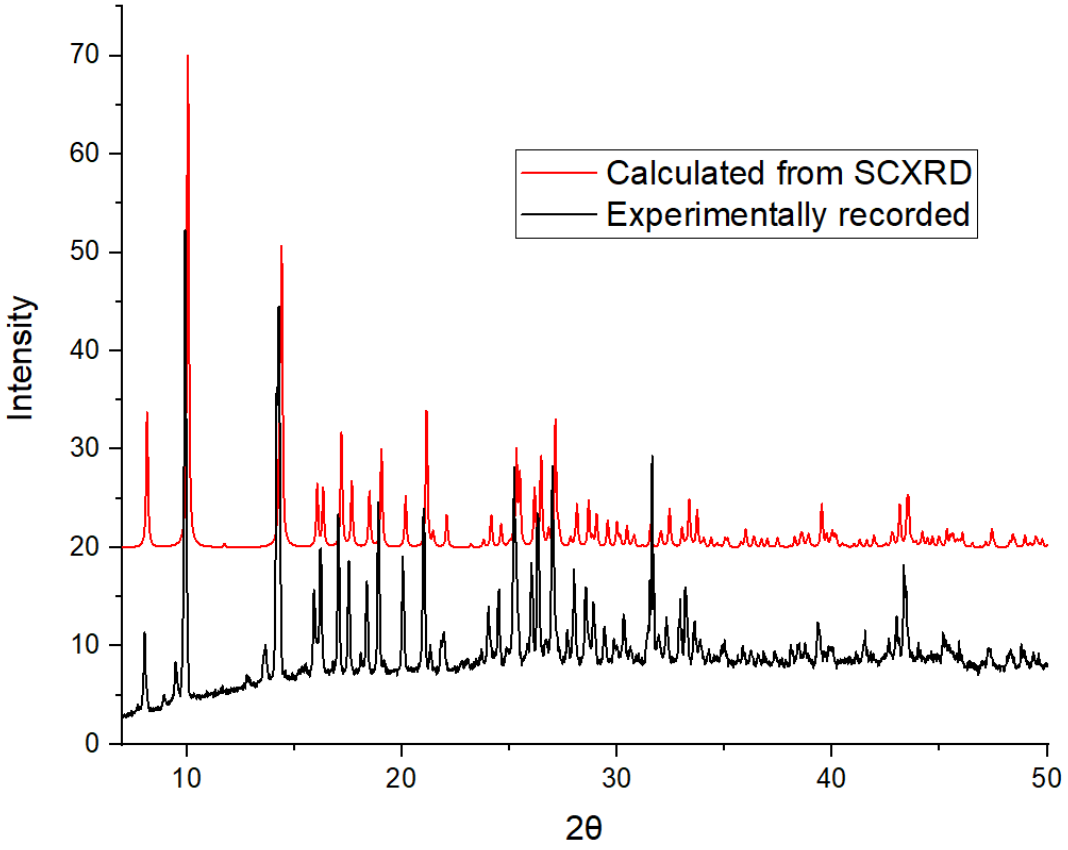

Figure 4.15: *Series of PXRD diffractograms in the range 5-50 2Θ, Red=Spectrum calculated from single crystal data of Cu(B1MTT)Cl(H_2O), Black= Experimentally recorded PXRD of Cu(B1MTT)Cl(H_2O)*

4.2.13 Thermal Behaviour

The thermal stability of Cu(B1MTT)(Cl)(H_2O) was investigated with DSC (See **Appendix 8.65**). The DSC calorigram of Cu(B1MTT))Cl).H_2O is fairly complex with 3 distinct endotherm / exothermic events. The endotherm at 101.6 ^oC could indicate a phase change / melting of the starting material, or decoordination of water; however, this has not been investigated further. The first exotherm at 237.0 ^oC is an indication of decomposition of the B1MTT ligand as its large enthalpy of is unlikely to be associated with the breakdown of Cu-Cl bonds. The smaller exotherm at 273.8 ^oC suggests that at high temperature a defined intermediate is formed that decomposes itself upon temperature increase. The high temperature of decomposition and large enthalpy of decomposition for the first exotherm point to a compound with desirable energetic properties. With a decomposition temperature smaller than that of

$Fe(B1MTT)_2.(CH_3)_2CO$, $Cu(B1MTT)(Cl)(H_2O)$ does not seem to fit the trend of short N2-N3 distances correlating to lower thermal stability, however with the Cu centre also containing bonds to chlorine it is more difficult to assess the first steps in thermal decomposition when compared to the series of $M(B1MTT)_2$ compounds known.

4.2.14 Substitution reactions with Cu(B1MTT)Cl(H_2O)

With one Cl still coordinated to the Cu centre of the compound, addition of a second more energetic (explosophoric) anion was undertaken in an attempt to increase the energetic nature of the compound by substitution of Cl^- and to see if precipitation of an energetic, water-insoluble $Cu(B1MTT)(X)_y$ coordination polymer could be induced (**Table 4.5**).

Cu-Triazenide used	**Explosophoric anion**	**Cu(B1MTT)(H_2O)Cl: Explosophore molar ratio**	**Observations**
$Cu(B1MTT)(H_2O)Cl$	K-4,5-DNI	1:2	Precipitation of green powder
$Cu(B1MTT)(H_2O)Cl$	$Na\text{-}NT.4H_2O$	1:2	No precipitation, only crystals of $Cu(B1MTT)(H_2O)Cl$ and $NaNT.4H_2O$ found. Blue solid also present

Table 4.5: *Results of the reactions of Cu(B1MTT)Cl(H_2O) with explosophoric ligands*

The attempt at synthesis of a mixed B1MTT-Nitrotetrazolate Cu(II) compound did not result in the isolation of any new solid. Instead, only crystalline $Cu(B1MTT)(H_2O)(Cl)$ and $NaNT.4H_2O$ was observed. A light blue solid was also observed which, after spectroscopic analysis, was deemed to be basic copper carbonate. The reason for the lack of substitution could be a result of the binding affinity of Cu(II) for nitrotetrazolate. With Cu(II) as a borderline hard acid and nitrotetrazolate assumed to be a soft base it

is sensible to suggest a stronger affinity for Cl^-(hard base) than for NT^- binding from the Cu(II) cation. Because of this, a strong driving force to induce substitution is required and not provided by the formation of NaCl from the reaction of Cu(B1MTT)(H_2O)Cl and Na-NT.4H_2O. For the addition of K-4,5-DNI to solutions of Cu(B1MTT)(H_2O)Cl, precipitation of a coloured solid is observed. While elemental analysis of this product could not be done prior to the end of the research project, FTIR does enable us to tentatively assign the identity of this product. The green powder isolated after addition of K-4,5-DNI.H_2O to a solution of Cu(B1MTT)(H_2O)(Cl) clearly shows the presence of two absorption bands (1527 cm^{-1} and 860 cm^{-1}) which can be associated to the asymmetric and bending NO_2 vibration modes found in K-4,5-DNI.H_2O (**Figure 4.16**). While the symmetric stretch is a key identifier of the NO_2 group it is unfortunately found in a part of the spectrum dominated by the vibrational modes of the B1MTT ligand and so cannot be used to accurately identify the presence of the 4,5-DNI moiety. Two bands found in K-4,5-DNI.H_2O, 1174 cm^{-1} and 950 cm^{-1} are absent from the spectrum of the precipitated product. These bands, as shown by Epishina are related to the v_{as} and v_{sym} stretches of a charged NO_2 group. The absence of these absorption bands in the spectrum of the precipitated product imply a shift in bonding environment from an ionic one to a more covalently bonded system as one would expect when going from a potassium salt to a covalently bound Cu(II)-4,5-DNI compound. Absorption bands associated with the B1MTT ligand are clearly present in the spectrum of the product and do not suggest that the addition of 4,5-DNI has resulted in displacement of the B1MTT ligand. Absorption bands of H_2O are also still present albeit reduced in intensity from both starting materials. Overall, the evidence from FTIR strongly suggests that substitution of the chloride has taken place with 4,5-DNI binding to the Cu(II) as shown by the disappearance of charge NO_2 absorptions. With the absorption bands of both B1MTT and water still present it is reasonable to suggest that the compound is of the formula Cu(B1MTT)(4,5-DNI)(H_2O)x. Full characterisation of the compound along with an assessment of its energetic properties could not be completed during the timeframe of this research project.

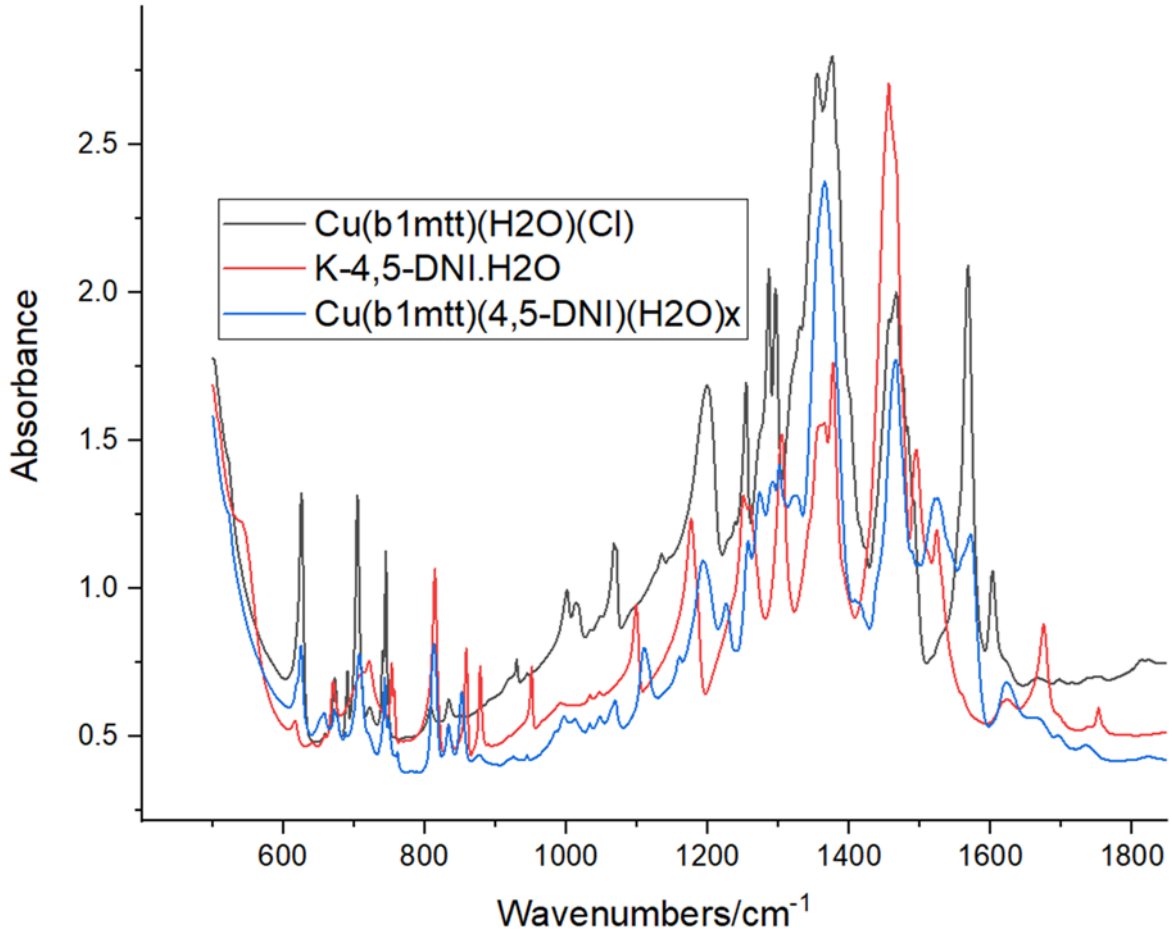

Figure 4.16: *Series of FTIR spectra in the range 4000-500 cm^{-1},* Cu(B1MTT)(H_2O)Cl (black), K-4,5-DNI.H_2O (red), Cu(B1MTT)(H_2O)(4,5-DNI) (blue)

4.2.15 Synthesis of PPN[bis(1-methyl-3-nitro-triazol-5-yl)-triazenate]

Following on from the work with bis(methyltetrazolyl)triazenes, we focused on the synthesis of new nitroazolate-containing triazenes which had not been reported in the open literature and could lead to some novel energetic materials with properties (in simple theory) that closely resemble known energetic triazenes such as B1MTT (seen as a prospective nitrogen rich rocket propellant). 1-Methyl-3-nitro-5-amino-1,2,4-triazole was chosen as the starting material for synthesis of novel triazenes. 1-methyl-3-nitro-5-amino-1,2,4-triazole was chosen as this would form a triazene with a single de-protonatable site and also because the methylated derivatives of amino containing azoles have been shown to work as precursors to triazenes. 3 Nitro-5-amino-triazole was synthesised as detailed in the paper by Liu et al.[23] 1-Methyl-3-nitro-5-amino-triazole was synthesised by the addition of dimethyl sulphate to 3-nitro-5-amino-

triazole according to the work of Klapötke et al.[24] Bis(1-methyl-3-nitro-triazol-5-yl)-triazene was synthesised by the addition of sodium nitrite to an acidic solution of 1-methyl-3-nitro-5-amino-triazole (**Figure 4.17**). After stirring overnight at room temperature, bis(1-methyl-3-nitro-triazol-5-yl)triazene (B1M3NTT) precipitated out as a pale yellow solid. The solid was dissolved in water with an equimolar amount of sodium hydroxide before the addition of (PPN)Cl to precipitate the ligand as its PPN salt (PPN = bis(triphenylphosphine)iminium). This would serve as an easily recrystallisable material which could be used to prove the synthesis of the novel triazene while also diluting the potential sensitiveness of the compound which allows for easy handling of an energetic ligand of unknown sensitiveness. This resulted in the immediate precipitation of a dark yellow solid.

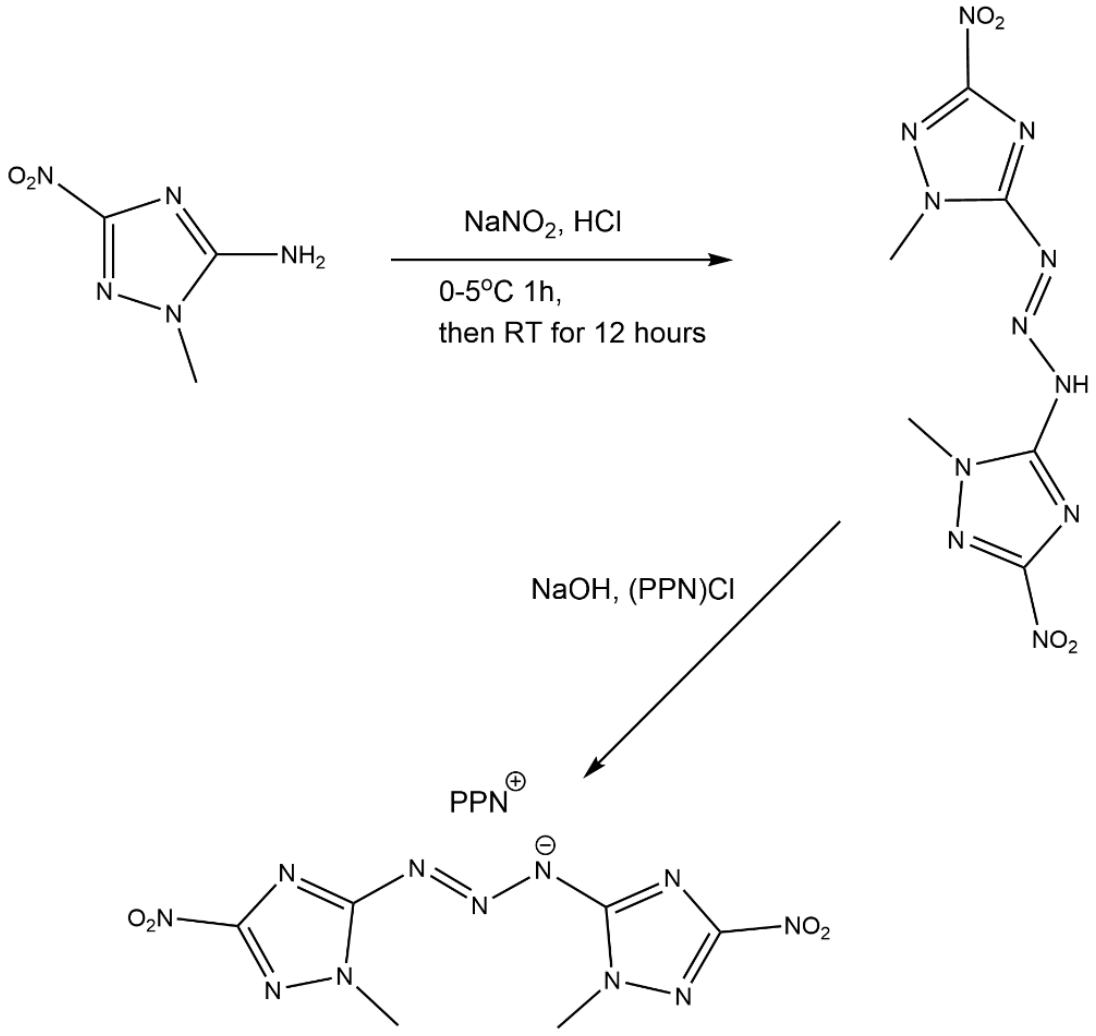

Figure 4.17: *Synthesis of (PPN)(bis(1-methyl-3-nitro-triazol-5-yl)-triazenide)*

4.2.16 ^{1}H and ^{13}C NMR Spectroscopy

^{1}H and ^{13}C NMR were used to assign product identity. The ^{1}H NMR shows large multiplets from 7.8-7.5 ppm, these are indicative of the PPN cation (**Figure 4.18**). Singlets at 3.84 and 3.37 ppm are assigned to the CH_3 of bis(1-methyl-3-nitro-triazol-5-yl)triazenide and H_2O respectively. Integration of the area under the peaks givens H ratios of 34(7.8-7.5): 5.6 (CH_3): 6.4 (H_2O) giving a tentative assignment of the compound as PPN[bis(1-methyl-3-nitro-triazol-5-yl)-triazenido].$3H_2O$. ^{13}C NMR shows 5 signals in the range 135-125 ppm, assigned to the PPN cation. 3 other non-solvent signals can be found in the spectrum at 35.4 (CH_3), 160.4 (C3 of triazole ring) and 162.4 ppm (C5 of the triazole ring).

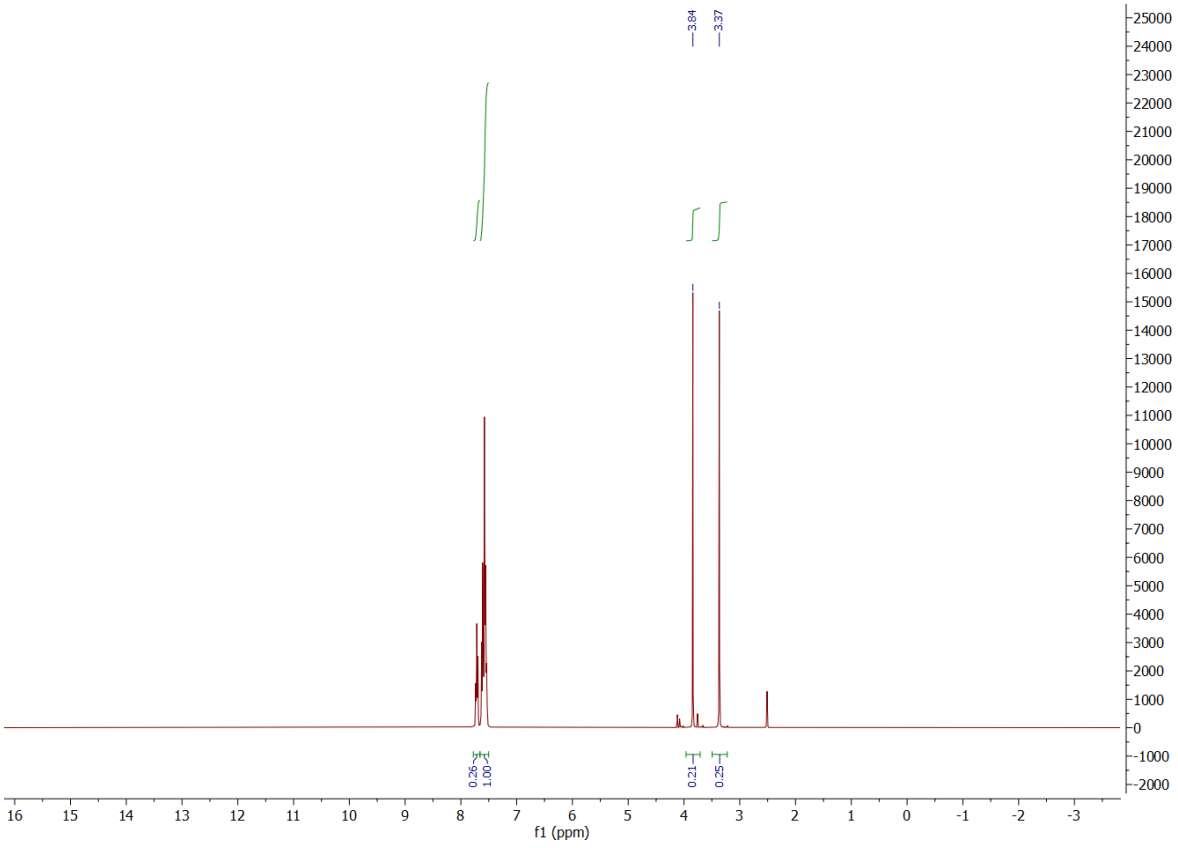

Figure 4.18: *^{1}H NMR spectrum of PPN[bis(1-methyl-3-nitro-triazol-5-yl)-triazenido].$3H_2O$*

4.2.17 Crystal Structure of PPN[bis(1-methyl-3-nitro-triazol-5-yl)-triazenido].3H₂O

Recrystallisation of this material in acetonitrile resulted in the formation of orange crystals. Single crystal X-ray diffraction gave the structure as PPN[bis(1-methyl-3-nitro-triazol-5-yl)-triazenido].3H_2O (**Figure 4.19**). PPN[bis(1-methyl-3-nitro-triazol-5-yl)-triazenido].3H_2O crystallises in the space group P $\bar{1}$ with two formula units per unit cell. Both nitrotriazolyl group are twisted out of the plane of the triazenide chain by 7° and 4.7°. No interactions between PPN cation and bis(1-methyl-3-nitro-triazol-5-yl)-triazenide can be found however fairly strong hydrogen bonds are found between N5/N5' and hydrogens of a water molecule (2.127 and 2.282 Å). As the only other PPN salt of an azolyltriazene known,[19] (PPN)(B1MTT) can be used to compare bond lengths in the triazenide chain. Trends between the two compounds are similar with one short N-N bond ((PPN)(B1MTT) : 1.308 (19), PPN[bis(1-methyl-3-nitro-triazol-5-yl)-triazenido].3H_2O : 1.307 (7)) and one long N-N bond ((PPN)(B1MTT) : 1.312 (18), PPN[bis(1-methyl-3-nitro-triazol-5-yl)-triazenido].3H_2O : 1.311 (8)) however the uncertainties attached to these bond lengths makes this analysis tentative.

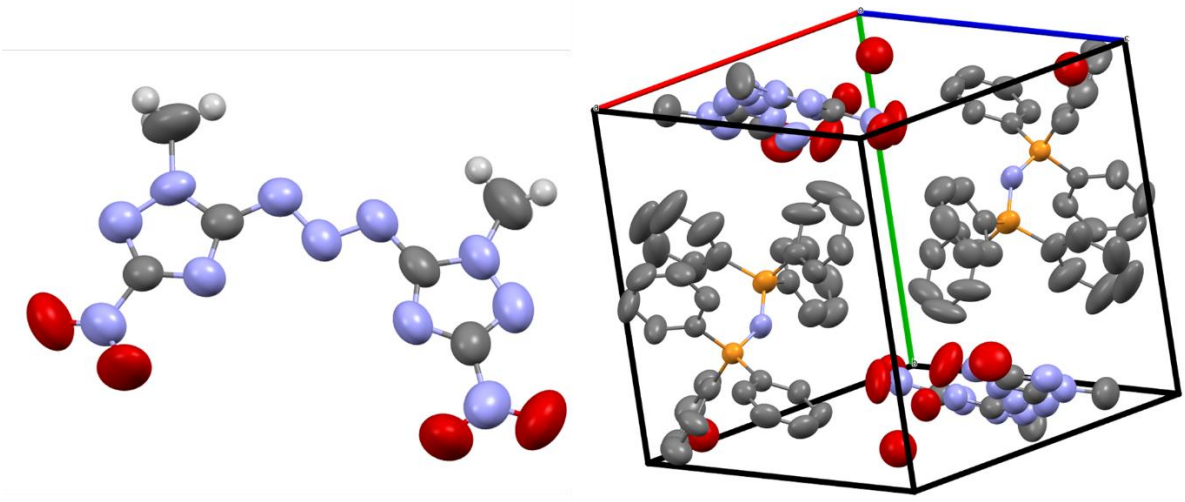

Figure 4.19: *Left: Projections of the thermal ellipsoid in the molecular structure of the crystals of (PPN)(bis(1-methyl-3-nitro-triazol-5-yl)-triazenido).3H_2O, PPN cation removed for clarity; Right: Unit cell of (PPN)(bis(1-methyl-3-nitro-triazol-5-yl)-triazenido).3H_2O, Atom Colours: Blue = Nitrogen, Grey = Carbon, Red = Oxygen, White = Hydrogen, Yellow= Phosphorus*

4.2.18 Thermal behaviour and detonation performance parameters of PPN[bis(1-methyl-3-nitro-triazol-5-yl)-triazenido].3H$_2$O

With the formation of a novel triazenide, an investigation of its potential as an energetic compound was required. Thermal analysis of PPN[bis(1-methyl-3-nitro-triazol-5-yl)-triazenido].3H$_2$O using DSC was compared to the same data recorded for the known PPN salt of bis(1-methyl-tetrazol-5-yl)triazene (See **Appendix 8.66 and 8.67**) . With bis(1-methyl-tetrazol-5-yl)triazene proving to be an energetic ligand capable of making water stable, high thermal stability energetic coordination compounds, comparison to PPN[bis(1-methyl-3-nitro-triazol-5-yl)-triazenido].3H$_2$O can help to draw conclusions about the prospective use of this novel azolyltriazene.

PPN-triazenide salt	Onset temperature, T_{on}/ °C	Peak temperature, T_{peak}/ °C
PPN[bis(1-methyl-tetrazol-5-yl)triazenide].MeCN	238.2	291.3
PPN[bis(1-methyl-3-nitro-1,2,4-triazol-5-yl)triazenide].3H$_2$O	281.5	322.8

Table 4.6: *T_{on} and T_{peak} of PPN[bis(1-methyl-tetrazol-5-yl)triazenide].MeCN and PPN[bis(1-methyl-3-nitro-1,2,4-triazol-5-yl)triazenide].3H$_2$O*

DSC measurements of PPN salts of bis(1-methyl-tetrazol-5-yl)triazenide and bis(1-methyl-3-nitro-1,2,4-triazol-5-yl)triazenide were recorded at a heating rate of 3K min^{-1} in the temperature range 50-400 °C. The PPN salt of B1MTT proved to be highly thermally stable with an onset of decomposition recorded at 238.2 °C and a peak temperature at 291.3 °C (**Table 4.6**). The decomposition of PPN(B1MTT) was not quick and occurred over a range of approximately 80 °C. PPN(B1MTT) also had a melting point of ~115 °C. The PPN salts of novel triazenides ideally would show similar T_{on} and T_{peak} to PPN(B1MTT) so as to have similarly temperature stable triazenes. PPN[bis(1-methyl-3-nitro-1,2,4-triazol-5-yl)triazenide] has T_{on} and T_{peak} at 281.5 °C

and 322.8 °C respectively. This suggests that bis(1-methyl-3-nitro-1,2,4-triazol-5-yl)triazene (B1M3NTT) is a highly temperature stable compound and could be a useful ligand in the synthesis of high energy metal coordination compounds.

Calculated heats of formation can also be used to assess the potential of these compounds as energetic materials. With B1MTT showing great potential as both a rocket propellant and as an energetic ligand it was important to compare calculated values of Q, D and P for the proligand bis(1-methyl-3-nitro-triazol-5-yl)-triazene (B1M3NTT) to the experimentally derived values for B1MTT. As heats of decomposition for the free acid triazene was not known the methods used for both novel Cu(I) compounds and the $M(B1MTT)_2$ compounds could not be applied. Instead heats of formation were estimated using the Atom Pair Contribution Method devised by Mathieu.[25] In this method, enthalpies of atomisation, bond enthalpy contributions and enthalpy contributions from 1,3 geminal interactions are added together to approximate heats of formation with bond enthalpy contributions determined through training of the method on a dataset of 50 compounds. As triazenes were not part of this training set it was important to assess the accuracy of the APC method against triazenes with known heats of formation and against those calculated through more expensive computational methods. $B1MTT.H_2O$ and B2MTT provide good examples of triazenes with experimentally determined heats of formation with bis(2-methyl-4-nitro-2H-1,2,3-triazole)triazene (B2MNTT) providing an example of computational determined heats of formation.[16][17]

Triazene	**Experimental ΔH_f/ kJ mol^{-1}**	**Calculated ΔH_f/ kJ mol^{-1}**	**APC/ kJ mol^{-1}**	**Deviation/ kJ mol^{-1}**	**% Difference**
$B1MTT.H_2O$	514	-	548.42	34.42	6.70
B2MTT	792	-	751.54	-40.46	-5.11
B2MNTT	-	685	643.05	-41.95	-6.12

Table 4.7: *Comparison of experimentally determined ΔH_f ($B1MTT.H_2O$, B2MTT) and calculated ΔH_f using the EXPLO5 computer code (B2MNTT) versus that calculated from the APC method*

The assessment of APC versus both experimental and calculated heats of formation show that the APC method gives values within a ± 7% margin of error (**Table 4.7**). This shows that the APC method can be viewed as a viable estimation of heat of formation for CHNO compounds if bomb calorimetry is unavailable. It also helps establish APC as an alternative to computational calculations for unknown CHNO compounds. For these reasons APC was used to make estimations of heat of formation for B1M3NTT.

Crystal densities are also required for the calculation of Q, D and P. As for the metal compounds of B1MTT crystal densities of the novel triazenes were estimated according to the methods of Ammon and Hofmann.[21][22] Crystal densities of B1MTT.H_2O, B2MTT and B2MNTT were also calculated to assess the accuracy of the method for CHNO compounds (**Table 4.8**).

Triazene	**ρ, crystal density / g cm^{-3}**	**ρ, estimated / g cm^{-3}**	**% Difference**
B1MTT.H_2O	1.528	1.515	-0.85
B2MTT	1.532	1.549	1.11
B2MNTT	1.64	1.659	1.16

Table 4.8: *Comparison of the crystal density derived from unit cell data to that derived from the methods of Hofmann and Ammon*[21][22]

In all cases the estimated densities for the triazenes are under ±1.2% compared to the structurally derived densities. This provides reasonable confidence in the accurate estimation of densities of novel triazenes. B1M3NTT is calculated to have properties close to or exceeding those found for B2MTT (**Table 4.9**). B1M3NTT is predicted to have higher density, heat of detonation and detonation pressure than that found for B2MTT. While the predicted detonation velocity is lower than for B2MTT, it is still within the range expected of both secondary explosives and propellants. The predicted properties of the synthesised B1M3NTT seem to position it as an ideal competitor to B2MTT as potential nitrogen rich solid rocket propellants. While the prediction of impact sensitiveness without a high-quality crystal structure is not possible with a high

degree of accuracy it is not unreasonable to suggest that B1M3NTT could possess a similar impact sensitiveness to those found for both B1MTT.H_2O and B2MTT. Because of this, the high decomposition temperature of its PPN salt and the high predicted densities of the ligand, B1M3NTT could also serve a dual purpose as a high energy ligand for the synthesis of novel metal-triazenido primary explosives (with a potential use in either detonators or igniters)

Triazene	**ρ/ g cm^{-3}**	**ΔH_f/ kJ mol^{-1}**	**Q/ J g^{-1}**	**D/ km s^{-1}**	**P/ kbar**
B2MTT	1.532	792	3879.0	7.982	221
B1M3NTT	1.658	427.3	4576.0	7.320	230.34

Table 4.9: *Q, D and P values calculated for B1M3NTT from the estimated crystal density and heat of formation, compared to the Q, D and P values calculated for B2MTT from experimentally derived heat of formation and crystal density derived from unit cell data*

4.3 Conclusion

Metal compounds of bis(1-methyl-tetrazol-5-yl)triazene can be formed. $Fe(B1MTT)_2$, $Co(B1MTT)_2$ and $Ni(B1MTT)_2$ all form as their monohydrates. $Zn(B1MTT)_2$ and $Pb(B1MTT)_2$ precipitate with no water in the crystal. Ni and Zn compounds precipitate as impure microcrystalline powders. Crude $Ni(B1MTT)_2$ can be extracted with hot acetone to give a compound with an FTIR spectrum closely matching that of the crude material except for 3 new prominent absorption bands. The cause of these absorption bands is currently unknown. All compounds prove to be highly temperature stable with T_{on} between 260 °C and 320 °C. Compounds are also calculated to have detonation velocities and pressures in the range expected of primary explosives. Ni, Co and Fe compounds can be recrystallised in acetone from which their crystal structures can be determined. Analysis of thermal stability and crystal structure seems to suggest that thermal stability is tied to N2-N3 bond length, the presumed first step in thermal decomposition. Impact sensitiveness could not be determined during this project, as such these compounds cannot be claimed as primary explosives until sensitiveness can eb proven. Compounds must also be desolvated prior to these tests to prevent desensitisation. The Cu compound is distinct from the other metal compounds in that it forms not the 1:2 metal-triazenide seen previously but instead forms $Cu(B1MTT)(Cl)(H_2O)$. If a sufficient driving force is present Cl^- can be substituted to form mixed explosophore compounds as shown by FTIR. Stochiometric ratios of the explosophores has yet to be determined. Bis(1-methyl-3-nitro-triazol-5-yl)-triazenide has been formed as its PPN salts. The identity of PPN[bis(1-methyl-3-nitro-triazol-5-yl)-triazenido].$3H_2O$ has been determined by ^1H and ^{13}C NMR alongside the determination of the crystal structure. PPN[bis(1-methyl-3-nitro-triazol-5-yl)-triazenido].$3H_2O$ proves to be a highly temperature stable compound surpassing the T_{on} and T_{peak} of PPN(B1MTT). Estimated crystal density and heats of formation of bis(1-methyl-3-nitro-triazol-5-yl)-triazenide was used to calculate Q, D and P values. Bis(1-methyl-3-nitro-triazol-5-yl)-triazenide is predicted to have higher densities, heats of detonation and detonation pressures than that found for B2MTT, a compound proposed to be a rocket propellant. Impact sensitiveness could not be determined for the bis(1-methyl-3-nitro-triazol-5-yl)-triazene but contingent on this testing this compound could prove to have a dual use as an explosophoric ligand for forming energetic coordination compounds.

4.4 Experimental

Synthesis of 1-methyl-5-amino-tetrazole

NaOH (10.261 g, 0.257 mol) and 5-aminotetrazole hydrate (25.156 g, 0.250 mol) were added to a two necked RB flask and dissolved in H_2O (60 ml) to give a colourless solution. A condenser and dropping funnel were attached to the flask, and the flask heated in an oil bath set to 95 °C. Dimethyl sulphate (12.5 ml, 0.132 mol) was added to the dropping funnel and added dropwise to the colourless solution over a period of 20 minutes. The solution was then stirred for 1hr at 95 °C after which the solution was allowed to slowly cool to room temperature overnight. On cooling, small, white crystals of 1-methyl-5-aminotetrazole (3.500 g, 35.3 mmol) had precipitated out of solution. The solid was filtered, washed with cold water, and dried under vacuum. Yield 3.5 g, 26.7% with respect to dimethyl sulphate IR (nujol) v / cm^{-1} = 3386, 3361, 3328, 3278, 3151, 2729, 2117, 2042, 1683, 1665, 1596, 1561, 1492, 1483, 1322, 1281, 1238, 1157, 1120, 1092, 1044, 970, 955, 844, 790, 742, 690, 680, 673, 639

Synthesis of bis(1-methyl-tetrazol-5-yl)triazene

1-Methyl-5-aminotetrazole (3.500 g, 35.3 mmol) was suspended in 100 mL water and cooled to 0 °C. After adding concentrated HCl (5 ml, 37%), 1-methyl-5-aminotetrazole was solved completely giving a colourless solution. A solution of $NaNO_2$ (1.218 g, 17.65 mmol) in 40 mL water was added drop wise within 20 min whilst maintaining the temperature at 0°C. Thereafter the solution was stirred for 24 h. After stirring for 24 hours a pale-yellow solution with a white solid had formed. The resulting white solid was isolated by filtration and washed with cold water before drying under vacuum. (1.520 g, 40.62 % with respect to $NaNO_2$) IR (nujol) v / cm^{-1} = 3607, 3451, 3380, 3190, 2724, 2671, 2033, 1664, 1633, 1531, 1503, 1440, 1363, 1351, 1309, 1274, 1247, 1227, 1196, 1172, 1154, 1103, 1036, 1005, 983, 936, 892, 808, 772, 748, 701.

Synthesis of sodium bis(1-methyl-tetrazol-5-yl)triazenide.5H_2O

Bis(1-methyl-tetrazol-5-yl)triazene (1.520 g, 7.2 mmol) was added to an aqueous solution of NaOH (20 ml H_2O, 0.288 g NaOH, 7.2 mmol). This gave a pale-yellow solution. Removal of H_2O *in vacuo* resulted in the precipitation of a pale yellow solid. Dissolution of the solid in warm (60°C) H_2O and subsequent slow cooling in ice led to the formation of an off-white powder. FTIR spectra confirms the identity of the powder as Na- bis(1-methyl-tetrazol-5-yl)triazene pentahydrate by comparison to known IR values. Yield = 1.05, 45.42% g, IR (nujol) v / cm^{-1} = 3585, 3536, 3458, 3413, 3275, 3199, 1681, 1656, 1620, 1519, 1483, 1456, 1343, 1314, 1287, 1267, 1245, 1217, 1205, 1151, 1124, 1104, 1062, 1046, 1010, 808, 750, 704, 670.

Synthesis of Ni(B1MTT)$_2$.H_2O

Na-bis(1-methyl-tetrazol-5-yl)triazenide.5H_2O (0.154 g, 4.8x10^{-4} mol) was added to an aqueous solution of $NiCl_2$ (0.03 g, 2.4x10^{-4} mol) at 60 °C. This resulted in immediate precipitation of a red solid. Solid was stirred for 1 hour at this temperature before being filtered, washed with cold water (2 X 10 ml) and dried under vacuum. Yield 0.06 g, 52.2%. (Elemental analysis calculated for $NiC_8H_{14}N_{22}O$, 493.3 g mol^{-1}): C, 19.48%, H, 2.89%, N, 62.48%; found: C,18.58%, H, 2.90%, 58.06%. IR (nujol) v / cm^{-1} = 3618, 3587, 3554, 1798, 1749, 1624, 1597, 1557, 1496, 1481, 1411, 1338, 1325, 1295, 1252, 1191, 1124, 1068, 1061, 1055, 1018, 1000, 994, 939, 928, 892, 823, 807, 769, 746, 710, 706, 690, 672, 623, 522. DSC, T_{on} = 321.8 °C (dec.), T_{peak} = 324.4 °C, ΔH = 1304.5 J g^{-1} , 3 K min^{-1}. Ni(B1MTT)$_2$.H_2O can be recrystallised in acetone to form Ni(B1MTT)$_2$.$(CH_3)_2CO$. 150 mg of Ni(B1MTT)$_2$.H_2O were loaded onto a sintered Soxhlet extractor. Allowing hot acetone vapour to condense and extract Ni(B1MTT)$_2$.H_2O lead to formation of large red crystals in the centre of the sinter bed where contact is only with hot acetone vapour. This serves to extract H_2O from the crystals forming Ni(B1MTT)$_2$.$(CH_3)_2CO$. IR (nujol) v / cm^{-1} = 1718, 1561, 1475, 1467, 1456, 1343, 1324, 1294, 1283, 1254, 1236, 1225, 1200, 1126, 1089, 1058, 1016, 996, 807, 748, 706, 691, 674, 623, 535, 519 Yield 0.068 mg, 36.47%.

Synthesis of $Zn(B1MTT)_2$

Na-bis(1-methyl-tetrazol-5-yl)triazenide.$5H_2O$ (0.154 g, $4.8x10^{-4}$ mol) was added to a solution of $ZnBr_2$ (0.054 g, $2.4x10^{-4}$ mol) at room temperature. This resulted in immediate precipitation of a pale yellow solid. Solid was stirred for 1 hour at room temperature before being filtered, washed with cold water (2 X 10 ml) and dried under vacuum. Yield (0.054 g, 46.6%).(Elemental analysis calculated for $ZnC_8H_{12}N_{22}$, 481.98 g mol^{-1}): C, 19.95%, H, 2.51%, N, 63.97%; found: C,18.02%, H, 3.00%, 55.74%. IR (nujol) v / cm^{-1} = 1663, 1623, 1548, 1517, 1484, 1413, 1363, 1337, 1326, 1318, 1299, 1292, 1284, 1251, 1242, 1221, 1196, 1109, 1055, 1043, 1009, 994, 920, 896, 845, 801, 777, 747, 710, 693, 675, 671, 613. DSC, T_{on} = 268 °C (dec.), T_{peak} = 276.4 °C, ΔH = 1545.3 J g^{-1} , 3 K min^{-1}

Synthesis of $Pb(B1MTT)_2$

Na-bis(1-methyl-tetrazol-5-yl)triazenide.$5H_2O$ (0.154 g, $4.8x10^{-4}$ mol) was added to a solution of $Pb(NO_3)_2$ (0.079 g, $2.4x10^{-4}$ mol) at room temperature. This resulted in immediate precipitation of a pale yellow solid. Solid was stirred for 1 hour at room temperature before being filtered, washed with cold water (2 X 10 ml) and dried under vacuum. Yield (0.120 g, 80.2 %). (Elemental analysis calculated for $PbC_8H_{12}N_{22}$, 481.98 g mol^{-1}): C, 15.41%, H, 1.94%, N, 49.92%; found: C,15.18%, H, 1.85%, 49.20%. IR (nujol) v / cm^{-1} = 1613, 1543, 1523, 1481, 1468, 1448, 1418, 1406, 1361, 1341, 1308, 1280, 1274, 1271, 1247, 1210, 1195, 1143, 1119, 1110, 1095, 1043, 1005, 985, 946, 924, 808, 745, 704, 667, 611. DSC, T_{on} = 312.4 °C (dec.), T_{peak} = 319.0 °C, ΔH = 1138.7 J g^{-1} , 3 K min^{-1}

Synthesis of $Fe(B1MTT)_2.H_2O$

Na-bis(1-methyl-tetrazol-5-yl)triazenide.$5H_2O$ (0.323 g, $4.8x10^{-4}$ mol) was added to a solution of $FeCl_2.4H_2O$ (0.1 g, $2.4x10^{-4}$ mol) at room temperature. This resulted in immediate precipitation of a dark green solid. Solid was stirred for 1 hour at room temperature before being filtered, washed with cold water (2 X 10 ml) and dried under vacuum. Yield (0.178g, 72.3%). (Elemental analysis calculated for $FeC_8H_{14}N_{22}O$,

490.461 g mol^{-1}): C, 19.59%, H, 2.88%, N, 62.87%; found: C, 19.67%, H, 2.71%, 63.36%. IR (nujol) v / cm 1 = 3598, 3538, 1637, 1574, 1540, 1450, 1366, 1309, 1284, 1250, 1238, 1188, 1073, 1016, 995, 828, 742, 730, 716, 687, 675, 641, 573. DSC, T_{on} = 268.26 °C (dec.), T_{peak} = 279.0 °C, ΔH = 1303.1 J g^{-1} , 3 K min^{-1}. $Fe(B1MTT)_2.H_2O$ can be recrystallised in acetone to form $Fe(B1MTT)_2.(CH_3)_2CO$. Dissolution of 150 mg of $Fe(B1MTT)_2.H_2O$ in 150 ml of acetone followed by slow evaporation of the solvent resulted in the growth of large, dark green, rectangular crystals. Yield 0.143 g, 88.03%

Synthesis of $Co(B1MTT)_2.H_2O$

Na-bis(1-methyl-tetrazol-5-yl)triazenide.$5H_2O$ (0.154 g, $4.8x10^{-4}$ mol) was added to a solution of $Co(NO_3)_2.6H_2O$ (0.070 g, $2.4x10^{-4}$ mol) at room temperature. This resulted in immediate precipitation of a mauve coloured solid. Solid was stirred for 1 hour at room temperature before being filtered, washed with cold water (2 X 10 ml) and dried under vacuum. Yield (0.077 g, 65.3 %). (Elemental analysis calculated for $CoC_8H_{14}N_{22}O$, 490.461 g mol^{-1}): C, 19.47%, H, 2.86%, N, 62.47%; found: C, 19.41%, H, 2.84%, 62.80%. IR (nujol) v / cm 1 = 3618, 3587, 3554, 1798, 1749, 1624, 1597, 1557, 1496, 1481, 1411, 1338, 1325, 1295, 1252, 1191, 1124, 1068, 1061, 1055, 1018, 1000, 994, 939, 928, 892, 823, 807, 769, 746, 710, 706, 690, 672, 623, 522. DSC, T_{on} = 310.50 °C (dec.), T_{peak} = 311.49 °C, ΔH = 1331.3 J g^{-1} , 3 K min^{-1}. $Co(B1MTT)_2.H_2O$ can be recrystallised in acetone to form $Co(B1MTT)_2.(CH_3)_2CO$. Dissolution of 40 mg of $Co(B1MTT)_2.H_2O$ in 150 ml of acetone followed by slow evaporation of the solvent resulted in the growth of large, hexagonal, dark purple crystals. Yield 0.034 g, 78.46% IR (nujol) v / cm 1 = 1717, 1559, 1519, 1489, 1471, 1401, 1336, 1321, 1298, 1285, 1251, 1226, 1200, 1129, 1118, 1106, 1090, 1056, 1012, 996, 933, 812, 780, 748, 704, 690, 672, 622, 533, 515

Synthesis of Cu(bis(1-methyl-tetrazol-5-yl)triazenide)(Cl)(H_2O)

Na-bis(1-methyl-tetrazol-5-yl)triazene(0.350 g, 1.52x10-3 mol) was added to a solution of $CuCl_2$ (0.204 g, 1.52x10-3 mol). This gave a dark brown solution which was left for slow evaporation. Over the course of a week the solution evaporated to leave dark brown crystals of $Cu(B1MTT)Cl(H_2O)$ (0.317 g, 64.1 %) . IR (nujol) v / cm-1 =

3505, 3424, 1604, 1567, 1493, 1486, 1452, 1354, 1331, 1296, 1286, 1255, 1239, 1202, 1134, 1072, 1067, 1017, 1001, 930, 919, 892, 820, 808, 745, 740, 705, 690, 673, 626. DSC, T_{on} = 310.50 °C (dec.), T_{peak} = 311.49 °C, ΔH = 1331.3 J g^{-1} , 3 K min^{-1}.

Synthesis of Cu(bis(1-methyl-tetrazol-5-yl)triazenide)x(4,5-DNI)y(H_2O)z

Cu(B1MTT)(Cl)(H_2O) (0.1 g, 0.307 mmol) was dissolved in 25 ml H_2O at 50 °C. K-4,5-DNI.H_2O (0.132 g, 0.614 mmol) was added as an aqueous solution (5 ml H_2O) in one portion to the stirred solution of Cu(B1MTT)(Cl)(H_2O). Immediate precipitation of a dark green powder was observed. Suspension was stirred for 1 hour before cooling to room temperature, filtering, washing with water and dried under vacuum. Mass yield 0.102 g. IR (nujol) v / cm^{-1} = 3608, 3586, 3499, 3428, 3132, 3110, 2136, 1662, 1623, 1572, 1525, 1465, 1408, 1365, 1324, 1301, 1291, 1273, 1257, 1226, 1193, 1160, 110, 1069, 1048, 1033, 1012, 997, 852, 834, 813, 743, 707, 673, 657, 624

Synthesis of 3,5-diamino-1H-1,2,4-triazole

The synthesis of 3,5-diamino-1-H-1,2,4-triazole from hydrazine dihydrochloride and cyanamide / dicyandiamide has been described by in ref[26]. The procedure given here is an adaptation of these earlier descriptions and differs in the nature of starting materials, solvent volumes and pH control. In a round-bottomed single-neck flask, dicyandiamide or 2-cyanoguanidine (8.426 g, 100 mmol) and H_2N-NH_2.HCl (6.864 g, 100 mmol) were dissolved in a mixture of deionised water (25 ml) and aqueous HCl (8.3 ml, 37%) giving a clear and colourless solution. During the initial stages of the reaction upon mixing of the reactant, reaction heat caused a temperature rise in the mixture up to 45 °C. Once the temperature had stopped rising, the flask was immersed in a water bath set to 50 °C and the mixture was left to stir for 2 h. After this time, the resultant solution appeared clear and colourless. To this mixture, an aqueous solution of NaOH (8.5 g in 200 ml) was added causing the pH to change to a value of 12. At this stage, the colour of the solution had changed to a pale yellow. All volatiles were then removed in vacuo to produce a pale-yellow solid. The raw product was purified by recrystallisation from a saturated solution of MeOH which was cooled slowly from

r.t. to −20 °C. Compound 1 crystalised as colourless, rectangular crystals. The synthesis has been carried out five times with yields ranging from 5.5 g to 6.3 g, average yield 6.0 g (M = 99.10 g mol^{-1}, 61 mmol, 61% with respect to dicyandiamide). IR (nujol) v / cm^{-1} = 3584, 3394, 3369, 3307, 3233, 3114, 2194, 2153, 1725, 1626, 1584, 1563, 1486, 1415, 1350, 1310, 1150, 1123, 1060, 1015, 844, 806, 767, 739, 655, 621.

Synthesis of Sodium-3,5-dinitro-1,2,4-triazolate dihydrate[23]

This procedure follows closely that given by of Liu et al., ref [21], as part of the synthesis of 3-amino-5-nitro-1,2,4. A solution of 3,5-diamino-1,2,4-triazole (4.00 g, 40 mmol, 1 eq.) in dilute sulphuric acid (134 ml, 0.68 mol) was added dropwise to a solution of sodium nitrite (26.22 g, 0.38 mol, 9.5 eq.) in water (30 ml) with vigorous stirring at a temperature range of 0 to −5 °C over the course of 2 h. This produced an orange-coloured, opaque solution with an orange-coloured solid in suspension. After the addition had completed, the reaction mixture was warmed up to 60 °C and stirred for another 1 h (NB: Depending on the control of temperature during the addition of sodium nitrite, two different observations were made. If temperature was not allowed to exceed the range 0 to −5 °C, then the orange solid dissolved and a red solution was formed. If temperature exceed this range, then not all of the orange solids would dissolve after 1 h of heating. In the latter case, the lack of dissolution did not affect the isolation of pure sodium-3,5-dinitrotriazole, but would reduce the reaction yield). The reaction solution was then cooled again by immersion of the reaction vessel in an ice bath, after which sulphuric acid (13 ml, 6 mol dm^{-3}) was added, followed by the addition of urea (2.00 g, 0.03 mol) in small portions. After the resultant reaction mixture was stirred overnight at r.t., the mixture was filtered, and the filtrate neutralized by sodium bicarbonate. The volume of the filtrate was then diminished in vacuo to leave an orange solid which was extracted by addition of acetone. The resultant suspension was stirred and then filtered into a new round-bottomed flask. Additional acetone was added to the orange solid filter residue until the filtrate ran clear. The volatile component of the combined extracts was removed in vacuo to yield sodium-3,5-dinitro-1,2,4-triazolate as an orange solid (4.0-5.5 g, 55.22-75.9 % raw yield with respect to 3,5-diamino-1,2,4-triazole). The solid can be purified through

recrystallisation as a dihydrate by cooling of a solution in hot water (70 ˚C) to 0 °C. This affords Na(DNT).2H_2O as orange irregular shaped crystals (yields range from 3.1 g to 4.0 g, average 3.65 g, 35.7-46.1 % with respect to 3,5-diamino-1,2,4-triazole)) IR (nujol) v / cm^{-1} = 3564, 3360, 3266, 3192, 2673, 2474, 2201, 2143, 1648, 1548, 1542, 1504, 1424, 1395, 1360, 1310, 1107, 1053, 846, 832, 772, 767, 672, 647, 615. Handling of the material gave no indication of high sensitiveness. Na(DNT).2H_2O can be scraped off a sinter filter without explosion. It can also be ground with pestle and mortar without any explosion. Direct exposure to a flame lead to decomposition into a black material without initiation.

Synthesis of 3-amino-5-nitro-1H-1,2,4-triazole.H_2O[23]

Crude (prior to recrystallization) sodium 3,5-dinitro-1,2,4-triazolate (5.21g, 28.8 mmol) was stirred in 80 % hydrazine monohydrate (5.71 ml 98% hydrazine monohydrate + 1.29 ml H_2O), giving a dark red solution, for 1.5 h in a stoppered RBF at 80 °C. Stopper was removed for another 30 minutes of heating to concentrate solution. Solution was concentrated in vacuo to remove all traces of hydrazine (N.B failure to remove all traces of hydrazine prevents the isolation of 3-amino-5-nitro-1H-1,2,4-triazole during acidification and instead results in the precipitation of a white, unidentified solid) Water (20 mL) was added, and the solution was acidified with hydrochloric acid to pH = 1 to give precipitation of a yellow solid. After stirring for 15 minutes, the precipitate was filtered, washed with water, and dried to yield 3-amino-5-nitro-1H-1,2,4-triazole.H_2O as a yellow powder (2.03 g, 22.5 mmol, 54.64% yield). ^{1}H-NMR (400 MHz, DMSO-d_6): 13.16 (s, 1H), 6.81 (s, 2H), 3.52 (2H, s); ^{13}C-NMR (400 MHz, DMSO-d_6): 160.91, 157.47 ppm. IR (nujol) v/cm^{-1} = 3584, 3442, 3330, 3293, 3278, 3232, 3168, 2149, 1655, 1641, 1586, 1568, 1548, 1536, 1511, 1400, 1319, 1173, 1127, 1102, 1091, 1037, 1014, 849, 754, 734, 607. Flame test: discoloration to light brown, no initiation.

Synthesis of 1-methyl-3-Amino-5-nitro-1,2,4-triazole[24]

3-Amino-5-nitro-1H-1,2,4-triazole monohydrate (1.50 g, 10.2 mmol) was dissolved in an aqueous NaOH solution (0.816 g in 20 mL H_2O, 20.4 mmol) forming a dark orange

solution. Dimethyl sulfate (1.29 g, 10.2 mmol, 0.97 mL) was added dropwise, and the reaction mixture was stirred under reflux conditions for 16 hours. No colour changes were observed during this period. The solution was then slowly cooled to 0 °C, resulting in the formation of a bright, microcrystalline, orange precipitate. The orange precipitate was filtered off, washed with water, and dried under vacuum to give 5-amino-1-methyl-3-nitro-1,2,4-triazole. Yields range from 1.03-1.23 g, 70.5-84.22 %. ^{1}H-NMR (400 MHz, DMSO-d_6): 7.01 (s, 2H), 3.64 (s, 3H) ppm; ^{13}C-NMR (400 MHz, DMSO-d_6): 158.92, 156.42, 34.44 ppm

Synthesis of (PPN)(bis(1-methyl-3-nitro-1,2,4-triazol-5-yl)triazenide).3H_2O

5-amino-1-methyl-3-nitro-1,2,4-triazole (1.00 g, 6.99 mmol) was dissolved in 15 ml 37% HCl to give an orange solution. The solution was cooled to 0-5 °C by immersion in an ice bath. $NaNO_2$ (0.241 g, 3.495 mmol) dissolved in 2 ml H_2O was added dropwise to this solution, with care paid to maintaining the temperature between 0-5 °C. Time of addition was 15 minutes. Solution was stirred at this temperature for 1 hour before removal of the ice bath and stirring at room temperature for 12 hours. This results in the precipitation of bis(1-methyl-3-nitro-1,2,4-triazol-5-yl)triazene as a pale yellow solid. The precipitate was filtered, washed with small amounts of cold water and dried under vacuum. Yield: 0.212 g, 20.4 % with respect to $NaNO_2$. Bis(1-methyl-3-nitro-1,2,4-triazol-5-yl)triazene (0.100 g, 0.337 mmol) was added to an aqueous solution of NaOH (0.015 g in 10 ml H_2O, 0.375 mmol) with stirring to form a pale yellow solution. This solution was heated to 60 °C. (PPN)Cl (0. 230 g, 0.4 mmol) as a solution in 5ml of H_2O at 60 °C was added in one portion resulting in the immediate precipitation of a yellow-brown solid. Suspension was stirred for 10 minutes at 60 °C before filtering, washing with small amount of cold water and drying under vacuum to give (PPN)(bis(1-methyl-3-nitro-1,2,4-triazol-5-yl)triazenide).3H_2O as a yellow solid. Yield 0.168 g, 59.7%. ^{1}H-NMR (400 MHz, DMSO-d_6): 7.66 (7H, m, Ar-H), 7.62-7.53 (26H, m, Ar-H), 3.84(6H, s, R-CH_3), 3.37 (9H, s, H-OH) ppm; ^{13}C-NMR (400 MHz, DMSO-d_6): 162.36, 160.64, 134.14, 132.54, 132.51, 132.45, 132.39, 132.36, 130.09, 130.06, 129.99, 129.92, 129.89, 127.82, 126.75, 35.38 ppm. DSC: T_{on}: 282.89 °C, T_{peak}: 322.96 °C

4.5 References

1. P. Portius, M. Davis, Coord. Chem. Rev., 2013, 257, 5-6, 1011-1025
2. P. Portius, B. Peerless, M. Davis, R. Campbell, Inorg. Chem. 2016, 55, 17, 8976–8984
3. C. Zhang, C. Sun, B. Hu, C. Yu, M. Lu, Science, 2017, 355, 6323, 374-376
4. Y. Xu, Q. Wang, C. Shen, Q. Lin, P. Wang, M. Lu, Nature, 2017, 549, 78-81
5. D. S. Moore, S. D. Robinson, Advances in Inorganic Chemistry: Catenated Nitrogen Ligands Part I, 1986, 30, 1-68
6. P. Gantzel, P. J. Walsh, Inorg. Chem., 1998, 37, 3450-3451
7. T. V. Serebryanskaya, L. S. Ivashkevich, A. S. Lyakhov, P. N. Gaponik, O. A. Ivashkevich, Polyhedron, 2010, 29, 2844-2850
8. S. D. Robinson, M. F. Uttley, J. Chem. Soc., Chem. Commun., 1971, 1315
9. S. D. Robinson, M. F. Uttley, J. Chem. Soc., Chem. Commun., 1972, 184
10. J. Kuyper, P. I. Van Vliet, K. Vrieze, J. Organomet. Chem., 1976, 105, 379
11. J. Kuyper, P. I. Van Vliet, K. Vrieze, J. Organomet. Chem., 1975, 96, 289
12. V. P. Hanot, T. D. Robert, J. G. Haasnoot, H. Kooijman, A. L. Spek, J. Chem. Cryst., 1999, 29, 3, 299-308
13. M. Hauser, J. Org. Chem., 1964, 29, 3449
14. V. P. Hanot, T. D. Robert, J. Coord. Chem., 1994, 32, 349-352
15. V. P. Hanot, T. D. Robert, J. Kolnaar, J. G. Haasnoot, J. Reedijk, H. Kooijman, A. L. Spek, Dalton Trans., 1996, 4275-4281
16. T. M. Klapötke, N. K. Minar, J. Stierstorfer, Polyhedron, 2009, 28, 13-26
17. S. Feng, F. Li, X. Zhao, Y. Qian, T. Fei, P. Yin, S. Pang, Energetic Materials Frontiers, 2021, 2, 125-130
18. V. P. Hanot, T. D. Robert, J. Kolnaar, J. G. Haasnoot, H. Kooijman, A. L. Spek, Inorg. Chim. Acta., 1997, 256, 327-329
19. B. Peerless, PhD Thesis, University of Sheffield, 2017
20. R. Essman, G. Kreiner, A. Niemann, D. Rechenbach, A. Schmieding, T. Sichla, U. Zachwieja, H. Jacobs, Z. Anorg. Allg. Chem., 1996, 622, 1161-1166
21. H. L. Ammon, S. Mitchell, Propellants, Explosives, Pyrotechnics, 1998, 23, 260-265
22. D. W. M. Hofmann, Acta Cryst., 2002, B57, 489-493
23. T. Liu, X. Q, K. Wang, J. Zhang, W. Zhang, Q. Zhang, New. J. Chem., 2017, 41, 9070-9076
24. A. A. Dippold, T.M. Klapötke, F. A. Martin, S. Wiedbrauk, Eur. J. Inorg. Chem., 2012, 14, 2429-2443
25. D. Mathieu, J. Chem. Inf. Model., 2018, 58, 1, 12–26
26. J. J. Roemer, D. W. Kaiser, 1953, US Patent No. 2648671

5. Synthesis and characterisation of azidonitroazoles and their use as energetic materials

5.1 Introduction

The azido group has proven to be a useful explosophore albeit less widely used than the nitro group in azole chemistry. Introduction of an azido group is known to increase ΔH_f of a compound by approximately 325 kJ mol^{-1} per azido group.[1] This increase in energy is due to the difference in bond dissociation energy of N-N, N=N and N≡N bonds. Because of this, introduction of the azido group into azoles could result in high performance energetic compounds. Synthesis of organic azides has been shown to occur through a variety of routes. By far the most widely used is reaction of sodium azide (NaN_3) with an organic compound containing a diazonium group by way of nucleophilic aromatic substitution (**Figure 5.1)**.[2] In some select cases this reaction does not take place with substitution of the diazonium group but occurs with attack of the azide on the diazonium ion with formation of pentazene chains, which decomposes to form azides or cyclises to form pentazoles.[3] Nucleophilic substitution of the diazonium groups has been used to synthesise many azidoazolates including azidoimidazole, pyrazole, triazole and tetrazole.[4]

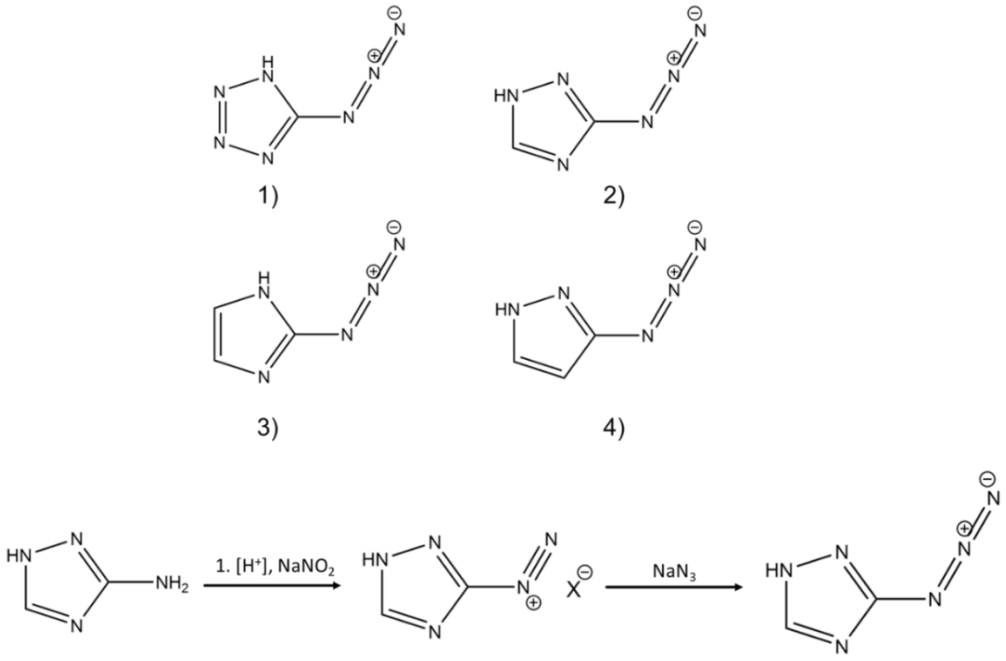

Figure 5.1: *Top 1): 5-Azidotetrazole; 2): 3-Azido-1,2,4-1H-triazole; 3): 2-Azidoimidazole; 4): 3-Azidopyrazole, Bottom: Synthesis to form 3-azido-1,2,4-1H-triazole*

While these reactions proceed easily and in good yield for imidazoles and triazoles, pyrazoles and tetrazoles suffer from some issues which make direct substitution not suitable in some cases.[5][6] Unsubstituted 3-aminopyrazole readily undergoes diazotisation followed by substitution to form 3-azidopyrazole. However it has been shown that some substituted pyrazoles can undergo substitution at a different carbon centre to the one hosting the diazonium group.[5] In the case of 3,5-dinitro-4-aminopyrazole this results in substitution of a nitro group and formation of a zwitterionic product.[5] In the case of azidotetrazole, substitution of a diazonium group is not used due to the formation of highly explosive tetrazole diazonium intermediates.[6] Azidotetrazole is instead synthesised by the reaction of cyanogen bromide with 2 equivalents of sodium azide followed by acidic work up (**Figure 5.2**).[7]

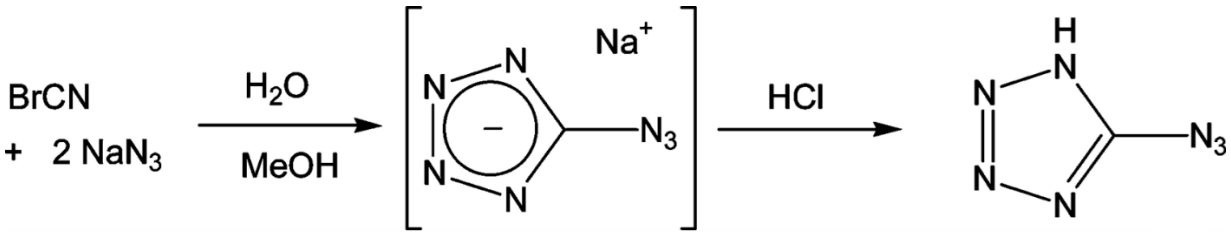

Figure 5.2: *Synthesis of azidotetrazole, image reproduced from ref [7]*

Direct substitution of a group other than a diazonium is also known for certain substituted azoles. Substitution of halogens by the azido anion has been shown to work for multiple different substituted imidazoles, pyrazoles, triazoles and tetrazoles.[8] It has also been shown in some unique cases that azides can be introduced to azoles through cine substitution.[9] Cine substitution occurs when a nucleophile attacks the ring at a position adjacent to the atom which has the intended leaving group.[10] This has been shown to work in azoles possessing an N-bound nitro group which serves as the leaving group (**Figure 5.3**). This is used to form azidoazolates in select cases most notably in forming 5-azido-3,4-dinitropyrazole, an important precursor to trinitropyrazole.[11]

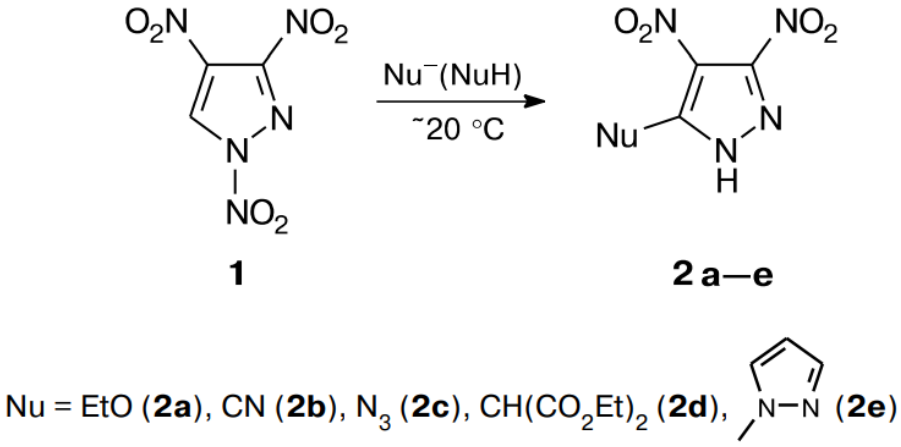

Figure 5.3: *Synthesis of various substituted dinitropyrazoles including 5-azido-3,4-dinitropyrazole, image reproduced from ref [9] with permission*

5.1.1 Identification of Organic azides

FTIR spectroscopy of azides is the simplest and quickest method of identifying azido groups. Azides have two stretching vibrations; the asymmetric stretch, (ν_{as}), which can be found from 2200-2000 cm^{-1} and the symmetric stretch, (ν_{sym}), which appears in the range 1350-1200 cm^{-1} (**Figure 5.4**). Azide deformation modes are also known and are thought to appear at ~700 cm^{-1} however these have not been studied in detail and are usually not assigned. [12]

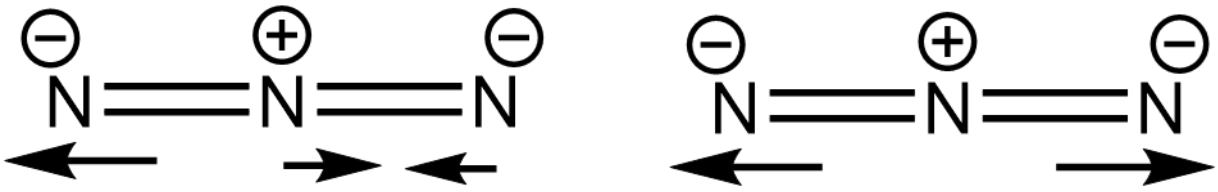

Figure 5.4: *Stretching modes of the azide anion; Left: Asymmetric stretching mode Right: Symmetric stretching mode*

As the symmetric stretch is found in the fingerprint region it can be difficult to assign. The asymmetric stretch is the primary absorption used for azide identification as it appears in a relatively quiet area of the IR spectrum. In ionic azides only the $\nu_{as}(N_3)$ is IR active however upon coordination or bonding to R groups $\nu_{sym}(N_3)$ also

becomes IR active. The location of the asymmetric stretch is dependent on the bonding present in the compound. In azides where bonding is purely ionic, $\nu_{as}(N_3)$ can be found closer to 2000 cm^{-1} ($(PPN)N_3$ found at 2000 cm^{-1}) whereas in the case of covalently bound azides they can be found as high as 2208 cm^{-1} as is the case with the triazidocarbonium cation.[13][14] The degree of ionicity or covalency in the bond can be denoted with the 4 resonance forms of XN_3 (**Figure 5.5**). Organic azides, such as the azidoazolates, can therefore be expected to show an asymmetric stretch dominated by the more covalent resonance forms.

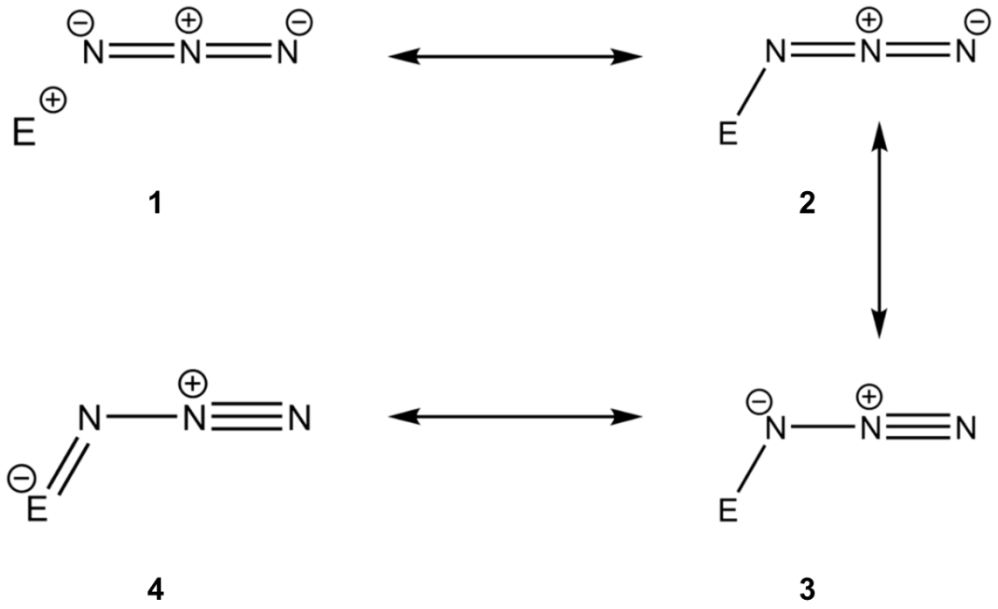

Figure 5.5: *Resonance hybrids of XN3, with 1 representing a purely ionic azide and 4 representing a purely covalent azide*

While organic azides generally have only one absorption associated with $\nu_{as}(N_3)$ there are known cases where two absorption bands are present. According to the work of Lieber, these can be interpreted as the Fermi resonance of $\nu_{as}(N_3)$ and either an overtone or a combination band mostly likely comprised of $\nu_{sym}(N_3)$ and another band of sufficient intensity in the region 1050-850 cm^{-1}.[15] The wavefunctions for the two resonant vibrations mix and result in a shift in frequency and a change in intensity of the two absorption bands. As a result, two strong bands

($v_{as}(N_3)$ is still noticeably more intense) are observed in the spectrum, instead of a strong and weak band (**Figure 5.6**). This effect is also known to occur for $v_{sym}(N_3)$.[15]

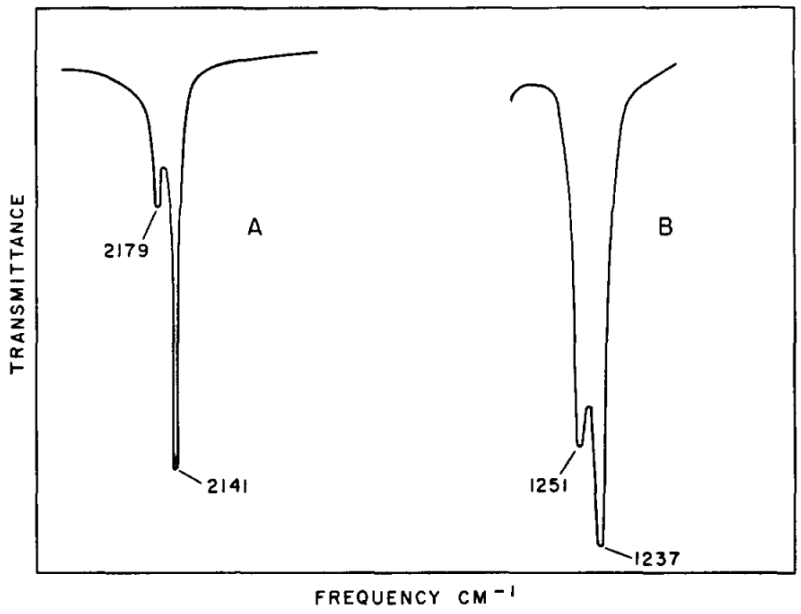

Figure 5.6: *FTIR spectra showing Fermi resonance affecting the peak positions of the $v_{as}(N_3)$ of organic azides, image reproduced from ref [15] with permission*

5.1.2 Azidoazolates and Azidonitroazolates as energetic materials

Azidoazolates have a long history but a relatively small number of papers, especially in the last 10 years, have been dedicated towards their synthesis, coordination chemistry and their use as energetic materials. Azidotetrazole has been known since 1939 with a patent by Friedrich and Flick detailing its synthesis.[16] As the tetrazole with the highest nitrogen content (88.3%), azidotetrazole has attracted some interest as an energetic material. However, azidotetrazole is rarely synthesised and finds no practical use due to its extremely high sensitiveness. Nevertheless, azidotetrazole does have some salts reported with either nitrogen rich cations or as coordination compounds with the alkali metals (**Figure 5.7**).[7] Azidotriazole has been synthesised in multiple papers and has shown to be a useful energetic compound as its energetic cation.[17] Diazidotriazole has a much sparser publication history with only two reports detailing its synthesis.[18] As with azidotetrazole, further work with this

compound seems to have been inhibited by its high sensitiveness and lower melting point/decomposition temperature which make a practical use for this compound unlikely. Both azidopyrazole and imidazole have attracted little interest as energetic compounds and have only found use in this field as energetic cations.[17]

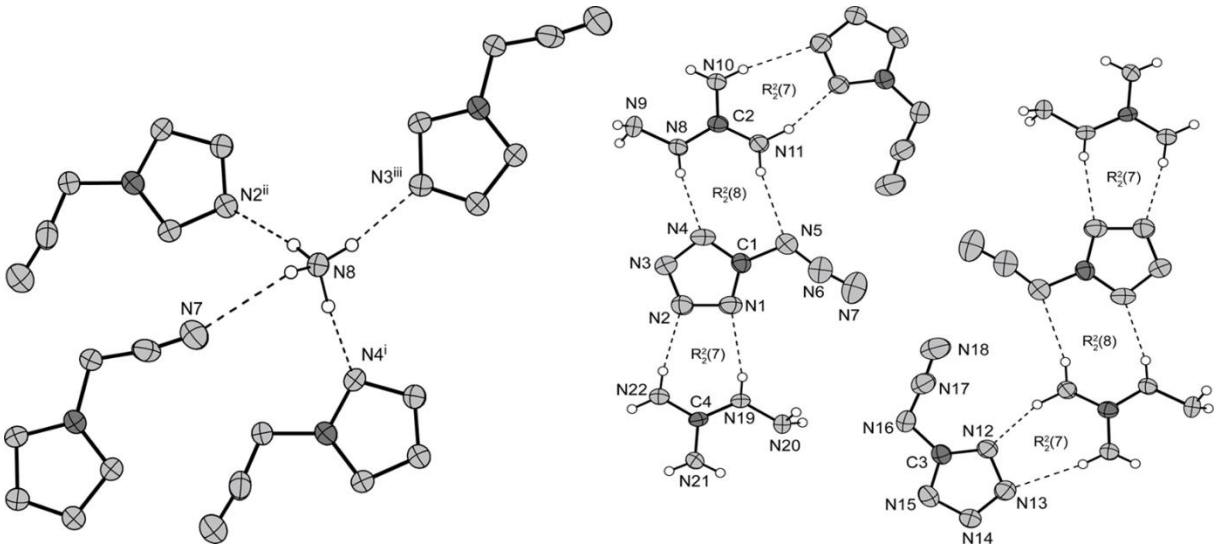

Figure 5.7: *Left: Hydrogen bonds in the packing of ammonium azidotetrazolate; Right: Hydrogen bonding present within the layers of aminoguanidinium tetrazolate, both images reproduced with permission from ref [7]*

Azidonitroazoles represent a related class of compound that could occupy a middle ground between the high decomposition temperature, low sensitiveness nitroazoles and the low decomposition temperature, high sensitiveness azidoazoles. This, along with the multiple coordination sites available to azoles, makes the azidonitroazolates ideal candidate energetic ligands. Much like the azidoazolates, many of the azidonitroazolates have reported syntheses but have attracted little interest beyond their initial publication. The synthesis of 3-azido-4-nitropyrazole has been reported in just two publications and has received no interest as an energetic material.[19] 3-azido-4,5-dinitropyrazole has also been synthesised and has found interest primarily as a precursor to 3,4,5-trinitropyrazole.[11] 3-azido-4,5-dinitropyrazole has been shown to be synthesised via two methods: diazotisation of 3-amino-4,5-dinitropyrazole followed by reaction with sodium azide or via the cine substitution of 1,3,4-trinitropyrazole by the azide anion (**Figure 5.8**).[11][20] Outside of reports of its

synthesis and use as a precursor, 3-azido-4,5-dinitropyrazole has also not been investigated as an energetic material.

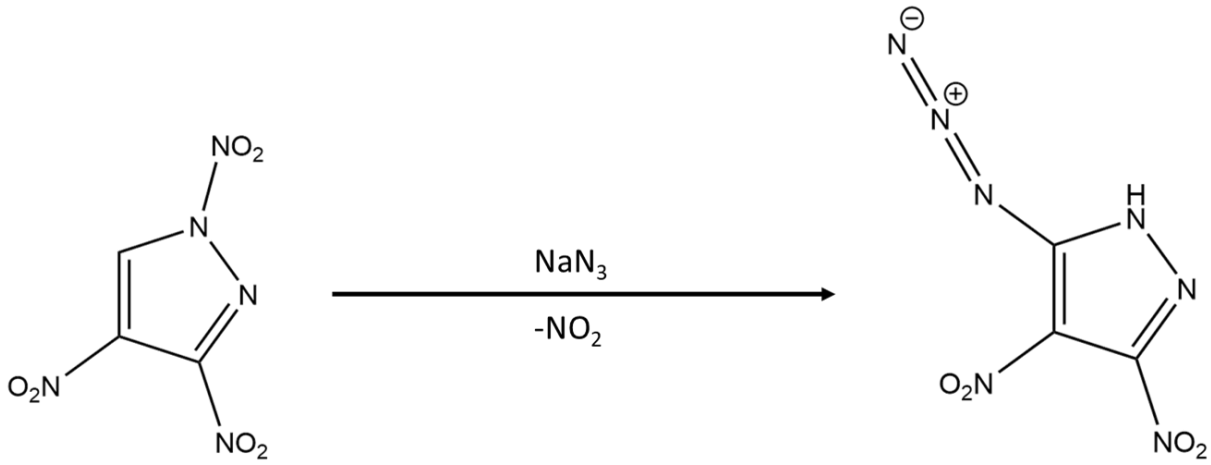

Figure 5.8: *Cine substitution of 1,3,4-trinitropyrazole by sodium azide to from 3-azido-4,5-dinitropyrazole*

Azidonitroimidazoles also possess published synthetic procedures. Both 2-azido-4-nitroimidazole and 2-azido-4,5-dinitroimidazole were synthesised and their energetic properties explored in a series of papers by Hou et al. [21][22] Both compounds were synthesised by direct nitration of their immediate precursor: 2-azidoimidazole for 2-azido-4-nitroimidazole and 2-azido-4-nitroimidazole for 2-azido-4,5-dinitroimidazole. While the compounds were explored as energetic compounds, neither were explored as potential energetic ligands. 4-azido-5-nitroimidazole also possess a short history of published work. Two papers have detailed the synthesis of this compound but outside of its use as a precursor to other compounds it has found no other use in the literature.[23][24]

The azidonitroazole with the most development as an energetic material is 3-azido-5-nitrotriazole (ANT). Known since 1974 the compound was recently reinvestigated in a series of papers by Klapötke et al.[25][26][27] Synthesis and crystal structures of the free acid and potassium salt were first discussed before the group went on to investigate the coordination chemistry of ANT by making a series of energetic coordination compounds.[27] While alkali metal, silver and lead salts were

made, the homoleptic transition metal compounds weren't investigated and remain unknown in the literature.

Due to the sparseness of research into azidonitroimidazoles/pyrazoles, we set out to investigate the synthesis, energetic properties of and coordination chemistry of these compounds.

Research Questions

- Can known azidonitroazoles be synthesised to form pure starting material for further reaction in good yield?
- Can these pro-ligands be deprotonated to form potassium or sodium salts, their crystal structure recorded and do the properties of these potassium/sodium-azidonitroazolates allow them to be classified as lead-free initiators?

5.2 Results and Discussion

5.2.1 Synthesis and characterisation of 2-azidoimidazole

Both 2-azido-4-nitroimidazole and 2-azido-4,5-dinitroimidazole have attracted little interest as energetic materials outside of the first publication of their syntheses. Therefore, both compounds have been reinvestigated during this work to improve the knowledge of both their energetic properties and of their potential use as energetic ligands. The synthesis of both 2-azido-4-nitroimidazole and 2-azido-4,5-dinitroimidazole were attempted according to the syntheses detailed by Hou et al (**Figure 5.9**).[21][22]

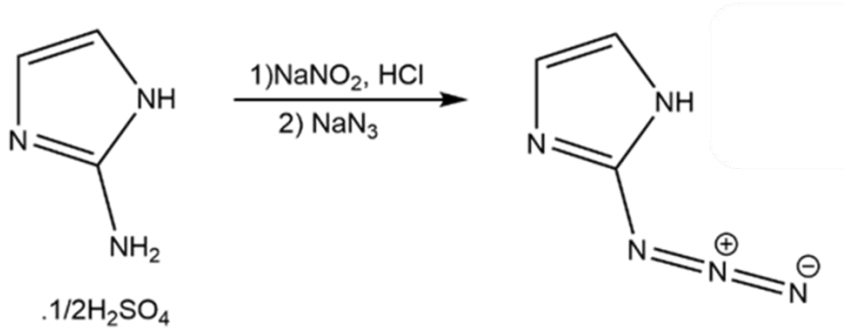

Figure 5.9: *Synthesis of 2-azidoimidazole from 2-aminoimidazole hemisulphate*[21][22]

The starting material for nitration, 2-azidoimidazole, was synthesised according to the method of Chen (**Figure 5.9**).[4] Product identity and purity was determined by comparison of $^{1}H/^{13}C$ NMR spectra to the published values of Chen. 2-Azidoimidazole shows two singlets in the ^{1}H NMR at 6.88 and 12.02 ppm (**Figure 5.10**) which are assigned to the C-H and N-H of azidoimidazole as per the reference paper.[4] This, along with the signals in the ^{13}C NMR at 139.92, 124.75 and 105.59 (**Figure 5.11**) which also match those reported for the three carbon signals of azidoimidazole[4], prove that the majority component of the crude product is 2-azidoimidazole. Two doublets at 7.97 and 7.63 are also present in the ^{1}H NMR. These doublets are also present in all repeats of the same reaction proving these peaks to be a result of a consistently produced by-product. The amount of these impurities range from 1% to 3% of the intensity of the signal associated with the N-H of 2-azidoimidazole. The identity of the impurity was not investigated further and currently remains unknown. Small peaks at 4.03, 1.99 and 1.17 are assigned to residual ethyl acetate present in the sample. As these impurities make up a negligible amount of the sample the crude 2-azidoimidazole was deemed pure enough for further reaction.

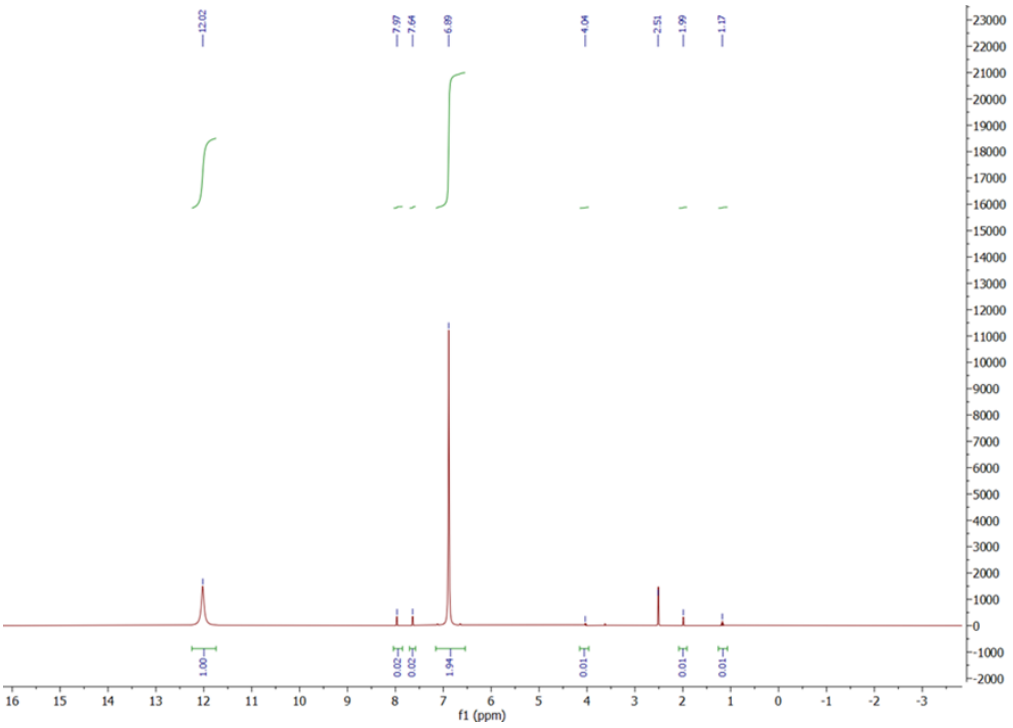

Figure 5.10: *^{1}H NMR spectra in dmso-d_6 of 2-azidoimidazole*

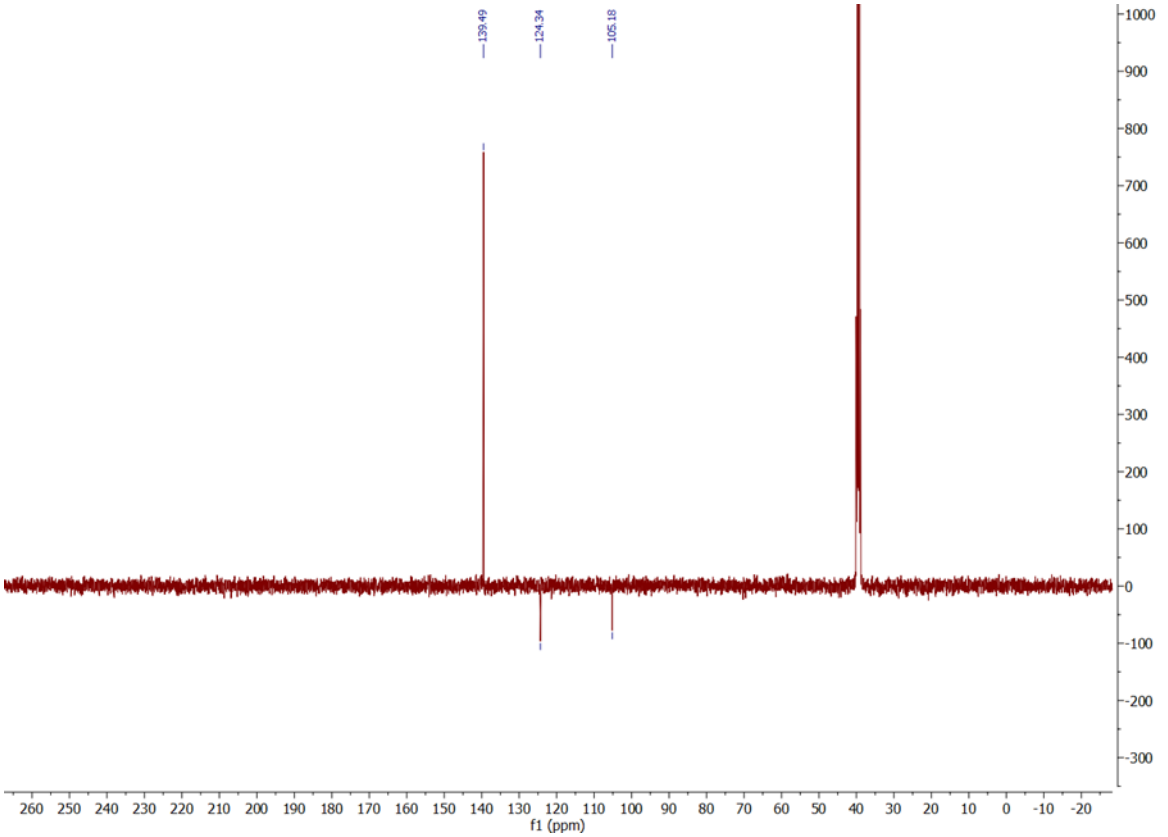

Figure 5.11: *^{13}C NMR spectra in dmso-d_6 of 2-azidoimidazole*

5.2.2 Synthesis and characterisation of 2-azido-4-nitroimidazole

The crude 2-azidoimidazole was nitrated according to a modified procedure published by Hou et al., [22] (**Figure 5.12**) resulting in the formation of a pale-yellow oil which, upon standing over the course of 12 hours, slowly crystallised to form bright yellow, crystalline 2-azido-4-nitroimidazole. 2-Azido-4-nitroimidazole was investigated using ^{1}H and ^{13}C NMR

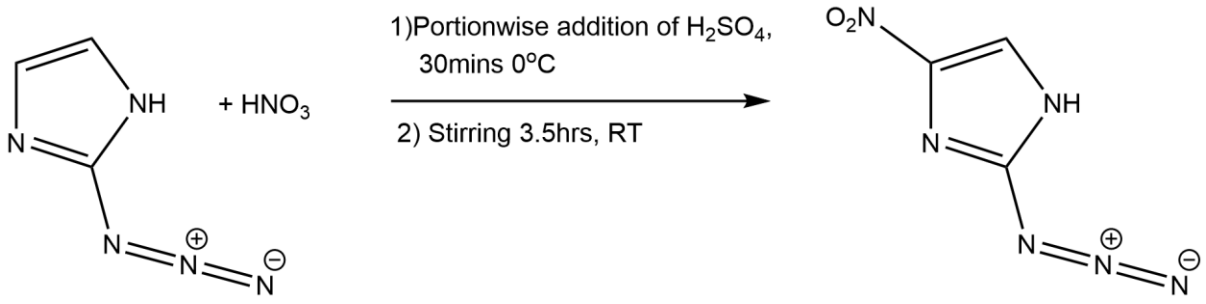

Figure 5.12: *Modified reaction to form 2-azido-4-nitroimidazole*

5.2.2.1 NMR spectroscopy

The ^{1}H and ^{13}C NMR were compared to literature values to prove 2-azido-4-nitroimidazole had formed and to assess its purity. 2-azido-4-nitroimidazole has two singlets in the ^{1}H NMR with a sharp singlet at 8.26 ppm and a broad singlet at 13.43 ppm (**Figure 5.13).** These are assigned to the C-H of the imidazole ring and the N-H of the imidazole ring respectively. These values closely match the published values of 8.27 ppm for the C-H and 13.46 ppm for the N-H of 2-azido-4-nitroimidazole.

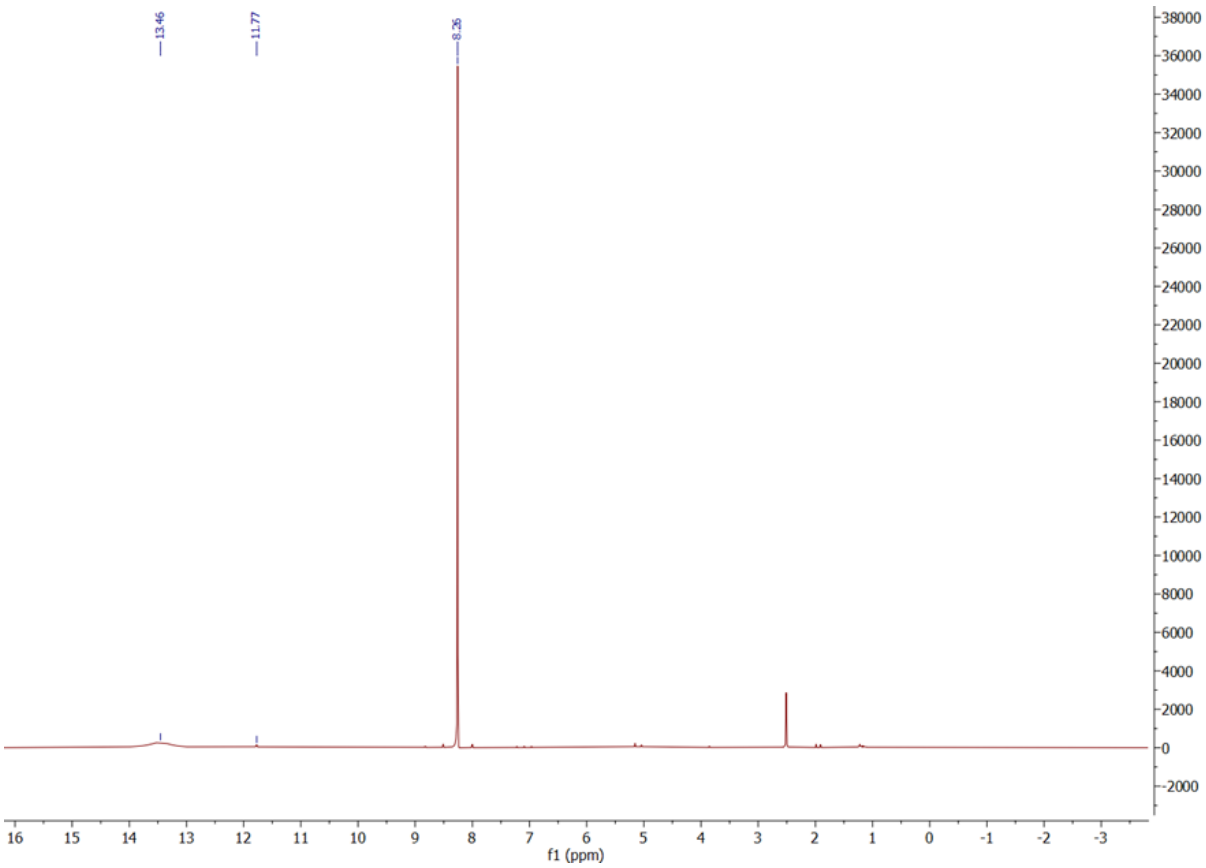

Figure 5.13: *^{1}H NMR spectra in dmso-d_6 of 2-azido-4-imidazole*

2-azido-4-nitroimidazole produces 3 signals in the ^{13}C NMR at 145.03, 140.62 and 119.21 ppm (**Figure 5.14**). Each signal is shifted by approximately 0.5 ppm compared to the values published by Hou et al. (145.03 to 144.50 ppm, 140.62 to 140.06 ppm and 119.21 to 118.63 ppm). With all signals in the ^{13}C NMR shifting by

approximately the same amount this does not cast doubt on the assignment of the product as 2-azido-4-nitroimidazole but rather is most probably due to the ^{13}C NMR experiment set up used. While both ^{1}H NMR and ^{13}C NMR confirm that the product is 2-azido-4-nitroimidazole, there are small amounts of impurities also present. Noticeably there is also a small impurity (<1% of the intensity of the signal for the C-H of 2-azido-4-nitroimidazole) at 11.76 ppm in the ^{1}H NMR. This is exactly the position of the N-H of 2-azido-4,5-dinitroimidazole as reported by Hou et al. This suggests that at room temperature complete nitration of 2-azidoimidazole starts to occur without the need for the stronger nitration conditions (HNO_3/Oleum mixture) required in the synthesis by Hou et al.[22]

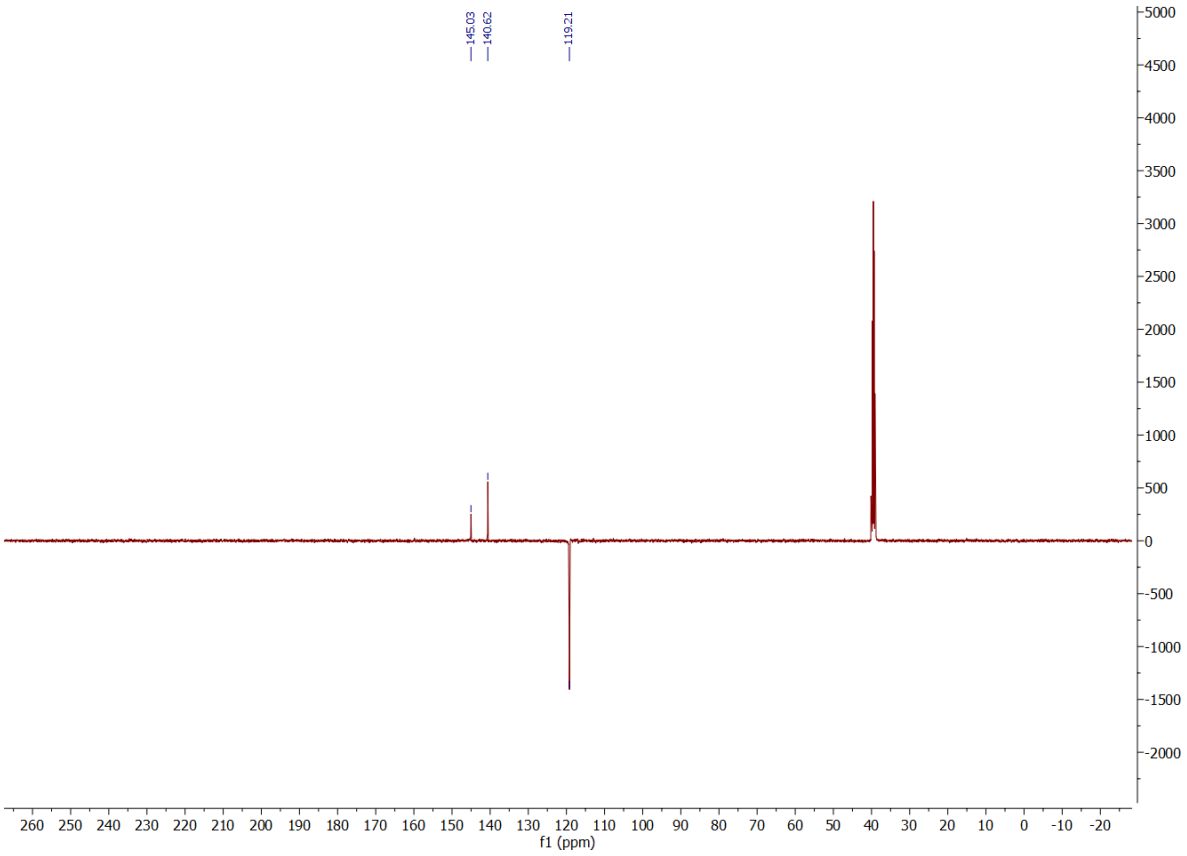

Figure 5.14: *^{13}C NMR spectra in dmso-d_6 of 2-azido-4-imidazole*

5.2.3 Investigation into improving the synthesis of 2-azido-4-nitroimidazole

The yield of 2-azido-4-nitroimidazole obtained after 4 hours of stirring was only 14.17%, much lower than reported yields of 85.7% (**Experiment 1, Table 5.1**). The cause of the lowered yield is not well understood. The reaction was repeated with differing time of reaction, temperature of reaction and H_2SO_4 addition scheme to observe the effect on the yield (**Table 5.1**).

Experiment Number	**Temperature of Reaction/ K**	**Time of reaction/ hours**	**H_2SO_4 addition scheme**	**2-A-4NI: 2-A-4,5-DNI product ratio**	**Mass Yield/ mg**
1	290	4	Added potion wise over 30 mins at ice bath temperature	40:1	40
2	290	4	Dropwise addition at room temperature over 4 hours	39:1	70
3	290	24	A	5:1	72
4	290	72	A	2.5:1	130
5	323	4	A	1:2.5	65
6	323	8	A	1:15	153
7	323	16	A	0:1	220

Table 5.1: *Preparative conditions for the nitration of 2-azidoimidazole to form 2-azido-4-nitroimidazole for experiments numbered in chronological order (Experiment Number), Mass yield give in milligrams, molar yields given in %, A= Added potion wise over 30 mins at ice bath temperature*

The first repeat of the reaction added H_2SO_4 dropwise, over the course of the total 4-hour reaction time with room temperature maintained in the solution throughout the reaction. This was done to more accurately match the experimental conditions detailed by Hou et al.[22] This did increase the yield to 24% but was still not approaching the published yields (**Experiment 2, Table 5.1**). The peak at 11.76 ppm in the ^{1}H NMR did not noticeably increase/decrease in intensity relative to the same peak present in Experiment 1 (**Table 5.1**). As more stringent following of reaction conditions still had

not resulted in good yields of the product, the nitration conditions were altered by differing lengths of reaction time and temperature of reaction to observe the impact this had upon product yield and selectivity. Increasing the reaction time or increasing the temperature resulted in a larger mass yield relative to Experiment 1 in all cases (**Experiments 3-7, Table 5.1**). However, the increase in reaction time and temperature also resulted in a growth of the peak at 11.76 ppm relative to the C-H peak of 2-azido-4-nitroimidazole. Heating at 50 °C for 16 hours was needed for all 2-azido-4-nitroimidazole to be consumed and only the product associated with the peak at 11.76 ppm to be present. It was assumed that this peak was the 2-azido-4,5-dinitroimidazole when compared to the literature values published by Hou et al. These results seemed to suggest that nitration of 2-azido-4-nitroimidazole was very facile and that the strong nitrating conditions used by Hou et al. were not needed to bring about full conversion to the full nitrated analogue.[22]

The product isolated from Experiment 6 was recrystallised in water to form clear, colourless crystals of a uniform crystal morphology. All crystals investigated were found to have a unit cell matching that of parabanic acid, an oxidation product of imidazole (**Figure 5.15**).[28]

Figure 5.15: *Left: Lewis Structure of parabanic acid, Right: Amorphous parabanic acid produced from Experiment 6(Table 5.1)*

Published ^{1}H NMR data for parabanic acid shows a single ^{1}H environment at 11.76 ppm,[31] the same as that assigned to the N-H of 2-azido-4,5-dinitroimidazole by Hou et al. while also matching the signal found in the spectra of Experiments 1-6 (**Table 5.1**).[22] Similarly the ^{13}C NMR for parabanic acid (two signals at 159.7 and 154.6 ppm) closely match the carbon environments found in the spectra of experiments 1-6 which cannot be assigned to 2-azido-4-nitroimidazole carbon signals.[29] The values also closely match two of the three carbon signals reported by Hou et al.[22] From the available data it is concluded that attempted nitration of 2-azido-4-nitroimidazole at 50 °C for 16 hours does not result in the formation of 2-azido-4,5-dinitroimidazole but instead forms parabanic acid. With the spectra of experiments 1-6 recorded prior to any recrystallisation attempt it is also clear that it is the reaction conditions which cause this oxidation and is not the attempted recrystallisation in water resulting in hydrolysis of 2-azido-4,5-dinitroimidazole. It is the opinion of this author that the published data for 2-azido-4,5-dinitroimidazole are incorrectly assigned and that the stronger nitrating conditions (and more oxidising) used in these syntheses result in formation of parabanic acid and another unknown by-product (which accounts for the third ^{13}C NMR peak seen by Hou et al.[22]).

In conclusion, 2-azido-4-nitroimidazole can be formed according to the synthesis reported by Hou et al.[22] The yield of this reaction is low at 14-24% depending on the H_2SO_4 addition scheme used. Increasing the temperature or time of the reaction leads to a greater mass yield but also a growth in the peak at 11.76 ppm in the ^{1}H NMR, initially assigned to 2-azido-4,5-dinitroimidazole, relative to the peak at 8.26 ppm, assigned to the C-H of 2-azido-4-nitroimidazole. Upon recrystallisation of the products of Experiment 6 the peak at 11.76 ppm was found to correspond to the N-H of parabanic acid and not 2-azido-4,5-dinitroimidazole. This is in direct contrast to the reports of Hou et al. and leads to the conclusion that the published procedures for synthesis of 2-azido-4,5-dinitroimidazole result only in the synthesis of parabanic acid and another unknown impurity leaving 2-azido-4,5-dinitroimidazole as a yet to be isolated potential energetic material.

5.2.4 Future exploration into the synthesis of 2-azido-4-nitroimidazole and 2-azido-4,5-dinitroimidazole

The investigations into the synthesis of 2-azido-4-nitroimidazole and 2-azido-4,5-dinitroimidazole lead to two further research questions:

1. Can the synthesis of 2-azido-4-nitroimidazole be improved upon to give better yields and prevent the production of parabanic acid?

2. Can an alternative synthesis of 2-azido-4,5-dinitroimidazole be found and the identity of the compound proved beyond doubt?

Due to time constraints these questions could not be investigated during this research project. However, the research conducted so far can be used to inform and guide future attempts to synthesise these compounds. Routes to the target compounds by nitration of 2-azidoimidazole should not be considered due to the likelihood of producing parabanic acid. Instead, reactions should focus on intergroup conversion to form azidonitroimidazoles. Reaction of a nitroaminoimidazole with $NaNO_2$/HCl followed by reaction with NaN_3 would seemingly be the simplest way to achieve this (**Figure 5.16**). This method has been reported by Hou et al. as an alternative route to 2-azido-4-nitroimidazole via the partial reduction of 2,4-dinitroimidazole to form 2-amino-4-nitroimidazole but was not investigated in this research project.[30] A similar reaction can be envisioned for 2-azido-4,5-dinitroimidazole. 2-amino-4,5-dinitroimidazole is currently unknown in the literature but would serve as an ideal starting material for the synthesis of 2-azido-4,5-dinitroimidazole. With many nitro group reductants known, partial reduction of trinitroimidazole should be considered as a viable route towards the target precursor. An alternative route involves the well-established Curtius rearrangement.[31] If the precursors 2-acyl-4-nitroimidazole/2-acylazide-4,5-dinitroimidazole can be formed, the reaction to form the 2-amino derivative should occur through simply heating the precursor to form the 2-isocyanate derivative followed by reaction with water to form the amino group (**Figure 5.17**). This would then be reacted with $NaNO_2$/HCl and NaN_3 to form 2-azido-4,5-dinitroimidazole.

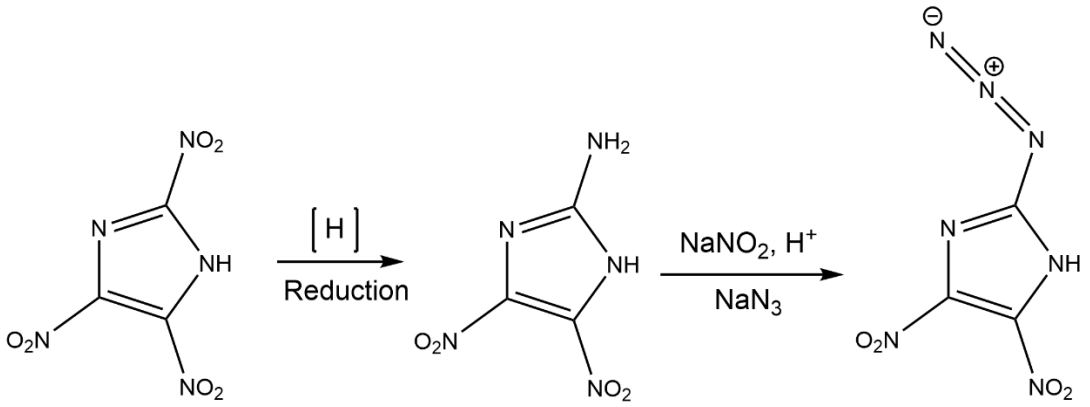

Figure 5.16: *Proposed reaction to form 2-azido-4,5-dinitroimidazole through partial reduction of trinitroimidazole followed by diazotisation and reaction with NaN_3*

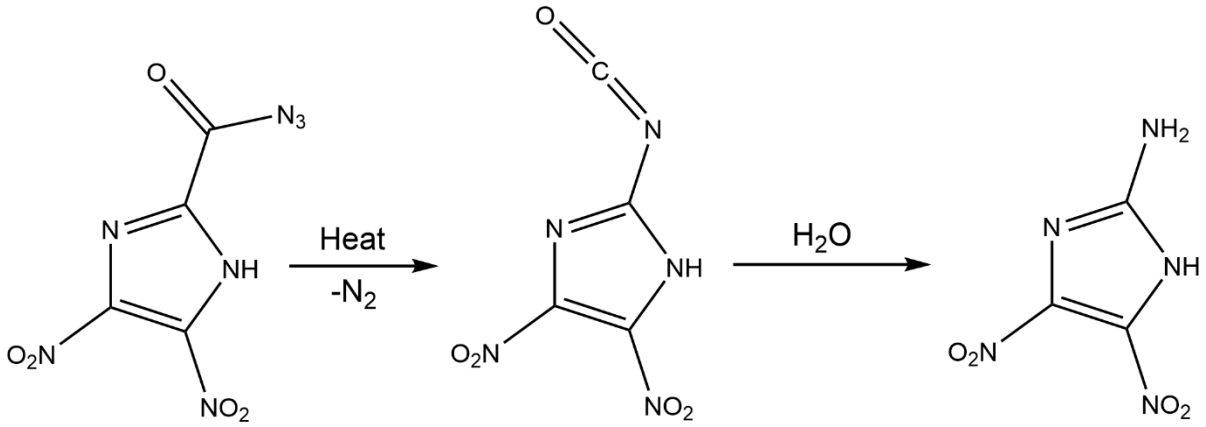

Figure 5.17: *Proposed reaction to form 2-amino-4,5-dinitroimidazole via the Curtius rearrangement, a precursor to 2-azido-4,5-dinitroimidazole*

A third potential route, inspired by the synthesis of 4-amino-3,5-dinitropyrazole, can also be conceived.[32] Here, 2-aminoimidazole would be protected by reaction with ethyl chloroformate to form 2-Ethylcarbethoxyamino-1-ethylcarbethoxyimidazole. This product could then be nitrated before removal of the protecting ethylcarbethoxy groups (**Figure 5.18**). Depending on the strength of the nitrating mixture this could as a route to either 2-amino-4-nitroimidazole or 2-amino-4,5-dinitroimidazole. This product would then be converted to 2-azido-4,5-dinitroimidazole as stated above.

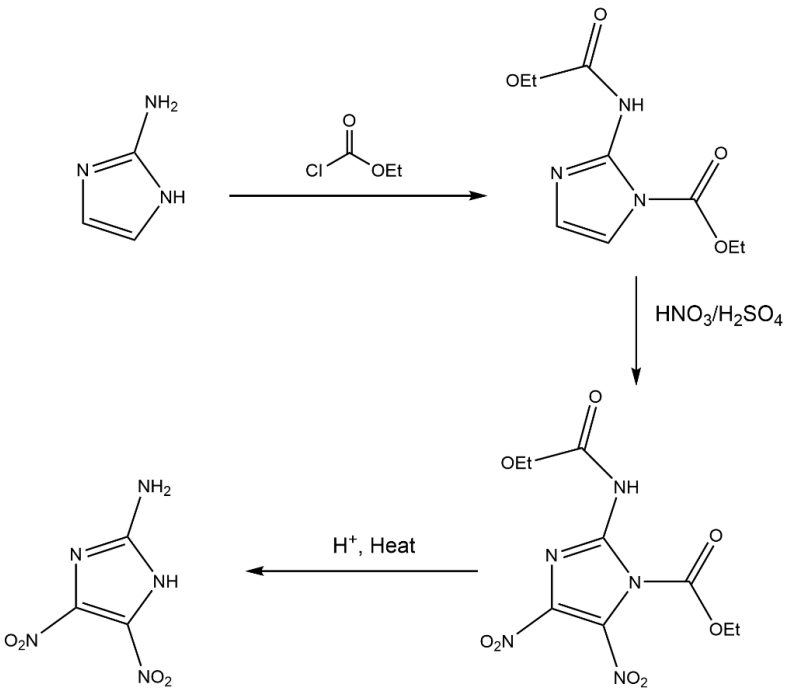

Figure 5.18: *Proposed route to 2-amino-4,5-dinitroimidazole via protection, nitration and finally deprotection of 2-amino-4,5-dinitroimidazole*

Alternatively, Shreeve reports on the synthesis of 5-amino-2,4-dinitroimidazole from ammonium-2,4,5-trinitroimidazole.[33] While using this as the starting material would result in the formation of a different isomer of azidodinitroimidazole, it would result in the first synthesis of 5-azido-2,4-dinitroimidazole and should be considered as a potential energetic azidonitroazolate (**Figure 5.19**).

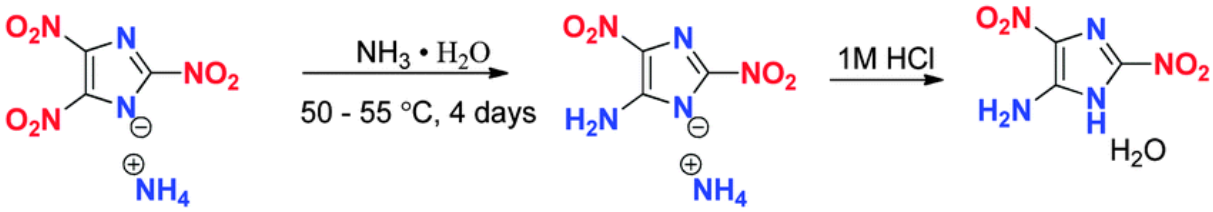

Figure 5.19: *Published procedure detailing the synthesis of 5-amino-2,4-dinitroimidazole, a precursor to 5-azido-2,4-dinitroimidazole, image reproduced with permission from ref [33]*

5.2.5 Synthesis and characterisation of potassium-2-azido-4-nitroimidazolate

A route to 2-azido-4-nitroimidazole affording higher yields could not be found. However, the synthesis of the potassium salt was attempted to assess the prospective properties of this compound as an energetic material and to serve as a starting material for transition metal coordination chemistry. Potassium-2-azido-4-nitroimidazolate(K-2-A-4-NIM) was synthesised according to a modified literature synthesis using K_2CO_3 as a base (**Figure 5.20**).[27] Following deprotonation, ethanolic solutions of potassium-2-azido-4-nitroimidazolate were allowed to slowly evaporate over five days to afford irregularly shaped orange crystals. Products were identified by comparison of NMR and FTIR spectra to starting materials and by determination of the crystal structure.

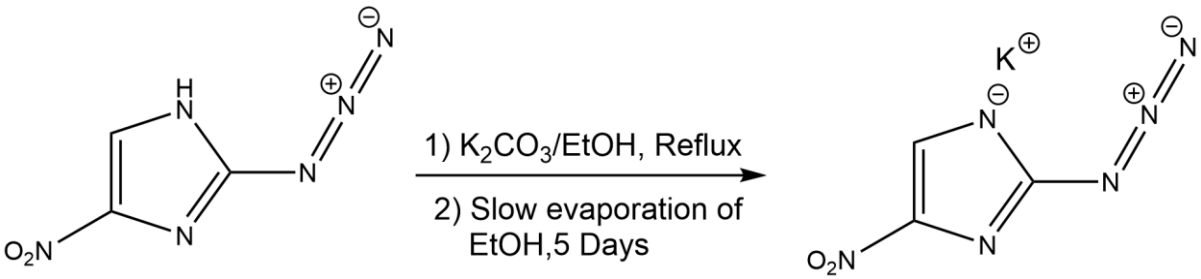

Figure 5.20: *Reaction of 2-azido-4-nitroimidazole with K_2CO_3 to form potassium-2-azido-4-nitroimidazolate*

5.2.5.1 NMR spectroscopy

Potassium-2-azido-4-nitroimidazolate was investigated using ^{1}H and ^{13}C NMR spectroscopy. These spectra were then compared to those of the starting material 2-azido-4-nitroimidazole. Potassium 2-azido-4-nitroimidazolate has two ^{1}H NMR singlets at 3.37 and 7.63 ppm (**Figure 5.21**). These are assigned to the C-H of the imidazolate ring and an O-H of water, respectively. Water presumably combines with the potassium-2-azido-4-ntroimidazole as a solvent of crystallisation. By comparison to the spectrum of 2-azido-4-nitroimidazole it can be shown that the signal at 13.43 ppm, which is assigned to the N-H of 2-azido-4-nitroimidazole, is not present in the spectrum of potassium 2-azido-4-nitroimidazole and thus confirms that deprotonation has occurred. The shift in the spectral position of the C-H resonance from 8.26 ppm in 2-azido-4-nitroimidazole to 7.63 ppm in the potassium salt is a result of the increased

electron density of the anion causing more shielding and shifts to smaller chemical shifts. Both potassium-2-azido-4-nitroimidazole and 2-azido-4-nitroimidazole have 3 carbon environments. Potassium 2-azido-4-nitroimidazole produces peaks at 148.26, 146.27 and 132.50 ppm in the ^{13}C NMR spectrum (**Figure 5.22**). All these resonances are shifted to higher chemical shifts when compared to the respective signals in 2-azido-4-nitroimidazole. The signals at 148.26 and 146.27 ppm are assumed to be related to the C-NO_2 and C-N_3 groups, respectively. Their intensity is reduced compared to the analogous signals in 2-azido-4-nitroimidazole. Shifts to higher ppm values implies a *decreased* shielding. This could indicate that electron density in potassium-2-azido-4-nitroimidazolate is localised over the NO_2 group rather than being concentrated in the imidazole ring which is the case for 2-azido-4-nitroimidazole. It is currently still unclear how localisation of electron density over the NO_2 group would result in the greater shielding of the C-H seen in the ^1H NMR.

An analysis of the NMR spectra leads to the conclusion that potassium 2-azido-4-nitroimidazolate has been formed. Integration of the ^1H NMR signals shows a 1 : 3 ratio of C-H to H_2O leading to a tentative formulation of the product as a trihydrate: potassium-2-azido-4-nitroimidazolate.$3H_2O$. Crystal structure determination is needed to prove conclusively the amount of water of crystallisation, however.

5.2.5.2 Vibrational Spectroscopy

FTIR spectra of both 2-azidoimidazole, 2-azido-4-nitroimidazole and potassium-2-azido-4-nitroimidazolate were recorded and compared to allow for an assignment of the observed absorption bands to bond vibrational modes (**Figures 5.23 and 5.24**). All three compounds exhibit intense bands for the $\nu_{as}(N_3)$ stretching vibration. Deprotonation (as realised in the potassium salt) results in a shift of the $\nu_{as}(N_3)$ frequency to higher wavenumbers and the appearance of a shoulder to the main absorption band. The cause of this new shoulder to the absorption band is not well understood, however, it is not uncommon for organic azides to have secondary absorptions in the same region as $\nu_{as}(N_3)$ due to Fermi resonance. Deprotonation to form the potassium salt could result in combination bands involving two bands in the fingerprint region resulting in a combination band of similar energy and symmetry to $\nu_{as}(N_3)$ resulting in Fermi resonance and the appearance of a shoulder. Assignment of

$v_{sym}(N_3)$ is much more challenging due to the area of the spectral region within which it can be expected to appear. This vibrational mode could be assigned to the absorption band at 1293 cm^{-1} in potassium-2-azido-4-nitroimidazolate, which has shifted ~10 cm^{-1} from the respective position in both 2-azidoimidazole and 2-azido-4-nitroimidazolate. The reason for this shift is currently unknown. Nitro group asymmetric and symmetric stretches for 2-azido-4-nitroimidazole can be observed at 1523 cm^{-1} and 1358 cm^{-1} respectively. These were assigned from comparison of the FTIR spectra of 2-azioimidazole and 2-azido-4-nitroimidazole. Potassium-2-azido-4-nitroimidazole can be seen to lack both absorption bands. Instead, potassium-2-azido-4-nitroimidazole has two new absorption bands at 1197 cm^{-1} and 991 cm^{-1}. These are assigned to $v_{as}(NO_2)$ and $v_{sym}(NO_2)$ of a charged nitro group(Introduction, **Effects of nitroazole salt formation on IR absorption bands**). Both $C\text{-}N_3$ and $C\text{-}NO_2$ deformation modes are not assigned in the spectra and would require much greater analysis than has been done during the course of this research for confident assignment to absorption bands. Absorption associated with N-H stretching modes is absent from the spectrum of potassium-2-azido-4-nitroimidazolate again showing that deprotonation has taken place (**Appendix 8.44**). Strong, broad O-H absorptions can be found for the O-H stretch(~3430 cm^{-1}) and for the O-H bend(~1665 cm^{-1}) in the expected ranges which corroborates the conclusions drawn from the NMR spectra which found water to have crystallised with potassium-2-azido-4-nitroimidazole (**Appendix 8.45**).

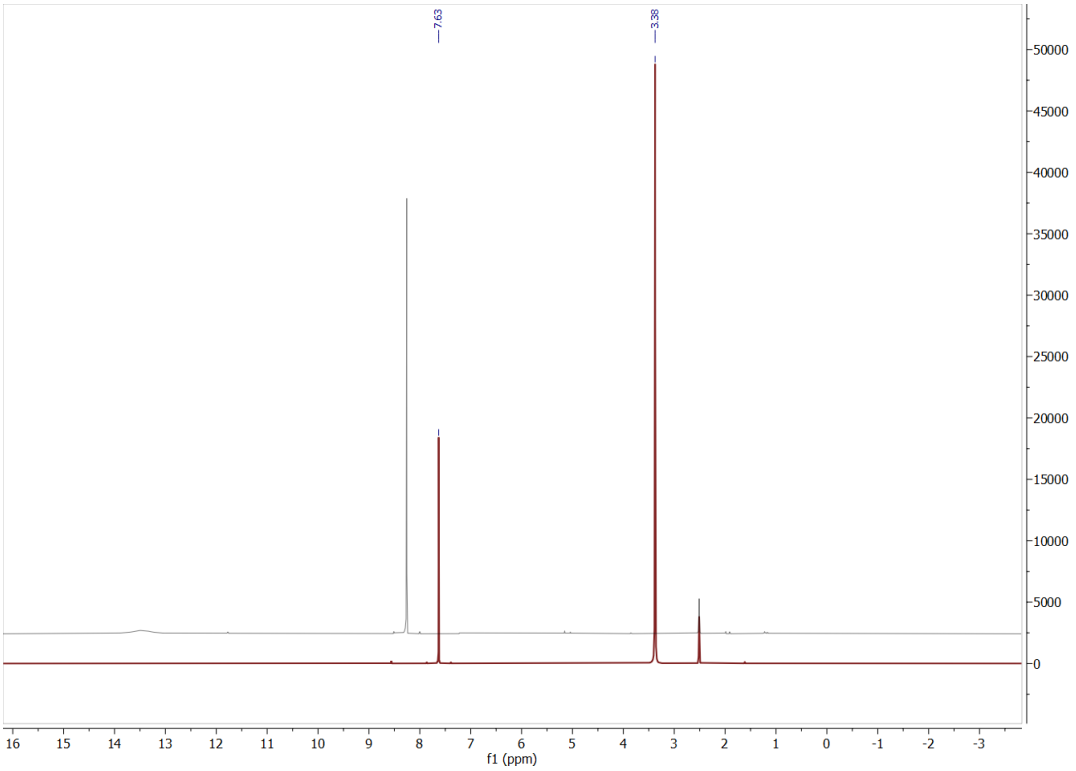

Figure 5.21: *Stacked ^{1}H NMR spectra in dmso-d_6 of 2-azido-4-nitroimidazole (black line) and the product obtained from the reaction of 2-azido-4-nitroimidazole with K_2CO_3 (red line)*

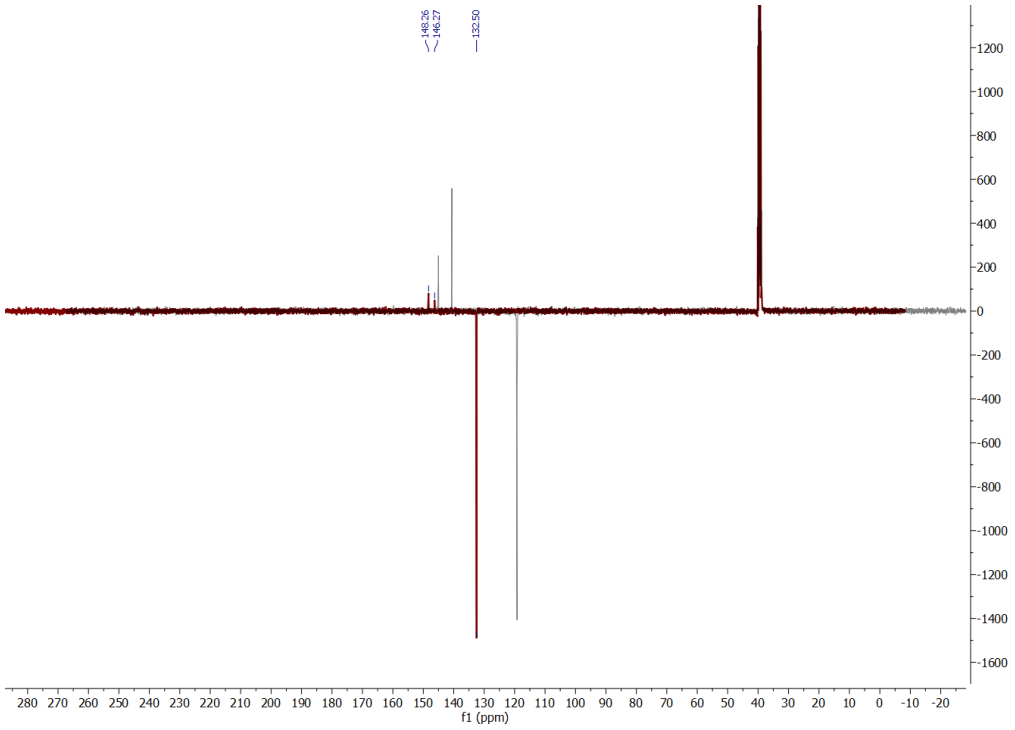

Figure 5.22: *Stacked ^{13}C NMR spectra in dmso-d_6 of 2-azido-4-nitroimidazole (black line) and the product obtained from the reaction of 2-azido-4-nitroimidazole with K_2CO_3 (red line)*

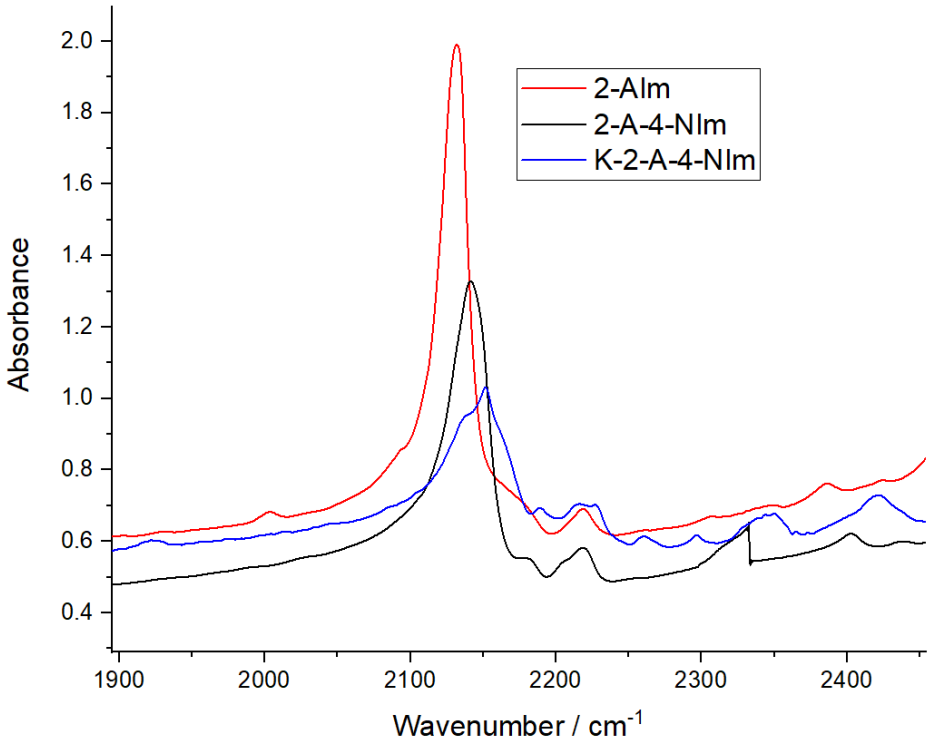

Figure 5.23: *Series of FTIR spectra (range 2500 to 1900 cm^{-1}) showing the spectra of 2-azioimidazole (red line), 2-azido-4-nitroimidazole (black line) and potassium-2-azido-4-nitroimidazolate.H_2O (blue line)*

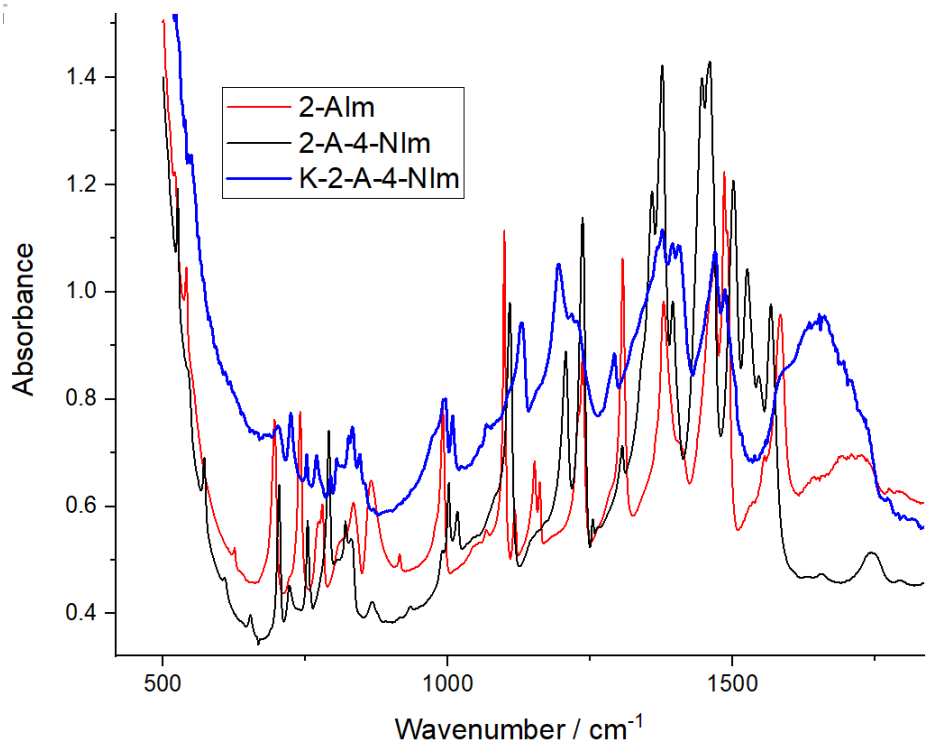

Figure 5.24: *Series of FTIR spectra (range 1750-500 cm^{-1}) showing the spectra of 2-azioimidazole(red), 2-azido-4-nitroimidazole (black) and potassium-2-azido-4-nitroimidazolate.H_2O(blue)*

5.2.6 Crystal structure of potassium-2-azido-4-nitroimidazolate monohydrate

Potassium-2-azido-4-nitroimidazolate (grown from evaporation of ethanolic solutions) crystallises in the space group $P2_12_12$ as a 1 : 1 potassium-azidonitroazolate compound with one water present per formula unit (**Figure 5.25**). This opposes the earlier ^1H NMR findings whereby 3 waters per azidonitroimidazolato moiety were expected. The azidonitroimidazolato anion is present in only one crystallographically independent site and engages in multiple coordination modes. It binds to K1 in an monodentate fashion via N2. N1 and O3 of the nitro group take part in a κ2 bidentate bond to K1. O2 of the nitro group also binds to K1 in a monodentate manner. The azido group also takes part in bonding by N3 and N5 binding to K1. H_2O acts as a bridge between two adjacent K1 atoms and takes part in strong (strong defined as a hydrogen bond between 1.5-2.2 Å with the bond length smaller than the sum of the Van der Waals radii and shows a significant effect on the crystal packing)[34] hydrogen bonding between hydrogen atoms and either the N1 or N2 of the imidazolate ring. Bonds to N2 are longer than that for N1 at 2.003 Å vs 2.158 Å. A claim for a weak hydrogen bond between N5 and H00D of the imidazole ring can be made due to the impact it can be seen to have on the crystal packing however at a bond length of 2.926 Å this is questionable.[34] Bond lengths of potassium-2-azido-4-nitroimidazolate.H_2O were compared to published data for 2-azido-4-nitroimidazole monohydrate and to data for azidoimidazole recorded during the course of this work (**Table 5.2**).[22] Potassium-2-azido-4-nitroimidazolate(K-2-A-4-NIm) possess the longest N_α-N_β bond at 1.257(4) Å compared to 1.248(5) Å and 1.207(1) Å for 2-azido-4-nitroimidazole monohydrate and 2-azidoimidazole respectively. The N_β-N_γ bond lengths of the potassium salt sits between that of the free acid and azidoimidazole at 1.125 Å whilst possessing the longest C-N_α at 1.426(4) Å respectively. The C-NO_2 bond of K-2-A-4-NIm is also shorter than that for the free acid, whilst also having longer N-O bonds. The ring C-N bonds of K-2-A-4-NIm have a smaller range than that found for either 2-A-4-NIm.H_2O or 2-AIm. Both 2-A-4-NIm and 2-AIm have one short C-N length whilst the longest C-N of 2-AIm is the longest found in any of the three structures. K-2-A-4-NIm also possesses the longest C-C length at 1.382(5) Å. From the available data observations can be made about the type of bonding and electronic structure in these compounds. Both K-2-A-4-NIm and 2-A-4-NIm.H_2O have longer N_α-N_β bonds than 2-

AIm while also having shorter N_β-N_γ lengths. This implies a greater contribution of electronic resonance forms where N_α-N_β and N_β-N_γ are present as double bonds in the case of 2-Aim. For K-2-A-4-Nim and 2-A-4-Nim, the azido group is clearly present with a triple bond between N_β-N_γ. 2-A-4-NIm possesses the shortest N_β-N_γ bond and could be more liable to N_2 elimination than K-2-A-4-NIm, however the differences between the two values are small and this effect is presumed to be weak. However, with a longer and weaker C-N_α bond, K-2-A-4-NIm could be more susceptible to the loss of the N_3 fragment than either of the other compounds in the discussed triad. Shorter C-NO_2 bonds for K-2-A-4-NIm compared to 2-A-4-NIm indicate an R-NO_2 group with a greater contribution of the C-NO_2 resonance form. This conclusion is also corroborated in the increased N-O bond lengths. The C-NO_2 distances can also be compared to those found in nitroazolates such as K-2,4-DNI, K-2,4,5-TNI and K-4,5-DNI (**Table 5.3**).

Bond	**Bond length/ Å**		
	K-2-A-4-NIm.H_2O	**2-A-4-NIm.H_2O[21]**	**2-AIm**
R-N_3(N_α-N_β)	1.257(4)	1.248(5)	1.207(1)
R-N_3(N_β-N_γ)	1.125(4)	1.113(5)	1.146(1)
C-N_α	1.426(4)	1.391(4)	1.422(1)
C-NO_2	1.407(5)	1.418(4)	-
N-O	1.247(4), 1.248(4)	1.231(4), 1.234(4)	-
Ring C-N	1.322(4)-1.38(4)	1.308(4)-1.373(4)	1.305(1)-1.395(1)
C-C	1.382(5)	1.352(5)	1.347(1)

Table 5.2: *Selected Bond lengths of potassium-2-azido-4-nitroimidazolate.H_2O, 2-azido-4-nitroimidazole[21] and 2-azidoimidazole*

Bond Type	**Bond Length/ Å**			
	K-2-A-4-NIm.H_2O	**K-2,4-DNI[35]**	**K-4,5-DNI[36]**	**K-2,4,5-TNI[37]**
C-NO_2	1.407(5)	1.421, 1.437	1.437, 1.438	1.420, 1.440, 1.458
N-O	1.247(4), 1.248(4)	1.226-1.241	1.216-1.233	1.216-1.238

Table 5.3: *Selected Bond lengths of potassium-2-azido-4-nitroimidazolate.H_2O, potassium-2,4-dinitroimidazolate (K-2,4-DNI), potassium-4,5-dinitroimidazolate (K-4,5-DNI) and potassium-2,4,5-trinitroimidazolate (K-TNI)*

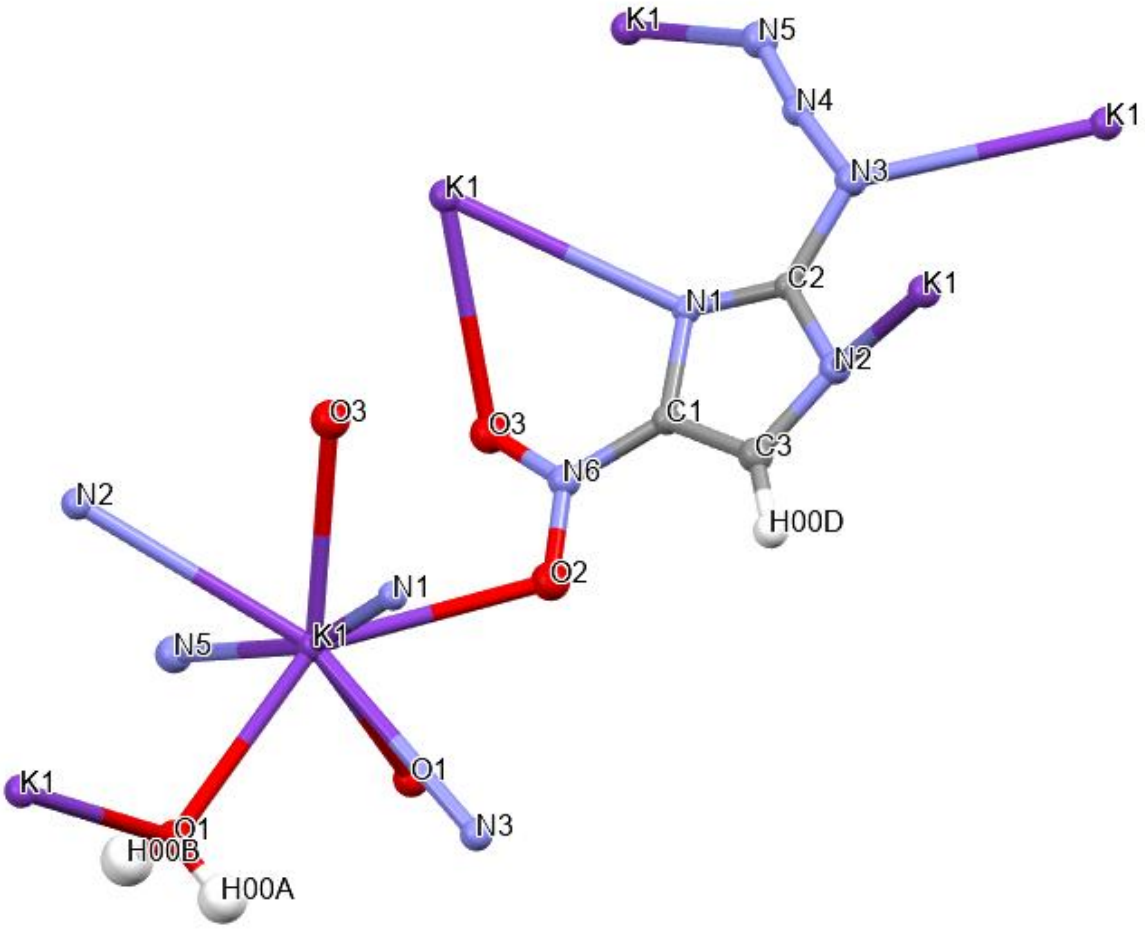

Figure 5.25: *Projections of the thermal ellipsoid in the molecular structure of the crystals of Potassium-2-azido-4-nitroimidazolate monohydrate. Thermal ellipsoids set at the 67% probability level. Selected bond lengths (Å): K1 O1 2.764(3) K1 O2 2.817(3) K1 O1 2.851(3) K1 O3 2.844(3) K1 N1 3.047(3) K1 N3 3.007(3) K1 N5 2.925(3) K1 N2 3.158(3) O1 K1 2.851(3) O2 N6 1.247(4) O3 N6 1.248(4) O3 K1 2.844(3) N1 C1 1.380(4) N1 C2 1.322(4) N1 K1 3.047(3) N6 C1 1.407(5) N3 N4 1.256(4) N3 C2 1.426(4) N3 K1 3.007(3) N4 N5 1.125(4) N5 K1 2.925(3) N2 C2 1.355(4) N2 C3 1.350(5) N2 K1 3.158(3) C1 C3 1.382(5), Atom Colours: Blue = Nitrogen, Grey = Carbon, Red = Oxygen, White = Hydrogen, Purple = Potassium*

From the comparison of bond lengths of these potassium salts, K-2-A-4-NIm has by far the shortest C-NO_2 length of any of the dinitro / trinitro imidazolates. This strongly suggests that the C-NO_2 group of K-2-A-4-NIm is present as the 'charged' NO_2 resonance form (i.e. localised formal charges on N and O) (**Figure 5.26**) with the negative charge gained upon deprotonation being localised primarily on the NO_2 group.

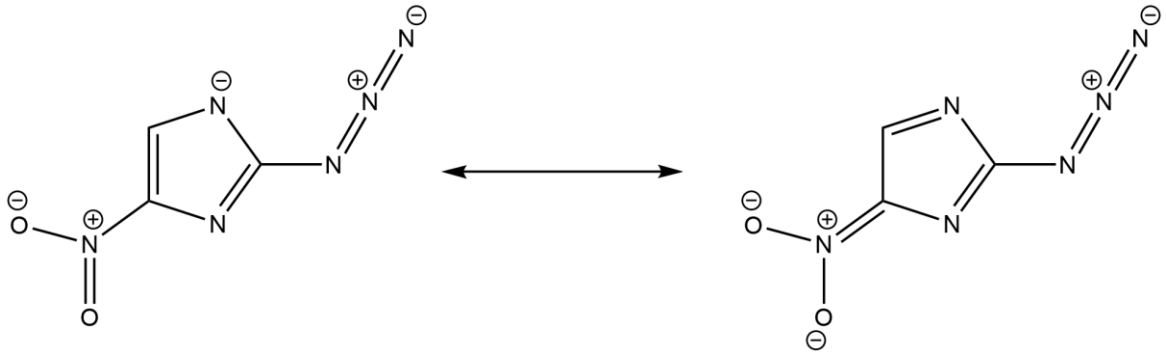

Figure 5.26: *Resonance forms of the azidonitroimidazolato anion; Left: Resonance form A displaying a ring nitrogen atom carrying a formal negative net charge of -1, Right: Resonance form B of the azidonitroimidazolato anion displaying a nitro group that carries a formal negative net charge of -1, the suspected dominant resonance form adopted by potassium-2-azido-4-nitroimidazolate.H_2O*

5.2.7 Synthesis and characterisation of metal salts of azidonitropyrazolates

Following the synthesis of K-2-A-4-NIm as energetic materials efforts were turned towards a similar treatment of azidonitropyrazoles. Two azidonitropyrazoles are known in the literature: 3-azido-4-nitropyrazole and 3-azido-4,5-dinitropyrazole. The synthesis of 3-azido-4-nitro-pyrazole was first published by Latypov et al. [19] However, as the starting material used by Latypov, 3-amino-4-nitro-pyrazole, is reported to be synthesised in low yields,[38] we elected to synthesis 3-azido-4-nitropyrazole via a novel route. The direct nitration of 3-azidopyrazole was chosen as the alternative synthesis due to the apparent ease of synthesis of starting materials (**Figure 5.27**).

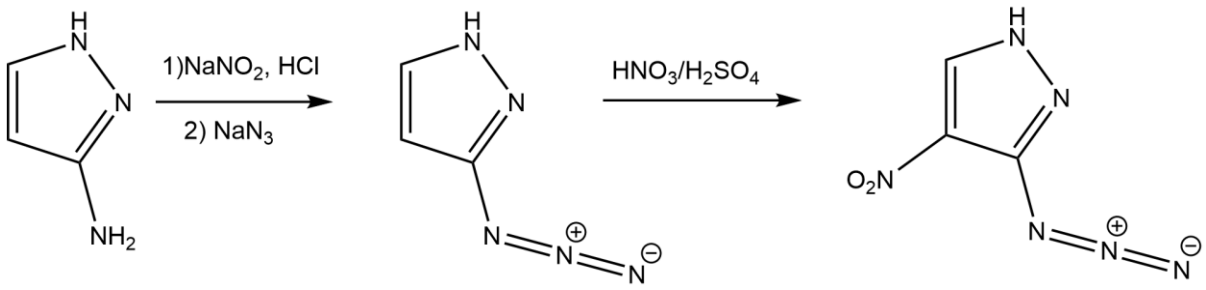

Figure 5.27: *Synthesis of 3-azido-4-nitropyrazole from the starting material 3-aminopyrazole*

3-azidopyrazole was synthesised according to the methods of Chen.[4] 3-aminopyrazole was diazotised by the action of $NaNO_2$ and HCl. Product purity was proven through both FTIR and NMR spectral analysis.

5.2.7.1 Vibrational Spectroscopy

The IR spectrum of 3-azidopyrazole is dominated by the $\nu_{as}(N_3)$ stretching mode (**Figure 5.28**). This is shown by the strong absorption at 2120 cm^{-1}, exactly matching that of the reported value.[4] Comparison to the IR spectrum of 3-aminopyrazole shows a drastic reduction in the absorption bands associated with the stretching (3328 cm^{-1}) and bending (1616 cm^{-1}) modes of C-NH_2. No absorption associated with these two vibrations can be found in the spectrum of 3-azidopyrazole. This is clear evidence for the successful diazotisation-substitution of 3-aminopyrazole with NaN_3 to form 3-azidopyrazole and implies that no 3-aminopyrazole remains in the product.

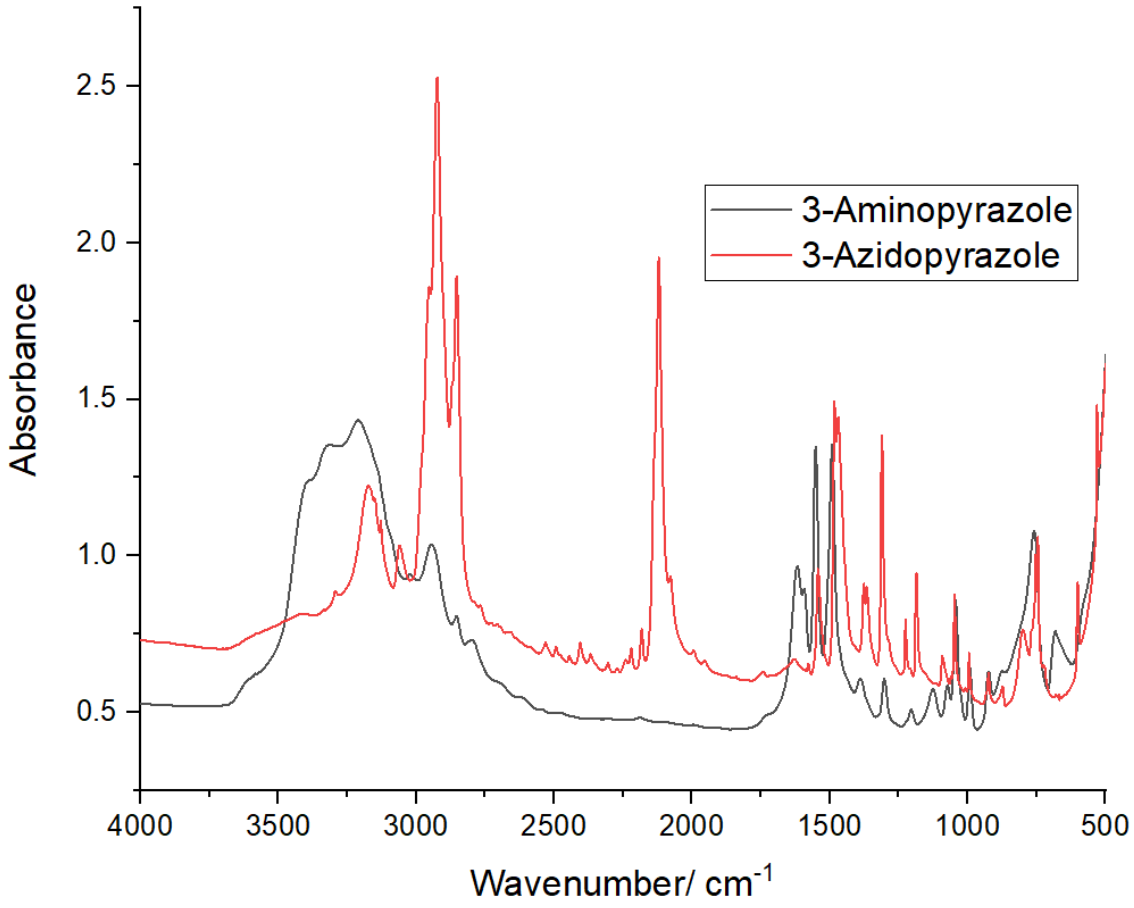

Figure 5.28: *Series of layered FTIR spectra (range 4000 to 500 cm^{-1}) showing the spectra of 3-azidopyrazole (red line) and 3-aminopyrazole (black)*

5.2.7.2 NMR spectroscopy

3-azidopyrazole was investigated with ^{1}H and ^{13}C NMR spectroscopy (**Figure 5.29**). Spectra were then compared to literature values to ascertain product identity and purity.[21] 3-azidopyrazole has 3 singlets in the ^{1}H NMR, one for the N-H (12.71 ppm) and two C-H signals (7.73 and 6.00 ppm). These match well to the reported values of 12.72, 7.74 and 6.01 ppm. A small amount of water is also present in the spectrum. Integration of the individual signals shows water makes up <5% of the spectrum. It is possible the product crystallises as a hydrate however, the presence of the water is more likely due to insufficient drying of the product prior to recording the spectra or H_2O present in the deuterated solvent used to dissolve the sample. 3-azidopyrazole produces shows three peaks at 147.06, 131.61 and 95.72 ppm in the ^{13}C NMR. These values all match well to the published data from Chen (146.53, 131.14, 95,24 ppm).[4]

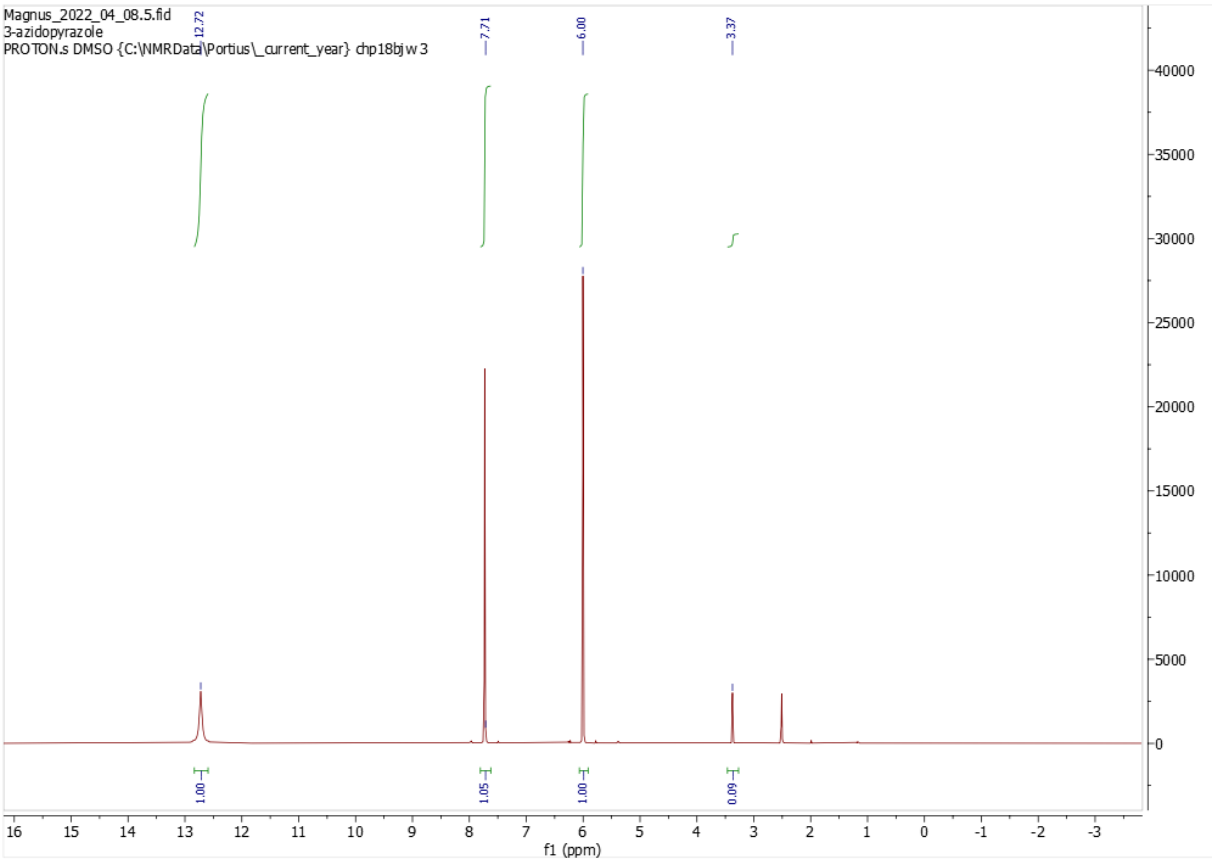

Figure 5.29: *^{1}H NMR spectra in dmso-d_6 of 3-azidopyrazole*

The NMR spectra, alongside investigation of the compound with FTIR, confirms the identity of the product as 3-azidopyrazole. As the NMR spectra show no substantial impurities, 3-azidopyrazole as synthesised by this method was used without further purification in subsequent reactions.

5.2.8 Synthesis and characterisation of 3-azido-4-nitropyrazole

3-azidopyrazole was nitrated according to the same procedures used for the synthesis for 2-azido-4-nitroimidazole.[22] This results in the formation of an orange oil. Oil formation is likely the result of residual acetic acid in the sample preventing crystallisation with the formation of acetic acid most likely happening due to acid catalysed hydrolysis of ethyl acetate. Removal of acetic acid with high vacuum over the course of several hours resulted in the crystallisation of clear rectangular pale-

yellow crystals alongside a microcrystalline yellow solid. The product was characterised through NMR, FTIR and crystallographic studies.

5.2.8.1 NMR spectroscopy

A sample containing both pale-yellow crystalline material and the microcrystalline yellow solid was investigated with ^{1}H and ^{13}C NMR. The sample has 4 singlets in its ^{1}H NMR spectrum at 13.90, 8.84, 3.64 and 1.91 ppm. Signals at 3.64 and 1.91 ppm were assigned to H_2O and AcOH respectively. H_2O presumably is found as a solvent of crystallisation. Signals at 13.90 and 8.84 ppm were assigned through comparison to the spectrum of 3-azidopyrazole. The signal at 8.84 ppm is assigned to the C-H of 3-azido-4-nitropyrazole. This signal is shifted to higher ppm values as expected of a C-H attached to a less electron rich ring. The loss of one of the C-H environments in 3-azidopyrazole is clear evidence for the formation of 3-azido-4-nitrpyrazole. The signal at 13.90 ppm is assigned to the N-H of 3-azido-4-nitropyrazole and again is shifted to higher ppm values as is expected. The N-H of 3-azido-4-nitropyrazole is also much broader than in 3-azidopyrazole, possibly due to greater deuterium/hydrogen exchange with the deuterated NMR solvent. The simplicity of the spectrum also suggests that both the pale-yellow crystals and the microcrystalline material are the same compound. If two products were forming more peaks would be expected in the ^{1}H NMR spectrum. ^{13}C NMR of the yellow solid shows 3 signals at 142.46, 132.22 and 124.63 ppm. These are assigned to the 3 carbon environments of 3-azido-4-nitropyrazole. Comparison to the ^{13}C NMR spectrum of 3-azidopyrazole shows that, upon nitration one signal moves downfield (147.06 to 142.46 ppm) and two signals move up field (131.61 to 132.22 ppm, 95.72 to 124.63 ppm) The signal at 124.63 ppm is assigned to C-NO_2. The substitution of a C-H for a C-NO_2 would lead to substantially reduced shielding and thus the largest shift up field. The signal at 132.22 ppm is assigned to the remaining C-H and the signal at 142.46 ppm is assigned to C-N_3. Once again, with no additional signals in the spectrum one can have confidence that the pale-yellow crystals and the microcrystalline material are the same compound.

5.2.8.2 Vibrational spectroscopy

FTIR spectra of 3-azidopyrazole and 3-azido-4-nitropyrazole were recorded and compared to allow for an assignment of the observed absorption bands to bond vibrational modes. Both compounds exhibit an intense band for the $\nu_{as}(N_3)$ stretching vibration. Nitration of the pyrazole ring has resulted in a shift of ~15 cm^{-1} to 2134 cm^{-1} in 3-azido-4-nitropyrazole (**Figure 5.30**). Assignment of $\nu_{sym}(N_3)$ can also be made with the compounds showing absorption at 1225 and 1219 cm^{-1} in 3-azidopyrazole and 3-azido-4-nitropyrazole respectively (**Figure 5.31**). The reason for the relatively small shift in wavenumbers of the band between 3-azidopyrazole and 3-azido-4-nitropyrazole compared to the asymmetric stretch is unknown. Assignment of the nitro group stretching vibrations is challenging in pyrazoles due to the proximity of ring vibrations to the spectral regions of interest, but tentative assignment of the bands can still be made. The symmetric NO_2 stretch is assigned to the band at 1283 cm^{-1}. While low in the spectrum, it is not uncommon for symmetric NO_2 stretches to appear this low in the FTIR, though symmetric NO_2 stretches in this region are more usually due to the presence of N-NO_2 groups rather than C-NO_2. The NO_2 asymmetric stretch can be assigned to the band at 1554 cm^{-1}. While close to a ring vibration, the increased intensity of the band in the spectrum of 3-azido-4-nitropyrazole makes this more likely to be the NO_2 asymmetric stretch. While not assigned in the analysis of 2-azido-4-nitroimidazole, C-NO_2 deformation modes in 3-azido-4-nitropyrazole could prove to be indicative of the presence of the NO_2 group. Bands of medium intensity can be found at 838 and 847 cm^{-1}. As discussed previously (Introduction, **IR spectroscopic properties of the -NO_2 group**) these fall in the range of the symmetric bend. With the appearance of these bands in a previously empty part of the spectrum, tentative assignment of one or both bands to the NO_2 symmetric bend can be made. Overall, both FTIR and NMR spectra suggest that the intended 3-azido-4-nitropyrazole has been synthesised. Both spectra also point to water presumably combining with the 3-azido-4-nitropyrazole as a solvent of crystallisation. Due to broadening of the signals in the NMR as a result of deuterium/hydrogen exchange, an accurate value for the amount of crystallised water could not be determined. Crystal structure determination was needed to conclusively prove the amount of water.

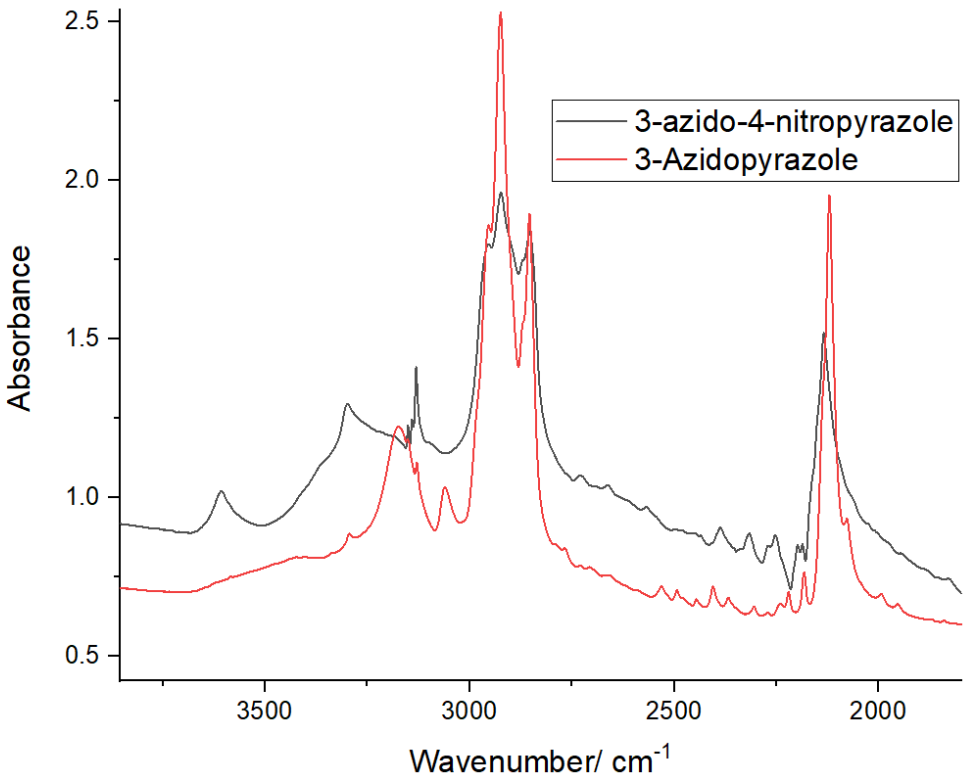

Figure 5.30: *Series of layered FTIR spectra (range 3750 to 2000 cm^{-1}) showing the spectra of 3-azidopyrazole (red line) and 3-azido-4-nitro-pyrazole (black)*

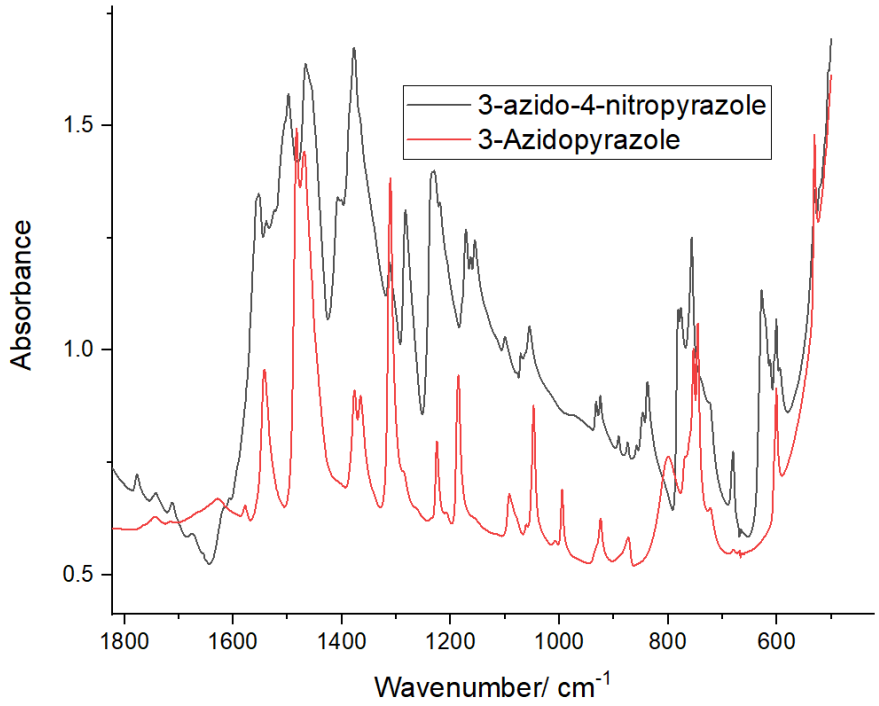

Figure 5.31: *Series of layered FTIR spectra (range 1800 to 500 cm^{-1}) showing the spectra of 3-azidopyrazole (red line) and 3-azido-4-nitropyrazole (black)*

5.2.9 Crystal structure determination of 3-azido-4-nitropyrazole.H_2O

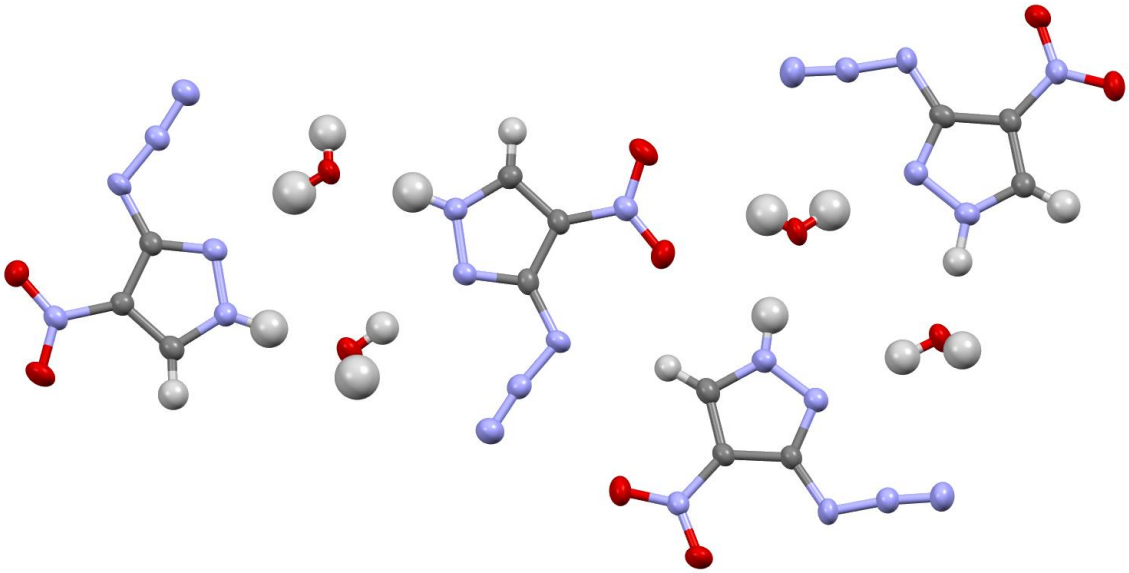

Figure 5.32: *Projections of the thermal ellipsoid in the molecular structure of the crystals of 3-azido-4-nitroprazole monohydrate. Thermal ellipsoids set at the 67% probability level, Atom Colours: Blue = Nitrogen, Grey = Carbon, Red = Oxygen, White = Hydrogen*

Crystals were grown from the yellow oil obtained following nitration by removal of acetic acid under vacuum. The compound crystallises as 3-azido-4-nitropyrazole.H_2O (**Figure 5.32**). As the work by Latypov did not investigate the structure of 3-azido-4-nitropyrazole this constitutes the first known crystal structure of this compound The asymmetric unit of 3-azido-4-nitropyrazole consists of 8 molecules, 4 of 3-azido-4-nitropyrazole and 4 of H_2O. These arrange as two dimers held together by hydrogen bonds between O-H and the pyrazole ring nitrogen and between the N-H of pyrazole and the oxygen atom of water. All the H bonds (2.017-2.081 A) are within the expected range for strong H-bonds (1.5-2.2 A). 3-Azido-4-nitropyrazole arranges itself in layers and is held together by H-bonds present *between* the layers. Overall, all characterisation techniques conclusively prove the synthesis of 3-azido-4-nitroimidazole by a new synthetic route. This also constitutes the first structure of 3-azido-4-nitropyrazole known in the literature with 3-azido-4-nitropyrazole crystallising as its monohydrate.

5.2.10 Attempted synthesis and characterisation of potassium-3-azido-4-nitropyrazolate

Following the synthesis of 3-azido-4-nitropyrazole.H_2O (3-A-4-NP.H_2O) via a new synthetic route, attempts at synthesising the potassium salt were made. The potassium salt of 3-azido-4-nitropyrazole was desired both as a precursor to transition metal-azidonitroazolates and as a potential energetic material itself. Potassium-3-azido-4-nitropyrazolate(K-3-A-4-NP) was synthesised according to a modified literature synthesis using potassium carbonate as a base (**Figure 5.33**).[27] Following deprotonation, ethanolic solutions of potassium-3-azido-4-nitropyrazolate were allowed to slowly evaporate over five days to afford irregularly shaped orange crystals. Products were identified by comparison of NMR and FTIR spectra to starting materials and by determination of the crystal structure.

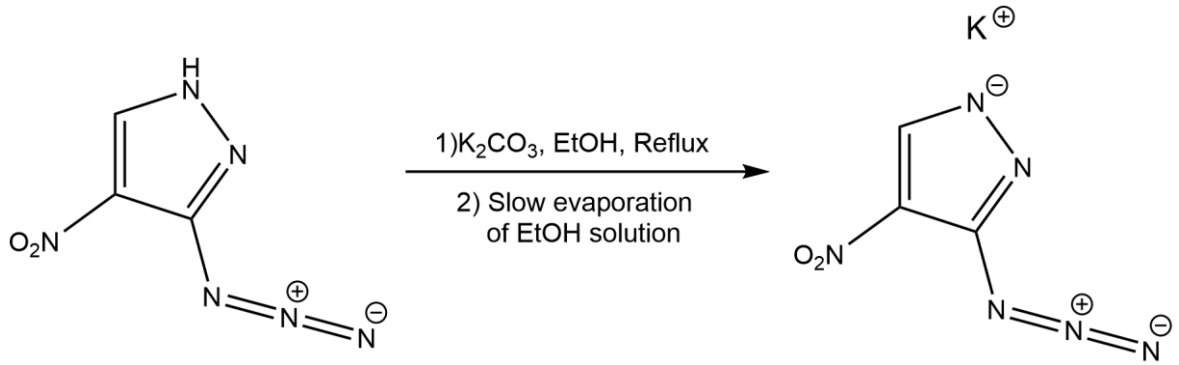

Figure 5.33: *Attempted synthesis of potassium-3-azido-4-nitropyrazolate*

5.2.10.1 NMR Spectroscopy

The crystals were investigated by ^{1}H and ^{13}C NMR. Two singlets in the ^{1}H NMR can be seen at 8.34 and 3.37 ppm. These are assigned to the C-H of the imidazole ring and to an O-H of water presumably present as a solvent of crystallisation. By comparison to the ^{1}H NMR spectra 3-azido-4-nitro-pyrazole it can be seen that the C-H has shifted downfield by 0.5 ppm, as expected of a proton in a more shielding environment due to the increased electron density of the presumed 3-azido-4-nitropyrazolato moiety. Comparison of the two spectra also makes clear the absence of any signal associated to the N-H of 3-azido-4-nitropyrazole confirming that complete

deprotonation had taken place. ^{13}C NMR of the orange crystalline product shows two signals at 145.19 and 142.55 ppm. This is inconsistent with the expected three carbon environments of potassium-3-azido-4-nitropyrazole and with the three carbon environments of the starting material 3-azido-4-nitroimidazole (signals at 142.46, 132.22 and 124.63). From comparison of the two spectra, it appears that the missing signal is assigned to the C-NO_2 carbon while the C-H and C-N_3 carbon environments shift up field in the spectrum by 2.73 and 10.33 ppm respectively. While it is not uncommon for tertiary carbons of azolates to have weak or non-detectable signals in ^{13}C NMR experiments, the ability to identify all 3 environments in the precursor to the potassium salt does imply a change, too big to assign to increased/decreased shielding alone, in the environment of one of the carbon atoms of the ring. Comparison of the IR spectra of K-3-A-4-NP and 3-A-4-NP.H_2O was used to help contextualise this apparent change in carbon environment.

5.2.10.2 FTIR spectroscopy

FTIR spectra of the orange crystalline product was recorded and compared to that of the starting material. Upon deprotonation, no absorption band assigned to the $\nu_{as}(N_3)$ stretching vibration can be found in the orange product (**Figure 5.34**). Neither can a band be assigned to the $\nu_{sym}(N_3)$ stretching vibration present in both 3-azidopyrazole and 3-azido-4-nitropyrazole (1225 cm^{-1} and 1219 cm^{-1} respectively). The assignment of NO_2 stretching vibrations is once again challenging. The FTIR of the product has three low intensity bands in the region 1560-1585 cm^{-1} (**Figure 5.35**). While one of these bands could be assigned to the $\nu_{as}(NO_2)$ stretching vibration, it is unlikely due to the intensity of the band relative to the other bands of the fingerprint region. Therefore, it is more likely that these bands are pyrazole ring vibrations. If this assignment is true then there are no other intense bands that can confidently be assigned to the $\nu_{as}(NO_2)$ stretching vibration. The band assigned to the $\nu_{sym}(NO_2)$ stretching vibration in 3-azido-4-nitropyrazole (1283 cm^{-1}) can be seen to completely disappear in the spectrum of the product. However, two new absorption bands at 980 and 1113 cm^{-1} in the spectrum of the product. These, much like for K-2-A-4-NIm, are indicative of the $\nu_{sym}(NO_2)$ and $\nu_{as}(NO_2)$ stretching vibrations of a charged NO_2 group. C-NO_2 deformation modes can also be observed in the spectrum of the orange crystalline

product. The C-NO_2 symmetric bend can be found at 832 cm^{-1} in the product, a shift of 5 cm^{-1} from the starting material. Overall, the identity of the product was not clear from NMR and FTIR. FTIR proves the absence of $\nu_{as}(N_3)$ and $\nu_{sym}(N_3)$ stretching vibrations indicating loss of the azido group. However, the ^{13}C NMR shows only a small shift to higher wavenumbers of the carbon of C-N_3. If the azido group has been substituted, the replacing group has only had a small effect on the carbon environment. The absence of the C-NO_2 signal in the ^{13}C NMR implies a change in environment compared to the starting material. This could be related to the charged NO_2 group resonance which can be plausibly assigned to absorption bands in the fingerprint region.

The loss of absorption bands assigned to stretches of the azido group is explained through tautomerisation of 3-azido-4-nitropyrazole to form 4-nitropyrazolo[1,5 d]tetrazole (**Figure 5.36**).

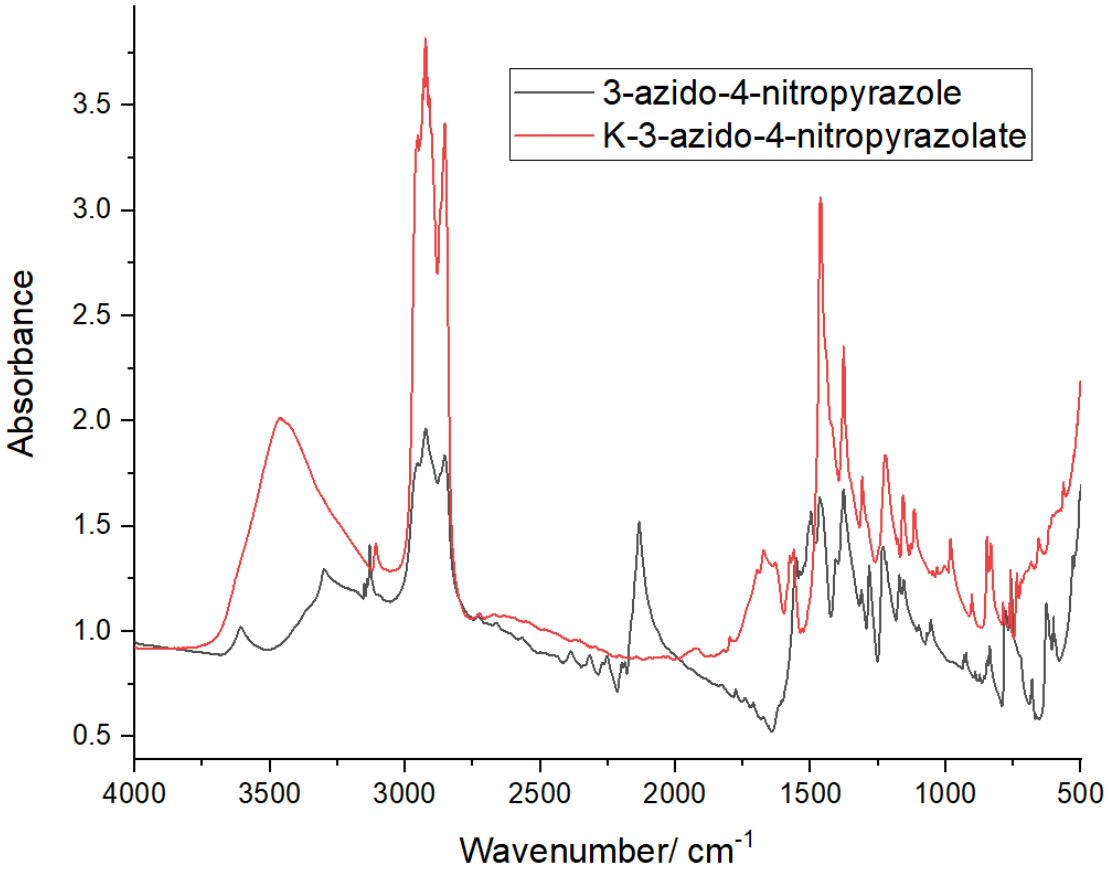

Figure 5.34: *Series of layered FTIR spectra (range 4000 to 500 cm^{-1}) showing the spectra of 3-azido-4-nitropyrazole (black) and a spectrum of the orange crystalline material initially assumed to be potassium-3-azido-4-nitropyrazolate (red)*

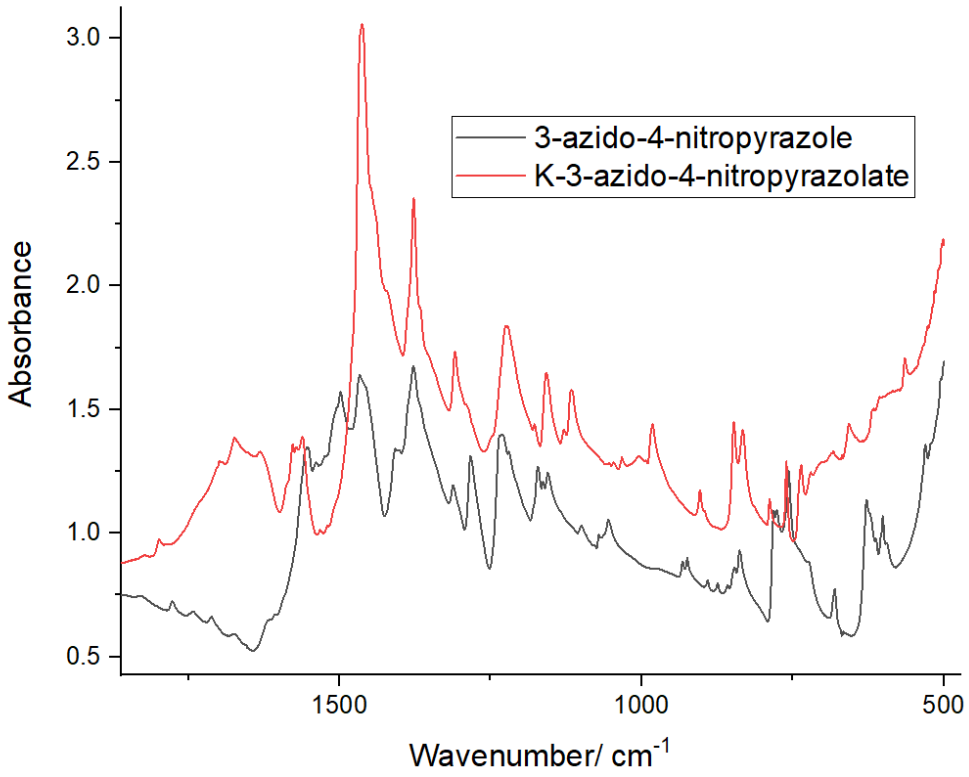

Figure 5.35: *Series of layered FTIR spectra (range 1750 to 500 cm^{-1}) showing the spectra of 3-azido-4-nitropyrazole (black) and a spectrum of the orange crystalline material initially assumed to be potassium-3-azido-4-nitropyrazolate (red)*

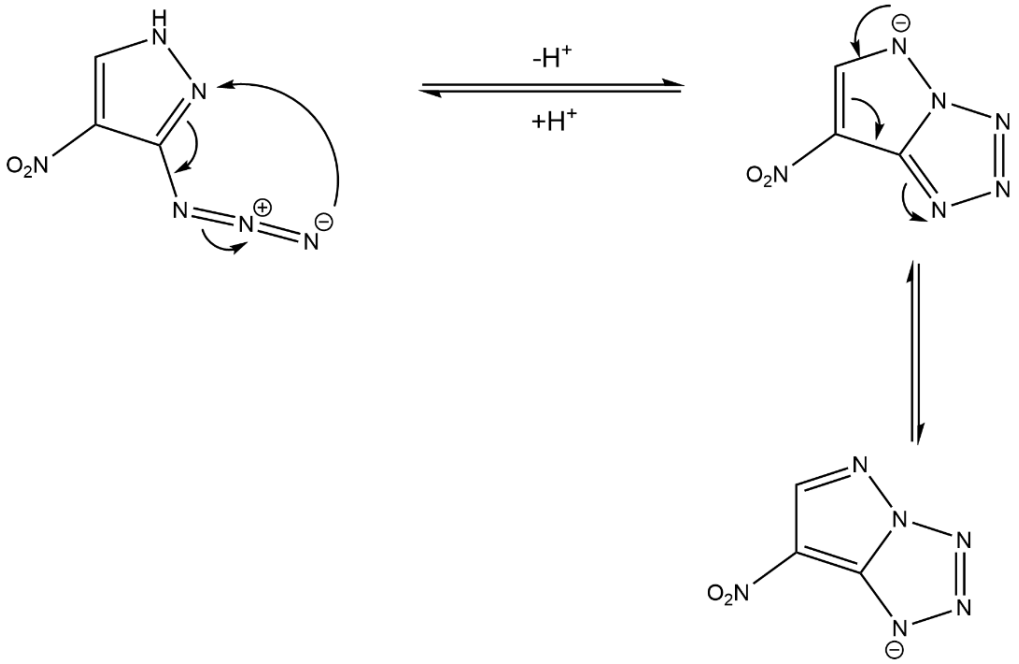

Figure 5.36: *Proposed azide-tetrazole tautomerisation of 3-azido-4-nitropyrazole upon deprotonation*

Azide-tetrazole tautomerisation is a known phenomenon and has been quite extensively studied in a series of azide/tetrazole-pyrimidine complexes.[39] It has also been shown that this equilibrium is in favour of tetrazole formation for anions of azidopyrazoles.[40] To assess whether azide/tetrazole tautomerisation was the cause of the disappearance of the azide absorption, 0.235 g of the orange crystalline material was dissolved in water and reacidified to pH 1. If the tetrazole containing product was forming rather than decomposition occurring, reacidification should result in the reformation of 3-azido-4-nitropyrazole. Upon addition of HCl to the reaction mixture small amounts of bubbling was observed and a white solid precipitated out after 1 hr of stirring. The solid was investigated with FTIR spectroscopy. The product has an FTIR spectrum which almost exactly matches that of 3-azido-4-nitropyrazole with only a few additional bands present (**Figure 5.37**). Most notable is the reformation of an intense $\nu_{as}(N_3)$ stretching vibration at the same value found for 3-azido-4-nitropyrazole. This is strong evidence to suggest that upon deprotonation the formed product is not potassium-3-azido-4-nitroimidazole but is instead potassium-4-nitro-pyrazolo[1,5 d]tetrazole (**Figure 5.38**).

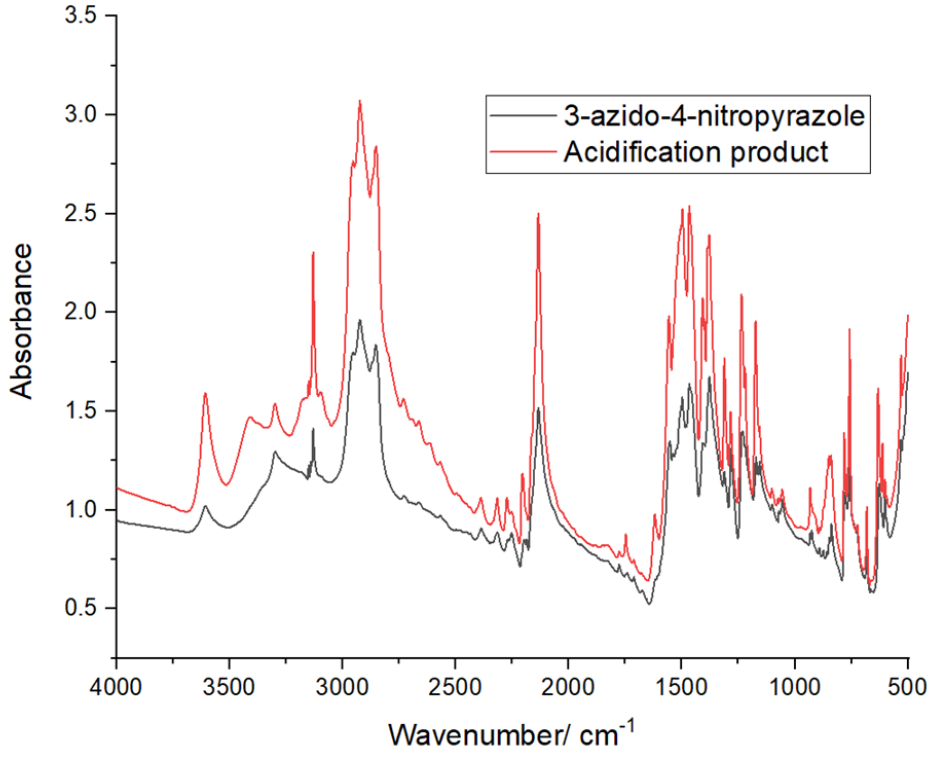

Figure 5.37: *Series of layered FTIR spectra (range 4000 to 500 cm^{-1}) showing the spectra of 3-azido-4-nitropyrazole (black) and a spectrum of the orange crystalline material initially assumed to be potassium-3-azido-4-nitropyrazolate (red)*

Acidification pushes the azide-tetrazole equilibrium towards the side of the azide which is shown by the intense $v_{as}(N_3)$ stretching vibration.

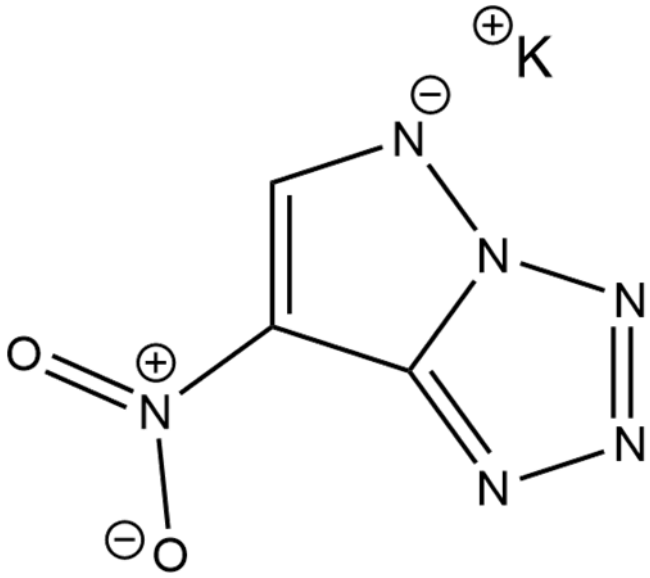

Figure 5.38: *Structure of potassium-4-nitro-pyrazolo[1,5 d]tetrazole*

5.2.11 Crystal structure of potassium-4-nitro-pyrazolo[1,5 d]tetrazole

To prove the identity of the product as potassium-4-nitro-pyrazolo[1,5 d]tetrazole, crystals formed upon slow evaporation of ethanolic solutions product were taken and used for single crystal X-ray diffraction studies. From the evaporation of the ethanolic solution two crystal types could be identified. Long, pale yellow rectangular needles were evident and when investigated with SCXRD proved to be potassium nitrate. Orange irregularly shaped crystals were also present in the crystalline solid. Investigation of these crystals allowed for the first structural determination of a non-substituted pyrazolotetrazole and confirmed the orange crystals to be potassium-4-nitropyrazolo[1,5 d]tetrazolate monohydrate(K-NPT.H_2O)(**Figure 5.39**). K-NPT.H_2O crystallises in the C2 space group. Potassium is present in one crystallographically independent site and forms bonds between tetrazole ring nitrogens, nitro group oxygen atoms and to one water molecule which bridges between potassium centres. The nitro groups of K-NPT.H_2O sit almost co-planar with the bicyclic ring structure with a twist out of plane by only 1.77 degrees. Nitro group oxygens (O1 and O2) bind in a bidentate manner towards two K1 atoms. All ring nitrogen of the pyrazolo[1,5

d]tetrazolate are involved in bonding except for N1. Only N3 and N5 of the tetrazole ring engage in bonds towards potassium centres with the bonding on N1 and N4 restricted to hydrogen bonding. N1 hydrogen bonds to one of the hydrogen atoms on H_2O. This forms a relatively strong hydrogen bond (2.3 Å) with N4 forming a weak hydrogen bond to the lone C-H of the bicyclic ring (2.5 Å). N5 of the tetrazolate ring forms a single bond to K1 whereas N3 bridges between two separate K1 atoms. As for K-2-A-4-NIm, bond lengths associated with the NO_2 group were taken and compared to the free acid and other known nitropyrazolates to assess the bonding present within the pyrazolo-tetrazole ring structure (**Table 5.4**). K-NPT.H_2O has by far the shortest C-NO_2 bond length of any of the nitroazolates with structures available to this author. K-NPT.H_2O also has the longest N-O bond length at 1.257(9) Å. Both bond lengths corroborate the FTIR analysis and support the hypothesis that in the nitropyrazolo-tetrazole anion, NO_2 is present as a 'charged' NO_2 group. The localisation of the negative charge over the NO_2 group is also supported by comparison of the N-K and O-K bond lengths. K-NPT.H_2O has both the longest N-K distance and the shortest O-K bond length. Compared to other potassium nitropyrazolates this suggests that less electron density is present on the ring nitrogens and more is localised over the NO_2 group. If negative charge were localised on one of the ring nitrogen atoms we would expect the shortest N/O-K length to be from ring nitrogen to potassium and not nitro group oxygen to potassium. Change to ring bond lengths can also be observed. C-C and N-N bond lengths are found to be longer in K-NPT.H_2O when compared to the potassium nitroazolates (**Table 5.4**).

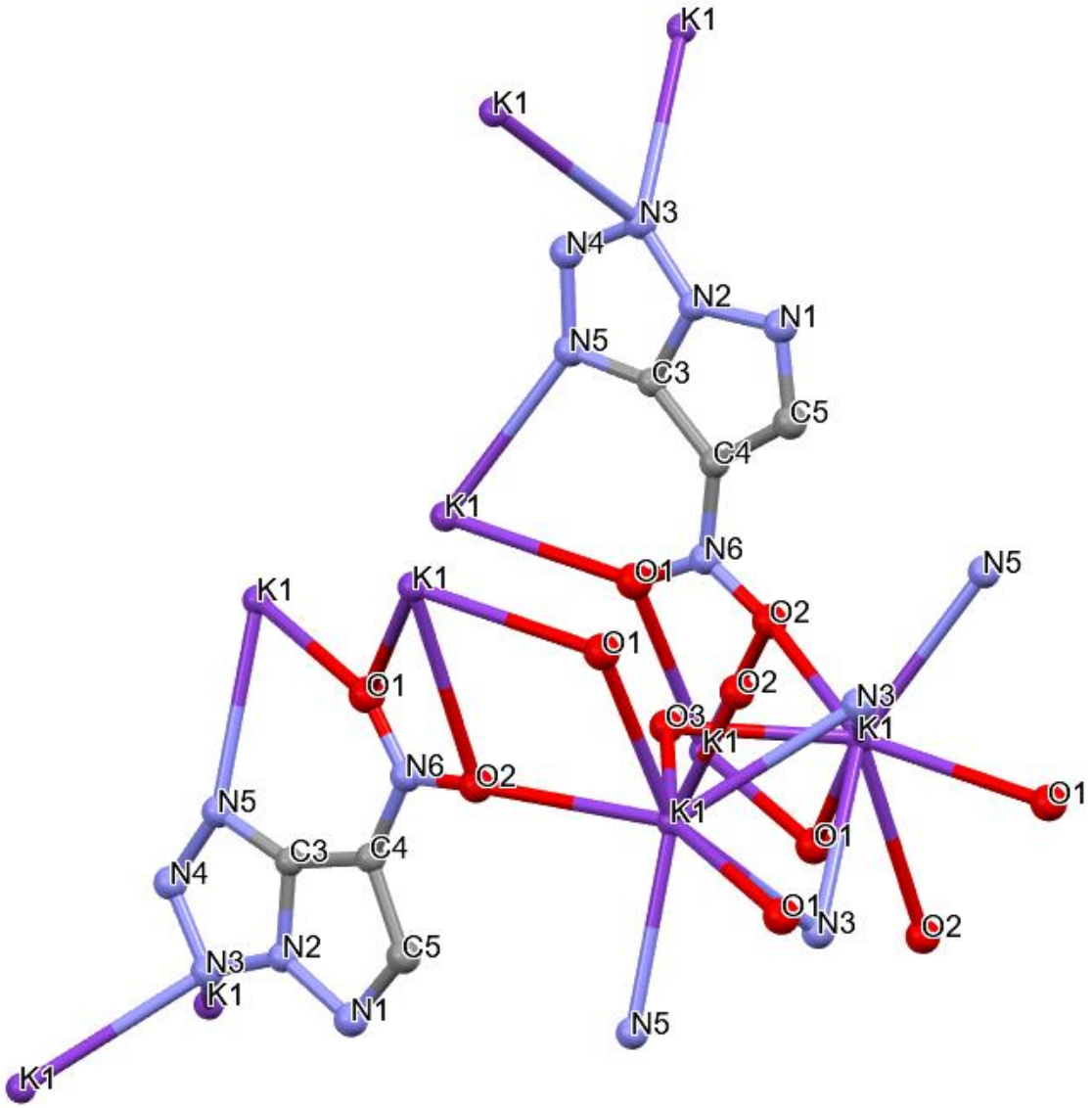

Figure 5.39: *Projections of the thermal ellipsoid in the molecular structure of the crystals of potassium-4-nitropyrazolo[1,5 d]tetrazolate monohydrate. Thermal ellipsoids set at the 67% probability level. Selected bond lengths K1 O3 2.732 K1 O2 2.745(5) K1 O2 3.145(5) K1 O1 2.766(5) K1 O1 2.868(6) K1 N5 2.919(6) K1 N3 2.980(6) K1 N3 3.121(6) O3 K1 2.732 O2 N1 1.257(9) O2 K1 3.145(5) O1 N1 1.240(9) O1 K1 2.766(5) O1 K1 2.868(6) N2 N3 1.356(8) N2 N1 1.395(9) N2 C3 1.340(8) N4 N5 1.370(8) N4 N3 1.313(8) N5 C3 1.351(9) N5 K1 2.919(6) N3 K1 2.980(6) N3 K1 3.121(6) N1 C5 1.327(9) C3 C4 1.418(9) C4 C5 1.41(1) C4 N1 1.381(8) 0.930 K1 O2 2.745(5) K1 O2 3.145(5) K1 O1 2.766(5) K1 O1 2.868(6) K1 N5 2.919(6) K1 N3 3.121(6) K1 N3 2.980(6) O2 N1 1.257(9) O2 K1 3.145(5) O1 N1 1.240(9) O1 K1 2.766(5) O1 K1 2.868(6) N2 N3 1.356(8) N2 N1 1.395(9) N2 C3 1.340(8) N4 N5 1.370(8) N4 N3 1.313(8) N5 C3 1.351(9) N5 K1 2.919(6) N3 K1 3.121(6) N3 K1 2.980(6) N1 C5 1.327(9) C3 C4 1.418(9) C4 C5 1.41(1) C4 N1 1.381(8) K1 O1 2.766(5) K1 O1 2.766(5), Atom Colours: Blue = Nitrogen, Grey = Carbon, Red = Oxygen, Purple = Potassium, Hydrogen atoms removed for clarity*

Bonds and Angles	Bond lengths and angles			
	K-NPT.H_2O	**K-TNP[41]**	**K-3, 5-DNP.H_2O[42]**	**K-3, 4-DNP.H_2O[42]**
C-NO_2	1.381(8)	1.432(2), 1.446(2), 1.452(2)	1.429(2), 1.432(2)	1.421(2), 1.452(2)
N-O	1.24(9), 1.257(9)	1.222(2)-1.233(2)	1.230(2)-1.236(2)	1.220(2)-1.224(2)
Pyrazole Ring C-C	1.413(1), 1.418(9)	1.392(2), 1.391(2)	1.376(3), 1.379(2)	1.386(3), 1.392(2)
Pyrazole Ring C-N	1.327(9), 1.34(8)	1.338(2), 1.340(3)	1.352(2), 1.352(2)	1.324(2), 1.317(2)
Pyrazole Ring N-N	1.395(9)	1.343(2)	1.346(2)	1.378(2)
N-K	2.919(6)-3.121(6)	2.785(2)-2.828(2)	2.816(2)-2.941(2)	-
O-K	2.745(5)-3.145(5)	2.782(2)-3.205(1)	2.924(2)-3.370(2)	2.974(2)-3.285(2)

Table 5.4: *Selected bond lengths of K-NPT.H_2O, K-TNP, K-3, 5-DNP.H_2O and K-3, 4-DNP.H_2O*

5.2.12 Synthesis and characterisation of 3-azido-4,5-dinitropyrazolate

With the synthesis of 3-azido-4-nitropyrazole and K-NPT.H_2O confirmed, efforts turned towards the synthesis of 3-azido-4,5-dinitropyrazole according to the methods of Herve (**Figure 5.40**).[11]

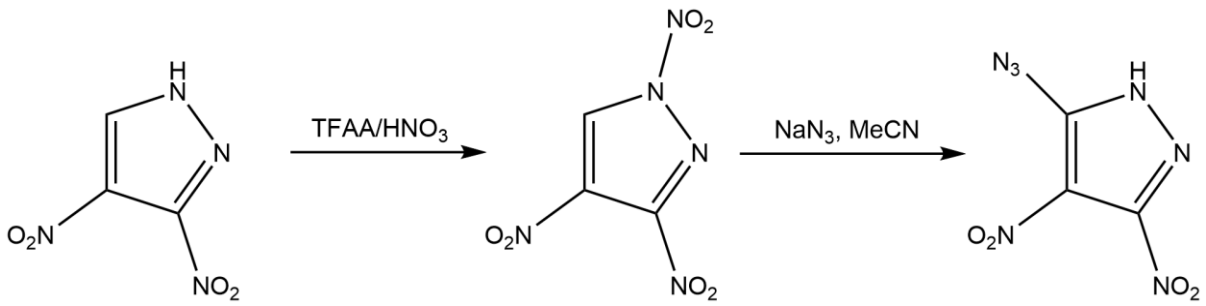

Figure 5.40: *Synthesis of 3-azido-4,5-dinitropyrazole starting from 3,4-dinitropyrazole*

1,3,4-trinitropyrazole(1,3,4-TNP) was synthesised by the in-situ generation of trifluoroacetylnitrate and subsequent nitration on the ring nitrogen in position 1.[11] Product identity and purity was confirmed solely by FTIR spectroscopy through comparison to the reported values and to FTIR spectra of 3,4-DNP.

5.2.12.1 FTIR Spectroscopy of 1,3,4-TNP

The FTIR spectrum of 1,3,4-TNP shows two intense absorption bands at 1676 and 1284 cm^{-1} (**Figure 5.41**). These bands are indicative of the $\nu_{as}(NO_2)$ and $\nu_{sym}(NO_2)$ stretching vibrations of an N bound NO_2 group. These bands can be seen to be completely absent from the spectrum of 3,4-dinitropyrazole and also match the reported values for 1,3,4-TNP of 1674 and 1285. All other IR absorptions can be found within 1-10 cm^{-1} of the reported values. Small shifts in band position can be attributed to the different forms of sample preparation (thin film versus KBr pellets). This was used as proof of the successful N-nitration of 3,4-dinitropyrazole to form 1,3,4-TNP.

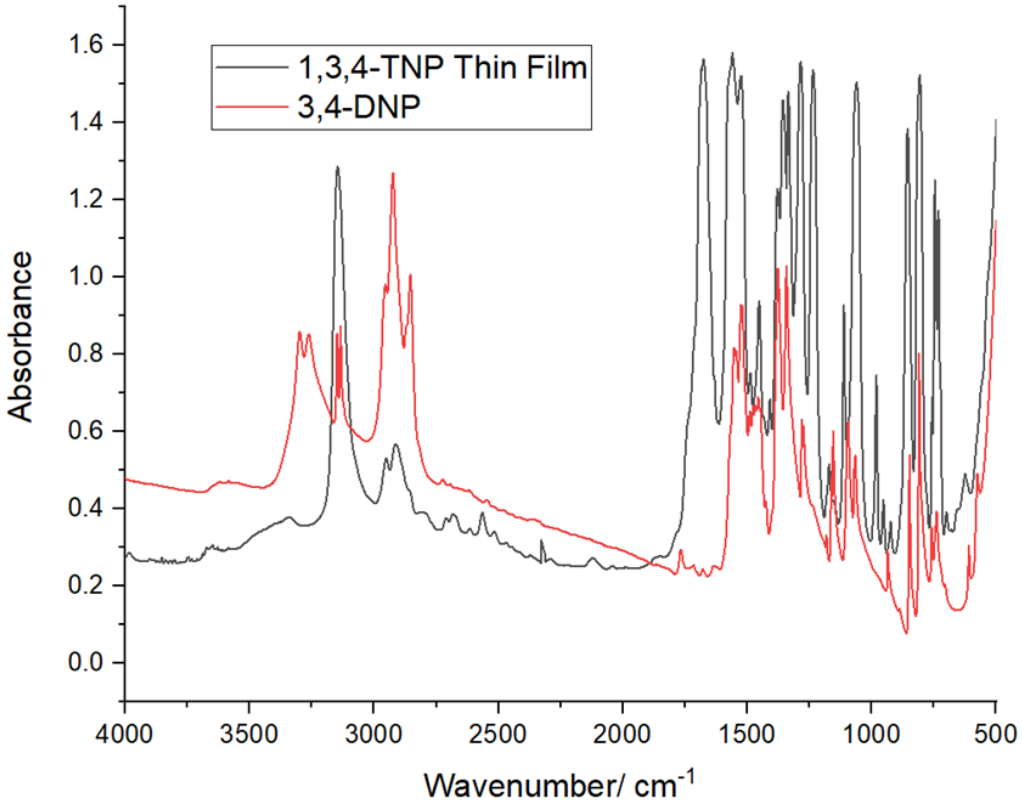

Figure 5.41: *Series of layered FTIR spectra (range 4000 to 500 cm^{-1}) showing the spectra of 1,3,4-trinitropyrazole (black) and a spectrum of 3,4-dinitropyrazole (red)*

5.2.13 Synthesis and FTIR spectroscopy of 3-azido-4,5-dinitropyrazole

1,3,4-TNP was used without further purification in the synthesis of 3-azido-4,5-dinitroimidazole (**Figure 5.40**). This resulted in the cine substitution of the N-bound nitro group. Product identity was confirmed solely by comparison of an FTIR spectrum of the product to that of the starting material and by comparison to known values for absorption bands published by Herve.[11]

5.2.13.1 Vibrational Spectroscopy

The FTIR spectrum of the product shows an intense absorption band at 2168 cm^{-1} (**Figure 5.42**). There is also a second slightly less intense band at 2144 cm^{-1}. The band at 2168 cm^{-1} is indicative of the $\nu_{as}(N_3)$ stretching vibration with the sharp band at 2143 cm^{-1} assigned as a product of the fermi resonance of the $\nu_{as}(N_3)$ stretching vibration with a combination band comprised of absorption bands appearing in the fingerprint region.

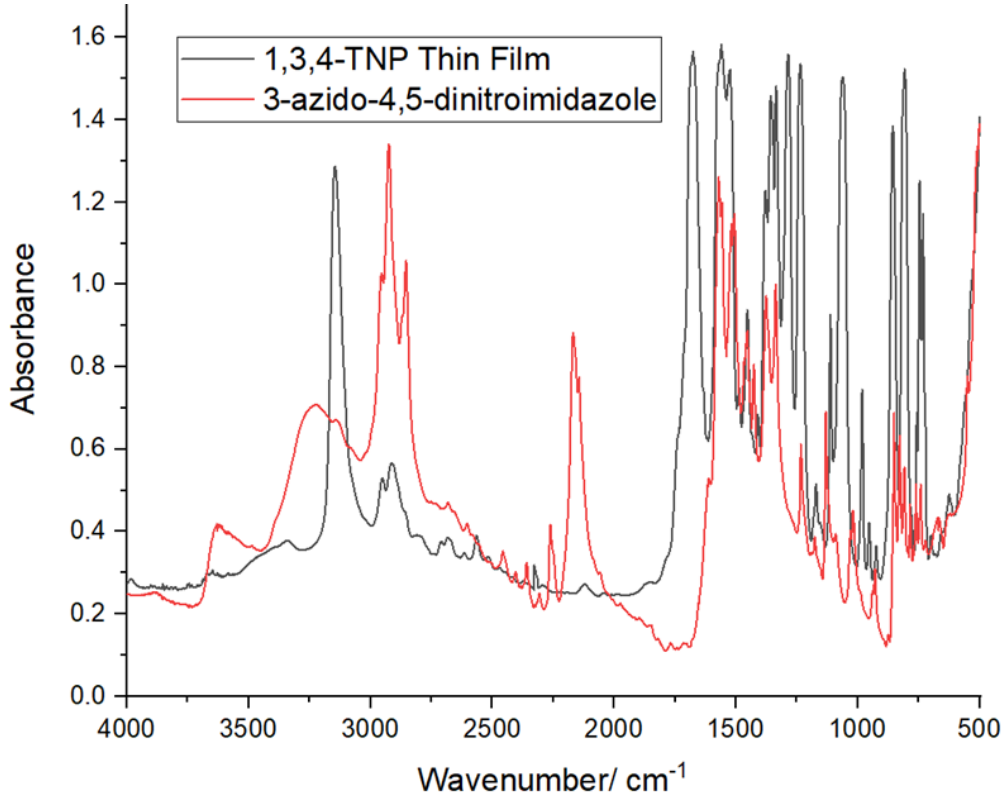

Figure 5.42: *Series of layered FTIR spectra (range 4000 to 500 cm^{-1}) showing the spectra of 1,3,4-trinitropyrazole (black) and a spectrum of 3-azido-4,5-dinitropyrazole (red)*

Bands assigned to the $v_{as}(NO_2)$ and $v_{sym}(NO_2)$ stretching vibrations of the N bound NO_2 group in 1,3,4-TNP are completely absent from the spectrum of the product. Absorption bands assigned to C-NO_2 groups in 1,3,4-TNP (855, 1335, 1379, 1525 and 1558 cm^{-1}) and are still present in the spectrum of the product (851, 1336, 1517, 1571 cm^{-1}) except for the absorption band at 1379 cm^{-1} which is indistinguishable from the absorption band of nujol used in sample preparation. The comparison of the FTIR spectra clearly points to the substitution of an N-NO_2 group in favour of a C-N_3. Comparison to the reported IR absorbances of 3-azido-4,5-dinitropyrazole also supports the formation of this compound with small band shifts accounted for by the difference in sample preparation (**Table 5.5**)

Absorption band assignment	**3-azido-4,5-dinitropyrazole(Published values[11])/ cm^{-1}**	**Product absorption bands/ cm^{-1}**
$v_{as}(N_3)$	2168	2168
Fermi resonance of $v_{as}(N_3)$ and combination band	2142	2143
$v_{as}(N_3)$	1572	1571
$v_{sym}(NO_2)$	1379	-
$v_{sym}(N_3)$	1232	1234
Not assigned	1130	1130
Not assigned	1019	1019
NO_2 symmetric bend	851	851
Not assigned	826	828
Not assigned	784	785
Not assigned	761	760
Not assigned	741	741
Not assigned	670	668
Not assigned	513	518

Table 5.5: *Comparison of published absorption bands for 3-azido-4,5-dinitropyrazole and the product obtained in Sheffield of the reaction of 1,3,4-TNP and NaN_3*

5.2.13.2 Attempted synthesis of sodium-5-azido-4,5-dinitropyrazolate

With evidence to suggest 5-azido-3,4-dinitropyrazolate had been isolated, formation of its sodium salt was attempted (**Figure 5.43**). To this end 5-azido-3,4-dinitropyrazole and a two-fold molar excess of Na_2CO_3 were added to ethanol and

refluxed for one hour to produce a bright orange coloured solution. Filtering and removal of the ethanoic solution in vacuo gave a dark orange solid. FTIR spectra of 5-azido-3,4-dinitropyrazole and the orange solid were compared to determine reaction outcome.

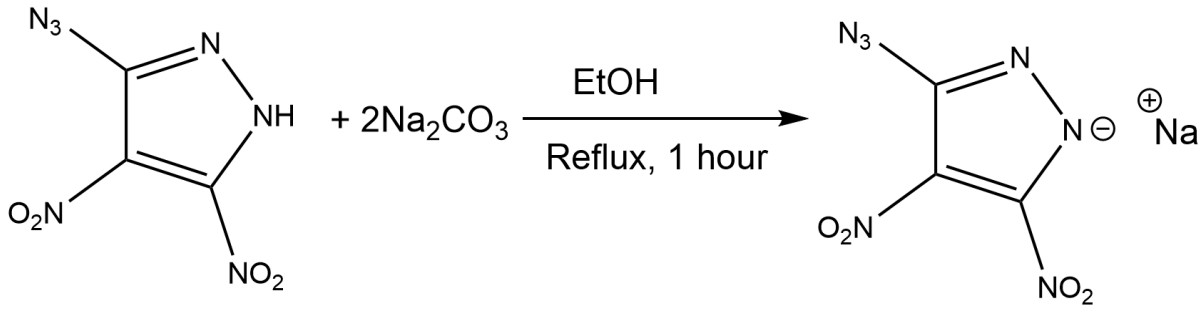

Figure 5.43: *Synthesis of Na-3-azido-4,5-dinitropyrazolate*

5.2.13.3 FTIR spectroscopy

The broad band associated with the N-H stretch of 3-azido-4,5-pyrazole can be seen to be absent from the product (assumed to be Na-3-A-4,5-DNP). This confirms that deprotonation has taken place (**Figure 5.44**). An intense $\nu_{as}(N_3)$ stretching vibration can be seen in the spectrum of Na-3-A-4,5-DNP at 2158 cm^{-1}. The Fermi resonance present in 3-azido-4,5-dinitropyrazole can still be seen in the spectrum of Na-3-A-4,5-DNP at 2135 cm^{-1}. Assuming the assignment of the product as Na-3-A-4,5-DNP is correct, the appearance of the $\nu_{as}(N_3)$ stretching vibration shows that for Na-3-A-4,5-DNP, the azide-tetrazole equilibrium is shifted towards the azide, unlike what is seen in the case of 3-azido-4-nitropyrazole. This is likely due to the nucleophilicity of 3-azido-4-nitropyrazolate versus 5-azido-3,4-dinitropyrazole. An additional nitro group attached to the ring reduces the nucleophilicity of the nitrogen formally carrying the negative charge to the extent that cyclisation cannot take place. In the case of 3-azido-4-nitropyrazolate, the C-H does not have the same electron withdrawing effect and so cyclisation can occur.

To identify both the composition and structure of Na-3-A-4,5-DNP, single crystals were grown from slow evaporation of aqueous solutions of 5-azido-3,4-dinitropyrazole and NaOH over the course of 21 days. This resulted in the growth of

yellow, rectangular needle crystals. These crystals proved to be of sufficient quality to undergo SCXRD studies which gave the structure of the compound

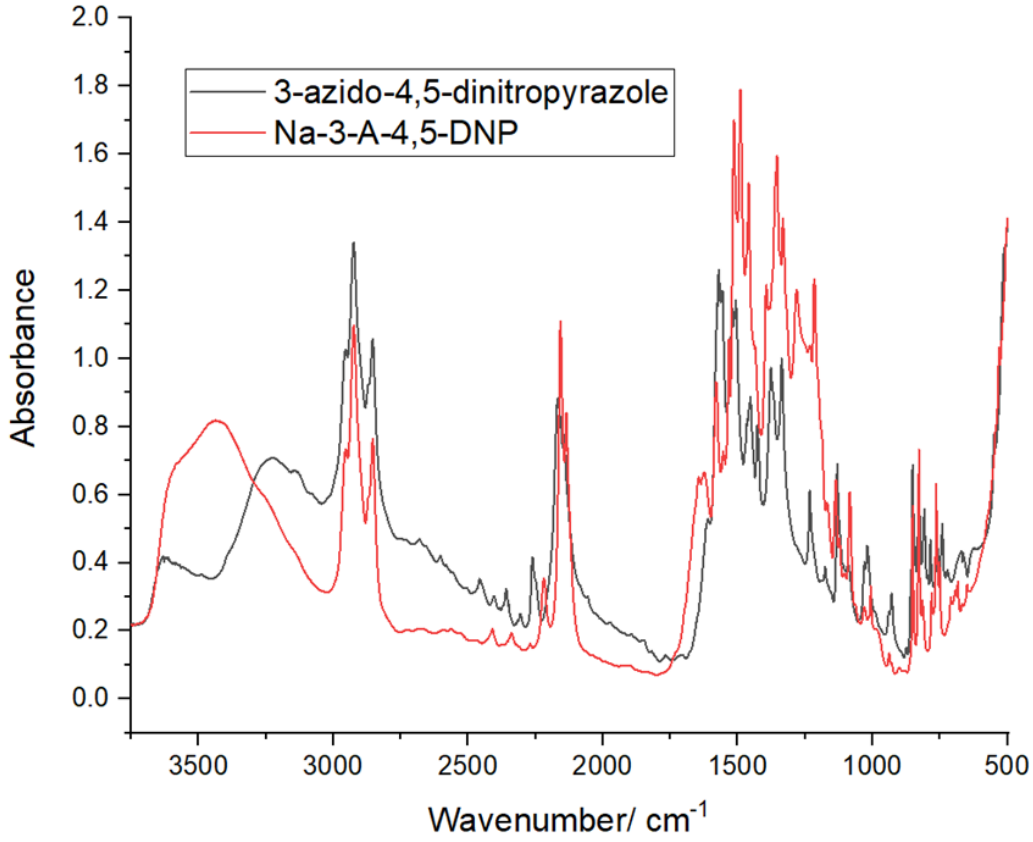

Figure 5.44: *Series of layered FTIR spectra (range 4000 to 500 cm^{-1}) showing the spectra of 3-azido-4,5-dinitropyrazolate (black) and sodium-3-azido-4,5-dinitropyrazolate (red)*

5.2.14 Crystal structure of disodium-3-oxido-4-nitropyrazolo[1,5 d]tetrazolate.5H_2O

Instead of obtaining Na-5-azido-3,4-dinitropyrazolate the structure solution confirmed the compound to instead be disodium-3-oxido-4-nitropyrazolo[1,5 d]tetrazolate.5H_2O (**Figure 5.45**). This is the first reported synthesis of this compound and represents the discovery of a potential new energetic ligand. Clearly, dissolution in alkali solutions over long periods of weeks results in substitution of one of the nitro groups. Substitution by OH^- occurs at the 3-nitro group rather than the 4-nitro group as seen in trinitropyrazole.[43]

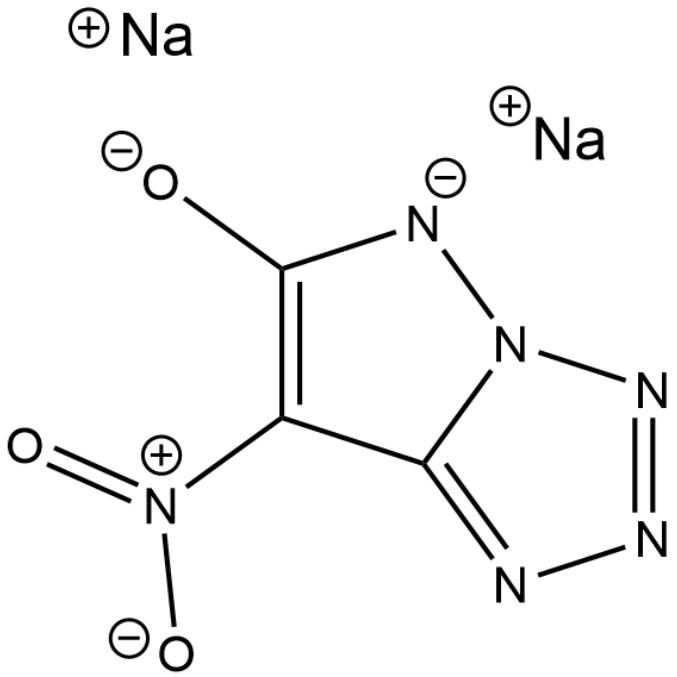

Figure 5.45: *Structure of disodium-3-oxido-4-nitropyrazolo[1,5 d]tetrazole*

The crystal structure of sodium-3-oxido-4-nitropyrazolo[1,5 d]tetrazolate is an interesting discovery when compared to Na-5-azido-3,4-dinitropyrazole. While only a tentative assignment, the FTIR of Na-5-azido-3,4-dinitropyrazole confirms the presence of an organic azide in a comparable position to that found for the free acid. The oxido group does not reduce the nucleophilicity of the nitrogen carrying the formal negative charge as much as a nitro group and so does not prevent cyclisation from occurring. Disodium-3-oxido-4-nitropyrazolo[1,5 d]tetrazolate.5H_2O forms as an infinitely extending coordination polymer in the $P2_1/c$ space group (**Figure 5.46**). Long chains are held together by bonds between sodium, 3-oxido-4-nitropyrazolo[1,5 d]tetrazolate and water with hydrogen bonding present between layers. There are two crystallographically independent sodium atoms in the structure. Na1 is bound in a distorted octahedron. Na1 forms bonds to three H_2O molecules and two units of 3-oxido-4-nitropyrazolo[1,5 d]tetrazolate. Two of the H_2O molecules bridge between Na1 and Na2 with the final H_2O molecule bound equatorially and trans to one of the bridging H_2O molecules.

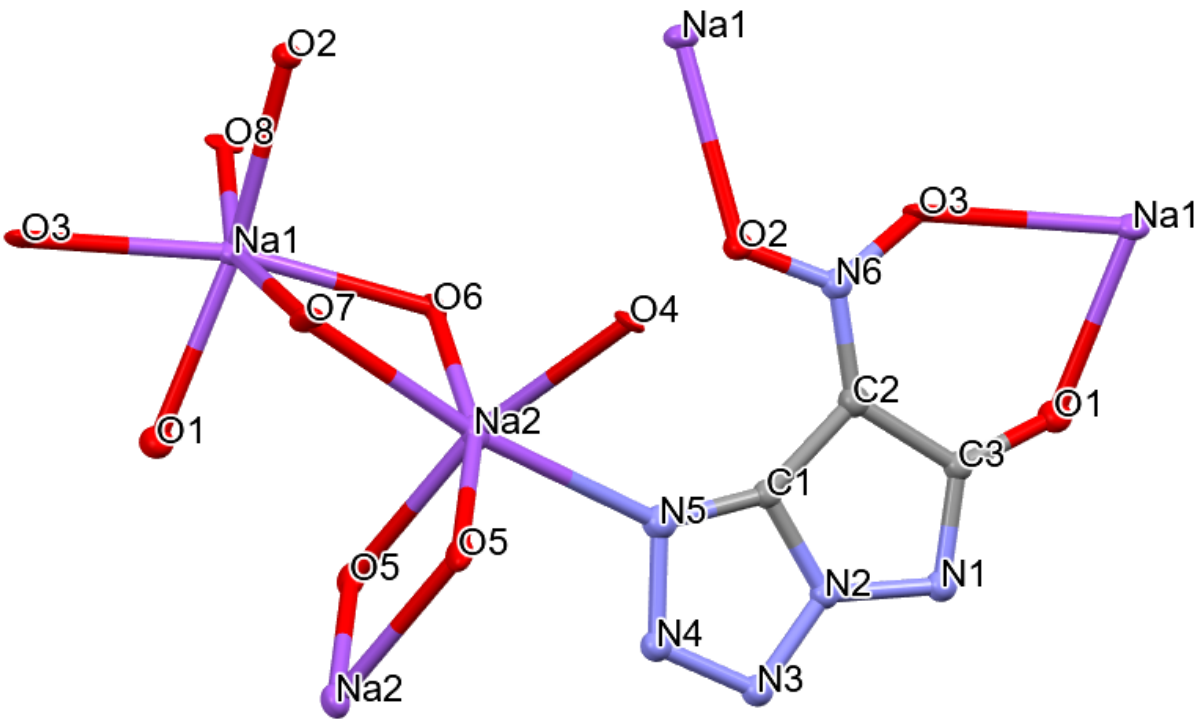

Figure 5.46 : *Projections of the thermal ellipsoid in the molecular structure of the crystals of disodium-3-oxido--4-nitropyrazolo[1,5 d]tetrazolate pentahydrate. Thermal ellipsoids set at the 67% probability level. Selected bond lengths Na1 O6 2.418(9) Na1 O7 2.379(9) Na1 O8 2.432(8) Na1 O1 2.325(8) Na1 O3 2.429(9) Na1 O2 2.436(8) Na2 O3 2.383(9) Na2 O6 2.333(9) Na2 O3 2.39(1) Na2 O7 2.457(9) Na2 N5 2.58(1) Na2 O3 2.358(8) O3 Na2 2.358(8) O1 C3 1.28(1) O1 Na1 2.325(8) O3 N6 1.26(1) O3 Na1 2.429(9) O2 N6 1.26(1) O2 Na1 2.436(8) N5 N4 1.39(1) N5 C1 1.33(1) N1 N2 1.41(1) N1 C3 1.35(1) C2 N6 1.34(1) C2 C3 1.46(2) C2 C1 1.45(2) N3 N4 1.33(1) N3 N2 1.33(1) N2 C1 1.34(1) Na2 O3 2.383(9), Atom Colours: Blue = Nitrogen, Grey = Carbon, Red = Oxygen, Purple = Sodium, hydrogen atoms removed for clarity*

The final three bonds making up the coordination sphere of Na1 are bonds to nitro group and oxido group oxygen atoms of two 3-oxido-4-nitropyrazolo[1,5 d]tetrazolato moieties. One unit of 3-oxido-4-nitropyrazolo[1,5 d]tetrazolate binds in a chelating manner through the oxygen atom, O1, of the oxido group and O3 of the nitro group. The other unit of 3-oxido-4-nitropyrazolo[1,5 d]tetrazolate binds through O2 to Na1 completing the distorted octahedron. Na2 also forms a distorted octahedron but forms its coordination sphere via five bonds to water and one to 3-oxido-4-nitropyrazolo[1,5

d]tetrazolate. Four of the water molecules are engaged in bridging between sodium centres with two involved in the bridge towards Na1 with another two H_2O molecules bridging between two Na2 centres. The final H_2O is bound equatorially and trans to one of the H_2Os bridging to Na2. Na2 only forms one bond to 3-oxido-4-nitropyrazolo[1,5 d]tetrazolate with N5 binding axially. No other ring nitrogen atom takes part in bonding to Na1/Na2. N1, N3 and N4 all engage in strong hydrogen bonding towards H_2O molecules with bond lengths between 1.944-2.196 Å. Much like in the case of K-4-nitropyrazolo[1,5 d]tetrazolate.H_2O the nitro group of Na_2-3-oxido-4-nitropyrazolo[1,5 d]tetrazolate sits almost perfectly in plane with only a minor twist by 0.77 degrees out of plane. This is in stark contrast to many known pyrazoles/pyrazolates with a nitro group bound in the 4-position and another substituent in the 3-position as this tends to produce a nitropyrazole/ate with a nitro group heavily twisted out of plane, as seen in the earlier discussed K-TNP. The tetrazole rings of both of K-4-nitropyrazolo[1,5 d]tetrazolate.H_2O and disodium-3-oxido-4-nitropyrazolo[1,5 d]tetrazolate.$5H_2O$ are very similar in regard to their bond lengths and angles. Small differences can be seen in the bond angles between K-4-nitropyrazolo[1,5 d]tetrazolate.H_2O and disodium-3-oxido-4-nitropyrazolo[1,5 d]tetrazolate.$5H_2O$ but the rings follow the same trends in bond angles. However, both compounds deviate significantly compared to potassium-tetrazolate. While N4-N5-C angles are generally consistent across all compounds, bond angles N3-N4-N5, N2-N3-N4, C-N2-N3 and N5-C-N2 all have much larger discrepancies with C-N2-N3 having a large bond angle change between pyrazolo-tetrazoles (110.6(5)°-111.59(9)°) and potassium tetrazolate (103.64°-104.85°). Changes in bond length can also be observed with potassium tetrazolate having the shortest C-N and N2-N3/N4-N5 lengths while disodium-3-oxido-4-nitropyrazolo[1,5 d]tetrazolate.$5H_2O$ has the longest N1-N2 bond length observed at 1.388. These bond lengths and angles highlight the distorted tetrazole present in pyrazolo-tetrazoles compared to the symmetrical tetrazolate found in potassium tetrazolate. disodium-3-oxido-4-nitropyrazolo[1,5 d]tetrazolate.$5H_2O$ is also found to have by far the shortest C-NO_2 bond of any of the compared nitropyrazoles at 1.339 Å. N-O lengths are similar to that found in K-NPT.H_2O however the average N-O length in disodium-3-oxido-4-nitropyrazolo[1,5 d]tetrazolate.$5H_2O$ can be seen to be longer (**Table 5.6**).

	K-4-nitropyrazolo[1,5 d]tetrazolate.H_2O	Disodium-3-oxido-4-nitropyrazolo[1,5 d]tetrazolate.5H_2O	Potassium-Tetrazolate[44]	K-TNP[41]
C-NO_2/ Å	1.381(8)	1.339(1)	-	1.432(2), 1.446(2), 1.452(2)
N-O/ Å	1.24(9)-1.257(9)	1.258(1)-1.264(1)	-	1.222(2)-1.233(2)
ONO-K/Na/ Å	2.745(5)-3.145(5)	2.429(9)-2.436(8)	-	2.782(2)-3.205(1)
N-K/Na/ Å	2.919(6)-3.121(6)	2.580(1)	2.88(5)-2.981(1)	2.785(2)-2.828(2)
N_4-N_5-C/ °	103.60(5)	104.29(9)	103.64-104.85	-
N_3-N_4-N_5/ °	113.64(5)	112.60(9)	109.27-109.89	-
N_2-N_3-N_4/ °	103.68(5)	103.50(8)	109.27-109.89	-
C-N_2-N_3/ °	110.60(5)	111.59(9)	103.64-104.85	-
N_5-C-N_2/°	108.45(6)	108.13(1)	112.4-114.15	-
C-N/ Å	1.34(8)-1.351(9)	1.328(1)-1.336(1)	1.308(1)-1.333(1)	-
N_2-N_3/N_4-N_5/ Å	1.356(8)-1.37(8)	1.334(1)-1.388(1)	1.331(8)-1.349(5)	-
N_3-N_4/ Å	1.313(8)	1.328(1)	1.300(5)-1.309(5)	-

Table 5.6: *Comparison of selected bond lengths and angles of nitro groups and tetrazole rings in K-NPT.H_2O, Na_2-3-O-4-NPT.5H_2O, potassium tetrazolate and potassium trinitropyrazolate*

These bond lengths heavily suggest the presence of the 'charged' NO_2 group in disodium-3-oxido-4-nitropyrazolo[1,5 d]tetrazolate.5H_2O. FTIR spectra could not be recorded during the timeframe of this research to corroborate this claim. Differences between Na-N/ K-N bond lengths and ONO-Na/K bond lengths in K-NPT.H_2O and disodium-3-oxido-4-nitropyrazolo[1,5 d]tetrazolate.5H_2O can be prescribed to the differing strengths of attraction of the respective to anions to Na/K with Na binding much more strongly than K. A similar effect can be seen in the crystal structures of potassium tetrazolate and sodium tetrazolate monohydrate.[44]

5.2.15 Thermal analysis, impact sensitiveness and detonation performance parameter calculations of novel salts

With potassium-2-azido-4-nitroimidazolate (K-2-A-4-NIm.H_2O), potassium-4-nitropyrazolo[1,5 d]tetrazolate.H_2O (K-NPT.H_2O) and disodium-3-oxido-4-nitropyrazolo[1,5 d]tetrazolate.5H_2O (Na_2-3-O-4-NPT.5H_2O) constituting a class of compound not previously investigated as energetic materials it is important to analyse sensitiveness, thermal behaviour and calculate P and D values for these materials and compare them to known alkali metal primary explosives to assess the potential of these compounds for application as LFI's (as either lead azide or lead styphnate replacements).

5.2.15.1 Thermal analysis

The thermal behaviour of all three compounds was investigated by differential scanning calorimetry. All compounds were sealed in closed stainless-steel high-pressure DSC capsules and heated at a heating rate of 3 K min^{-1}. Onset temperatures for exotherms were calculated by the intersection of the tangent of maximum gradient with the projected baseline. Peak temperatures were taken from the point of highest heat flow.

Potassium-4-nitropyrazolo[1,5 d]tetrazolate.H_2O has three thermal events in the temperature range scanned (**Figure 5.47**). A small endothermic peak in the region 110-140 °C could indicate loss of the H_2O molecule. It could also be an indication that a melting of the material is taking place though usually melts appear much sharper than this endothermic peak. The large exothermic peak can be assumed to be relating to the decomposition of K-4-nitropyrazolo[1,5 d]tetrazolate.H_2O. The compound has a peak temperature of decomposition at 204.9 °C with an onset temperature of 198.2 °C and possess a molar enthalpy of decomposition at 278.9 kJ /mol. There exists a second exothermic peak in the spectrum though this one is much less sharp than the first. This could be a decomposition of the decomposition product of K-4-nitropyrazolo[1,5 d]tetrazolate.H_2O. An onset temperature of 198.2 °C for the main exotherm is almost at the required 200 °C for potential lead free initiators and so as

far as decomposition temperature is concerned K-NPT.H_2O can be considered a potential LFI.

Disodium-3-oxido-4-nitropyrazolo[1,5 d]tetrazolate.$5H_2O$ was shown to have two thermal events in the temperature range scanned (**Figure 5.48**). A small, two stage endothermic peak in the region 75-100 °C could indicate either loss of water or that the sample is melting. The large exothermic peak was assumed to be the decomposition of Na_2-3-oxido-4-nitropyrazolo[1,5d]tetrazolate. The onset temperature of Na_2-3-oxido-4-nitropyrazolo[1,5 d]tetrazolate was 233.7 °C with a peak temperature of 240.4 °C. This is above that required of primary explosives and so does suggest that Na_2-3-oxido-4-nitropyrazolo[1,5 d]tetrazolate may be a viable sodium based alternative to lead explosives. The molar enthalpy of decomposition is 405.4 kJ/mol. This is above that for DBX-1 when recorded on the same instrument.

K-2-A-4-NIm was found to have 3 thermal events in the temperature range scanned (**Figure 5.49**). The large exothermic peak was assumed to be the decomposition of the 2-azido-4-nitroimidazolato moiety. This peak was found to have an onset temperature of 116.5 °C and a peak temperature of 134.2 °C with a molar enthalpy of decomposition of 128.1 kJ/mol.

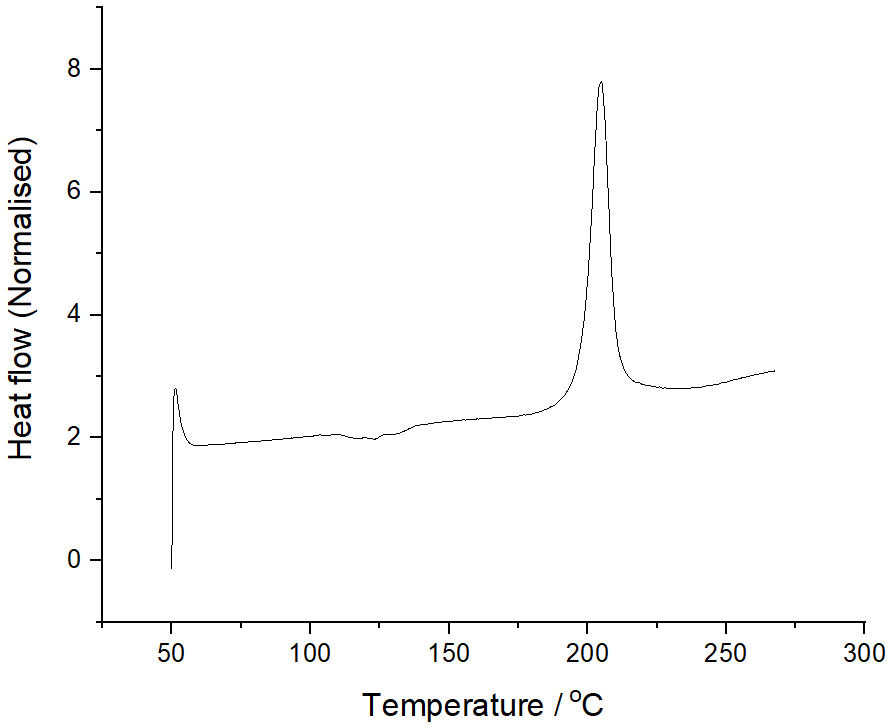

Figure 5.47: *DSC calorigram for K-NPT.H_2O (exothermic events show as an increase of heat flow).*

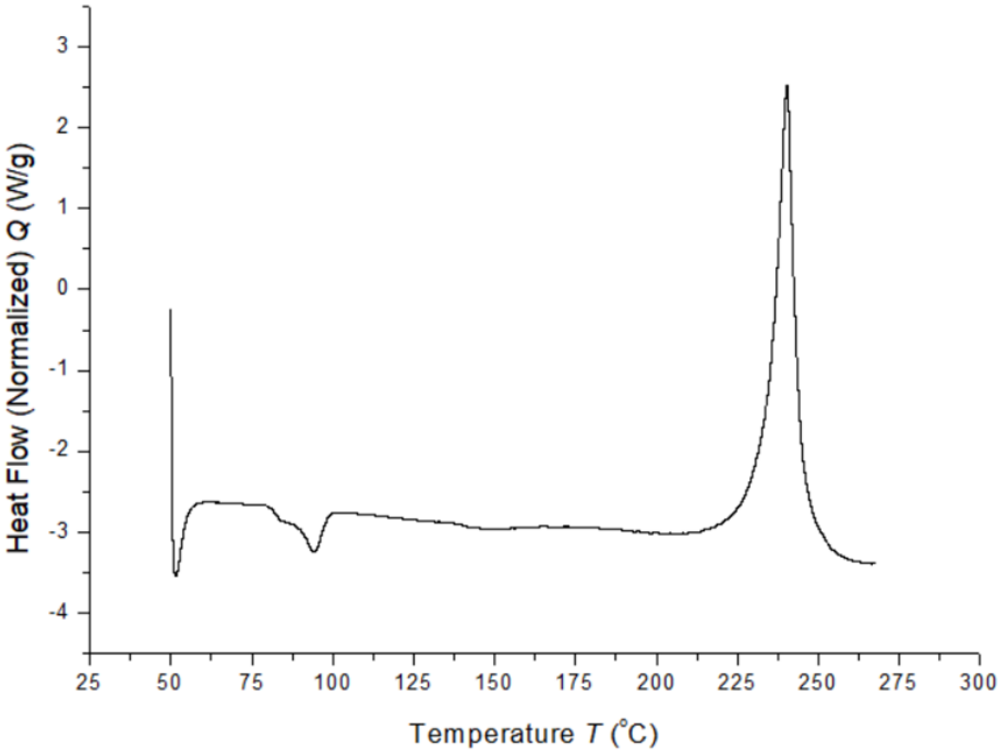

Figure 5.48: *DSC calorigram for Na_2-3-O-4-NPT.5H_2O (exothermic events show as an increase of heat flow).*

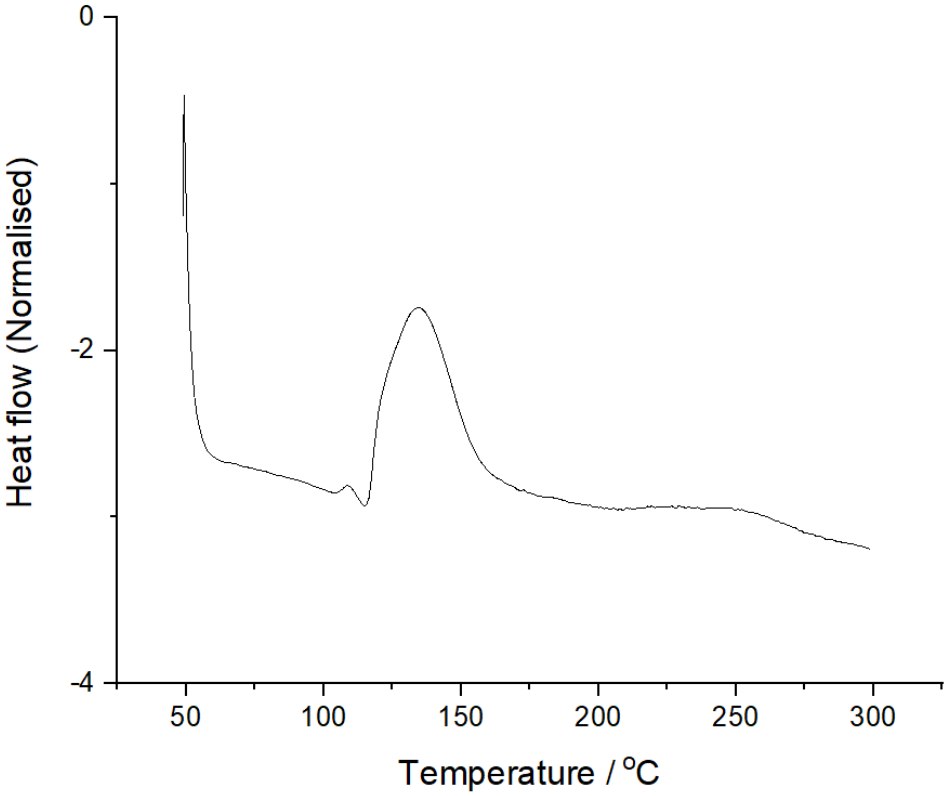

Figure 5.49: *DSC calorigram for K-2-A-4-NIm (exothermic events show as an increase of heat flow).*

5.2.15.2 DSC and Detonation performance parameter calculations

By making similar assumptions as has been shown for the novel Cu(I)-nitroazolates and transition metal-triazenido compounds the values for enthalpy of decomposition (ΔH_d) measured by DSC can be used to estimate heat of formation (ΔH_f) for the novel compounds. DSC can also be used to find thermal decomposition temperatures for each of the novel salts. As the crystal structure of each of these compounds is known, crystal density can be calculated from the unit cell volume. For these calculations crystal density is taken as the maximum loading density.

Compound	**T_{dec}/ °C**	**ΔH_f/ kJ mol^{-1}**	**D/ km s^{-1}**	**P/ kbar**
K-NPT.H_2O	198	-653.2	4.871	110.23
Na_2-ONPT.5H_2O	233.4	-706.2	4.944	107.46
K-2-A-4-NIm	116.5	-804.0	3.970	72.61
K_2DNABT[45]	200	326.40	8.33	317
KDNP[46]	285	-197.07	-	117
KDNBF[47]	217	-	-	-
$Pb(N_3)_2$[48]	313	-	5920	338

Table 5.7: *Comparison of T_{dec}, ΔH_f, D and P values for K-NPT.H_2O, Na_2-3-O-4NPT.5H_2O and K-2-A-4-NIm against known alkali metal primary explosives and lead azide*

K-NPT.H_2O and Na_2-3-O-4-NPT both have predicted detonation velocities and pressures lower than that for other known alkali metal LFI's (**Table 5.7**). However, the values for D and P are still within the expected ranges for primary explosives. K-NPT.H_2O has a decomposition temperature close to that of the proposed LFI K_2DNABT whilst Na_2-3-O-4-NPT has a decomposition temperature exceeding that of two of the known alkali metal LFI's. This, provided both K-NPT.H_2O and Na_2-3-O-4-NPT have sufficient sensitivity to stimuli to initiate secondary explosives, along with

the calculated Q and P values does make K-NPT.H_2O and Na_2-3-O-4-NPT interesting as potential LFI's. With values for D and P much lower than that found for K2DNABT (a proposed replacement for lead azide) it is likely K-NPT.H2O and NA2-3-O-4-NPT would instead serve as lead styphnate replacements and find use in igniters (ignition to burning) over detonators (ignition to detonation and shockwave generation). K-2-A-4-NIm suffers a very low thermal decomposition temperature when compared to lead azide and the alkali metal LFI's. This can be attributed to the azide-tetrazole equilibrium favouring azide formation in imidazolates, resulting in lower decomposition temperatures. This seemingly rules out a practical use for K-2-A-4-NIm.

5.2.15.3 Drop weight testing of K-NPT.H_2O

The impact sensitiveness of K-NPT.H_2O was recorded on the Sheffield Drop Weight Tester (**Figure 5.50**). A weight of mass 0.9kg with a shaped striker pin was dropped on samples of K-NPT.H_2O sealed in aluminium foil with masses ranging from 8-12(±1) mg. Drops were recorded as "go's" or "no-go's" determined by observed flashes, auditory events (crack, bangs etc) and noticeable changes to sample (formation of detonation residues usually as a black soot-like material, smoke give off etc). When "go's" are recorded of K-NPT.H_2O, an audible crack can be heard, smoke is given off, a black soot-like material is deposited on the striker pin and in the drop weight crater and a red flash can on occasion be observed. K-NPT.H_2O is recorded to have an IS of 4.3 J. K-NPT.H_2O is therefore as sensitive as many recorded primary explosives including DBX-1 (4 J, recorded on the Sheffield Drop Weight tester) but is found to be less sensitive than lead azide (1J).[49] The water that crystallises along with K-NPT can be assumed to have a phlegmatizing effect, reducing IS. If K-NPT can be desolvated under vacuum, it is predicted that the IS will increase resulting in an even more impact sensitive material. This result shows that even with the azide-tetrazole tautomer favouring tetrazole formation in nitropyrazolates, the high sensitiveness of the azido group is retained. The impact sensitiveness of Na_2-3-O-4-NPT.5H_2O was not recorded and so it is unclear if it also shares the high sensitiveness of K-NPT.H_2O, however until drop weight testing can be done it is sensible to assume a high IS for this compound for safety purposes.

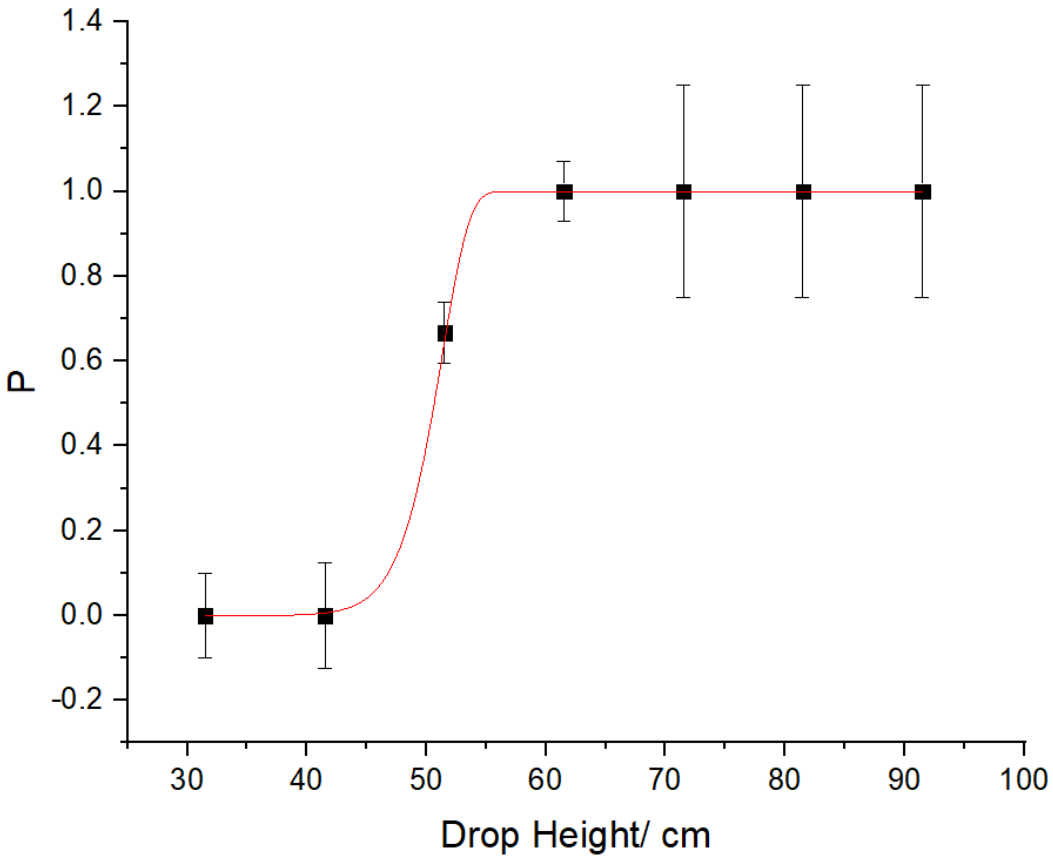

Figure 5.50: *Graph showing the probability of initiation of samples of K-NPT.H_2O at different drop heights. The E_{50} values were determined by curve-fitting using the Weibull function* $y = a - (a - b)\exp(-(k\,x)^d)$.

Overall, both K-NPT.H_2O and Na_2-3-O-4-NPT can be treated as prospective LFIs (Specifically lead styphnate replacements) with further investigation needed. K-2-A-4-NIm suffers from low thermal stability and so cannot be seen as a viable LFI. The formation of tetrazole rather than azide is seen as the cause of the higher thermal stability of K-NPT.H_2O and Na_2-3-O-4-NPT compared to K-2-A-4-NIm. For K-NPT.H_2O, formation of tetrazole does not result in a largely reduced IS; K-NPT.H_2O is a compound that matches the IS of well know LFI's such as DBX-1. While K-NPT.H_2O and Na_2-3-O-4-NPT have lower performance parameters than many known alkali metal LFI's they are still within the range of values expected of primary explosives and warrant further investigate into their practical use as such.

5.3 Conclusions

Following previous publications detailing the synthesis of 2-azido-4-nitroimidazole results in the isolation of a yellow oil which upon standing and allowing for evaporation of residual acetic acid results in the crystallisation of 2-azido-4-nitroimidazole. However, even with strict adherence to the published procedures yields of 2-azido-4-nitroimidazole were insufficient to allow for scale up and bulk synthesis. Altering the reactions conditions did result in a higher mass yield however this was due to formation of parabanic acid, a side product which forms due to oxidation of the imidazole ring. If the reaction is heated to 50 °C for 16 hours all 2-azido-4-nitroimidazole and 2-azidoimidazole starting material is consumed and only parabanic acid forms. Parabanic acid has 1 signal in the ^{1}H NMR at 11.76 ppm and two signals in the ^{13}C NMR at 160.26 and 155.18 ppm. This matches closely to the published ^{1}H and ^{13}C NMR spectra for 2-azido-4,5-dinitroimidazole, the synthesis of which was first detailed by the same authors as for 2-azido-4-nitroimidazole. Therefore, it is believed that 2-azido-4,5-dinitroimidazole has not in fact been synthesised by these authors and remains a non-synthesised potential energetic material. Potassium-2-azido-4-nitroimidazole can be synthesised from the reaction of 2-azido-4-nitroimidazole with K_2CO_3. Potassium 2-azido-4-nitroimidazolate crystallises from ethanol as its monohydrate. 3-azido-4-nitropyrazole can be synthesised via a new synthetic route in high yields through nitration of 3-azidopyrazole. Reaction with K_2CO_3 does not result in the formation of potassium-3-azido-4-nitropyrazolate but instead forms K-4-nitropyrazolo[1,5 d]tetrazolate. Recrystallisation from ethanol allowed for the determination of the crystal structure as K-4-nitropyrazolo[1,5 d]tetrazolate.H_2O. 3-azido-4,5-dinitropyrazole can be formed and reacted with Na_2CO_3 to form Na-3-azido-4,5-dinitropyrazolate. However, if allowed to stand in alkali aqueous solution for two weeks substitution of the nitro group in the five position by hydroxide occurs forming Na_2-3-oxido-4-nitropyrazolo[1,5 d]tetrazolate.$5H_2O$. The thermal behaviour and detonation performance parameters of K-2-azido-4-nitroimidazolate, K-4-nitropyrazolo[1,5 d]tetrazolate.H_2O and Na_2-3-oxido-4-nitropyrazolo[1,5 d]tetrazolate were investigated. K-4-nitropyrazolo[1,5 d]tetrazolate.H_2O and Na_2-3-oxido-4-nitropyrazolo[1,5 d]tetrazolate proved to be thermally stable enough to potentially have use as primary explosives. Potassium 2-azido-4-nitroimidazolate has a very low decomposition temperature and so will find no practical use as an energetic

compound. All salts proved to have detonation performance characteristics in the ranges expected of primary explosives but are lower than that found for other alkali metal lead free initiators. Impact sensitiveness was also measured for K-4-nitropyrazolo[1,5 d]tetrazolate.H_2O. K-4-nitropyrazolo[1,5 d]tetrazolate.H_2O was found sensitive towards impact with an IS similar to that of DBX-1. Dehydrating both K-NPT.H_2O and Na_2-3-oxido-4-nitropyrazolo[1,5 d]tetrazolate.$5H_2O$ could potentially result in compounds with extremely high impact sensitiveness.

5.4 Experimental

5.4.1 Synthesis of 2-azidoimidazole[4]

2-Aminoimidazole hemisulphate (6.60 g, 50.0 mmol) was dissolved in HCl (5.0 mol L^{-1}, 40 mL) and stirred at 0 °C under ice-water bath cooling. An aqueous solution (30 mL) of $NaNO_2$ (3.46 g, 50.2 mmol) was then added portion wise, maintaining the temperature at 0°C. This resulted in the formation of a clear yellow solution. An aqueous solution of NaN_3 (3.26 g, 50.2 mmol, 10 ml of H_2O) was then added dropwise, maintaining the temperature at 0 °C. This results in the formation of an orange solution. The mixture was stirred at 0 °C for 1 hours before stirring at room temperature for another 20 hours. Following the 20 hour stir, the solution had turned yellow. $NaHCO_3$ was added until pH 7 was reached (large amounts of foam form during this process), at which point the reaction mixture was extracted by ethyl acetate (3 × 100 mL) (foam dissolves into ethyl acetate). The combined organic layers were dried over anhydrous Na_2SO_4. After filtration and evaporation of ethyl acetate in vacuo, an orange solid was obtained. The crude solid was not purified before any further reactions. Yield: 4.43 g, 81.21 % yield. ^{1}HNMR (400 MHz, DMSO-d_6, δ): 6.89 (s, 1H), 12.03 (s, 1H); ^{13}CNMR (400 MHz, DMSO-d_6, δ): 139.49, 124.312, 105.28.)) IR (nujol) v / cm^{-1} = 3156, 3144, 3119, 3042, 2131, 1707, 1583, 1485, 1467, 1307, 1236, 1161, 1152, 1116, 1099, 991, 865, 834, 811, 780, 770, 740, 695

5.4.2 Synthesis of 2-azido-4-nitroimidazole (ANI) [22]

2-azidoimidazole (0.2 g, 1.83 mmol) was added to nitric acid (68%, 2 mL) at room temperature to form an orange solution. H_2SO_4 (98%, 3 ml) was added dropwise over the course of 4 h with temperature maintained at room temperature. By the end od addition the solution had turned yellow. The reaction mixture was poured into an ice–water mixture, then extracted with ethyl acetate (200 ml). The extracts were dried over anhydrous magnesium sulfate and evaporated to leave a yellow oil. Allowing the oil to slowly desolvate resulted in the growth of bright yellow crystals of 2-azido-4-nitroimidazole. Yield: 70mg, 24.8%; ^{1}H NMR (400 MHz, DMSO-d_6): δ 8.27 (s, 1H), 13.44 (s, 1H); ^{13}C NMR (400 MHz, DMSO-d_6): δ 119.21, 140.61, 145.02. IR (nujol) v / cm^{-1} = 3147, 2142, 1567, 1546, 1526, 1501, 1460, 1446, 1394, 1358,

1306, 1255, 1236, 1207, 1108, 1016, 1002, 865, 830, 820, 791, 754, 722, 704, 573, 526

5.4.3 Synthesis of potassium-2-azido-4-nitro-imidazolate monohydrate

2-azido-4-nitroimidazole (0.5 g, 3.24 mmol) and K_2CO_3 (0.897 g, 6.49 mmol) were added to ethanol (50 ml) and stirred for 6 hours. The suspension was then filtered and allowed to slowly evaporate for 3 days resulting in the growth of irregularly shaped orange crystals. The crystals were identified as potassium-2-azido-4-nitro-imidazolate monohydrate. Yield: 0.511 g, 75.03%; ^{1}H NMR (400 MHz, DMSO-d_6): δ 7.63(s, 1H); ^{13}C NMR (400 MHz, DMSO-d_6): δ 132.50, 141.28, 148.27. IR (nujol) v / cm^{-1} = 3421, 2422, 2151, 1661, 1486, 1468, 1404, 1394, 1376, 1292, 1225, 1218, 1194, 1129, 1066, 1008, 991, 845, 833, 825, 794, 769, 752, 724, 702. DSC, T_{on} = 134.2 °C (dec.), T_{peak} = 116.5 °C, ΔH = 609.2 J g^{-1} , 3 K min^{-1}

5.4.4 Synthesis of 3-azidopyrazole[4]

3-aminopyrazole (4.15 g, 50.0 mmol) was dissolved in HCl (5.0 mol L^{-1}, 40 mL) and stirred at 0 °C under ice-water bath cooling. An aqueous solution (30 mL) of $NaNO_2$ (3.46 g, 50.2 mmol) was then added portion wise, maintaining the temperature at 0°C. An aqueous solution of NaN_3 (3.26 g, 50.2 mmol, 10 ml of H_2O) was then added dropwise, maintaining the temperature at 0°C. The mixture was stirred at 0°C for 1 hours before stirring at room temperature for another 20 h. $NaHCO_3$ was added until pH 7 was reached, at which point the reaction mixture was extracted by ethyl acetate (3 × 100 mL). The combined organic layers were dried over anhydrous Na_2SO_4. After filtration and evaporation of ethyl acetate in vacuo, an orange solid. The crude solid was not purified before any further reactions. Yield: 3.3 g , 60.5%. ^{1}HNMR (400 MHz, DMSO-d_6, δ): 6.00 (s, 1H), 7.73(s, 1H), 12.71(s, 1H); ^{13}CNMR (400 MHz, DMSO-d_6, δ): 95.28, 131.16, 146.62. IR (nujol) v / cm^{-1} = 3173, 3129, 3060, 2182, 2120, 2078, 1542, 1484, 1467, 1380, 1365, 1311, 1225, 1185, 1092, 1048, 993, 920, 870, 800, 769, 753, 746, 601, 531

5.4.5 Synthesis of 3-azido-4-nitropyrazole monohydrate

3-Azidopyrazole (0.8 g, $7.33x10^{-3}$ mol) is dissolved in HNO_3(68%, 8 ml) at room temperature to form a dark brown solution. H_2SO_4 (98%, 12 ml) is added portionwise keeping temperature between 20-30 °C to form an orange solution. Solution is stirred at room temperature for 8 hours. The still orange solution is quenched in 250g of ice water and extracted with ethyl acetate (3 X 100 ml). The extract is dried over $MgSO_4$ before filtering and removal of ethyl acetate in vacuo to leave a brown oil with an odour of acetic acid. The acetic acid was removed in vacuo over 3 hours until the oil began to crystallise. Oil was removed from the vacuum and allowed to slowly evaporate for 24 hours which resulted in the growth of pale-yellow rectangular crystals and a microcrystalline yellow powder. The product was identified as 3-azido-4-nitropyrazole monohydrate. Yield 1.04 g, 82.4% ^{1}HNMR (400 MHz, DMSO-d_6, δ): 3.64 (s, 2H), 8.84 (s, 1H), 13.90(s, 1H); ^{13}CNMR (400 MHz, DMSO-d_6, δ): 124.63, 132.22, 142.43. IR (nujol) v / cm^{-1} = 3603, 3419, 3300, 3130, 2121, 1621, 1555, 1540, 1522, 1499, 1467, 1407, 1387, 1378, 1312, 1283, 1235, 1220, 1174, 1156, 1100, 1055, 996, 931, 927, 848, 835, 781, 756, 709, 680, 629, 529

5.4.6 Synthesis of potassium-4-nitropyrazolo[1,5 d]tetrazolate.H_2O

3-azido-4-nitropyrazole monohydrate (2.492 g, 0.0145 mol) and K2CO3 (4 g, 0.029 mol) were added to acetone (150 ml) and stirred for 6 hours. The suspension was then filtered and allowed to slowly evaporate for 3 days resulting in the growth of irregularly shaped orange crystals. The crystals were identified as potassium-4-nitropyrazolo[1,5 d]tetrazolate.H_2O. Yield 2.392 g, 78.48% ^{1}HNMR (400 MHz, DMSO-d_6, δ): 3.37 (s, 2H), 8.34 (s, 1H); ^{13}CNMR (400 MHz, DMSO-d_6, δ): 142.54, 145.18. IR (nujol) v / cm^{-1} = 3451, 3106, 1696, 1674, 1628, 1576, 15621463, 1422, 1309, 1225, 1177, 1158, 1116, 1009, 982, 903, 847, 833, 789, 760, 736, 653. DSC, T_{on} = 198.2 °C (dec.), T_{peak} = 204.9 °C, ΔH = 278.87 kJ mol^{-1}, 3 K min^{-1}

5.4.7 Synthesis of 1,3,4-trinitropyrazole[11]

3,4-dinitropyrazole (410 mg, 2.6 mmol) is added in small portions into a cold mixture of trifluoroacetic anhydride (10.5 mL) and fuming nitric acid (2.825 g, 1.85 mL) at 0 °C. The temperature is allowed to rise to 15 °C over 3 hours. The reaction mixture is

poured onto 50 g of ice and then the product is extracted with dichloromethane (2x 100 ml). The organic phases are combined, dried over magnesium sulphate, filtered and concentrated under vacuum. The crude product is isolated as a pale-yellow oil (336 mg, 32% yield) and was used without further purification. IR (nujol) v / cm^{-1} = 3146, 2952, 2904, 1678, 1562, 1520, 1452, 1379, 1357, 1335, 1285, 1236, 1171, 1112, 1063, 981, 953, 923, 855, 807, 758 743, 731, 700.

5.4.8 Synthesis of 3-azido-4,5-dinitroprazole[11]

A solution of 1,3,4-trinitropyrazole (336 mg, 1.65 mmol) in 40 mL of acetonitrile is poured slowly into a stirred suspension of sodium azide (0.534 g , 8.22 mmol) suspended in acetonitrile (6.5 mL) at 0°C. After 1 hour, the solvent is removed in vacuo before dissolution of the solids in the minimum amount of water. The solution is then acidified to pH 1 at 0 °C with 37% hydrochloric acid solution. The mixture is extracted with 60 mL of diethyl ether 3 times. The organic phases are combined, washed with brine, dried over magnesium sulphate, filtered and concentrated under vacuum to leave an orange oil. 2 ml of DCM was added to aid crystallisation. Upon addition and stirring at room temperature a yellow-orange solid crystallises. 5-Azido-3,4-dinitropyrazole is collected by filtration and dried in vacuo to yield a yellow-orange crystalline solid (244 mg, 74.9% yield). IR (nujol) v / cm^{-1} = 3648, 3234, 2251, 2166, 2143, 1566, 1514, 1455, 1427, 1338, 1233, 1179, 1131, 1092, 1021, 927, 855, 826, 806, 785, 763, 745, 673, 630, 548

5.4.9 Synthesis of Sodium-3-azido-4,5-dinitropyrazolate.XH_2O

3-azido-4,5-dinitropyrazole (0.200 g, 1.006 mmol) and K_2CO_3 (0.139 g, 2.012 mol) were added to acetone (15 ml) and stirred for 6 hours. The suspension was then filtered and allowed to slowly evaporate for 3 days resulting in the growth of irregularly shaped orange crystals. The crystals were identified as sodium-3-azido-4,5-dinitropyrazolate.XH_2O. Mass yield: 198 mg. IR (nujol) v / cm^{-1} = 3441, 2212, 2160, 2132, 1620, 1583, 1534, 1512, 1488, 1457, 1393, 1353, 1334, 1285, 1218, 1138, 1085, 1007, 851, 826, 761.

5.4.10 Synthesis of disodium-3-oxido-4-nitropyrazolo[1,5 d]tetrazolate.5H_2O

3-azido-4,5-dinitroprazole (0.100 g, 0.503 mmol) was dissolved in 10 ml H_2O. NaOH(0.2 g 0.503 mmol) was added and the solution left to slowly evaporate over 21

days. After 21 days orange needle crystals had formed. Crystals were stable when stored in the mother liquor but deteriorated if left to fully desolvate. Single crystal data are given in the SI. Yield: 40 mg, 22.5%. DSC, T_{on} = 233.7 °C (dec.), T_{peak} = 240.4 °C, ΔH = 405.4 kJ mol^{-1}, 3 K min^{-1}

5.5 References

1. M. S. Elioff, J. Hoy, J. A. Bumpus, Journal of Chemistry, 2016, 1-11
2. S. Brase, K. Banert, Organic Azides: Synthesis and Applications, Wiley, 2009
3. S. Brase, C. Gil, K. Knepper, V. Zimmermann, Angew.Chem.Int.Ed., 2005,44, 5188 – 5240
4. X. Chen, Q. Jin, L. Wu, C.H. Tung, X. Tang, Angew. Chem. Int. Ed., 2014, 53, 46, 12542-12547
5. I. L. Dalinger, T. I. Cherkasova, S. A. Shevelev, Mendeleev Commun., 1997, 7, 2, 58-59
6. T. M. Klapötke, J. Stierstorfer, A. Hammerl, R. D. Chapman, Z. Anorg. Allg. Chem., 2008, 634, 1051-1057
7. T. M. Klapötke, J. Stierstorfer, J. Am. Chem. Soc.,2009, 131, 3, 1122-1134
8. S. Angerer, Science of Synthesis, 2004, 16, 528
9. I. L. Dalinger, T. I. Cherkasova, G. P. Popova, T. K. Shkineva, I. A. Vatsadze, S.A. Shevelev, and M. I. Kanishchev, Russ. Chem. Bull. Int. Ed., 2009, 58, 2, 410-413
10. J. W. Suwiński, Arkivoc, 2017, part i, 402-435
11. G. Hervé, C. Roussel, H. Graindorge, Angew. Chem. Int. Ed., 2010, 49, 3177 –3181
12. J. E. Gurst, The Azido Group: Characterisation and determination of organic azides, Wiley, 1971, 3, 191-202
13. U. Muller, H. Barnighausen, Acta Crystallogr. Sect. B Struct. Crystallogr. Cryst. Chem., 1970, 26, 1671-1679
14. U. Muller, W. Kolitsch, Spectrochim. Acta, 1975, 31, 1455-1461
15. E. Lieber, C. N. R. Rao, A. E. Thomas, E. Oftedahl, R. Minnis, C. V. N. Nambury, Spectrochimica Acta., 1963, 19, 1135-1144
16. W. Friederich, K. Flick, US-Pat. 2179783
17. H. Xue, Y. Gao, B. Twamley, J. M. Shreeve, Chem. Mater. 2005, 17, 191-198
18. N. Fischer, T. M. Klapötke, J. Stierstorfer, E. N. Wiedemann, New Trends in Research of Energetic Materials, Proceedings of the Seminar, 14th, Pardubice, Czech Republic, Apr. 13-15, 2011

19. N. V. Latypov, V. A. Silevich, P. A. Ivanov, M. S, Pevzner, Khim. Getero. Soed., 1976, 12, 1649-53
20. I. L. Dalinger, I. A. Vatsadse, T. K. Shkineva, G. P. Popova, B. I. Ugrak, S. A. Shevelev, Russ. Chem. Bull. Int. Ed., 2010, 59, 8, 1631-1638
21. K. Hou, C. Ma, Z. Liu, Chin. Chem. Lett., 2014, 25, 438-440
22. K. Hou, C. Ma, Z. Liu, Chin. J. Chem. 2013, 31, 1539—1545
23. P. Yin, Q. Zhang, J. Zhang, D. A. Parrish, J. M. Shreeve, J. Mater. Chem. A . Mater. Energy. Sustain., 2013, 1, 25, 7500-7510
24. V. S. Mokrushin, I. S. Selezneva, T. A. Pospelova, V. K. Usova, S. M. Malinskaya, G. M. Anoshina, T. E. Zubova, Z. V. Pushkareva, Khim. Farma. Zhurn., 1982, 16, 3, 303-307
25. M. S. Pevzner, M. N. Martynova, Y. N. Timofeeva, Khim. Getero. Soed., 1974, 9, 1288-91
26. D. Izsak, T. M. Klapötke, J. Stierstorfer, R. Scharf, Z. Anorg. Allg. Chem., 2013, 639, 10, 1746-1755
27. D. Izsak, T. M. Klapötke, Crystals, 2012, 2, 294-305
28. D. R. Davies, J. J. Blum, Nature, 1954, 173,993
29. M. Matsui, K. Kamiya, K. Shibata, H. Muramatsu, H. Nakazumi, J. Org. Chem., 1990, 55, 4, 1396-9
30. K. Hou, Z. Liu, H. Zhang, J. Cheng, Chin. J. Energ. Mat., 2012, 20, 3, 289-291
31. D. Ginsburg, Concerning Amines, Pergamon, 1967, 17-62
32. S. Ek, N. V. Latypov, J. Heterocyclic Chem., 51, 1621 (2014)
33. C. He, L. A. Mitchell, D. A. Parrish, J. M. Shreeve, Chem. Comm., 2016, 52, 52, 8123-8126
34. G. Desiraju, T. Steiner, The Weak Hydrogen bond: In Structural Chemistry and Biology, 2001, Oxford University Press.
35. G. Zhang, Y. Wang, M. Cai, D. Din, K. Yan, A. Ma, P. Chen, R. Wang, P. Li, J. Yi, J.Coord. Chem., 2010, 63, 9, 1480-1491
36. A. Kowalski, Z. Krist., 1993, 208, 244-245
37. B. Westwater, 2021
38. H. Dorn, H. Dilcher, Liebigs Ann. Chem., 1967, 707, 141-146
39. E. B. Nikolaenkova, N. V. Aleksandrova, V. I. Mamatyuk, V. P. Krivopalov, Russ. Che. Bull., 2018, 67, 893-901

40. E. Alcalde, R. M. Claramunt, J. Elguero, Anales de Quimica, Serie C: Quimica Organica y Bioquimica, 1983, 79, 2, 248-50
41. B. Westwater, 2022
42. M. F. Bolter, A. Harter, T. M. Klapötke, J. Stierstorfer, ChemPlusChem, 2018,83,804– 811
43. I. L. Dalinger, R. A. Vatsadze, T. K. Shkineva, G. P. Popova, S. A. Shevelev, U. V. Nelyubina, J. Het. Chem, 2013, 50, 4, 911-924
44. T. M. Klapötke, M. Stein, J. Stierstorfer, Z. Anorg. Allg. Chem., 2008, 1711-1723
45. D. Fischer, T. M. Klapötke, J. Stierstorfer, Angew. Int. Ed., 2014, 53, 31, 8172-8175
46. J. W. Fronabarger, M. D. Williams, W. B. Sanborn, D. A. Parrish, M. Bichay, Propellants Explos. Pyrotech.2011,36, 459 – 470
47. Q. Nisa-Tariq, S. Manzoor, M. Nisa-Tariq, W. Cao, J. Zhang, Defence Technology, 2021
48. D. J. Whelan, R. J. Spear, R. W. Read, Thermochim. Acta., 1984, 80, 149-163
49. T. M. Klapötke, C. M. Sabate, J. M. Welch, Dalton Trans., 2008, 6372-6380

6. Conclusion

Investigations into the use of nitroazoles, azidonitroazoles and azolyltriazenes as lead free initiators have been conducted. As reported problems in the synthesis of DBX-1 were preventing its adoption as the go to lead free initiator, we conducted a thorough investigation into the synthetic conditions needed for consistent DBX-1 production. It was found that the use of $NaNT.2H_2O$, purified only through Soxhlet extraction, in the Cu(II)/Cu(I) reduction reaction does not result in the formation of DBX-1. Using NaNT.4H2O was required for any successful synthesis of DBX-1. A secondary product, DBX-X, a wine-red chlorine-containing copper nitrotetrazolate, $Cu_3Cl(N_4C\text{-}NO_2)_2$, was discovered. Crystalline DBX-X forms as an infinitely extending coordination polymer with a density higher than that reported for DBX-1. Control over the reaction products could be attained but required careful control over the presence of seed crystals. Seeding the reaction vessel with DBX-1 crystals allowed for consistent formation of pure DBX-1 in high yield. DBX-X can be selectively made but the thermodynamic favouring of DBX-1 formation makes consistent large scale synthesis problematic DBX-X proves be highly friction and impact sensitive, much more so than either DBX-1 ($Cu(N_4C\text{-}NO_2)$) or lead azide and decomposes violently upon rapid heating or shock. $Cu_3Cl\ (N_4C\text{-}NO_2)_2$ is a powerful explosive but has lower energetic parameters than DBX-1. Both DBX-1 and DBX-X prove to be stable in air indefinitely, however, $Cu_3Cl(N_4C\text{-}NO_2)_2$ decomposes under water within weeks. Due to this its lower decomposition temperature, and its lower detonation performance parameters $Cu_3Cl(N_4C\text{-}NO_2)_2$ is ruled out as an alternative to DBX-1.

With the difficulties in DBX-1 synthesis fully explored, novel Cu(I)-nitroazolates were synthesised with the intention of forming viable DBX-1/ $Pb(N_3)_2$ alternatives. Six new Cu(I)-nitroazolates were formed through the use of the same reaction scheme that produced DBX-1. $Cu_4(DNT)_3Cl$ was formed through the addition of $NaDNT.2H_2O$ to aqueous $CuCl_2$ solutions followed by addition of sodium ascorbate. The crystal structure of $Cu_4(DNT)_3Cl$ was determined and compared to DBX-X as the only other know Cu-chlorido-nitroazolato coordination polymer. Cu_2-TNBI was synthesised and although the crystal structure could not be determined, product purity and identity were proven through EA and Cu content analysis. Likewise, Cu-2,4-DNI and Cu-4,5-DNI were also synthesised and product identity was proven through FTIR and EA. Cu-3,5-

DNP and Cu-ADNP were synthesised and each had their crystal structure recorded with Cu-3,5-DNP forming as a coordination polymer whereas Cu-ADNP formed as trimeric Cu_3ADNP_3 units. All compounds proved highly temperature stable with the most thermally unstable, $Cu_4(DNT)_3Cl$, still being 67 °C above the threshold for lead free initiators (~200 °C). The detonation parameters for all compounds were calculated with some (Cu_2-TNBI, $Cu_4(DNT)_3Cl$ and Cu-ADNP) proving to have high predicted Q, D and P values. The impact sensitiveness of Cu_2-TNBI, $Cu_4(DNT)_3Cl$ and Cu-ADNP was also tested with all compounds being much more sensitive to impact than DBX-1. Cu_2-TNBI and Cu-ADNP can both be considered viable alternatives to DBX-1 with $Cu_4(DNT)_3Cl$ suspected to suffer similar water instability issues as seen for DBX-X. Cu-3,5-DNP, Cu-2,4-DNI and Cu-4,5-DNI are highly interesting compounds and may, provided they are proven to possess the sensitiveness's required of primary explosives, come to be regarded as other DBX-1 alternatives.

As triazenes represent a class of nitrogen rich ligand with a short history of use as energetic materials, we researched the use of bis(1-methyl-tetrazol-5-yl)triazene as an explosophoric ligand. Six new metal-triazenido compounds were synthesised and their properties recorded. $Fe(B1MTT)_2.H_2O$ and $Co(B1MTT)_2.H_2O$ form as water insoluble, pure microcrystalline powders, $Ni(B1MTT)_2.H_2O$ forms as an impure, water insoluble powder. $Zn(B1MTT)_2$ and $Pb(B1MTT)_2$ form as water free powders though $Zn(B1MTT)_2$ forms with a substantial impurity present. The crystal structures of $Fe(B1MTT)_2$, $Ni(B1MTT)_2$ and $Co(B1MTT)_2$ can be formed as their acetone solvates. All compounds prove to be highly thermally stable compounds, with onset temperatures of decomposition far above that expected of prospective LFI's. All compounds have detonation performance parameters in the range expected of primary explosives. $Cu(B1MTT)(Cl)(H_2O)$ can be formed by the addition of $Na(B1MTT).5H_2O$ to aqueous solutions of $CuCl_2$. The crystal structure of $Cu(B1MTT)(Cl)(H_2O)$ was recorded and found to have a similar structure to other copper(II)-triazenido-chlorido compounds. Substitution of the chloride for other explosophores can occur provided there is a large enough driving force. The novel nitroazolyl-triazene, bis(1-methyl-3-nitro-1,2,4-triazol-5-yl)triazene was formed as its PPN salt. The crystal structure of the PPN salt was recorded. Estimated detonation performance parameters of bis(1-methyl-3-nitro-1,2,4-triazol-5-yl)triazene were

calculated and compared to values known for other triazenes. B1M3NTT is calculated to have properties close to or exceeding those found for B2MTT.

The azidonitroazoles were investigated as explosophoric ligands. 2-Azido-4-nitroimidazole can be synthesised but yields never match those of the published literature. It was found that parabanic acid is produced by the oxidation of 2-azidoimdazole/2-azido-4-nitroimidazole by the acidic reaction solution. Parabanic acid is determined to be the product formed by reported syntheses of 2-azido-4,5-dinitroimidazole. Potassium-2-azido-4-nitroimidazole was synthesised and had its crystal structure determined. A new, high yielding route to 3-azido-nitroimidazole was found and the crystal structure of 3-azido-4-nitroimidazole monohydrate determined. Deprotonation of 3-azido-4-nitroimidazole leads to the formation of potassium-4-nitropyrazolo[1,5 d] tetrazole which can be crystallised to as its monohydrate, the crystal structure of which was recorded. The synthesis and crystal structure of the related Na_2-3-oxido-4-nitropyrazolo[1,5 d]tetrazolate.$5H_2O$ was also discovered. The three novel alkali metals salts were investigated as energetic materials. Potassium-4-nitropyrazolo[1,5 d] tetrazole monohydrate and Na_2-3-oxido-4-nitropyrazolo[1,5 d]tetrazolate.$5H_2O$ were found to be worse performing than other alkali metal LFI's but still within the ranges for Q, D and P expected of primary explosives. The impact sensitiveness of potassium-4-nitropyrazolo[1,5 d] tetrazole monohydrate was recorded and was found to be almost as impact sensitive as DBX-1. Potassium-4-nitropyrazolo[1,5 d] tetrazole monohydrate and Na_2-3-oxido-4-nitropyrazolo[1,5 d]tetrazolate.$5H_2O$ can be regarded as energetic materials warranting further investigation. Potassium-2-azido-4-nitroimidazole should find no practical use on account of its low thermal stability.

6.1 Outlook

The synthesis of DBX-1 has been clearly shown to be a complex process with multiple possible reaction products depending on various factors. While DBX-X, a compound with a far higher sensitiveness to impact than DBX-1, should not be viewed as a viable alternative to DBX-1/$Pb(N_3)_2$, its discovery must be considered in any future synthesis of DBX-1. If DBX-1 is to be synthesised in the quantities needed to fully replace $Pb(N_3)_2$ (requiring large-scale industrial set-ups), a lack of appreciation for the

potential production of the much more sensitive DBX-X could lead to catastrophic incidents. It is crucial that a further investigation into the conditions that control the synthesis of both DBX-1 and DBX-X is performed before large scale synthesis should be attempted.

All 6 novel Cu(I)-nitroazolates detailed in Chapter 3 require further investigation before they can truly be considered as DBX-1/lead azide replacements. Cu_2-TNBI is arguably the most promising, with predicted Q, D and P values all higher than those recorded for DBX-1. Elucidation of the crystal structure of Cu_2-TNBI is crucial to obtain more accurate values for Q, D and P. Provided this can be recorded, Cu2-TNBI should be tested as a part of initiatory compositions used for detonators. Likewise, all other Cu(I)-nitroazolates detailed in Chapter 3 require full characterisation prior to their tests in initiatory compositions.

The work of Chapter 3 is by no means exhaustive and should instead be treated as a preliminary investigation into Cu(I)-nitroazolato complexes. Cu(I) complexes of trinitroimidazolate, trinitropyrazolate and tetranitrobispyrazolate are obvious continuations of the work detailed. Further work in this area should not be limited to these targeted ligands and should consider the wide variety of explosophoric ligands whose syntheses have been published. It is highly likely that novel, lead azide replacements with performance parameters meeting or exceeding that of both DBX-1 and lead azide can be found with further investigation into Cu(I) based primary explosives.

The synthesis of transition metal-triazenido complexes shows that compounds with promising properties as primary explosives can be synthesised when exploiting the capabilities of energetic triazenes as ligands. Further work on these compounds must focus on full characterisation (specifically drop weight testing) to determine if they hold practical use as primary explosives. However, it is the synthesis of a novel nitroazolyltriazene which should inspire the future of work into this class of compound. With only five known triazenes that can be viewed as energetic materials, there exist a wealth of novel compounds which can targeted in this underexplored class of energetic compound such as the nitropyrazolyl/imidazolyl-triazenes. Synthesis of further novel, energetic triazenes could result in compounds fit for a variety of purposes from nitrogen rich rocket propellants to explosophoric ligands for the formation of coordination compounds for use in detonators or igniters. With a

continued focus from the energetic material community on the synthesis of new classes of compound, an investigation of an overlooked but known class of compound in the triazenes should be of increased interest.

The investigation into the synthesis of azidonitroazolates can be continued in a number of ways. While 2-azido-4-nitroimidazole can be synthesised, the low yields reported in this thesis show that an improved synthetic route needs to be explored. Specifically, the conversion of 2-amino-4-nitroimidazole to 2-azido-4-nitroimidazole (first reported by Hou et al.) should be reinvestigated as an alternative route. With the work of this thesis also showing the reported synthesis of 2-azido-4,5-dinitroimidazole was likely to have been unsuccessful, first synthesis of this novel energetic compound should be attempted following the proposed syntheses outlined in Chapter 5.

With K-NPT.H_2O proving to have potential as a lead styphnate replacement, further investigation of this compound is warranted. Full sensitiveness testing (FS and ESD) should be done prior to testing the compound as a part of initiatory formulations used in igniters. K-NPT.H_2O also could serve as an ideal starting material for the synthesis of transition metal complexes. Future work with Na_2-3-O-4-NPT must centre on further characterisation and larger scale syntheses. If full characterisation is obtained (and depending on the results of this characterisation), Na_2-3-O-4-NPT can be treated in a similar way to K-NPT.H_2O.

More generally the work of Chapter 5 serves to show that while azidonitroimidazoles may hold no practical use as energetic materials, the nitropyrazolotetrazoles possess the sensitivity of azidoazoles while retaining the higher thermal stabilities of nitroazoles. Synthesis of novel pyrazolotetrazoles with different explosophoric groups could result in the isolation of high performance energetic materials. With no other records of these compounds in literature regarding energetic materials, further investigation into these compounds can be viewed as the development of an entirely new class of energetic compound.

7. General Experimental Methods and Instrumentation

Infrared absorption spectra were recorded in the range 500-4000 cm^{-1} on a Bruker Tensor 27 Fourier Transform Infrared Spectrometer running the Bruker OPUS software package at a spectral resolution of 2 cm^{-1} either as a nujol mull or as a thin film between NaCl plates. Elemental analyses were carried out by the University of Sheffield elemental analysis service on a Elementar vario EL MICRO cube elemental analyser in an atmosphere of pure oxygen. ^{1}H, ^{13}C NMR were recorded using a 400 MHz Bruker Advance 400 Spectrometer. ^{1}H and ^{13}C NMR were calibrated against the residual solvent peak according to ref.[1] NMR spectra were processed using the MestreNova software package. DSC measurements were recorded on a TA DSC25 operated under nitrogen flow in sealed stainless-steel capsules fitted with Au-plated Cu Seals. The instrument was calibrated against a pure indium reference (99.999%) with a sharp transition at 156.60 °C, with a well know enthalpy change of 28.45 J g^{-1} Onset temperatures for decomposition were calculated by the intersection of the tangent of maximum gradient with the projected position of the baseline. Peak temperatures were determined at maximum heat flow of the inspected exotherm. Enthalpy of decomposition was determined by the integration of the recorded trace. The uncertainties associated with calculation of enthalpies of decomposition are at least ±10%. Single crystal X-ray diffraction (XRD) data collections recorded at The University of Sheffield were collected on one of three diffractometers: A Bruker Small Molecule Analytical Research Tool (SMART) or Bruker Kappa diffractometer equipped with a CCD detector and an Oxford Cryosystems Cryocooler using MoK_{α} radiation (λ= 0.71073) at or a Bruker D8 Venture diffractometer using CuK_{α} radiation (λ=1.54056 Å) equipped with a Bruker PHOTON CMOS detector and an Oxford Cryosystems Cryocooler. Data was collected using Bruker APEX2/3 software and integrated using the APEX 2/3 software. Structures were solved using Olex2 using either the XT (Intrinsic phasing) or XS (Direct methods) functions. Data collected at either 100 K or at room temperature. Powder X-ray diffraction data was recorded at the University of Sheffield using 0.7 mm borosilicate glass capillaries prior to being mounted and aligned on a D8 Advance powder X-ray diffractometer with a $Cu\text{-}K_{\alpha}$ sealed source (λ=1.54056 Å). Data was recorded using a rotating capillary stage. Powder patterns were recorded using the Bruker DIFFRac.EVA software suite. SEM

imaging recorded at The University of Sheffield was performed using a TESCAN VEGA3 LMU SEM instrument, operating at 5 kV and using the secondary electron detector. Samples were prepared by loading onto a carbon sticky tab on an aluminium stub via pipetting of an IPA suspension of the sample onto the tab and allowing the IPA to evaporate. These samples are then sputter coated with approximately 20 nm of gold using an Edwards S150B sputter coater before being imaged at a distance of 9mm.

7.1 References

1. G. R. Fulmer, A. J. Miller, N. H. Sherdan, H. E. Gottlieb, A. Nudelman, B. M. Stoltz, J. E. Bercaw, K. I. Goldberg, Organometallics, 2010, 29, 2176-79

8. Appendix

8.1 FTIR of NaNT.2H_2O, range 4000-500 cm^{-1}

8.2 FTIR of NaNT.4H_2O, range 4000-500 cm^{-1}

8.3 FTIR of DBX-1, range 4000-500 cm^{-1}

8.4 FTIR of DBX-X, range 4000-500 cm^{-1}

8.5 FTIR of DBX-1/DBX-X mixed powder, range 4000-500 cm^{-1}

8.6 PXRD of DBX-1

8.7 PXRD of DBX-X

8.8 Table of all experimental repeats and their results for Chapter 2

8.9 FTIR of Sodium-3,5-dinitro-1,2,4-triazolate dihydrate, range 4000-500 cm^{-1}

8.10 FTIR of $Cu_4(DNT)_3Cl$, range 4000-500 cm^{-1}

8.11 FTIR of K_2-TNBI, range 4000-500 cm^{-1}

8.12 FTIR of Cu_2-TNBI, range 4000-500 cm^{-1}

8.13 FTIR of Cu(I)-ADNP

8.14 FTIR of Na-3,5-DNP.2H2O, range 4000-500 cm^{-1}

8.15 FTIR of K-3,4-DNP.2H2O, range 4000-500 cm^{-1}

8.16 FTIR of Cu-3,5-DNP, range 4000-500 cm^{-1}

8.17 FTIR of K-4,5-DNI.H2O, range 4000-500 cm^{-1}

8.18 FTIR of Cu-4,5-DNI.H2O, range 4000-500 cm^{-1}

8.19 FTIR of K-2,4-DNI, range 1600-500 cm^{-1}

8.20 FTIR of Cu-2,4-DNI, range 4000-500 cm^{-1}

8.21 PXRD of Cu_2-TNBI

8.22 PXRD of Cu-4,5-DNI

8.23 PXRD of Cu-ADNP

8.24 FTIR of Na-b1mtt.5H_2O, range 4000-500 cm^{-1}

8.25 FTIR of $Fe(b1mtt)_2.H_2O$, range 4000-500 cm^{-1}

8.26 FTIR of $Pb(b1mtt)_2$, range 4000-500 cm^{-1}

8.27 FTIR of $Zn(b1mtt)_2$, range 4000-500 cm^{-1}

8.28 FTIR of $Co(b1mtt)_2.H_2O$, range 4000-500 cm^{-1}

8.29 FTIR of $Co(b1mtt)_2.(CH_3)_2CO$, range 4000-500 cm^{-1}

8.30 FTIR of $Ni(b1mtt)_2.H_2O$, range 4000-500 cm^{-1}

8.31 FTIR of $Ni(b1mtt)_2.(CH_3)_2CO$, range 4000-500 cm^{-1}

8.32 FTIR of $Fe(b1mtt)_2.H_2O$ after 2 month water immersion, range 4000-500 cm^{-1}

8.33 FTIR of $Pb(b1mtt)_2$. after 2 month water immersion, range 4000-500 cm^{-1}

8.34 FTIR of $Zn(b1mtt)_2$ after 2 month water immersion, range 4000-500 cm^{-1}

8.35 FTIR of $Ni(b1mtt)_2.H_2O$ after 2 month water immersion, range 4000-500 cm^{-1}

8.36 FTIR of $Co(b1mtt)_2.H_2O$ after 2 month water immersion, range 4000-500 cm^{-1}

8.37 FTIR of $Cu(b1mtt)(Cl)(H_2O)$, range 4000-500 cm^{-1}

8.38 FTIR of Cu(b1mtt)(4,5-DNI) , range 4000-500 cm^{-1}

8.39 ^{1}H NMR of (PPN)(bis(1-methyl-3-nitro-1,2,4-triazol-5-yl)triazenide).$3H_2O$

8.40 ^{13}C NMR of (PPN)(bis(1-methyl-3-nitro-1,2,4-triazol-5-yl)triazenide).$3H_2O$

8.41 FTIR of 2-Azido-4-nitroimidazole, range 4000-500 cm^{-1}

8.42 ^{1}H NMR of 2-Azido-4-nitroimidazole

8.43 ^{13}C NMR of 2-Azido-4-nitroimidazole

8.44 FTIR of Potassium-2-azido-4-nitroimidazolate, range 4000-500 cm^{-1}

8.45 ^{1}H NMR of Potassium-2-azido-4-nitroimidazolate

8.46 ^{13}C NMR of Potassium-2-azido-4-nitroimidazolate

8.47 FTIR of 3-Azido-4-nitropyrazole.H_2O, range 4000-500 cm^{-1}

8.48 ^{1}H NMR of 3-Azido-4-nitropyrazole.H_2O

8.49 ^{13}C NMR of 3-Azido-4-nitropyrazole.H_2O

8.50 FTIR of Potassium-4-nitropyrazolo[1,5 d]tetrazolate.H_2O, range 4000-500 cm^{-1}

8.51 ^{1}H NMR of Potassium-4-nitropyrazolo[1,5 d]tetrazolate.H_2O

8.52 ^{13}C NMR of Potassium-4-nitropyrazolo[1,5 d]tetrazolate.H_2O

8.53 FTIR of Sodium-3-azido-4,5-dinitropyrazolate, range 4000-500 cm^{-1}

8.54 DSC calorigram of Cu4(DNT)3Cl

8.55 DSC calorigram of Cu2-TBI

8.56 DSC calorigram of Cu-ADNP

8.57 DSC calorigram of Cu-3,5-DNP

8.58 DSC calorigram of Cu-2,4-DNI

8.59 DSC calorigram of Cu-4,5-DNI

Figure 8.1: *FTIR of NaNT.2H_2O, range 4000-500 cm^{-1}*

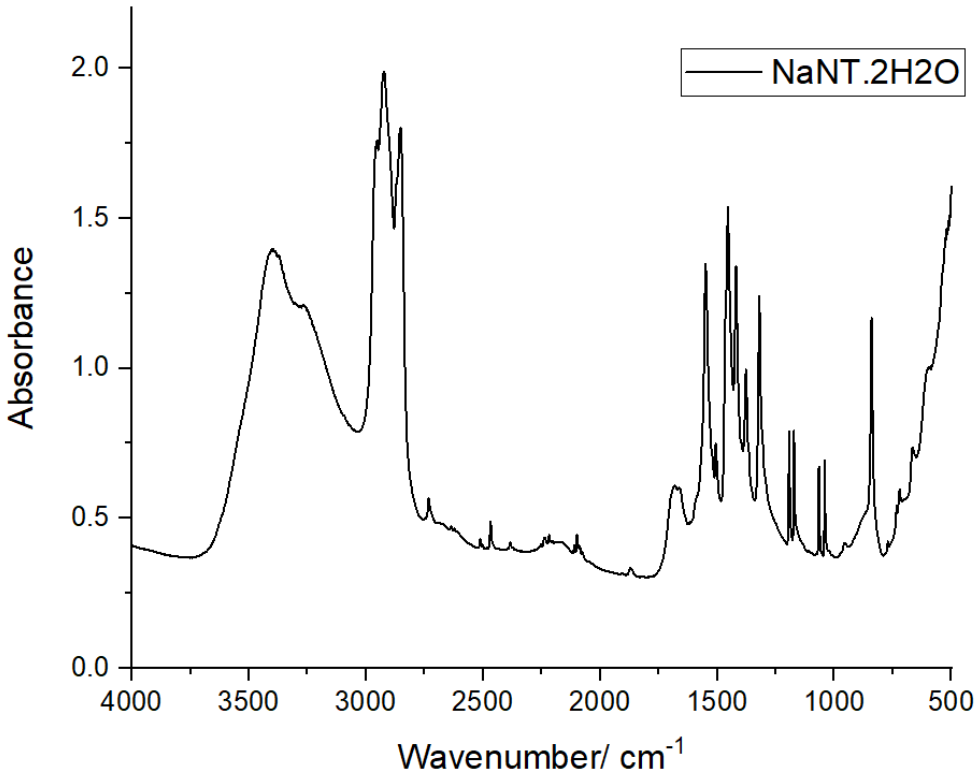

Figure 8.2: *FTIR of NaNT.4H_2O, range 4000-500 cm^{-1}*

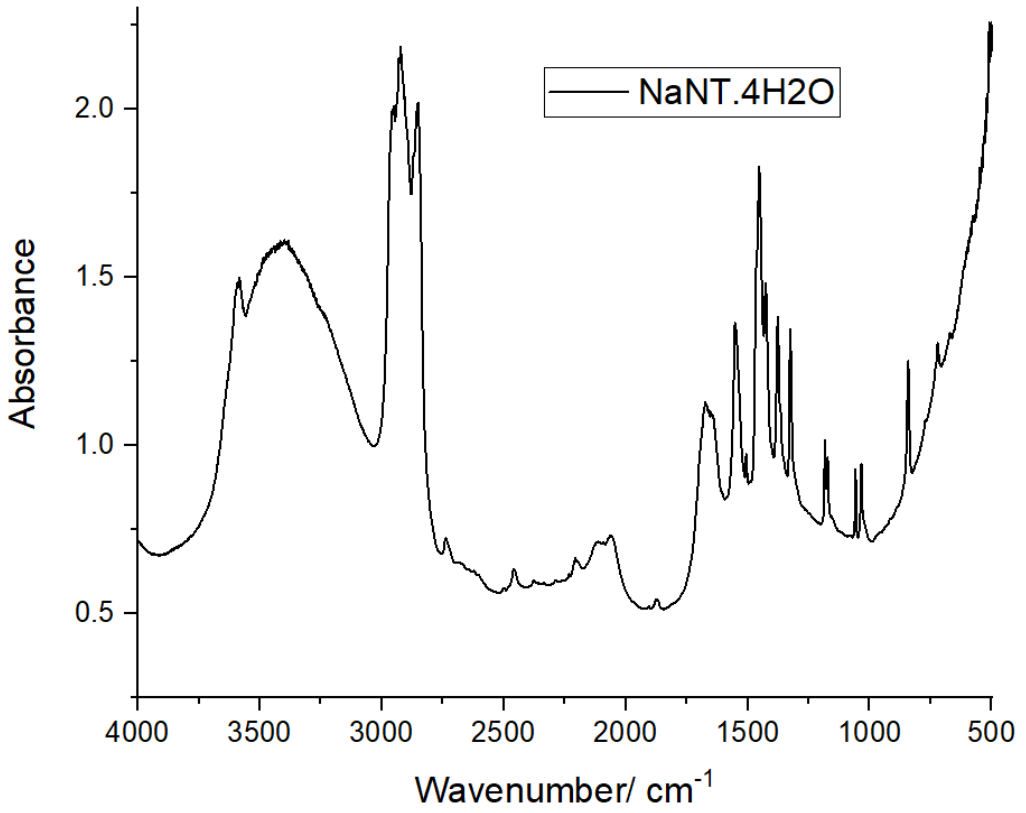

Figure 8.3: *FTIR of DBX-1, range 4000-500 cm^{-1}*

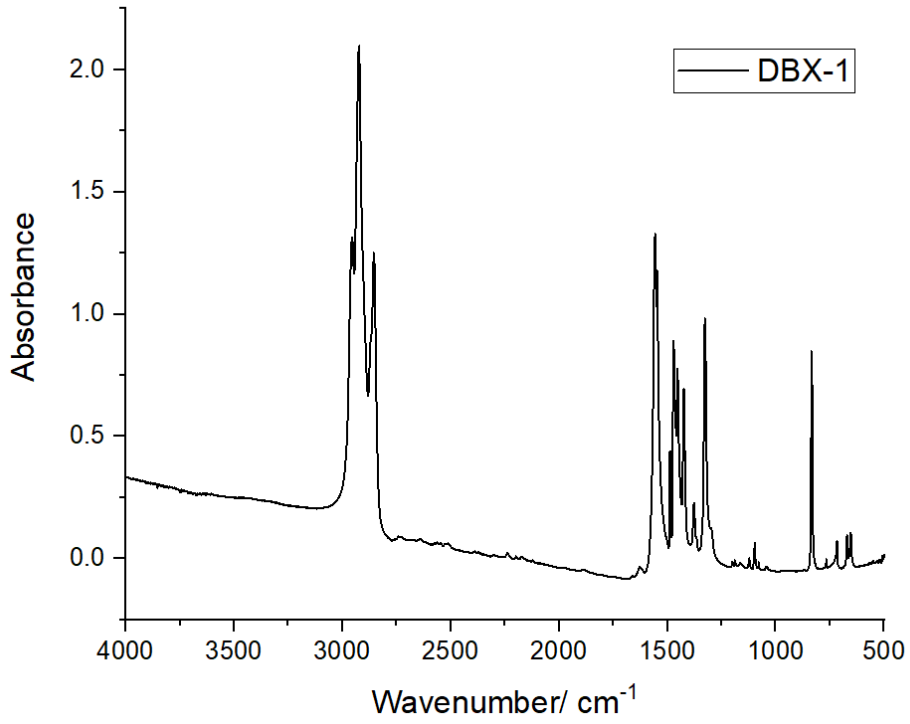

Figure 8.4: *FTIR of DBX-X, range 4000-500 cm^{-1}*

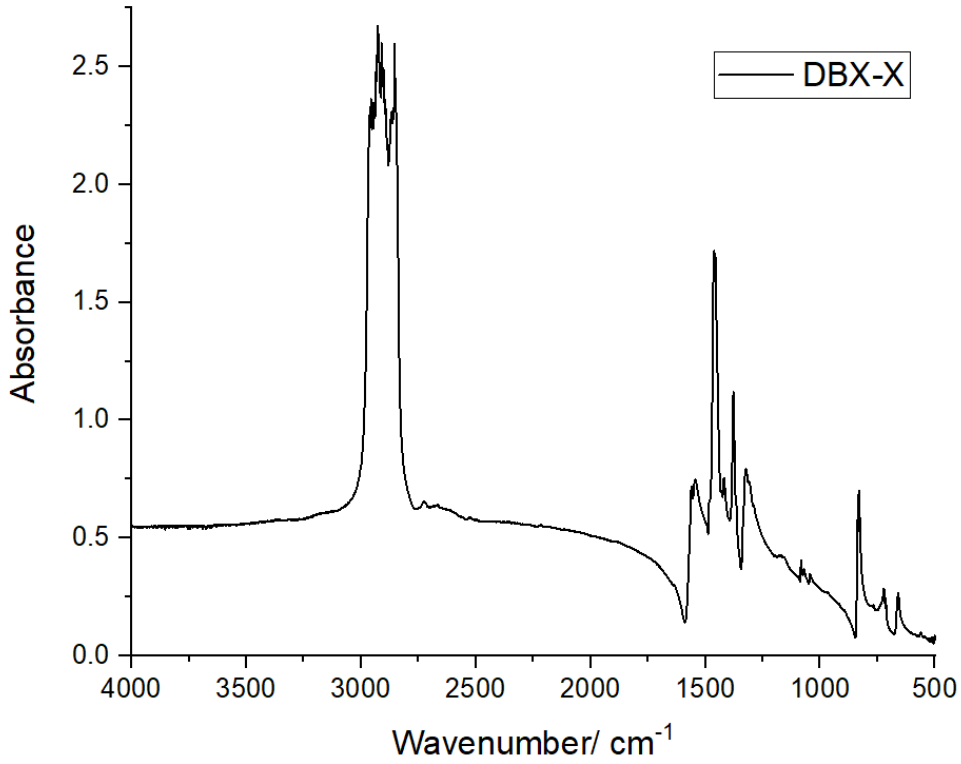

Figure 8.5: *FTIR of DBX-1/DBX-X mixed powder, range 4000-500 cm^{-1}*

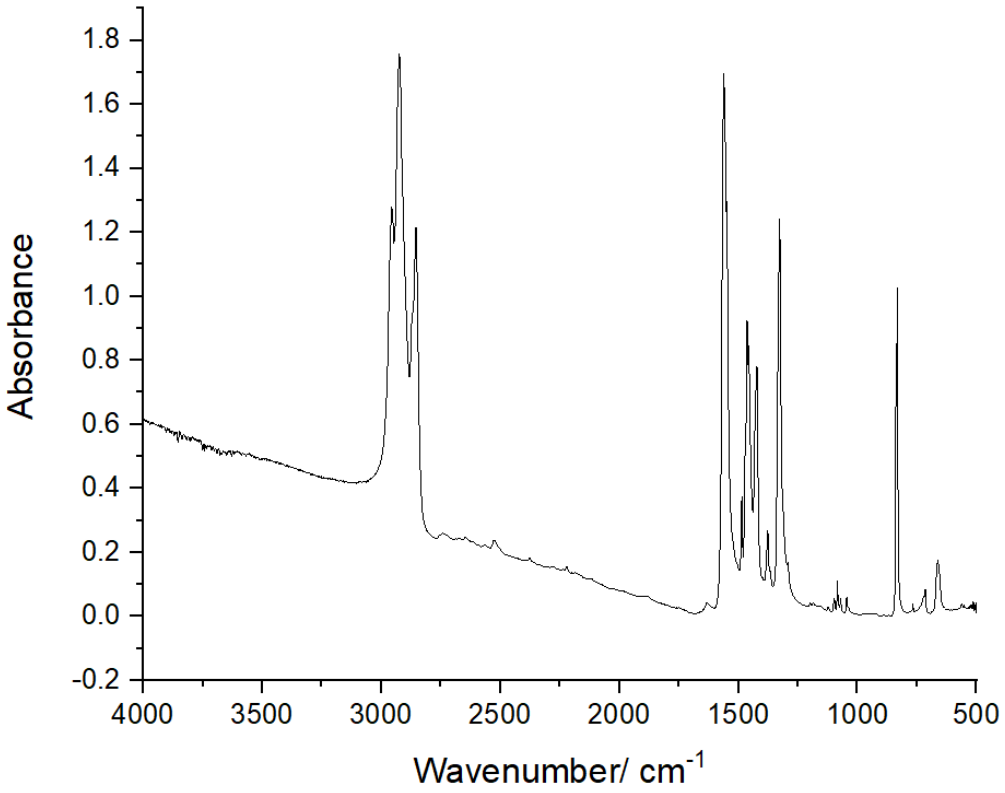

Figure 8.6: *PXRD of DBX-1*

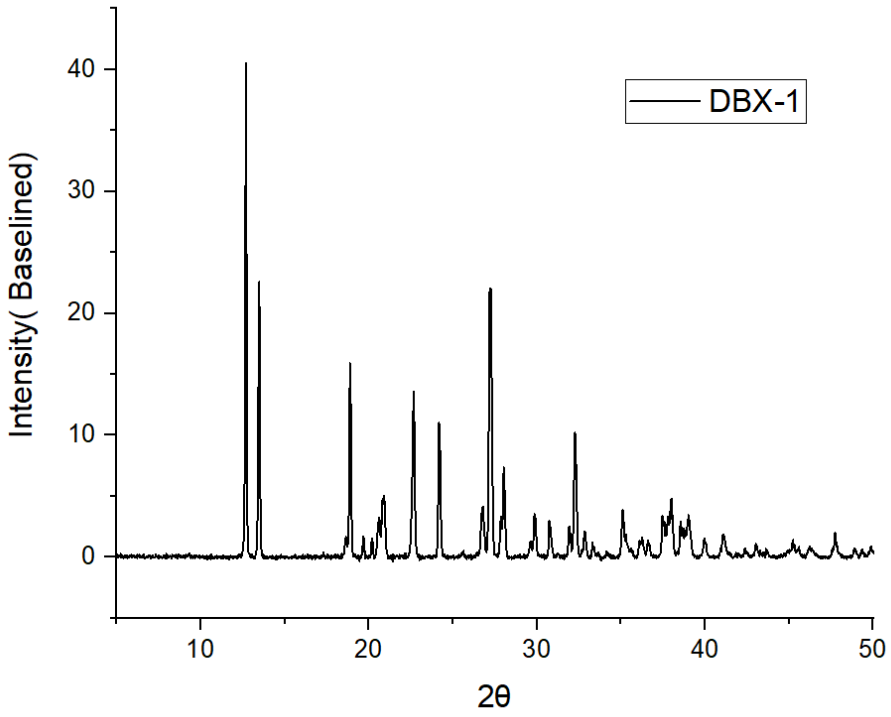

Figure 8.7: *PXRD of DBX-X*

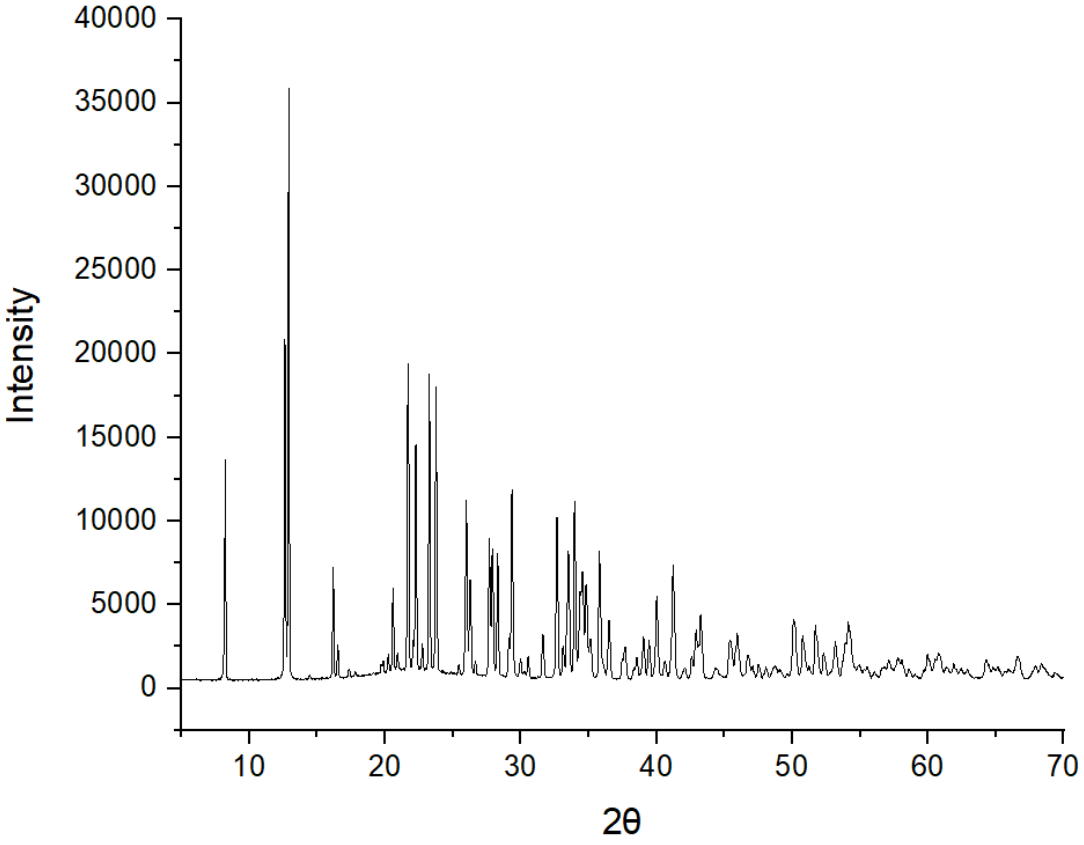

Figure 8.8: *Table of all experimental repeats of DBX-1 synthesis and their results*

No	Conditions	Reagent 1	c	v	Reagent 2	c	v	Reagent 3	c	v	Product	Yield
1	vessel and stir bar rinsed with water and mechanically cleaned with cellulose paper	$CuCl_2$	1.02	1.00	$NaNT(H_2O)_2$ batch 1	0.46	0.93	Na H-Asc	1.00	0.50	amorphous air sensitive solid	-
2	vessel and stir bar rinsed with water and mechanically cleaned with cellulose paper	$CuCl_2(H_2O)_2$	1.00	1.00	$NaNT(H_2O)_4$ batch 1	0.47	0.82	Na H-Asc	1.00	0.50	$Cu_3Cl(N_4CNO_2)_2$	86
3	vessel and stir bar rinsed with water and mechanically cleaned with cellulose paper	$CuCl_2(H_2O)_2$	0.18	1.00	$NaNT(H_2O)_4$ batch 1	0.66	1.17	Na H-Asc	1.00	0.50	$Cu_3Cl(N_4CNO_2)_2$	86
4	vessel and stir bar rinsed with water and mechanically cleaned with cellulose paper; only deionised water used that was purified further by distillation	$CuCl_2$	0.15	1.00	$NaNT(H_2O)_4$ batch 1	0.57	1.00	Na H-Asc	0.99	0.50	$Cu_3Cl(N_4CNO_2)_2$	83
5	vessel and stir bar rinsed with water and mechanically cleaned with cellulose paper	$CuCl_2$	0.15	1.00	$NaNT(H_2O)_4$ batch 1	0.46	0.94	Na H-Asc	1.00	1.00	Amorphous	-
6	vessel and stir bar rinsed with water and mechanically cleaned with cellulose paper	$CuCl_2$	0.14	1.00	$NaNT(H_2O)_4$ batch 1	0.46	1.00	Na H-Asc	0.97	0.50	$Cu_3Cl(N_4CNO_2)_2$	67
7	vessel and stir bar rinsed with water and mechanically cleaned with cellulose paper; only deionised water used that was purified further by distillation	$CuCl_2$	0.15	1.00	$NaNT(H_2O)_4$ batch 1	0.57	1.00	Na H-Asc	0.99	0.50	$Cu_3Cl(N_4CNO_2)_2$ / $CuCN_4NO_2$	73-86
8	vessel and stir bar rinsed with water and mechanically cleaned with cellulose paper	$CuCl_2$	0.15	1.00	$NaNT(H_2O)_4$ batch 1	0.45	1.00	Na H-Asc	0.50	0.50	$CuCN_4NO_2$	72
9	vessel and stir bar rinsed with water and mechanically cleaned with cellulose paper	$CuCl_2$	0.15	1.00	$NaNT(H_2O)_4$ batch 1	0.46	1.00	Na H-Asc	0.49	0.50	$CuCN_4NO_2$	71
10	vessel and stir bar rinsed with water and mechanically cleaned with cellulose paper	$CuCl_2$	0.15	1.00	$NaNT(H_2O)_4$ batch 1	0.47	1.00	Na H-Asc	1.00	0.50	$CuCN_4NO_2$	71
11	vessel treated with 65% aqueous HNO_3 and neutralised with deionised water	$CuCl_2$	0.15	1.00	$NaNT(H_2O)_4$ batch 2	0.46	1.00	Na H-Asc	0.98	0.50	amorphous solid	-

Figure 8.8b: *Table of all experimental repeats of DBX-1 synthesis and their results cont.*

12	vessel and stir bar rinsed with water and mechanically cleaned with cellulose paper	CuCl2	0.15	1.00	$NaNT(H_2O)_2$ batch 2	0.47	1.00	Na H-Asc	0.99	0.50	amorphous solid	-
13	beaker treated with 65% aqueous HNO_3 and neutralised with deionised water; seeded with 10 – 15 mg $Cu(N_4CNO_2)$	$CuCl_2$	0.15	1.00	$NaNT(H_2O)_4$ batch 2	0.46	1.00	Na H-Asc	0.98	0.50	CuN_4CNO_2	65
14	beaker treated with 65% aqueous HNO_3 and neutralised with deionised water; seeded with 10 – 15 mg $Cu_3Cl(N_4CNO_2)_2$	$CuCl_2$	0.15	1.00	$NaNT(H_2O)_4$ batch 2	0.46	1.01	Na H-Asc	0.99	0.50	CuN_4CNO_2	69
15	beaker treated with 65% aqueous HNO_3 and neutralised with deionised water; seeded with 10 – 15 mg $Cu_3Cl(N_4CNO2)_2$	$CuCl_2$	0.15	1.00	$NaNT(H_2O)_4$ batch 2	0.46	1.01	Na H-Asc	0.98	0.50	$Cu_3Cl(N_4CNO_2)_2$ / $CuCN_4NO_2$	67-79
16	beaker only rinsed with deionized water	$CuCl_2$	0.15	1.00	$NaNT(H_2O)_4$ batch 2	0.47	1.00	Na H-Asc	0.98	0.50	$CuCN_4NO_2$	61
17	seeded with 10 to 15 mg $Cu(N_4CNO_2)$	$CuCl_2$	0.15	1.00	$NaNT(H_2O)_2$ batch 3	0.56	1.20	Na H-Asc	0.99	0.50	amorphous air sensitive solid	-
18	vessel and stir bar rinsed with water and mechanically cleaned with cellulose paper	$CuCl_2$	0.14	1.00	$NaNT(H_2O)_4$ batch 3	0.56	1.20	Na H-Asc	0.88	0.50	CuN_4CNO_2	72
19	vessel and stir bar rinsed with water and mechanically cleaned with cellulose paper	$CuCl_2$	0.15	1.00	$NaNT(H_2O)_4$ batch 4	0.31	0.67	Na H-Asc	1.00	0.50	amorphous air sensitive solid	-
20	seeded with 10 to 15 mg $Cu_3Cl(N_4CNO_2)_2$	$CuCl_2$	0.15	1.00	$NaNT(H_2O)_4$ batch 4	0.31	0.67	Na H-Asc	0.99	0.50	amorphous solid; red material deposited on vessel walls	-
21	beaker only rinsed with deionized water	$CuCl_2$	0.15	1.00	$NaNT(H_2O)_4$ batch 4	0.47	1.00	Na H-Asc	0.98	0.50	amorphous solid; 64 mg dark red material deposited on vessel walls	15

Figure 8.9: *FTIR of Sodium-3,5-dinitro-1,2,4-triazolate dihydrate, range 4000-500 cm^{-1}*

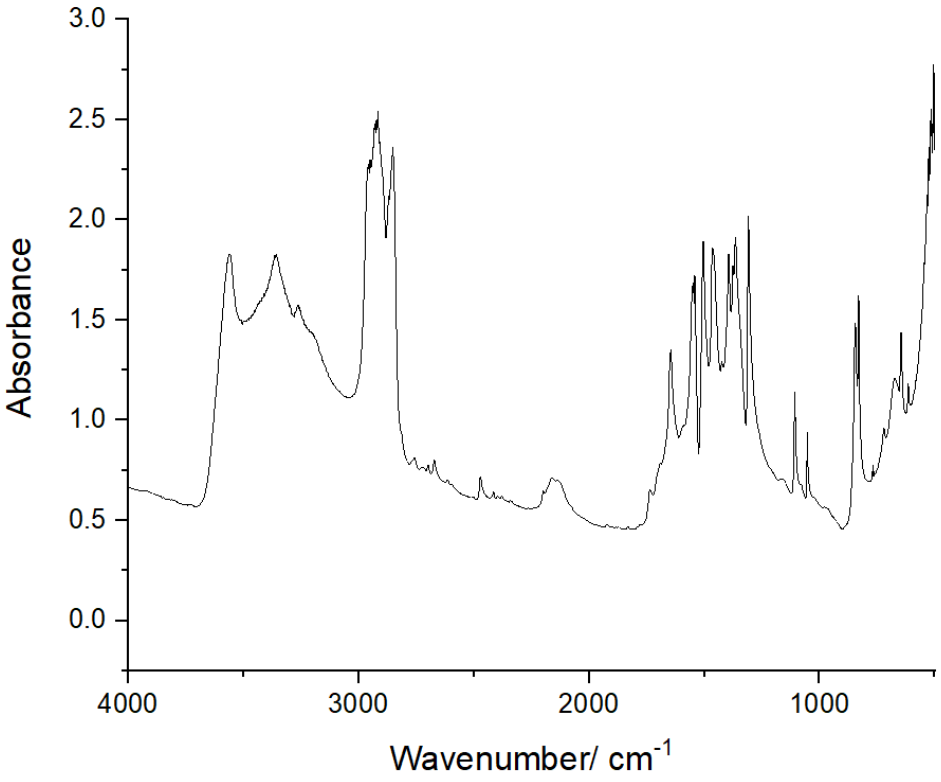

Figure 8.10: *FTIR of $Cu_4(DNT)_3Cl$, range 4000-500 cm^{-1}*

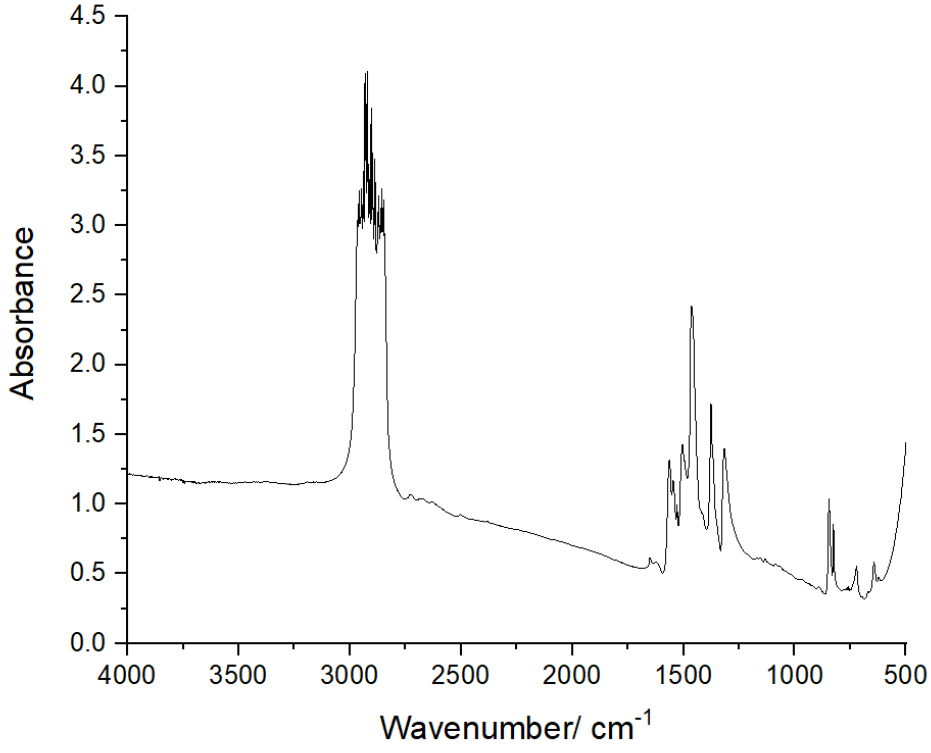

Figure 8.11: *FTIR of K_2TNBI, range 4000-500 cm^{-1}*

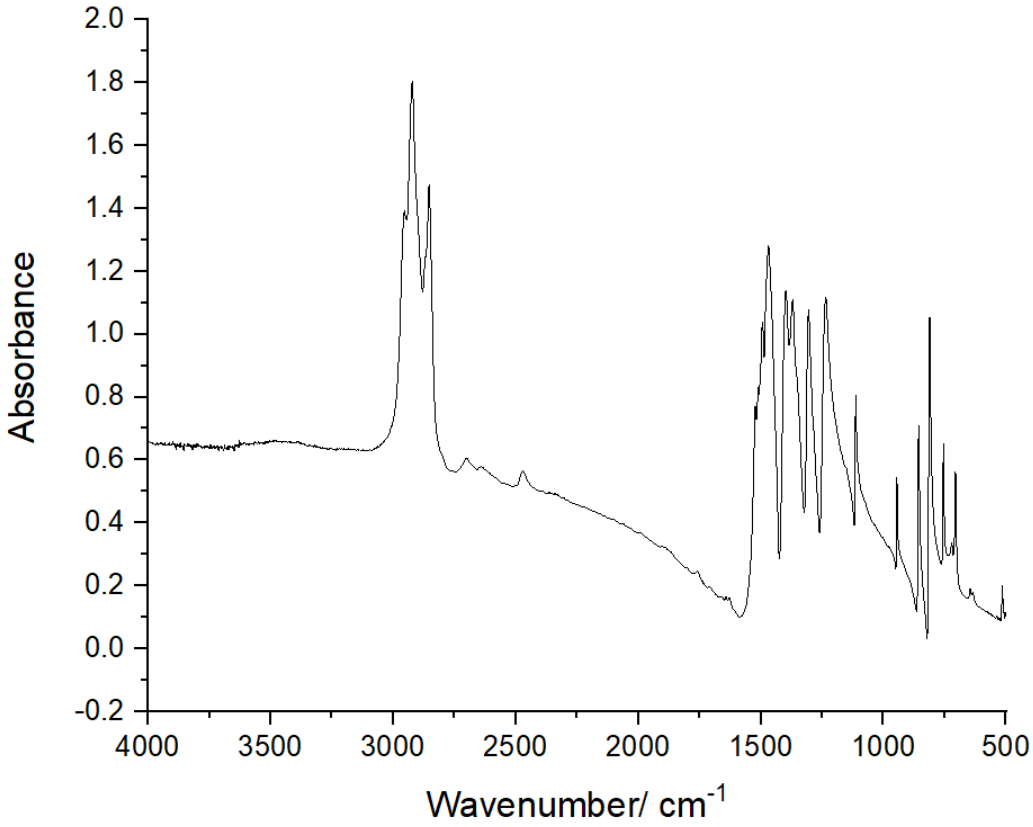

Figure 8.12: *FTIR of Cu_2TNBI, range 4000-500 cm^{-1}*

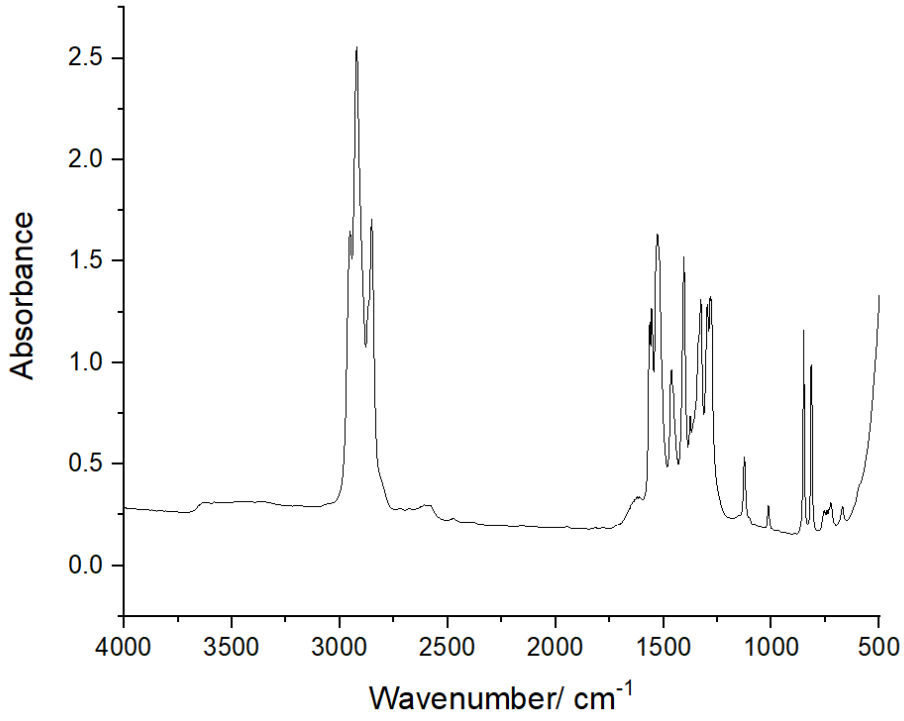

Figure 8.13: *FTIR of Cu-ADNP, range 4000-500 cm^{-1}*

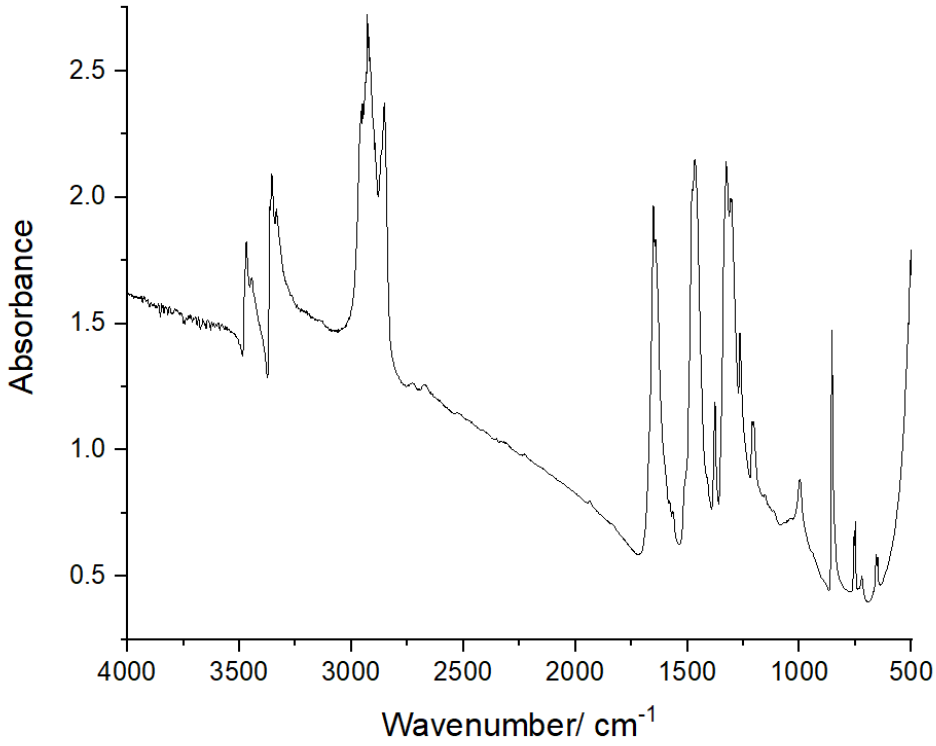

Figure 8.14: *FTIR of Na-3,5-DNP.2H2O, range 4000-500 cm^{-1}*

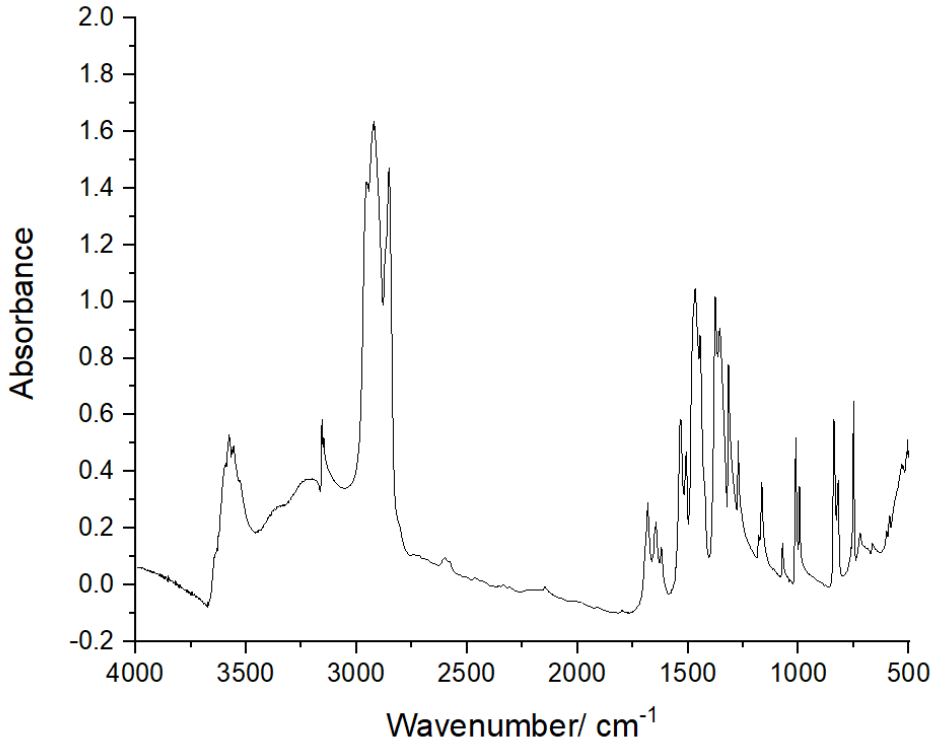

Figure 8.15: *FTIR of K-3,4-DNP.2H2O, range 4000-500 cm^{-1}*

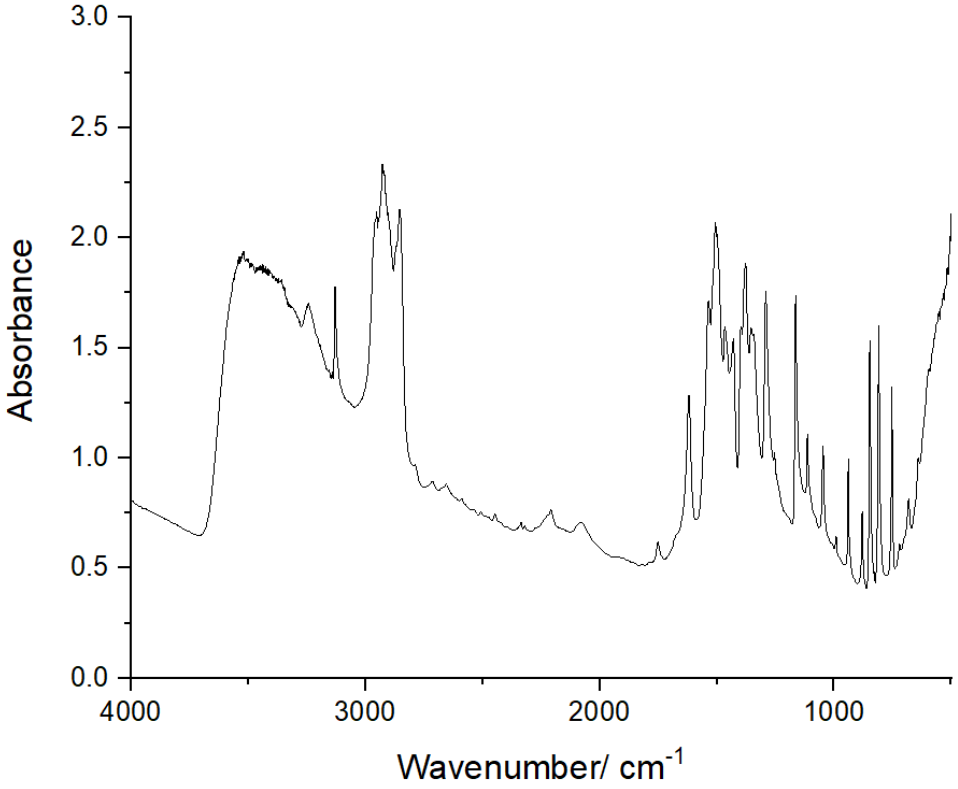

Figure 8.16: *FTIR of Cu-3,5-DNP, range 4000-500 cm^{-1}*

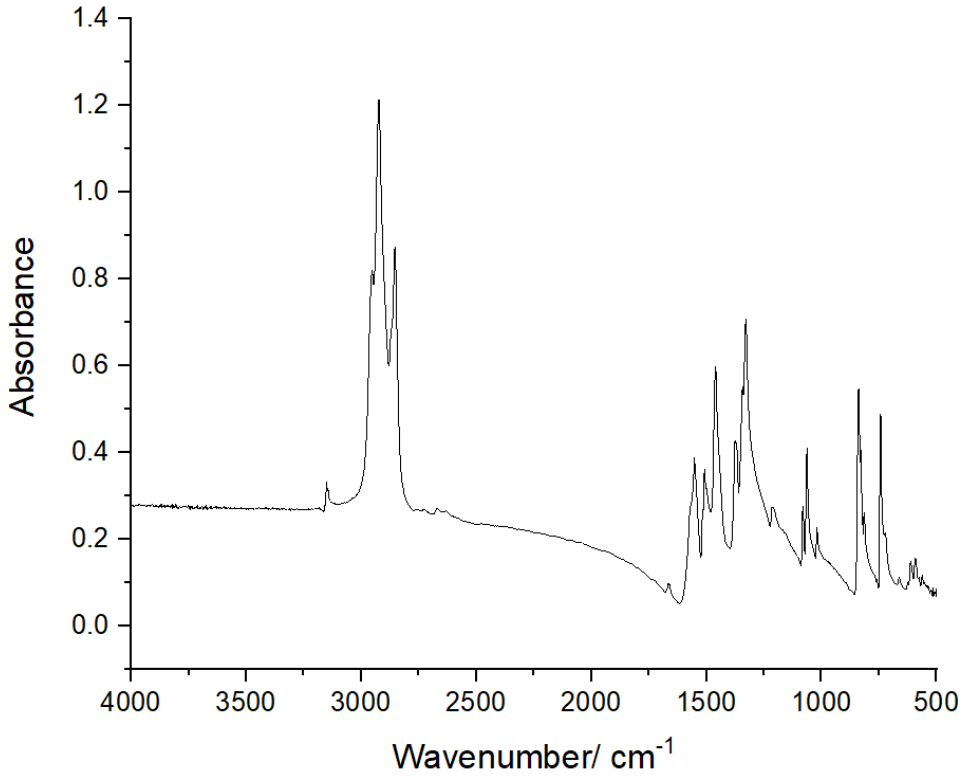

Figure 8.17: *FTIR of K-4,5-DNI.H2O, range 4000-500 cm^{-1}*

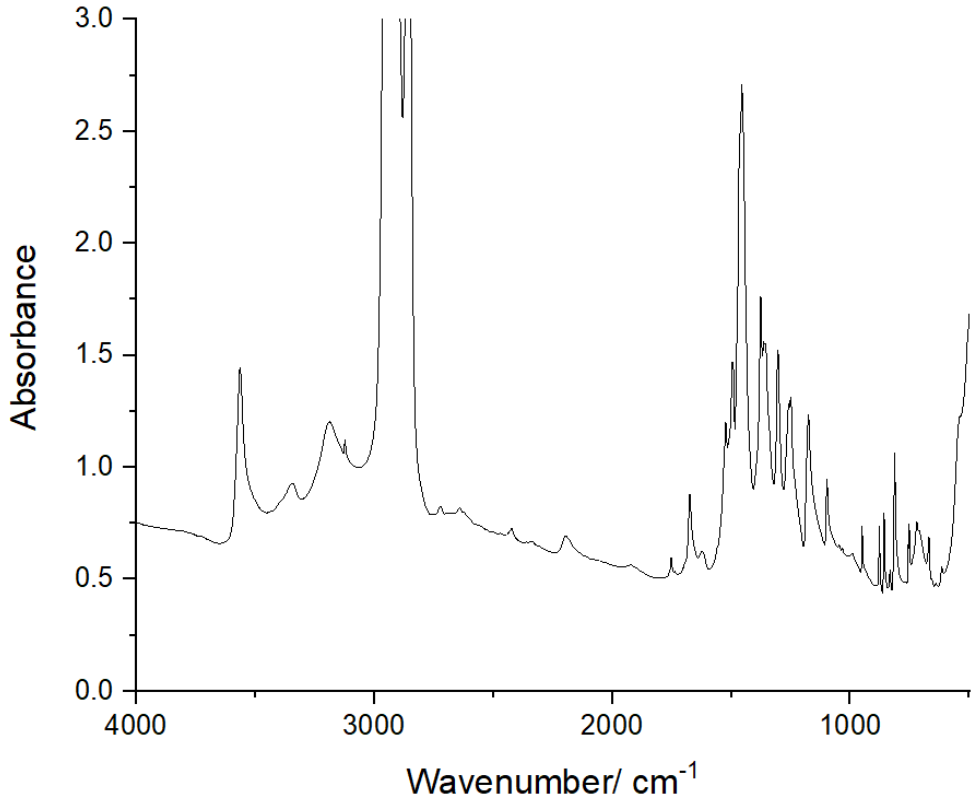

Figure 8.18: *FTIR of Cu-4,5-DNI, range 4000-500 cm^{-1}*

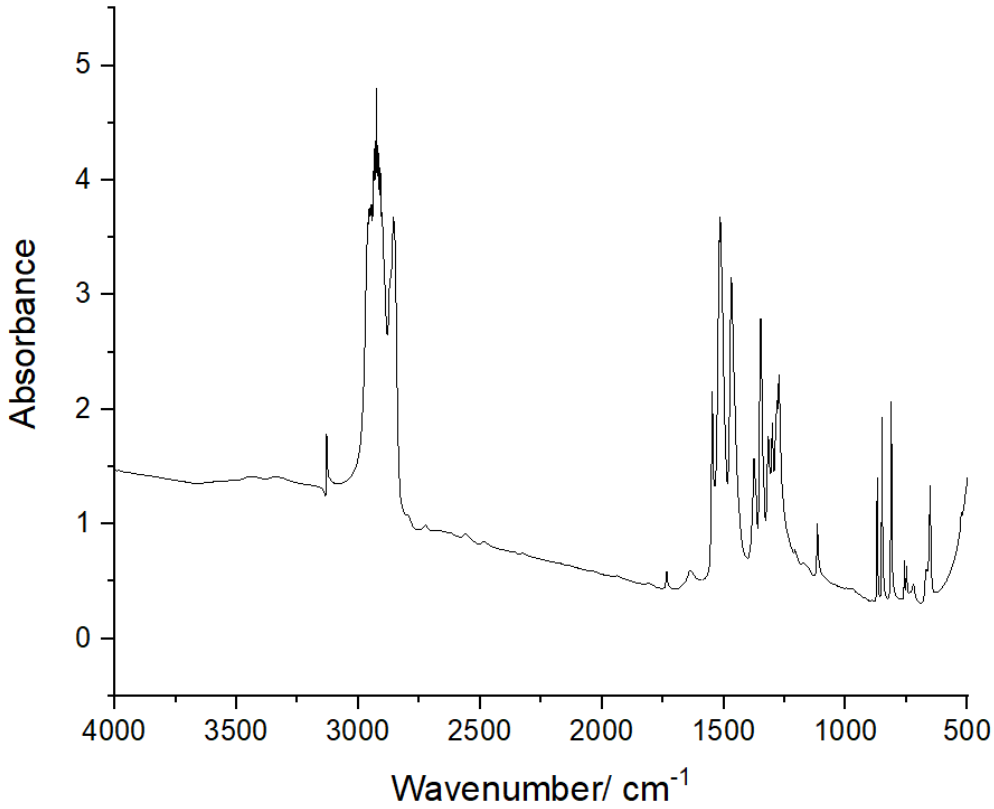

Figure 8.19: *FTIR of K-2,4-DNI, range 1600-500 cm^{-1}*

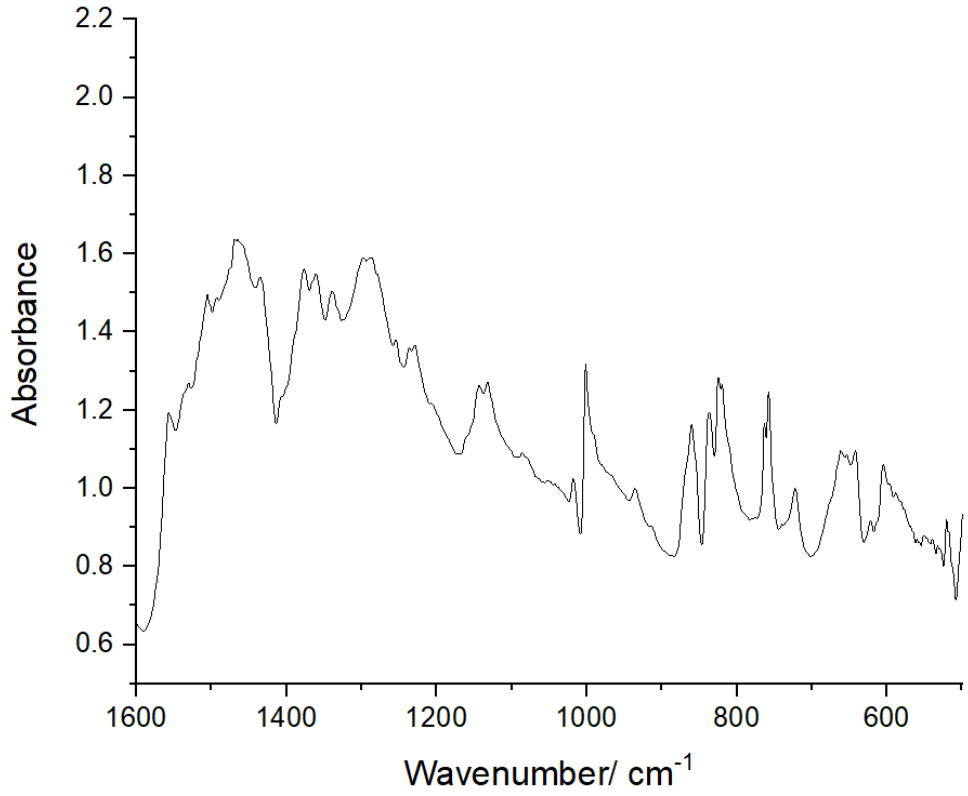

Figure 8.20: *FTIR of Cu-2,4-DNI, range 4000-500 cm^{-1}*

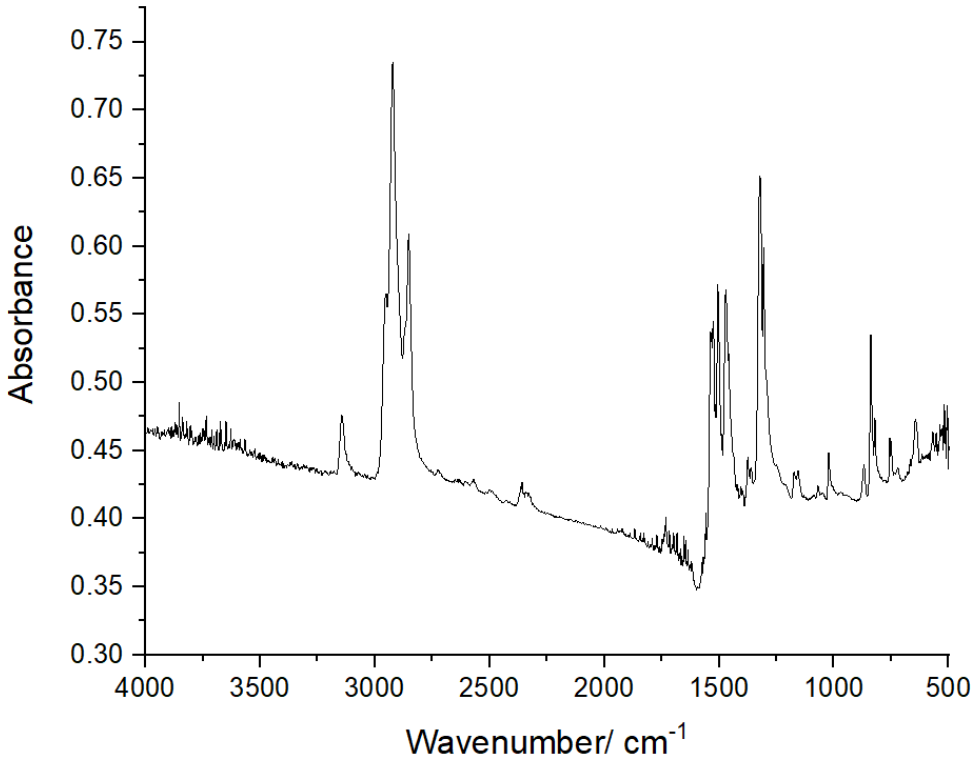

Figure 8.21: *PXRD of Cu2TNBI*

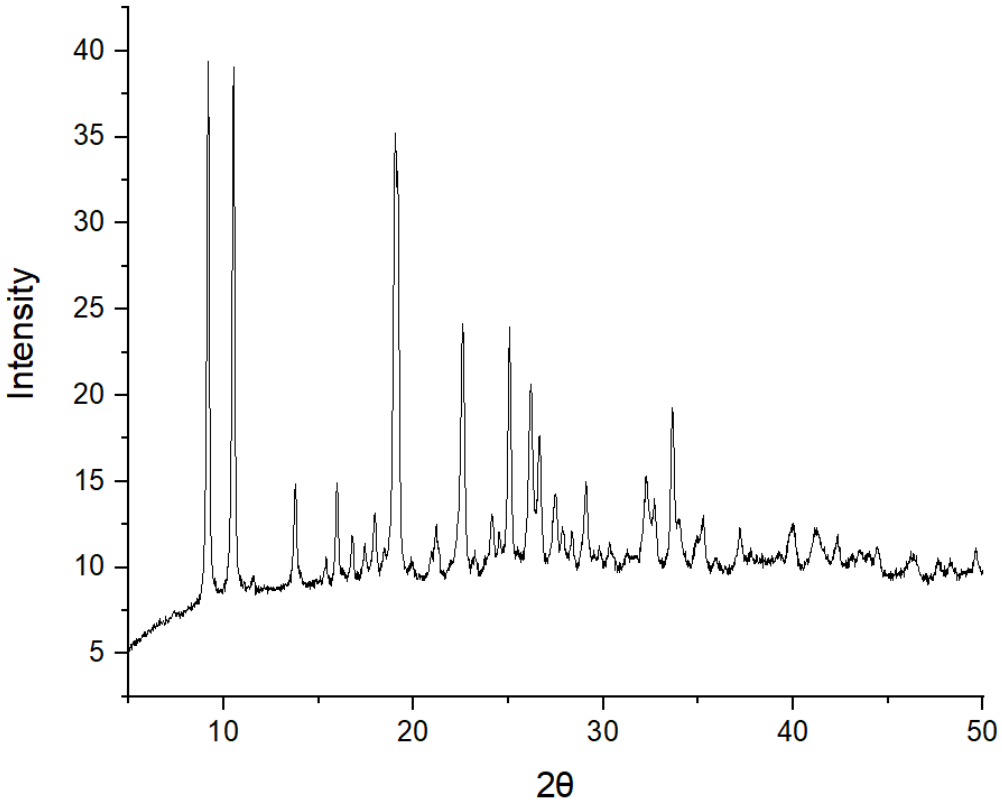

Figure 8.22: *PXRD of Cu-ADNP*

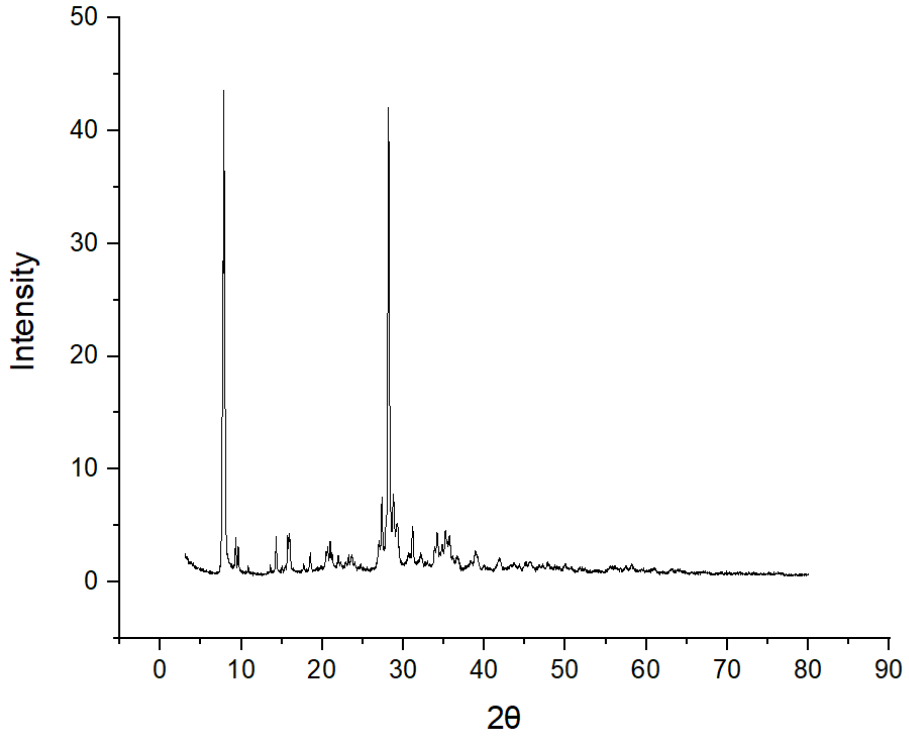

Figure 8.23: *PXRD of Cu-4,5-DNP*

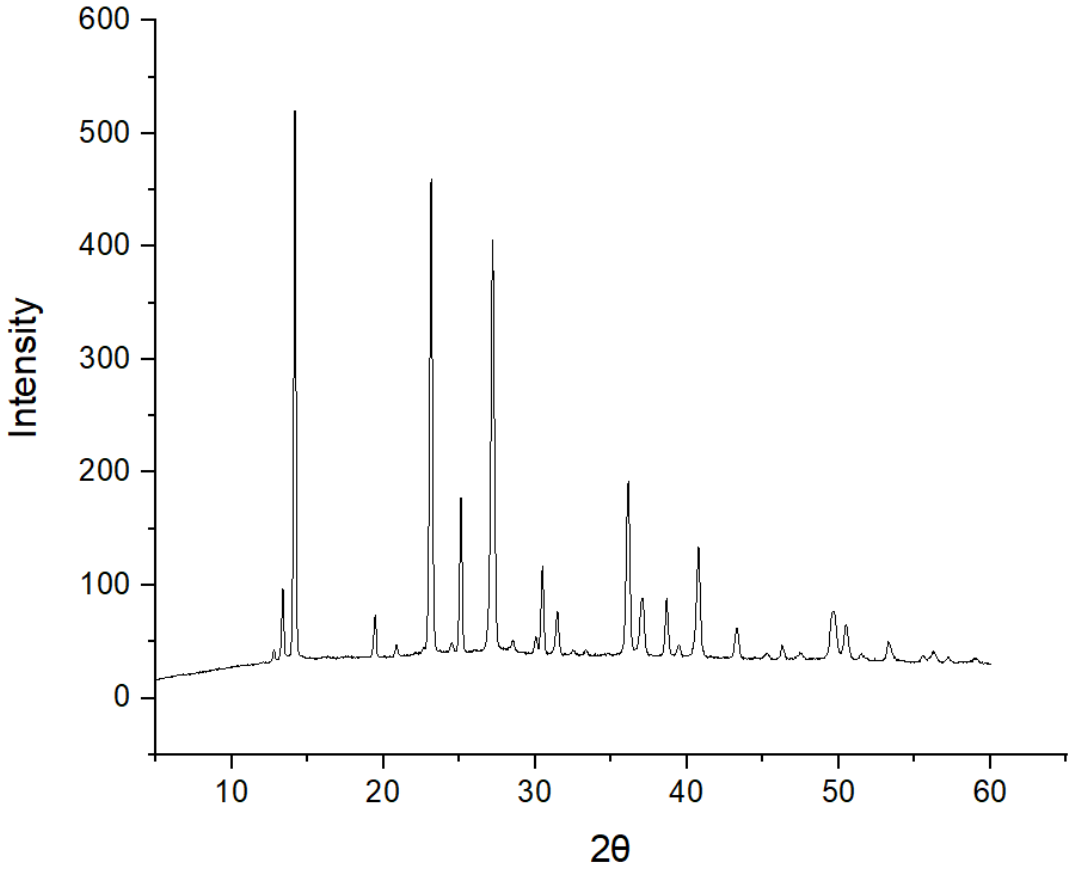

Figure 8.24: *FTIR of Na-B1MTT.5H2O, range 4000-500 cm^{-1}*

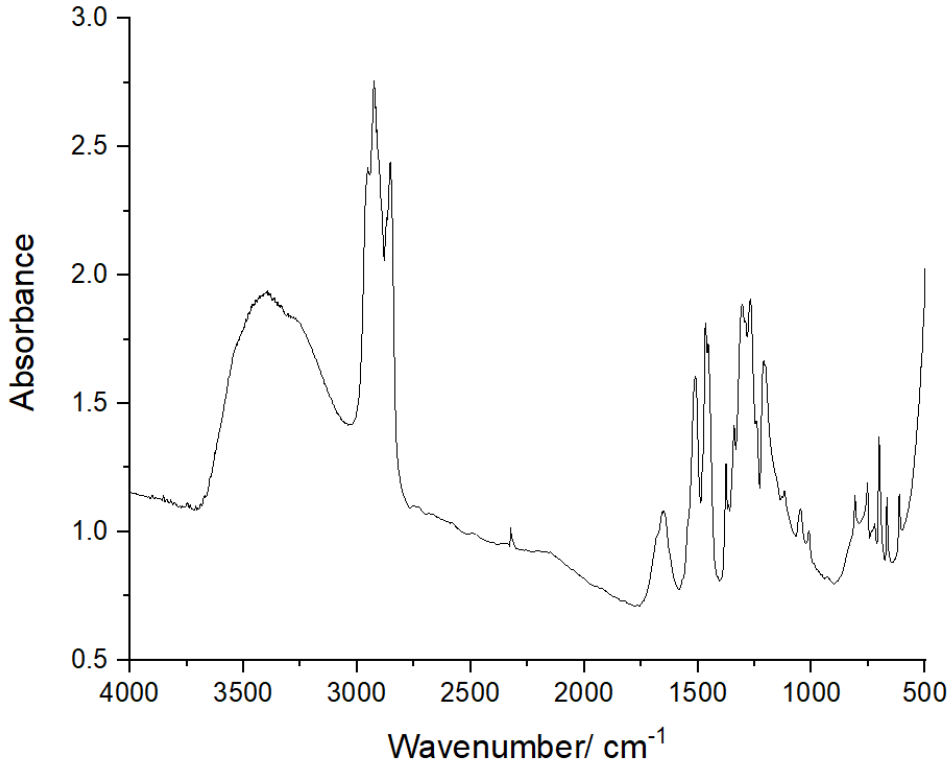

Figure 8.25: *FTIR of $Fe(B1MTT)_2.H_2O$, range 4000-500 cm^{-1}*

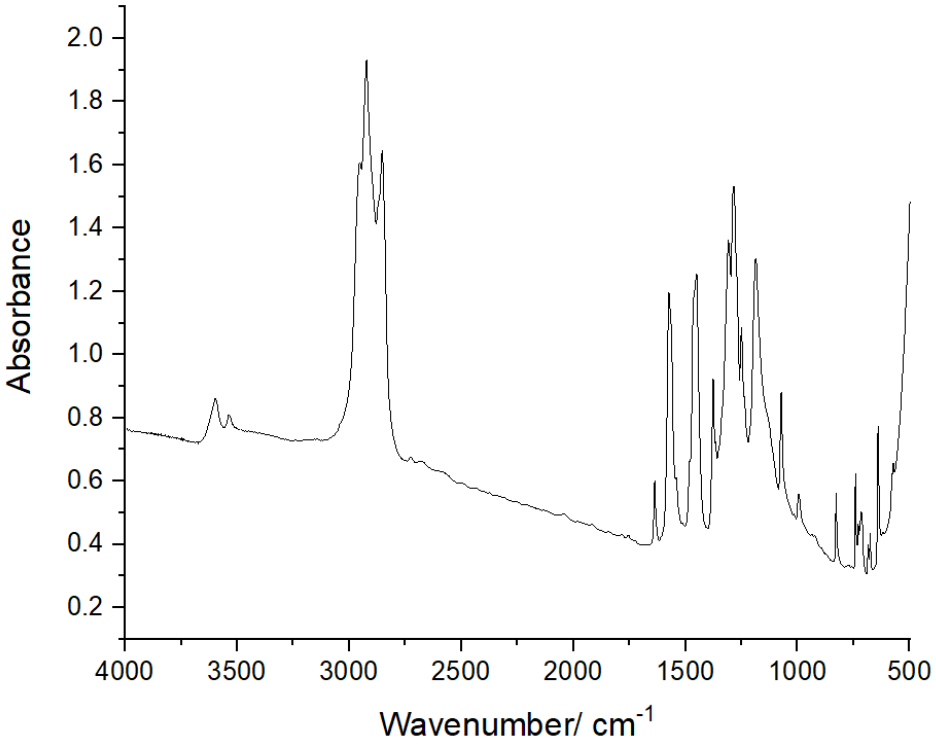

Figure 8.26: *FTIR of $Pb(B1MTT)_2$, range 4000-500 cm^{-1}*

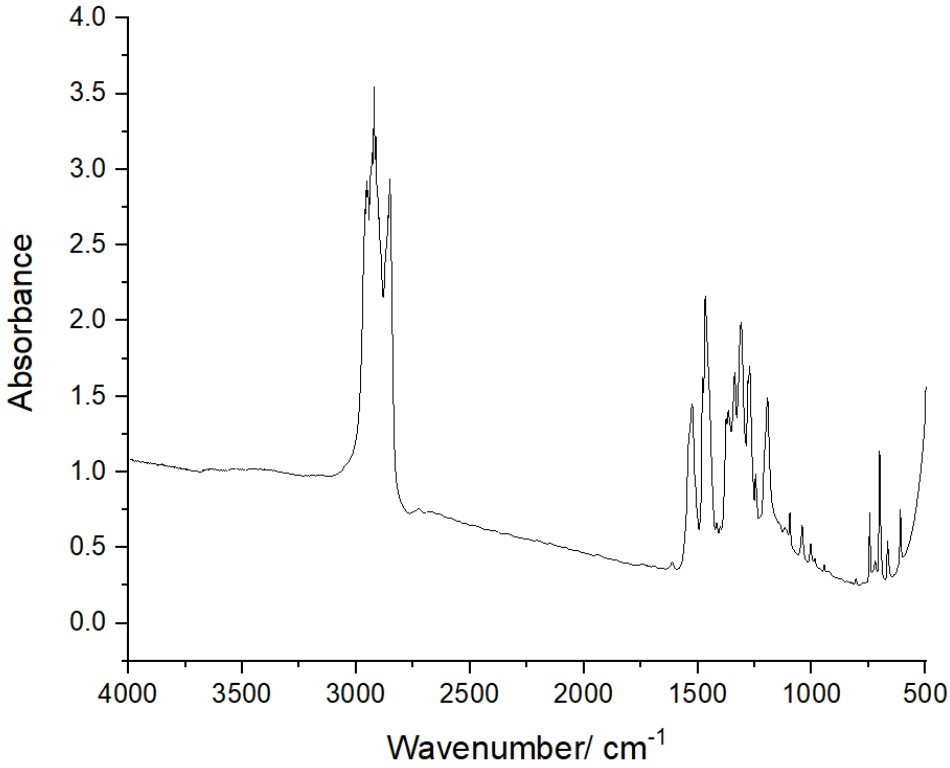

Figure 8.27: *FTIR of $Zn(B1MTT)_2$, range 4000-500 cm^{-1}*

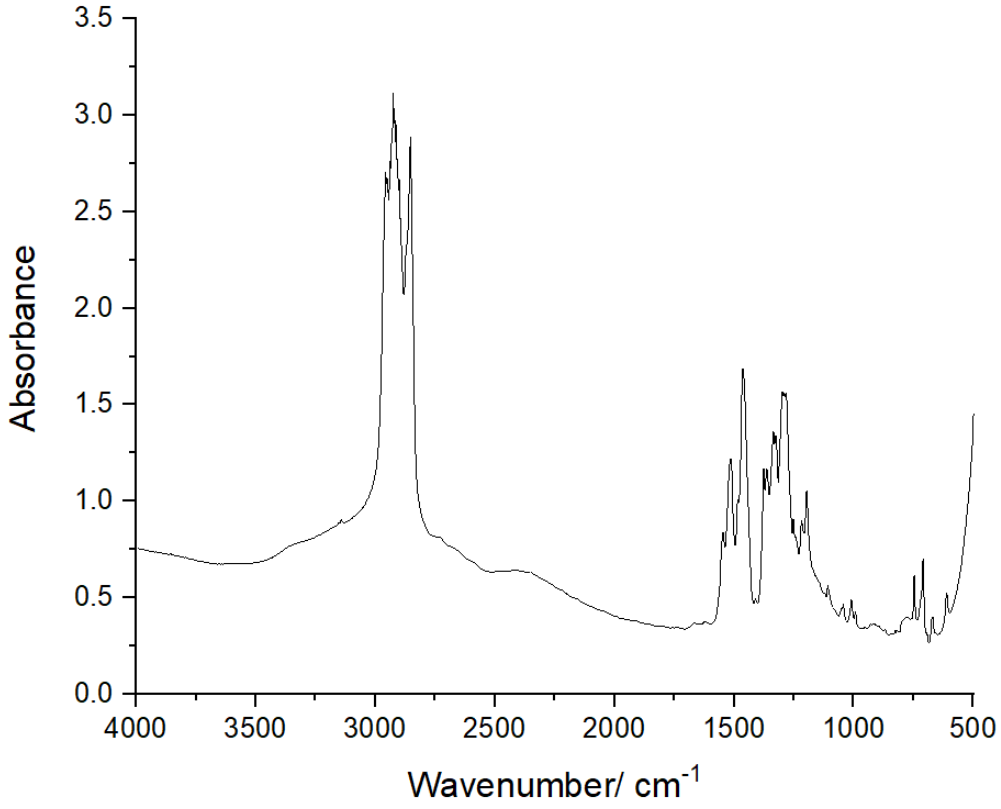

Figure 8.28: *FTIR of $Co(B1MTT)_2.H_2O$, range 4000-500 cm^{-1}*

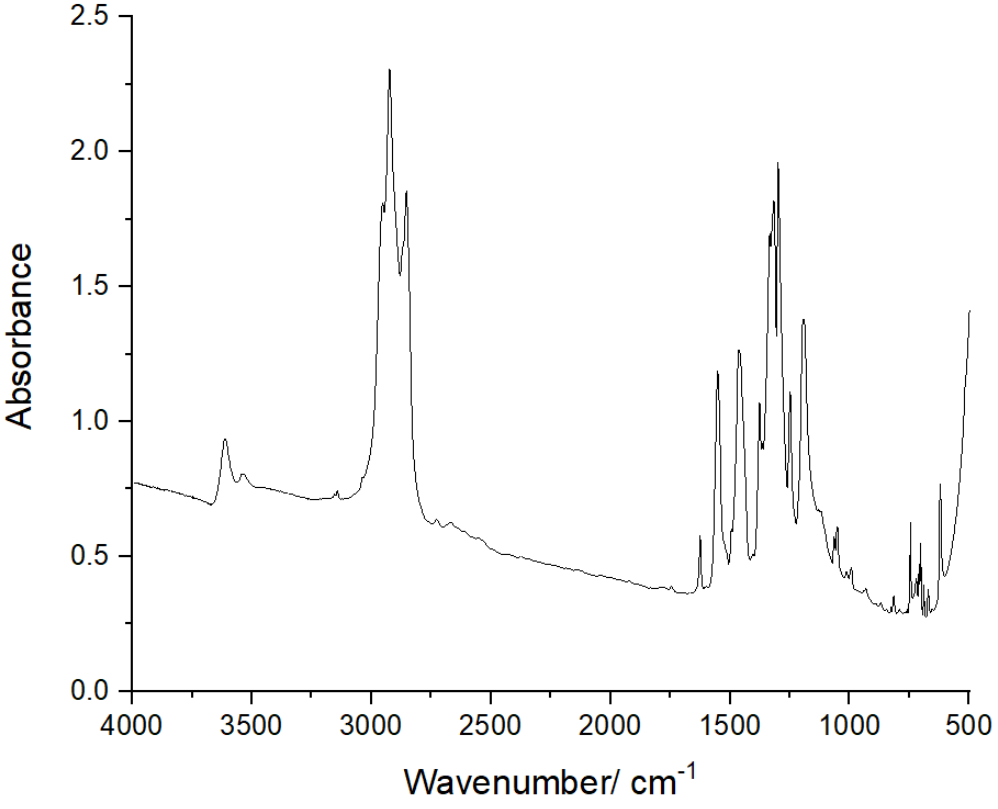

Figure 8.29: *FTIR of $Co(B1MTT)_2.(CH_3)_2CO$, range 4000-500 cm^{-1}*

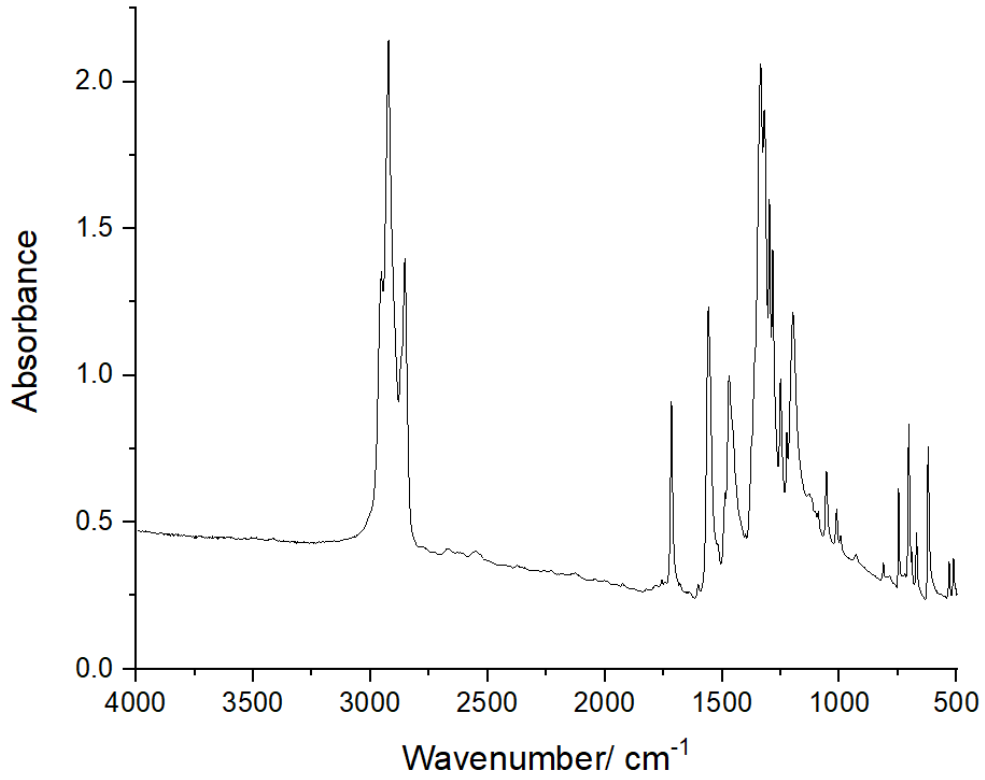

Figure 8.30: *FTIR of $Ni(B1MTT)_2.H_2O$, range 4000-500 cm^{-1}*

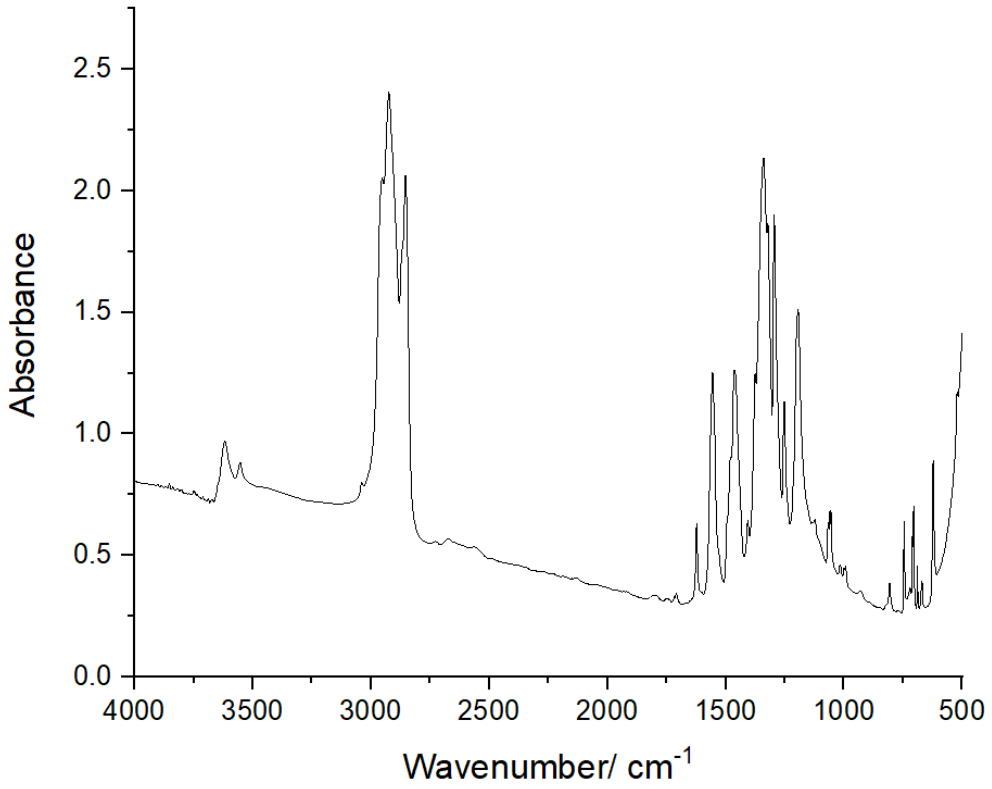

Figure 8.31: *FTIR of $Ni(B1MTT)_2.(CH_3)_2CO$, range 4000-500 cm^{-1}*

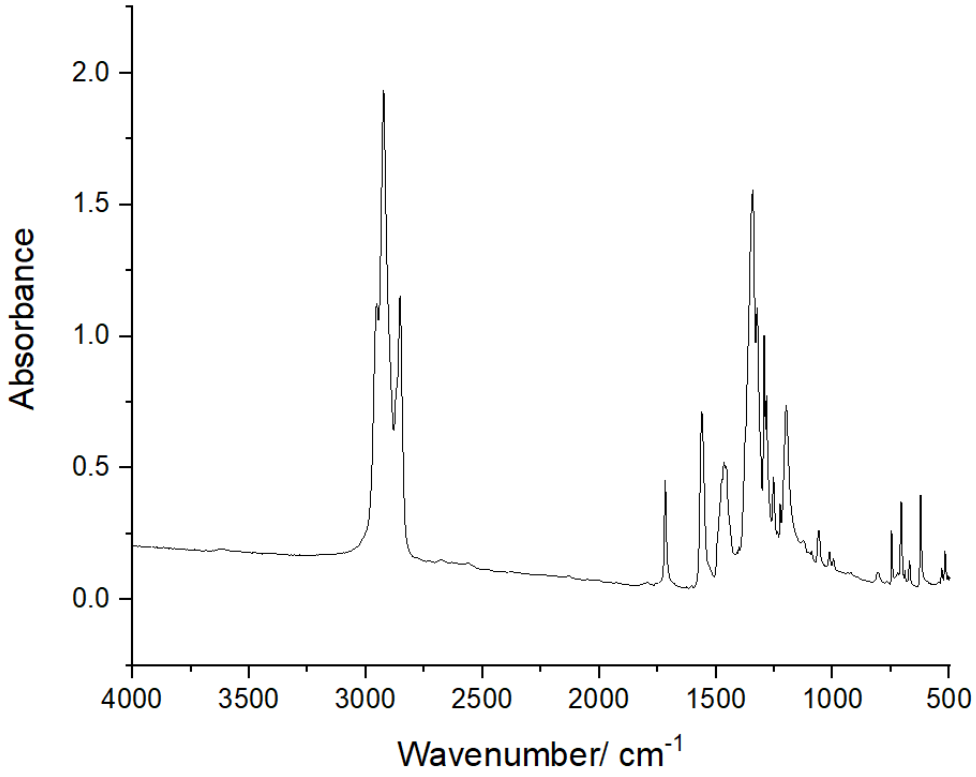

Figure 8.32: *FTIR of $Fe(b1mtt)_2.H_2O$ after 2 month water immersion, range 4000-500 cm^{-1}*

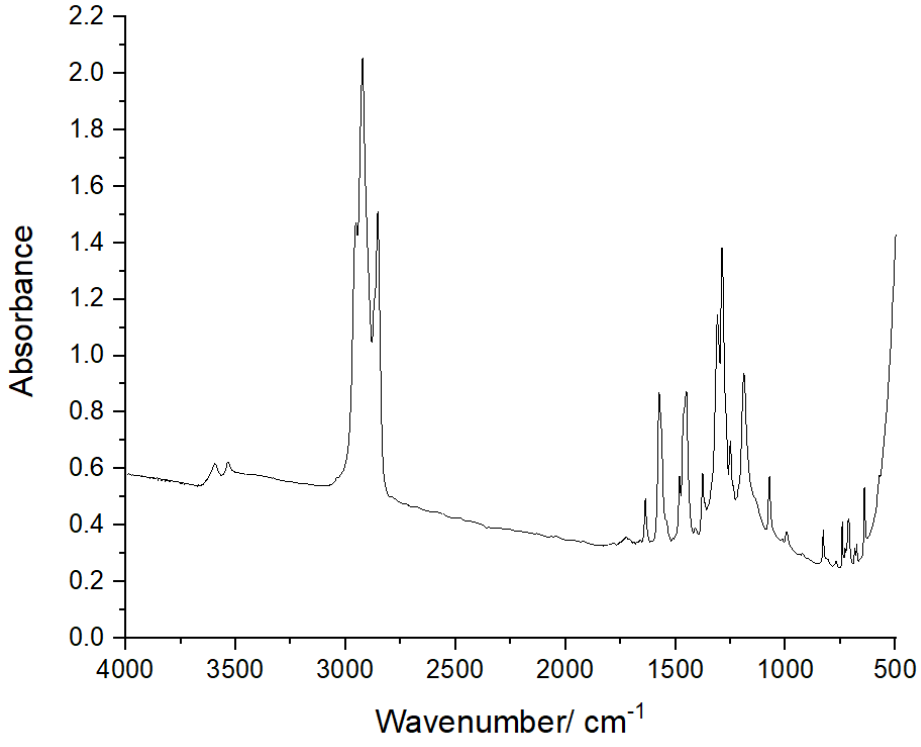

Figure 8.33: *FTIR of $Pb(b1mtt)_2$ after 2 month water immersion, range 4000-500 cm^{-1}*

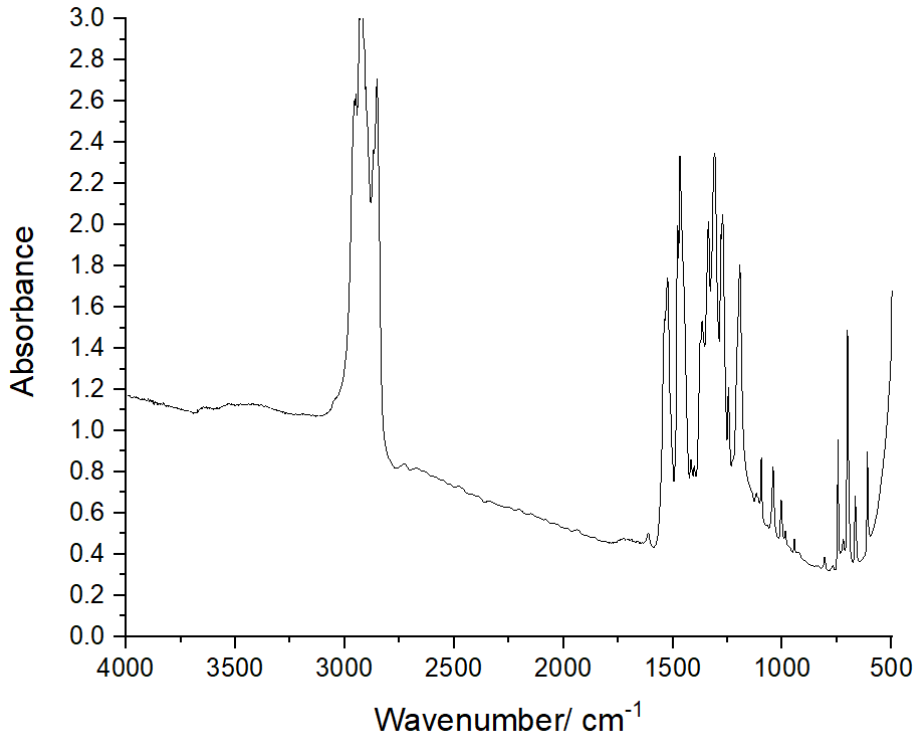

Figure 8.34: *FTIR of $Zn(b1mtt)_2$ after 2 month water immersion, range 4000-500 cm^{-1}*

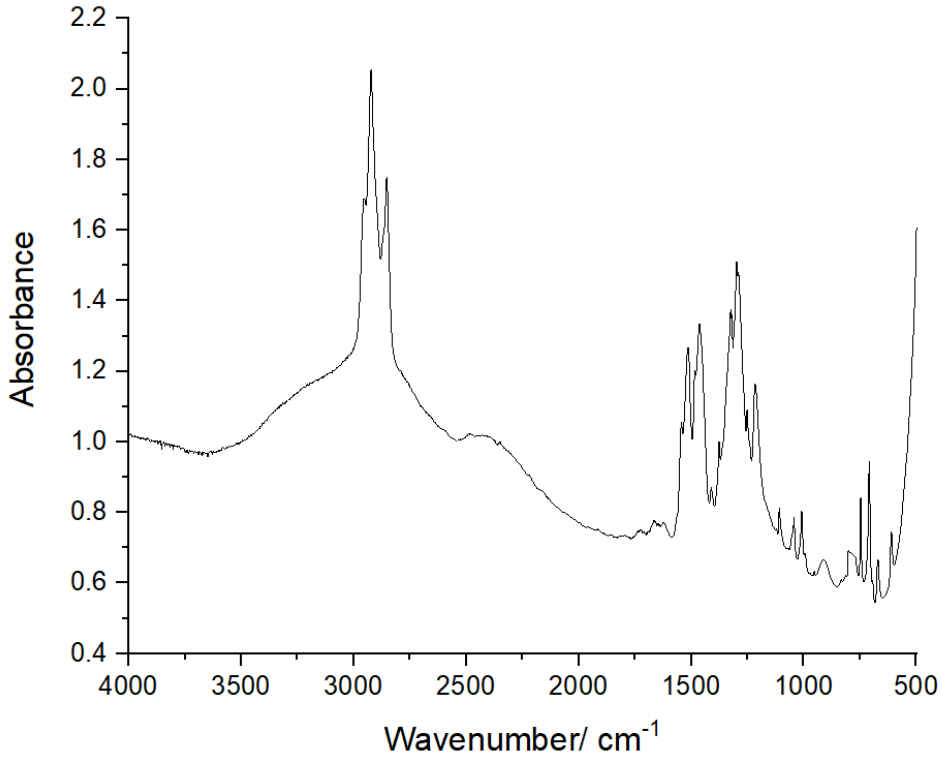

Figure 8.35: *FTIR of $Ni(b1mtt)_2.H_2O$ after 2 month water immersion, range 4000-500 cm^{-1}*

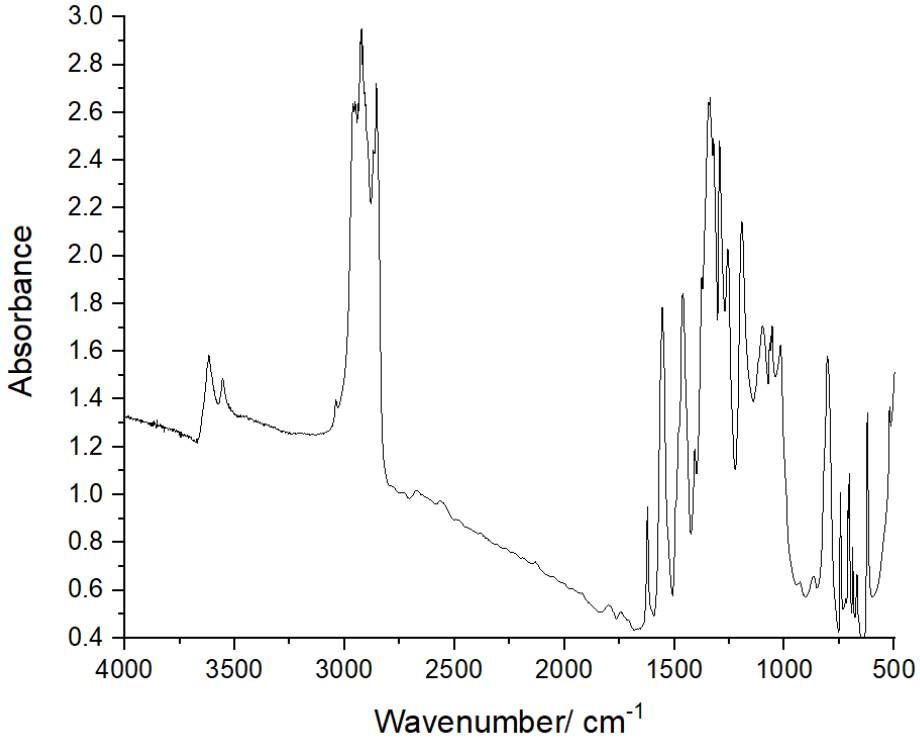

Figure 8.36: *FTIR of $Co(b1mtt)_2.H_2O$ after 2 month water immersion, range 4000-500 cm^{-1}*

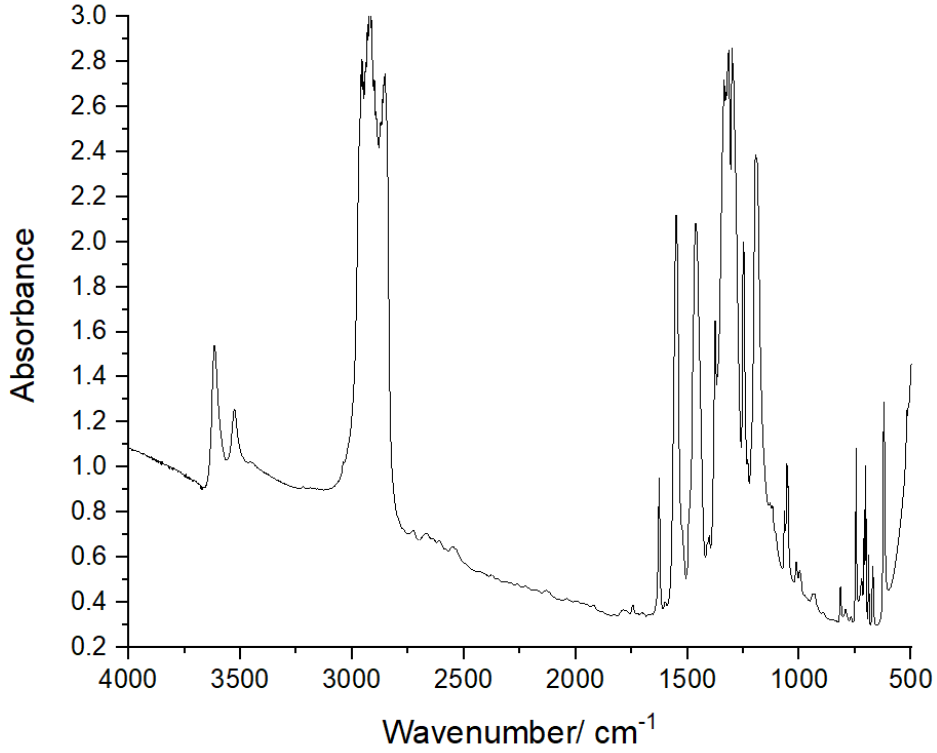

Figure 8.37: *FTIR of Cu(b1mtt)(Cl)(H_2O) , range 4000-500 cm^{-1}*

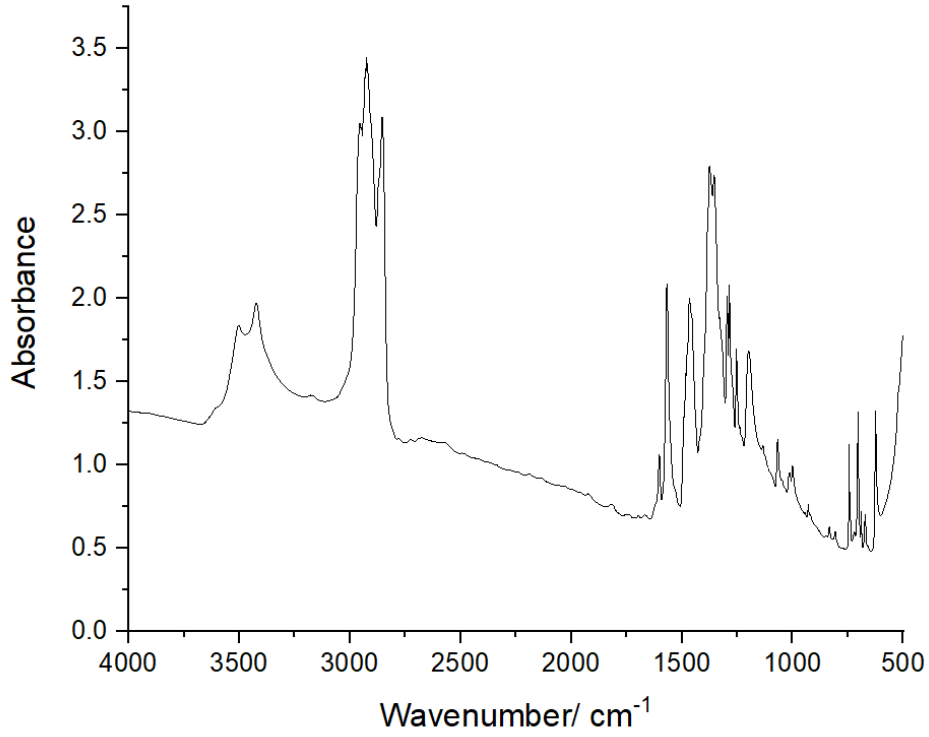

Figure 8.38: *FTIR of Cu(b1mtt)x(4,5-DNI)y(H_2O)z , range 4000-500 cm^{-1}*

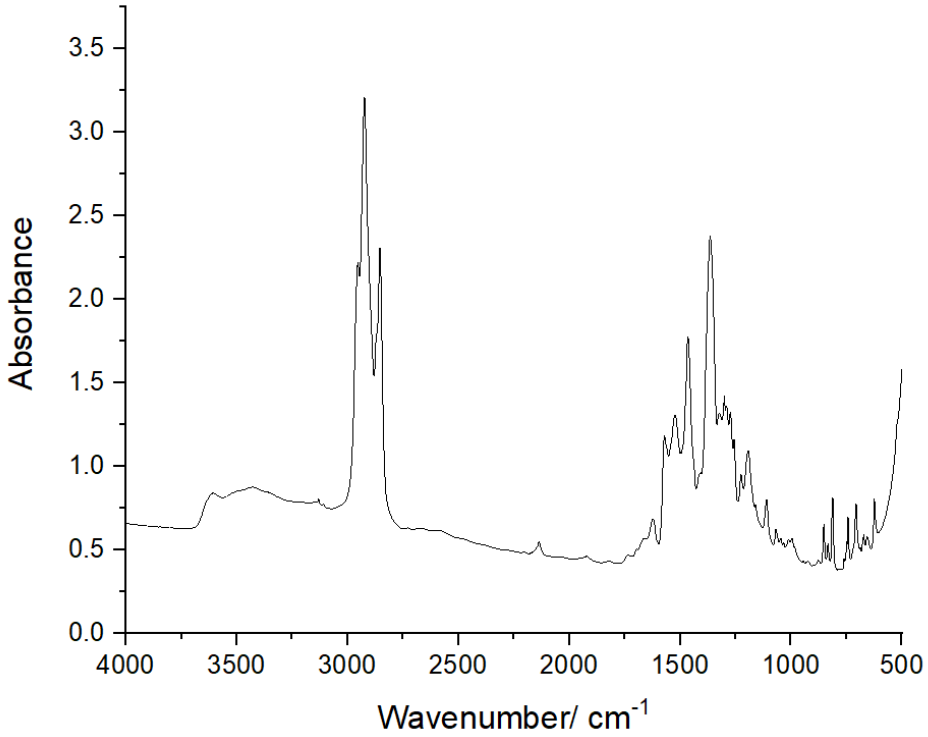

Figure 8.39: *^{1}H NMR of (PPN)(bis(1-methyl-3-nitro-1,2,4-triazol-5-yl)triazenide).3H_2O*

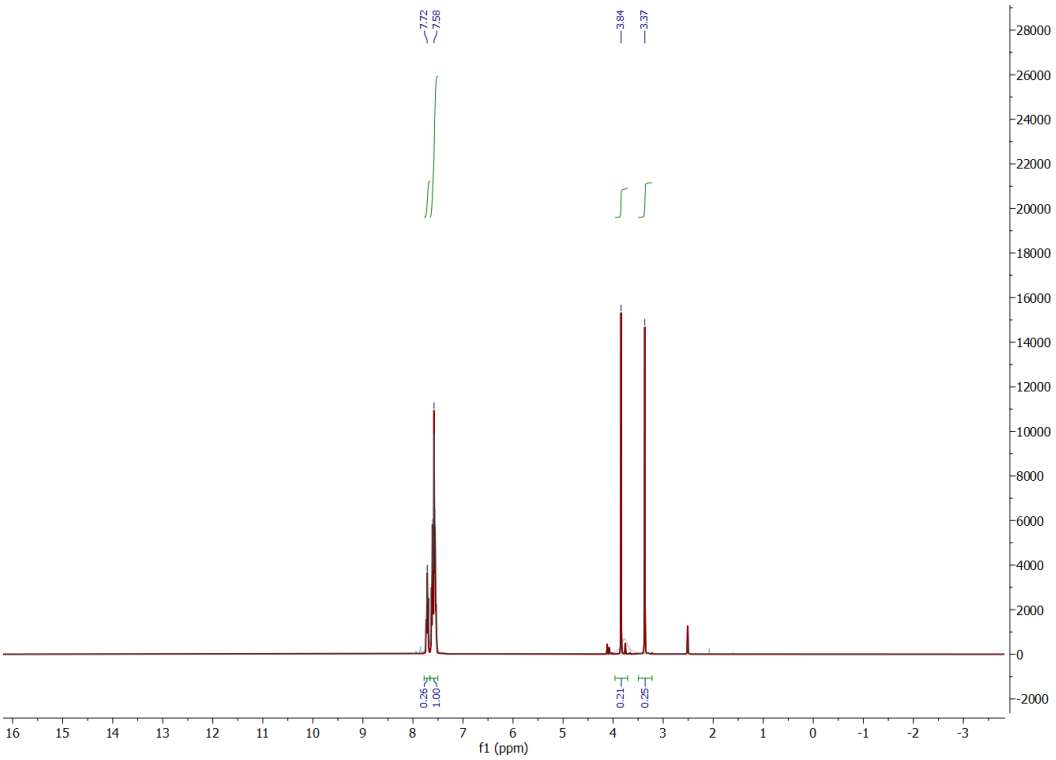

Figure 8.40: *^{13}C NMR of (PPN)(bis(1-methyl-3-nitro-1,2,4-triazol-5-yl)triazenide).3H_2O*

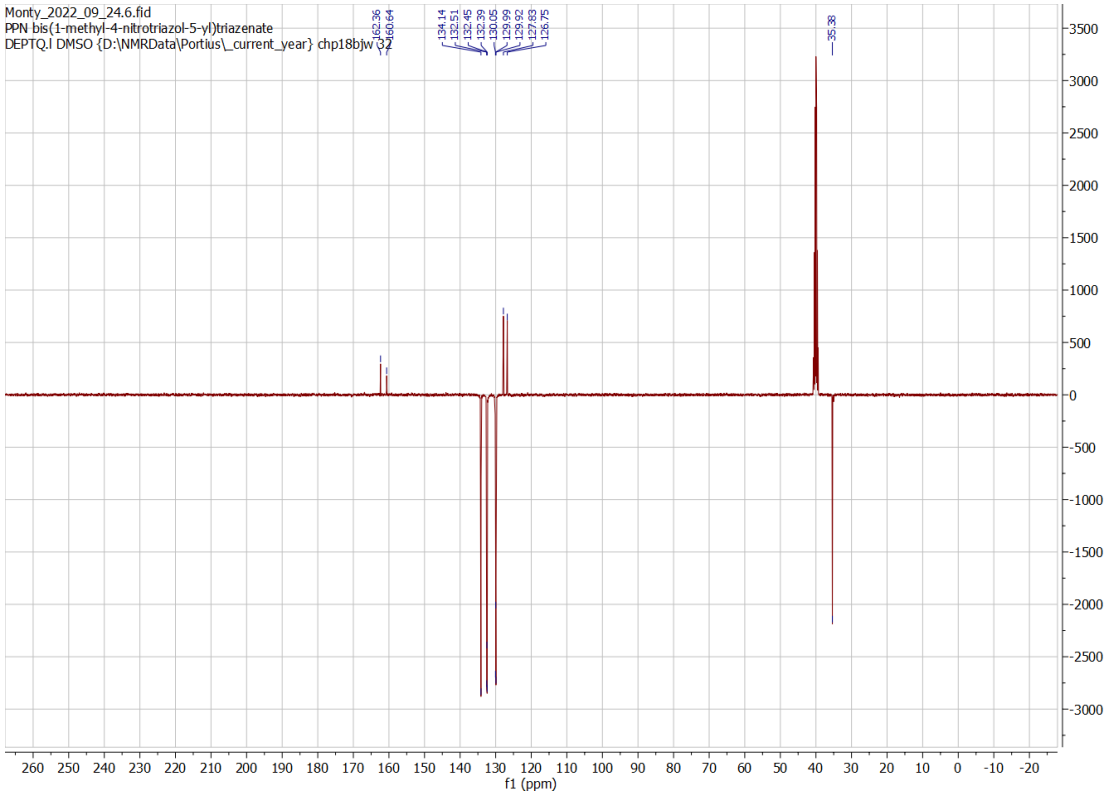

Figure 8.41 FTIR of 2-Azido-4-nitroimidazole, range 4000-500 cm^{-1}

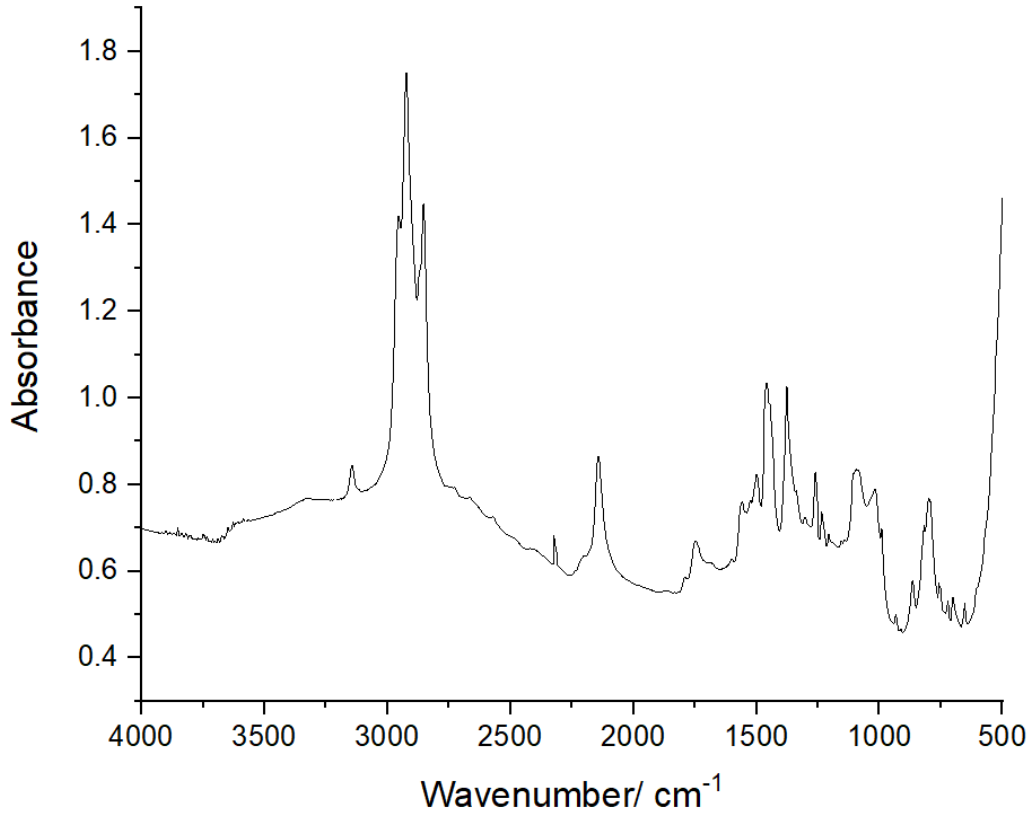

Figure 8.42 ^{1}H NMR of 2-Azido-4-nitroimidazole

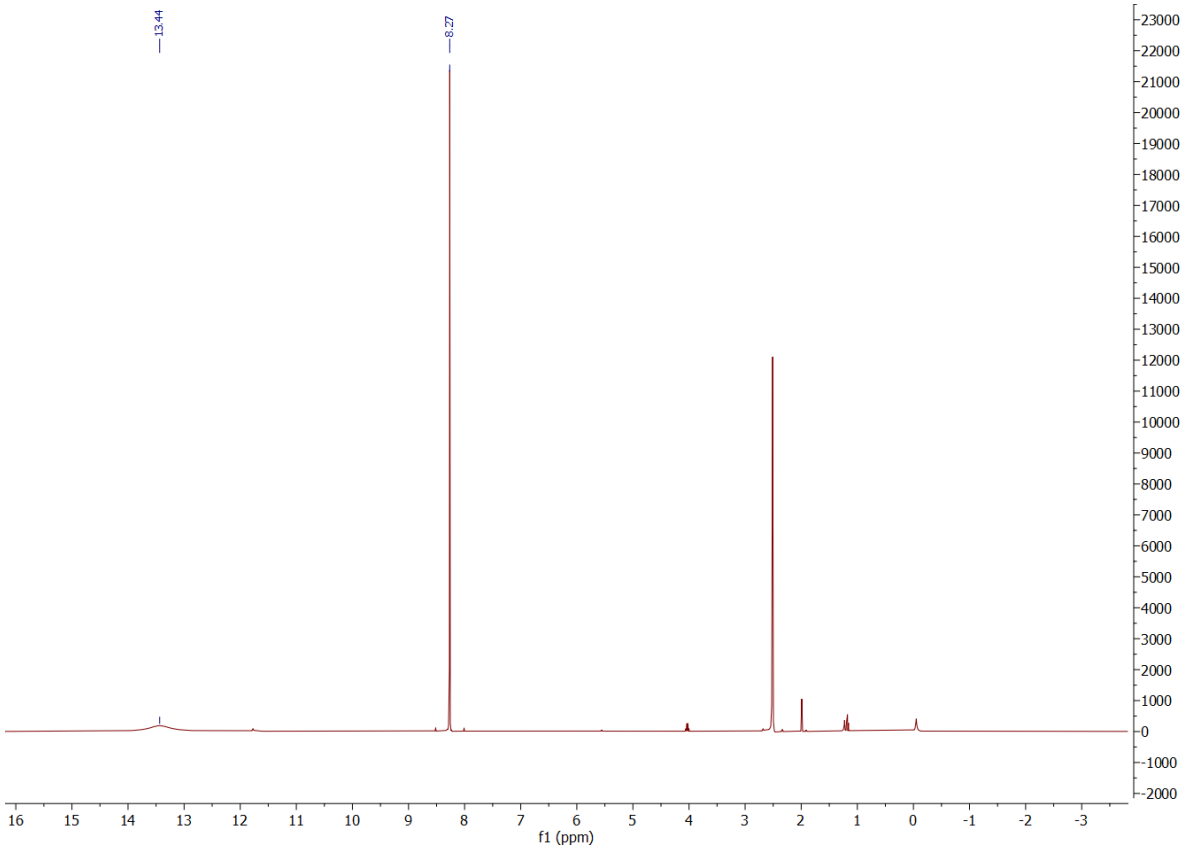

Figure 8.43 ^{13}C NMR of 2-Azido-4-nitroimidazole

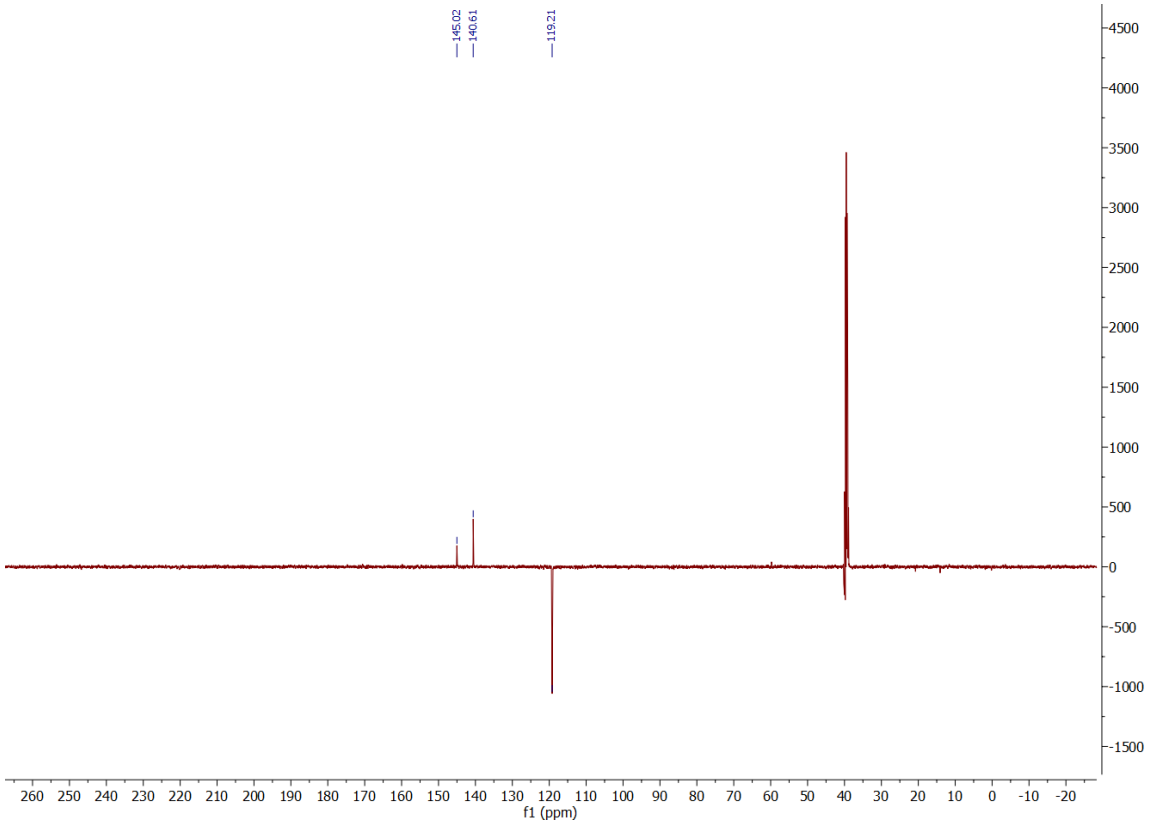

Figure 8.44 FTIR of Potassium-2-azido-4-nitroimidazolate, range 4000-500 cm^{-1}

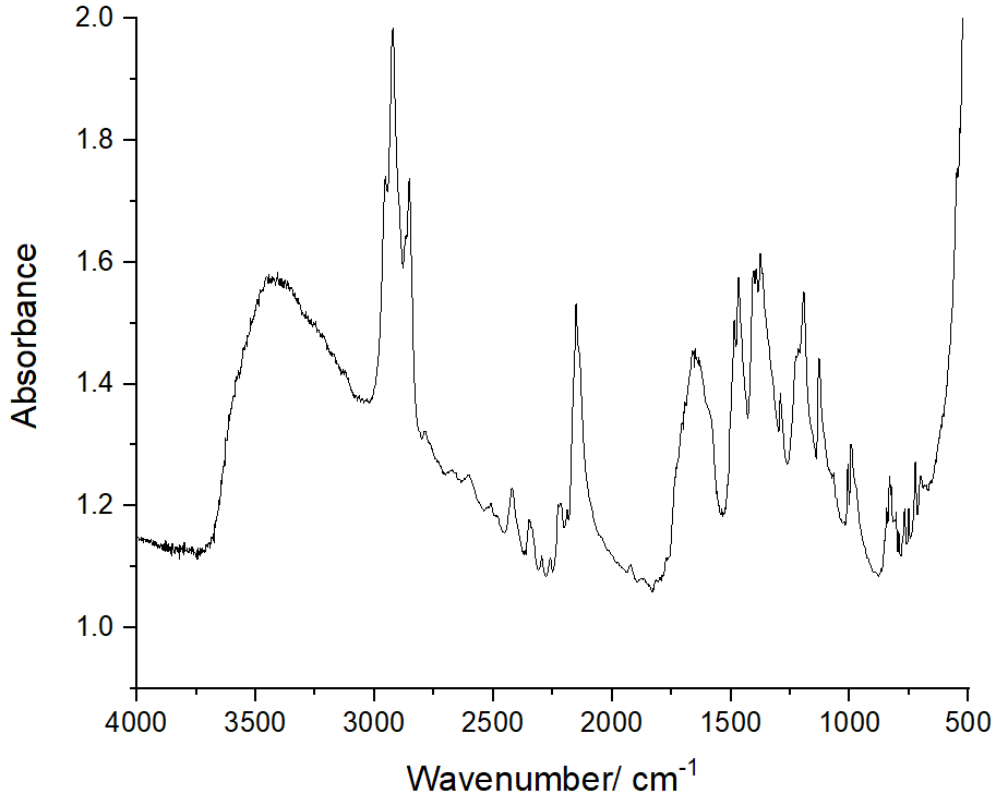

Figure 8.45 ^{1}H NMR of Potassium-2-azido-4-nitroimidazolate

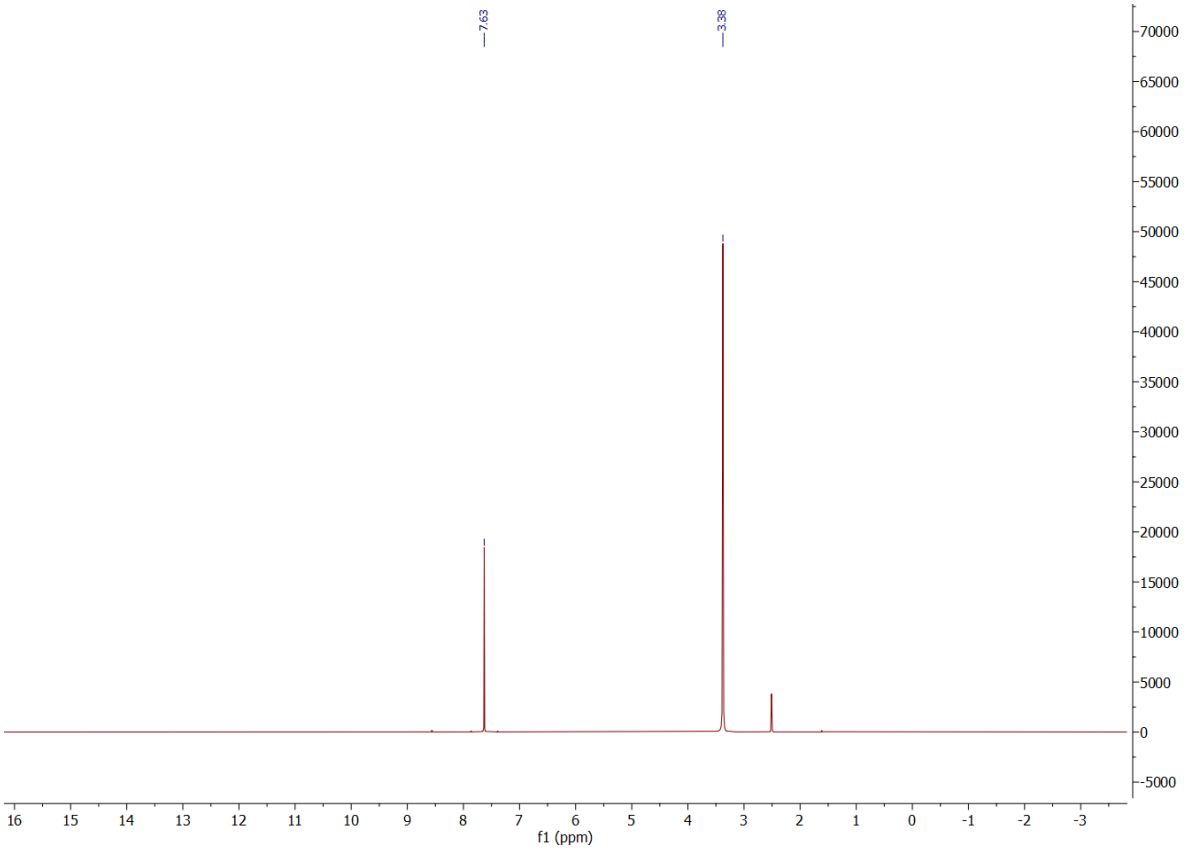

Figure 8.46 ^{13}C NMR of Potassium-2-azido-4-nitroimidazolate

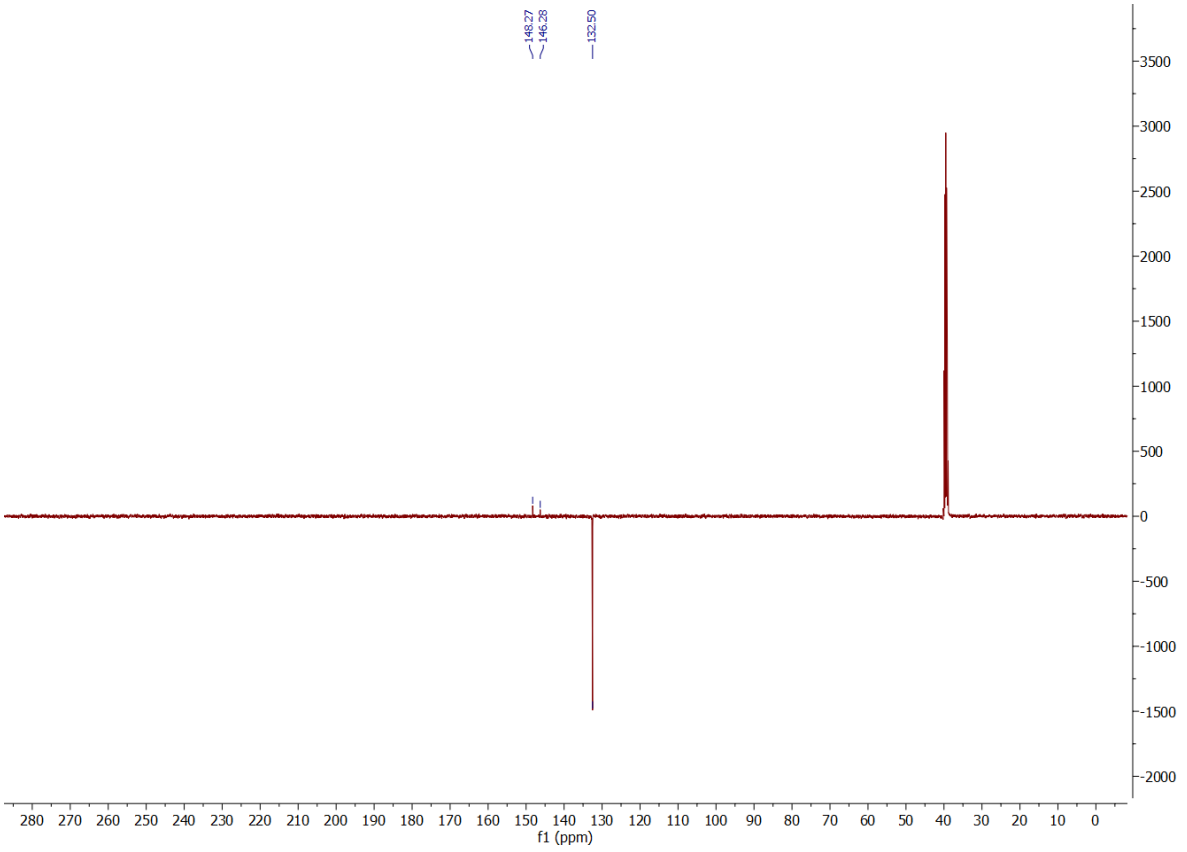

Figure 8.47 FTIR of 3-Azido-4-nitropyrazole.H_2O, range 4000-500 cm^{-1}

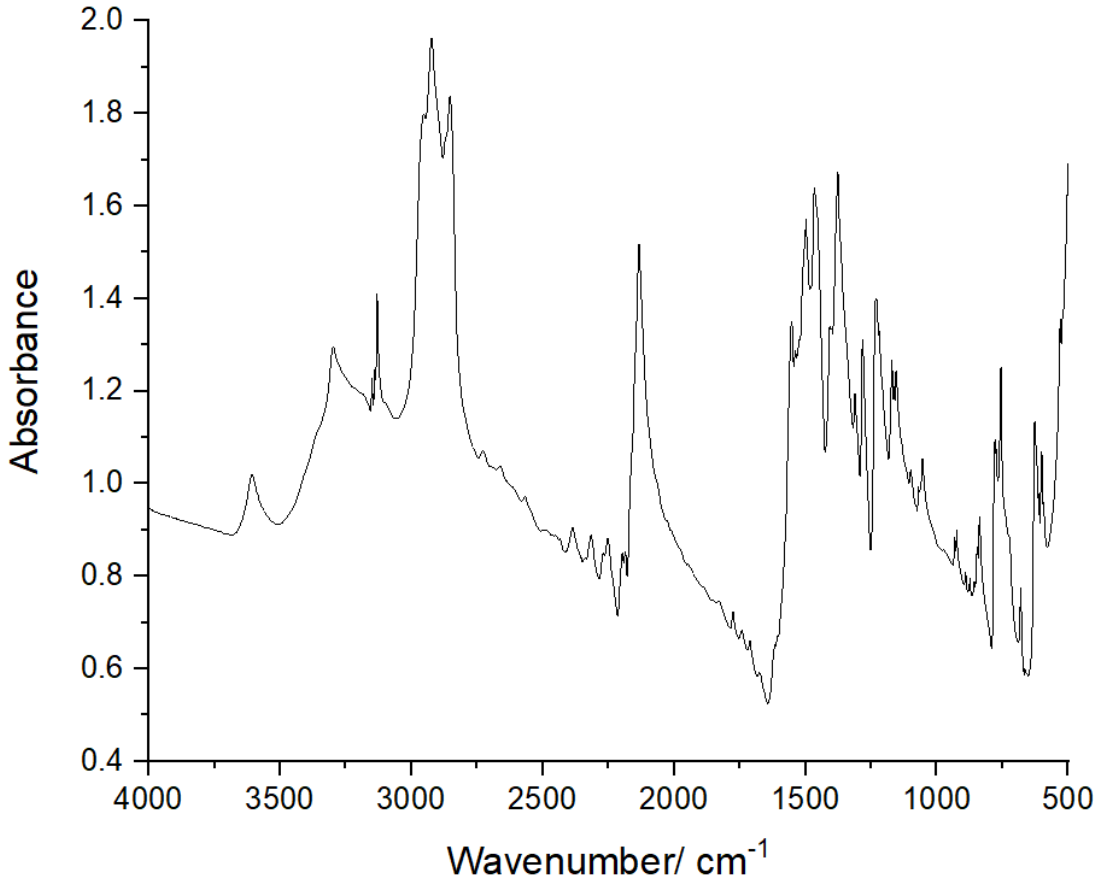

Figure 8.48 ^1H NMR of 3-Azido-4-nitropyrazole.H_2O

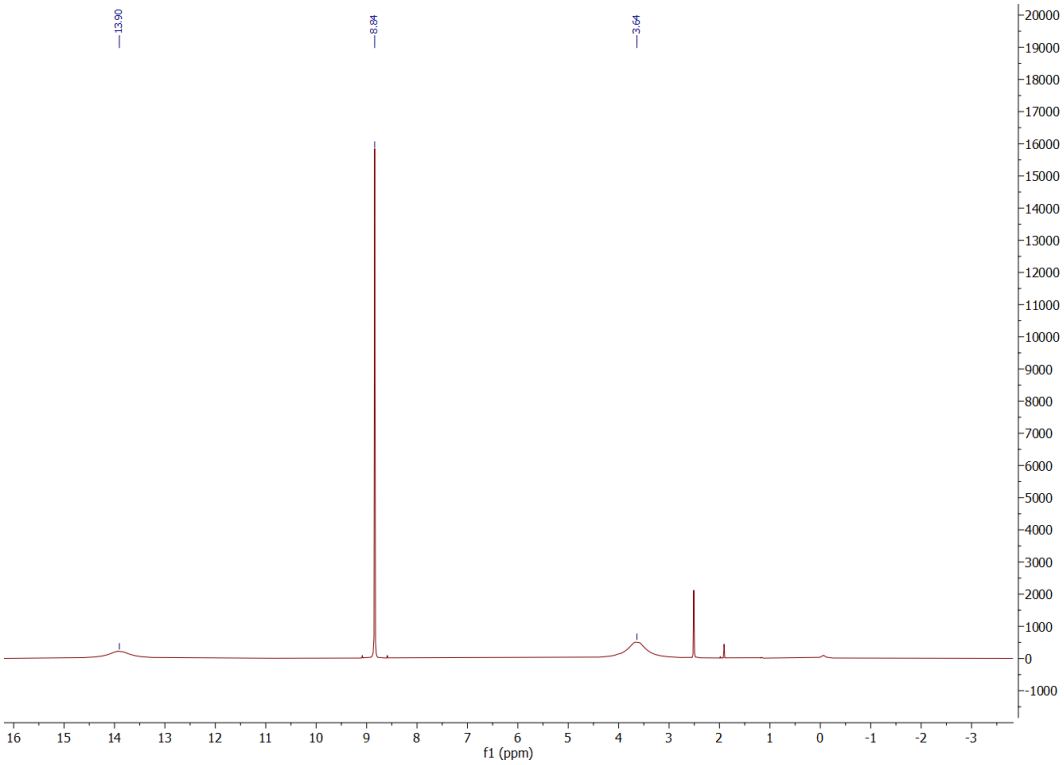

Figure 8.49 ^{13}C NMR of 3-Azido-4-nitropyrazole.H_2O

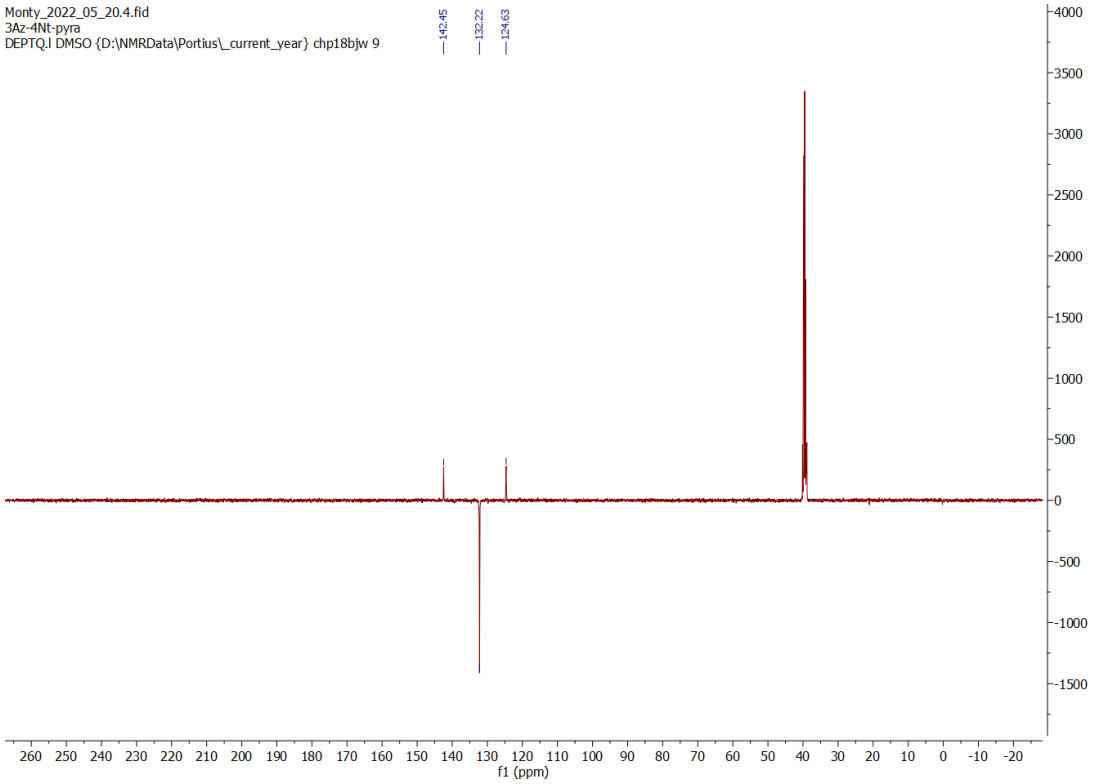

Figure 8.50 FTIR of Potassium-4-nitropyrazolo[1,5 d]tetrazolate.H_2O, range 4000-500 cm^{-1}

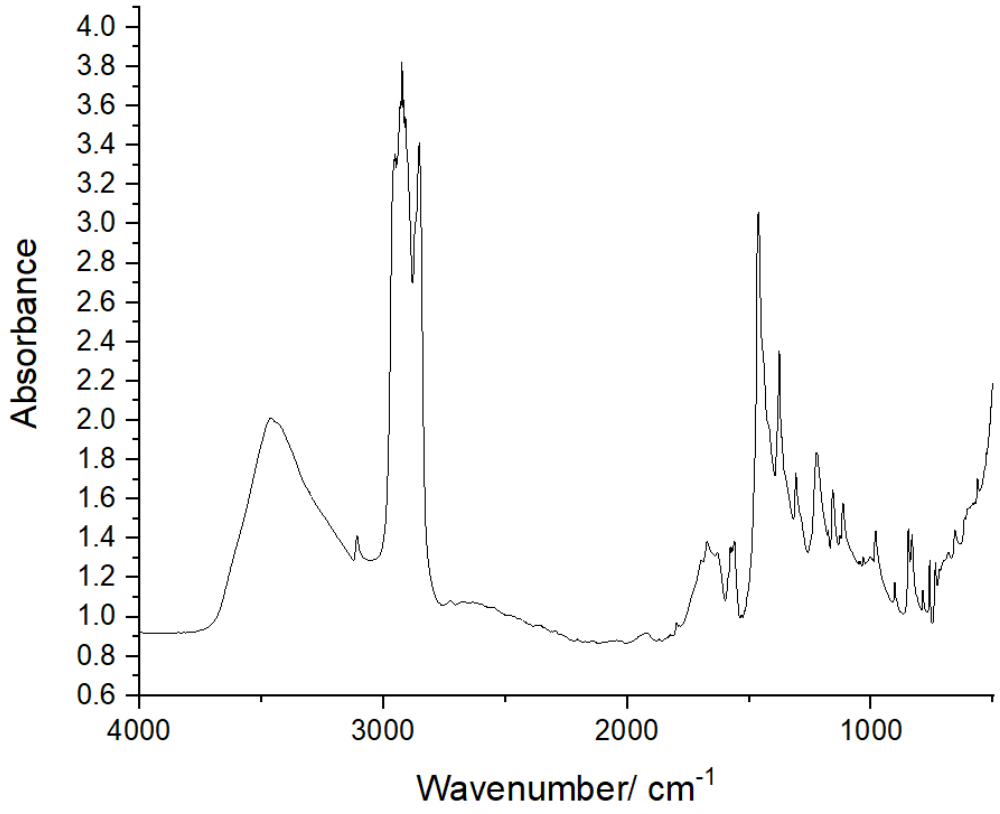

Figure 8.51 ^{1}H NMR of Potassium-4-nitropyrazolo[1,5 d]tetrazolate.H_2O

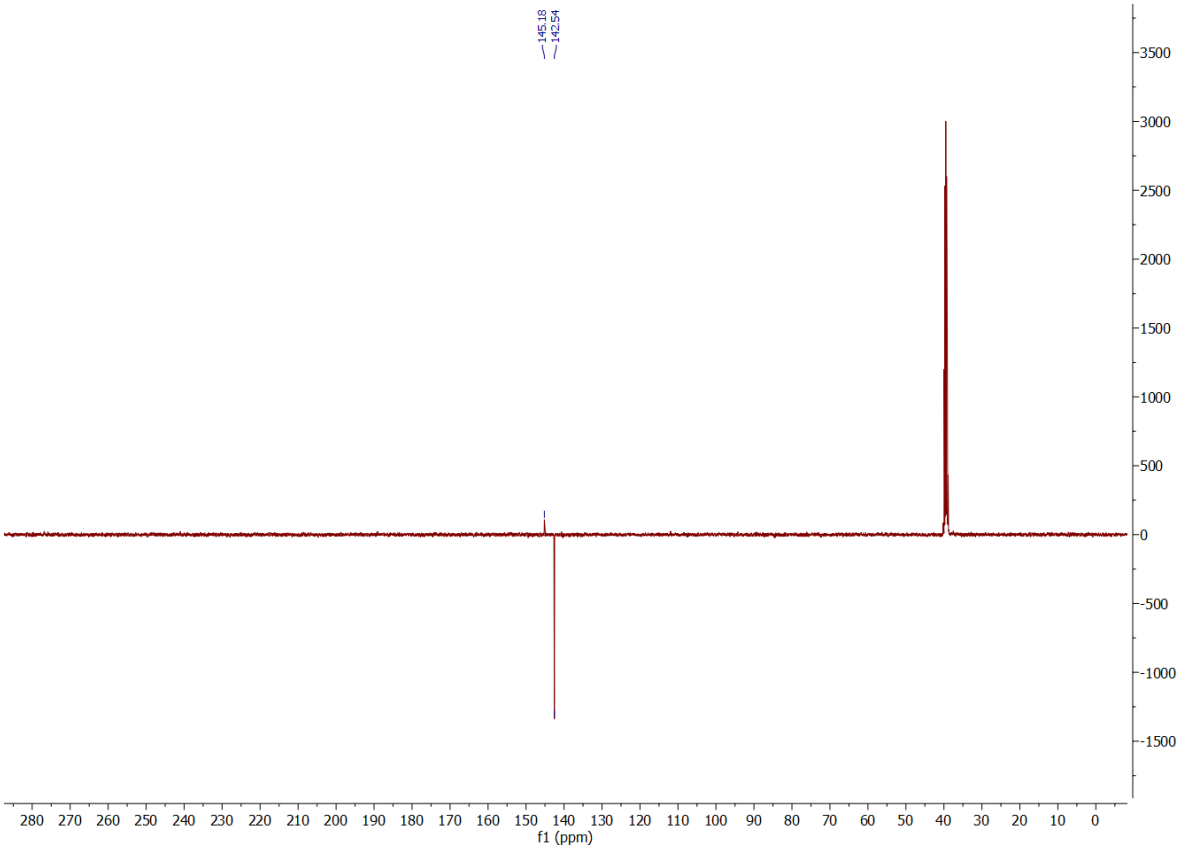

Figure 8.52 ^{13}C NMR of Potassium-4-nitropyrazolo[1,5 d]tetrazolate.H_2O

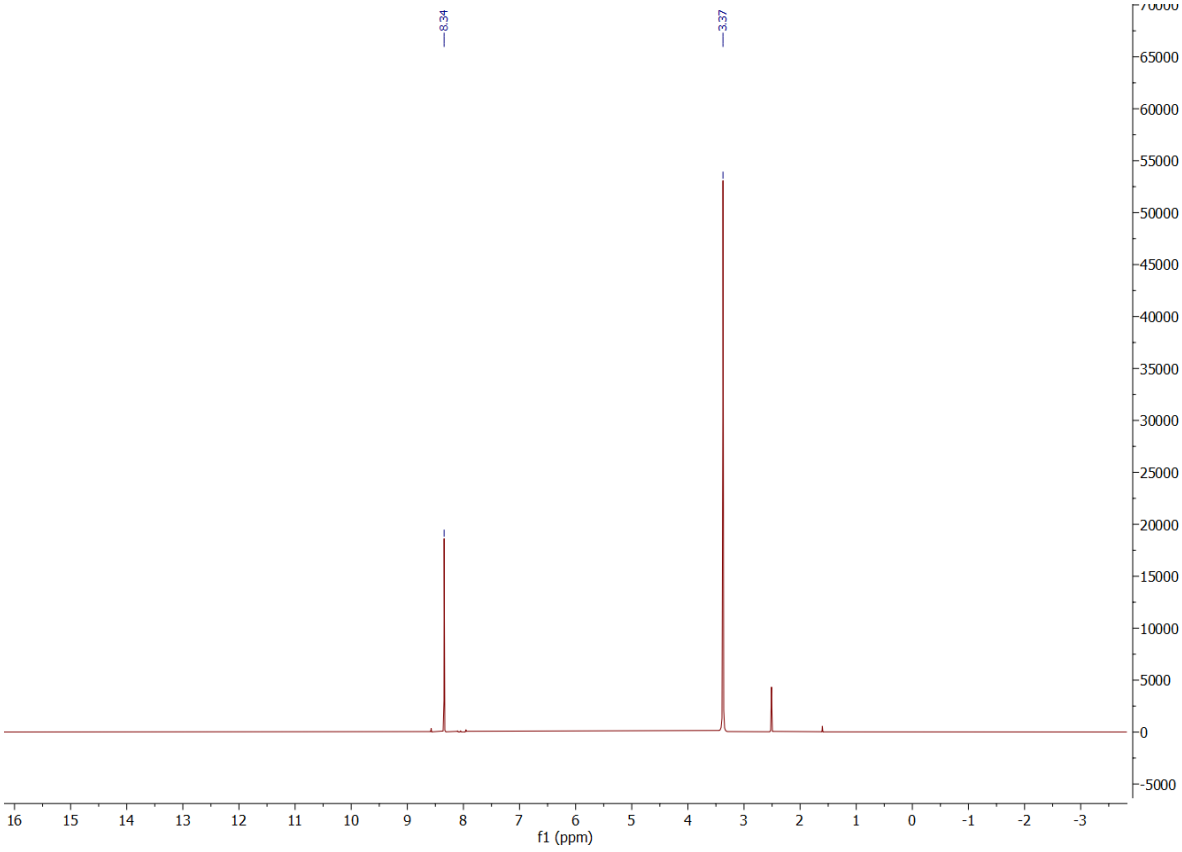

Figure 8.53 FTIR of Sodium-3-azido-4,5-dinitropyrazolate, range 4000-500 cm^{-1}

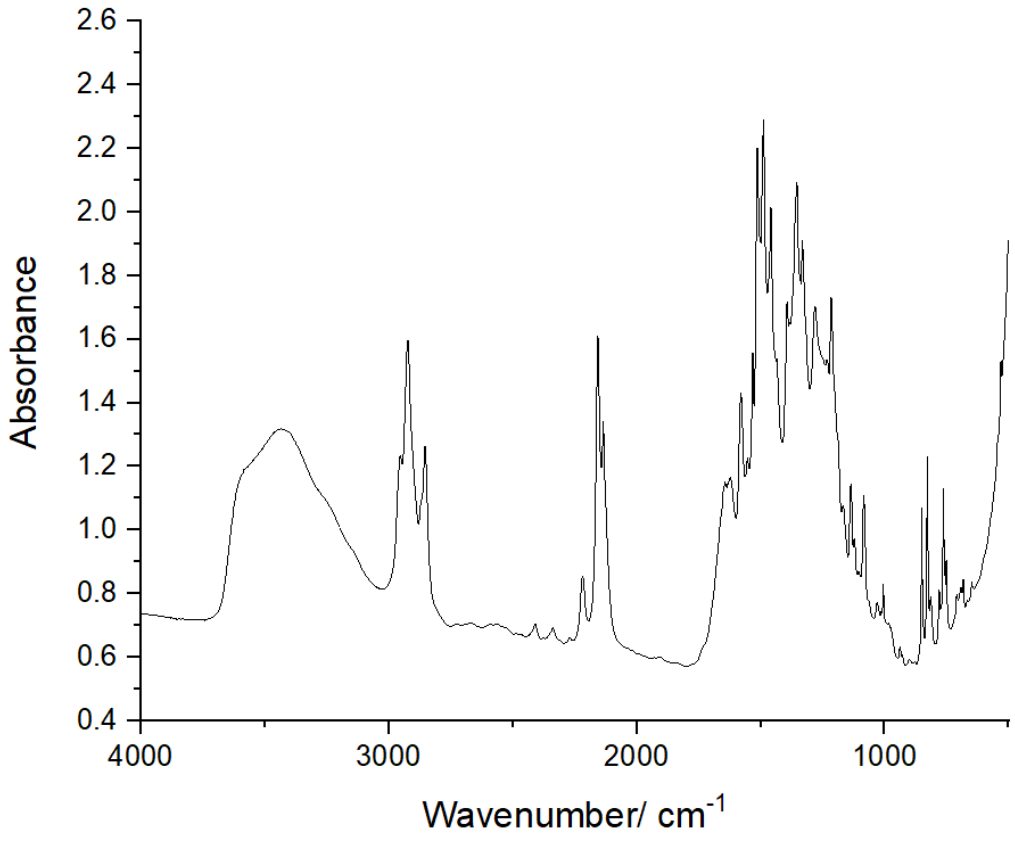

Figure 8.54 DSC calorigram of $Cu_4(DNT)_3Cl$

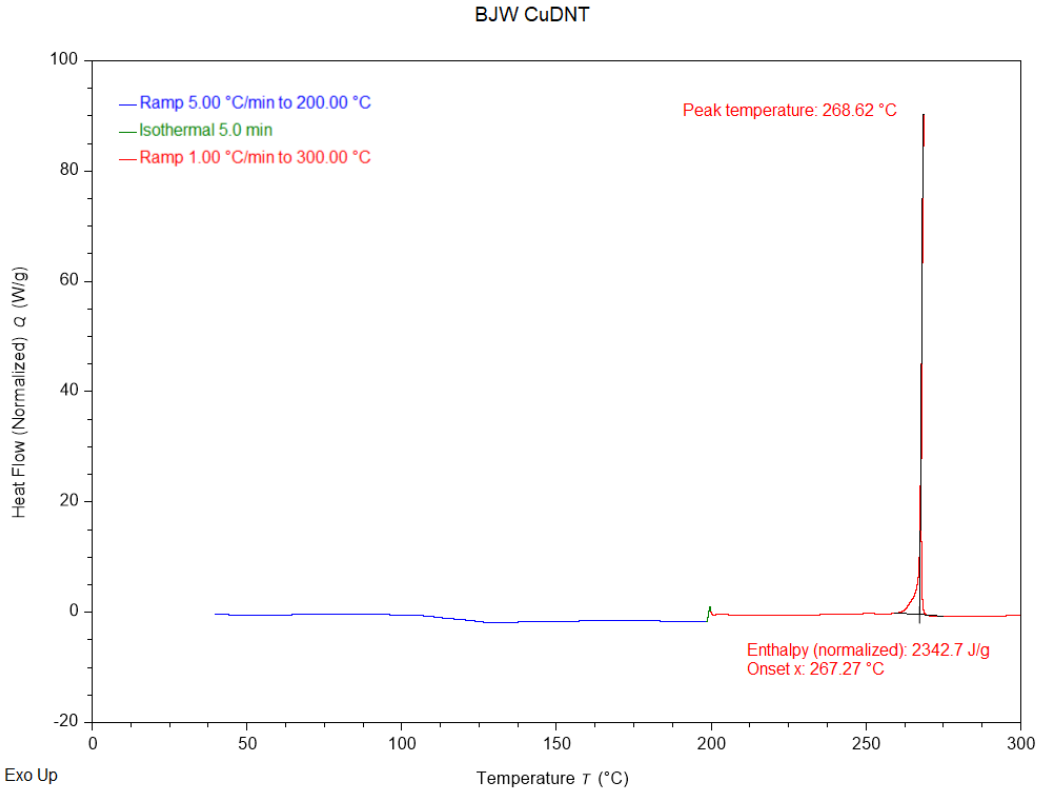

Figure 8.55 DSC calorigram of Cu_2-TBI

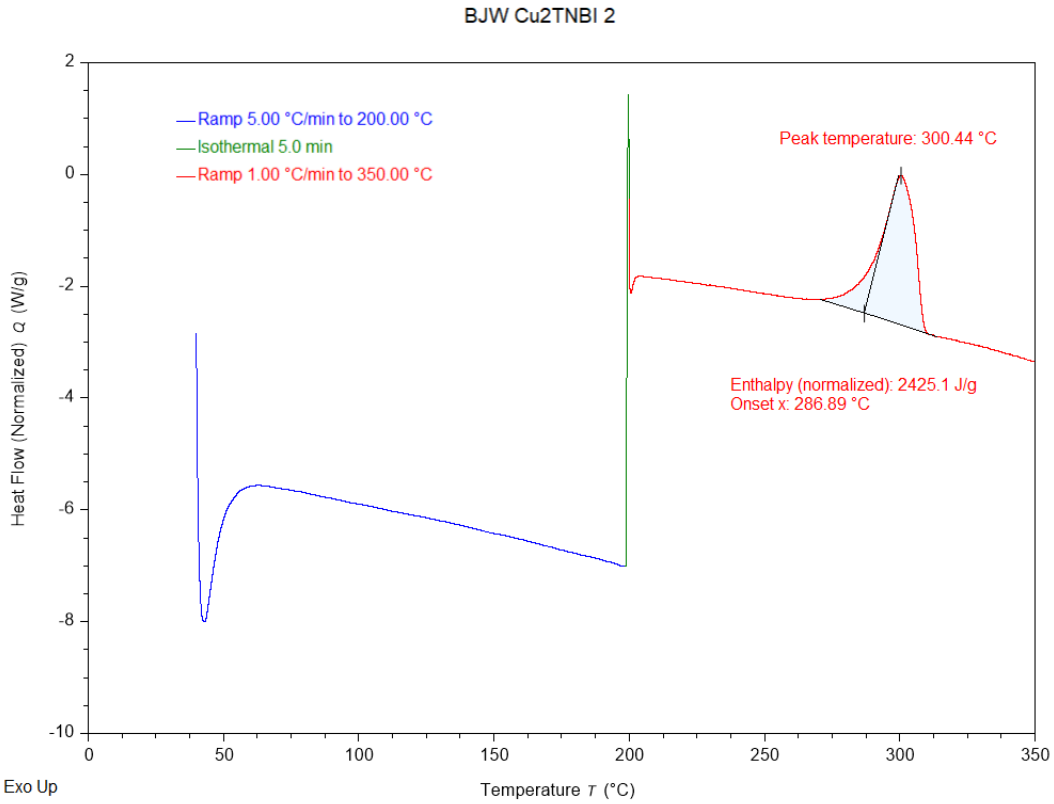

Figure 8.56 DSC calorigram of Cu-ADNP

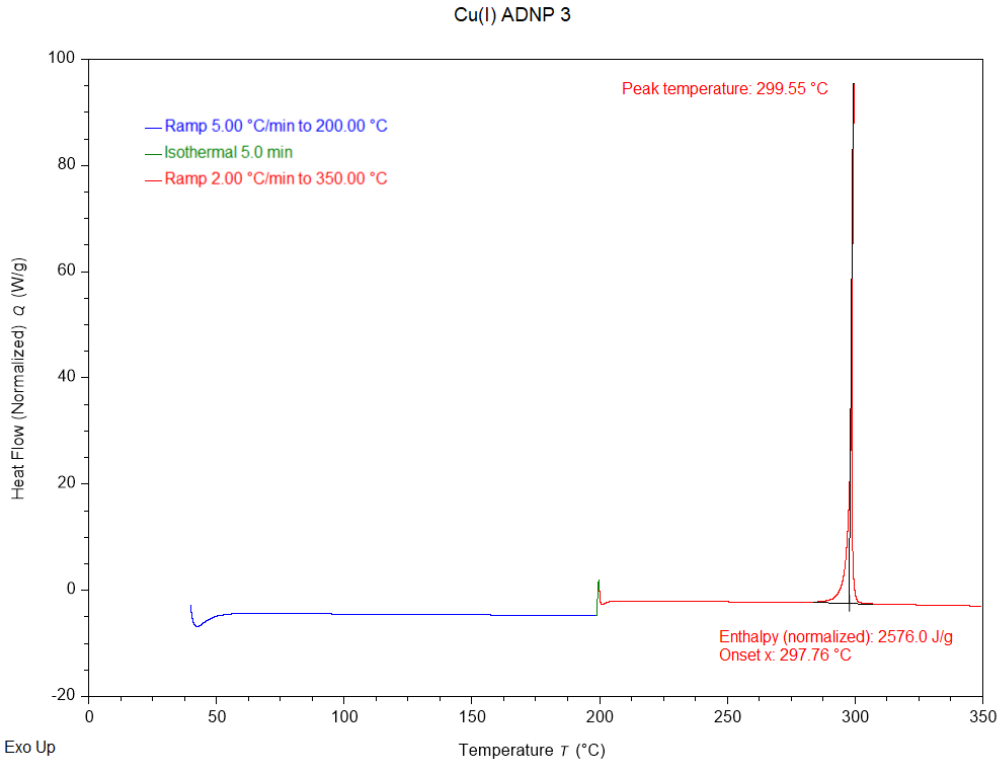

Figure 8.57 DSC calorigram of Cu-3,5-DNP

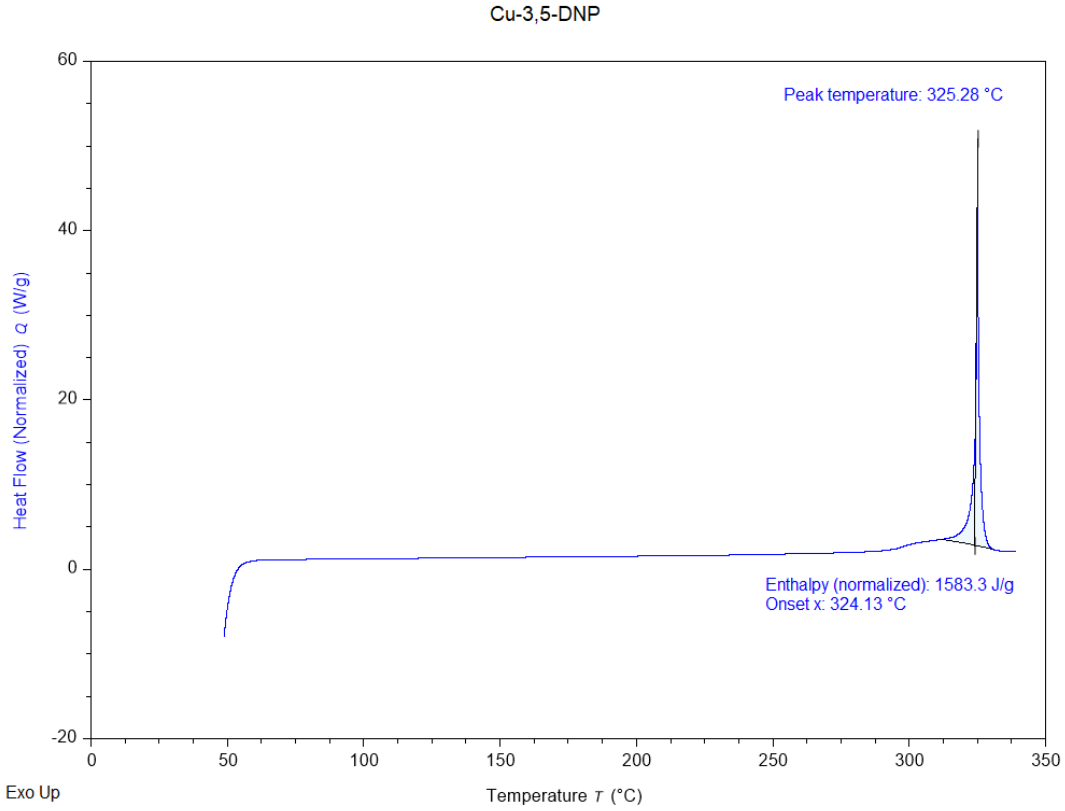

Figure 8.58 DSC calorigram of Cu-2,4-DNI

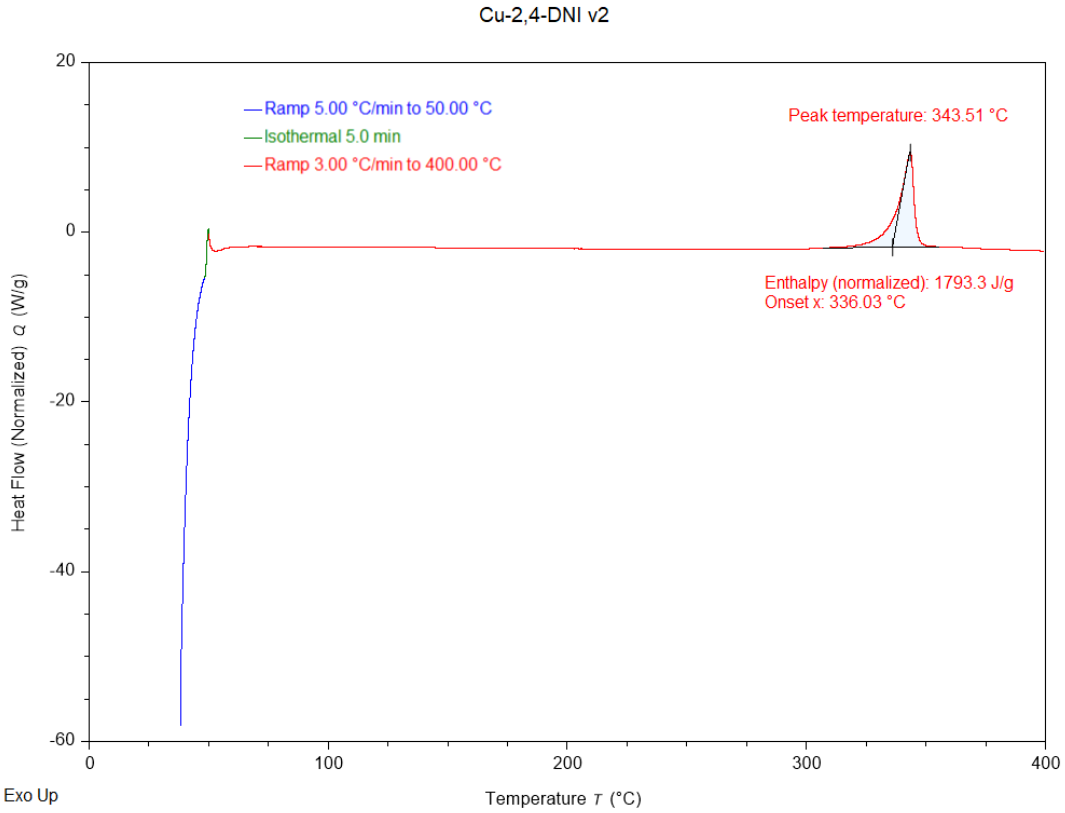

Figure 8.59 DSC calorigram of Cu-4,5-DNI

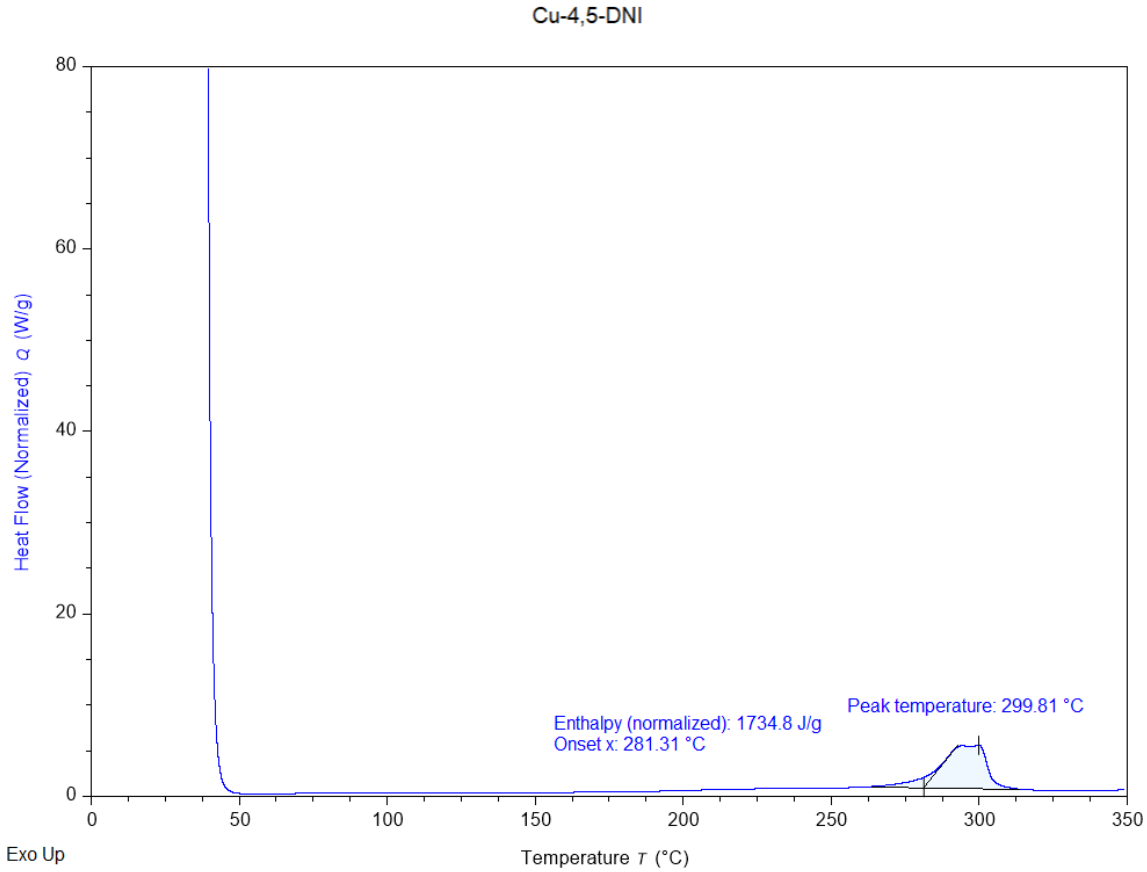

Figure 8.60 DSC calorigram of $Fe(B1MTT)_2.(CH_3)_2CO$

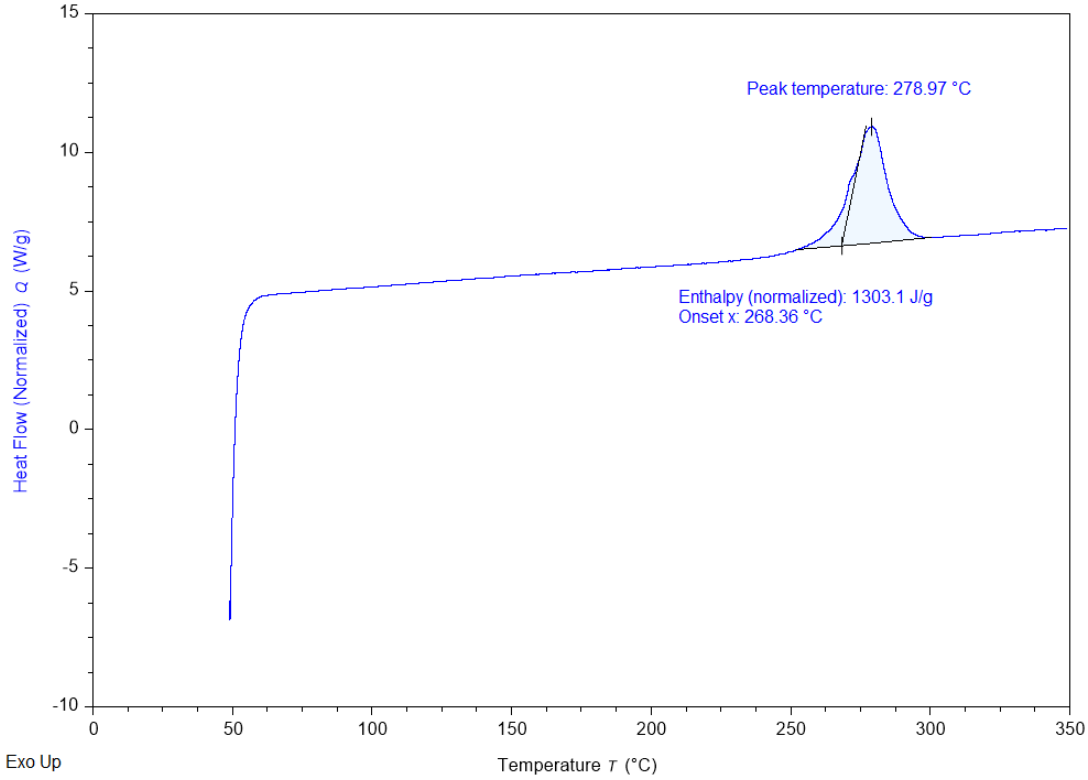

Figure 8.61 DSC calorigram of $Co(B1MTT)_2.H_2O$

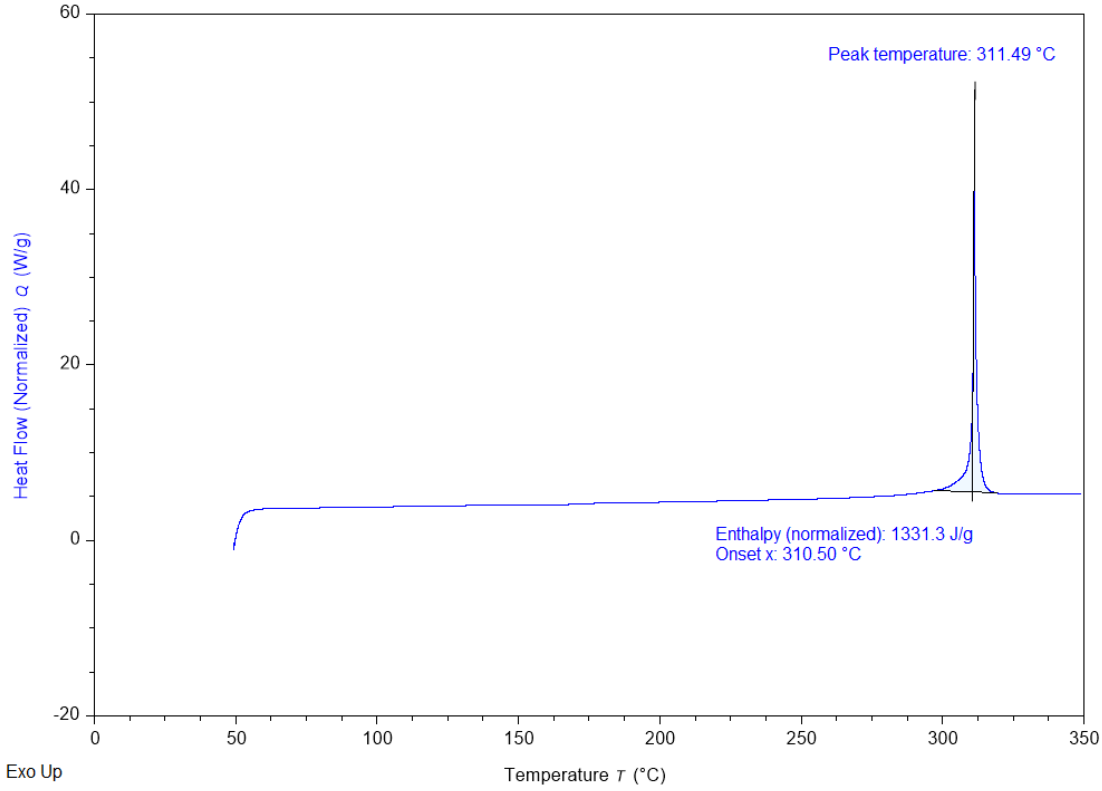

Figure 8.62 DSC calorigram of $Co(B1MTT)_2.H_2O$

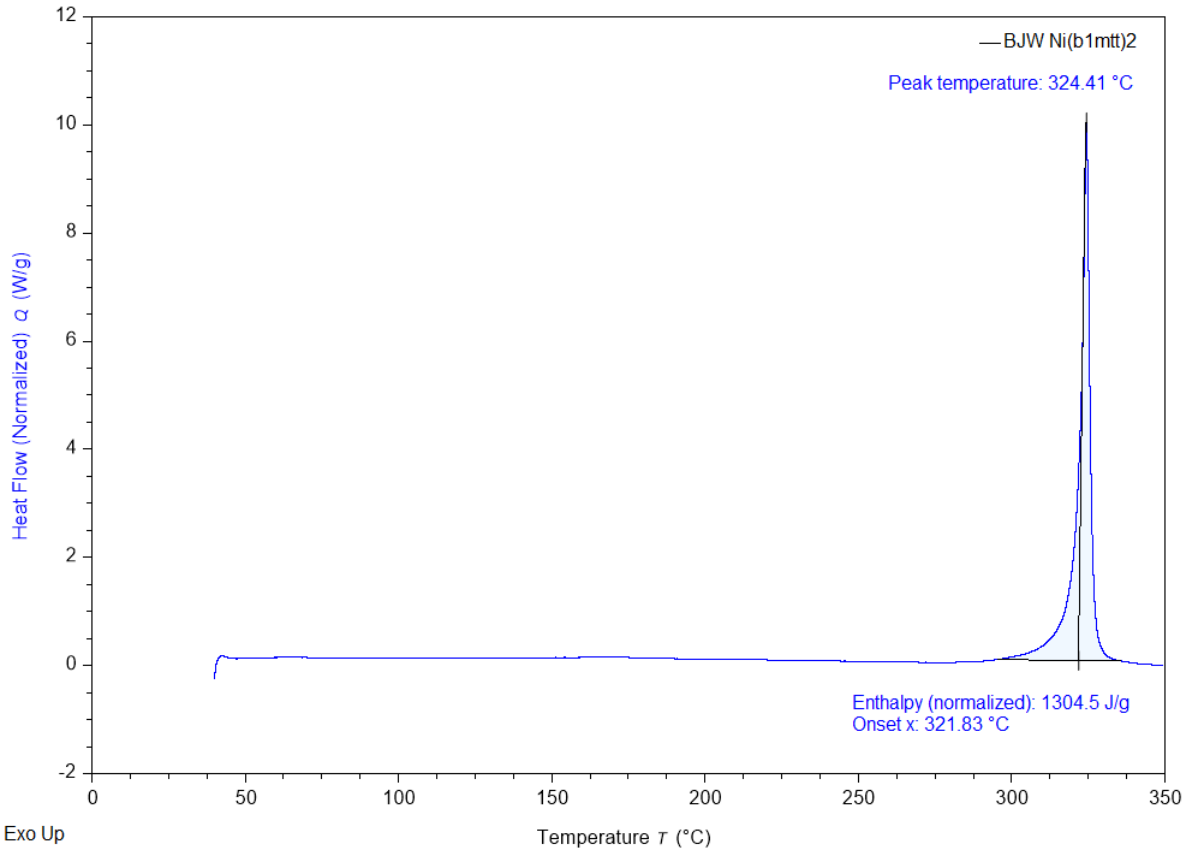

Figure 8.63 DSC calorigram of $Pb(B1MTT)_2$

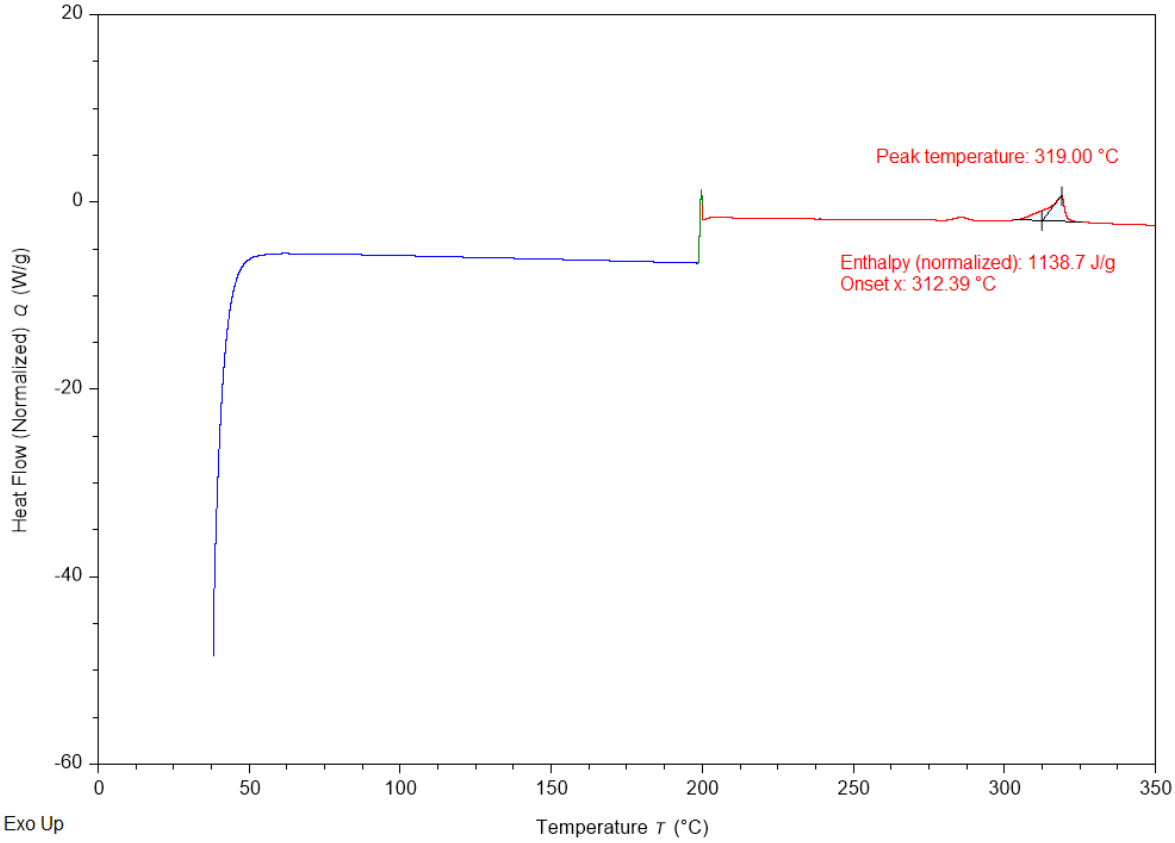

Figure 8.64 DSC calorigram of $Zn(B1MTT)_2$

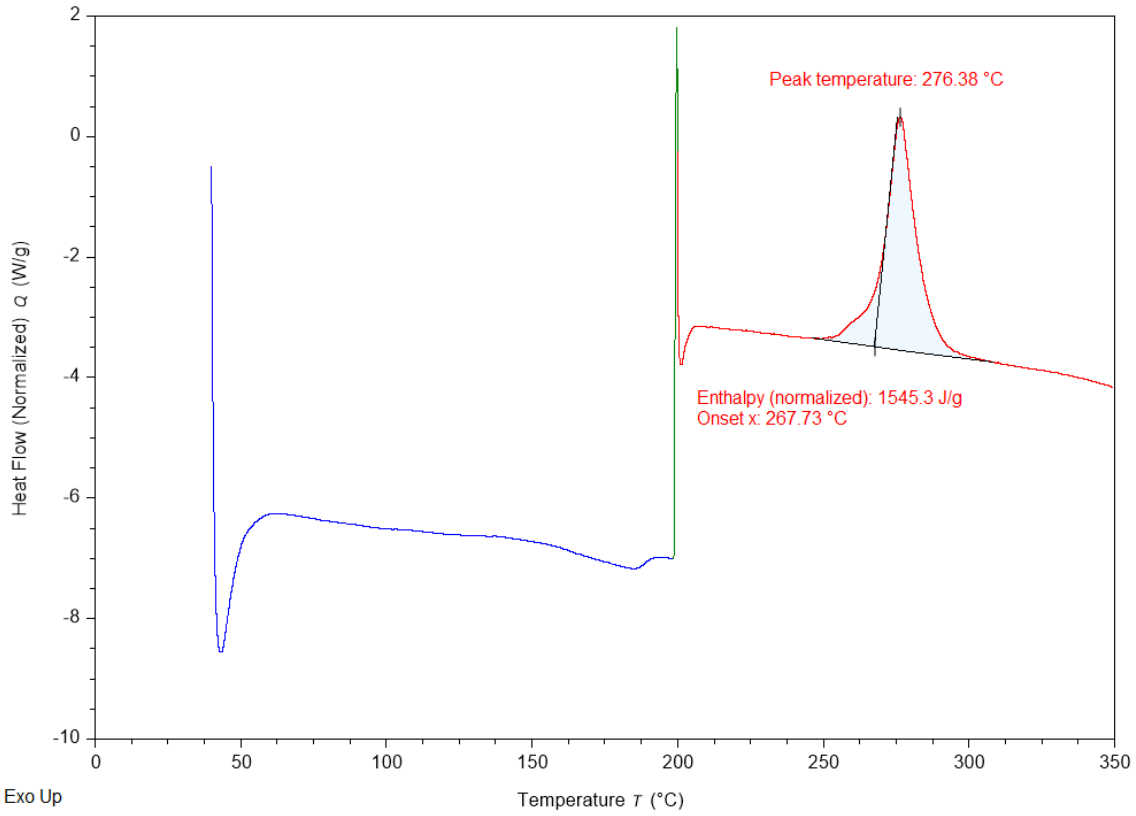

Figure 8.65 DSC calorigram of Cu(B1MTT)(Cl)(H_2O)

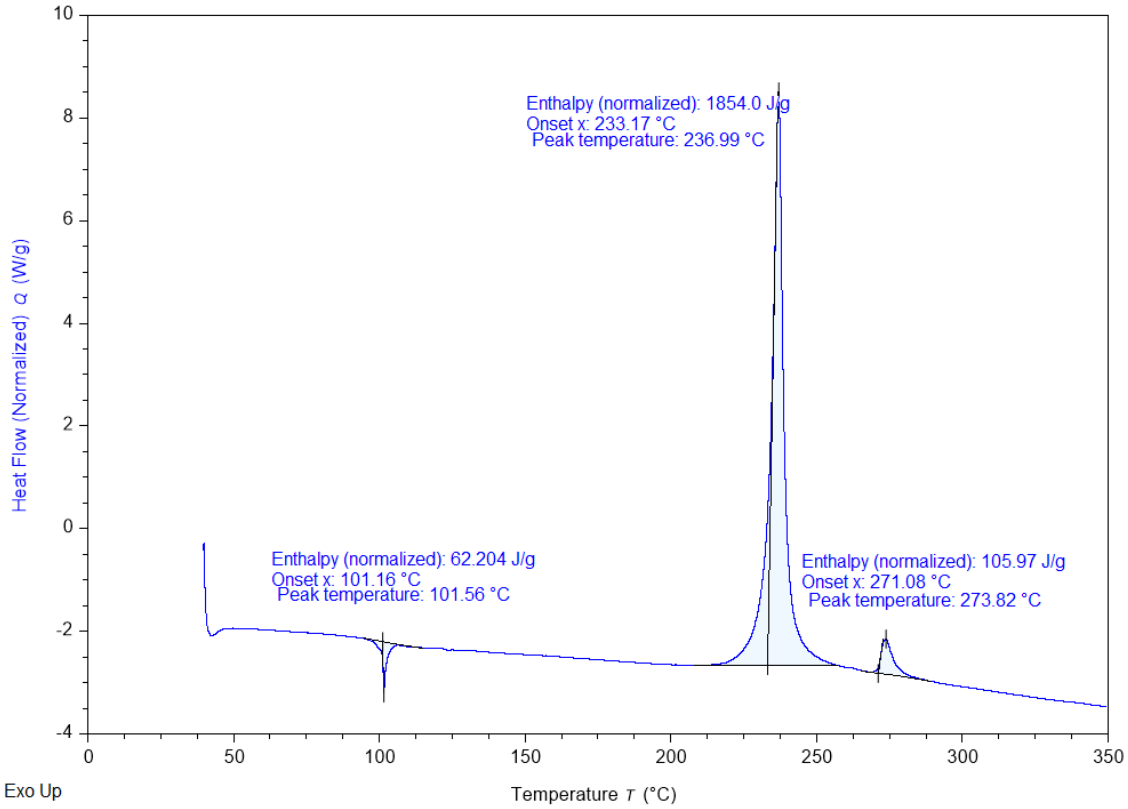

Figure 8.66 DSC calorigram of PPN(B1MTT).MeCN

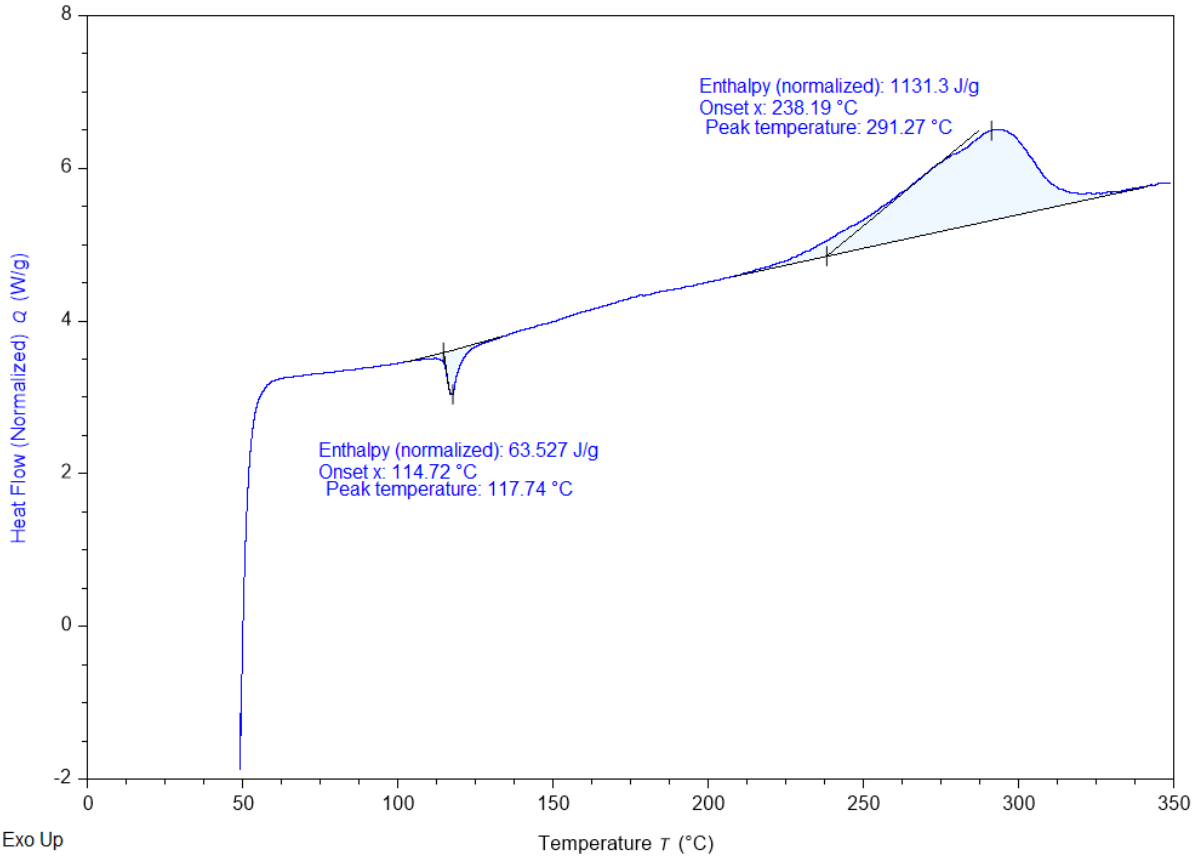

Figure 8.67 DSC calorigram of PPN(B1M3NTT).3H_2O

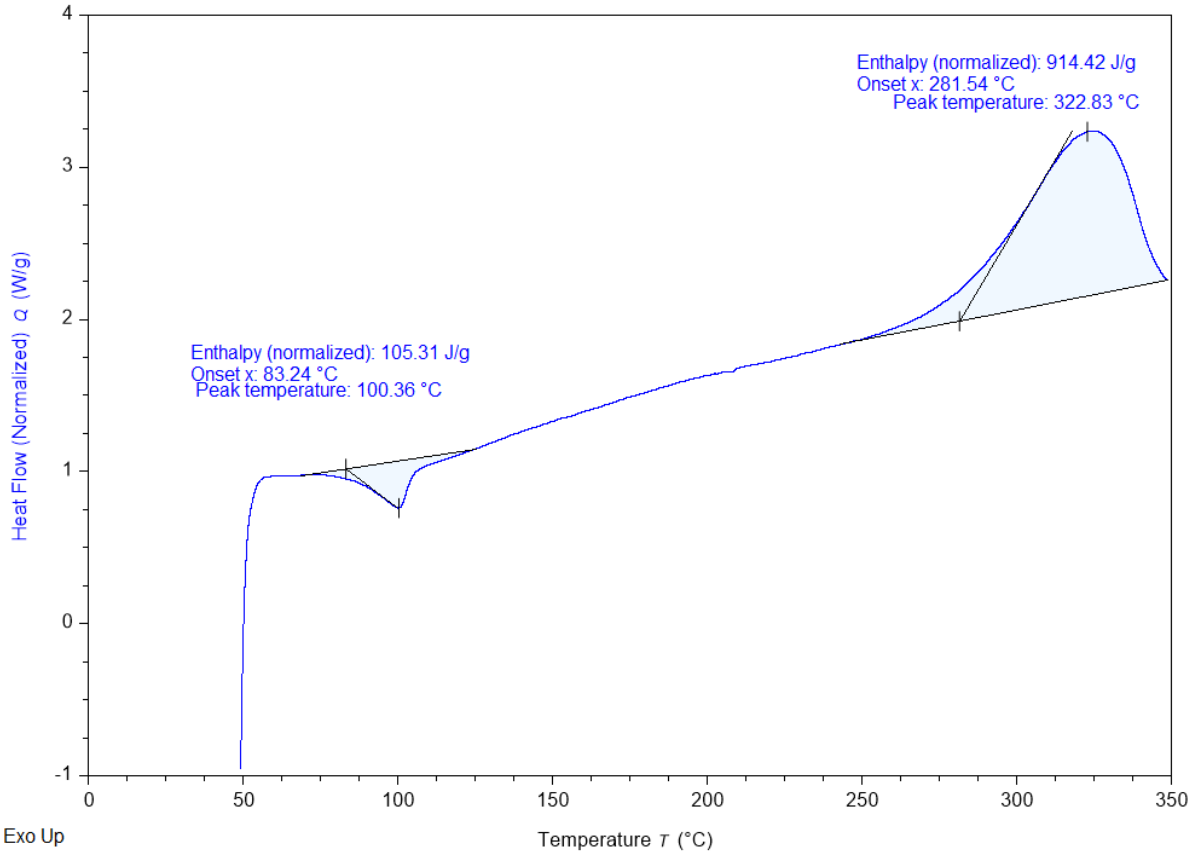

9. X-ray Data Tables

9.1 Crystal data for $Cu_3(NT)_2Cl$, DBX-X

Empirical formula	$C_2ClCu_3N_{10}O_4$
Formula weight	454.19
Temperature/K	100.0(3)
Crystal system	monoclinic
Space group	$P2_1/c$
a/Å	10.8980(10)
b/Å	9.2377(9)
c/Å	10.3680(10)
α/°	90
β/°	100.493(10)
γ/°	90
Volume/Å^3	1026.32(17)
Z	4
ρ_{calc}g/cm^3	2.939
μ/mm^{-1}	10.046
F(000)	872.0
Crystal size/mm^3	0.01 × 0.01 × 0.01
Radiation	CuKα (λ = 1.54184)
2Θ range for data collection/°	8.252 to 152.288
Index ranges	$-10 \leq h \leq 13$, $-11 \leq k \leq 11$, $-11 \leq l \leq 12$
Reflections collected	4254
Independent reflections	2060 [R_{int} = 0.0827, R_{sigma} = 0.1114]
Data/restraints/parameters	2060/84/181
Goodness-of-fit on F^2	1.066
Final R indexes [I>=2σ (I)]	R_1 = 0.0569, wR_2 = 0.1200
Final R indexes [all data]	R_1 = 0.1046, wR_2 = 0.1429
Largest diff. peak/hole / e Å^{-3}	1.01/-0.93

9.2 Crystal data for $Cu_4(DNT)_3Cl$

Empirical formula	$Cu_4ClC_6N_{15}O_{12}$
Formula weight	N/A
Temperature/K	N/A
Crystal system	hexagonal
Space group	$P6_3$
a/Å	11.2866(5)
b/Å	11.2866(5)
c/Å	9.0555(6)
α/°	90
β/°	90
γ/°	120
Volume/$Å^3$	999.00(11)
Z	1
$\rho_{calc}g/cm^3$	N/A
μ/mm^{-1}	N/A
F(000)	N/A
Crystal size/mm^3	N/A × N/A × N/A
Radiation	N/A (λ = N/A)
2Θ range for data collection/°	N/A to N/A
Index ranges	$100 \leq h \leq -100$, $100 \leq k \leq -100$, $100 \leq l \leq -100$
Reflections collected	N/A
Independent reflections	N/A [R_{int} = N/A, R_{sigma} = N/A]
Data/restraints/parameters	N/A/N/A/N/A
Goodness-of-fit on F^2	N/A
Final R indexes [I>=2σ (I)]	R_1 = N/A, wR_2 = N/A
Final R indexes [all data]	R_1 = N/A, wR_2 = N/A
Largest diff. peak/hole / e $Å^{-3}$	N/A/N/A

NB: Data table is incomplete due to method of collection (See 3.4 Experimental)

9.3 Crystal data for Cu(ADNP)

Empirical formula	$C_{4.25}Cu_{1.5}N_{7.75}O_6$
Formula weight	350.93
Temperature/K	107.17
Crystal system	triclinic
Space group	P1
a/Å	8.2914(8)
b/Å	10.3466(10)
c/Å	12.5252(12)
α/°	112.620(5)
β/°	104.719(7)
γ/°	90.112(6)
Volume/Å^3	953.31(16)
Z	4
ρ_{calc}g/cm^3	2.445
μ/mm^{-1}	4.931
F(000)	685.0
Crystal size/mm^3	? × ? × ?
Radiation	CuKα (λ = 1.54178)
2Θ range for data collection/°	7.956 to 133.652
Index ranges	$-9 \leq h \leq 9$, $-12 \leq k \leq 12$, $-14 \leq l \leq 14$
Reflections collected	7866
Independent reflections	4909 [R_{int} = 0.1074, R_{sigma} = 0.1569]
Data/restraints/parameters	4909/3/260
Goodness-of-fit on F^2	1.161
Final R indexes [I>=2σ (I)]	R_1 = 0.2497, wR_2 = 0.4912
Final R indexes [all data]	R_1 = 0.2612, wR_2 = 0.5013
Largest diff. peak/hole / e Å^{-3}	3.32/-4.32
Flack parameter	0.39(10)

9.4 Crystal data for Cu(b1mtt)(Cl)(H_2O)

Empirical formula	$C_4H_8ClCuN_{11}O$
Formula weight	325.20
Temperature/K	298.73
Crystal system	orthorhombic
Space group	Pbca
a/Å	15.0488(7)
b/Å	7.0782(3)
c/Å	21.6852(10)
α/°	90
β/°	90
γ/°	90
Volume/$Å^3$	2309.87(18)
Z	8
$\rho_{calc}g/cm^3$	1.870
μ/mm^{-1}	4.946
F(000)	1304.0
Crystal size/mm^3	? × ? × ?
Radiation	CuKα (λ = 1.54178)
2Θ range for data collection/°	11.76 to 133.26
Index ranges	$-17 \leq h \leq 17$, $-7 \leq k \leq 8$, $-25 \leq l \leq 25$
Reflections collected	12510
Independent reflections	2032 [R_{int} = 0.0621, R_{sigma} = 0.0411]
Data/restraints/parameters	2032/0/166
Goodness-of-fit on F^2	1.098
Final R indexes [I>=2σ (I)]	R_1 = 0.0389, wR_2 = 0.0975
Final R indexes [all data]	R_1 = 0.0471, wR_2 = 0.1023
Largest diff. peak/hole / e $Å^{-3}$	0.38/-0.68

9.5 Crystal data for $Co(B1MTT)_2.(CH_3)_2CO$

Empirical formula	$C_{11}H_{18}CoN_{22}O$
Formula weight	533.40
Temperature/K	296.15
Crystal system	monoclinic
Space group	$P2_1/n$
a/Å	9.7917(9)
b/Å	15.3747(14)
c/Å	14.9248(13)
α/°	90
β/°	100.1260(10)
γ/°	90
Volume/$Å^3$	2211.8(3)
Z	4
$\rho_{calc}g/cm^3$	1.602
μ/mm^{-1}	0.834
F(000)	1092.0
Crystal size/mm^3	? × ? × ?
Radiation	MoKα (λ = 0.71073)
2Θ range for data collection/°	3.834 to 55.002
Index ranges	$-12 \leq h \leq 12$, $-19 \leq k \leq 19$, $-19 \leq l \leq 19$
Reflections collected	26108
Independent reflections	5070 [R_{int} = 0.0246, R_{sigma} = 0.0179]
Data/restraints/parameters	5070/36/359
Goodness-of-fit on F^2	1.345
Final R indexes [I>=2σ (I)]	R_1 = 0.0890, wR_2 = 0.2388
Final R indexes [all data]	R_1 = 0.0930, wR_2 = 0.2501
Largest diff. peak/hole / e $Å^{-3}$	0.82/-0.88

9.6 Crystal data for $Ni(B1MTT)_2.(CH_3)_2CO$

Empirical formula	$C_{11}H_{18}N_{22}NiO$
Formula weight	417.10
Temperature/K	296.15
Crystal system	orthorhombic
Space group	Pbca
a/Å	8.4341(3)
b/Å	17.7531(7)
c/Å	29.8766(11)
α/°	90
β/°	90
γ/°	90
Volume/$Å^3$	4473.5(3)
Z	8
$\rho_{calc}g/cm^3$	1.239
μ/mm^{-1}	0.903
F(000)	1657.0
Crystal size/mm^3	? × ? × ?
Radiation	MoKα (λ = 0.71073)
2Θ range for data collection/°	2.726 to 57.41
Index ranges	$-8 \leq h \leq 11$, $-23 \leq k \leq 22$, $-38 \leq l \leq 39$
Reflections collected	26691
Independent reflections	5739 [R_{int} = 0.0661, R_{sigma} = 0.0592]
Data/restraints/parameters	5739/0/322
Goodness-of-fit on F^2	1.124
Final R indexes [I>=2σ (I)]	R_1 = 0.0439, wR_2 = 0.1175
Final R indexes [all data]	R_1 = 0.0801, wR_2 = 0.1593
Largest diff. peak/hole / e $Å^{-3}$	0.74/-1.02

9.7 Crystal data for $Fe(B1MTT)_2.(CH_3)_2CO$

Empirical formula	$C_{11}H_{18}FeN_{22}O$
Formula weight	530.32
Temperature/K	296.15
Crystal system	monoclinic
Space group	$P2_1/n$
a/Å	15.490(6)
b/Å	8.096(3)
c/Å	17.220(5)
α/°	90
β/°	97.778(18)
γ/°	90
Volume/$Å^3$	2139.7(13)
Z	4
$\rho_{calc}g/cm^3$	1.646
μ/mm^{-1}	0.765
F(000)	1088.0
Crystal size/mm^3	? × ? × ?
Radiation	MoKα (λ = 0.71073)
2Θ range for data collection/°	3.32 to 55.426
Index ranges	$-18 \leq h \leq 20$, $-10 \leq k \leq 5$, $-22 \leq l \leq 16$
Reflections collected	13517
Independent reflections	4871 [R_{int} = 0.1630, R_{sigma} = 0.2003]
Data/restraints/parameters	4871/0/322
Goodness-of-fit on F^2	1.082
Final R indexes [I>=2σ (I)]	R_1 = 0.1411, wR_2 = 0.3165
Final R indexes [all data]	R_1 = 0.2162, wR_2 = 0.3511
Largest diff. peak/hole / e $Å^{-3}$	1.47/-1.18

9.8 Crystal data for (PPN)(B1M3NTT)

Empirical formula	$C_{42}H_{42}N_{12}O_7P_2$
Formula weight	888.81
Temperature/K	295.76
Crystal system	triclinic
Space group	P-1
a/Å	10.5766(15)
b/Å	14.228(2)
c/Å	15.742(2)
α/°	108.021(7)
β/°	96.295(8)
γ/°	94.408(8)
Volume/Å^3	2223.7(6)
Z	2
ρ_{calc}g/cm^3	1.327
μ/mm^{-1}	1.418
F(000)	928.0
Crystal size/mm^3	? × ? × ?
Radiation	CuKα (λ = 1.54178)
2Θ range for data collection/°	5.964 to 134.166
Index ranges	$-12 \leq h \leq 12$, $-16 \leq k \leq 16$, $-18 \leq l \leq 18$
Reflections collected	65802
Independent reflections	7831 [R_{int} = 0.1354, R_{sigma} = 0.0676]
Data/restraints/parameters	7831/0/579
Goodness-of-fit on F^2	1.104
Final R indexes [I>=2σ (I)]	R_1 = 0.0861, wR_2 = 0.2322
Final R indexes [all data]	R_1 = 0.1365, wR_2 = 0.2621
Largest diff. peak/hole / e Å^{-3}	0.45/-0.37

9.9 Crystal data for K-2-Az-4-NIm

Empirical formula	$C_3H_3KN_6O_3$
Formula weight	167.86
Temperature/K	100.03
Crystal system	orthorhombic
Space group	$P2_12_12$
a/Å	17.2060(7)
b/Å	6.2551(3)
c/Å	6.9757(2)
α/°	90
β/°	90
γ/°	90
Volume/Å^3	750.76(5)
Z	4
ρ_{calc}g/cm^3	1.485
μ/mm^{-1}	2.425
F(000)	335.0
Crystal size/mm^3	? × ? × ?
Radiation	CuKα (λ = 1.54178)
2Θ range for data collection/°	10.282 to 133.048
Index ranges	$-20 \leq h \leq 17$, $-5 \leq k \leq 7$, $-8 \leq l \leq 8$
Reflections collected	2648
Independent reflections	1241 [R_{int} = 0.0375, R_{sigma} = 0.0589]
Data/restraints/parameters	1241/0/130
Goodness-of-fit on F^2	1.107
Final R indexes [I>=2σ (I)]	R_1 = 0.0327, wR_2 = 0.0817
Final R indexes [all data]	R_1 = 0.0338, wR_2 = 0.0826
Largest diff. peak/hole / e Å^{-3}	0.43/-0.42
Flack parameter	0.124(12)

9.10 Crystal data for 3-azido-4-nitropyrazole monohydrate

Empirical formula	$C_3H_4N_6O_3$
Formula weight	172.12
Temperature/K	296.15
Crystal system	triclinic
Space group	P-1
a/Å	8.227(16)
b/Å	12.02(2)
c/Å	14.59(3)
α/°	81.56(5)
β/°	73.84(5)
γ/°	82.81(6)
Volume/Å^3	1365(4)
Z	8
ρ_{calc}g/cm^3	1.675
μ/mm^{-1}	0.148
F(000)	704.0
Crystal size/mm^3	? × ? × ?
Radiation	MoKα (λ = 0.71073)
2Θ range for data collection/°	2.928 to 57.484
Index ranges	$-10 \leq h \leq 11$, $-16 \leq k \leq 16$, $-19 \leq l \leq 19$
Reflections collected	49322
Independent reflections	6944 [R_{int} = 0.0980, R_{sigma} = 0.0692]
Data/restraints/parameters	6944/0/497
Goodness-of-fit on F^2	1.024
Final R indexes [I>=2σ (I)]	R_1 = 0.0639, wR_2 = 0.1549
Final R indexes [all data]	R_1 = 0.1206, wR_2 = 0.1861
Largest diff. peak/hole / e Å^{-3}	0.66/-0.41

9.11 Crystal data for K-NPT.H_2O

Empirical formula	$C_3H_2KN_6O_{2.5}$
Formula weight	201.21
Temperature/K	296.15
Crystal system	monoclinic
Space group	C2
a/Å	13.301(5)
b/Å	7.247(3)
c/Å	7.377(3)
α/°	90
β/°	94.331(7)
γ/°	90
Volume/$Å^3$	709.1(5)
Z	4
$\rho_{calc}g/cm^3$	1.885
μ/mm^{-1}	0.725
F(000)	404.0
Crystal size/mm^3	? × ? × ?
Radiation	MoKα (λ = 0.71073)
2Θ range for data collection/°	5.538 to 55.15
Index ranges	$-17 \leq h \leq 17$, $-9 \leq k \leq 9$, $-9 \leq l \leq 9$
Reflections collected	4315
Independent reflections	1657 [R_{int} = 0.0601, R_{sigma} = 0.0796]
Data/restraints/parameters	1657/1/113
Goodness-of-fit on F^2	1.092
Final R indexes [I>=2σ (I)]	R_1 = 0.0530, wR_2 = 0.1024
Final R indexes [all data]	R_1 = 0.0658, wR_2 = 0.1173
Largest diff. peak/hole / e $Å^{-3}$	0.57/-0.42
Flack parameter	0.02(6)

9.12 Crystal data for Na_2-3-O-4-NPT.5H_2O

Empirical formula	$C_3N_6Na_2O_8$
Formula weight	294.07
Temperature/K	99.99
Crystal system	monoclinic
Space group	$P2_1/c$
a/Å	6.7771(4)
b/Å	17.6146(10)
c/Å	10.1712(5)
α/°	90
β/°	106.356(3)
γ/°	90
Volume/Å^3	1165.06(11)
Z	4
ρ_{calc}g/cm^3	1.677
μ/mm^{-1}	2.067
F(000)	584.0
Crystal size/mm^3	? × ? × ?
Radiation	CuKα (λ = 1.54178)
2Θ range for data collection/°	10.042 to 133.696
Index ranges	$-8 \leq h \leq 8$, $-20 \leq k \leq 20$, $-11 \leq l \leq 12$
Reflections collected	8831
Independent reflections	2020 [R_{int} = 0.0843, R_{sigma} = 0.0627]
Data/restraints/parameters	2020/0/77
Goodness-of-fit on F^2	1.460
Final R indexes [I>=2σ (I)]	R_1 = 0.1775, wR_2 = 0.3565
Final R indexes [all data]	R_1 = 0.1819, wR_2 = 0.3583
Largest diff. peak/hole / e Å^{-3}	0.75/-0.70